ANNUAL REPORTS ON

NMR SPECTROSCOPY

Edited by

G. A. WEBB

Department of Chemistry, University of Surrey, Guildford, Surrey, England

VOLUME 38

ACADEMIC PRESS

San Diego ● London ● Boston
New York ● Sydney ● Tokyo ● Toronto

This book is printed on acid-free paper.

Academic Press
24–28 Oval Road, London NW1 7DX, UK
http://www.hbuk.co.uk./ap/

Academic Press
A division of Harcourt Brace & Company
525 B Street, Suite 1900, San Diego, California 92101-4495, USA
http://www.apnet.com

ISBN 0-12-505338-X

A catalogue for this book is available from the British Library

Typeset by Keyset Composition, Colchester, Essex
Printed in Great Britain by MPG Books Ltd, Bodmin, Cornwall

99 00 01 02 03 04 MP 9 8 7 6 5 4 3 2 1

List of Contributors

Toshihide Baba, *Department of Chemical Engineering, Tokyo Institute of Technology, Ookayama, Meguro-ku, Tokyo 152-8552, Japan*

Jeremy R. Everett, *Department of Physical Sciences and Computational Chemistry, Pfizer Central Research, Sandwich, Kent CT13 9NJ, UK*

Dietrich Gudat, *Institut für Anorganische Chemie der Universität Bonn, Gerhard-Domagk-Strasse 1, D-53121 Bonn, Germany*

James F. Hinton, *Department of Chemistry/Biochemistry, University of Arkansas, Fayetteville, Arkansas 72701, USA*

John C. Lindon, *Biological Chemistry, Biomedical Sciences Division, Imperial College of Science, Technology and Medicine, University of London, Sir Alexander Fleming Building, South Kensington, London SW7 2AZ, UK*

John Malito, *Department of Chemistry, Cork Institute of Technology, Rossa Avenue, Bishopstown, Cork, Ireland*

Jeremy K. Nicholson, *Biological Chemistry, Biomedical Sciences Division, Imperial College of Science, Technology and Medicine, University of London, Sir Alexander Fleming Building, South Kensington, London SW7 2AZ, UK*

Yoshio Ono, *Department of Chemical Engineering, Tokyo Institute of Technology, Ookayama, Meguro-ku, Tokyo 152-8552, Japan*

William S. Price, *Water Research Institute, Sengen 2-1-6, Tsukuba, Ibaraki 305-0047, Japan*

Bernd Wrackmeyer, *Laboratorium für Anorganische Chemie der Universität Bayreuth, D-95440 Bayreuth, Germany*

Preface

It is a very great pleasure for me to introduce Volume 38 of Annual Reports of NMR Spectroscopy. As in previous volumes in this series, the refulgence of NMR in tackling a wide range of molecular problems is amply demonstrated by the topics chosen by the authors of the present reports.

The first chapter by J. C. Lindon, J. K. Nicholson and J. R. Everett covers the NMR Spectroscopy of Biofluids. This is followed by an account of Studies of Biological Ion Transporting Channels from J. F. Hinton. The third chapter by D. Gudat relates to Applications of Heteronuclear X,Y-correlation Spectroscopy in Organometallic and Organoelement Chemistry. B. Wrackmeyer reports on Applications of ^{119}Sn NMR Parameters. ^{63}Cu NMR Spectroscopy is the area covered in the chapter by J. Malito. The penultimate account is by W. S. Price on Water Signal Suppression in NMR Spectroscopy. In the final chapter, T. Baba and Y. Ono discuss Variable Temperature ^{1}H MAS NMR: A Powerful Tool for the Investigation of Dynamic Properties of Acidic Protons in Zeolites and Heteropoly Compounds.

My thanks are due to all of these authors for the efforts which they have invested in producing such interesting accounts which suffer neither from asperity nor prolixity. I am also extremely grateful for the cooperation of the production staff at Academic Press (London) in the timely appearance of this volume.

University of Surrey
Guildford, Surrey
England

G. A. WEBB
October 1998

NMR Spectroscopy of Biofluids

JOHN C. LINDON,[1] JEREMY K. NICHOLSON[1] and JEREMY R. EVERETT[2]

[1]Biological Chemistry, Biomedical Sciences Division, Imperial College of Science, Technology and Medicine, University of London, Sir Alexander Fleming Building, South Kensington, London SW7 2AZ, UK
[2]Department of Physical Sciences and Computational Chemistry, Pfizer Central Research, Sandwich, Kent CT13 9NJ, UK

ANNUAL REPORTS ON NMR SPECTROSCOPY
VOLUME 38 ISBN 0-12-505338-X

1. INTRODUCTION

Analysis of biofluids provides a unique window into the biochemical status of a living organism since the composition of a given biofluid will be modulated according to the level of function of the cells that are intimately concerned with its manufacture and secretion. For that reason the composition of a particular fluid carries biochemical information on many of the modes and severity of organ dysfunction. Dietary and diurnal variations may also influence biofluid compositions, and it is clearly important to differentiate these effects if correct biochemical inferences are to be drawn from their analysis. Knowledge of the composition of biofluids can also be important in toxicological studies and in experiments on the metabolism, disposition and fate of drugs and other xenobiotics. One of the most successful approaches to biofluid analysis has been the application of NMR spectroscopy[1] and studies can be divided into those that are largely *analytical* or *dynamic* in nature. Analytical biofluid NMR studies are concerned primarily with the collection,

assignment, and quantitation of NMR spectra and their interpretation in biochemical terms; such studies are the most numerous by far in the literature. Dynamic biofluid NMR studies cover the detailed understanding of the interactions of the components in the whole biological matrix. The types of dynamic interactions amenable to NMR study include enzymatic biotransformations, metal complexation reactions, binding of small molecules to macromolecules, and cellular and micellar compartmentation which occur in different biofluids to varying degrees.

The information content of biofluid spectra is very high and the complete assignment of the ^{1}H NMR spectrum of most biofluids is not possible (even by use of 900 MHz NMR spectroscopy) due to the enormous complexity of the matrix. However, the assignment problems vary considerably between biofluid types. For instance, seminal fluids are highly regulated with respect to metabolite composition and concentrations and the majority of the NMR signals have been assigned at 600 and 750 MHz for normal human individuals. Urine composition is much more variable because its composition is normally adjusted by the body in order to maintain homeostasis and hence complete analysis is much more difficult. There is also enormous variation in the concentration range of NMR-detectable metabolites in urine samples. Clearly those metabolites present in concentration close to the limits of detection for 1-dimensional (1D) NMR spectroscopy (~100 nM for many metabolites at 800 MHz giving a 3×10^8 metabolite concentration range) pose severe NMR spectral assignment problems. With every new increase in available spectrometer frequency the number of resonances that can be resolved in a biofluid increases and although this has the effect of solving some assignment problems, it also poses new ones. Furthermore, there are still important problems of spectral interpretation that arise due to compartmentation and binding of small molecules in the organized macromolecular domains that exist in some biofluids such as blood plasma and bile. This does not, however, reduce the diagnostic capabilities and potential of the technique, merely drawing attention to problems of biological variation and the influence of variation on diagnostic certainty.

All biological fluids have their own characteristic physicochemical properties, and these partly dictate the types of NMR experiment that may be employed to maximize the biochemical information from each fluid type and a summary of some of these is given in Table 1 for normal biofluids. ^{1}H NMR spectra of biofluids are usually highly complex with signals from protons with a wide range of chemical shifts, scalar couplings and relaxation properties, due to differences in molecular structure, mobility and dynamics. It has been argued[2] that NMR studies of body fluids should ideally be performed at the highest field available to obtain maximal dispersion and sensitivity and most work has been performed at 400 MHz or greater. Although lower field strength measurements can be useful for the detection of the most abundant metabolites and, in certain circumstances, give

Table 1. Normal biofluids and their physicochemical properties.

Sample	Function	Water content[1]	Viscosity	Protein content[2]	Lipid content[2]	Peak overlap[3]
Urine	Excretion Homeostasis	+++	–	–	–	–
Bile	Excretion Digestion	++	++	+	+	+++
Blood plasma	Transport Homeostasis Mechanical	+++	++	+++	+++	++
Whole blood[4]	Transport Oxygenation	+++	+++	+++	++	+++
Cerebrospinal fluid	Transport Homeostasis Mechanical	+++	+	+	+	++
Milk	Nutrition	++	+	++	+++	+++
Saliva	Excretion Digestion	+++	++	++	++	+
Sweat	Excretion Homeostasis					
Gastric juice	Digestion	+++	+++	+++	–	++
Pancreatic juice	Digestion	++	++	+++	+	+++
Seminal fluid	Support for spermatozoa	+	+++	+	+	+++
Prostatic fluid	Support for spermatozoa	+	++	+	+	++
Seminal vesicle fluid	Support for spermatozoa	+	+++	+++	+	+++
Amniotic fluid	Protection of fetus	+++	+	+	+	+
Follicular fluid	Reproduction	+++	+	+	+	+
Synovial fluid	Joint protection	+++	+++	++	+	+
Aqueous humour	Eye function	+++	+	++	–	+

Key

1. Relative water intensity when compared with concentrations of metabolites of interest, +++ indicates that few metabolite signals can be observed without water suppression due to dynamic range problems.
2. In biofluids with high protein or lipid contents, spin-echo spectra must normally be employed to eliminate broad resonances.
3. A subjective indication of spectral crowding (at 600 MHz) due to abundance of endogenous metabolites with a wide range of shifts.
4. Presence of cells and process of cell sedimentation gives rise to magnetic field inhomogeneity problems.

quantitatively accurate results, comparable higher field ^{1}H NMR measurements are generally more accurate. Even the dispersion gain on going from 600 MHz to 800 MHz is significant in ^{1}H NMR spectroscopy of biofluids and allows more signals to be assigned, considerably easing the analysis of complex biofluid spectra. An illustration of the complexity of biofluid spectra, and hence the need for ultra-high-field measurements, is given in Fig. 1 which shows 800 MHz ^{1}H NMR spectra of normal human urine, bile and blood plasma.

There are two types of noise that may be evident in ^{1}H NMR spectra of biological fluids namely *instrument noise* and *chemical noise*. Unlike instrument noise, chemical noise is related to the sample itself and is the result of the extensive overlap of signals from compounds that are low in abundance in the matrix and, individually, close to the detection limits of the spectrometer. Nonetheless, they give rise to apparently broad and weakly featured ^{1}H NMR responses due to their frequency superimposition. It is generally true that for ^{1}H NMR work on biofluids it is the chemical noise rather than instrument noise that usually limits the amount of recoverable spectral information. Normally only increasing the NMR frequency can allow recovery of the information that was in the chemical noise at lower frequencies. Furthermore, the problem of chemical noise interference varies in severity according to the biofluid type and chemical shift ranges that are under consideration for each fluid.

There are also two types of accessible information available in an NMR experiment on a biological fluid. These have been termed *latent* and *patent* biochemical information.[2] Patent biochemical information is defined as being that which can be measured quantitatively in a single pulse experiment. Latent information in an NMR spectrum measured at a particular field is not available in the single pulse spectrum and the biochemical data contained therein can only be obtained by careful selection of appropriate multipulse sequences to achieve either spectral editing or frequency dispersion in a second or higher dimension. Latent information can also be transformed into patent data by increasing the measurement field strength. Biochemical information can be latent in two ways, namely, through multiple peak overlap and by undergoing some type of dynamic molecular interaction resulting in the lack of resolved signals for a compound present at levels in the NMR detection range for the spectrometer involved. On increasing the frequency at which an NMR experiment is performed there is a consequent increase in sensitivity and so signals from molecules in solution that were too dilute to be measured may become measurable at higher frequency and become latent or patent information. Thus there is an effective increase in the amount of information of all levels on increasing field strength, thereby increasing the amount of useful biochemical data in the NMR spectrum.

It is clear that at even the present level of technology in NMR, it is not yet possible to detect many important biochemical substances, e.g. hormones, in

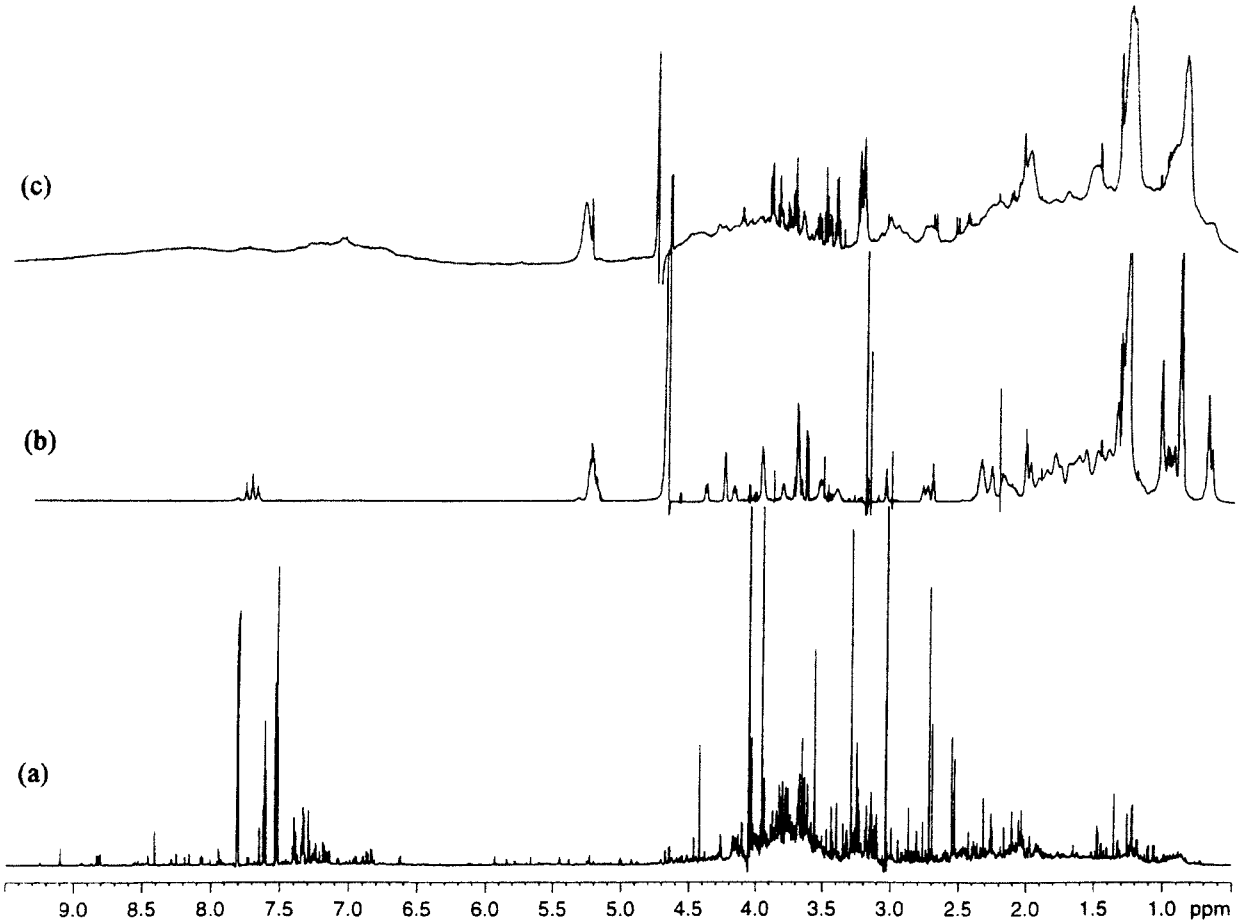

Fig. 1. 800 MHz ^{1}H NMR spectra of control human biofluids: (a) urine, (b) gall bladder bile and (c) blood plasma.

body fluids because of problems with sensitivity, dispersion and dynamic range and this area of research will continue to be technology-limited. With this in mind, it would seem prudent to interpret quantitative ^{1}H NMR measurements of intact biological materials and assignment of resonances in 1D spectra with considerable caution even when measured at ultrahigh field.

2. RESONANCE ASSIGNMENT IN NMR SPECTRA OF BIOFLUIDS

Usually in order to assign ^{1}H NMR spectra of biofluids, comparison is made with spectra of authentic materials and by standard addition to the biofluid sample. This has served to assign the major peaks in biofluids. Additional confirmation of assignments is usually sought from the application of 2-dimensional (2D) NMR methods, particularly COSY and TOCSY and, increasingly, inverse-detected heteronuclear correlation methods such as HMQC and HSQC. Thus the application of the 2D J-resolved (JRES) pulse sequence is important for spreading out the coupling patterns of the multitude of small molecules in a biofluid. Even 2D correlation NMR spectra of complex biofluids show much overlap of cross-peaks and further editing is often desirable. Thus simplification of NMR spectra of biofluids can also be achieved using (i) spin-echo methods particularly for fluids containing high levels of macromolecules, (ii) relaxation editing in general based on T_1 and/or T_2, (iii) diffusion editing, (iv) multiple quantum filtering. To this end, a method based on the separation of ^{1}H NMR resonances into subspectra according to whether the protons arise from CH, CH_2 or CH_3 groups via use of maximum quantum coherence spectroscopy (MAXY)[3–5] has been demonstrated. This has been extended to produce 2D NMR spectra such as MAXY–TOCSY, MAXY–NOESY and MAXY–JRES.[5] Editing of NMR spectra based on differences in relaxation rates and diffusion coefficients will be covered later in the section devoted to NMR spectroscopy of blood plasma (Section 5.6).

One major advantage of using NMR spectroscopy to study complex biomixtures is that measurements can often be made with minimal sample preparation (usually with only the addition of 5–10% D_2O) and a detailed analytical profile can be obtained on the whole biological sample.[1] Hence, much effort has been expended in discovering efficient new NMR pulse sequence techniques for spectral simplification and water suppression especially for biofluids.[6]

Detailed ^{1}H NMR spectroscopic data for a wide range of metabolites and biomolecules found in biofluids are given in Table 2. Many of these have been confirmed by addition of authentic material and others are identified by 2D NMR methods and valuable supplementary information is available in several literature compilations of data.[7,8]

Table 2. ^{1}H NMR chemical shifts and signal assignments of low-molecular-weight metabolites found in biofluids.

	Assignment	$\delta(^1H)$	Multiplicity	$\delta(^{13}C)$	Biofluid[1]
α-Hydroxyisovalerate	CH_3	0.81	d		C,U
α-Hydroxy-*n*-butyrate	CH_3	0.90	t		C,U
n-Butyrate	CH_3	0.90	t		U
α-Hydroxy-*n*-valerate	CH_3	0.92	t		U
Isoleucine	δ-CH_3	0.94	t		A,C,P,S,U
Leucine	δ-CH_3	0.96	t		A,C,P,U
Leucine	δ-CH_3	0.97	t		A,C,P,U
α-Hydroxyisovalerate	CH_3	0.97	d		C,U
Valine	CH_3	0.99	d	19.6	C,P,U
Isoleucine	β-CH_3	1.01	d	14.6	A,C,P,S,U
Valine	CH_3	1.04	d		A,C,P,U
Ethanol	CH_3	1.11	t		C,P,U
Propionate	CH_3	1.12	t		U
Isobutyrate	CH_3	1.13	d		P
β-Hydroxybutyrate	CH_3	1.20	d		C,P,S,U
Isoleucine	γ-CH_2	1.26	m		A,C,P,S,U
Fucose	CH_3	1.31	d		P
Lactate	CH_3	1.33	d	20.9	A,C,P,S,U
Threonine	CH_3	1.34	d		A,C,P,S,U
α-Hydroxyisobutyrate	CH_3	1.36	s		U
α-Hydroxy-*n*-valerate	γ-CH_2	1.37	m		U
Alanine	CH_3	1.48	d	16.8	A,C,P,S,U
Lysine	γ-CH_2	1.48	m		C,P,S,U
Isoleucine	γ-CH_2	1.48	m		C,P,S,U
n-Butyrate	β-CH_2	1.56	d		P,U
Adipate	CH_2	1.56	m		P,U
Citrulline	γ-CH_2	1.58	m		C,U
α-Hydroxy-*n*-valerate	β-CH_2	1.64	m		U
α-Hydroxybutyrate	CH_2	1.70	m		U

Arginine	γ-CH_2	1.70	m		U
Leucine	CH_2	1.71	m	40.7	C,P,S,U
Lysine	δ-CH_2	1.73	m		C,P,S,U
Ornithine	γ-CH_2	1.81	m		C,P,S,U
Citrulline	β-CH_2	1.88	m		C,P,S,U
N-Acetylglutamate	β-CH_2	1.89	m		C,P,S,U
γ-Amino-*n*-butyrate	β-CH_2	1.91	m		C,P,S,U
Lysine	β-CH_2	1.91	m	30.3	C,P,S,U
Arginine	β-CH_2	1.93	m		C,P,S,U
Ornithine	β-CH_2	1.95	m		A,S,U
Acetate	CH_3	1.95	s		A,C,P,S,U
Isoleucine	β-CH	1.98	m		C,P,U
Acetamide	CH_3	2.01	s		U
N-Acetyl groups (glycoproteins)	CH_3	2.02	s	23.0	P,U
α-Hydroxyisovalerate	β-CH	2.02	m		U
N-Acetylaspartate	CH_3	2.03	s		C,U
Proline	γ-CH_2	2.01	m		C,S,U
N-Acetyl groups (glycoproteins)	CH_3	2.05	s		P,U
Proline	β-CH_2	2.07	m		C,S,U
N-Acetylglutamate	CH_3	2.04	s		U
N-Acetylglutamate	β-CH_2	2.06	m		U
Glutamate	β-CH_2	2.10[2]	m	30.1	A,C,P,S,U
Glutamine	β-CH_2	2.14[2]	m		C,P,S,U
Methionine	S-CH_3	2.14	s		A,C,P,S,U
n-Butyrate	α-CH_2'	2.16	t		C,P,S,U
Methionine	β-CH_2	2.16	m		A,C,P,S,U
Adipate	CH_2COOH	2.22	m		U
N-Acetylglutamate	γ-CH_2	2.23	t		U
Acetone	CH_3	2.23	s		P,U
Valine	β-CH	2.28	m		C,P,S,U
Acetoacetate	CH_3	2.29	s		C,P,S,U
γ-Amino-*n*-butyrate	α-CH_2	2.30	t		C
β-Hydroxybutyrate	CH_2	2.31	ABX		C,P,S,U

Table 2.—*Continued*

	Assignment	$\delta(^1H)$	Multiplicity	$\delta(^{13}C)$	Biofluid[1]
Proline	β-CH_2	2.35	m		A,C,S,U
Glutamate[4]	γ-CH_2	2.36	m	34.5	*in PBS*
Oxalacetate	CH_2	2.38	s		C,P,U
Pyruvate	CH_3	2.38	s		C,P,U
Malate	CH_2	2.39	dd		U
β-Hydroxybutyrate	CH_2	2.41	ABX		C,P,S,U
Succinate	CH	2.43	s		C,P,S,U
Carnitine	CH_2(COOH)	2.44	dd		C,P,S,U
α-Ketoglutarate	γ-CH_2	2.45	t		C,P,S,U
Glutamine	γ-CH_2	2.46[2]	m	31.9	C,P,S,U
Glutamate[4]	γ-CH_2	2.50	m		A,C,P,S,U
N-Acetylaspartate	CH_2	2.51	ABX		C,U
Methylamine	CH_3	2.54	s		P
Citrate	$\frac{1}{2}CH_2$	2.67	AB		A,C,P,S,U
Methionine	S-CH_2	2.65	t		C,P,S,U
Aspartate	β-CH_2	2.68[3]	ABX		C,P,S,U
Malate	CH_2	2.69	ABX		U
N-Acetylaspartate	CH_2	2.70	ABX		C,U
Dimethylamine	CH_3	2.72	s		C,P,S,U
Sarcosine	CH_3	2.74	s		U
Dimethylglycine	CH_3	2.78	s		P,U
Citrate	$\frac{1}{2}CH_2$	2.80	AB		A,C,P,S,U
Aspartate	β-CH_2	2.82	ABX		C,P,S,U
Methylguanidine	CH_3	2.83	s		U
Asparagine	β-CH_2	2.86	m		C,P,S,U
Trimethylamine	CH_3	2.88	s		U
Asparagine	β-CH_2	2.96	m		C,P,S,U
α-Ketoglutarate	β-CH_2	3.01	t		C,P,S,U
γ-Amino-*n*-butyrate	γ-CH_2	3.02	t		C
Lysine	ε-CH_2	3.03	t	40.3	C,P,S,U

Cysteine	CH_2	3.04	m		C,U
Creatine	CH_3	3.04	s		A,C,P,S,U
Phosphocreatine	CH_3	3.05	s		S
Creatinine	CH_3	3.05	s		A,C,P,S,U
Tyrosine	CH_2	3.06	ABX		C,P,S,U
Ornithine	δ-CH_2	3.06	t		C,S,U
Cysteine	CH_2	3.12	ABX		C,U
Malonate	CH_2	3.13	s		U
Phenylalanine	β-CH_2	3.13	m		C,P,S,U
Histidine	β-CH_2	3.14	ABX		C,P,S,U
Citrulline	α-CH_2	3.15	m		C,U
cis-Aconitate	CH_2	3.17	s		U
Tyrosine	CH_2	3.20	ABX		C,P,S,U
Choline	$N(CH_3)_3$	3.21	s	55.0	C,P,S,U
Phosphorylethanolamine	NCH_2	3.23	t		S
β-Glucose	C-H2	3.24	dd		A,C,P,S,U
Histidine	β-CH_2	3.25	ABX		C,P,S,U
Arginine	δ-CH_2	3.25	t	41.3	C,S,U
Trimethylamine-*N*-oxide	$N(CH_3)_3$	3.27	s		C,P,S,U
Taurine	CH_2SO_3	3.25	t		A,C,P,S,U
Betaine	$N(CH_3)_3$	3.27	s		C,P,S,U
Phenylalanine	β-CH_2	3.28	m		C,P,S,U
Myo-Inositol	H5	3.28	t		P
Tryptophan	CH_2	3.31	ABX		P,S,U
Glycerophosphorylcholine	$N(CH_3)_3$	3.35	s		S
Proline	δ-CH_2	3.33	m		A,P,U
β-Glucose	C-H4	3.40	t	70.6	A,C,P,S,U
α-Glucose	C-H4	3.41	t	70.6	A,C,P,S,U
Proline	δ-CH_2	3.42	m		A,P,U
Carnitine	NCH_2	3.43	m		C,P,S,U
Taurine	NCH_2	3.43	t		A,C,P,S,U

Table 2.—*Continued*

	Assignment	$\delta(^1H)$	Multiplicity	$\delta(^{13}C)$	Biofluid[1]
Acetoacetate	CH_2	3.45	s		C,P,S,U
β-Glucose	C-H5	3.47	ddd	76.7	A,C,P,S,U
trans-Aconitate	CH_2	3.47	s		U
β-Glucose	C-H3	3.49	t	76.7	A,C,P,S,U
Tryptophan	CH_2	3.49	ABX		P,U
Choline	NCH_2	3.52	m		C,P,S,U
Glycerophosphorylcholine	NCH_2	3.52	m		S
α-Glucose	C-H2	3.53	dd	72.3	A,C,P,S,U
Glycerol	CH_2	3.56	ABX	63.5	C,P
Myo-inositol	H1/H3	3.56	dd		P
Glycine[4]	CH_2	3.57	s		C,P,S,U
Threonine	α-CH	3.59	d		U
Fructose (β-furanose)	H1	3.59	d		S
Fructose (β-furanose)	H1′	3.59	d		S
Fructose (β-pyranose)	H1	3.60	d		S
Sarcosine	CH_2	3.61	s		C,P,S,U
Ethanol	CH_2	3.61	q		C,P,S,U
Valine	α-CH	3.62	d	64.2	C,P,S,U
Myo-inositol	H4/H6	3.63	dd		P
Fructose (β-pyranose)	H6′	3.63	m		S
Fructose (β-pyranose)	H3	3.64	m		S
Glycerol	CH_2	3.65	ABX	63.5	C,P
Isoleucine	α-CH	3.68	d		A,C,P,S,U
Fructose (β-furanose)	H6′	3.70	m		S
Fructose (β-furanose)	H1	3.70	m		S
α-Glucose	C-H3	3.71	t	73.6	C,P,S,U
β-Glucose	C-H6′	3.72	dd	61.6	A,C,P,S,U
Leucine	α-CH	3.73	t	55.1	A,C,P,S,U

α-Glucose	C-H6′	3.74	m	61.4	A,C,P,S,U
Ascorbate	CH_2	3.74	d		U
Ascorbate	CH_2	3.76	d		U
Citrulline	α-CH	3.76	t		C,U
Lysine	α-CH	3.76	t		C,P,S,U
Glutamine	α-CH	3.77	t	55.4	C,P,S,U
Glutamate	α-CH	3.77	t		A,C,P,S,U
Arginine	α-CH	3.77	t		C,U
Glycerol	CH	3.79	ABX	72.6	C,P
Alanine	CH	3.79	q		A,C,P,S,U
Ornithine	α-CH	3.79	t		C,P,S,U
Guanidoacetate	CH_2	3.80	s		U
Mannitol	CH3	3.82	d		C
Fructose (β-furanose)	H4	3.82	m		S
Fructose (β-pyranose)	H3	3.84	m		S
α-Glucose	C-H6	3.84	m	61.4	A,C,P,S,U
α-Glucose	C-H5	3.84	ddd	72.3	A,C,P,S,U
Fructose (β-furanose)	H6	3.85	m		S
α-Hydroxyisovalerate	α-CH	3.85	d		U
Serine	α-CH	3.85	ABX		U
Methionine	α-CH	3.86	t		A,C,P,S,U
β-Glucose	C-H6	3.90	dd	61.6	A,C,P,S,U
Fructose (β-pyranose)	H4	3.90	m		S
Betaine	CH_2	3.90	s		C,P,S,U
Aspartate	α-CH	3.91	ABX		C,U
4-Aminohippurate	CH_2	3.93	d		U
Creatine	CH_2	3.93	s		P
Glycolate	CH_2	3.94	s		U
Tyrosine	CH	3.94	ABX		C,P,S,U
Phosphocreatine	CH_2	3.95	s		–
Serine	β-CH_2	3.95	ABX		U

Table 2.—*Continued*

	Assignment	$\delta(^1H)$	Multiplicity	$\delta(^{13}C)$	Biofluid[1]
Hippurate	CH_2	3.97	d		C,P,S,U
Histidine	α-CH	3.99	ABX		C,P,S,U
α-Hydroxybutyrate	CH	4.00	ABX		U
Asparagine	α-CH	4.00	ABX		C,S,U
Cysteine	CH	4.00	ABX	69.2	U
Serine	β-CH_2	4.00	ABX		C,U
Phosphorylethanolamine	OCH_2	4.00	m		S
Phenylalanine	α-CH	4.00	m		C,P,S,U
Fructose (β-pyranose)	H5	4.01	m		S
Ascorbate	CH	4.03	m		U
Fructose (β-pyranose)	H6	4.01	m		S
α-Hydroxy-*n*-valerate	α-CH	4.05	m		U
Creatinine	CH_2	4.06	s		A,C,P,S,U
Tryptophan	CH	4.06	ABX		S,U
Myo-Inositol	H2	4.06	t		C,S,U
Choline	OCH_2	4.07	m		C,P,S,U
Lactate	CH	4.12	q		A,C,P,S,U
Fructose (β-furanose)	H5	4.13	m		S
Proline	α-CH	4.14	m		A,C,P,S,U
β-Hydroxybutyrate	CH	4.16	ABX		C,P,S,U
Threonine	β-CH	4.26	ABX		A,C,P,S,U
Malate	CH	4.31	dd		U
N-Methylnicotinamide	CH_3	4.48	s		U
Glycerophosphorylcholine	NCH_2	3.52	m		S
N-Acetylaspartate	CH	4.40	ABX		C,U
β-Galactose	CH1	4.52	d		C
Ascorbate	CH	4.52	d		U
β-Galactose	CH1	4.53	d		P
β-Glucose	CH1	4.64	d		A,C,P,S,U
Water	H_2O	4.79	s		all fluids

Phospho(enol)pyruvate	CH	5.19	t		–
α-Glucose	CH1	5.23	d	92.9	A,C,P,S,U
Allantoate	CH	5.26	s		–
Phospho(enol)pyruvate	CH	5.37	t		–
Allantoin	CH	5.40	d		U
Urea	NH_2	5.78	s		P,U
Uridine	H5	5.80	d		C,S,U
Uridine	H1′	5.82	d		C,S,U
cis-Aconitate	CH	5.92	s		U
Urocanate	CH(COOH)	6.40	d		U
Fumarate	CH	6.53	s		U
trans-Aconitate	CH	6.62	s		U
4-Aminohippurate	CH3/5	6.87	d		U
3,4-Dihydroxymandelate	cyclic H	6.87	d		U
3,4-Dihydroxymandelate	cyclic H	6.90	s		U
Tyrosine	H3/H5	6.91	d′	116.7	C,P,S,U
3,4-Dihydroxymandelate	cyclic H	6.94	d		U
3-Methylhistidine	H4	7.01	s		P
Histidine	C4H	7.08	s		C,P,S,U
1-Methylhistidine	H4	7.05	s		P
Tyrosine	H2/H6	7.20	d		C,P,S,U
Tryptophan	C5H/C6H	7.21	t		S,U
Indoxyl sulfate	H5	7.20	m		U
Indoxyl sulfate	H6	7.28	m		C,U
Tryptophan	C5H/C6H	7.29	t		S,U
Urocanate	CH(ring)	7.31	d		U
Tryptophan	C2H	7.33	s		S,U
Phenylalanine	H2/H6	7.33	m		C,P,S,U
Phenylalanine	H4	7.38	m		C,P,S,U
Urocanate	C5H	7.41	s		U
Phenylalanine	H/H5	7.43	m		C,P,S,U

Table 2.—*Continued*

	Assignment	$\delta(^1H)$	Multiplicity	$\delta(^{13}C)$	Biofluid[1]
Nicotinate	cyclic H	7.53	dd		U
Hippurate	CH3/CH5	7.55	t		U
Tryptophan	C7H	7.55	d		S,U
3-Methylhistidine	H2	7.61	s		P
Hippurate	CH4	7.64	t		U
4-Aminohippurate	CH2/6	7.68	d		U
Tryptophan	C4H	7.74	d		S,U
1-Methylhistidine	H2	7.77	s		P
Uridine	H6	7.81	d		C,S,U
Histidine	C2H	7.83	s		C,P,S,U
Hippurate	CH2/6	7.84	d		U
Urocanate	cyclic C3H	7.89	s		U
N-Methylnicotinamide	CH5	8.19	t		U
Nicotinate	cyclic H	8.26	dt		U
Formate	CH	8.46	s		C,P,S,U
Nicotinate	cyclic H	8.62	dd		U
N-Methylnicotinamide	CH4	8.90	d		U
Nicotinate	cyclic H	8.95	d		U
N-Methylnicotinamide	CH6	8.97	d		U
N-Methylnicotinamide	CH2	9.28	s		U

Key

1. Main biofluid in which compounds are found or have been observed; U, P, C, A and S refer to observation in urine, serum, CSF, amniotic and seminal fluids respectively.
2. Varies according to the presence of divalent metal ions (especially Ca, Mg and Zn).
3. Highly variable over physiological pH range.
4. Significant shift differences due to the formation of fast exchanging complexes with divalent metal ions in biofluids.

3. NMR STUDIES OF DYNAMIC INTERACTIONS

3.1. Introduction

Although NMR spectroscopy of biofluids is now a well-established technique for probing a wide range of biochemical problems, there are still many poorly understood physicochemical phenomena occurring in biofluids, particularly the subtle interactions occurring between small molecules and macromolecules or between organized multiphasic compartments. The understanding of these dynamic processes is of considerable importance if the full diagnostic potential of biofluid NMR spectroscopy is to be realized. Many studies of dynamics require a precise knowledge of the sample temperature, and a method of obtaining the true sample temperature, as opposed to the thermocouple temperature outside the NMR tube, has been proposed for biofluids.[9]

3.2. Enzymatic reactions

Many biological fluids contain significant amounts of active enzymes. This may be because they fulfil a biological function in the fluid, e.g. the esterase and peptidases present in prostatic fluid. Additionally, they may have leaked into the fluid due to disease or toxin-induced organ damage such as raised plasma alanine transaminase levels in liver and kidney disease, or raised urinary *N*-acetylglucosaminidase in kidney disease. When provided with the appropriate substrates these enzymes will manufacture new products which can be NMR detectable. Collection of sequential NMR data may then allow the time-course of this enzymatic conversion to be followed. This may yield important kinetic data on the activity of the enzyme in a "real" biological medium and may also provide indirect NMR evidence of organ damage. Whole blood is a biofluid containing red blood cells that have active metabolism catalysed by a range of enzymes, mainly the glycolytic cycle. Much study of these reactions has been undertaken (see Section 5.9.2).

3.3. Chemical reactions and biofluid instability

Many biofluids are not chemically stable and for this reason care should be taken in their collection and storage. For example, cell lysis in erythrocytes can easily occur. In addition, if the biofluid has been reconstituted into D_2O after freeze-drying or if a substantial amount of D_2O has been added to provide an NMR field lock, then it is possible that certain ^1H NMR resonances will be lost. These include not only NH and OH protons as expected but CH groups where the C–H bond is labile such as H2 of imidazole moieties (as in histidine or histidinyl-containing proteins such as

haemoglobin) or the CH_2 groups of acetoacetate which participates in keto–enol tautomerism. It should be noted that freeze-drying of biofluid samples also causes the loss of volatile components such as acetone.

3.4. Microbiological activity in biofluids

Biofluids are very prone to microbiological contamination, especially fluids such as urine, which are difficult to collect under sterile conditions. Samples should be stored deep frozen to minimize the effects of such contamination but evidence of bacterial growth will be seen in a time-dependent pattern of metabolites if NMR spectra are measured over a period of time or if the sample is kept at room temperature for extended periods. It has been noticed that bacteria can incorporate a ^2H atom from D_2O into metabolites and the presence of isotopically labelled acetate ($CH_2D.COOH$ and $CD_2H.COOH$ observable in the ^1H NMR spectrum) for example is a good indication of bacterial contamination.[10]

3.5. Macromolecular binding of small molecules

Some biofluids such as blood plasma contain high levels of proteins and many endogenous metabolites are bound to such macromolecules. There are many examples of this such as aromatic amino acids binding to serum albumin in blood plasma and this has a direct consequence of making the detection and quantitation of such species less easy.[11] This is also an important problem for detection and quantitation of drug metabolites in such biofluids. In NMR terms, the molecule can appear to be in fast, intermediate or slow exchange with the macromolecule. Thus interpretation of metabolite levels by NMR spectroscopy must always be undertaken after consideration of whether the result is perturbed by macromolecule binding with resulting relaxation and line width changes.

Binding of aromatic amino acids to blood plasma appears to occur by both non-polar and electrostatic interactions, but electrostatic interactions only are important for the binding of lactate,[11,12] citrate and acetate.[11] These examples appear to be nonspecific at mmol l^{-1} concentration levels and do not appear to be stereochemically selected[11] and so this would appear to preclude specific molecular recognition.

3.6. Membrane-based compartmentation

Some biofluids, particularly blood, contain cells with intact cell membranes. Other fluids such as bile or blood plasma have high levels of lipids organized into supramolecular particles such as micelles in bile and lipoproteins in

blood plasma. Small molecules can therefore be inside or outside of the lipid membrane or even inside the lipid membrane itself. In the extreme case of micellar aggregations, e.g. in bile, this can be regarded as compartmentation as the small molecule can be outside the micelles, in the micelle wall or within the micelle itself. Many small molecules are more freely soluble in biological fluids than they are in water alone (e.g. cholesterol and its esters in blood plasma). In all cases compartmentation of small molecules results in changes in the rotational correlation times and hence relaxation properties of their nuclei with respect to free solution conditions, and in some cases chemical shift and coupling constant changes as well. Observation of such species may be further complicated by chemical exchange. Visualization of the signals from compartmentalized molecules usually requires some physical perturbation of the sample to make the NMR lines sharp enough to be detected, e.g. methanolic extraction to observe cholesterol in blood or seminal plasma.[11]

3.7. Metal complexation

All biological fluids contain a variety of potential metal-chelating agents, sometimes at very high concentrations. The most ubiquitous metal chelators in biofluids are the free amino acids (especially, glutamine, glutamate, cysteine, histidine and aspartate) and organic acids such as citrate and succinate. Ca^{2+}, Mg^{2+} and Zn^{2+} are the main endogenous metal ions involved in complexation reactions[11] with organic biofluid components and many of these reactions can be studied using NMR. Chelation reactions and the physicochemical effects of other metals such as Fe^{3+}/Fe^{2+} metallodrugs and toxic metals such as Cd^{2+} in red blood cells and whole blood can also be studied under certain circumstances (see Section 5.9.2). Paramagnetic ions such as Gd^{2+} and Mn^{2+} can also be used to effect chemical editing of NMR spectra (and spin-echo-based solvent suppression) by selectively binding to endogenous metal-chelating agents such as citrate and hence broadening their signals.[13] The metal-chelating agent ethylenediaminetetraacetic acid (EDTA) is very effective for many di- and trivalent metal ions and can be added to biological fluids to remove metal from the endogenous chelating species with consequent changes in the NMR signal pattern and the appearance of signals from metal EDTA complexes.[11] EDTA addition also results in a general sharpening of NMR signals from biofluids because it also complexes trace levels of paramagnetic ions.

3.8. Chemical exchange processes

Biofluids contain many endogenous species that can participate in chemical exchange processes covering a variety of exchange time scales. These

processes may be connected with macromolecular binding or with metal complexation reactions or, more simply, involve exchange of protons with each other and/or solvent water. Some molecules such as citrate may be involved with all three types of chemical exchange phenomena, and hence signal positions vary considerably according to solution conditions. Depending on the exchange rate, spectral lines may be broadened or shifted from their free solution condition. Citrate signals are generally broadened in the presence of the metal ions present in biofluids (usually Ca^{2+}, Mg^{2+} and Zn^{2+}), and this broadening is reversed by the addition of EDTA which outcompetes citrate for binding of divalent metal ions.

4. ^{1}H NMR SPECTROSCOPY OF CEREBROSPINAL FLUID (CSF)

4.1. Properties and biochemical composition of CSF

The CSF surrounds the brain and spinal cord, where it acts as a barrier against mechanical shock, as a lubricant between the brain surface and the meninges, and helps support the weight of the brain. By means of CSF, substances are removed from the brain and spinal tissue and returned to the bloodstream. Drugs may also be distributed within the brain with the aid of the CSF circulation. CSF is a normally crystal-clear, low-viscosity liquid of pH 7.3 to 7.4. Because CSF is an ultrafiltrate it usually has a much lower protein content than plasma, although this may be elevated significantly in various disease states. Altered composition and physical characteristics of CSF can reflect damage to the central nervous system or meninges, and CSF is often sampled for microbiological, haematological, serological and biochemical analysis in patients with suspected cerebral disease. In general, the biochemical composition of CSF reflects the composition of the ultrafiltered blood plasma, but it also contains a number of metabolites that are secreted by the CNS tissue. It may also be depleted of certain constituents (e.g. glucose) relative to plasma, because of their utilization by the cerebral cells. It is, therefore, good practice to compare concentrations of metabolites in CSF with those in the plasma, because alterations in the latter may be reflected in the CSF even if cerebral metabolism is normal.

CSF is normally collected for diagnostic purposes by lumbar puncture, with a needle being inserted into the subarachnoid space. Given the invasive and delicate nature of this intervention, lumbar puncture is only performed with good reason and it is extremely rare to obtain CSF from a truly healthy donor. CSF may also be collected at postmortem, but the composition may be very different to that found antemortem. After collection of CSF, samples can be measured directly by NMR or freeze-dried and reconstituted in D_2O. In the latter case, the preconcentration step allows many more minor metabolites to

be detected. Unlike plasma, most CSF samples can be concentrated by up to 10 times after freeze drying because of the low protein content, and this allows collection of good-quality NMR data in reasonable times. Fluoride can be added to the CSF soon after collection where glucose measurements are required as this strongly inhibits glycolysis.

4.2. Assignment of the ^{1}H NMR spectra of CSF

Due to the low protein content of normal human CSF, it is possible to use single-pulse ^{1}H NMR experiments to obtain biochemical information without recourse to the spin-echo techniques often required for studies on blood and plasma (see Section 5). However, where serious cerebral damage has occurred, or in the presence of an acute infection, spectra may become dominated by protein resonances. Problems may also arise from protein binding and metal binding of some metabolites, with a consequential broadening of their proton resonances.

There are a number of ^{1}H NMR studies of CSF in the literature. The earliest report was by Bales *et al.*[14] and later Petroff *et al.*,[15] Bell *et al.*[16] and Kriat *et al.*[17] reported the assignment of a number of resonances. Also, Petroff and co-workers have shown that high-quality 2D ^{1}H NMR spectra can be obtained from human CSF, and that changes in NMR patterns can be roughly related to disease states in the donor.[15] In addition, many resonances have been assigned through the use of 2D JRES spectra and COSY45 spectra[18,19] and these are listed in Table 2. Examination of a number of *ex vivo* control samples showed high consistency in the aliphatic region of the 1D ^{1}H NMR spectra of CSF and many assignments could be made by inspection but glutamate and glutamine had distinctly broadened resonances. Wevers *et al.* have proposed a standardized method for acquiring NMR spectra of CSF and identified 50 compounds in CSF.[20] In addition, issues relating to sample handling have been reviewed.[17]

4.3. NMR spectroscopy of CSF in disease studies

Koschorek *et al.*[21] have measured ^{1}H NMR spectra of CSF from 84 patients at 360 MHz and quantified the levels of 19 signals, some of which were assigned to specific metabolites. For 42 patients with lumbar disk herniations, no significant differences from controls were found. However, they observed differences between controls and one patient with a medulloblastoma that showed a decreased glucose level plus new signals in the δ0.8–1.0 and δ1.28–1.42 regions which they assigned to valine and alanine. They also reported a ^{1}H NMR study on the CSF of 19 controls, 42 patients with disk herniations and 23 with cerebral tumours.[22] A semiquantitative analysis

of metabolites was conducted but relative metabolite concentrations were derived by dividing each metabolite signal intensity by that of lactate, the level of which can vary widely. No significant differences were found between the CSF of controls and disk herniation patients, but the CSF of the tumour patients were found to have significantly lower glucose–lactate ratios and higher valine–lactate ratios than in the controls. Population overlap prohibited diagnosis based on any one ratio, and so, in a subsequent study[22] with an enlarged patient population, discriminant analysis using 16 metabolite concentration ratios was performed to investigate the diagnostic potential of NMR. The results demonstrated good predictive capability, except for tumour diagnosis, in contrast to the previous results.[21] The poor discrimination of tumours was ascribed both to their inherent variability and to the fact that the tumours will usually contain a good blood supply and hence will tend to be confused with bleedings.[22]

Petroff and co-workers[15] reported a quantitative analysis of the ^{1}H NMR spectra of six CSF samples from three patients. These included a 34-year-old man presenting with seizures several hours after injecting heroin and cocaine while intoxicated with alcohol, and a 7-month-old girl who presented as a febrile, cyanotic hypotensive in a coma. The ^{1}H NMR spectrum of the CSF of the drug overdose victim showed clear and abnormally elevated signals for citrate, *myo*-inositol, creatinine/creatine and lactate.

Another study[12] also showed that human cerebrospinal fluid ^{1}H NMR spectra were different between normals (three subjects) and mildly diabetic people (two subjects), with the spectra of the latter group showing elevations in glucose and glycine. This study also included the ^{1}H NMR spectra of CSF from three infants with bacterial meningitis and found greatly increased lactate, but lowered glucose signals, relative to normal adults, with a complete absence of signals from citrate. CSF samples from patients with Huntingdon's disease have been compared with that from controls using ^{1}H NMR spectroscopy and a significant increase in glycine detected using 11 patients and 12 controls.[23] Hiraoka *et al.* have also studied a number of different neurological conditions using ^{1}H NMR spectroscopy of human CSF and identified raised glutamine in a case of hepatic encephalitis.[24] One study of CSF from rats in a model of stroke has been reported using 500 MHz ^{1}H NMR spectroscopy including 2D COSY methods and a number of spectral changes could be observed as a result of the experimentally induced lesion.[25]

NMR spectroscopy of CSF has been used in a number of studies of multiple sclerosis (MS). In one study a total of 19 patients with multiple sclerosis, 12 patients with degenerative dementia and 17 controls were examined. They showed increased lactate and fructose levels in multiple sclerosis patients but no correlations between NMR spectra and the differentiation of relapsing, remitting and primary, progressive multiple sclerosis.[26] Another study examined 53 cases of multiple sclerosis plus others with a variety of neurological disorders and showed that the observed level of lactate correlated with the

number of CSF mononuclear cells in patients with clinical activity. Also a decrease in formate was detected during active and inactive clinical phases of multiple sclerosis.[27] A third study examined CSF from 30 patients with actively progressing multiple sclerosis and found that acetate levels were higher in patients whilst formate levels were lower in patients compared to controls. There were no significant differences between spectra from early and longstanding MS patients. An unidentified peak, probably from an *N*-methyl compound, was seen in spectra from patients with actively progressing disease. However, this was not found in spectra of CSF from patients with AIDS dementia complex or Parkinson's disease but it did appear in one out of three Creutzfeld–Jakob disease patients and one out of seven patients with Guillain–Barre syndrome.[28]

Commodari *et al.*[29] have detected changes in the ^{1}H NMR spectra of CSF in nine patients suffering a variety of conditions including the detection of methylmalonate in a patient with vitamin B_{12} deficiency.

One study[30] has reported 500 and 600 MHz ^{1}H NMR data on the postmortem CSF from 23 Alzheimer's disease patients and controls. The main differences between the spectra of the two groups were found to be in the region δ2.4–2.9, where the resonances of aspartate, *N*-acetylaspartate, citrate, glutamate and methionine occur. Principal components analysis showed that separation of the two groups was possible and that citrate was the principal marker with citrate levels in the Alzheimer's disease patients much reduced compared with the controls. Patient age and the time interval between death and autopsy were examined to see whether these factors might account for the differences between the Alzheimer's disease and control groups. Allowing for these factors, the inter-group differences were reduced but still significant ($p<0.05$). It was hypothesized that the reduction in CSF citrate found in the Alzheimer's disease patients may be due to the reductions in pyruvate dehydrogenase (PDH) reported in the parietal cortex and temporal cortex of Alzheimer's disease patients. A decrease in PDH activity could result in a drop in mitochondrial citrate and a corresponding drop in the secretion of citrate to the CSF from the CNS.

5. ^{1}H NMR SPECTROSCOPY OF BLOOD PLASMA AND WHOLE BLOOD

5.1. Properties of blood and blood plasma

Vertebrate blood consists of cellular elements suspended in a complex fluid matrix of proteins, principally of albumin, immunoglobulins, glycoproteins and lipoproteins, together with a large number of inorganic and low-molecular-weight organic solutes. The functions of blood include the transport of oxygen, carbon dioxide, products of metabolism and hormones.

It is through the medium of the circulating blood that the constancy of the internal environment is maintained; disease processes or abnormalities anywhere in the body are reflected to various extents in altered blood composition. The dominant cell type is the erythrocyte that normally makes up about 45–50% of the blood volume. Other cell types normally make up only about 1% of the packed cell volume. The remaining volume of the blood is the plasma. "Serum" is the term given to the fluid separated from whole, untreated blood by centrifugation, whereas "plasma" is separated from whole blood after the addition of an anticoagulant (normally trisodium EDTA or lithium heparin). Serum is depleted in fibrinogen (the major clotting protein precursor) and is consequently less viscous than plasma. Serum and plasma consist mainly of water in which there are a number of distinct domains. These include an essentially isotropic, free-solution environment, which contains colloidal structures and aggregates of macromolecules including proteins, lipids and immunoglobulins. The complex mixture of fatty and nonfatty structures has a significant influence on the physicochemical behaviour of water itself and the substances dissolved in it.

The physicochemical complexity of plasma is expressed in its ^{1}H NMR spectra by the range of linewidths of the signals. This means that a number of different multiple pulse NMR experiments and/or physicochemical interventions must be applied to extract useful biochemical information. Numerous high-resolution ^{1}H NMR studies have been performed on the biochemistry of blood and its various cellular components and plasma. The physical properties of whole blood pose serious limitations on direct NMR investigations, but packed erythrocytes yield more useful information on cell biochemistry. The best resolved spectra are given by plasma, and ^{1}H NMR measurements on blood serum and plasma can provide a plethora of useful biochemical information on both low-molecular-weight metabolites and macromolecular structure and organization. The usefulness of ^{1}H NMR spectra of blood plasma for metabolic studies has been highlighted recently[31] and the difficulties of obtaining quantitative determinations of substances in blood plasma using ^{1}H NMR spectroscopy have been noted.[32] However, a quantitative method for determining glucose levels in blood plasma has been published.[33] The relative benefits of using formate over the more widely used trimethylsilylpropionate sodium salt (TSP) as an internal standard has been evaluated.[34]

5.2. ^{1}H NMR spectroscopy and comparative biochemistry of blood plasma

Single-pulse spectra of human blood plasma are very complex, and resonances of metabolites, proteins, lipids and lipoproteins are heavily overlapped even at 800 MHz ^{1}H observation frequency (Fig. 1). Most blood plasma samples are quite viscous and this gives rise to relatively short T_1

relaxation times for small molecules compared to simple aqueous solutions allowing relatively short pulse repetition cycles without signal saturation. The complex spectral profile given in the single-pulse ^{1}H NMR spectrum of blood plasma can be simplified by use of spin-echo experiments with an appropriate T_2 relaxation delay to allow signals from broad macromolecular components and compounds bound to proteins to be attenuated.[2] The effect of applying the Carr–Purcell–Meiboom–Gill (CPMG) spin-echo pulse sequence to blood plasma results in a substantial reduction in the contribution from the albumin, lipoprotein and lipid. By the early 1980s many metabolites had been detected in normal blood plasma using 400 MHz spectrometers; these included alanine, isoleucine, valine, lactate, acetate, creatinine, creatine, glutamine, 3-D-hydroxybutyrate, choline, glucose, acetoactetate and acetone.[1] Assignments were, in general, based on the observation of only one or two resonances for each metabolite.[35,36] In adddition, peaks from certain macromolecules such as α_1-acid glycoprotein, *N*-acetylneuraminic acid and related sialic acid fragments[36] have been assigned and used diagnostically, in particular their *N*-acetyl groups which give rise to relatively sharp resonances presumably due to less-restricted molecular motion.[37] In most ^{1}H NMR studies on blood plasma, the occurrence of two major acetyl signals is seen in spin-echo spectra. The resolution-enhanced, 750 MHz CPMG spectrum indicates that there are many resolved lines from low-molecular-weight species, and possibly other glycoproteins, in the region δ1.9–2.1.[2] These are not resolved in 400 MHz spin-echo spectra and thus use of the "glycoprotein" lines for diagnostic purposes observed at lower fields may be unreliable. Furthermore, in single-pulse spectra the *N*-acetyl signal from glycoproteins centred at δ2.04 is also partially overlapped with the broad $CH_2C{=}C$ signals from several plasma lipids which will not be resolved at 400 MHz (Table 3). The signals from some lipid and lipoprotein components, e.g. very-low-density lipoprotein (VLDL), low-density lipoprotein (LDL), high-density lipoprotein (HDL) and chylomicrons, have also been partially characterized. However, the assignment has been limited by the use of lower-frequency spectrometers, the extensive chemical shift overlap and the broadness of the signals due to the short proton T_2 relaxation times of these large supramolecular species.[35] In the single-pulse NMR spectrum of blood plasma in the chemical shift region δ0.7–1.5, there are many overlapping signals from small organic species such as lactate, 3-D-hydroxybutyrate, alanine and branched-chain amino acids together with those from terminal CH_3 and long-chain $(CH_2)_n$ groups of fatty acids and triglycerides integral to the various lipoprotein particles, especially VLDL, LDL and HDL.[38]

Two approaches can be adopted for dealing with the overlap problem. Firstly, simple sample preparation such as centrifugal ultrafiltration can be used to remove the macromolecules. This results in a spectrum of all the nonprotein-bound metabolites contributing to the spectrum. Alternatively, to avoid sample manipulation, a spectral editing technique can be applied. It has

Table 3. Resonances of lipid and macromolecule components found in blood plasma.

Molecule	Assignment	$(\delta)^1$H	Multiplicity	$(\delta)^{13}$C
Cholesterol	C18 (in HDL)	0.66	m	12.6
Cholesterol	C18 (in VLDL)	0.70	m	
Cholesterol	C26 and C27	0.84	m	23.3
Lipid (mainly LDL)	$\mathbf{CH_3}(CH_2)_n$	0.84	t	14.7
Lipid (mainly VLDL)	$\mathbf{CH_3}CH_2CH_2C$=	0.87	t	
Cholesterol	C21	0.91		19.4
Lipid	$\mathbf{CH_3}CH_2$	0.93	m	
Lipid	$CH_3CH_2\mathbf{CH_2}$	1.22	m	32.7
Lipid (mainly LDL)	$(CH_2)_n$	1.25	m	30.6
Lipid	$CH_3\mathbf{CH_2}\ (CH_2)_n$	1.26	m	23.2
Lipid (mainly VLDL)	$\mathbf{CH_2}CH_2CH_2CO$	1.29	m	
Lipid	CH_2	1.30	m	19.7
Lipid	$\mathbf{CH_2}CH_2CH_2CO$	1.32	m	
Lipid (mainly VLDL)	$\mathbf{CH_2}CH_2CO$	1.57	m	25.6
Lipid	$\mathbf{CH_2}.CH_2.C$=C	1.69	m	27.4
Lipid	CH_2.C=C	1.97	m	
Lipid	CH_2.C=C	2.00	m	27.8
Lipid	CH_2.C=C	2.00	m	
Glycoprotein*	$NHCOCH_3$	2.04	s	23.0
Lipid	CH_2.CO	2.23	m	34.6
Lipid	C=C.CH_2.C=C	2.69	m	
Lipid	C=C.CH_2.C=C	2.71	m	26.2
Albumin lysyl	ε-CH_2	2.89	t	40.3
Albumin lysyl	ε-CH_2	2.96	t	40.3
Albumin lysyl	ε-CH_2	3.01	t	40.3
Choline (lipid)	NCH_2	3.66	m	66.7
Glyceryl of lipids	CH_2.O.COR	4.06	m	62.5
Glyceryl of lipids	CH_2.O.COR	4.25	m	62.5
Glyceryl of lipids	CH.O.COR	5.20	m	
Unsaturated lipid	$-CH=\mathbf{CH}.CH_2.\mathbf{CH}=CH-$	5.23	m	128.6
Unsaturated lipid	$-CH=\mathbf{CH}.CH_2.\mathbf{CH}=CH-$	5.26	m	128.6
Unsaturated lipid	$=\mathbf{CH}.CH_2.CH_2$	5.27	m	
Unsaturated lipid	$=\mathbf{CH}.CH_2.CH_2$	5.31	m	130.1
Unsaturated lipid	$=\mathbf{CH}.CH_2.CH_2$	5.33	m	

Key: s, singlet; t, triplet; m, multiplet; * mainly α_1-acid glycoprotein; chemical shifts referenced to H1 and C1 of α-glucose at δ5.233 for ^{1}H and at δ92.9 for ^{13}C. The bold font denotes the proton assignment.

been shown that Hahn spin-echo (HSE) and CPMG spin-echo methods are both highly effective means of editing plasma ^{1}H NMR spectra according to solute T_2 relaxation times. Many signals from low-molecular-weight species are readily detected in the HSE experiment that cannot be resolved in the single-pulse experiment (e.g. 3-D-hydroxybutyrate and 3-D-hydroxyisobutyrate).

The HSE spectrum gives phase modulation of signals that is dependent on the spin–spin coupling multiplicity so that singlets are always phased upright as are triplets when the spin-echo delay is selected to be 1/2J. With a delay of about 68 ms, doublets and quartets with coupling constants of approximately 7.4 Hz appear phase-inverted. The CPMG spin-echo pulse sequence does not J-modulate signal phases and losss of signal intensity during the T_2 relaxation delays by diffusion through field gradients are minimized by virtue of the short delays employed. In either type of spin-echo experiment, total spin–spin relaxation delays of <120 ms are usually sufficient to attenuate protein resonances by factors of 10^3 and hence allow low-molecular-weight species to be measured without interference.[1] Characteristic signals from many molecules are seen in the spectral region to low frequency of the water signal plus resonances from the olefinic protons in lipoproteins, aromatic amino acids and formate. For normal plasma at pH 7, the largest peak in the spectral region to high frequency of water is that of the α-anomeric H1 resonance of glucose at δ5.223 (which provides a useful internal chemical shift reference). Through the increased spectral dispersion available from the use of 600, 750 and 800 MHz ^{1}H NMR measurements[39] and through the use of a variety of 2D methods, the assignment of resonances in blood plasma spectra in normal individuals is now extensive (see Table 2).

The use of 2D NMR methods is important for spectral assignment. The application of the J-resolved (JRES) experiment results in a dramatic simplification of the blood plasma spectrum, and hence enables the complex overlapped resonances in the chemical shift range δ3–4 to be more completely resolved.[40] Furthermore, the protein resonances are attenuated as effectively as was seen in the application of the simple spin-echo experiment. The skyline projection through the JRES map results in a greatly simplified spectral profile of the effectively ^{1}H-decoupled ^{1}H NMR spectrum of the motionally unconstrained metabolites in plasma. The skyline projection might therefore offer an attractive method for quantitating minor metabolites in plasma where attenuation due to T_2 relaxation can be accounted for or calibrated. It should be noted that signals from any small molecules that are extensively protein-bound are also severely attenuated due to constrained molecular tumbling and a shortening of the T_2 relaxation time.

^{1}H–^{1}H COSY spectra provide an additional assignment aid enabling the confirmation of the presence of a number of amino acid resonances including all those of valine, alanine, leucine, isoleucine, threonine and glutamine and the majority of the resonances of others especially those in particularly diagnostic regions of the spectrum. A number of other small molecules can be readily observed in the COSY spectrum and these include the acids 3-D-hydroxybutyrate, citrate, taurine and lactate as well as polyols such as *myo*-inositol and all other resonances of α- and β-glucose. In addition, the resolving power of the COSY experiment is demonstrated by the connectivities observed for many of the lipidic resonances which are not observable

in the 2D-JRES experiment because of their short T_2 relaxation times. The total correlation spectrum (TOCSY) of human blood plasma allows the assignment of extra metabolites because of the narrower lineshape of the TOCSY spectrum and because the coupling connectivity along complete chains of protons provided a more certain indication of the molecular identity. The ^1H–^{13}C 2D HMQC and HSQC experiments applied to blood plasma are also useful for metabolite identification giving information on ^{13}C chemical shifts using ^1H detection.

An assay for ethanol in blood plasma has been published[41] and a comprehensive listing of the ^1H NMR-detectable metabolites observed in the various 1D and 2D experiments, together with their spin systems and their ^1H chemical shifts (and ^{13}C shifts where available) in plasma, is given in Table 2.

5.3. Effects of temperature variation on the ^1H NMR spectra of blood plasma

With increasing temperature all the lipidic methyl and methylene group peaks sharpen and increase in intensity. This is consistent with a general reduction in the plasma viscosity and increased motional freedom of the lipoprotein particles which also significantly increase the ^1H–^{13}C 2D HMQC peak intensities. Selective changes are also visible, e.g. the cholesteryl C18 axial methyl group of HDL progressively sharpens, as do the signals from ring current-shifted methyl groups of albumin. The LDL methyl signal also increases selectively at higher temperature and dominates the low-frequency lipoprotein methyl signal complex at 308 K. This is consistent with the known selective temperature dependence of the LDL signal linewidths.[42] From these measurements it is also apparent that spin-echo spectral editing will be more efficient at lower temperatures as the signals from albumin and lipoproteins are significantly broader. In effect, this means that a shorter relaxation delay period in the spin-echo pulse sequence is required to attenuate the macromolecular signals with less T_2 relaxation distortion introduced into the spectra of the low-molecular-weight metabolites under study (see also Section 5.7).

5.4. Metal complexes in blood plasma

EDTA forms stable complexes with Ca^{2+} and Mg^{2+} ions in aqueous solution. Ca^{2+} and Mg^{2+} are present in blood plasma at about 2.2–2.5 mmol l^{-1} and 0.6–0.8 mmol l^{-1} respectively and about 30–40% of both metals is protein bound. The 400 MHz ^1H NMR spectra of human blood plasma collected using an EDTA anticoagulant has been reported to give well-resolved signals from

both the octahedral EDTA complexes of Ca^{2+} and Mg^{2+} which are in slow exchange on the NMR time-scale.[11] EDTA gives rise to two ^1H NMR singlets in the intensity ratio 2:1 at δ3.62 and δ3.21 respectively at pH 7. The $-NCH_2CH_2N-$ protons of the Ca-EDTA^{2-} and Mg-EDTA^{2-} complexes give singlets at δ2.57 and δ2.76 respectively (plasma pH 7.4) whereas in the metal complexes the NCH_2CO protons become magnetically nonequivalent (AB spin system) with the shifts for the Ca-EDTA^{2-} and Mg-EDTA^{2-} complexes being centred at δ3.12 and δ3.23 respectively.[11] The changes in shifts and magnetic nonequivalence of the EDTA signals are due to the formation of octahedral metal complexes. Integrations of the $-NCH_2CH_2N-$ peaks of the Ca-EDTA^{2-} and Mg-EDTA^{2-} complexes in spin-echo spectra of plasma when calibrated by standard additions of metal ion give quantitatively accurate results for the total Ca^{2+} and Mg^{2+} present in plasma.[11]

5.5. Protein–ligand binding in blood plasma

Many plasma components can exist either free in solution or in a more organized physicochemical domain such as a micelle or lipoprotein complex. On changing from one environment to another, the motional properties of the compound under study are altered with a concomitant change in the T_2 relaxation times of their protons. Consequently, it is possible to monitor some of these transitions by observing line width changes, or by use of spin-echo techniques to edit the spectra according to molecular mobility.

Bell *et al.*[43] have shown that a significant proportion of plasma lactate is present in an "NMR-invisible" pool due to binding to transferrin, α_1-antitrypsin and possibly other high-molecular-weight plasma proteins and it has been suggested that this may have an important role in lactate transfer in plasma. The spin-echo NMR assay of serum lactate is reported to underestimate by about 30% when compared with conventional biochemical procedures whereas previous studies[11] have shown that NMR assays of alanine and valine give values nearly identical to conventional amino acid analysis procedures. Lactate can be liberated from its protein binding site by the addition of 0.5 mmol l^{-1} ammonium chloride or the anionic detergent sodium dodecyl sulfate (SDS) and then becomes NMR-detectable in spin-echo spectra together with nonprotein-bound lactate; a similar effect was reported for 3-D-hydroxybutyrate and acetoacetate.

In single pulse and spin-echo spectra of normal human and animal plasma, there are few resonances in the chemical shift range to high frequency of δ5.3 when measured in the pH range 3 to 8.5. However, on acidification of the plasma to pH <2.5, resonances from histidine and phenylalanine become detectable.[44] In plasma from patients with Wilson's disease (liver degeneration secondary to an inborn error of caeruloplasin/copper metabolism), weak signals from histidine and tyrosine are seen in spin-echo spectra at pH 7.6, but

increase in strength on acidification and signals from phenylalanine appear at pH 1.8 or below. Experiments with model solutions suggested that serum albumin has a high capacity for binding aromatic amino acids and histidine at neutral pH and this is responsible for their NMR-invisibility in normal human blood plasma. Serum albumin also binds a large number of other species of both endogenous and xeniobiotic origin. Even commercial "purified" bovine serum albumin (BSA) can be shown to contain a significant amount of bound citrate and acetate which become NMR detectable in BSA solutions at pH 2. Acidification (without protein precipitation) of human plasma also renders citrate NMR detectable in spin-echo spectra as it becomes mobilized from the protein binding sites.

Blood plasma also has intrinsic enzymatic activities although many of these are not stable (particularly if the sample is not frozen immediately on collection). It has been noted that under certain pathological conditions, such as those following liver or kidney damage, enzymes that are present at elevated levels in the plasma because of leakage from the damaged tissue, can cause NMR-detectable alterations to spin-echo spectra of plasma. The levels of these enzymes, e.g. alanine transaminase (ALT), are often used as primary evidence for organ damage. In order to observe the effect of elevated ALT it is necessary to freeze dry the plasma sample soon after collection and then to reconstitute the sample in D_2O. The metabolites involved are at equilibrium in the plasma when collected. However, reconstitution in D_2O is then associated with the establishment of an isotopic equilibrium that results in the progressive incorporation of deuterons at the α-CH position of alanine.[45] Consequently, the alanine methyl protons no longer experience the coupling to the CH and the signal changes from a doublet to a singlet with a small deuterium isotope shift. This is clearly observed in Hahn spin-echo spectra because the phase of the signal is shifted by 180° and this can also be monitored by adding ALT to normal blood plasma redissolved in D_2O. More complex signal modulations also occur on enzymatic incorporation of deuterons into glutamine.

5.6. Molecular diffusion in blood plasma

Molecular diffusion coefficients are parameters that are not related directly to NMR spectral intensities under normal conditions. However, molecular diffusion can cause NMR signal intensity changes when pulsed field gradients are applied during the FT NMR experiment.[46] A number of pulse sequence developments, particularly the LED sequence, have meant that measurement of diffusion coefficients is relatively routine.[47,48] The editing of ^1H NMR spectra of biofluids based on diffusion alone or on a combination of spin relaxation and diffusion has been demonstrated.[49,50] This has been termed the Diffusion and Relaxation Editing (DIRE) pulse sequence. This approach is

complementary to the editing of ^{1}H NMR spectra based on differences in T_1 and T_2 first reported by Rabenstein *et al.* (see Section 5.9).

New methods for editing TOCSY NMR spectra of biofluids have been proposed based on differences in molecular diffusion coefficients and this has been termed Diffusion Edited TOCSY (DETOCSY). This approach complements the editing of TOCSY NMR spectra based on coherence selection and promises to provide an efficient alternative strategy for assignment of resonances in complex mixtures such as biofluids and cell extracts.[49,50]

The ^{1}H–^{1}H TOCSY NMR spectra of human blood plasma shown in Fig. 2 were acquired using the DETOCSY pulse sequence.[49] When a very low gradient strength is used, the spectrum is similar to that in the absence of gradients. Increasing the gradient strength causes the resonances from the small molecules to be reduced substantially due to their relatively fast diffusion compared to those of the larger molecules that give rise to the broad peaks in the spectrum. The various lipoprotein resonances arise from different positions within the fatty acid chains. In a 1-dimensional diffusion edited experiment, relatively sharp peaks near $\delta 2$ arise from the *N*-acetyl groups of the carbohydrate component of glycoproteins, and their appearance in this edited spectrum confirms that they are from macromolecular systems. Other peaks are observed in the region $\delta 3.4$–3.9 and these have been assigned to the glycerol protons and to the methylene groups of the choline group in phospholipids in lipoproteins, based on the measurement of NMR spectra of model compounds. The ability to remove the resonances from the small molecules may be important in view of the increasing number of studies reporting lipoprotein analyses in whole plasma by using lineshape fitting algorithms (see Section 5.7). It is possible to combine relaxation and diffusion editing in the DIRE pulse sequence such that molecules in a given window of mobility give rise to NMR resonances.

5.7. Lipoprotein analysis in plasma from NMR spectra

Much study has been devoted to the problem of lipoprotein analysis in blood plasma using ^{1}H NMR spectroscopy. This has been comprehensively reviewed recently by Ala-Korpela[51] and so extensive discussion is not repeated here. Lipoproteins are complex particles that transport molecules normally insoluble in water. They are spherical with a core region of triglyceride and cholesterol ester lipids surrounded by phospholipids in which are embedded various proteins known as apolipoproteins. In addition, free cholesterol is found in both the core and surface regions. The lipoproteins are in a dynamic equilibrium with metabolic changes going on *in vivo*. Lipoproteins are usually classified into five main groups: chylomicrons, very-low-density lipoprotein (VLDL), low-density lipoprotein (LDL), intermediate-density lipoprotein (IDL) and high-density lipoprotein (HDL) based on physical separation

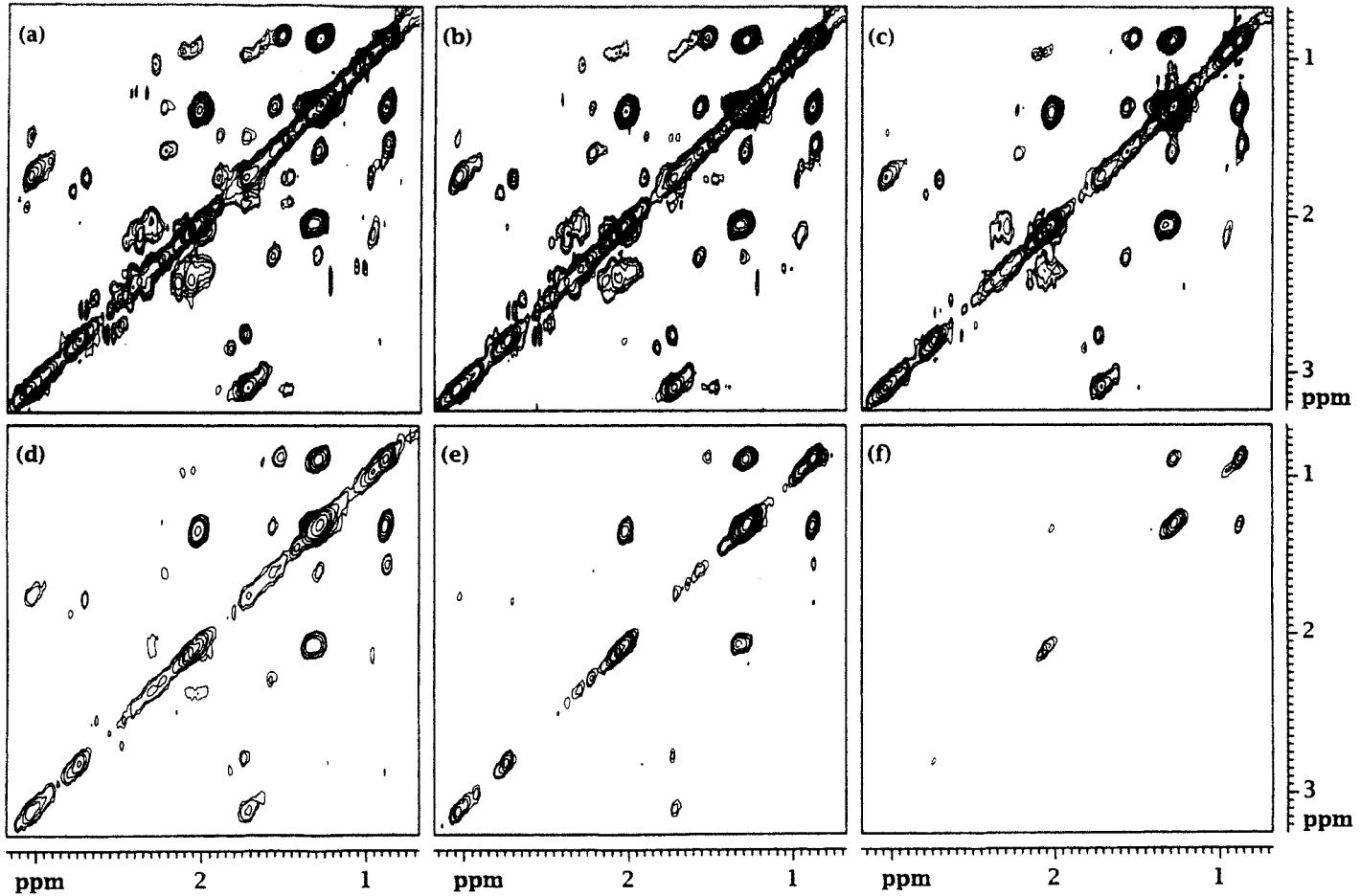
(a)
(b)
(c)
(d)
(e)
(f)
1
2
3
ppm
ppm
2
1

using centrifugation. Based on the measurement of ^{1}H NMR spectra of the individual fractions and using lineshape fitting programs, it has been possible to identify the chemical shifts of the CH_2 and CH_3 groups of the fatty acyl side chains.[52–56] Quantification can be carried out using either time domain or frequency domain NMR data.[55] For example, in the time domain the Hankel–Lanczos single-value decomposition method (HLSVD) has been used to model the damped sinusoidal signals observed in an FID both to remove the residual water resonance and to quantify the lipoprotein fractions.[55] Another widely used algorithm is VARPRO which also works on the time domain signal.[55,57] Alternatively a frequency domain approach has used the program FITPLA[52,53,57] which uses resonance positions and linewidths from model solutions to fit the overall lineshape of the CH_2 and CH_3 signal region. The usefulness of ^{1}H NMR spectra for lipoprotein analysis[59,60] and ^{31}P NMR spectroscopy for phospholipid analysis in blood plasma has been explored.[61] More recently, a neural network software approach has been used to provide rapid lipoprotein analyses.[62]

5.8. NMR spectra of blood plasma in pathological states

Cancer

The very first publication on biofluid NMR spectroscopy was concerned with the detection of cancer.[63] In it Ohsaka *et al.* reported that 100 MHz ^{1}H NMR spectra of human blood serum showed high lactate levels for patients with malignant tumours. This method has not been widely used due to two factors: (i) lactate is not 100% NMR visible in blood serum or plasma and (ii) variability in lactate levels due to many factors other than cancer.[64,65] However, Nagasawa *et al.*[66] have also reported analogous results for lactate elevation in the urine from mice with mammary tumours.

A good deal of excitement was generated by the publication of a paper which reported that ^{1}H NMR spectroscopy of human blood plasma could be used to discriminate between patients with malignant tumours and other groups, namely normals, patients with nontumour disease and a group of patients with certain benign tumours.[67] This paper stimulated many other research groups around the world to investigate this approach to cancer detection. However, many of these groups were unable to repeat the original observations, either wholly or in part, and a major controversy soon erupted.

Fig. 2. A series of partial 600 MHz ^{1}H–^{1}H DETOCSY NMR spectra of human blood plasma. A range of gradient strengths was used to illustrate the progressive signal attenuation. Gradients strengths were, (a)–(f), 21.3, 95.8, 170.3, 244.8, 319.3 and 393.8 mT m^{-1}.

The test as originally published involved the measurement of the averaged width at half signal height of the two composite signals at δ1.2 and δ0.8 in the single-pulse ^{1}H NMR spectrum of human blood plasma. On comparing the averaged signal width, *W*, for normal subjects with those for patients with a variety of diseases and with those for pregnant women, it was reported that several statistically significant differences existed between the groups. It was proposed that the lowering of *W* observed in the malignant group was due to an increase in the T_2^* of the lipoprotein signals at δ0.8 and δ1.2, due in turn to "lack of supramolecular ordering of lipoprotein lipids" in the plasma of the patients with malignant tumours. However, excitement soon turned into controversy as many workers found difficulty in reproducing the results. A mass of literature now exists on this subject and it is impossible to thoroughly review all of the many important contributions. It was immediately apparent that the perfect 100% sensitivity and specificity reported in the early publications has never been repeated by any group.

In addition to the presence of cancer, a number of other factors have been found to cause changes in the linewidth index, *W*. These include diet,[64,68–70] age and sex,[65,71,73] pregnancy[65,67] and trauma[70] as well as hyperlipidaemia.[69,71–77] In all cases the observed changes in *W* are caused by alterations in the plasma lipoprotein composition, especially the VLDL/HDL ratio. These additional factors all contribute to the low specificity and sensitivity observed for the test and thus it appears that the changes in *W* are due to elevations in the levels of VLDL in the plasma of patients with cancer.

Much useful information on the variation of blood plasma lipoprotein content as a function of malignancy was obtained during studies on the cancer test. After the realization that this test was unlikely to be of any clinical utility, attention has again focused on the changes that occur to the profiles of plasma metabolites. The Cozzone group has conducted a series of experiments which have focused on changes in the ratios of signals from lipoproteins and glycoproteins in the ^{1}H NMR spectra of the plasma from patients with a variety of different cancers. A "star plot" pattern recognition method was used to distinguish three types of metabolic alterations induced by the cancer metabolism: (i) an "inflammatory" pattern, (ii) a "lipid modified" pattern and (iii) a "sarcoma" pattern.[78]

Other studies of ^{1}H NMR spectra of blood plasma in cancer have included general studies,[79–85] comparison of NMR and chromatographic methods,[86] testicular cancer,[87] effects on plasma sialic acids,[88] use of both ^{1}H and ^{13}C NMR spectra,[89] lung cancer,[90] the effect of trauma[91] and dyslipoproteinemia.[92]

In 1987, Mountford and co-workers[93] reported the isolation by ultracentrifugation of two lipoprotein bands, lying between the HDL and LDL bands of the plasma of a patient with a borderline ovarian tumour. These bands were later termed "malignancy-associated lipoprotein" (MAL). ^{1}H NMR spectroscopy studies on these bands showed that they contained a

methyl signal at δ1.3 which correlated in 2D ^{1}H COSY NMR spectra with a methine signal at δ4.2. The methyl signal had an abnormally long T_2^* value (>400 ms) whilst none of the conventional lipoproteins had a T_2^* of above 160 ms. The signal was consistent with that of a fucose moiety, a carbohydrate that is often found in the antigenic compounds on the surface of cancer cells, but this identification is not yet proven.[94] Nine months after surgery the long T_2^* lipoprotein component had disappeared. It was suggested that this MAL could provide a noninvasive and specific method of assaying for cancer. A simple method for removing the interfering signals from lactate and threonine from the fucose region of the spectrum has been developed and this could be useful in further work in this area.[95]

Further results were reported later for a breast cancer patient but, in a larger study,[96] less than 50% of the cancer patients had the MAL band, but so did the same number of normal controls. No correlation was found between the linewidth index W and the appearance of the MAL, although no T_2^* measurements were made. Mountford and co-workers have presented further results on blood serum and plasma from patients with tumours of the colon and ovary.[96] In this study 85% of the patients had a long T_2^* value for the signal at δ1.3 in the spectrum of the MAL band. However, problems were reported with the isolation of the MAL. The fractions of interest are dialysed for up to two hours to remove KBr and any free lactate prior to analysis. The long T_2^* signal was reported to be removed if the dialysis was too extensive. It was suggested that the MAL particle may be disassociating during the dialysis, but other explanations are possible. Lipoprotein-bound lactate, which would slowly dissociate during dialysis, would be one possibility. Kriat *et al.*[97] failed to detect any signals from fucosylated lipids in the 2D ^{1}H NMR spectra of the plasma from 12 cancer patients, including three patients with ovarian cancer. Until the nature and origin of the MAL band are conclusively defined, its significance for cancer detection and diagnosis remains unclear.

Heart transplantation

The success of heart transplantation has improved recently with the chronic use of cyclosporin A to suppress rejection, and the better treatment of acute rejection episodes when they do occur. However, the early detection of acute cardiac graft rejection still relies on invasive and iterative right ventricular endomyocardial biopsies. In 1988 Eugene *et al.* reported a new application of the measurement of the linewidth index, W; the assessment of heart graft rejection after transplantation.[98] The methodology was exactly the same as for the cancer test except that the width at half-height of the composite lipoprotein lipid methyl and methylene signals was summed rather than averaged, leading to all the results being reported as $2W$ values rather than W.

A more detailed study on an enlarged patient population was reported

shortly after,[99] and showed similar results. Patients in moderate and severe rejection showed $2W$ values that were significantly different from those of the light rejection patients. However, as occurred in the test for cancer, the wide overlap between the values observed for each group meant that the $2W$ value alone could not be used to classify the patients into the four rejection grades. A third report from the same group[100] reported the results of 410 measurements on a total of 46 patients. For these heart transplant patients, and the other transplant patients discussed below, it was hypothesized that the altered values of $2W$ observed were due to the presence of a graft-associated lipoprotein (GAL), rather than being due to changes in the abundance of normal plasma lipoproteins. This GAL would be a direct analogue of the MAL proposed by Mountford and co-workers to occur in the plasma of cancer patients.

It has also been reported[101] that the areas of two glycoprotein signals in the spin-echo ^{1}H NMR spectra of blood plasma from heart transplant patients correlated with a standard echocardiography parameter used to monitor rejection. The sum of the areas of the *N*-acetyl signals of *N*-acetylglucosamine (NAG) and *N*-acetylneuraminic acid (NANA) moieties of plasma glycoproteins (NAG + NANA) was measured and then this area was divided by that of the methyl signal of alanine. When this area ratio was plotted against isovolumetric left ventricular relaxation times (measured by Doppler echocardiography), a good correlation was found in five patients and an acceptable correlation in three patients, but only a poor correlation in five further patients. It was noted that infections and inflammatory states unrelated to rejection interfered with the correlation.

Other organ transplants

Some preliminary results have also been reported on kidney and liver transplant patients.[99] Plasma linewidth measurements were reported on 28 samples from 10 kidney transplant patients at up to 15 days post-transplantation with the lowering of $2W$ values being ascribed to immunomodulation. $2W$ values were also reported for the plasma of three patients who underwent liver transplantation.

Malaria

Malaria is caused by several species of *Plasmodium* parasites which enter the human bloodstream after penetration of the skin by anopheline mosquitos. Nishina *et al.* have reported[102] 270 MHz W and lactate concentration measurements on the blood sera from 20 Nigerians seropositive to *Plasmodium*, 13 seronegative Nigerians and six healthy Japanese controls. Significantly lower W values and high lactate concentrations were reported for the sera of the malaria-positive group than for the other two groups.

Diabetes

In human beings diabetes is a relatively common condition which can have serious, complex and far-reaching effects if not treated. It is characterized by polyuria, weight loss in spite of increased appetite, high plasma and urinary levels of glucose, metabolic acidosis, ketosis and coma. The muscles and other tissues become starved of glucose, whilst highly elevated levels of glucose are found in the urine and plasma. This deficiency in glucose leads to ketosis and acidosis and in many cases diabetes can be controlled by the administration of insulin.

Based on NMR spectra,[36] there are marked elevations in the plasma levels of the ketone bodies and glucose, postinsulin withdrawal. The levels of these metabolites, as well as lactate, valine and alanine, were also measured by standard clinical chemistry methods, in order to test the accuracy of the NMR method. In general, the NMR results were in good agreement with the conventional assay results. The CH_3 and CH_2 resonances of the lipoproteins VLDL and chylomicrons decreased significantly in intensity relative to the CH_3 signal of HDL and LDL, indicating the rapid metabolism of the mobile pool of triglycerides in VLDL and chylomicrons. By fluorimetric measurements, the concentration of the so-called "free fatty acids" rose from 0.33 to 1.92 mmol l^{-1} in the period from 0 to 12 hours post withdrawal. However, these free fatty acids are immobile (due to binding to albumin) and NMR-invisible.

In the same paper, the ^1H NMR spectrum of the plasma of a non-insulin-dependent obese diabetic was shown to be dominated by signals from glucose and mobile triglycerides in lipoproteins with no signals visible from the ketone bodies. In uncontrolled diabetes, the plasma levels of "free fatty acids", triglycerides and lipoproteins rise markedly due to decreased removal of triglycerides from the plasma into fat depots. This effect was also observed in the case of a diabetic with hypertriglyceridaemia and Type IV hyperlipoproteinaemia. The spectra clearly showed the very elevated triglyceride levels decreasing as the patient responds to a better diet and insulin regime.

Renal failure

The ^1H NMR spectra of the blood plasma from nine patients with chronic renal failure during dialysis, two patients in the early stages of renal failure and six normals have been analysed.[103] For patients on acetate dialysis, the method clearly showed how the acetate was accumulated and metabolized during the course of the dialysis, as well as allowing changes in the relative concentrations of endogenous plasma components to be monitored. In nine of the 11 cases it was reported that plasma betaine levels were elevated but this is possibly a misassignment for trimethylamine-*N*-oxide (TMAO) as no resonances can be seen for the CH_2 group of betaine in the figure published

in this paper. It had been shown by Holmes *et al.*[104] that the N-CH_3 resonances of betaine and TMAO are very close together at normal plasma pH and that it is the TMAO level that is elevated in renal failure patients. A subsequent ^1H, ^{13}C and ^{14}N NMR study of the plasma and urine from 16 chronic renal failure patients[105] showed that the plasma levels of TMAO correlated with those of urea and creatinine, suggesting that the presence of TMAO is closely related to the degree of renal failure. Differences in the interaction of lactate with the plasma proteins were also observed in the uraemic patients. The study by Holmes *et al.*[104] of 15 renal failure patients also showed increased levels of lactate in the plasma, ascribed to metabolic disturbances (mainly acidoses) associated with decreased renal function. Elevated creatinine levels were found in the plasma of renal failure patients (levels of $>1000\,mmol\,l^{-1}$ are possible, compared with 45–120 $mmol\,l^{-1}$ for normals). The patients undergoing haemodialysis were differentiated by the presence of elevated dimethylamine, whilst glycine was predominantly raised in the plasma of the peritoneal dialysis patients. Matsushita and coworkers[106] reported that urinary levels of trimethylamine were elevated in six out of 50 patients with unspecified renal disease, many of whom may have been renal failure patients, but details were not provided.

A 750 MHz ^1H NMR comparison of blood plasma between a normal control and a patient with chronic renal failure has also been described.[107] At this high field strength, signals for free phenylalanine, tyrosine, histidine, 3-methylhistidine, 1-methylhistidine, *p*-hydroxyphenylacetic acid and other unassigned molecules were observed in the CPMG spectrum of the plasma from the uraemic patient which had not been observed at lower field strengths and were absent from the control spectrum. It was hypothesized that some of these abnormal molecules could be uraemic toxins but further work is necesary in order to substantiate this.

The uraemic syndrome is associated with a complex set of biochemical and pathophysiological changes that remain poorly understood. The first application of 750 MHz NMR for studying the biochemical composition of plasma has been reported from patients on haemodialysis and peritoneal dialysis.[108] Increased plasma levels of low-molecular-weight metabolites including methylhistidine, glycerol, choline, TMAO, dimethylamine and formic acid were found. The concentrations of these metabolites, and ratios to others, varied with the type of dialysis therapy. For example, the biochemical composition of plasma from patients on peritoneal dialysis was remarkably consistent whereas pre- and post-haemodialysis significant fluctuations in the levels of TMAO, glucose, lactate, glycerol, formate and lipoproteins (VLDL, LDL and HDL) were observed. Patients who take paracetamol (acetaminophen) long term for pain control had abnormally high plasma levels of paracetamol glucuronide, which may correlate with the presence of anorexia and wasting in this group of patients. Elevated concentrations of glycoprotein fragments were also observed and may relate to the presence

of high levels of *N*-acetylglucosaminidase, and other glycoprotein cleaving enzymes, in the plasma originating from damaged kidney cells. These observations lead to the hypothesis that the biochemical changes associated with uraemic symptoms and dialysis therapy include: (i) the elevation, and incomplete removal by dialysis, of a group of toxic methylamine species; (ii) the dialysis-dependent alterations in the metabolism of groups of physiologically important compounds such as choline and the lipoproteins and (iii) the generation of formate.

5.9. ^{1}H NMR spectroscopy of whole blood and red blood cells

Introduction

Single-pulse ^{1}H NMR measurements on whole blood give very little biochemical information due to the presence of a broad envelope of resonances from haemoglobin and plasma proteins. Spin-echo spectroscopy of whole blood can give rise to moderately well-resolved signals from plasma metabolites and those present inside erythrocytes, notably glutathione. However, whole-blood spectra are not easily reproducible because of erythrocyte sedimentation which progressively (within a few minutes) degrades the sample field homogeneity during the course of collecting a series of FIDs. Furthermore, there are substantial intracellular/extracellular field gradients which give a major contribution to the T_2 relaxation processes for the nuclei of molecules diffusing through those gradients. In spin-echo spectra this results in the signal echoes not refocusing at the end of the second delay in the pulse sequence and very weak spectra are obtained.[11] Spin-echo NMR measurements on packed erythrocyte samples do give rise to well-resolved signals from intracellular metabolites and a variety of transport and cellular biochemical functions can be followed by this method.

Erythrocyte metabolism, pH and membrane transport studied using NMR spectroscopy

The first paper which showed that NMR spectra of endogenous small molecules could be obtained from erythrocytes appeared in 1977[109] and this also showed how, using a spin-echo approach, the large broad haemoglobin resonances could be eliminated. In cells which were washed with H_2O and D_2O, time courses for the conversion of glucose to lactate were determined. In another study, the cells were washed to remove all glucose and lactate and the intracellular glutathione (GSH) was oxidized to GSSG and the conversion monitored by ^{1}H NMR of the GSH resonances, principally the CH_2S and CH_2 of the glycyl residue. After conversion to GSSG, glucose was added to the suspension and the reformation of GSH was determined as a function of time.

Isotope exchange methods have been developed and used to study the kinetic effects of intra-erythrocyte enzymes by adding a labelled compound to a suspension of red blood cells and then monitoring the subsequent distribution of label with time.[110–116] Enzymes studied include the lactate dehydrogenase interconversion of lactate to pyruvate and the exchange of label between lactate and solvent to investigate properties of fructose bisphosphate aldolase, triose phosphate isomerase, glyceraldehyde phosphate dehydrogenase and lactate dehydrogenase.[114] Pyruvate–water exchange has also been studied[115] as has the NAD-dependent lactate–malate reaction[116] and alanine aminotransferase reaction for lactate–pyruvate conversion.[117] Reactions of GSH have been studied also. In erythrocytes, GSH and its constituent amino acids (cysteine, glycine and glutamate) are in dynamic exchange and this has been followed using 2H-labelled glycine.[118,119]

One major parameter which can be obtained from NMR is the intracellular pH and the pH inside erythrocytes can be measured using ^{1}H NMR spectroscopy using a suitable ^{1}H NMR pH indicator which has an NMR chemical shift which varies with pH in the range desired. Candidates include the C2-H protons from histidines in haemoglobin[109] but also an exogenous compound can be added as an indicator and imidazole has been used here.[120]

The transport of substances between the inside and outside of the red cell can be monitored using NMR if the resonances from the two environments have different chemical shifts or intensities. In spin-echo NMR spectra of erythrocytes, the intensity of resonances from metabolites inside the cells is less than outside because of magnetic susceptibility differences inside and outside the cells.[121] Also, resonances outside the cell can be selectively broadened by the addition of paramagnetic species that do not cross the red cell membrane. Those used include the ferric complex of desferrioxamine, dysprosium-DTPA and the copper-cyclohexanediaminetetraacetic acid complex.[117,120–122] To measure the rate of influx of a compound into red cells, the compound is added with the paramagnetic agent to a red cell suspension and the intensity of the resonance from the intracellular component is monitored as a function of time. This approach has been used to study the transport of glycerol,[122] alanine, lactate and choline[123] and glycylglycine.[124] The time scale that can be addressed covers the range of milliseconds to hours.[125]

Kuchel and co-workers have used NMR spectroscopy of erythrocytes to study the effect of lithium treatment in manic-depressive patients[123–126] showing an increase in choline. In heavy-metal poisoning, a considerable proportion of the metal is found in the blood and the binding of heavy metals inside erythrocytes has received much attention.[127–131] For example, methylmercury(II) was shown to cross the red cell membrane rapidly and be complexed principally to the thiol groups of GSH and haemoglobin.[130] The anti-arthritic gold drug aurothiomalate has also been studied in intact red cells using NMR spectroscopy.[132] Rabenstein has reviewed much of the work

in the area of red blood cell NMR spectroscopy.[133] More recently diffusion coefficient measurement has been used to study the binding between diphosphoglycerate and haemoglobin inside intact red blood cells.[134]

Very recently, the Kuchel group has been applying a new form of analysis called "diffusion–diffraction" to suspensions of red blood cells. This approach is based on the pulsed-field gradient diffusion NMR experiment[46] and demonstrated that the cells are aligned by the static magnetic field of the NMR spectrometer. In addition conversion of the intracellular haemoglobin caused a predictable change in the diffraction pattern and it was also shown that water transport inhibition affected the results.[135] Finally the cell diameter and intercell spacing could be measured from the diffraction plots and these have been compared with electron micrographs.[136]

The technique of magic angle spinning (MAS) has also been applied to ^{1}H NMR spectra from red blood cell suspensions and under the MAS conditions two water peaks can be observed, corresponding to intra- and extracellular water.[137]

6. ^{1}H NMR SPECTROSCOPY OF HUMAN AND ANIMAL URINE

6.1. Sample details for NMR spectroscopy

The kidneys have a key role in the maintenance of body homeostasis and effectively regulate whole-body biochemistry by the reactive elimination of a wide variety of unwanted organic and inorganic compounds in the urine, i.e. the constancy of the internal environment is maintained at the expense of varying urinary composition. This variation in composition is, therefore, a reflection of a large number of biochemical processes taking place both in the kidney and elsewhere in the body and, as such, NMR urinalysis is potentially of enormous diagnostic importance.

The composition and physical chemistry of urine is complex and highly variable both between species and within species according to lifestyle. A wide range of organic acids and bases, simple sugars and polysaccharides, heterocycles, polyols, low-molecular-weight proteins and polypeptides is present together with inorganic species such as Na^+, K^+, Ca^{2+}, Mg^{2+}, HCO_3^-, SO_4^{2-} and phosphates. It is possible to detect large numbers of the organic species with modern NMR spectrometers. Many of these moieties also interact extensively, forming complexes that may undergo chemical exchange reactions on a variety of different time scales, some of which are amenable to NMR study. The ionic strength of urine varies considerably and may be high enough to affect adversely the tuning and matching of the RF circuits of a spectrometer probe, particularly at high field strengths. Therefore, it may be necessary to retune the spectrometer probe for each urine sample especially at fields of 14.1 T or more. Because of its high ionic strength it is sometimes

counterproductive to concentrate urine samples by freeze-drying and subsequent reconstitution in smaller volumes of solvent, unless this is performed conservatively. Urinary osmolalities vary from about 150 to 1300 mOsmoles in normal human urine,[138] but animal urines can have much higher osmolarities (up to 2000 mOsmoles in rodents and >3000 mOsmoles in desert species). The viscosity of human urine samples is normally low, but may be higher in laboratory rodents that are physiologically proteinuric; this will generally shorten relaxation times in comparison with pure aqueous solutions of metabolites. The presence of high concentrations of protein in the urine, e.g. due to renal glomerular or tubular damage, can result in the broadening of resonances from low-molecular-weight compounds which may bind to these urinary proteins.

Urinary pH may vary from pH 5 to 8, according to the physiological condition in the individual, but usually lies between 6.5 and 7.5. High urinary pH values (>9) may indicate partial decomposition of the sample due to contamination by bacteria which secrete the enzyme urease which decomposes urea to release ammonia. Urine samples should, therefore, be frozen as soon as possible after collection if NMR measurements cannot be made immediately. When experiments involve collections from laboratory animals housed in metabolic cages, urine samples should be collected into receptacles that are either cooled with dry ice or have a small amount of sodium azide present as a bacteriocide. However, both these procedures may inhibit or destroy urinary enzymes that may frequently be assayed by conventional biochemical methods for assessment of kidney tubular integrity in toxicological experiments. Correction of urinary pH to a standard value of 7.4 can be attempted for normalization of chemical shifts. However, pH correction can be time consuming and it can be shown experimentally that urinary pH values are unstable (even with added strong buffer) because of the progressive and highly variable precipitation of calcium phosphates which may be present in urine close to their solubility limits. One possible solution to this problem is the addition of 100–200 mmol l^{-1} phosphate buffer in the D_2O added for the lock signal followed by centrifugation to remove precipitated salts. This has the effect, in most cases, of normalizing the pH to a range of 6.7–7.6 which is stable for many hours during which NMR measurements can be made. Relatively few metabolites show major chemical shift variations over this pH range (with the exception of histidine and citrate).

Good signal-to-noise ratios for the major metabolites can usually be obtained in single-pulse spectra of urine by collecting only 16–32 FID on 600 or 800 MHz spectrometers. The vast majority of urinary metabolites have ^1H T_1 relaxation times of 1 to 4 s, the relaxation process being slightly more efficient than in pure aqueous solutions due to the presence of small amounts of paramagnetic metal ions in the urine. Given this range of T_1 values, the general rule of applying a $5 \times T_1$ relaxation delay between successive 90° transients to obtain >99% relaxation and hence quantitative accuracy cannot

be applied routinely. Applying this delay to the longest T_1 signal in the sample unnecessarily compromises the best signal-to-noise ratios for most metabolites (unless the measurement of a selected group of metabolites is particularly important, in which case the delays are optimized for those). Therefore, by using 30–45° pulse angles and leaving a total T_1 relaxation delay of 5 s between successive pulses, spectra with good signal-to-noise ratios can usually be obtained for most metabolites in 5–10 minutes at high field with a generally low level of quantitative signal distortion. Clearly, for a particular quantitative problem on a defined set of metabolites, the instrumental conditions and relaxation delays would be optimized for those measurements. But it is the overall speed (and lack of necessity of rigorous optimization) with which biofluids can be screened and fingerprinted that makes ^{1}H NMR particularly useful in studies on the comparative biochemistry and physiology of animals. Recently, it has become standard practice to replace simple solvent resonance presaturation with pulse methods which either induce such saturation or which leave the solvent water resonance unexcited. One popular method involves using simply the first increment of a 2D NOESY sequence and, as a consequence, this requires the use of only 90° pulses.

A vast number of metabolites may appear in urine samples, and problems due to signal overlap can occur in single-pulse experiments. The magnitude of the signal assignment problem in urine is also apparent at ultra high field. There are probably > 5000 resolved lines in single-pulse 750 or 800 MHz ^{1}H NMR spectra of normal human urine (Fig. 1), but there is still extensive peak overlap in certain chemical shift ranges. Thus chemical noise is still a significant feature of NMR spectra of urine even at 800 MHz and many signals remain to be assigned. The dispersion gain at 800 MHz even over 600 MHz spectra is particularly apparent in 2D (or 3D) experiments that can be used to aid signal assignment and simplify overlapped spectra. The endogenous compounds that have been detected in NMR spectra of human and animal urines are shown in Table 2.

6.2. NMR comparisons of biochemistry of urine from different species

The biochemical composition of urine varies considerably from species to species and also with the age of the animal as almost all species have age-related changes in renal function. Rats and other rodents have much higher levels of taurine, citrate, succinate, 2-oxoglutarate and allantoin than humans and this is clearly apparent in the ^{1}H NMR spectra. Rat urine (and that of other rodents) is generally much more concentrated than human urine, and so NMR signal-to-noise ratios may be better for many metabolites. All animals have physiological processes which are modulated by biological rhythms. This includes excretory processes and the urinary composition of an

animal may vary considerably according to the time it is collected. Given these types of variation it is obviously of paramount importance to have closely matched (and in many cases timed) control samples where toxicological or disease processes are being studied.

Dietary composition also affects the urinary metabolite profiles of man and animals, and it is important to distinguish these from disease-related processes in clinical or toxicological studies. For example, persons consuming large quantities of meat/poultry before urine collection may have NMR-detectable levels of carnosine and anserine in their urine; consumption of cherries is associated with elevated urinary fructose, and consumption of shellfish and fish is associated with high levels of betaine and trimethylamine in the urine.[1] The age of a laboratory animal can also influence the excretion profiles of urinary metabolites, for instance the increasing age of a rat is associated with increased urinary taurine but a decrease in urinary citrate.[1] These variations due to age or diet must be accounted for in biochemical or toxicological studies, in which it is very important to match controls as closely as possible to the experimental subjects with respect to age and weight.

6.3. NMR observation of chemically exchanging species in urine

In urine samples, T_2 relaxation times for some metabolites are dominated by chemical exchange contributions and can be variable according to the pH and endogenous metal ion concentrations. For example, the T_2 of citrate CH_2 protons is dependent on pH, and the relative concentrations of the acid itself and the Ca^{2+} and Mg^{2+} ions which are present in concentrations ranging from 1 to 10 mmol l^{-1}. The T_2 relaxation time of water in urine is highly dependent both on pH and the presence of the more abundant endogenous species which have exchangeable protons. In normal human subjects, the most important of these are urea, uric acid (and allantoin in most nonprimates), phosphate and ammonium ions. Urea is the most abundant proton-exchanging solute and is often present at concentrations of up to 0.7 mmol l^{-1} in human urine, and possibly twice this in rodents.[139] The urinary water NMR linewidth is typically about 4 Hz at 400 MHz, broadening to >10 Hz at 600 MHz. Supplementation of the natural amounts of these compounds in urine and adjustment of pH can give water linewidths of >30 Hz and allow efficient water suppression via the selective augmented T_2 relaxation (WATR method).[139] At low pH (i.e. < 1) proton-exchange reactions are slower and T_2 relaxation times become longer for water, ammonium and urea protons. Ammonium ions (present as an endogenous metabolite in all animal urines) can be detected directly in urine at low pH values, as the proton exchange rate is slow and the lines sharpen to give a 1:1:1 triplet (due to the ^{14}N–^{1}H coupling) at δ7.2. If deuterium oxide is present in the sample (e.g. at 20% for a field frequency lock) the ammonium signals may show additional splittings

due to the presence of various deuterium/proton isotopomers of ammonium (i.e. NH_4^+, NH_3D^+, $NH_2D_2^+$ and NHD_3^+).

In addition, paramagnetic species can be added to urine samples. The paramagnetic ions bind to polar species such as the water, causing a considerable shortening of the water T_2 relaxation time and a consequent line broadening. The water peak can then be eliminated simply by measuring a spin-echo spectrum using a suitable delay between the 90° and 180° pulses. This process will of course also attenuate the resonances of any other species which interacts with the paramagnetic ion.

6.4. Effects of solvation changes on metabolite spectra in urine

An effective method of changing the solvation conditions of a biofluid sample is to freeze-dry samples and reconstitute with the desired solvent. There are several reasons for undertaking such procedures including replacement of water with deuterium oxide as a method of avoiding the dynamic range caused by the water resonance. This is a facile procedure but may result in selective deuteration of exchangeable metabolite protons, mainly NH, NH_2, SH, COOH, OH but also certain CH or CH_2 protons can exchange, e.g. CH_2 of acetoacetate, which undergoes keto–enol tautomerism, and the CH_2 of creatinine which is mildly acidic. Changing to a deuterated aprotic solvent, e.g. dimethyl sulfoxide (DMSO), prior to NMR study confers the benefit of being able to observe protons which are normally exchange-broadened in aqueous solutions or to observe protons which are coincident with the water resonance frequency. Yamamoto *et al.*[140] proposed freeze-drying urine samples followed by their reconstitution in deuterated DMSO as a method for eliminating the water signal in order to detect signals from glycerol which were otherwise masked by the solvent resonance at very low magnetic field. One of the problems of such reconstitutions is the differential solubility of metabolites in nonaqueous solvents, i.e. the metabolites of interest may not dissolve at all. This can be shown by reconstituting freeze-dried rat urine in DMSO in which citrate resonances are noticeably absent.[140] The benefit of this type of reconstitution lies in the extra information forthcoming in the form of, for example, the resolved resonances of NH groups and their proton couplings.

6.5. Physiological effects on urine composition by NMR spectroscopy

Effects of diet

Dietary composition affects the urinary metabolite profiles, and it is important to distinguish this from disease-related processes in clinical or toxicolo-

gical studies. The effects of diet on urinary metabolites can be quite marked as for urine from a rat on a standard laboratory diet for rodents to one that was fed on a 15% casein diet and a rat that was fed on a diet depleted in sulfur amino acids.[1] The sulfur amino-acid-deficient diet leads to low urinary taurine because of the depletion of the taurine biosynthetic pathway, whereas the casein diet leads to elevated levels of TMAO, and dimethylamine due to the catabolism of excess dietary choline. The age of a laboratory animal can also influence the excretion profiles of urinary metabolites for instance increasing the age of a rat is associated with increased urinary taurine but a decrease in urinary citrate.[1] These variations due to age or diet must be accounted for in biochemical or toxicological studies, in which it is very important to match controls as closely as possible to the experimental subjects with respect to age and weight.

More subtle interactions of dietary factors with the metabolism of xenobiotic compounds can also be studied using ^{1}H NMR spectroscopy of urine. For instance rats fed on diets containing 1% paracetamol become anorexic, but supplementation of the diet with methionine protects against the weight loss.[141] Insight into the biochemical basis of this phenomenon was given by ^{1}H NMR urinalysis studies which showed that rats dosed chronically with paracetamol excreted large amounts of 5-oxoproline (prevented by dietary methionine supplementation) which was consistent with a defect in the glutathione cycle. This defect was caused by the chronic depletion of sulfur amino acids because of the heavy requirement for these imposed by the metabolism of paracetamol to sulfate, glutathione and cysteine conjugates.[142]

Fetal renal metabolism

The study of renal development has major implications for understanding further the aetiology of a range of renal disorders that include inherited polycystic kidney disease. The stages of development of renal function (i.e. glomerular filtration and tubular reabsorption/secretion processes) however remain ill defined with respect to cellular development and therefore NMR is particularly appropriate for the investigation of the metabolite composition of valuable microvolumes of fluids that are obtainable from fetuses.

The 500 MHz and 600 MHz ^{1}H NMR spectra of neonate urines are characterized by strong signals from amino acids, organic acids, amines, sugars and polyols.[143,144] In particular, high concentrations of *myo*-inositol were detected in both pre- and full-term urines. This is an important intracellular organic osmolyte in renal cells, present in high concentrations in the renal inner medulla. The turnover of *myo*-inositol in the human, however, is substantially greater than can be accounted for by dietary intake alone. The high neonatal urinary excretion of *myo*-inositol observed, prior to any form of nutritional intake, may be significant in understanding further the clinical

implications of *myo*-inositol metabolism. These include, in addition to lung immaturity, neonatal growth and development, diabetes mellitus and chronic renal disease. *Myo*-inositol is ultimately synthesized from D-glucose and the structural similarity between glucose and *myo*-inositol results in competition for high-affinity *myo*-inositol transporters. Hyperglycaemic-induced alterations in polyol metabolism (e.g. depletion of *myo*-inositol) may be contributory factors to the development of diabetic renal complications. The response of the fetal kidney to hypoxia has also been investigated using NMR spectroscopy of urine.[145] The levels of betaine in human neonatal urine and in developing rat urine have been studied.[146]

Fasting

Fasting and starvation lead to a condition known as ketosis or metabolic acidosis, characterized by high levels of the ketone bodies (acetone, acetoacetate and 3-D-hydroxybutyrate) in the biofluids. This condition is potentially life threatening due to the impact that high levels of the ketone body acids have on the blood plasma bicarbonate buffering system. Thus clinical chemistry methods for the analysis of the ketone bodies are important. Unfortunately, many of the standard methods for the analysis of the ketone bodies are time-consuming and require considerable sample preparation steps. In view of this, the utility of ^{1}H NMR spectroscopy of biofluids has been investigated as an alternative monitor of clinical condition.

Following on from initial ^{1}H NMR studies on the serum and urine from a single volunteer in 1984, a detailed study of the effects of fasting on the ^{1}H NMR spectra of the urines from five normal human volunteers was reported in 1986.[147] These volunteers underwent a 48-hour period of fasting. ^{1}H NMR analysis was able to detect simultaneously the rise in levels of all three ketone bodies as well as those of acetylcarnitine, dimethylamine and creatinine. The excretion rates of dimethylamine and creatinine remained relatively constant throughout the course of the entire experiment whilst the excretion rate of 3-D-hydroxybutyrate measured by ^{1}H NMR was in reasonable agreement with conventional enzyme assay methods. However, the levels of acetylcarnitine excretion determined by ^{1}H NMR, i.e. up to 600 μmole d^{-1}, were much higher than those measured by conventional assay. The conventional method is complex and involves ion-exchange chromatography, treatment with three enzymes and a final fluorescence assay.

6.6. NMR spectra of urine in disease

Inborn errors of metabolism

Given the serious outcome of many inborn errors of metabolism, if not diagnosed and treated at an early stage, there has been a search for a rapid,

sensitive and general method for the detection and diagnosis of inborn errors of metabolism in neonates. Conventional methods including specific enzyme assays and gas chromatography/mass spectrometry are sensitive but time consuming, involve considerable sample preparation and are not general. However, NMR spectroscopy of biofluids has been shown to be a very powerful and general method for the detection of inborn errors of metabolism.

Many metabolic disorders have been studied by the use of biofluid NMR and these are summarized in Table 4 which lists most significant studies.[148–166] Most of the work listed has involved ^{1}H NMR studies on human urine. In many cases the disease diagnosis had been made by gas chromatography/mass spectrometry and in some cases further confirmed by enzymology on cultured skin fibroblasts. For ^{1}H NMR at 250 MHz Lehnert and Hunkler[150] had problems with signal overlap so operation at 360 MHz or above is recommended. Lehnert and Hunkler also recommended that all urine samples should be adjusted to a standard pH of 2.5 in order to avoid the problem of chemical shifts varying slightly with the pH of the urine. This approach has not been adopted by others. The adjustment of pH should be avoided if possible, as it adds to the sample preparation time and can lead to accelerated degradation of biofluid components. Changing the pH also interferes with subtle intermolecular interactions in biofluids, which may themselves carry important biochemical and clinical information. A few key examples serve to illustrate the approach.

In individuals with a deficiency in methylacetoacetyl CoA thiolase (MACT), the conversion of 2-methylacetoacetyl-CoA into acetyl-CoA and propionyl-CoA is inhibited and an accumulation of abnormal catabolic products is observed in the urine. Williams *et al.*[160] have successfully used both 1D and 2D ^{1}H NMR spectroscopy to investigate the urinary metabolites of two unrelated patients with this disorder. The urine spectra from both patients clearly showed the presence of both 2-methyl-3-hydroxybutyrate and tiglylglycine, which is characteristic for MACT deficiency due to the build-up of metabolites close to the position of enzyme deficiency. However, at 360 MHz, the ^{1}H NMR spectra are quite crowded and difficult to interpret fully. This difficulty was overcome by the use of the 2D JRES ^{1}H NMR experiment, which resolved all the proton–proton couplings into the second dimension, allowing much clearer spectral interpretation. In addition to the spin-echo and 2D ^{1}H J-resolved NMR spectra, 2D ^{1}H COSY NMR spectroscopy was used to determine the spin–spin coupling connectivities between the protons in the various urinary components.

A similar success was observed for studies of branched-chain ketoaciduria in which the second stage of the catabolism of leucine, valine and isoleucine involves an oxidative decarboxylation. In patients with branched-chain ketoaciduria, this step is blocked for all three of these amino acids. The urine of these patients takes on the odour of maple syrup and hence this condition

is also known as maple syrup urine disease. Iles *et al.*[152] have used ^{1}H NMR spectroscopy to study the urines of three patients with branched-chain ketoaciduria. The spectra showed several abnormal metabolites including the amino acids leucine, isoleucine and valine and their corresponding transamination products. It was noted that 2-hydroxyisovalerate levels were very high in the urines of all the patients studied and that, as in other inborn errors of metabolism, the levels of urinary glycine were elevated. Similar results have been reported by Lehnert and Hunkler in ^{1}H NMR studies at 250 MHz.[150] Also urine from a patient with maple syrup urine disease has been studied using 750 MHz ^{1}H NMR spectroscopy. The increased dispersion provided at this frequency leads to increased confidence in the assignment of the abnormal metabolites such as hydroxy and keto acids.[158]

Iles *et al.*[165,166] have reported the use of ^{1}H NMR to monitor the effects of carnitine therapy on patients with methylmalonic aciduria and propionic acidaemia, disorders characterized by the accumulation of acyl-CoA intermediates. Acylcarnitine excretion is much increased in these disorders and it is likely that this results in intracellular carnitine insufficiency. The administration of carnitine in large quantities to these patients is designed to reduce the harmful excess of acyl-CoA intermediates by increased excretion of acylcarnitine conjugates. In these NMR studies the adult patients and controls were given oral or intravenous L-carnitine at a variety of doses. Spectra from a methylmalonic aciduria patient not only showed a fall in methylmalonate excretion as a result of therapy but also established that a large fraction of the "propionyl pool" had combined with the carnitine to produce propionylcarnitine, which was excreted in the urine. The patient showed a marked clinical improvement as the level of propionylcarnitine excretion rose. By contrast, a patient with propionic acidaemia exhibited little clinical improvement with carnitine therapy. Full results of studies on two boy patients with propionic acidaemia and one girl with methylmalonic acidaemia were also reported.[167] The studies describe the response of the patients to both carnitine challenges given when the patients were clinically stable and to carnitine therapy given in periods of metabolic instability.

High-field ^{1}H NMR spectroscopy has shown itself to be a very powerful tool with which to diagnose inborn errors of metabolism and to monitor the clinical response of patients to therapeutic interventions. Characteristic patterns of abnormal metabolites are observed in the patient's urine for each disease. The main advantages of using ^{1}H NMR spectroscopy in this area are (i) it is fast, with spectra being obtained in 5 to 10 minutes, (ii) minimal sample preparation is required, which again speeds sample throughput, but also ensures minimal perturbation to sensitive compounds in the biofluid, and (iii) it provides a nonselective detector for all the abnormal metabolites in the biofluid regardless of their structural type, providing only that they are present above the detection limit of the NMR experiment. The speed advantage is of crucial importance in this area of work as the clinical

Table 4. Inborn errors of metabolism studied by NMR spectroscopy.

Inborn error of metabolism	Diagnostic metabolites	Ref.
Alkaptonuria	Homogentisate	148,149
Argininosuccinic aciduria	Argininosuccinate	149
Biotinidase deficiency	3-Hydroxyisovalerate	150
Cytochrome *b* deficiency	Lactate	151
Cytochrome *c* oxidase deficiency	Alanine, valine	151
Glutaric aciduria type I	Glutarate, 2-ketoglutarate	152
Glutaric aciduria type II	Glutarate, isovalerate	150
Homocysteinuria	Homocystine	153
L-2-Hydroxyglutaric aciduria	2-Hydroxyglutarate	150
3-Hydroxy-3-methylglutaconyl CoA lyase deficiency	3-Hydroxy-3-methylglutarate, 3-methylglutaconate, 3-methylglutarate	150
3-Hydroxy-3-methylglutaryl CoA lyase deficiency	3-Hydroxyisovalerate, 3-hydroxy-3-methylglutarate, 3-methylglutarate *cis*-3-methylglutaconate, *trans*-3-methylglutaconate	154,155
Hyperornithinaemia	Ornithine	149
Idiopathic haemochromatosis	Iron–citrate complex	156
Isovaleric acidaemia	Acetone, isovalerylglycine, 3-hydroxyisovalerate, 3-hydroxybutyrate	150,152,157
Lactic acidosis (congenital)	Alanine, lactate	150

Maple syrup urine disease (branched-chain ketoaciduria)	Leucine, isoleucine, valine, 2-keto-isocaproate, 2-keto-3-methyl-*n*-valerate, 2-ketoisovalerate, 2-hydroxyisovalerate	152,158
Medium-chain acyl-CoA dehydrogenase deficiency	Adipate, hexanoylglycine, 5-hydroxyhexanoic acid, octanoyl camitine, sebacate, suberate, suberylglycine	159
2-Methylacetoacetyl CoA thiolase (MACT) deficiency	Butanone, tiglylglycine, 2-methyl-3-hydroxybutyrate, 2-methylacetoacetate	150,160
3-Methyicrotonyl CoA carboxylase defiency	3-Hydroxyisovalerate, 3-methylcrotonylglycine	150
Methylmalonic aciduria	Methylmalonate, glycine	150,152,161, 165,166
Multiple carboxylase deficiency	3-Hydroxypropionate	149
Non-ketotic hyperglycinaemia	Glycine	150
5-Oxoprolinuria	5-Oxoproline	162
Phenylketonuria	Phenylalanine	150
Propionic acidaemia	3-Hydroxypropionate, propionylglycine, glycine, propionylcarnitine, tiglylglycine	150,152,161, 165,166
Pyruvate decarboxylase E_1 deficiency	Acetate, lactate, pyruvate	151
Pyruvate decarboxylase E_3 deficiency	Acetate, dimethylglycine, pyruvate, succinate, trimethylamine-*N*-oxide	151
Vitamin B_{12} deficiency	Methylmalonate	163
Wilson's disease	Histidine, tyrosine	164

condition of a patient can change very rapidly and correspondingly rapid changes must be made to the therapy provided. Overall, the characteristics of NMR spectroscopy make it an ideal tool with which to obtain an analytical overview of abnormal metabolites in a biofluid and it may therefore be of value for large-scale screening for a variety of these diseases in the population at large. In addition to the potential for the rapid and accurate diagnosis of inborn errors of metabolism, further advantages are associated with the NMR approach. In particular, NMR spectroscopy may facilitate the understanding of the changes that occur in the profiles of minor, secondary biofluid metabolites in many of the disease states. This is of importance in gaining a greater insight into the clinical condition.

Set against these advantages are, however, the drawbacks of insensitivity relative to the conventional GC/MS assays and the fact that the ^{1}H NMR spectra are rather crowded, even at very high field. Thus ^{1}H NMR is very much complementary to the conventional assay methods, and GC/MS will still be required for confirmation of diagnosis and the differentiation of variant forms of diseases, some of which are characterized by the excretion of low levels of diagnostic metabolites. With the advent of even higher-field NMR spectrometers with much enhanced sensitivity, it is envisaged that the use of NMR spectroscopy in this area, which has already been very successful, will increase.

Disease studies

Videen and Ross have recently emphasized the usefulness of ^{1}H NMR spectroscopy of urine for disease diagnosis.[168] The use of ^{1}H NMR spectra of mouse urine to monitor the course of spontaneous mammary tumorigenesis has been proposed.[169]

Knubovets and co-workers reported a statistical analysis of the ^{1}H NMR spectral data from the urines of 52 patients with glomerulonephritis and eight healthy volunteers on a pseudonephrological diet.[170,171] Peak intensities in the spectra were normalized relative to the creatinine signal and were given as so-called "excretion indices". This approach was selected because creatinine is not secreted or reabsorbed in the renal tubules and is only filtered in the renal glomeruli. Thus daily creatinine excretion is stable for each person and is independent of external factors such as the protein content of meals. Using the excretion indices eliminates the dependence of signal intensities on the glomerular filtration rate and specifically reveals changes in metabolite concentration due to renal tubular dysfunction. The urine of glomerulonephritis patients was characterized by increased levels of amino acids, ketone bodies, TMAO, dimethylamine and lactate but decreased levels of citrate and α-ketoglutarate. The elevated amino acids, TMAO and dimethylamine were interpreted as being due to renal tubular interstitial changes. Progression of glomerulonephritis was shown to be accompanied by

a change in the amino aciduria from involving non-essential amino acids to essential amino acids. The ^{1}H NMR urinalysis was found to be more sensitive than standard biopsy techniques in certain cases and was capable of establishing tubular and papillary damage in glomerulonephritis patients with clinically preserved kidney function, especially those with the nephrotic variant of the disease.

Foxall *et al.*[172] used 500 and 600 MHz ^{1}H NMR spectroscopy to study the urine samples from 33 kidney transplant patients over a period of 14 days postoperation. For each of the patients the NMR data were correlated with clinical observations, graft biopsy pathology and conventional renal function tests. All of the patients received immunosuppressive treatment, although none of the patients showed clinical or histopathological signs of cyclosporin A nephrotoxicity. Currently, the assessment of renal graft dysfunction following transplantation relies on plasma creatinine concentration measurements (to assess creatinine clearance) and graft biopsy results, which are often inconclusive. A statistically significant ($p < 0.025$) increase in urinary TMAO was found for patients with graft when compared with either normal controls or patients with good graft function. However, there was an overlap between the TMAO concentrations of each of the groups, indicating that TMAO measurements alone would not be a reliable marker of graft dysfunction. Urinary levels of dimethylamine were also elevated in the patients with graft dysfunction, but this was not statistically significant. In patients with clinical evidence of renal ischaemia and acute tubular necrosis, the ^{1}H NMR of the urine showed high levels of lactate, acetoacetate, hippurate and acetoacetate but minimal aminoaciduria.

In a similar study, Le Moyec *et al.*[173] reported an analysis of the ^{1}H NMR spectra of urine and plasma from 39 patients following renal transplantation. Peak heights of several urinary metabolite signals were compared with the peak height of the creatinine signal for two groups of patients, divided according to their renal function (Group 1, creatinine clearance greater than or equal to 17 ml min^{-1}; Group 2, less than 17 ml min^{-1}). It was suggested that the use of three parameters could provide a means of discriminating between patients with rejection, cyclosporin A nephrotoxicity or cyclosporin A overdose. The three parameters were: (i) the ratio TMAO/creatinine in the urine, (ii) the presence of TMAO in plasma and (iii) the ratio of a peak at δ3.7 to that of creatinine in the urine ^{1}H NMR spectrum. From the above two studies it is apparent that urinary TMAO concentrations are an important marker of renal transplant dysfunction, although the sensitivity and specificity of the measurement are insufficient for clinical diagnosis. Eugene *et al.*[174] have studied urine from fetuses with uropathologies using ^{1}H NMR spectroscopy and another study investigated levels of urinary betaine in patients with vascular disease.[175]

Paracetamol (acetaminophen) is a very widely used analgesic and antipyretic and it has little toxicity when taken at therapeutic doses. The

metabolism of paracetamol in normal men, after a typical therapeutic dose, has been studied by both 1D[176] and 2D NMR spectroscopy,[177] as well as many other techniques. The patterns of metabolite excretion determined by NMR spectroscopy are in agreement with the results of other methods and show that the relative proportions of the glucuronide, sulfate, *N*-acetyl-L-cysteinyl and free drug plus L-cysteinyl metabolites were approximately 50, 38, 3 and 9% respectively. ^{1}H NMR spectroscopy has also been used to study the profiles of both drug and endogenous metabolites in the urine (and plasma) from patients suffering from paracetamol self-intoxification after overdose with suicidal intent.[178] Ingestion of more than 10 g of the drug results in centrilobular necrosis of the liver, which can lead to fatal liver failure several days postingestion. The toxicity of paracetamol is associated with a reactive metabolite produced by the cytochrome P450 mixed-function oxidase system. However, after a normal therapeutic dose of paracetamol, the metabolite is detoxified by glutathione conjugation, which leads to the formation of the L-cysteinyl and *N*-acetyl-L-cysteinyl metabolites. In cases of paracetamol overdose, glutathione depletion occurs. If admitted to hospital within 12 hours of overdose, the toxic damage can be limited by dosing the patient with glutathione precursors such as *N*-acetyl-L-cysteine or L-methionine. The pattern of drug metabolites in the urine following a paracetamol overdose is very different to that after a normal dose as the excretion of the sulfate metabolite is decreased greatly relative to the glucuronide. The spectrum from a "massive overdose" patient (admitted to hospital in a coma but subsequently recovered) showed a different pattern again. The most abundant drug-related signals now come from the cysteinyl and *N*-acetylcysteinyl metabolites, and disturbances are evident in the levels of a number of endogenous components. For instance, the levels of lactate, tyrosine, alanine and other amino acids are elevated, suggesting that hepatic catabolic-transamination reactions are disturbed: a sign of drug-induced liver failure. Similar spectra were obtained on the urines from patients whose overdose was subsequently fatal at this timepoint. The ^{1}H NMR spectrum of the blood plasma of the "massive overdose" patient, two days after overdose, showed large elevations in plasma amino acid levels, consistent with suffering acute liver failure. These elevations in plasma amino acid concentrations would cause the high amino acid and organic acid levels observed in the urine of this patient.

^{1}H NMR spectroscopy has also been used, in conjunction with standard clinical biochemical analyses, to monitor renal function in an unusual case of phenol poisoning.[179] A 41-year-old man fell into a shallow vat containing 40% phenol in dichloromethane, at his place of work. He did not ingest any solvent and was partially immersed for only a few seconds. However, he was found collapsed and badly burned in the nearby shower unit. Subsequently, his plasma creatinine levels began to rise, and he did not pass urine. This acute renal failure was treated by haemodialysis and the i.v. administration

of furosemide. Not only were metabolites of phenol clearly visible in the spectra taken within a few days of the incident, but the abnormally high levels of lactate, amino acids such as alanine and valine and glucose were all indicative of severe proximal tubular damage (see Section 6.7). Recovery from these cortical renal lesions was relatively rapid (about four weeks). However, levels of dimethylamine and dimethylglycine began to rise after two to three weeks. These metabolites are not normally measured in clinical chemical studies, but have recently been shown to be markers for experimentally induced renal papillary lesions (see Section 6.7). The patient was discharged from hospital after six weeks, when renal function was judged to be normal by standard clinical chemistry criteria (blood plasma levels of urea, potassium, sodium, creatinine, calcium, phosphate, and urine levels of glucose and protein), but ^{1}H NMR revealed residual renal papillary damage. One year after the incident, the patient was still polyuric and passing 3 litres of urine per day.

Vermeersch and co-workers have reported[180] the case of a 4-month-old girl who presented with agitation, hyperexcitation, fever, dehydration, polypnea and metabolic acidosis. ^{1}H NMR spectroscopy of the lyophilized urine from the patient showed the presence of 2-hydroxybenzoic acid (salicylic acid), *o*-hydroxyhippuric acid and 2,5-dihydroxyhippuric acid, which indicated that she had been poisoned with salicylate (aspirin). It is notable that this study was completed at 80 MHz, a relatively low field strength.

Malhotra and co-workers[181] reported on the ^{1}H NMR analysis of urine (and plasma) from five patients presenting with metabolic acidoses and elevated anion gaps at a hospital renal consultation service. Analysis of the biofluids by NMR was found to be extremely beneficial in the rapid determination of the causes of the metabolic disturbances. In three of the patients, alcohol ingestion (paint thinner, antifreeze) was identified in only 10 to 15 minutes allowing prompt decisions on treatment to be taken with increased chances of patient recovery. Case 1 from this report is typical. A young male in a comatose state was brought into the hospital by his wife, who had observed him drinking a can of paint thinner (containing methanol, toluene and methylene dichloride). Ethanol infusion was begun in order to protect against methanol intoxification and a sample of the patient's urine was analysed by NMR. Characteristic resonances from the methanol, toluene and methylene dichloride in the paint thinner were readily observed confirming the cause of the symptoms. Signals were also observed from the ethanol in the infusion. After haemodialysis the patient recovered and was discharged.

Pappas *et al.*[182] have recently reported a similar ^{1}H NMR application, identifying and quantitating ethanol, isopropanol, acetone and methanol in biofluids from 15 patients.

Few cases have been reported of the application of high-resolution NMR spectroscopy to the study of clinical toxicological problems. However, the reports discussed above were so successful that it seems certain that ^{1}H NMR

spectroscopy with its attributes of speed, lack of sample preparation and detection of a very wide range of metabolites will enjoy much increased usage in this area in the future.

6.7. Evaluation of toxic effects of xenobiotics using NMR spectroscopy of urine

The successful application of ^{1}H NMR spectroscopy of biofluids to study a variety of metabolic diseases and toxic processes has now been well established[183–213] and many novel metabolic markers of organ-specific toxicity have been discovered. The method is based on the fact that the biochemical composition of a biofluid is altered when organ damage occurs. This is particularly true for NMR spectra of urine in situations where damage has occurred to the kidney[195,203,210] or liver.[184,201] It has been shown that specific and identifiable changes can be observed which distinguish the organ that is the site of a toxic lesion. Also it is possible to focus in on particular parts of an organ such as the cortex of the kidney and even in favourable cases to very localized parts of the cortex. Finally, it is possible to deduce the biochemical mechanism of the xenobiotic toxicity, based on a biochemical interpretation of the changes in the urine.

A wide range of toxins has now been investigated including the kidney cortical toxins mercury chloride,[188,192,200] *p*-aminophenol,[202,211] ifosfamide,[189,190] the kidney medullary toxins propyleneimine[191] and 2-bromoethanamine hydrochloride[193] and the liver toxins hydrazine, allyl alcohol, thioacetamide and carbon tetrachloride.[185,186] The testicular toxin cadmium chloride has also been investigated in detail.[187,208] The aldose reductase inhibitor HOE-843 has also been studied.[194]

6.8. Use of combined NMR spectroscopy–pattern recognition (NMR–PR) to evaluate biochemical changes in urine

Introduction

One of the prerequisites for automatic use of NMR spectra as descriptors to enable sample classification has been the need to reduce the spectra to a series of multidimensional coordinates. One way is to segment the spectrum and integrate over each segmented region, thereby removing the effects of minor chemical shift changes as a result of changes, e.g. in pH.[214]

Studies of xenobiotic toxicity

The first studies of using PR to classify biofluid samples were those of Gartland *et al.*[215–217] Here a simple scoring system was used to describe the

levels of 18 endogenous metabolites in urine from rats which were either in a control group or had received a specific organ toxin which affected the liver, the testes, the renal cortex or the renal medulla. The ^{1}H NMR spectra were measured at 400 MHz using presaturation for water resonance suppression. Scores were generated for acetate, alanine, 3-hydroxybutyrate, creatinine, citrate, glucose, glutamine, 2-oxoglutarate, hippurate, lactate, succinate, trimethylamine-*N*-oxide, valine, dimethylamine, lysine, taurine, dimethylglycine and creatine. The data were used to construct nonlinear maps and various types of principal components scores plots in 2D or 3D. The samples were divided into two subsets, a training set and a test set. This study showed that samples corresponding to different organ toxins mapped into distinctly different regions and that in particular the renal cortical and renal medullary toxins showed good separation, as can be seen in Fig. 3. Various refinements in the data analysis were investigated, including taking scored data at three time points after the toxin exposure for the nephrotoxins only (this used only 16 metabolites as taurine and creatine were not altered in this data subset) as well as using a simple dual scoring system (the time and magnitude of the greatest change from control). The maps derived from the full time-course information provided the best discrimination between toxin classes.

The study described above was further extended[218] to incorporate actual metabolite NMR resonance intensities rather than simple scores. This was carried out for the nephrotoxins in the earlier group plus additional nephrotoxic compounds. The aim was to discover whether the NMR–PR approach could also distinguish mechanism of toxicity and site of lesion within an organ rather than simply differentiate different organ toxicities. A total of 15 different renal cortical and medullary toxins and a control group were used and the relative levels of 16 endogenous metabolites in the rat urine were quantified. NMR spectral intensities were measured at three time points: 0–8 hours, 8–24 hours and 24–48 hours after dosing. A good separation of renal medullary from renal cortical toxins was achieved. In addition, it was possible to differentiate cortical toxins according to the region of the proximal tubule which was affected and also by the biochemical mechanism of the toxic effect. A comparison was also made between the use of an added internal standard, TSP, and the use of internal glucose which could be calibrated using an independent assay for its quantitation; this showed that the derived toxic classification was independent of which method was used.

In order to test the NMR–PR approach further, the time course of metabolic urinary changes induced by two renal toxins has been investigated in detail.[219,220] In this case, toxic lesions were induced in Fisher 344 rats by a single acute dose of the renal cortical toxin mercury(II) chloride and the medullary toxin 2-bromoethanamine. The rat urine was collected for up to 9 days after dosing and was analysed using ^{1}H NMR spectroscopy. The onset, progression and recovery of the lesions were also followed using histopath-

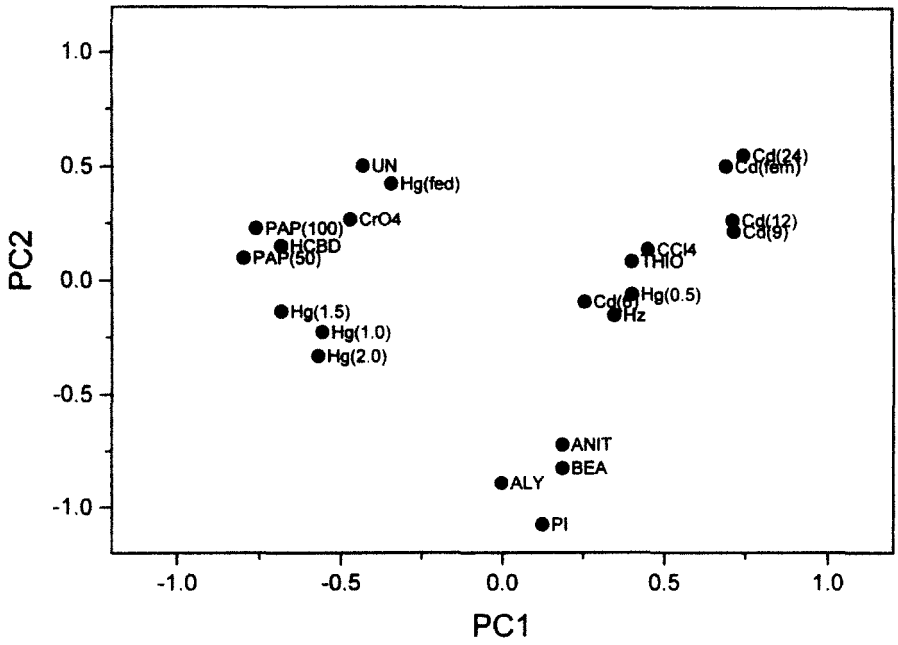

Fig. 3. A plot of principal component scores (PC1 versus PC2) for a set of rat urine samples using simple scored levels of 16 metabolites as the descriptor set. A cluster of renal cortical toxins is seen at the left, whilst the testicular and liver toxins are to the right. At the bottom the two renal papillary toxins (BEA = 2-bromoethanamine; and PI = propyleneimine) appear to cluster with liver toxins (ALY = allylalcohol; and ANIT = α-napthylisothiocyanate) but are well separated in the third principal component.

ology to provide a definitive classification of the toxic state relating to each urine sample. The concentrations of 20 endogenous urinary metabolites were measured at eight time points after dosing using internal TSP as a quantitation standard. Principal components analysis (PCA) and nonlinear maps (NLM) were used to reduce the data dimensionality. A number of ways of presenting the data were investigated and by taking the animal group mean value for the 20 metabolite concentrations it was possible to construct principal component scores plots which showed metabolic trajectories which were quite distinct for the two toxins (Fig. 4). These show that the points on the plot can be related to the development of, and recovery from, the lesions. These trajectories allowed the time points at which there were maximal metabolic differences to be determined and provided visualization of the treated groups of animals. The control group animals showed no distinct metabolic trajectory and remained in a cluster throughout all time points. Unlike the trajectory for mercury, the trajectory for

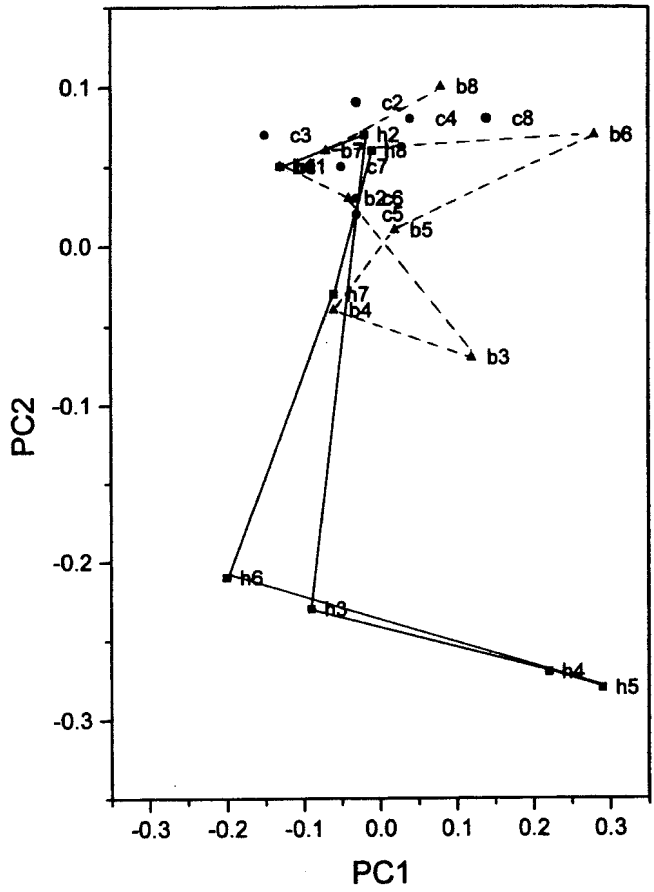

Fig. 4. A plot of PC1 versus PC2 for a set of rat urine samples using levels of 20 metabolites as the descriptor set. Each point is labelled with the day of collection and distinct biochemical trajectories can be seen for the mercury-treated (h) and the 2-bromoethanamine-treated (b) animals.

2-bromoethanamine showed different routes for onset of, and recovery from, toxicity. It was suggested that the NMR-detectable biochemical changes after mercury toxicity mainly reflect the proportions of functional cells lining the nephron, whereas the biochemical abnormalities associated with renal medullary damage probably relate to functional integrity. A statistical analysis of the NMR-based metabolites which were responsible for defining the trajectories was also made. These discriminatory metabolites (using a paired *t*-test at $p < 0.001$) included valine, taurine, TMAO, and glucose for mercury toxicity and acetate, methylamine, dimethylamine, lactate and creatine for 2-bromoethanamine toxicity. In addition a number of other resonances were significant in defining trajectories for both toxins and these

included citrate, succinate, hippurate, alanine, 2-oxoglutarate and *N*-acetyl resonances from glycoproteins released into the urine.

A toxicological assessment approach based on neural network software was tested by analysing the toxin-induced changes in endogenous biochemicals in urine as measured using ^{1}H NMR spectroscopy to ascertain whether the methods provide a robust approach which could lead to automatic toxin classification.[221] The neural network approach to sample classification was in general predictive of the sample class. It appears to be reasonably robust and once the network is trained, the prediction of new samples is rapid and automatic. It is possible to tune the network with respect to improving its predictive power and optimizing its architecture (i.e. the number of nodes in the hidden layer). However, the principal disadvantage is common to all neural network studies in that it is difficult to ascertain from the network which of the original sample descriptors are responsible for the classification.

Recently, similar studies have been published using pattern recognition to predict and classify drug toxicity effects including lesions in the liver[222] and kidney[223] and using supervised methods as an approach to an expert system.[224]

Normal physiological variance of human urine

The complexity of ^{1}H NMR spectra can make sample classification difficult and especially, if one is looking for differences in biochemistry which may be the result of a disease process, it becomes necessary to be able to define the normal physiological variation in human urine. This is also true for animal urines used for toxicological studies especially if the NMR spectroscopic approach is used for rapid screening of xenobiotic compounds for possible abnormal effects. To this end the variations in human urine caused by water loading and deprivation and by diet and exercise have been investigated using NMR–PR[225] with spectra segmented to provide a series of descriptors for each sample. In general, the spectra were mapped using NLM or PCA.

The 600 MHz ^{1}H NMR spectra generated from urine samples were for the most part similar. However, some intraperson differences could be observed in the spectra. For example one effect could be related to diet in that one sample showed a highly elevated level of TMAO following a meal containing a high proportion of fish. Several interpersonal differences were observed in that two of the volunteers had consistently low urinary citrate, whilst others had above-average concentrations of lactate in their urine. The urinary metabolites that exhibited the greatest proportional variation between people were acetate, citrate, hippurate, lactate and glycine. Spectra obtained from urine samples after exercise in general showed a higher concentration of lactate when compared to pre-exercise samples, and this could be indicative of increased anaerobic metabolism. Both TMAO and taurine showed a variation

from sample to sample but no consistent pattern in this variation could be deduced which could be attributed to either interperson or physiological differences.

In a principal components (PC) map produced from a selected set of descriptors, it was noted that the samples obtained post exercise mapped separately to all groups, except for the group of samples classified as normal which accounted for all the urines which did not fall into any other class. Samples collected from subjects in a water-deprived state could be separated from the corresponding samples representing the water-restored state. Samples from water-loaded subjects were partially separated from those representing water deprivation, with the exception of three samples from the water-loaded class, two of which were subsequently found to have osmolalities within the normal (non-water-loaded) range. Whereas no appreciable classification was obtained on the basis of subject or physiological status using unsupervised PR methods, the application of supervised learning procedures proved partially successful both in classifying individual subjects and in separating samples obtained under different physiological conditions. These supervised procedures also highlighted metabolites responsible for the observed class separations.[225]

Inborn errors of metabolism

The usefulness of the NMR–PR approach to the classification of urine samples from patients with inborn errors of metabolism has been attempted.[225] Urine samples from adult patients with inborn errors of metabolism were obtained from clinics for metabolic disorders. These comprised cystinuria ($n = 3$), oxalic aciduria ($n = 3$), Fanconi syndrome ($n = 1$), porphyria ($n = 1$) and 5-oxoprolinuria ($n = 1$). In this study, each 600 MHz ^{1}H NMR spectrum was segmented as before.

PCA mapping produced a condensed grouping for control samples and showed a well-defined separation of the inborn errors of metabolism samples, with the exception of the samples from oxalic aciduria patients which grouped along the edge of the main body of samples in the PC1 versus PC2 map. Two of the three oxalic acid samples grouped together, separate from the control samples in PC3. The oxalic aciduric samples were classified by conventional methods as being of two different types which was supported by their separate mapping positions. As with oxalic aciduria, only two of the three cystinuria samples mapped closely, a result in agreement with their NMR spectra as that of the separated cystinuria was found to be different from the other two. The data were also predefined into three classes [(a) cystinuria samples ($n = 3$); (b) oxalic aciduria samples ($n = 3$) and (c) control samples ($n = 23$)] thereby excluding any samples for which there was only one member per class. Descriptors were selected which were significant for class separation. The maps generated from these reduced numbers of descriptors

showed improved classification. The descriptors principally responsible for classification of cystinuria samples corresponded to spectral regions for lysine, whereas glyoxalate was found to heavily influence the classification of the oxalic aciduria samples.

Human renal transplantation

The rapid and unambiguous distinction of the various clinical situations that can occur following a kidney transplant remains a problem. For example, it is necessary to distinguish rejection which requires increased immunosuppressive therapy such as cyclosporin A (CyA), from tubular necrosis which can be caused by too high levels of CyA. At present, kidney function is generally characterized using the level of blood plasma creatinine as a monitor. However, the balance between rejection and tubular necrosis remains a difficult distinction and the only clear diagnosis is an invasive kidney biopsy.

A study of patients after renal transplantation has shown that NMR can reveal new markers of abnormality and in particular that high levels of TMAO in the urine are correlated with rejection episodes.[172,173] However, the use of TMAO as a single diagnostic marker of rejection is probably not sufficiently discriminatory for clinical use because of interpatient variability. It is likely that TMAO is only one of a number of potential markers of rejection and that a combination of other low-molecular-weight metabolites present in urine will provide a new differential diagnosis of rejection and CyA toxicity. A combination of high-field ^{1}H NMR urinalysis, automatic data reduction and PR methods has been applied to investigate the biochemical consequences of renal allograft dysfunction. The specific objectives were to evaluate the use of NMR–PR techniques in the differential diagnosis of graft rejection and CyA toxicity, to identify novel urinary markers of graft dysfunction, and to monitor the biochemical changes occurring with time following transplantation.[226]

Ten patients who received a renal transplant were selected for this study because of their clearly defined transplant outcome. All patients were in end-stage renal failure at the time of transplantation and had immediate graft function within three days of receiving the allograft. After exclusion of regions which contained drug metabolite, urea and water resonances, each urine ^{1}H NMR spectrum was divided into segments of equal chemical shift range, and the total intensity of the signals within each segment was calculated. Initially, unsupervised PR analysis, requiring no *a priori* assumptions regarding patient classification, was performed. A nonlinear mapping (NLM) technique was used to display the data in the form of a 2D map. Supervised PR techniques were then used to identify the descriptors which best separated and defined normal transplant function, acute graft rejection and CyA-toxic episodes, based upon advance knowledge of patient

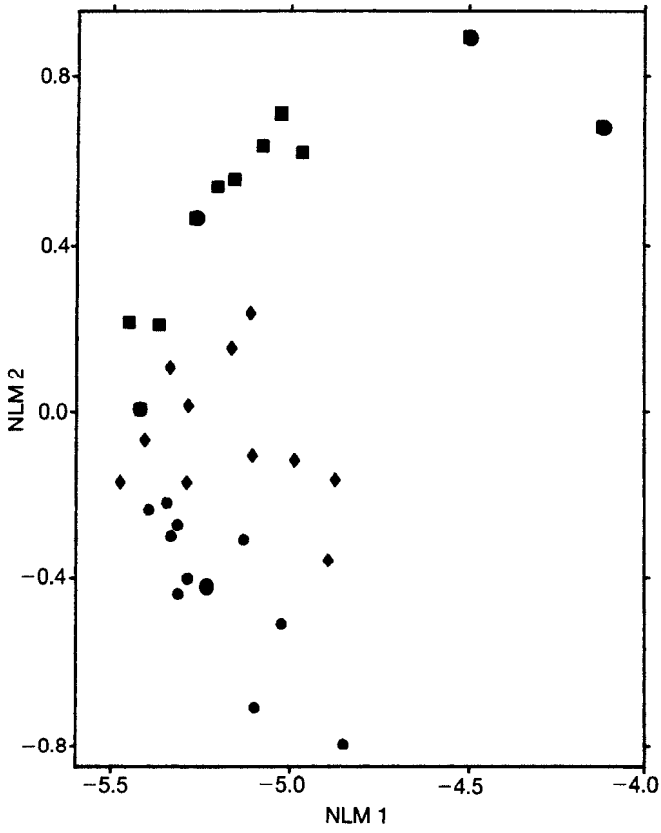

Fig. 5. A nonlinear map (NLM) of 33 human urine samples from patients after kidney transplantation based on the levels of six urinary metabolic descriptors. The diamonds correspond to patients showing good kidney graft function after transplantation, the squares are from patients showing cyclosporin nephrotoxicity and the circles are from patients with kidney rejection.

classification, and these were used to provide an improved mapping method. Six patients, generating 33 urine samples, were selected to form a training set for PR analysis and an NLM showing these urines is given in Fig. 5. The original clinical classification of the cause of the dysfunction is represented using diamond symbols for normal function, circles for rejection and squares for CyA toxicity. Quite clearly, supervised NMR–PR is seen to separate these samples into three distinct groups with the greatest separation being between the CyA toxicity group and the rejection group. It was also notable that, in general, the greater the degree of allograft dysfunction (as assessed by conventional means) the further the samples plotted away from the control group.

Identification of the compounds that gave rise to the significant descriptors has not been conclusively proven. However, close examination of spectra from samples from the various classes using both 600 MHz and 750 MHz ^{1}H NMR spectroscopy suggested that these were 3-hydroxyisovaleric acid, *N*-acetylated glycoproteins, TMAO, hippuric acid and a molecule related to *N*-methylnicotinamide.

A second object of the exercise was to determine if NMR–PR analysis could be used to monitor renal allograft dysfunction as a function of time. With the use of NLM techniques, it is possible to construct a plot of the longitudinal time course variations in the ^{1}H NMR spectral profile of urine from a patient following transplantation, i.e. a trajectory of the pattern of renal allograft function. These trajectories were constructed using the six descriptors of the spectrum chosen by the NMR–PR method and could be used successfully to predict the clinical status of the patients.

7. ^{1}H NMR SPECTROSCOPY OF SEMINAL FLUIDS

7.1. Composition of seminal fluids

Seminal plasma is biochemically distinct from other mammalian body fluids in that it contains unusually high levels of small peptides, organic and amino acids as well as a range of polyols and compounds with positively charged quaternary nitrogen atoms such as choline and glycerophosphorylcholine. These substances are secreted by the testis and the other accessory glands of the genital tract, particlarly the prostate and seminal vesicles and the reasons for the high concentrations of the components are poorly understood. The complexity of seminal plasma confers a severe problem in analysis on those attempting to define the composition of the fluid, and the relationship between altered composition and impaired reproductive function.

Seminal plasma contains many organic compounds and inorganic ions, some of which (e.g. Zn^{2+}) and amino acids, spermine and citrate, are present in concentrations up to two orders of magnitude higher than any other mammalian body fluid. The protein composition of seminal fluid is also varied and complex. The seminal fluid is predominantly formed by the secretions of the prostate (45–50%) and the seminal vesicles (45–50%), and to a lesser extent the testis ($< 5\%$). The composition of each secretion being biochemically distinct and the exact proportion of each varies considerably from subject to subject. Seminal vesicle fluid forms the later part of the ejaculate. Obtaining pure samples of this can only be achieved by invasive means (surgery or aspiration with a wide-bore needle). With the difficulty in obtaining seminal vesicle fluid, it then becomes necessary to maximize the information obtained through the use of modern analytical methods such as NMR, which are not restricted to *a priori* selection of analyte and which can give information on

molecular dynamics, protein binding and chemical exchange processes. Each of the contributory fluids to seminal fluid is biochemically active and a series of enzymatic reactions is initiated on mixing (prior to ejaculation) which result in major alterations to the biochemical composition.

7.2. Seminal fluid NMR resonance assignment

The 750 MHz ^{1}H NMR spectra of seminal fluid obtained from a healthy individual is complex but many of the signals have been assigned (see Table 2). Samples are usually left standing for 30 minutes for enzymatic gel liquefaction to occur[227] prior to freezing and then diluted by 50% with D_2O before NMR measurement. Fresh undiluted seminal fluid gives rise to NMR spectra with very broad and poorly resolved signals due to the presence of high concentrations of peptides (which are cleaved to amino acids by endogenous peptidase activity) and the high viscosity of the matrix. The complexity of the biochemical composition of seminal fluids together with their reactivity poses a number of assignment and quantitation problems. Some metabolite signals in seminal fluids also appear to have anomalous chemical shifts when compared to simple standard solutions measured at the same pH or even when compared to other body fluids. The signals from glutamate (particularly the γ-CH_2) appear to high frequency of the γ-CH_2 of glutamine (the reverse of standard solutions). The reason for this is as yet unclear but is likely to involve the formation of a stable carbamate complex by reaction with bicarbonate under the alkaline conditions (pH 7.5) that generally prevail in seminal fluids.

The application of the JRES experiment on human seminal fluids either at 600 or 750 MHz results in a dramatic simplification of the spectrum due to the dispersion of the chemical shift and coupling constant data in two orthogonal frequency domains.[227] This experiment enables the complex overlapped resonances in some of the chemical shift ranges (especially δ3–4) to be more completely resolved. The 600 MHz ^{1}H single pulse and JRES NMR spectra of normal human seminal fluid are shown in Fig. 6, illustrating the levels of assignment achieved for the endogenous species. The 600 MHz ^{1}H–^{1}H TOCSY spectrum of human seminal fluid was particularly useful for showing the connectivity maps for arginine and lysine that are extensively overlapped with each other and other metabolites. The inverse-detected ^{1}H–^{13}C HMQC spectrum provides dispersion in the ^{13}C frequency domain with its much greater chemical shift range. Many of the major amino and organic acid signals can be assigned based on their ^{1}H chemical shifts in the 2D experiments but some are much more easily distinguished and separated in the heteronuclear 2D ^{1}H–^{13}C HMQC experiment, e.g. the spermine CH_2N groups, that from the CH_2N group of arginine and the choline $N^+(CH_3)_3$ group. Some variation in the exact ^{13}C NMR shifts in 2D ^{1}H–^{13}C HMQC

spectra have been noted which are consistent with the normal pH variations in that fluid. The combination of the various homonuclear and heteronuclear techniques has resulted in the assignment of most of the major and many of the minor resonances in the spectrum (see Table 2). Therefore, this provides the basis of the use of NMR for probing biochemical interactions of the seminal fluid components in the intact matrix or the use of NMR as a diagnostic probe of altered male reproductive gland function.

Seminal fluid contains moderate concentrations of amino acids and these, because their α-CH proton resonances fall into a narrow range of chemical shifts, contribute to the severe overlap in the NMR spectral region between δ3.5 and 4.2. Although it is possible to investigate this region using 2D experiments such as COSY and TOCSY, these require significant data accumulation times and need large amounts of computer disk space. On the other hand, the 1D TOCSY experiment is rapid and economical of disk space and has been used to assign some peaks in the 750 MHz ^{1}H NMR spectrum of seminal fluid, namely valine, lactate, glutamate, pyroglutamate, uridine and uracil.[228] The simplification of the biofluid ^{1}H NMR spectrum which is effected by the application of this pulse sequence is dramatic and highly informative. The success of the method, which is rapid and of high sensitivity, relies on the molecule under study having a clearly resolved resonance which is spin coupled to others in an unbroken chain of couplings. The method should be applicable to other biofluids for the assignment of endogenous species and is best suited to those molecules which because of extended couplings are most difficult to observe in the highly overlapped 1D NMR spectrum.

An investigation of dynamic molecular processes that occur in seminal fluid has been undertaken using ^{1}H NMR spectroscopy. Reactions that could be followed included hydrolysis of phosphorylcholine and nucleotides and zinc complexation.[229]

In view of the importance of artificial insemination in farming, it is somewhat surprising that so few studies of animal seminal fluid have been reported. However, there are studies on boar seminal plasma giving details of resonance assignments.[230,231]

7.3. NMR studies of seminal fluids from infertile men

The comparison of ^{1}H NMR spectra of seminal fluid from normal controls with those from patients with vasal aplasia (obstruction of the vas deferens

Fig. 6. 600 MHz ^{1}H NMR spectra of human seminal fluid: (a) JRES spectrum, (b) single-pulse spectrum with assignments as marked.

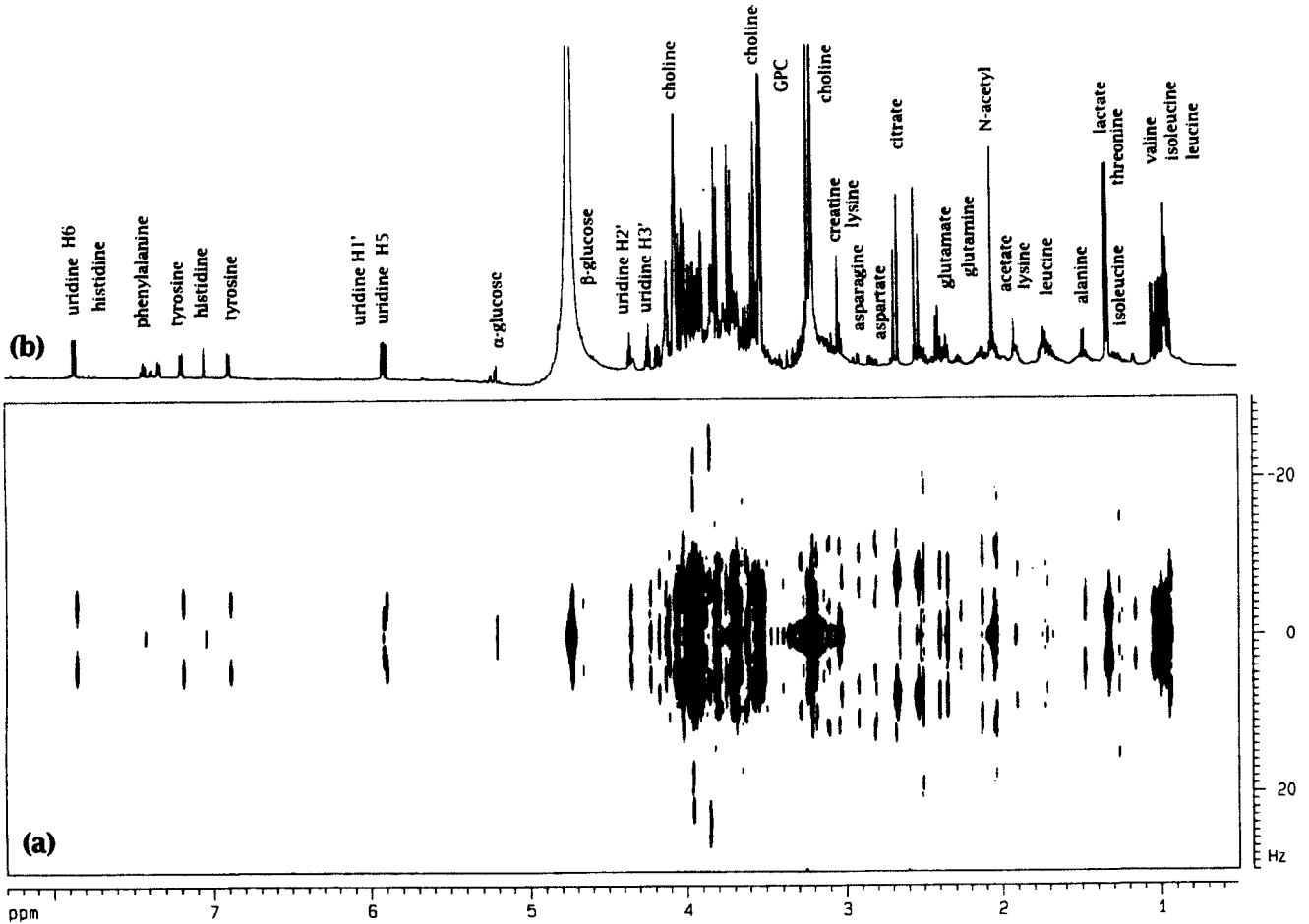
(b)
uridine H6
histidine
phenylalanine
tyrosine
histidine
tyrosine
uridine H1'
uridine H5
α-glucose
β-glucose
uridine H2'
uridine H3'
choline
choline
GPC
choline
creatine
lysine
asparagine
aspartate
citrate
glutamate
glutamine
N-acetyl
acetate
lysine
leucine
alanine
lactate
threonine
isoleucine
valine
isoleucine
leucine
(a)
-20
0
20
Hz
ppm
7
6
5
4
3
2
1

leading to blockage of the seminal vesicles) and those with nonobstructive infertility has been reported.[227] The ^{1}H NMR spectra of the seminal fluid from patients with nonobstructive infertility were similar to those of normal subjects. However, the ^{1}H NMR spectra of the seminal fluid from patients with vasal aplasia were grossly different from those of normal subjects and corresponded closely to those of prostatic secretions from normals, due to the lack of seminal vesicle secretion into the fluid. In the ^{1}H NMR spectra of the vasal aplasia patients, signals from amino acids were either absent or present at very low levels. Similarly, choline is at a low level or absent in the seminal fluid from vasal aplasia patients, as it derives (indirectly) from the seminal vesicle component. Very significant differences were observed between the normal and vasal aplasia patient groups for the molar ratio of citrate : choline and spermine : choline.

Other studies of infertility include a procedure providing automatic diagnosis based on NMR spectroscopy[232] and work on azoospermic subjects[233,234] and prostate cancer.[235] In addition ^{31}P NMR spectroscopy has also been used to distinguish semen from healthy and infertile men.[236,237]

8. ^{1}H NMR SPECTROSCOPY OF BILE

8.1. Composition of bile

One important function of the liver is bile formation. Bile is both a secretory and an excretory fluid and, as such, its composition is complex and varies according to the nutritional state of the individual. The secretory functions most prominently include the delivery to the intestinal tract of bile salts and their associated lipids to aid fat digestion and absorption, while the excretory functions include the excretion of liver-derived metabolites of potentially toxic endogenous (e.g. steroid hormones, bilirubin) or exogenous (e.g. drugs, environmental chemicals) materials. The analysis of bile by conventional biochemical techniques is a difficult procedure since it has complex physicochemical properties including a micellar substructure with a lipid-rich matrix, together with detergent properties. The chief emulsifying action is provided by the bile salts that consist of different types of free bile acids and each of these acids may in turn conjugate with glycine or taurine to form more complex acids and salts. Bile is one of the most complex and least understood of all the body fluids in terms of physicochemical properties. The bile acids are present in a matrix which contains cholesterol, cholesterol esters, phosphatidylcholine, neutral fats, fatty acids (all present in micelles) and glycoproteins together with inorganic salts including large amounts of bicarbonate.

8.2. NMR spectroscopy of bile and dynamic interactions of metabolites

The single-pulse NMR spectra of bile are dominated by broad resonances that arise from bile acids that are present in mixed micelles with phospholipids and cholesterol (Fig. 1). They are broad as a result of short spin–spin (T_2) relaxation times reflecting constrained molecular motions within micellar particles. On lyophilization and reconstitution with water, the molecular mobility of a number of biliary metabolites changes significantly due to disruption of the micellar compartments. In particular the T_2 relaxation times of the aliphatic side-chains of lipid moieties are increased in lyophilized bile suggesting greater mobility of these molecules. Reduction or disappearance of signal intensity reflects loss of volatile or unstable components (e.g. acetoacetate and acetone) which occur during the lyophilization process. Some compounds may also be unstable under freeze-drying conditions and may degrade. Increases in signal intensities that occur on lyophilization reflect changes in compartmentation of molecules which is related to the disruption/reorganization of the biliary micellar compartments. Interestingly, signals from β-hydroxybutyrate, valine and other branched-chain amino acids do not contribute significantly to the ^{1}H NMR spectra of nonlyophilized bile, but resonances from these components are clearly resolved after lyophilization indicating a dramatic lengthening of their T_2 and consequently their molecular mobility in untreated bile. The sharper signals in bile give rise to well-resolved 2D COSY spectra that allow a comprehensive assignment of the bile salt signals.[238]

Variable-temperature ^{1}H NMR studies on human bile show that considerable dynamic structural information is available, particularly at very high fields, e.g. 600 MHz. The micellar cholesteryl esters that are abundant in bile appear to show liquid crystal behaviour, and it is possible to use NMR measurements to map the phase diagram for the complex biliary matrix.

A number of studies have used both ^{1}H and ^{13}C NMR spectroscopy of bile to aid characterization of its composition and structure. Thus, ^{13}C spectra of bile from fish exposed to petroleum have been studied.[239] ^{31}P NMR spectra of human bile have also been investigated.[240] ^{1}H NMR spectroscopy of bile has been used to investigate the micellar cholesterol content[241,242] and lipids[243] and both ^{1}H and ^{31}P NMR have been used to study the distribution of lecithin and cholesterol.[244]

8.3. NMR spectroscopy of bile in pathological states

The use of ^{1}H NMR spectroscopy of bile as a means of monitoring liver function has been proposed.[245] Khristianovitch and co-workers[240] have studied the ^{31}P NMR spectra of the bile from 17 patients with primary biliary cirrhosis of the liver and from 14 clinically healthy men. Multistage fractional

duodenal catheterization was used to obtain the bile and the cystic and hepatic portions were examined separately. Also the level of lactate in bile from patients with hepatobiliary diseases including cancer has been investigated using ^{1}H NMR spectroscopy.[246]

9. ^{1}H NMR SPECTROSCOPY OF MISCELLANEOUS BODY FLUIDS

9.1. Amniotic and follicular fluids

The first study of human amniotic fluid using ^{1}H NMR spectroscopy detected 18 small molecule metabolites in samples of human amniotic fluid including clinically important glucose, leucine, isoleucine, lactate and creatinine.[247] Following this, other studies used a combination of 1D and 2D COSY spectroscopy to assign resonances, assess NMR methods of quantitation and to investigate the effects of freezing and thawing.[248,249] In addition, NMR results have been correlated with other clinical chemical analyses. A total of 70 samples were measured using ^{1}H NMR at 600 MHz at different stages of gestation and with different clinical complications, and significant correlations between the NMR spectral changes and maternal pre-eclampsia and fetal open spina bifida were observed.[250] The effects of various pathological conditions in pregnancy were investigated using ^{1}H NMR spectroscopy of human amniotic fluid by Lemoyec *et al.*[251] A similar study was also carried out at an observation frequency of 300 MHz.[252]

Several studies of amniotic fluid using ^{31}P NMR spectroscopy have also been carried out, principally to analyse the phospholipid content.[253–255]

One study of the metabolic profiling of ovarian follicular fluids from sheep, pigs and cows has been reported.[256]

9.2. Milk

Surprisingly very little has been published on the NMR spectroscopy of milk given that it is both a biofluid and a food substance. The studies generally focus on milk as a food and the first spectra were given in 1986[257] by Eads and Bryant. Since then, Belton has also reviewed the information content of NMR spectra of milk.[258] Very recently, ^{19}F NMR spectroscopy has been used to detect trifluoroacetic acid in milk.[259]

9.3. Synovial fluid

Williamson and co-workers[260] have used ^{1}H NMR to measure the levels of a variety of endogenous components in the synovial fluid aspirated from the knees of patients with osteoarthritis (10), rheumatoid arthritis (18) and

traumatic effusions (11 patients). The spin-echo 400 MHz NMR spectrum of synovial fluid shows the signals of a large number of endogenous components. Many potential markers of inflammation could not be monitored because of their low concentrations (e.g. prostaglandins) or because of their slow tumbling (hyaluronic acid, a linear polysaccharide that imparts a high viscosity to synovial fluid). The low-molecular-weight endogenous components showed a wide patient-to-patient variability and showed no statistically significant correlation with disease state. However, correlations were reported between the disease states and the synovial fluid levels of the *N*-acetyl signals from acute phase glycoproteins. These molecules have a high molecular weight and their signals are not observed in spin-echo ^{1}H NMR spectra. However, most glycoproteins contain *N*-acetylneuraminic acid or *N*-acetylglucosamine units and the *N*-acetyl signals from these units are NMR detectable, if the carbohydrate side-chains are sufficiently mobile.[37] Correlations between the disease state and the levels and type of triglyceride in the synovial fluid were also reported. Triglyceride CH_3, CH_2 and vinylic CH group signals are observed in the ^{1}H NMR of synovial fluid. In osteoarthritis, the CH_3 and CH_2 levels were very low compared with rheumatoid arthritis or traumatic effusions, and, in addition, the ratio of intensities CH_2:CH_3 was lower in osteoarthritis than in rheumatoid arthritis or traumatic effusions, thus implying a shorter chain length for the fatty acid chains. The levels of triglycerides in rheumatoid arthritis were slightly lower than in traumatic effusions and thus, on the basis of literature data for triglyceride levels in traumatic effusions, the rheumatoid arthritis levels are greater than those expected in controls.

The ^{1}H NMR spectra of the synovial fluid of a female patient with seronegative erosive rheumatoid arthritis and of another female patient with sarcoidosis and independent inflammatory osteoarthritis were followed over the course of several months and standard clinical tests were performed on paired blood serum samples taken at the same time. It was found that the synovial fluid levels of triglyceride CH_3, CH_2 and CH, glycoprotein *N*-acetyl signals and creatinine all correlated well with one another, and with standard clinical measures of inflammation. The correlation of disease state with creatinine level is of particular interest, and the altered triglyceride composition and concentration in osteoarthritis were suggested as potential markers for the disease in synovial fluid.[261]

Parkes and co-workers have also conducted ^{1}H NMR studies on synovial fluid from patients with rheumatoid arthritis.[262,263] The nature of the non-transferrin-bound iron in the synovial fluid of patients with inflammatory joint disease was investigated. Transferrin is an iron ion transport protein. In these patients the synovial fluid contains non-transferrin-bound iron which appears to be in low-molecular-mass, redox-active complexes of unknown type. This form of iron has the adverse effect of stimulating free-radical lipid peroxidations involving oxygen. 500 MHz spin-echo ^{1}H NMR spectroscopy was used to show that the incubation of patient synovial fluid with the powerful Fe(III)

chelator desferrioxamine resulted in small increases in intensity of the resonances from citrate, indicating that at least some of the non-transferrin-bound iron is present as Fe(III) citrate. Furthermore, the addition of Fe(III) ions to these samples resulted in the marked broadening and disappearance of the citrate signals from the spectrum. Subsequent addition of excess desferrioxamine resulted in the reappearance of the citrate signals in the synovial fluid spectrum after 6 hours at ambient temperature.

Also, 500 MHz spin-echo ^{1}H NMR spectroscopy was used to detect the production of formate and a low-molecular-weight, *N*-acetyl-containing oligosaccharide, derived from the oxygen radical-mediated depolymerization of hyaluronate, in the synovial fluid of patients with rheumatoid arthritis, during exercise of the inflamed joint. Gamma radiolysis of rheumatoid synovial fluid and of aqueous hyaluronate solutions was also shown to produce formate and the oligosaccharide species. It was proposed that the hyaluronate-derived oligosaccharide and formate could be novel markers of reactive oxygen radical injury during hypoxic reperfusion injury in the inflamed rheumatoid joint.

Albert *et al.*[264] showed that ^{13}C NMR could usefully be used to monitor the synovial fluids from patients with arthritis. In contrast to the ^{1}H NMR studies discussed above, signals are seen from hyaluronic acid, the main determinant of the viscoelasticity of the synovial fluid, even though the molecular weight is in the region 500 to 1600 kD. ^{13}C NMR spectra of synovial fluids from patients with rheumatoid arthritis, osteoarthritis, traumatic effusions and cadaver controls were compared with one another and with spectra of authentic hyaluronic acid, both before and after the incubation of the latter with hyaluronidase, an enzyme which depolymerizes the hyaluronic acid. Depolymerization of the hyaluronic acid was accompanied by a decrease in the half-bandwidths of its ^{13}C resonances. The synovial fluid NMR spectra from the patients with rheumatoid arthritis had sharper signals for the C-1 and C-1′ carbons of hyaluronic acid than those from the osteoarthritic patients, which in turn exhibited sharper signals than those from the cadavers or the joint trauma patients. Thus the degree of polymerization of hyaluronic acid was deduced to decrease in the order controls/joint trauma patients > osteoarthritic patients > rheumatoid arthritis patients. Since it is known that the consequence of hyaluronate depolymerization may be articular cartilage damage, it was concluded that ^{13}C NMR spectroscopy may be a valuable method for studying these clinical relevant biophysical changes in synovial fluid.

9.4. Aqueous humour and vitreous humour

The first study by NMR spectroscopy on aqueous humour was on nine samples taken during surgery for other conditions and NMR spectra were

measured at 400 MHz.[265] A number of metabolites were detected, including acetate, acetoacetate, alanine, ascorbate, citrate, creatine, formate, glucose, glutamine or glutamate, β-hydroxybutyrate, lactate, threonine and valine. Following this, there have been a number of other studies. These include ^{1}H NMR spectra from aqueous humour of rabbits,[266,267] cod fish,[268] ^{31}P NMR spectra of aqueous and vitreous humour from pigs[269] and ^{23}Na NMR spectra of vitreous humour.[270] Finally, the penetration of dexamethasone phosphate into the aqueous humour has been followed using ^{1}H and ^{19}F NMR spectroscopy.[271]

9.5. Saliva

Only limited studies using NMR spectroscopy of saliva have been reported. Initially Harada *et al.* used ^{1}H NMR spectroscopy of human saliva in a forensic study[272] and following this another Japanese group reported that only parotid gland saliva gave a well-resolved ^{1}H NMR spectrum showing significant circadian effects. No age- or sex-related differences were observed for saliva from healthy subjects but marked differences were observed in cases of sialodentitis.[273] Finally, the biochemical effects of an oral mouthwash preparation have been studied using ^{1}H NMR spectroscopy.[274]

9.6. Digestive fluids

The analysis of pancreatic juice and small bowel secretions using ^{1}H NMR spectroscopy has been reported.[275]

9.7. Pathological cyst fluid in polycystic kidney disease

Foxall and co-workers[276] have reported a ^{1}H NMR study of the fluid from the cysts of six patients with autosomal dominant polycystic kidney disease (ADPKD). ADPKD in adults is characterized by the slow progressive growth of cysts in the kidney which are lined by a single layer of renal tubular epithelium. When these cysts reach a large size they can significantly distort the kidney, and disrupt both the blood supply and renal function. ADPKD is one of the commonest causes for renal transplantation in adults. Little was known about the exact biochemical composition of cyst fluids prior to this study, or about the relationship between cyst fluid composition and the pathogenesis of the disease. The ^{1}H NMR spectra of the cyst fluids were assigned by standard methods developed earlier for other biofluids and by the use of 600 MHz ^{1}H spin-echo and 2D J-resolved experiments. The spectra revealed a number of unusual features and showed the cyst fluids to be

distinct from both blood plasma and urine. Isoleucine, lysine, threonine and valine were present at millimolar concentrations. High concentrations of acetate, lactate, succinate, creatinine and dimethylamine were also found in the cyst fluids, and in ratios different from those of blood plasma or urine. Glucose concentrations varied from 3.4 to 9.6 mmol l^{-1}, and the majority of the fluids contained signals from the *N*-acetyl groups of mobile glycoprotein sugar side-chains. Unusually, the fluids from all six patients contained high levels of ethanol, which was not related to consumption of alcoholic beverages or drug preparations. In general there was little variation in the composition of the cyst fluids as revealed by ^{1}H NMR, although the protein signal intensity did vary somewhat. It was hypothesized that this constancy of composition reflected the chronic nature of the accumulation of the cyst fluid and a long turnover time of the cyst components, which thus has the effect of averaging the compositions. The unique biochemical composition of the cyst fluids was ascribed to abnormal transport processes occurring across the cyst epithelial wall, reflecting polarity reversal of the cystic epithelium.

10. DRUG METABOLITES IN BIOFLUIDS

10.1. Drug metabolites in bile

Several studies have used NMR spectroscopy to determine the number and identity of drug metabolites in bile. These include the use of ^{19}F NMR spectroscopy to study doxifluridine catabolites in human bile,[277] ^{19}F and ^{13}C NMR spectroscopy of perfluorinated fatty acids in rat bile[278] and ^{13}C NMR for monitoring the formation of formaldehyde from demethylation of antipyrine.[279] ^{1}H NMR spectroscopy of rat bile has been used to monitor the excretion of paracetamol metabolites.[280,281] A combination of ^{1}H and ^{1}H–^{13}C 2D NMR methods has allowed identification of 4-cyano-*N*,*N*-dimethylaniline, cefoperazone and benzyl chloride in rat bile.[282,283]

10.2. Drug metabolites in urine

Nicholls *et al.* have used NMR spectroscopy of urine combined with labelling with stable isotopes such as ^{13}C and ^{2}H to monitor the silent process of deacetylation and subsequent reacetylation (futile deactylation) in the rat as this has implications for the toxicity of paracetamol[284,285] and phenacetin.[286] Hull *et al.* have monitored the metabolites of 5-fluorouracil in plasma and urine using ^{19}F NMR spectroscopy in patients receiving chemotherapy.[287] Akira *et al.* have used ^{2}H NMR to study the pharmacokinetics of benzoic

acid in relation to liver function.[288] The metabolism of hydrazine in rats has been probed using ^{15}N NMR spectroscopy of urine.[289] Often it is advantageous to carry out a partial extraction of metabolites using a solid-phase separation cartridge. In this case, the urine containing the drug metabolites is loaded on to a C18 cartridge that is then washed with acidified water to remove very polar endogenous components. The metabolites of interest can then be selectively washed off using methanol or water/methanol mixtures.[290]

10.3. HPLC–NMR studies

Introduction

The direct coupling of HPLC with NMR spectroscopy has waited for a number of technological developments to make it a feasible routine technique. Since then, major advances have made the routine use of on-line NMR detection of HPLC fractions a useful adjunct to the armoury of analytical methods.[291–295] Experiments can be carried out in one of three modes, direct on-line NMR detection of the HPLC eluent (on-flow), a stopped-flow approach or finally the eluted fractions can be stored in capillary tubes for later recall for detailed NMR spectroscopic studies. No compromise needs to be made in the chromatographic conditions, and programmed gradient elution profiles can be accommodated. The extension of the method to nanolitre scale separations has also been discussed.[296]

The simplest of operating modes is continuous-flow detection, but this is usually only practicable when using ^{1}H or ^{19}F NMR for detection unless isotopically enriched compounds are available. If the retention times of the analytes are known, or there is a good method for their detection on-line, such as UV or radioactivity, stop-flow HPLC–NMR becomes a viable option. In the stop-flow technique, all the usual techniques available for high-resolution NMR become available to the analyst. In particular, these include valuable techniques for structure determination such as the 2D NMR experiments such as TOCSY or HMQC. There are two further special categories of stop-flow experiment. Firstly, fractions eluting from the column can be stored in capillary loops for later off-line NMR study ("peak picking"). Secondly, the flow can be halted at short intervals during the passage of the eluting peak through the NMR flow cell ("time-slicing") in a manner analogous to the use of diode-array UV detector to obtain spectra from various portions of the peak. This allows chromatographic peak purity to be estimated. Time-slicing is most useful where the separation is poor, or where the compounds under study have weak/no UV chromophores making it difficult to determine the retention times.

The detection limits of HPLC–NMR are continually being revised downwards as new technical advances are made. Recently, these have

included the use of ultra-high magnetic field strengths (operating at 750 MHz and 800 MHz for ^{1}H NMR spectroscopy), the incorporation of digital filtering and oversampling into NMR data acquisition and the introduction of microbore HPLC methods. By combining the use of digital electronics with microbore HPLC, it appears that detection limits for structural characterization are in the region of 5 ng even at lower observation frequencies of 500 MHz and 600 MHz.

To date, HPLC–NMR spectroscopy has been applied to the profiling and identification of the metabolites of a number of drugs and xenobiotics present in biofluids such as plasma, urine and in bile samples from rat and man.[293] In general the simple stop-flow approach has predominated in these studies. The HPLC–NMR method is most useful for compounds and their metabolites, with suitable NMR reporter groups. This includes the use of ^{19}F NMR spectroscopy for molecules containing fluorine and diagnostic ^{1}H NMR resonances in regions of the NMR spectrum where solvent signals do not cause interference. For example, the pattern of NMR resonances from glucuronide conjugates is particularly diagnostic.

Endogenous substances

HPLC–NMR of biofluids has been employed to identify the unusual endogenous metabolites found in rat urine after administration of compounds that induce liver enzymes leading to elevated urinary levels of a number of carbohydrates and related molecules.[297]

Xenobiotic substances

A wide range of ^{1}H and ^{19}F HPLC–NMR studies has been carried out on human and animal biofluids, predominantly urine and bile, to characterize the metabolites of exploratory drugs and marketed pharmaceuticals. In some cases, the biofluid has been subjected to solid-phase extraction to remove many of the very polar materials and which hence facilitates the HPLC separation by avoiding overloading the column. These studies include the identification and structuring of metabolites of antipyrine,[298] ibuprofen,[299] flurbiprofen,[300] paracetamol (acetaminophen),[284,285,301,302] the anti-HIV compound GW524W91,[303] iloperidone[304] and tolfenamic acid.[305] Other studies using HPLC–NMR on bile include the identification of a metabolite of 7-(4-chlorobenzyl)-7,8,13,13a-tetrahydroberberine chloride in rat bile[306] and metabolites of a drug LY335979, under development to prevent multidrug resistance to cancer chemotherapy.[307] In addition, ^{31}P HPLC–NMR has been used to study metabolites of ifosfamide,[308] and ^{2}H HPLC–NMR has been employed to detect metabolites of dimethylformamide-d_7.[309]

Many drugs containing carboxylate groups form β-1-*O*-acyl glucuronides as major metabolites. Such ester glucuronides are potentially reactive due to the

susceptibility of the acyl group to nucleophilic reactions and they can undergo hydrolysis, acyl migration and covalent adduct formation. The acyl migration reactions result in positional isomers and anomers and these may be reactive towards serum proteins with toxicological consequences. The acyl group migrates successively to the 2-, 3- and 4-hydroxyl groups of the glucuronic acid moiety, thereby allowing the formation of both α- and β-anomers of the positional isomers. The acyl migration of the glucuronide metabolite of the model drug 6,11-dihydro-11-oxo-dibenz(b,e)oxepin-2-acetic acid has been investigated in pH 7.4 buffer using directly coupled stop-flow HPLC–^{1}H NMR spectroscopy and also by studying the isomers present in urine.[310] The order of elution of the isomers from the C18 column was 4β, 4α, aglycone, 1β, 3α, 3β, 2β and 2α (α and β referring to the anomerization state at C1 on the glucuronide ring, the numbers referring to the carbon number on the glucuronide ring to which the drug moiety has migrated). It is clear that directly coupled HPLC–NMR spectroscopy offers a unique analytical approach to obtain structural information of interconverting compounds in a complex mixture of isomers. This method will be of value in the elucidation of the reactivity of drug glucuronides in terms of acyl migration and enable an investigation of the potential for protein binding.

The further coupling of HPLC–NMR with mass spectrometry has also been used to analyse drug metabolites in urine for the human excretion of paracetamol metabolites.[311] This approach has also been used to identify metabolites of substituted anilines in rat urine.[312,313]

10.4. Other types of separation coupled to NMR spectroscopy

Capillary electrophoresis, together with related techniques, is a relatively new technique but has been shown to be a very powerful addition to the armoury of separative methods.[314] The technique is very simple experimentally, with all that is required being a length of fused silica capillary with an optical window to enable detection, a detector (UV, fluorescence or mass spectrometry), a high-voltage source, two electrode assemblies and buffer solutions in suitable reservoirs. The technique has been shown to provide very high separation efficiencies, with hundreds of thousands of theoretical plates achievable. However, the small injection volume available to capillary electrophoresis (a few nanolitres) means that high sensitivity can only be achieved if concentrations of the analyte in the sample are high. Nevertheless, some results have been reported using capillary electrophoresis–NMR[315] and the method has been applied to the identification of paracetamol metabolites in human urine.[316] Finally the application of capillary electrochromatography directly coupled to NMR has been explored using the same paracetamol metabolite samples.[316]

REFERENCES

1. J. K. Nicholson and I. D. Wilson, *Prog. NMR Spectrosc.*, 1989, **21**, 449.
2. J. K. Nicholson, P. J. D. Foxall, M. Spraul, R. D. Farrant and J. C. Lindon, *Anal. Chem.*, 1995, **67**, 793.
3. M. Liu, R. D. Farrant, J. K. Nicholson and J. C. Lindon, *J. Magn. Reson.*, 1995, **106B**, 270.
4. M. Liu, R. D. Farrant, B. C. Sweatman, J. K. Nicholson and J. C. Lindon, *J. Magn. Reson.*, 1995, **A113**, 251.
5. M. Liu, R. D. Farrant, J. K. Nicholson and J. C. Lindon, *J. Magn. Reson.*, 1995, **A112**, 208.
6. M. Liu, X. Mao, C. Ye, H. Huang, J. K. Nicholson and J. C. Lindon, *J. Magn. Reson.*, 1998, **132**, 125.
7. T. W.-M. Fan, *Prog. NMR Spectrosc.*, 1996, **28**, 161.
8. D. Y. Sze and O. Jardetzky, *Immunomethods*, 1994, **4**, 113.
9. R. D. Farrant, J. C. Lindon and J. K. Nicholson, *NMR Biomed.*, 1994, **7**, 243.
10. B. C. Sweatman, R. D. Farrant and J. C. Lindon, *J. Pharm. Biomed. Anal.*, 1993, **11**, 169.
11. J. K. Nicholson, M. J. Buckingham and P. J. Sadler, *Biochem. J.*, 1983, **211**, 605.
12. J. D. Bell, J. C. C. Brown, G. Kubal and P. J. Sadler, *FEBS Lett.*, 1988, **235**, 81.
13. S. Connor, J. K. Nicholson and J. R. Everett, *Anal. Chem.*, 1987, **59**, 2885.
14. J. R. Bales, D. P. Higham, I. Howe, J. K. Nicholson and P. J. Sadler, *Clin. Chem.*, 1984, **30**, 426.
15. O. A. C. Petroff, R. K. Yu and T. Ogino, *J. Neurochem.*, 1986, **47**, 1270.
16. J. D. Bell, J. C. C. Brown, P. J. Sadler, A. F. Macleod, P. H. Sönksen, R. D. Hughes and R. Williams, *Clin. Sci.*, 1987, **72**, 56.
17. M. Kriat, F. Nicoli, J. Vion-Dury, S. Confort-Gouny, P. Dano, F. Grisoli, J. L. Gastaut and P. J. Cozzone, *Annales de Biol. Clin.*, 1991, **49**, 461–467.
18. B. C. Sweatman, R. D. Farrant, E. Holmes, F. Y. Ghauri, J. K. Nicholson and J. C. Lindon, *J. Pharm. Biomed. Anal.*, 1993, **11**, 651.
19. N. W. Lutz, S. Maillet, F. Nicoli, P. Viout and P. J. Cozzone, *FEBS Lett.*, 1998, **425**, 345.
20. R. A. Wevers, U. Engelke, U. Wendel, J. G. N. de Jong, F. J. M. Gabreëls and A. Heerschap, *Clin. Chem.*, 1995, **41**, 744.
21. F. Koschorek, H. Gremmel, J. Stelten, W. Offermann and D. Leibfritz, *Neuroradiology*, 1988, **167**, 813.
22. F. Koschorek, W. Offermann, J. Stelten, W. E. Braunsdorf, U. Steller, H. Gremmel and D. Leibfritz, *Neurosurg. Rev.*, 1993, **16**, 307.
23. F. Nicoli, J. Vion-Dury, J. M. Maloteaux, C. Delwaide, S. Confort-Gouny, M. Sciaky and P. J. Cozzone, *Neurosci. Lett.*, 1993, **154**, 47.
24. A. Hiraoka, I. Miura, M. Hattori, I. Tominaga, K. Kushida and M. Maeda, *Biol. Pharm. Bull.*, 1994, **17**, 1.
25. M. A. Yates, M. F. James, N. I. Woods, D. A. Middleton, L. A. Cottrell and D. G. Reid, *J. Magn. Reson. Anal.*, 1995, **1**, 13.
26. F. Nicoli, J. Vion-Dury, S. Confort-Gouny, S. Maillet, J. L. Gastaut and P. J. Cozzone, *Comptes Rendus Ser. III – Sci de la Vie*, 1996, **319**, 623.
27. I. L. Simone, F. Federico, M. Trojano, C. Tortorella, M. Liguori, P. Giannini, E. Picciola, G. Natile and P. Livrea, *J. Neurolog. Sci.*, 1996, **144**, 182.
28. J. Lynch, J. Peeling, A. Auty and G. R. Sutherland, *Can. J. Neurolog. Sci.*, 1993, **20**, 194.
29. F. Commodari, D. L. Arnold, B. C. Sanctuary and E. Shoubridge, *NMR Biomed.*, 1991, **4**, 192.
30. F. Y. K. Ghauri, J. K. Nicholson, B. C. Sweatman, C. R. Beddell and J. C. Lindon, *NMR Biomed.*, 1993, **6**, 163.
31. R. A. Wevers, U. Engelke and A. Heerschap, *Clin. Chem.*, 1994, **40**, 1245.
32. J. C. Lindon and B. C. Sweatman, *J. Magn. Reson. Anal.*, 1996, **2**, 66.

33. S. Y. Fan, W. Y. Choy, S. L. Lam, S. C. F. Au-Yeung, L. Tsang and C. S. Cockram, *Anal. Chem.*, 1992, **64**, 2570.
34. M. Kriat, S. Confort-Gouny, J. Vion-Dury, M. Sciaky, P. Viout and P. J. Cozzone, *NMR Biomed.*, 1992, **5**, 179.
35. J. K. Nicholson, M. P. O'Flynn, P. J. Sadler, A. F. MacLeod, S. M. Juul and P. H. Sonksen, *Biochem. J.*, 1984, **217**, 365.
36. J. D. Bell, J. C. C. Brown and P. J. Sadler, *NMR Biomed.*, 1989, **2**, 246.
37. M. Grootveld, A. W. D. Claxson, C. L. Chander, P. Haycock, D. R. Blake and G. E. Hawkes, *FEBS Letters*, 1993, **322**, 266.
38. J. D. Bell, P. J. Sadler, A. F. Macleod, P. R. Turner and A. La Ville, *FEBS Lett.*, 1987, **219**, 239.
39. P. J. D. Foxall, R. D. Farrant, J. C. Lindon, G. H. Neild, M. Spraul and J. K. Nicholson, *J. Pharm. Biomed. Anal.*, 1993, **11**, 267.
40. P. J. D. Foxall, J. A. Parkinson, I. H. Sadler, J. C. Lindon and J. K. Nicholson, *J. Pharm. Biomed. Anal.*, 1993, **11**, 21.
41. A. Davin, J. Vion-Dury, P. Viout and P. J. Cozzone, *Alcohol Alcoholism*, 1984, **29**, 479.
42. J. D. Otvos, E. J. Jeyarah, D. S. Freedman, P. J. Blanche and R. M. Krauss, *Circulation*, 1993, **88**, 519.
43. J. D. Bell, J. C. C. Brown, G. Kubal and P. J. Sadler, *FEBS Letters*, 1988, **235**, 81.
44. K. P. R. Gartland, PhD Thesis, University of London, 1988.
45. M. L. Anthony, C. R. Beddell, J. C. Lindon and J. K. Nicholson, *J. Pharm. Biomed. Anal.*, 1993, **11**, 897.
46. P. J. Stilbs, *Prog. NMR Spectrosc.*, 1987, **19**, 1.
47. S. J. Gibbs and C. S. Johnson Jr, *J. Magn. Reson.*, 1991, **93**, 395.
48. H. Barjat, G. A. Morris, S. Smart, A. G. Swanson and S. C. R. Williams, *J. Magn. Reson.*, 1995, **B108**, 170.
49. M. Liu, J. K. Nicholson and J. C. Lindon, *Anal. Chem.*, 1996, **68**, 3370.
50. M. Liu, J. K. Nicholson, J. A. Parkinson and J. C. Lindon, *Anal. Chem.*, 1997, **69**, 1504.
51. M. Ala-Korpela, *Prog. NMR Spectrosc.*, 1995, **27**, 475.
52. Y. Hiltunen, M. Ala-Korpela, J. Jokisaari, S. Eskelinen, K. Kiviniitty, M. Savolainen and Y. A. Kesaniemi, *Magn. Reson. Med.*, 1991, **21**, 222.
53. M. Ala-Korpela, Y. Hiltunen, J. Jokisaari, S. Eskelinen, K. Kiviniitty, M. Savolainen and Y. A. Kesaniemi, *NMR Biomed.*, 1993, **6**, 225.
54. M. Ala-Korpela, A. Korhonen, J. Keisala, S. Horkko, P. Korpi, L. P. Ingman, J. Jokisaari, M. Savolainen and Y. A. Kesaniemi, *J. Lipid Res.*, 1994, **35**, 2292.
55. A. van den Boogaart, M. Ala-Korpela, J. Jokisaari and J. R. Griffiths, *Magn. Reson. Med.*, 1994, **31**, 347.
56. R. de Beer, A. van den Boogaart, D. van Ormondt, W. W. F. Pijnappel, J. A. den Hollander, A. J. H. Marien and P. R. Luyten, *NMR Biomed.*, 1992, **5**, 171.
57. J. W. C. van der Veen, R. de Beer, P. R. Luyten and D. van Ormondt, *Magn. Reson. Med.*, 1988, **6**, 92.
58. Y. Hiltunen, M. Ala-Korpela, J. Jokisaari, S. Eskelinen and K. Kiviniitty, *Magn. Reson. Med.*, 1992, **26**, 89.
59. J. D. Otvos, E. J. Jeyarajah and D. W. Bennett, *Clin. Chem.*, 1991, **37**, 377.
60. J. D. Otvos, E. J. Jeyarajah, D. W. Bennett and R. M. Krauss, *Clin. Chem.*, 1992, **38**, 1632.
61. S. Bradamante, E. Barchiesi, L. Barenghi and F. Zoppi, *Anal. Biochem.*, 1990, **185**, 299.
62. Y. Hiltunen, E. Heiniemi and M. Ala-Korpela, *J. Magn. Reson.*, 1995, **B106**, 191.
63. A. Ohsaka, K. Yoshikawa and T. Matuhasi, *Japan. J. Med. Sci. Biol.*, 1979, **32**, 305.
64. J. D. Bell, J. C. C. Brown, R. E. Norman, P. J. Sadler and D. R. Newell, *NMR Biomed.*, 1988, **1**, 90.
65. T. Engan, J. Krane and S. Kvinnsland, *NMR Biomed.*, 1991, **4**, 142.

66. H. Nagasawa, Y. Fujii, H. Nishiyama, Y. Goto and H. Inatomi, *Anticancer Res.*, 1992, **12**, 993.
67. E. T. Fossel, J. M. Carr and J. McDonagh, *New Engl. J. Med.*, 1986, **315**, 1369.
68. G. N. Chmurny *et al.* (18 authors), *NMR Biomed.*, 1988, **1**, 136.
69. M. P. Mims, J. D. Morrisett, C. A. Mattioli and A. M. Gotto, *New Engl. J. Med.*, 1989, **320**, 1452.
70. R. B. Verdery, D. F. Benham, I. McLennan, M. J. Busby, J. P. Wehrle and J. D. Glickson, *Biochim. Biophys. Acta*, 1989, **1006**, 287.
71. T. Engan, J. Krane, O. Klepp and S. Kvinnsland, *New Engl. J. Med.*, 1990, **322**, 949.
72. Y. Hiltunen, M. Ala-Korpela, J. Jokisaari, S. Eskelinen and K. Kiviniitty, *Mag. Res. Med.*, 1992, **26**, 89.
73. F. G. Herring, P. S. Phillips, H. Pritchard, H. Silver and K. P. Whittal, *Mag. Res. Med.*, 1990, **48**, 35.
74. K. T. Holmes, W. A. Mackinnon, G. L. May, L. C. Wright, M. Dyne, M. H. N. Tattersall, C. E. Mountford and D. Sullivain, *NMR Biomed.*, 1988, **1**, 44.
75. P. Wilding, M. B. Senior, T. Inubushi and M. L. Ludwick, *Clin. Chem.*, 1988, **34**, 505.
76. M. Kriat, J. Vion-Dury, S. Confort-Gouny, R. Favre, P. Viout, M. Sciaky, H. Sari and P. J. Cozzone, *J. Lipid Res.*, 1993, **34**, 1009.
77. J. Vion-Dury, M. Kriat, M. Sciaky, S. Confort-Gouny, P. Viout, R. Favre, F. Grisoli, J. R. Harle, E. Fontanarara, J. Sarrage and P. J. Cozzone, *Cancer J.*, 1991, **4**, 131.
78. J. Vion-Dury, R. Favre, M. Sciaky, M. Kriat, S. Confort-Gouny, J. R. Harle, N. Gazziani, P. Viout, F. Grisoli and P. J. Cozzone, *NMR Biomed.*, 1993, **6**, 58.
79. S. Berger, K.-H. Pflüger, W. A. Etzel and J. Fischer, *Eur. J. Cancer Clin. Oncol.*, 1989, **25**, 535.
80. S. D. Buchtal, M. A. Hardy and T. R. Brown, *Am. J. Med.*, 1988, **85**, 528.
81. J. M. Nabholtz, A. Rossignol, M. Famier, P. Gambert, J. C. Tremeaux and J. Guerrin, *Acta Oncol.*, 1988, **27**, 479.
82. P. Okunieff, M. D. Greenberg, A. Zietman, J. Kahn, S. Westgate and L. J. Neuringer, *J. Clin. Oncol.*, 1990, **8**, 906.
83. P. Okunieff, A. Zietman, J. Kahn, S. Singer, L. Neuringer, R. A. Levine and F. E. Evans, *New Engl. J. Med.*, 1990, **322**, 953.
84. J. D. Otvos, M. C. Coffer, S. Chen and S. Wehrli, *Biochem. Biophys. Res. Comm.*, 1987, **145**, 1397.
85. J. D. Otvos, E. J. Jeyarajah, L. W. Hayes, D. S. Freedman, N. A. Janjan and T. Anderson, *Clin. Chem.*, 1991, **37**, 369.
86. G. W. Chmurny, M. L. Mellini, D. Halverson, H. J. Issaq, G. M. Muschik, W. J. Urba, G. N. McGregor, B. D. Hilton, N. Caporaso, I. C. P. Smith, T. Kroft and J. J. Saunders, *J. Liq. Chrom.*, 1988, **11**, 647.
87. H. Höfeler and M. E. Scheulen, *Eur. J. Cancer Clin. Oncol.*, 1989, **25**, 1141.
88. M. Kriat, J. Vion-Dury, R. Rafre, D. Maraninchi, J. R. Harle, S. Confort-Gouny, M. Sciaky, E. Fontanarava, P. Viout and P. J. Cozzone, *Biochimie*, 1991, **73**, 99.
89. J. Peeling, G. Sutherland, K. Marat, E. Tomchuk and E. Bock, *J. Neurosurg.*, 1988, **68**, 931.
90. J. H. Schuhmacher, D. Conrad, H. G. Manke, J. H. Clorius, E. R. Matys, H. Hauser, I. Zuna, W. Maier-Borst and W. E. Hull, *Mag. Res. Med.*, 1990, **13**, 103.
91. G. Sutherland and J. Peeling, *NMR Biomed.*, 1989, **2**, 66.
92. F. G. Herring, P. S. Phillips and P. H. Pritchard, *J. Lipid Res.*, 1989, **30**, 521.
93. C. E. Mountford, G. L. May, L. C. Wright, W. B. Mackinnon, M. Dyne, K. T. Holmes, C. van Haaften-Day and M. H. N. Tattersall, *Lancet*, 1987, 829.
94. I. C. P. Smith and G. N. Chmurny, *Anal. Chem.*, 1990, **62**, 853A.
95. J. K. Nicholson and F. Nicholson, *Lancet*, 1987, 280.
96. C. E. Mountford, K. T. Holmes, W. B. Mackinnon and L. C. Wright, in *Magnetic Resonance*

Spectroscopy of Biofluids; A New Tool in Clinical Biology (ed. J. D. de Certaines), World Scientific, Singapore, p. 103, 1989.
97. M. Kriat, S. Confort-Gouny, J. Vion-Dury, P. Viout and P. J. Cozzone, *Biochemie*, 1992, **74**, 913.
98. M. Eugene, J. de Certaines, L. Le Moyec, E. Le Rumeur, M. Desruennes, P. Lechat and C. Cabrol, *C. R. Acad. Sci. Paris*, 1988, **307(III)**, 41.
99. M. Eugene, L. Le Moyec and J. D. de Certaines, in *Magnetic Resonance Spectroscopy of Biofluids; A New Tool in Clinical Biology* (ed. J. D. de Certaines), World Scientific, Singapore, p. 179, 1989.
100. M. Eugene, L. Le Moyec, J. D. de Certaines, M. Desruennes, E. Le Rumeur, J. B. Fraysse and C. Cabrol, *Magn. Reson. Med.*, 1991, **18**, 93.
101. H. Pont, J. Vion-Dury, M. Kriat, A. Mouly-Bandini, M. Sciaky, P. Viout, S. Confort-Gouny, T. Messana, M. Goudart, J. R. Monties and P. J. Cozzone, *Lancet*, 1991, **337**, 792.
102. M. Nishina, E. Hori, K. Matsushita, M. Takahashi and A. Ohsaka, *Physiol. Chem. Phys. Med. NMR*, 1988, **20**, 269.
103. H. Grasdalen, P. S. Belton, J. S. Pryor and G. T. Rich, *Mag. Res. Chem.*, 1987, **25**, 811.
104. E. Holmes, P. J. D. Foxall and J. K. Nicholson, *J. Pharm. Biomed. Anal.*, 1990, **81**, 955.
105. J. D. Bell, J. A. Lee, P. J. Sadler, D. R. Wilkie and R. H. Woodham, *Biochim. Biophys. Acta*, 1991, **109**, 101.
106. K. Matsushita, K. Kato, A. Ohsaka, M. Kanazawa and K. Aizawa, *Physiol. Chem. Phys. Med. NMR*, 1989, **21**, 3.
107. P. J. D. Foxall, M. Spraul, R. D. Farrant, J. C. Lindon, G. H. Neild and J. K. Nicholson, *J. Pharm. Biomed. Anal.*, 1993, **11**, 267.
108. P. J. D. Foxall, PhD Thesis, University of London, 1993.
109. F. F. Brown, I. D. Campbell, P. W. Kuchel and D. L. Rabenstein, *FEBS Lett.*, 1977, **82**, 12.
110. F. F. Brown and I. D. Campbell, *Phil. Trans. R. Soc. Lond. B*, 1980, **289**, 395.
111. R. J. Simpson, K. M. Brindle, F. F. Brown, I. D. Campbell and D. L. Foxall, *Biochem. J.*, 1981, **193**, 401.
112. R. J. Simpson, K. M. Brindle, F. F. Brown, I. D. Campbell and D. L. Foxall, *Biochem. J.*, 1982, **202**, 573.
113. R. J. Simpson, K. M. Brindle, F. F. Brown, I. D. Campbell and D. L. Foxall, *Biochem. J.*, 1982, **202**, 581.
114. K. M. Brindle, F. F. Brown, I. D. Campbell, D. L. Foxall and R. J. Simpson, *Biochem. J.*, 1982, **202**, 589.
115. K. M. Brindle, I. D. Campbell and R. J. Simpson, *Biochem. J.*, 1982, **208**, 583.
116. R. J. Simpson, K. M. Brindle and I. D. Campbell, *Biochim. Biophys. Acta*, 1982, **707**, 191.
117. K. M. Brindle, J. Boyd, I. D. Campbell, R. Porteous and N. Soffe, *Biochem. Biophys. Res. Commun.*, 1982, **109**, 864.
118. A. A. Isab and D. L. Rabenstein, *FEBS Letters*, 1979, **106**, 325.
119. M. J. York, P. W. Kuchel, B. E. Chapman and A. J. Jones, *Biochem. J.*, 1982, **207**, 65.
120. D. L. Rabenstein and A. A. Isab, *Anal. Biochem.*, 1982, **121**, 423.
121. K. M. Brindle, F. F. Brown, I. D. Campbell, C. Grathwol and P. W. Kuchel, *Biochem. J.*, 1979, **180**, 37.
122. F. F. Brown, I. Sussman, M. Avron and H. Degani, *Biochim. Biophys. Acta*, 1982, **690**, 165.
123. A. J. Jones and P. W. Kuchel, *Clin. Chim. Acta*, 1980, **104**, 77.
124. G. F. King, M. J. York, B. E. Chapman and P. W. Kuchel, *Biochem. Biophys. Res. Commun.*, 1983, **110**, 305.
125. B. E. Chapman, G. R. Beilharz, M. J. York and P. W. Kuchel, *Biochem. Biophys. Res. Commun.*, 1982, **105**, 1280.

126. P. W. Kuchel, G. E. Hunt, G. F. S. Johnson, G. R. Beilharz, B. E. Chapman, A. J. Jones and B. S. Singh, *Affective Disorders*, 1984, **6**, 83.
127. D. L. Rabenstein and A. A. Isab, *FEBS Lett.*, 1980, **121**, 61.
128. D. L. Rabenstein, S. J. Backs and A. A. Isab, *J. Am. Chem. Soc.*, 1981, **103**, 2836.
129. D. L. Rabenstein, A. A. Isab and R. S. Reid, *Biochim. Biophys. Acta*, 1982, **696**, 53.
130. D. L. Rabenstein and A. A. Isab, *Biochim. Biophys. Acta*, 1982, **721**, 374.
131. D. L. Rabenstein, A. A. Isab, W. Kadima and P. Mohanakrishnan, *Biochim. Biophys. Acta*, 1983, **762**, 531.
132. G. Otiko, M. T. Razi, P. J. Sadler, A. A. Isab and D. L. Rabenstein, *J. Inorg. Biochem.*, 1983, **19**, 227.
133. D. L. Rabenstein, *J. Biochem. Biophys. Methods*, 1984, **9**, 277.
134. A. J. Lennon, N. R. Scott, B. E. Chapman and P. W. Kuchel, *Biophys. J.*, 1994, **67**, 2096.
135. P. W. Kuchel, A. Coy and P. Stilbs, *Magn. Reson. Med.*, 1997, **37**, 637.
136. P. W. Kuchel, *Magn. Reson. Imaging*, 1998, **16**, 423.
137. E. Humpfer, M. Spraul, A. W. Nicholls, J. K. Nicholson and J. C. Lindon, *Magn. Reson. Med.*, 1997, **38**, 334.
138. J. F Zilva and P. R. Pannall, *Clinical Chemistry in Diagnosis and Treatment*, 4th edn. Lloyd-Luke, London, 1984.
139. S. C. Connor, J. R. Everett and J. K. Nicholson, *Magn. Reson. Med.*, 1987, **4**, 461.
140. H. Yamamoto, N. Koda, S. Yamaguchi, Y. Eto and K. Aoki, *Clin. Chem.*, 1987, **33**, 714.
141. F. Y. K. Ghauri, A. E. M. McLean, D. Beales, I. D. Wilson and J. K. Nicholson, *Physiol. Chem. Phys. Med. NMR*, 1993, **25**, 209.
142. J. D. Bell, J. C. C. Brown, J. K. Nicholson and P. J. Sadler, *FEBS Letters*, 1987, **215**, 311.
143. P. J. D. Foxall, S. Bewley, G. H. Neild, C. H. Rodeck and J. K. Nicholson, *Arch. Dis. Childhood*, 1995, **73**, F153.
144. P. J. D. Foxall, J. C. P. Kingdom, C. H. Rodeck, G. H. Neild and J. K. Nicholson. *J. Am. Soc. Nephrol.*, 1995, **6**, 361.
145. P. J. D. Foxall, L. R. Green, L. Bennet, M. A. Hanson and J. K. Nicholson, *J. Am. Soc. Nephrol.*, 1996, **7**, A2887.
146. S. E. C. Davies, R. A. Chalmers, E. W. Randall and R. A. Iles, *Clin. Chim. Acta*, 1988, **178**, 241.
147. J. R. Bales, J. D. Bell, J. K. Nicholson and P. J. Sadler, *Magn. Reson. Med.*, 1986, **3**, 849.
148. S. Yamaguchi, N. Koda and T. Ohashi, *Tohoku J. Exp. Med.*, 1986, **150**, 227.
149. N. Koda, S. Yamaguchi and T. Mori, *Tokyo Jikeikai Med. J.*, 1987, **102**, 1269.
150. W. Lehnert and D. Hunkler, *Eur. J. Pediatr.*, 1986, **145**, 260.
151. J. E. Rafter, R. A. Chalmers and R. A. Iles, *Biochem. Soc. Trans.*, 1990, **18**, 551.
152. R. A. Iles, A. J. Hind and R. A. Chalmers, *Clin. Chem.*, 1985, **31**, 1795.
153. J. C. C. Brown, G. A. Mills, P. J. Sadler and V. Walker, *Mag. Res. Med.*, 1989, **11**, 193.
154. R. A. Iles, J. R. Jago, S. R. Williams and R. A. Chalmers, *FEBS Lett.*, 1986, **203**, 49.
155. J. R. Jago, S. R. Williams, R. A. Chalmers and R. A. Iles, *Biochem. Soc. Trans.*, 1986, **14**, 731.
156. M. Grootveld, J. D. Bell, B. Halliwell, O. I. Aruoma, A. Bomford and P. J. Sadler, *J. Biol. Chem.*, 1989, **264**, 4417.
157. J. C. C. Brown, P. J. Sadler, G. A. Mills and V. Walker, *Ann. Clin. Biochem.*, 1987, **24**, 101.
158. J. E. Rafter, R. A. Chalmers and R. A. Iles, *Biochem. Soc. Trans.*, 1990, **18**, 912.
159. E. Holmes, P. J. D. Foxall, M. Spraul, R. D. Farrant, J. K. Nicholson and J. C. Lindon, *J. Pharm. Biomed. Anal.*, 1997, **15**, 1647.
160. S. R. Williams, R. A. Iles and R. A. Chalmers, *Clin. Chim. Acta*, 1986, **159**, 153.
161. R. A. Iles, R. A. Chalmers and A. J. Hind, *Clin. Chim. Acta*, 1986, **173**, 173.
162. F. Y. K. Ghauri, H. G. Parkes, J. K. Nicholson, I. D. Wilson and D. P. Brenton, *Clin. Chem.*, 1991, **39**, 1341.

163. F. Commodari, D. L. Arnold, B. C. Sanctuary and E. Shoubridge, *NMR Biomed.*, 1991, **4**, 192.
164. J. K. Nicholson and I. D. Wilson, *NMR Biomed.*, 1989, **2**, 77.
165. R. A. Iles, J. R. Jago, S. R. Williams, T. E. Stacey, C. de Sousa and R. A. Chalmers, *Biochem. Soc. Trans.*, 1986, **14**, 702.
166. R. A. Iles and R. A. Chalmers, *Clin. Sci.*, 1988, **74**, 1.
167. S. E. C. Davies, R. A. Iles, T. E. Stacey, C. de Sousa and R. A. Chalmers, *Clin. Chim. Acta*, 1991, **204**, 263.
168. J. S. Videen and B. D. Ross, *Kidney Int.*, 1994, **46**, S122–S128.
169. H. Nagasawa, Y. Fujii, H. Nishiyama, Y. Goto and H. Inatomi, *Anticancer Res.*, 1992, **12**, 993.
170. T. L. Knubovets, T. A. Lundina, L. A. Sibeldina and K. R. Sedov, *Mag. Res. Imaging*, 1992, **10**, 127.
171. T. A. Lundina, T. L. Knubovets, K. R. Sedov, S. A. Markova and L. A. Sibeldin, *Clin. Chim. Acta*, 1993, **214**, 165.
172. P. J. D. Foxall, G. J. Mellotte, M. R. Bending, J. C. Lindon and J. K. Nicholson, *Kidney Int.*, 1993, **43**, 234.
173. L. Le Moyec, A. Pruna, M. Eugene, J. Bedrossian, J. M. Idatte, J. F. Huneau and D. Tomé, *Nephron*, 1993, **65**, 433.
174. M. Eugene, F. Muller, M. Dommergues, L. Le Moyec and Y. Dumez, *Am. J. Obstet. Gynecol.*, 1994, **170**, 595.
175. P. Lundberg, N. P. B. Dudman, P. W. Kuchel and D. E. L. Wicken, *Clin. Chem.*, 1995, **41**, 275.
176. J. R. Bales, J. D. Bell, J. K. Nicholson, P. J. Sadler, J. A. Timbrell, R. D. Hughes, P. Bennett and R. Williams, *Mag. Res. Med.*, 1988, **6**, 300.
177. J. R. Bales, P. J. Sadler, J. K. Nicholson and J. A. Timbrell, *Clin. Chem.*, 1984, **30**, 1631.
178. J. R. Bales, J. K. Nicholson and P. J. Sadler, *Clin. Chem.*, 1985, **31**, 757.
179. P. J. D. Foxall, M. R. Bending, K. P. R. Gartland and J. K. Nicholson, *Human Toxicol.*, 1989, **9**, 491.
180. G. Vermeersch, J. Marko, B. Cartigny, F. Leclerc, P. Roussel and M. L. Hermitte, *Clin. Chem.*, 1988, **34**, 1003.
181. D. Malhotra, J. I. Shapiro and L. Chan, *J. Am. Soc. Nephrol.*, 1991, **2**, 1046.
182. A. A. Pappas, J. R. Thompson, G. L. Fuller, W. H. Porter and R. H. Gadsen, *J. Anal. Toxicol.*, 1993, **17**, 273.
183. M. L. Anthony, C. R. Beddell, J. C. Lindon and J. K. Nicholson, *Arch. Toxicol.*, 1993, **67**, 696.
184. S. M. Sanins, J. K. Nicholson, C. R. Elcombe and J. A. Timbrell, *Arch. Toxicol.*, 1990, **64**, 407.
185. S. M. Sanins, J. A. Timbrell and J. K. Nicholson, *Human Toxicol.*, 1986, **5**, 123.
186. K. P. R. Gartland, J. K. Nicholson, J. A. Timbrell and F. W. Bonner, *Human Toxicol.*, 1986, **5**, 122.
187. J. A. Gray, J. K. Nicholson and J. A. Timbrell, *Human Toxicol.*, 1986, **5**, 402.
188. J. K. Nicholson, J. A. Timbrell, D. P. Higham and P. J. Sadler, *Human Toxicol.*, 1984, **3**, 334.
189. P. J. D. Foxall, J. M. Singer, J. M. Hartley, G. H. Neild, M. Lapsley, J. K. Nicholson and R. L. Souhami, *Clin. Cancer Res.*, 1997, **2**, 295.
190. P. J. D. Foxall, J. M. Hartley, J. M. Singer, R. L. Souhami, G. H. Neild and J. K. Nicholson, *J. Am. Soc. Nephrol.*, 1994, **5**, 392.
191. E. Holmes, F. W. Bonner and J. K. Nicholson, *Comp. Biochem. Physiol. C*, 1997, **116**, 125.
192. E. Holmes, F. W. Bonner and J. K. Nicholson, *Comp. Biochem. & Physiol. C*, 1996, **114**, 7.
193. E. Holmes, F. W. Bonner and J. K. Nicholson, *Arch. Toxicol.*, 1995, **70**, 89.

194. V. Hoyle, P. J. Gilbert, J. A. Troke, C. W. Vose and J. K. Nicholson, *Biochem. Pharmacol.*, 1992, **44**, 231.
195. E. Holmes, F. W. Bonner, K. P. R. Gartland and J. K. Nicholson, *J. Pharm. Biomed. Anal.*, 1990, **8**, 959.
196. M. L. Anthony, C. R. Beddell, J. C. Lindon and J. K. Nicholson, *Arch. Toxicol.*, 1995, **69**, 99.
197. M. L. Anthony, K. P. R. Gartland, C. R. Beddell, J. C. Lindon and J. K. Nicholson, *Arch. Toxicol.*, 1992, **66**, 525.
198. M. L. Anthony, K. P. R. Gartland, C. R. Beddell, J. C. Lindon and J. K. Nicholson, *Arch. Toxicol.*, 1994, **68**, 43.
199. M. L. Anthony, K. P. R. Gartland, J. C. Lindon, C. R. Beddell and J. K. Nicholson, *Hum. Experim. Toxicol.*, 1990, **9**, 350.
200. J. K. Nicholson, J. A. Timbrell and P. J. Sadler, *Mol. Pharmacol.*, 1985, **27**, 644.
201. S. Sequeira, P. W. So, J. R. Everett, C. R. Elcombe, A. S. Kelvin and J. K. Nicholson, *J. Pharm. Biomed. Anal.*, 1990, **8**, 945.
202. K. P. R. Gartland, F. Bonner, J. A. Timbrell and J. K. Nicholson, *Arch. Toxicol.*, 1989, **63**, 97.
203. K. P. R. Gartland, F. Bonner and J. K. Nicholson, *Mol. Pharmacol.*, 1989, **35**, 242.
204. M. L. Anthony, K. P. R. Gartland, C. R. Bedell, J. C. Lindon and J. K. Nicholson, *Arch. Toxicol.*, 1992, **66**, 525.
205. M. L. Anthony, C. R. Beddell, J. C. Lindon and J. K. Nicholson, *Arch. Toxicol.*, 1993, **67**, 696.
206. M. L. Anthony, C. R. Beddell, J. C. Lindon and J. K. Nicholson, *Arch. Toxicol.*, 1995, **69**, 99.
207. S. M. Sanins, J. A. Timbrell, C. R. Elcombe and J. K. Nicholson, *Arch. Toxicol.*, 1990, **64**, 407.
208. J. K. Nicholson, D. P. Higham, J. A. Timbrell and P. J. Sadler, *Mol. Pharmacol.*, 1989, **36**, 398.
209. K. P. R. Gartland, M. L. Anthony, C. R. Beddell, J. C. Lindon and J. K. Nicholson, *J. Pharm. Biomed. Anal.*, 1990, **8**, 951.
210. K. P. R. Gartland, F. W. Bonner and J. K. Nicholson, *Mol. Pharmacol.*, 1989, **35**, 242.
211. K. P. R. Gartland, C. T. Eason, F. W. Bonner and J. K. Nicholson, *Arch. Toxicol.*, 1990, **64**, 14.
212. E. Holmes, F. W. Bonner, B. C. Sweatman, J. C. Lindon, C. R. Beddell, E. Rahr and J. K. Nicholson, *Mol. Pharmacol.*, 1992, **42**, 922.
213. E. Holmes, S. Caddick, J. C. Lindon, I. D. Wilson, S. Kryvawych and J. K. Nicholson, *Biochem. Pharmacol.*, 1995, **49**, 1349.
214. M. Spraul, P. Neidig, U. Klauck, P. Kessler, E. Holmes, J. K. Nicholson, B. C. Sweatman, S. R. Salman, C. R. Beddell, R. D. Farrant and J. C. Lindon, *J. Pharm. Biomed. Anal.*, 1994, **12**, 1215.
215. K. P. R. Gartland, C. R. Beddell, J. C. Lindon and J. K. Nicholson, *Mol. Pharmacol.*, 1991, **39**, 629.
216. K. P. R. Gartland, S. M. Sanins, J. K. Nicholson, B. C. Sweatman, C. R. Beddell and J. C. Lindon, *NMR Biomed.*, 1990, **3**, 166.
217. K. P. R. Gartland, C. R. Beddell, J. C. Lindon and J. K. Nicholson, *J. Pharm. Biomed. Anal.*, 1990, **8**, 963.
218. M. L. Anthony, B. C. Sweatman, C. R. Beddell, J. C. Lindon and J. K. Nicholson, *Mol. Pharmacol.*, 1994, **46**, 199.
219. E. Holmes, J. K. Nicholson, F. W. Bonner, B. C. Sweatman, C. R. Beddell, J. C. Lindon and E. Rahr, *NMR Biomed.*, 1992, **5**, 368.
220. E. Holmes, F. W. Bonner, B. C. Sweatman, J. C. Lindon, C. R. Beddell, E. Rahr and J. K. Nicholson, *Mol. Pharmacol.*, 1992, **42**, 922.

221. M. L. Anthony, V. S. Rose, J. K. Nicholson and J. C. Lindon, *J. Pharm. Biomed. Anal.*, 1995, **13**, 205.
222. B. M. Beckwith-Hall, J. K. Nicholson, A. W. Nicholls, P. J. D. Foxall, J. C. Lindon, S. C. Connor, M. Abdi, J. Connelly and E. Holmes, *Chem. Res. Tox.*, 1998, **11**, 260.
223. E. Holmes, A. W. Nicholls, J. C. Lindon, S. Ramos, M. Spraul, P. Neidig, S. C. Connor, J. Connelly, S. J. P. Damment, J. Haselden and J. K. Nicholson, *NMR Biomed.*, 1998, **11**, 235.
224. E. Holmes, J. K. Nicholson, A. W. Nicholls, J. C. Lindon, S. C. Connor, S. Polley and J. Connelly, *Chemomet. Intel. Lab Systems*, **44**, 251.
225. E. Holmes, P. J. D. Foxall, J. K. Nicholson, G. H. Neild, S. M. Brown, C. R. Beddell, B. C. Sweatman, E. Rahr, J. C. Lindon, M. Spraul and P. Neidig, *Anal. Biochem.*, 1994, **220**, 284.
226. P. J. D. Foxall, G. J. Mellotte, C. R. Beddell, J. C. Lindon and J. K. Nicholson, unpublished.
227. M. J. Lynch, J. Masters, J. P. Pryor, J. C. Lindon, M. Spraul, P. J. D. Foxall and J. K. Nicholson, *J. Pharm. Biomed. Anal.*, 1994, **12**, 5.
228. M. Spraul, J. K. Nicholson, M. J. Lynch and J. C. Lindon, *J. Pharm. Biomed. Anal.*, 1994, **12**, 613.
229. A. M. Tomlins, P. J. D. Foxall, M. J. Lynch, J. Parkinson, J. R. Everett and J. K. Nicholson, *Biochim. Biophys. Acta*, 1998, **1379**, 367.
230. G. Kamp and J. Lauterwein, *Biochim. Biophys. Acta*, 1995, **1243**, 101.
231. M. Kalic, G. Kamp and J. Lauterwein, *NMR Biomed.*, 1997, **10**, 341.
232. J. Segalen, J. D. de Certaines, M. le Calve, D. Colleu, J. Y. Bansard and M. Rio, *J. Reprod. Fertil.*, 1995, **103**, 181.
233. S. Hamamah, F. Seguin, C. Barthelemy, S. Akoka, A. le Pape, J. Lansac and D. Royere, *J. Reprod. Fertil.*, 1993, **97**, 51.
234. S. Hamamah, F. Seguin, C. Barthelemy, S. Akoka, A. le Pape, D. Royere and J. Lansac, *Contracep. Fertil. Sexualité*, 1993, **21**, 374.
235. M. J. Lynch and J. K. Nicholson, *Prostate*, 1997, **30**, 248.
236. W. S. M. Arrata, T. Burt and S. Corder, *Fertility Sterility*, 1978, **30**, 329.
237. A. S. Levine, N. Foster and B. Bean, *Ann. NY Acad. Sci.*, 1987, **508**, 466.
238. B. Beckwith-Hall, PhD Thesis, University of London, 1998.
239. J. Hellou, J. H. Banoub and J. F. Payne, *Chemosphere*, 1986, **15**, 787.
240. D. S. Khristianovitch, V. I. Reshetnyak, A. S. Loginov, V. E. Yushmanov, M. A. Tumanyan and L. A. Sibeldina, *Bull. Exp. Biol. Med.*, 1988, **106**, 1707.
241. J. P. M. Ellul, G. M. Murphy, H. G. Parkes, R. Z. Slapa and R. H. Dowling, *FEBS Lett.*, 1992, **300**, 30.
242. S. S. Sequeira, H. G. Parkes, J. P. M. Ellul and G. M. Murphy, *Biochim. Biophys. Acta*, 1995, **1256**, 360.
243. S. S. Sequeira, H. G. Parkes, J. P. M. Ellul and G. M. Murphy, *Biochem. Soc. Trans.*, 1994, **22**, S114.
244. M. P. Degraaf, A. K. Groen and W. M. M. J. Bovee, *Gastroenterology*, 1993, **104**, 894.
245. J. J. Powell, K. P. R. Gartland, M. Lombard, R. Sallie, J. K. Nicholson and R. P. H. Thompson, *Clin. Sci.*, 1990, **78**, 13.
246. T. Nishijima, M. Nishina and K. Fujiowara, *Jap. J. Clin. Oncol.*, 1997, **27**, 13.
247. T. R. Nelson, R. J. Gillies, D. A. Powell, M. C. Schrader, D. K. Manchester and D. H. Pretorius, *Prenatal Diagnosis*, 1987, **7**, 363.
248. C. J. Sims, D. T. Fujito, D. R. Burholt, J. Dadok, H. R. Giles and D. A. Wilkinson, *Prenatal Diagnosis*, 1993, **13**, 473.
249. P. E. McGowan, J. Reglinski, R. Wilson, J. J. Walker, S. Wisdom and J. H. McKillop, *J. Pharm. Biomed. Anal.*, 1993, **11**, 629.
250. J. L. Bock, *Clin. Chem.*, 1994, **40**, 56.

251. L. Lemoyec, F. Muller, M. Eugene and M. Spraul, *Clin. Biochem.*, 1994, **27**, 475.
252. C. J. Sims, D. T. Fujito, D. R. Burholt, J. Dadok and D. A. Wilkinson, *J. Maternal-Fetal Invest.*, 1996, **6**, 62.
253. J. M. Pearce, M. A. Shifman, A. A. Pappas and R. A. Komoroski, *Magn. Reson. Med.*, 1991, **21**, 107.
254. J. M. Pearce and R. A. Komoroski, *Magn. Reson. Med.*, 1993, **29**, 724.
255. J. M. Pearce, J. T. Krone, A. A. Pappas and R. A. Komoroski, *Magn. Reson. Med.*, 1993, **30**, 476.
256. R. G. Gosden, I. H. Sadler, D. Reed and R. H. F. Hunter, *Experientia*, 1990, **46**, 1012.
257. T. M. Eads and R. G. Bryant, *J. Agric. Food Chem.*, 1986, **34**, 834.
258. P. S. Belton, *Pure Appl. Chem.*, 1997, **69**, 47.
259. A. Preiss, J. Kruppa and C. Mugge, *J. Pharm. Biomed. Anal.*, 1998, **16**, 1381.
260. M. P. Williamson, G. Humm and A. J. Crisp, *Br. J. Rheumatol.*, 1989, **28**, 23.
261. M. C. Grootveld, H. Herz, R. Haywood, G. E. Hawkes, D. Naughton, A. Perera, J. Knappitt, D. R. Blake and A. W. D. Claxson, *Radiat. Phys. Chem.*, 1994, **43**, 445.
262. H. G. Parkes, R. E. Allen, A. Furst, D. R. Blake and M. Grootveld, *J. Pharm. Biomed. Anal.*, 1991, **9**, 29.
263. H. G. Parkes, M. Grootveld, E. B. Henderson, A. Farrell and D. R. Blake, *J. Pharm. Biomed. Anal.*, 1991, **9**, 75.
264. K. Albert, S. Michele, U. Günther, M. Fial, H. Gall and J. Saal, *Magn. Reson. Med.*, 1993, **30**, 236.
265. J. C. C. Brown, P. J. Sadler, D. J. Spalton, S. M. Juul, A. F. MacLeod and P. H. Sönksen, *Exp. Eye Res.*, 1986, **42**, 357.
266. I. S. Gribbestad and A. Midelfart, *Graefes Arch. Clin. Exp. Ophthalmol.*, 1994, **232**, 494.
267. G. S. Srivatsa, M. F. Chan, D. S. Chien and B. Tobias, *Current Eye Res.*, 1991, **10**, 127.
268. A. Midelfart, I. S. Gribbestad, B. H. Knutsen and L. Jorgensen, *Comp. Biochem. Physiol. B, Biochem. Mol. Biol.*, 1996, **113**, 445.
269. J. V. Greiner, L. A. Chanes and T. Glonek, *Ophthalmol. Res.*, 1991, **23**, 92.
270. J. W. Pettegrew, T. Glonek, N. J. Minshew and D. E. Woessner, *J. Magn. Reson.*, 1985, **63**, 439.
271. A. Midelfart, A. Dybahl, N. Muller, B. Sitter, I. S. Gribbestad and J. Krane, *Exp. Eye Res.*, 1998, **66**, 327.
272. H. Harada, H. Shimizu and M. Maeiwa, *Forensic Sci. Int.*, 1987, **34**, 189.
273. A. Yamadanosaka, S. Fukutomi, S. Uemura, T. Hashida, M. Fujishita, Y. Kobayashi and Y. Kyogoku, *Arch. Oral Biol.*, 1991, **36**, 697.
274. E. Lynch, A. Sheerin, A. W. D. Claxson, M. D. Atherton, C. J. Rhodes, C. J. L. Silwood, D. P. Naughton and M. Grootveld, *Free Rad. Res.*, 1997, **26**, 209.
275. J. J. Powell, K. P. R. Gartland, J. K. Nicholson, C. C. Ainley and R. P. H. Thompson, *Gut*, 1990, **31**, A1197.
276. P. J. D. Foxall, R. G. Price, J. K. Jones, G. H. Neild, F. D. Thompson and J. K. Nicholson, *Biochim. Biophys. Acta*, 1992, **1138**, 305.
277. R. Martino, J. Bernadou, M. C. Malet-Martino, H. Roche and J. P. Armand, *Biomed. Pharmacother.*, 1987, **41**, 104.
278. C. M. Goeckeflora and N. V. Reo, *Chem. Res. Toxicol.*, 1996, **9**, 689.
279. P. Huetter, K. Albert, E. Bayer, K. P. Zeller and F. Hartmann, *Biochem. Pharmacol.*, 1987, **36**, 2729.
280. K. P. R. Gartland, C. T. Eason, K. E. Wade, F. W. Bonner and J. K. Nicholson, *J. Pharm. Biomed. Anal.*, 1989, **7**, 699.
281. T. D. Spurway, K. P. R. Gartland, A. Warrander, R. Pickford, J. K. Nicholson and I. D. Wilson, *J. Pharm. Biomed. Anal.*, 1990, **8**, 969.
282. D. A. Ryan, J. K. M. Sanders, G. C. Curtis and H. Hughes, *J. Pharm. Biomed. Anal.*, 1995, **13**, 735.

283. D. A. Ryan, J. K. M. Sanders, G. C. Curtis and H. Hughes, *J. Pharm. Biomed. Anal.*, 1995, **13**, 723.
284. A. W. Nicholls, S. T. Caddick, I. D. Wilson, R. D. Farrant, J. C. Lindon and J. K. Nicholson, *Biochem. Pharmacol.*, 1995, **49**, 1155.
285. A. W. Nicholls, R. D. Farrant, J. P. Shockcor, S. E. Unger, I. D. Wilson, J. C. Lindon and J. K. Nicholson, *J. Pharm. Biomed. Anal.*, 1997, **15**, 901.
286. A. W. Nicholls, J. C. Lindon, S. Caddick, R. D. Farrant, I. D. Wilson and J. K. Nicholson, *Xenobiotica*, 1997, **27**, 1175.
287. W. E. Hull, R. E. Port, R. Herrmann, B. Britsch and W. Kunz, *Cancer Res.*, 1988, **48**, 1680.
288. K. Akira, R. D. Farrant, J. C. Lindon, S. T. Caddick, A. W. Nicholls and J. K. Nicholson, *Anal. Biochem.*, 1994, **221**, 297.
289. N. E. Preece, J. K. Nicholson and J. A. Timbrell, *Biochem. Pharmacol.*, 1991, **41**, 1319.
290. I. D. Wilson and J. K. Nicholson, *J. Pharm. Biomed. Anal.*, 1988, **6**, 151.
291. J. C. Lindon, J. K. Nicholson and I. D. Wilson, *Prog. NMR Spectrosc.*, 1996, **29**, 1.
292. J. C. Lindon, J. K. Nicholson and I. D. Wilson, *Adv. Chromatogr.*, 1995, **36**, 315.
293. J. C. Lindon, J. K. Nicholson, U. G. Sidelman and I. D. Wilson, *Drug Metab. Reviews*, 1997, **29**, 705.
294. K. Albert, *Analusis*, 1996, **24**, M17.
295. K. Albert, *J. Chromatogr.*, 1995, **A696**, 1.
296. B. Behnke, G. Schlotterbeck, U. Tallarek, S. Strohschein, L. H. Tseng, T. Keller, K. Albert and E. Bayer, *Anal. Chem.*, 1996, **68**, 1110.
297. V. Hoyle, PhD Thesis, University of London, 1995.
298. I. D. Wilson, J. K. Nicholson, M. Hofmann, M. Spraul and J. C. Lindon, *J. Chromatogr.*, 1993, **617**, 324.
299. M. Spraul, M. Hofmann, P. Dvortsak, J. K. Nicholson and I. D. Wilson, *Anal. Chem.*, 1993, **65**, 327.
300. M. Spraul, M. Hofmann, I. D. Wilson, E. Lenz, J. K. Nicholson and J. C. Lindon, *J. Pharm. Biomed. Anal.*, 1993, **11**, 1009.
301. M. Spraul, M. Hofmann, J. C. Lindon, R. D. Farrant, M. J. Seddon, J. K. Nicholson and I. D. Wilson, *NMR Biomed.*, 1995, **7**, 295.
302. M. J. Seddon, M. Spraul, I. D. Wilson, J. K. Nicholson and J. C. Lindon, *J. Pharm. Biomed. Anal.*, 1994, **12**, 419.
303. J. P. Shockcor, R. W. Wurm, L. W. Frick, P. N. Sanderson, R. D. Farrant, B. C. Sweatrnan and J. C. Lindon, *Xenobiotica*, 1996, **26**, 189.
304. A. E. Mutlib, J. T. Strupczewski and S. M. Chesson, *Drug Metab. Disp.*, 1995, **23**, 951.
305. U. G. Sidelmann, U. Braumann, M. Hofmann, M. Spraul, J. C. Lindon, J. K. Nicholson and S. H. Hansen, *Anal. Chem.*, 1997, **69**, 607.
306. N. P. Feng, Z. X. Zhang, D. K. An, W. L. Huang, G. J. Wang, X. W. Han and X. H. Wao, *Chin. Chem. Letters*, 1997, **8**, 515.
307. W. J. Ehlardt, J. M. Woodland, T. M. Baughman, M. Vandenbranden, S. A. Wrighton, J. S. Kroin, B. H. Norman and S. R. Maple, *Drug Metab. Disp.*, 1998, **26**, 42.
308. P. J. D. Foxall, E. M. Lenz, J. C. Lindon, G. H. Neild, I. D. Wilson and J. K. Nicholson, *Therapeut. Drug Monit.*, 1996, **18**, 498.
309. R. D. Farrant, B. C. Cupid, J. K. Nicholson and J. C. Lindon, *J. Pharmaceut. Biomed. Anal.*, 1997, **16**, 1.
310. E. M. Lenz, D. Greatbanks, I. D. Wilson, M. Spraul, M. Hofmann, J. C. Lindon, J. Troke and J. K. Nicholson, *Anal. Chem.*, 1996, **68**, 2832.
311. J. P. Shockcor, S. E. Unger, I. D. Wilson, P. J. D. Foxall, J. K. Nicholson and J. C. Lindon, *Anal. Chem.*, 1996, **68**, 4431.
312. G. B. Scarfe, B. Wright, E. Clayton, S. Taylor, I. D. Wilson, J. C. Lindon and J. K. Nicholson, *Xenobiotica*, 1998, **28**, 373.

313. G. B. Scarfe, B. Wright, E. Clayton, S. Taylor, I. D. Wilson, J. C. Lindon and J. K. Nicholson, *Xenobiotica*, in press.
314. M. J. Gordon, X. Huang, S. L. Pentoney Jr and R. N. Zare, *Science*, 1988, **242**, 224.
315. N. Wu, T. L. Peck, A. G. Webb, R. L. Magin and J. V. Sweedler, *J. Am. Chem. Soc.*, 1994, **116**, 7929.
316. K. Pusecker, J. Schewitz, P. Gfrörer, L.-H. Tseng, K. Albert, E. Bayer, I. D. Wilson, N. J. Bailey, C. B. Scarfe, J. K. Nicholson and J. C. Lindon, *Anal. Comm.*, 1998, **35**, 213.

NMR Studies of Ion-transporting Biological Channels

JAMES F. HINTON

Department of Chemistry/Biochemistry, University of Arkansas, Fayetteville, Arkansas 72701, USA

1. INTRODUCTION

1.1. Biological membranes[1]

Eukaryotic cells have both an extracellular plasma membrane and a distinct nucleus and various intracellular vacuoles and organelles, each of which is contained by its own membrane systems. The viability of these organisms depends upon the ability of the membranes to isolate and protect the integrity of their contents and to provide regulatory, selective, permeation mechanisms for the transport of material in and out of the cellular membrane components. Most selective permeation mechanisms that have evolved are mediated by membrane-bound proteins that are incorporated into the structure of the lipid bilayer of the membrane. Membrane function plays a central role in the transformation of metabolic energy into osmotic, electrical and, to some extent, mechanical work, in the acquisition and processing of information. In living cells an electrical potential difference exists between the cytoplasm and the extracellular medium due to the unequal distribution of ions on both sides of the plasma membrane surrounding the cell. The electrical resistance of the cell membrane is several orders of magnitude smaller than the resistance of the lipid membrane. This suggests that cell membranes are equipped with special

ANNUAL REPORTS ON NMR SPECTROSCOPY
VOLUME 38 ISBN 0-12-505338-X

transport mechanisms (e.g. ion channels) which accelerate the passage of ions across the lipid barrier.

The physical nature of cell membranes was revealed by experiments in the late 1890s. These experiments showed that nonpolar lipid molecules were absorbed by cells more readily than polar molecules. It was proposed that molecules enter cells by penetrating or dissolving in a layer of lipid molecules that cover cell surfaces.

The first evidence for the arrangement of the lipid molecules on the cell surface came from surface area experiments in the 1920s. Mammalian erythrocytes of uniform size and shape and containing no internal organelles or nucleus were used in these experiments. The only lipid in these samples, therefore, came from the plasma membrane. A comparison of the surface area of a lipid monolayer with the surface area of the erythrocytes from which the lipid was extracted indicated that sufficient lipid was present to make a layer two molecules thick around each cell. It was proposed that the lipid molecules of cell membranes occur as a bilayer.

During the decade of the 1930s to 1940s, surface tension experiments were used to investigate further the physical nature of cell membranes. These experiments suggested that if cells were covered with a layer of lipids then the surface tension of the cells should be similar to that of triglyceride oil droplets. Measurements showed that the surface tension of the cells was lower than that of oil droplets. However, the surface properties of cells could be mimicked by the addition of proteins to the oil droplets. Thus, the proteins were thought to form a hydrophilic film over the surface of the oil droplets thereby reducing the surface tension. To account for the low surface tension of cells it was proposed that the bilayer is coated on the internal and external surfaces with a layer of unfolded and extended proteins. To account for the unexpectedly high rate of water transport through membranes, small pores extending through the membrane were included in the model. Later, this model was modified by introducing the idea of asymmetric cell membranes having glycoproteins coating the extracellular side and proteins coating the cytoplasmic side.

Experiments in the 1960s showed that as much as 30% of the amino acid chains of membrane proteins is twisted into an alpha helix. Thus, it is unlikely that membrane proteins could be spread over the membrane surface in completely extended form as proposed in the earlier model. The total alpha helix content of membrane proteins is typical of a spherical shape rather than a flattened one. Spherical proteins were thought to be incompatible with the earlier model because placing proteins in this form on both sides of a bilayer would create a membrane structure several times thicker than that experimentally observed. Furthermore, it was noted that unfolding proteins into fully extended form on membrane surfaces would expose hydrophobic amino acid side-chains to the aqueous environment, a very thermodynamically unfavourable condition.

Experimental investigation on aqueous phospholipid solutions showed that, unlike the triglyceride solutions previously used, the phospholipids can form a bilayer in which all of the exposed surfaces are hydrophilic. This structural arrangement reduces the surface tension with no requirement for a surface protein coat. Freeze-fracture experiments indicated that proteins were actually embedded in membranes as globular units rather than extended on membrane surfaces.

Finally, Singer and Nicolson produced the fluid mosaic model for membrane structure. This model retained the phospholipid bilayer as the basic structure underlying biological membranes and proposed that the bilayer is fluid. Proteins were considered to be suspended in the fluid bilayer as discrete, individual units. The fluid mosaic model is now accepted as an accurate representation of the fundamental structure of biological membranes.

1.2. Biological membranes and passive ion transport[1]

Biological membranes have complex effects on passive transport by diffusion because they are structured as a mosaic of regions with distinct hydrophobic and hydrophilic properties. Consequently, polarity affects the ability of molecules to pass through biological membranes by passive diffusion. The ability of membrane proteins specifically to admit some polar molecules and exclude others dramatically affects the responses of biological membranes to concentration gradients.

Many substances cross biological membranes according to their lipid solubility. Other polar molecules, such as amino acids and glucose, cross the membranes more rapidly than expected according to their solubility in lipids. Cations, such as Na^+ and K^+, also cross membranes rapidly in spite of their hydrophilic nature. This passive transport of substances at higher rates than predicted from their lipid solubility is termed facilitated diffusion. That proteins are directly involved in facilitated diffusion was shown by comparison of experiments with natural membranes and synthetic membranes produced with phospholipid films. With phospholipid films all molecules, except water, diffuse according to lipid solubility and molecular size. Ions are essentially impermeable. The addition of membrane proteins, however, frequently allowed many polar and charged species to penetrate the membrane at rates comparable to natural membranes.

The transport proteins of natural membranes are integral membrane proteins that completely span the lipid bilayer. The hydrophilic channels of these proteins are created by an arrangement of amino acid chains that opens the channels and lines their sides with polar groups. The channels may be formed by a polar opening through a single protein or by several proteins that combine to form a channel between them. There are several types of transporters that facilitate diffusion across biological membranes. One type

found in animal cells is involved with the transport of small organic molecules, such as glucose. Another transport protein facilitates the diffusion of anions across membranes. A third type forms channels for cation (e.g. Na^+, K^+ and Ca^{2+}) transport across membranes. Most of the ion channels are gated. A gated channel is one that is controllable and exists in an open or closed state. Gated channels are very important in animals because they provide the basis for such processes as conduction of impulses along and between nerve cells. All of the facilitated diffusion transporters share several structural characteristics.

All of the transporters are integral membrane proteins that contain several alpha helical segments that weave back and forth across the membrane. Most of the transporters are also glycoproteins with carbohydrate groups directed towards the cell exterior.

Proteins that form ion-transporting channels are quite common among eukaryotes. The majority of these channels transport positive ions, such as Na^+, K^+ and Ca^{2+}. However, Cl^- channels have been recently observed. The cation channels function in a selective, nonspecific manner. For example, a channel may transport Na^+ ions more efficiently than K^+ ions but both cations move through the channel.

The mechanism for selectively transporting ions through a channel is complex. It appears to involve a number of factors. The shape, size and polar nature of the channel surface, the size and charge of the cation, the thermodynamic driving force for the partial dehydration of the cation at the channel entrance and the subsequent binding of the cation at the channel entrance both of which depend upon cation charge and size, and the interaction of the cations with the polar groups that line the channel all have a role in determining the selective filter of a channel.

Most ion channels operate in a gated mode. Conformational changes produced by ligand binding, mechanical stress or voltage change open or close the channel for ion transport. The ligand-gated channel opens and closes in response to the binding of specific molecular species. Hormones and molecules released by nerve cells as neurotransmitters act as control molecules that open and close ligand-gated channels. Voltage-gated channels open and close in response to changes in membrane voltage or electrical potential. The mechanosensitive-gated channel functions by mechanical stresses on the membrane producing conformational changes which open and close the channel. Gating can be very rapid. Ion transport rates can change from essentially zero to millions of ions per second in a few milliseconds.

The Na^+ voltage-gated channels in cells (i.e. excitable cells) are opened by small voltage changes at some point on the plasma membrane and admit large inflows of Na^+ ions. The inflow of Na^+ ions produced when the channels open is responsible for much of the voltage change that is involved in conduction of nerve impulses. Many neurotoxins in poisons and venoms bind to the Na^+ channels in nerve and muscle. The channels are then blocked in an open or

closed state. In this manner the neurotoxins so perturb the channel function that their effects are generally fatal.

Many epithelia (e.g. kidney tubules, colon, lungs, trachea and sweat ducts) have ligand-gated Na^+ channels. The channels are regulated by hormones. Stretch-gated Na^+ channels have been found in muscles in mammals.

Almost all animal cells contain voltage-gated or ligand-gated K^+ channels. The voltage-gated channels are associated with generation and conduction of an impulse along nerve cells. The ligand-gated channels are associated with communication between nerve cells. Eukaryotic cells contain voltage-gated, ligand-gated and stretch-gated Ca^{2+} channels. The voltage-gated channels can serve as links between nerve impulses and the regulation of major cell functions such as muscle contraction. Ligand-gated Ca^{2+} channels are also important in many cellular regulatory pathways, especially those triggered by the activation of receptors at the cell surface. Stretch-gated Ca^{2+} channels have been found in the epithelia lining blood vessels, where their activity may be associated with the regulation of blood pressure.

Recently, Cl^- channels have been discovered. These channels have no sequence relationship to the voltage-gated Na^+, K^+ and Ca^{2+} channels. One such channel is involved in the disease, cystic fibrosis. In this disease, regulation of the channel is defective. The altered function of the channel in epithelia causes elevated levels of sodium and chloride ions in sweat and, through unknown processes, the accumulation of mucus in the respiratory tract and failure of exocrine secretion in glands, such as the pancreas. Blockage of airways leads to chronic lung infections that, with other effects of the Cl^- transport deficiency, can be fatal.

1.3. Strategies for studying ion channels

The determination of the correlation between channel structure and function is of considerable importance. The peptides of ligand-gated and voltage-gated channels from several species have been completely sequenced. The amino acid sequence analysis indicates that most ligand-gated channels are related proteins that have a cluster of three α-helical segments that extend across the membranes and form a hydrophilic channel. The voltage-gated Na^+, K^+ and Ca^{2+} channels appear to be members of a related group. The K^+ channel, the simplest of the three, is a relatively small polypeptide that contains a single domain. This domain contains six segments of hydrophobic amino acids that are capable of folding into membrane-spanning α-helices. The more complex channel-forming polypeptides of the Na^+ and Ca^{2+} channels contain four domains, each with six transmembrane segments arranged in a pattern that is similar to that of the K^+ channel. The amphipathic helices are thought to associate so that their polar surfaces form an inner channel through the core of the protein. Although some of the general features of the structure of

channels are known, not a single high-resolution structure of an ion channel protein from a eukaryotic cell is available,[2] with the one exception of the landmark 3.2 Å X-ray crystallographic structure determination of the K^+ channel from *Streptomyces lividans*.[3] A major reason for this is that proteins embedded into membrane bilayers are poor candidates for x-ray crystallography. Currently, these proteins are too large to be studied by conventional NMR techniques. It is hoped that the next generation of ultra-high magnetic field NMR spectrometers will provide the capability of obtaining significant structural information concerning ion channels. However, if or until that becomes a reality, other strategies are employed to investigate the structure–function relationship.

One strategy is to use small peptides that form channels in membranes or to use segments of protein channels that are associated with the channel formation. Channel-forming peptides, considered to be minimal models for the pore-forming structure of channel proteins, may be classified in three categories:[4] (i) naturally occurring channel-forming peptides, (ii) peptides that mimic structural elements predicted to form the channel lining of authentic channel proteins and (iii) minimally designed synthetic peptides. Another strategy that can be used to obtain information about channels is property-directed, nonpeptidic synthesis of channels.

Naturally occurring peptides, such as gramicidin A, can form channels that exhibit a wide range of structure and biological activity. These relatively small channels are also very useful in the study of the structure–function relationship of channels. Small, synthetic peptides of a limited number of types of hydrophobic and hydrophilic amino acids, which bear no relationship to the sequence of naturally occurring channels can serve as model channels. These systems are useful in the study of the general properties of channels.[4] The third class of channel-forming peptides represents part of a strategy involved with the design of pore proteins based upon sequence information and the oligomeric organization of naturally occurring channels.[4] This strategy is based upon the assumption that given the primary structure of channel proteins it may be possible to identify a segment associated with the ion-transporting pore. It is then assumed that such a sequence folds into a structure that has the channel characteristics of the natural protein channel.

A comprehension of how a channel structure is formed and how its structure affects the function of ion transport across membranes requires knowledge of many facets of this relationship. One must understand the interaction between a specific peptide or protein and the membrane environment which ultimately determines the folded structure that forms a channel. Single amino acid substitution in the sequence of the peptide or protein can be used to investigate the very delicate balance of forces that must exist between side-chains of the residues and the membrane environment to maintain a stable folded structure. The structure of these peptide or protein analogues in a membrane environment must be obtained to determine if there are structural differences that might

affect the transport process. Although the channel dimensions might not change with amino acid substitution, the long-range interaction between side-chains, such as the indole ring of tryptophan, and the ions to be transported can be modulated by substitution and, therefore, influence the binding and transport processes. Consequently, binding constants and transport energetics must be determined as a function of amino acid substitution.

There are relatively few physical techniques available for the characterization of the interaction of monovalent cations with biological molecules responsible for cation transport. However, nuclear magnetic resonance (NMR) spectroscopy has proven to be a very powerful technique for the study of the transport process and the molecular systems responsible for the transport. NMR techniques can be used to determine the three-dimensional structure of the channel, to determine the thermodynamic parameters for the incorporation of the transport system into the membrane environment, to obtain the thermodynamic parameters for the binding of the cations to the channel, to determine the kinetic activation enthalpy for the transport process, and to study the internal motion of the peptide or protein that forms the channel.

2. NATURALLY OCCURRING PEPTIDE CHANNELS

The gramicidin family of linear polypeptides represents a biologically viable channel system of related peptides in which specific changes in amino acid composition can be correlated with cation binding selectivity and transport. The parent molecule of this family of polypeptides, gramicidin A, has the amino acid sequence shown in Fig. 1. This relatively simple molecule is probably the best characterized ion channel (both structurally and functionally) and has, to date, been the principal proving-ground for many of our ideas about the molecular nature of ion conduction in membranes.[5]

The linear gramicidins A, B (Trp at position 11 in gramicidin A replaced by phenylalanine) and C (Trp at position 11 in gramicidin A replaced by tyrosine) are the main species synthesized by the aerobic spore-forming bacterium *Bacillus brevis*[6] (see Fig. 1). These peptides contain D-amino acids and are made *in vivo* by total enzymatic synthesis without the use of ribosomes or a template RNA.[7] A mixture of nine pentadecapeptides is synthesized by *Bacillus brevis*, the major component being gramicidin A.[8–11] Six of the peptides of the mixture have different amino acids at position 1 (Ile instead of Val) and/or at position 11 Phe or Tyr instead of Trp)[8] while three of the peptides are acylated gramicidins A, B and C.[9–12] The relative abundance of the various amino acids in the growth medium can affect the amounts of the linear gramicidins produced by *Bacillus brevis*[13] and, therefore, the proportions of gramicidins in different commercial lots. Typically, an A/B/C ratio of approximately 7/1/2 is produced. Further variations in amino acid sequence can

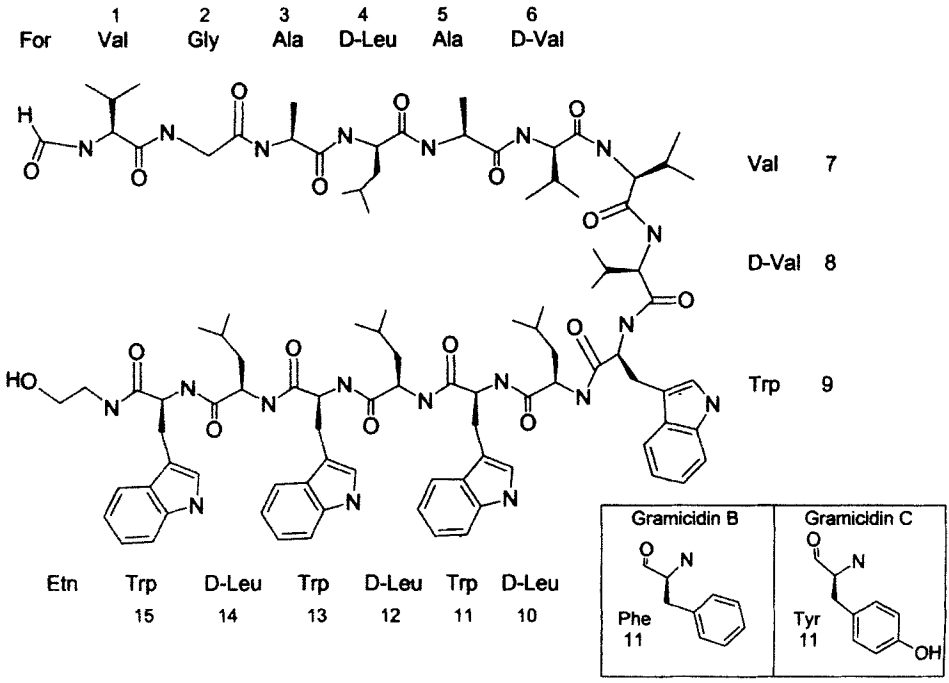

Fig. 1. The amino acid sequence of gramicidin A, B and C.

be produced by either total synthesis or semisynthesis.[14–16] Because these analogues provide subtle but well-defined perturbations of the properties of gramicidin, they represent a powerful means of deciphering the structure–function relationship of this channel system. Many investigations of the properties of the gramicidin channel and the interaction between gramicidin and its environment have been facilitated by the availability of naturally occurring and chemically synthesized analogues which differ from the parent peptide, gramicidin A, by only a single amino acid substitution.[17–39]

Gramicidin has been shown to induce monovalent cation permeability in both natural and artificial lipid membranes. Hladky and Haydon[40] found that the addition of small amounts of gramicidin A to bilayer membranes caused discrete conductance changes because of the formation of gramicidin channels. Gramicidin A became the first ion-selective transmembrane channel of known molecular structure. This channel is essentially impermeable to anions and multivalent cations and displays appreciable selectivity between monovalent cations.[41] Gramicidin A exhibits high single-channel ion fluxes (10^7 Na^+ s^{-1} at 25°C, 1 M NaCl and 100 mV)[42,43] producing a channel conductance of about 10 ps.[44] It has a number of characteristics similar to those of physiological channels such as monovalent cation selectivity, and blocking, saturation

effects, concentration dependence of permeability ratios,[45–47] multivalent anion screening effects[48] and divalent cation damping of the single-channel currents.[49] Gramicidin channels are ideally selective for monovalent cations. The single-channel conductance for alkali cations is ranked in the same order as the aqueous mobilities of these cations and follows the thermodynamic profile that describes the transfer of cations from an aqueous solution to the amide binding environment of the channel interior.[50,51] Divalent cations, such as Ca^{2+} and Ba^{2+}, block the channel by binding at the channel entrance.[51–53] Monovalent cations move through the channel in single file, as shown by tracer-flux measurements[54,55] and the mole-fraction dependence of the channel conductance in the presence of symmetric mixtures of KX, TlX and AgX.[56–60] The channel is filled with about six to seven water molecules, some of which are displaced when an ion is transported.[61–64] Protons are transported much more rapidly than other ions by means of a proton-hopping mechanism with no displacement of water molecules.[63] The gramicidin channel is selective for K^+ over Na^+.[50,51] For 10 mM Na^+ and K^+ at 25°C, the bionic potential is 27.7 mV.[65] This corresponds to a permeability ratio of 2.9, a value which agrees with the measured conductance ratio.[66]

The structural characteristics of the linear gramicidins remain as a subject of considerable interest. If Gly is counted as a D-amino acid, the gramicidin sequence consists of an alternating series of L- and D-amino acids. Early X-ray patterns associated predominate helical components to the structure of gramicidin,[67] yet none of the family of α-helices would be stable for an alternating L,D sequence of amino acids. In 1971, Urry[68] proposed that helical variations of peptide β sheets could provide stable environments for the side-chains of an alternating L,D sequence. In such single-stranded π-(L,D) or β helices the intramolecular hydrogen-bonding pattern resembles that of a parallel β-pleated sheet. Veatch[69] showed that various double-stranded β helices could be formed by intertwining two (L,D) peptides in either a parallel or an antiparallel manner. In all β-type helices, as in β sheet structures, the basic repeating unit is a dipeptide. The evidence indicates that gramicidin adopts single- and/or double-stranded helical conformations, depending upon the environment into which it is placed. Thin-layer chromatography, circular dichroism, infrared and NMR spectroscopy have shown that the conformation state of gramicidin is solvent, membrane and analogue dependent.[70–92]

Because gramicidin incorporated into membranes or membrane-like environments represents a model for channel activity, considerable interest has focused upon the interaction of gramicidin with the lipid membrane environment. The influence of gramicidin on the macroscopic organization of the lipid environment, the influence of gramicidin on acyl chain order and motion of a bilayer, the influence of the lipid environment upon the structure, dynamics and aggregation behaviour of gramicidin, the effect of added membrane constituents on gramicidin, and conformational transitions of gramicidin in a lipid environment have been investigated.[93–122]

The circular dichroism spectra of gramicidin incorporated into phospholipid vesicles and micelles are quite different than those obtained for gramicidin dissolved in nonpolar organic solvents,[123–125] indicating that the conformation in membrane-like environments is different from those present in solution. X-ray crystallographic studies of gramicidin A have been performed;[126–143] however, the structure of gramicidin in the crystalline form is not the same as that found in micelles and bilayers. Furthermore, the x-ray studies of gramicidin A in bilayers were able to provide only the overall dimensions of the channel, the helical pitch and the binding sites for mono- and divalent cations. Numerous other physical methods have been employed in the study of the structure and function of the linear gramicidins.[93,144–150] One of the first steps in defining the conformation of the membrane-bound gramicidin A channel was the demonstration that a dimer forms the transmembrane channel[151–163] and not a tetramer.[164,165] High-resolution two-dimensional ^{1}H[166–176] and ^{15}N, ^{13}C, ^{1}H and ^{2}H solid-state NMR spectroscopy[177–216] have been used to study the structure of gramicidin A incorporated into micelles and lipid bilayers, respectively. As the result of the NMR studies and the use of other physical techniques, the generally accepted model is one in which a gramicidin A dimer channel is formed by the formyl-to-formyl association of two single-stranded, right-handed, $\beta^{6.3}$-helical monomers.[68,93,144–230] The dimer which spans the lipid bilayer or is incorporated into micelles is approximately 26 Å long and has a diameter of about 4 Å.

The structure of gramicidin A, gramicidin B, gramicidin C, Phe-1 gramicidin A, Phe-1 gramicidin C and Gly-15 gramicidin A incorporated into sodium dodecyl sulfate (SDS) has been determined in the laboratory of the author. Sodium dodecyl sulfate micelles have been used extensively as a model membrane for NMR studies of incorporated peptides and proteins.[231–298]

A combination of two-dimensional NMR techniques (DQCOSY, TOCSY and NOESY) was used to make all proton chemical shift assignments. All of the NOESY spectra were obtained using a mixing time of 40 ms to avoid spin diffusion effects. A delay of 10 s was inserted after each acquisition of an FID to allow for relaxation. The distance restraints required for molecular modelling of the dimer channel were obtained from the NOESY spectra. Approximately 600 distance restraints were obtained for each gramicidin analogue dimer. Of these distance restraints, an average of 12 were associated with monomer–monomer interactions in the dimer. These do not count intermolecular hydrogen bond interactions. The backbone torsion angles (ω) were not fixed. The distance-restrained simulated annealing technique was used to obtain 100 dimer structures. The 10 best structures (i.e. lowest penalty functions) were then combined to obtain an averaged dimer structure. This averaged structure was used with the relaxation matrix technique to generate a theoretical NOESY spectrum. The theoretical NOESY spectrum of the averaged dimer structure was used to correct experimental cross-peaks, particularly those very close to the diagonal, and to resolve cross-peak

overlaps. The refined NOESY distance restraints were then used to obtain 100 new dimer structures, the 10 best structures again being used to obtain an averaged dimer structure. The final dimer structure was obtained by subjecting the averaged dimer structure to restrained minimization calculation. The dimer structure calculations were performed with a dielectric constant of 2 to represent the environment of the micelle. Figure 2 shows the structure of the gramicidin A dimer obtained by this method. The dimer structure obtained in this manner for gramicidin A incorporated into SDS micelles is in good agreement with that previously obtained for the identical system using essentially the same method.[166–176]

Cross[299] has pioneered the use of solid-state NMR spectroscopy to obtain orientational restraints used with the simulated annealing technique to determine the structure of gramicidin A. Isotopically labelled (^{2}H, ^{13}C and ^{15}N) gramicidin A is incorporated into planar dimyristoyl phosphatidylcholine (DMPC) bilayers held on a very thin glass plate. A number of these plates are stacked together, hydrated and then uniformly aligned with respect to the direction of the magnetic field of the NMR spectrometer. Each of the restraints orients the molecular frame of an atomic site with respect to the magnetic field and a unique molecular axis. This molecular axis is the lipid bilayer normal and the channel axis, both of which are aligned parallel to the direction of the magnetic field. The restraints are derived from the orientation dependence of the nuclear spin interactions. Each of these interactions is described in the molecular frame by a tensor or coordinate system.

Each peptide linkage is considered a plane and its orientation is defined by two dipolar interactions, ^{15}N–$^{13}C_1$ and ^{15}N–^{1}H. The unique axis of these spin interaction tensors is parallel to the internuclear vector (i.e. N–C_1 and N–H bonds). Therefore, the orientation of each plane is defined with respect to the magnetic field direction. Side-chains for the aliphatic amino acids were characterized by ^{2}H NMR. The Val-1 and Val-7 side-chains exhibited large amplitude dynamics; however, for the initial structures these side-chains were placed in their dominant χ_1 rotomeric state. For the Val-6 and Val-8 side-chains, unique rotomeric states were defined. The leucine side-chains showed no large amplitude dynamics and, therefore, unique χ_1 values were defined for each residue. Also, unique χ_2 values were defined for Leu-12 and Leu-14. Most probable values, based upon torsional energy, for Leu-4 and Leu-10, from two possible χ_2 values for each, were chosen. Orientational restraints for the indole side-chain of the tryptophan residues were obtained from ^{2}H and ^{15}N spectroscopy. For each indole side-chain, four possible sets of torsional angles (χ_1 and χ_2) were found to be consistent with the NMR data. Most probable values were used for each one. A total of 120 experimental restraints were imposed on the structure during refinement (i.e. 19 ^{15}N and 2 $^{13}C_1$ anisotropic chemical shifts, 14 ^{15}N–$^{13}C_1$ and 19 ^{15}N–^{1}H dipolar splittings, 12 C_α–^{2}H and 54 other quadrupolar splittings) together with intermolecular and intramolecular hydrogen distances.

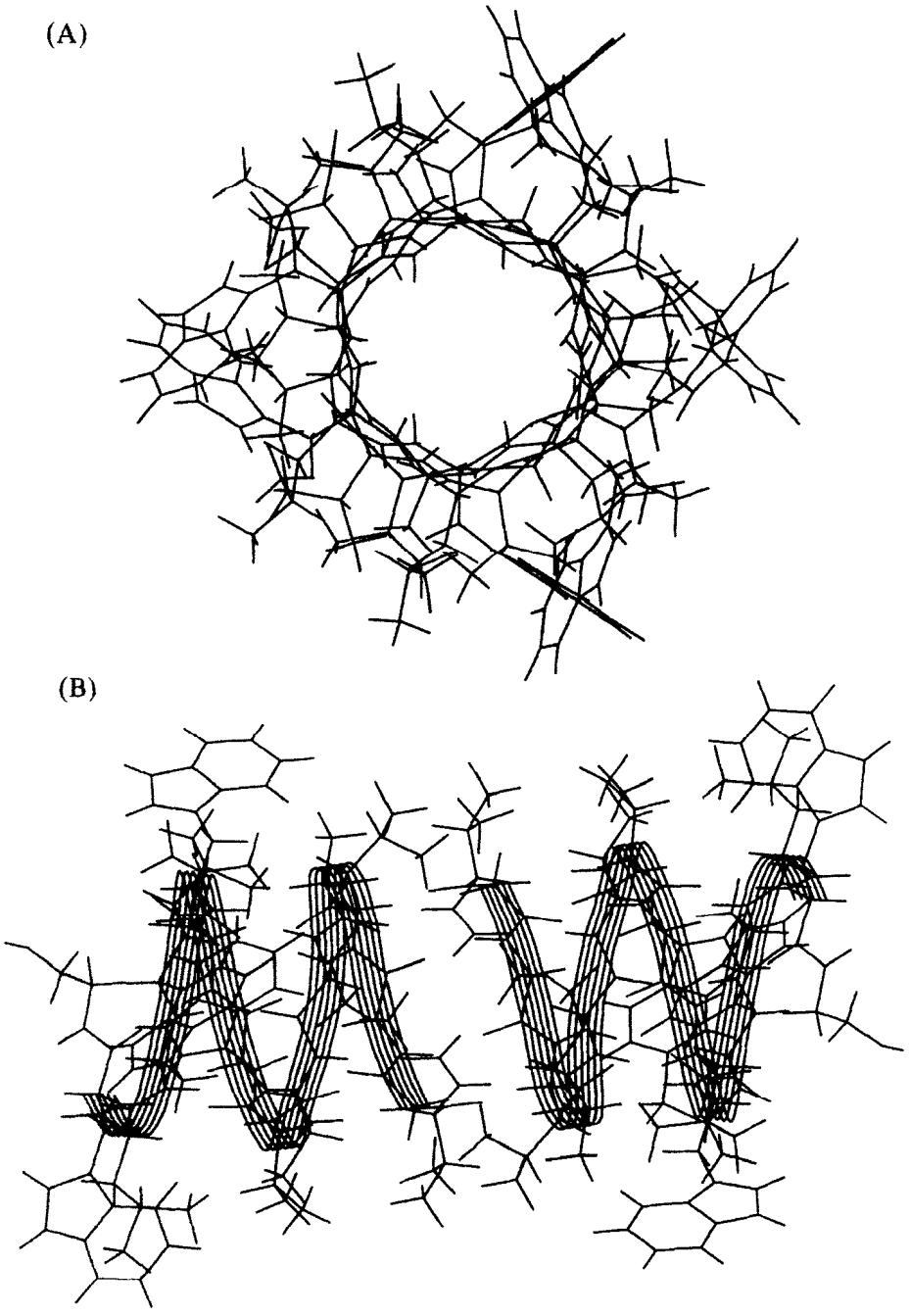

Fig. 2. (A) A view down the channel axis of the gramicidin A dimer. (B) A side view of the gramicidin A dimer channel showing the helical conformation of each monomer.

Initial structures were refined against both the experimental restraints and the CHARMM[300] energy using a novel simulated annealing protocol to define the torsion angle solutions to within an error of about ± 5°. Forty refined structures were used to obtain an average structure which was then further refined. A dielectric constant of 1 was used in the calculations.

An overlay of the backbone structure of the gramicidin A dimer in oriented DMPC bilayers of Cross[299] (coordinates deposited in the Protein Data Bank with accession code 1mag) with that of gramicidin A incorporated into SDS micelles obtained in the author's laboratory is shown in Fig. 3. With one exception, the structures are quite similar. One would expect to find small differences between the two structures for a number of reasons. The temperature for the two experiments was not the same, therefore, average side-chain positions could be slightly different. The structure determined in SDS micelles is that in the presence of 0.25 M Na^+ ions while no ions are present in the oriented bilayer system. There is experimental evidence that suggests Na^+ ions change the orientation of the carbonyl groups when ion binding occurs within the channel,[194,301,302] although there is some disagreement with this.[303] If the cation–carbonyl interaction produces changes in side-chain positions, changes in proton–proton distances could also occur. Consequently, one might expect small differences in side-chain positions when comparing the structure in the presence and absence of Na^+ ions. The dimer structure in SDS micelles was obtained with the use of proton–proton distances derived from NOESY cross-peaks related to protons on one monomer with those on the other monomer and not just hydrogen bond links between the two monomers. The inclusion of the NOESY-derived distance restraints linking the monomers has an effect on the proton positions of residues near the dimer interface. Differences in side-chain positions could also result from environmental change in going from a planar bilayer to a micelle of rather small radius of curvature. The effect of water on the structure must also be considered. The micelles containing gramicidin A are in an aqueous solution while the bilayers are just hydrated.

The one major difference in the two structures appears to be in the position of the Trp-9 indole ring. The structure of Cross[299] has the Trp-9 ring stacking with the Trp-15 ring whereas in SDS micelles there is no stacking of these two tryptophan indole rings (Fig. 4).

None of the above reasons for differences in structure in the two systems would seem to explain this difference. Other ^2H[204] and ^{13}C[180,304] solid-state NMR results for gramicidin A incorporated into oriented DMPC bilayers produced results that were interpreted as being consistent with the structure of gramicidin A incorporated into SDS micelles (i.e. no tryptophan 9/15 stacking). The results of a Raman spectroscopy study of water accessibility to the tryptophan indole NH sites of gramicidin A incorporated into a liposome (dilauroyl-L-α-phosphatidylcholine) aqueous suspension were interpreted as being consistent with the stacked tryptophan structure.[301] Obviously, the

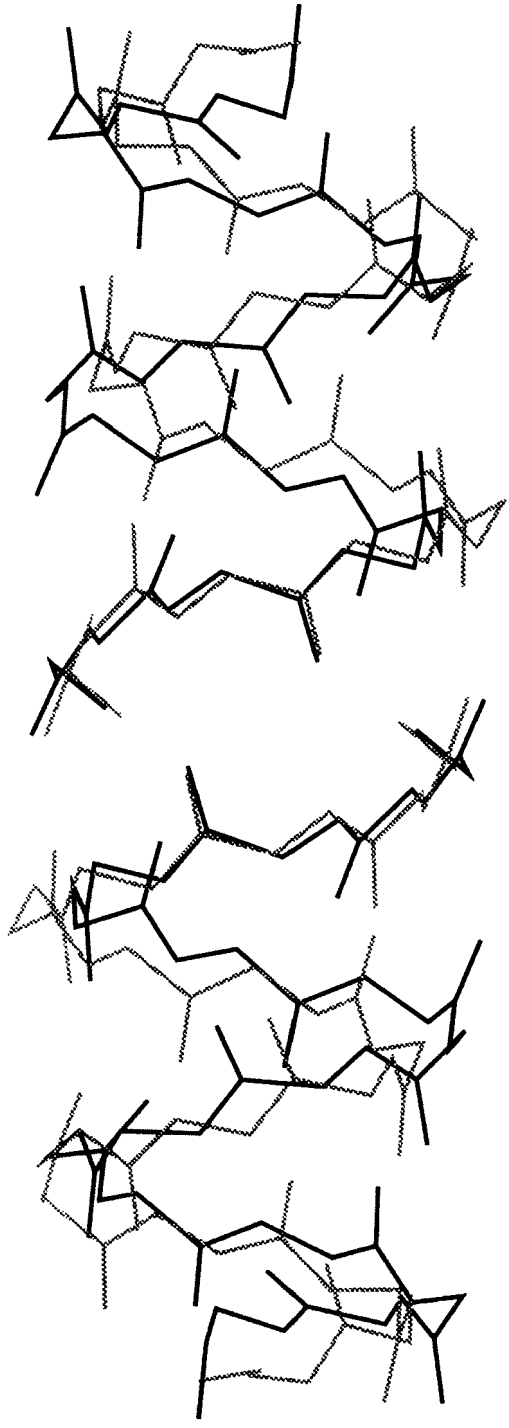

Fig. 3. Overlay of the backbone structure of gramicidin A in SDS micelles (black) and that in DMPC bilayers (grey).

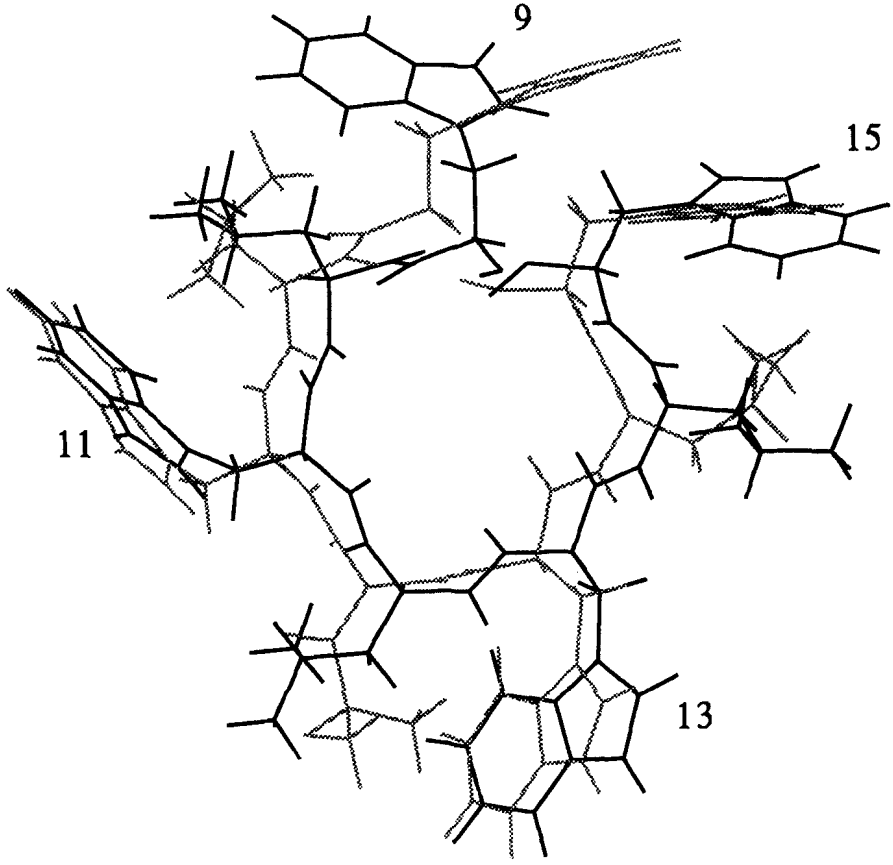

Fig. 4. Overlay of residues 9 to 15 for gramicidin A in SDS micelles (black) and in DMPC bilayers (grey).

importance of tryptophan residues in determining the structure–function relationship of gramicidin channels warrants further investigation of this difference in structure. However, in a recent review on the gramicidin channel Wallace[5] states: "Given the extreme sensitivity of gramicidin's molecular structure to environment, there was some concern that the micelles would produce a different structure from that in lipid bilayers. However, those fears now appear to be unfounded, since the structure in SDS micelles is very close to that found in lipid bilayers."

The structure of gramicidin B and gramicidin C incorporated into SDS micelles has been determined. No significant differences in the backbone of the channel are observed. A comparison of the tryptophan region (i.e. 9 to 15) reveals some small differences in residue orientation that may be of importance in ion binding and transport (Fig. 5). With the Gly-15 analogue of

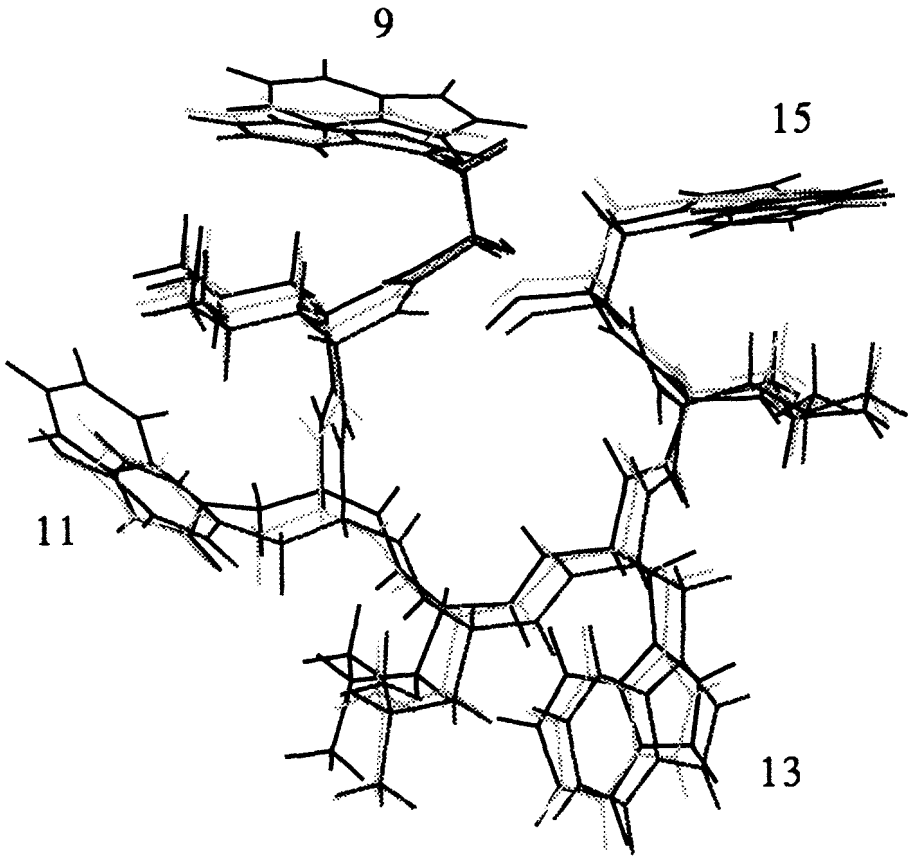

Fig. 5. Overlay of residues 9 to 15 for gramicidin A, B and C.

gramicidin A (Trp-15 replaced by Gly) significant differences are observed in the structure of this analogue and gramicidin A. The loss of the Trp-15 anchor at the aqueous interface results in an increased freedom of motion of the ethanolamine moiety at the end of the channel. These differences are probably responsible for the ion binding and transport characteristics of the Gly-15 analogue being so different from those of gramicidin A as will be discussed.

A detailed understanding of the transport of the linear gramicidins requires not only the structure of the channel but also a knowledge of channel properties. The dependence of channel properties on the amino acid residues, position in the sequence and side-chain orientation, have been used to assist in elucidating the molecular mechanism of ion transport through the channel. The side-chains are important contributors to the formation and stability of the channel in the membrane-like environments. They are regulators of the

channel conductance (i.e. transport), channel lifetime and cation binding at the channel entrance. For example, the introduction of a polar side-chain at position 1 tends to alter the energy barrier to ion transport,[305] while the replacement of tryptophan at position 11 by phenylalanine lowers the transport rate.[18] There have been many studies of the effect of single amino acid substitution on the conductance, lifetime behaviour of gramicidin channels.[305–361] For example, channels with branched side-chains at position 1 have longer lifetimes than channels with a corresponding straight chain. Since the movement of ions through a channel involves (i) diffusion of the ion through the aqueous medium to reach the channel entrance, (ii) association with the channel at the entrance, (iii) transport through the channel, (iv) dissociation from the channel and (v) diffusion away from the channel entrance, the determination of the binding constant for cation association with the channel entrance and the activation enthalpy for the transport process are very import quantities to be determined for gramicidin analogues. Although the channel is impermeable to divalent cations,[41,49,65,319,324,360,361] the channel does bind trivalent, divalent and monovalent cations.[50,51,56,362–391] The difference in binding constants obtained for the monovalent cations has been related to the overall cation transport selectivity of the channel. Differences in binding constants for the cations have also been related to side-chain polarity at the binding site of the channel. It is important to note that it is not the binding constant or a rate constant for the transport process at a single temperature that is most important to obtain but rather, the enthalpy and entropy of binding and transport. One must ultimately attempt to correlate the binding parameters, enthalpy of transport and the three-dimensional structure of the channel formed by gramicidin A and its analogues to understand more completely the structure–function relationship for this channel system.

Recently, the cation binding "pocket" for monovalent cations was mapped for gramicidin A and Phe-1 gramicidin A incorporated into SDS micelles using the NOESY11 pulse sequence.[392] The binding "pocket" involves the carbonyl groups of residues 10 to 15. These results are in agreement with those obtained from solid-state ^{2}H and solution-state ^{13}C labelled NMR experiments,[194,230,386,393–395] Raman spectroscopy[301,302] and molecular dynamics calculations.[396] The binding site for divalent cations is much nearer the channel entrance.[397,398]

The NOESY11 experiment also showed that in the presence of Na^+ ions, the indole NH sites of Trp-15 and Trp-13 are more accessible to water than Trp-9 and Trp-11. This has recently been confirmed from Raman spectra.[301]

To obtain a quantitative measure of cation binding to the gramicidin channel, one must determine the enthalpy and entropy for the binding process not just an equilibrium constant at a single temperature. These thermodynamic parameters (enthalpy and entropy) for the binding of cations to the channel entrance have been obtained by using the $^{205}Tl^+$ NMR-competitive binding method.[399–401] Briefly, this method involves the measurement of the $^{205}Tl^+$

chemical shift as a function of the Tl^+ thermodynamic activity in the presence of a constant amount of gramicidin incorporated into lipid vesicles made with lysophosphatidylcholine. The equilibrium binding constant is calculated from the chemical shift–activity relationship. The equilibrium binding constant, determined at a number of temperatures, is then used to calculate the enthalpy and entropy of binding the Tl^+ ion to the channel entrance. This procedure is repeated for the system that also contains a cation (e.g. Li^+, Na^+ or K^+) that competes with the Tl^+ ion for the same binding site at the channel entrance. The change in the chemical shift of the Tl^+ ion in the presence and absence of the competing cation at different temperatures is then used to calculate the enthalpy and entropy of binding for the competing cation. The binding constant and enthalpy of binding for monovalent cations was found to increase in the order: $Li^+ > Na^+ > K^+ > Tl^+$. The binding of a cation to the channel entrance requires the removal of waters of hydration and replacing them with carbonyl oxygen atoms from the backbone of the channel at the binding site. Both the enthalpy and entropy of binding were found to correlate very well with the enthalpy and entropy of transfer of these ions from water to dimethylformamide. The binding constants obtained for the alkali cations using the $^{205}Tl^+$ method were corroborated using ^{13}C NMR spectroscopy of ^{13}CO labelled gramicidin A.[364] The $^{205}Tl^+$ chemical shift technique was also used to study the binding of divalent cations to the channel entrance. The enthalpy of binding for divalent cations was found to be much larger than those for monovalent cations, reflecting the effect of ion charge on the binding process. The binding enthalpy for monovalent cations has also been found to increase proceeding from Gly-15 gramicidin A to gramicidin C to gramicidin A.

Having quantitatively measured the first step in the transport process, cation binding, the kinetic activation enthalpy for the transport of Li^+, Na^+ and K^+ ions can be determined for the same gramicidin A analogues using the magnetization inversion transfer (MIT) NMR technique.[402–416] If a membrane impermeable chemical shift reagent[417–419] $[Dy(P_3O_{10})_2]^{-7}$ is added to an aqueous salt solution of large unilamellar vesicles with incorporated gramicidin, the internal and external pools of cations (i.e. $^7Li^+$, $^{23}Na^+$ or $^{39}K^+$) can be distinguished by their individual NMR signals as shown in Fig. 6 for the $^7Li^+$ system. A typical MIT experiment for $^7Li^+$ is shown in Fig. 7. The decrease in the signal intensity of the inside signal with mixing time can be analysed by the method of McClung[420] to obtain the unidirectional rate constant for the transport of Li^+ ions through the channel. The MIT experiment is then repeated as a function of temperature to obtain the kinetic activation enthalpy for the transport process for a given analogue and cation. The activation enthalpy of transport through the gramicidin A channel increases in the order of cations: $^{39}K^+$(4.2 kcal mol^{-1}); $^{23}Na^+$(5.4 kcal mol^{-1}); $^7Li^+$(7.2 kcal mol^{-1}). This order is consistent with the results of conductance experiments[347] where the conductance order is: K^+ (14.0 ps); Na^+ (6.95 ps); Li^+(1.89 ps).

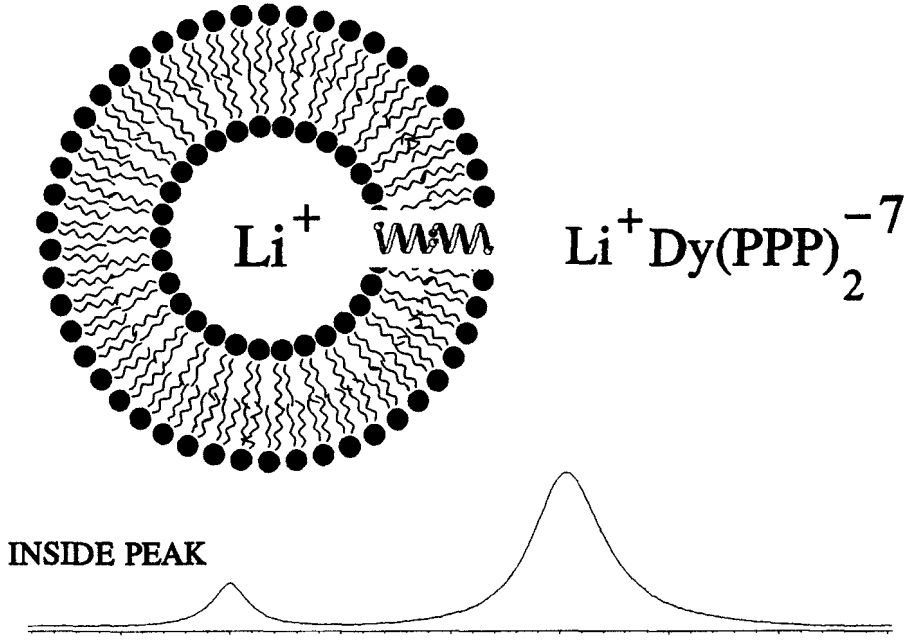

Fig. 6. $^{7}Li^{+}$ NMR spectrum of the ions on the inside and outside of a vesicle.

The activation enthalpy of transport for $^{7}Li^{+}$ by gramicidin A ~ gramicidin C < gramicidin B was found to be in agreement with conductance data.[347] The same type of correlation was found for $^{23}Na^{+}$ transport by the Phe-15, Phe-13, Phe-11 and Phe-9 gramicidin A analogues.[357,421] The activation enthalpy for the $^{23}Na^{+}$ ion through gramicidin A and Gly-15 gramicidin A is 5.4 and 10.0 kcal mol^{-1}, respectively. The binding enthalpy for the Na^{+} ion by the Gly-15 gramicidin A analogue is significantly less than that with gramicidin A. Obviously, the removal of a tryptophan residue at the channel entrance has a very significant effect on the transport process. Evidence for the transport of Xe atoms through the gramicidin A channel has been obtained with ^{129}Xe NMR spectroscopy.[422] Based upon the binding and transport NMR data obtained thus far, a correlation emerges indicating that the tighter the binding, the faster the transport rate. Therefore, the selective monovalent cation filter for the transport process involves a combination of the thermodynamics of binding and the kinetic barrier to transport.

The dynamic nature of the gramicidin channel has been the subject of much interest. The ^{15}N spin-lattice relaxation time (T_1) of the nitrogen atom at the Leu-4 position has been used to investigate the local dynamics about the Ala-3/Leu-4 linkage.[213] Evidence was obtained that suggests a correlation between the local dynamics and ion transport through the channel. The

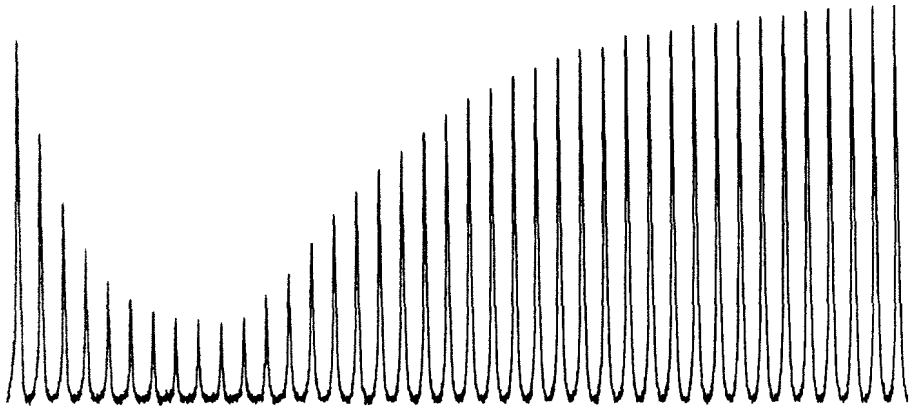

Fig. 7. The inside $^{7}Li^{+}$ NMR signal as a function of increasing mixing time (increasing from left to right).

backbone dynamics of gramicidin A in DMPC bilayers have been studied using low-temperature solid-state ^{15}N spectroscopy.[190] A ^{1}H T_1 and T_2 study of the tryptophan indole ring NH of the gramicidin analogues, gramicidin A, gramicidin B, gramicidin C, Phe-1 gramicidin A, Phe-1 gramicidin C, Gly-11 gramicidin A and Gly-15 gramicidin A, incorporated into SDS micelles showed that there is a systematic decrease in the overall motion of the indole ring from Trp-15 (at the aqueous interface) to Trp-9 (at the interior of the micelles) for all of the analogues.[423] However, a ^{2}H NMR study of the orientation of Trp-9 and Trp-11 in gramicidin A incorporated into oriented bilayers suggested that Trp-9 appears to have greater mobility than Trp-11.[204] It is not obvious as to why the two experiments appear to contradict one another.

There are several other areas of research that have provided further insight into the properties of the gramicidin channel and its interaction with a membrane-like environment. The effect of side-chains on the kinetics of the incorporation of gramicidin into a vesicle as a channel has been studied.[424–427] For example, the enthalpy for the incorporation of gramicidin A and gramicidin B into vesicles was found to be 11.8 and 14.6 kcal mol^{-1}, respectively. Photolytic and microwave modulation of gramicidin channels has been the subject of several investigations.[428–436] The transport of cations by gramicidin has been found to be dramatically reduced by photolytic degradation.[428] Direct observation of differential photolytic degradation among the tryptophan residues of gramicidin A in SDS micelles has been made.[431] It was found that Trp-9 degrades the fastest, in agreement with a chemical modification study[437] while Trp-11 degrades the slowest. Finally, there have been numerous theoretical studies of the structure and physical properties of the gramicidin channel.[438–462] These studies range from ^{15}N chemical shift calculations of the backbone nitrogen atoms, to the structure of

monomers and dimers, to molecular dynamics simulations of the motion and transport of the channel.

Finally, one note of caution. The small size and ease of synthesizing single amino acid substituted analogues make gramicidin an ideal molecule for studying the structure–function relationship for channels. However, recent NMR experiments have shown that some analogues produce multiple forms of the channel in micelles.[463,464] Consequently, there is the danger of making an analogue, incorporating it into some lipid environment, making measurements related to some physical property of the channel and assuming that only one form of the channel exists. The measured physical property may actually be an average value if more than one form of the channel exists. It would be advantageous to determine whether or not one has only a single or multiple forms before measuring the physical properties of the channel. The delicate balance of interactive forces that must exist between the side-chains of gramicidin and the lipid-like environment of the micelles, critical for the formation of a single species of the gramicidin channel, is a complex function of the type of substitution and position of substitution.

The peptaibols, a class of small, naturally occurring peptides, have been used as models of ion channels which consist of a bundle of transmembrane helices surrounding a central pore. Perhaps the most thoroughly studied member of this class of peptides is alamethicin. Alamethicin is a 20-residue linear peptide from the fungus *Trichoderma viride*.[465] The sequence[466] of this hydrophobic peptide is shown below:

Ac-Aib-Pro-Aib-Ala-Aib-Ala-Gln-Aib-Val-Gly-Leu-Aib-Pro-Val-Aib-Aib-Glu-Gln-Pheol

where Ac is an N-terminal acetyl, Aib is α-aminoisobutyric acid and Pheol is a C-terminal phenylalaninol. Alamethicin forms voltage-dependent channels in planar lipid bilayers.[467–469] Conformational studies show alamethicin to be helical.[470–485] An x-ray crystallographic study of alamethicin revealed that it is predominantly an α-helix with some 3.0_{10}-helical content.[470] The large α-helical content of alamethicin permits the coexistence of two regions, one hydrophilic and one hydrophobic, resulting in the formation of a channel that agrees with the "barrel-stave" model.[468,470,482,486–490] The analysis of conductance studies is also consistent with the "barrel-stave" model of channel formation, in which a bundle of helices with a varying number of monomers aligned to produce a central pore (i.e. channel).[489,491]

A number of NMR investigations of alamethicin in SDS micelles[481] and in methanol or aqueous methanol solution[476–480,482–485] have been conducted concerning the conformation of the monomers. The results of these investigations indicate that the N-terminal region is of α-helical character with several 3.0_{10} parts in the C-terminal region. The NOE distance restrained/simulated annealing study of alamethicin incorporated into SDS micelles produced data

that suggested that there was some structural variability between the Aib-10 and Leu-12 residues.[481] It was suggested that conformation rearrangements at or near residue 10 may play a role in the voltage gating of alamethicin. Heteronuclear NOE measurements[480] and ^{13}C studies[476] of the dynamics of alamethicin in methanol did not confirm a variation in dynamics along the length of the peptide.[489] This suggests that alamethicin behaves as a rigid rod, at least on the picosecond time scale.[489] However, it has been observed that these data do not necessarily rule out the interconversion of structural forms found in the simulated annealing study of alamethicin incorporated into SDS micelles.[481] If the forms observed in the simulated annealing study are interconverting on a slow time scale relative to the tumbling rate of alamethicin in methanol (~ 1 ns), they would not contribute to the spectral densities leading to relaxation and would not be observed. A change in environment might also produce the differences observed in mobility. Molecular dynamics simulations[489,492] also cast some doubt on the rigid rod character of alamethicin.[493]

An NOE analysis of a methanol solution of an analogue of alamethicin in which the Aib residues were replaced by Leu residues showed the analogue to be greater in the α-helical content (with no residual 3.0_{10} character) and to be shorter in length than alamethicin. This shortening in length was associated with a decrease in channel lifetime.[482] Because of the bend introduced in the conformation of alamethicin by Pro-14, the role of this residue has been assumed to be essential in the "barrel-stave" model for voltage gated ion channels. To investigate this, an alamethicin analogue with Abi replaced by Leu (as above) and Pro-14 replaced by Ala has been synthesized and studied by NMR spectroscopy.[494] An NOE distance restrained/molecular modelling study of this analogue in methanol showed that this analogue was better ordered than the Leu analogue, particularly in the region of the substitution and in the C-terminal region. The conductance behaviour and the structure of the Ala-14 analogue suggest that Pro-14 is not an essential residue in the "barrel-stave" model for ion channels formed by alamethicin.

The transmembrane movement of the C terminus of alamethicin and the Leu analogue (i.e. all Abi residues are replaced with Leu) from one bilayer surface to the other in a lipid vesicle has been investigated using NMR techniques.[495] One method involved the use of a spin-labelled alamethicin analogue which was used in small unilamellar vesicles to produce paramagnetic line-broadening of the inside and outside NMe protons of the palmitoyloleoylphosphatidylcholine (POPC) vesicles. Another technique employed the effect of unlabelled alamethicin on the ^{2}H NMR quadrupole splitting of POPC deuterated at the α position of the choline headgroup in POPC/cholesterol vesicles. These studies showed that the transmembrane migration rate for alamethicin is about 100 times slower than that of the Leu analogue. The equilibrium position of the Leu analogue was found to be about 3–4 Å deeper into the membrane than alamethicin.[496] The slow rate of migration of alamethicin was related to the

irregular nature of the helix at the C-terminal end and to hydrogen bonding to the solvent and lipid. On the other hand, the relatively fast migration rate of the Leu analogue was related to the fact that this analogue is already buried within the membrane interface. Consequently, this difference was explained by conformational differences between the Leu analogue and alamethicin rather than differences in hydrophobicity.

The membrane orientation of the N-terminal segment of alamethicin has been determined by solid-state ^{15}N NMR spectroscopy.[497] Alamethicin was synthesized with ^{15}N incorporated into alanine at position 6 in the peptide sequence. Solid-state ^{15}N NMR of the peptide in dispersions of hydrated DMPC gave an axially symmetric powder indicating that the peptide reorients with a single axis of symmetry when associated with the lamellar lipid. When incorporated into bilayers that are uniformly oriented with the bilayer normal parallel to the direction of the applied magnetic field, the position of the observed ^{15}N chemical shift was found to be at 171 ppm. This chemical shift is coincident with the sigma parallel to the edge of the axially symmetric powder pattern for the non-oriented sample. Consequently, the axis of motional averaging lies along the bilayer normal. Two-dimensional separated local field spectra were obtained that provided a measure of the N–H dipolar coupling in one dimension and the ^{15}N chemical shift in the other dimension. These data gave a dipolar coupling of 17 kHz corresponding to an average angle of 24° for the N–H bond with respect to the applied magnetic field axis. These results were found to be consistent with an α-helical conformation inserted along the bilayer normal. NMR studies of other peptaibols have shown that they exhibit the characteristic α-helical conformation.[498–505]

In summary, x-ray crystallography and spectroscopic studies clearly indicate that peptaibols form amphipathic helices when placed in a membrane-like environment, and that these helices are kinked in the region of the central proline residue. The aggregation state of peptaibols in bilayers is less certain. Orientations both parallel to and perpendicular to the bilayer plane appear to be possible, at least in the absence of an applied transbilayer potential.[489]

There are other naturally occurring peptides, such as melittin, magainin, cecropin and pardaxin, that can aggregate into bundles to produce channels. Melittin is a 26 amino acid cytolytic peptide from the *Apis mellifera* honey bee. It is known to exist as an α-helical tetramer, as an α-helical monomer, or as a monomeric random coil depending on solution conditions.[506,507] In aqueous solution mellitin adopts aggregation states and conformations that depend on peptide concentration, pH, ionic strength and the nature of the negative counterion since the peptide has a net charge of $^{+}6$. In aqueous solution mellitin is either a monomer or tetramer.[507,508–513] ^{1}H NMR spectroscopy showed that the monomer in aqueous solution exhibits chemical shifts typical of an extended flexible form with the fragments 5–9 and 14–20 more highly structured than the rest of the amino acid sequence.[511] CD results[510,514,515] are consistent with a random coil state in aqueous solution.

NMR studies (i.e. coupling constants, NOEs and amide proton exchange) showed that in methanol, melittin exists as an α-helical monomer.[516–518] The absence of NOEs characteristic of an α-helix through residues 10–12 suggests flexibility of the helical conformation around the Pro-14 residue.[493,516,517] No NOEs were found that would define the nature of the bend between the two helical segments.[516] NOE distance restrained/molecular dynamics simulations suggest that in the monomeric state the bend in the helical structure may be significantly smaller than in the crystal structure.[516] Additional support for the importance of the flexibility afforded by the Pro-14 residue to form transmembrane aggregates that are associated with ion transport has been obtained from NMR studies of an analogue of melittin in which Pro-14 was replaced by Ala-14.[519] The Ala-14 analogue in methanol was found to adopt a regular, stable α-helical conformation without the flexibility around found with the Pro-14 melittin. The Ala-14 analogue was also found to be less able to induce voltage-dependent ion conductance in planar bilayers.

A ^{1}H NMR study of amide proton exchange for melittin in methanol solution confirmed the conclusions about the structure of the peptide.[517] This exchange study also revealed a loosening in the helical structure in the last few residues. The dynamics of the main chain and side-chains of ^{13}C-enriched melittin in solution have been investigated using ^{13}C spin–lattice relaxation times (T_1) and NOE measurements.[520] From these measurements, the order parameter, a measure of the amplitude of internal motion, and an effective correlation time for the internal motion for several backbone and side-chain positions were obtained. For melittin in the monomeric random coil in water at pH 4, monomeric helical conformation in methanol, a tetramer in water and the tetramer in water in the presence of phosphate, overall rotational correlation times of 1.28, 1.4, 2.8 and 4.2 ns, respectively, were obtained. Motion of the backbone in the interior of the residue sequence was found to be most restricted in the monomeric helix and least restricted in the tetramer. In the monomeric random coil form, relatively less restricted backbone motion extending from the N terminus to the fourth residue was observed. Such end-effects continued only to the third residue in the monomeric helix and were observed just in the amino terminus glycine in the tetramer. The three Lys chains of the peptide showed the least restricted motion in the monomers and a differential restriction in the tetramers consistent with the tetramer structure. The motion of the Trp side-chain was more restricted than that of the Lys side-chains and generally as restricted as that of the interior backbone atoms. The agreement between the NMR data and Trp fluorescence anisotropy data, which also measures dynamics, was good for the monomer but not for the tetramer.

The structure of melittin bound to micelles and vesicles has been studied using ^{1}H, ^{13}C and ^{31}P NMR spectroscopy.[521–530] In general, the structure of melittin bound to micelles is the same as that in methanol. Micelle-bound melittin is an α-helix that has a relaxation in structure in the central region

of the peptide. Order parameters determined from ^{13}C relaxation measurements of melittin in lysomyristoyl phosphatidylcholine micelles showed that the backbone of the peptide is partially, but not completely, immobilized.[530] The order parameters were found to be larger for the residues in the N-terminal half of the molecule. The amino terminal glycine has about the same range of motion as the backbone carbons. The order parameters for the Trp side-chain were found to be similar to those of the peptide C_α moieties, as was verified by Trp fluorescence measurements. The motion of the Lys side-chains was found to be less restricted. The pH dependence of the dynamics in the micelles indicates that the α-helix lies near the surface of the micelle at low-to-neutral pH, but at higher pH its orientation changes, accompanied by deeper penetration of the Lys side-chains into the micelle interior. Although the vesicle-bound conformation of melittin is similar to that occurring in a methanol solution and in micelles, significant differences have been found in the conformation of the C-terminal residues and the helical bend angle, as determined from NOE distance restrained/simulated annealing calculations.[528]

X-Ray crystallographic analysis of two crystalline forms of tetrameric melittin showed that the conformation of the peptide is essentially the same in each form.[531,532] Melittin was found to adopt a helical conformation in the crystalline state. The presence of Pro-14 also caused the helix to bend with an angle of about 120° between residues 1–10 and 16–26. The large helix bend allows for the optimal packing of hydrophobic side-chains within the tetramer.[507] Melittin provides a rare example of a membrane-bound peptide whose structure has been determined in low dielectric solvents, micelles and in the crystalline state and found to be quite similar. The similarities of these structures lends confidence to the idea that they represent good models for the membrane-bound conformation.[507]

Obviously, one would like to be able to understand the mechanism by which the melittin monomers aggregate to form the tetramer which contains the ion-conducting central pore. Does the tetramer form in the membrane in the absence of a membrane voltage or is the membrane voltage necessary for the formation of the tetramer? There does not appear to be a definitive answer to these questions for the membrane environment. A very interesting experimental observation has been made that melittin channels can become activated for ion transport in vesicle membranes by the addition of the tricyclic tranquillizers, chlorpromazine and imipramine to the vesicle solution.[533] The dynamic ^{23}Na NMR technique of Riddell[412] was used to detect the tranquillizer-induced Na^+ transport through the melittin channel. Because the formation of a drug–melittin complex was detected by ^1H NMR, the activation of melittin channels was assumed to originate from the direct interaction of the drug and melittin. The model proposed for the drug activation of the channel involves an anchoring effect in which the drug molecule drags the aggregate deeper so as to span the membrane bilayer. A ^1H NMR study has also shown

that the addition of phosphatidic acid to vesicles containing melittin markedly increases ion transport through the channel.[534] Again, this effect was discussed in terms of specific interactions between the acid and melittin. The topography of the membrane-bound state of melittin, the effect of melittin on lipid membranes and the interaction of melittin with lipid membranes have been investigated using a number of NMR techniques and nuclei.[535–546] Unlike the membrane environment, factors affecting the aggregation process in aqueous solution have been determined.[507,510–513] The factors that appear to be the most important for the ultimate formation of the tetramer are the hydrophobic effect that acts to sequester the nonpolar amino acids in the interior of the aggregate and the factors opposing aggregation (i.e. high positive charge density of melittin and the entropic effect associated with the formation of the secondary structure in the tetramer). Factors that suppress ionic charge, such as high ionic strength and phosphate binding, promote aggregation.

Magainins are a family of 21–26-residue peptides isolated from the skin of the African clawed frog, *Xenopus laevis*. These peptides can form cationic amphipathic α-helices[547] and facilitate the transport of ions across protein-free phospholipid bilayers.[548,549] Ion transport is proposed to be facilitated by the formation of channels composed of aggregated transmembrane α-helices.[550] It has been suggested that ion channel formation by magainin is driven by the concentration gradient that exists between the inside and outside of the bilayer.[551] Magainin is thought to bind initially to the outer surface of the vesicles as α-helices, then insert as oligomeric ion channels across the bilayer and finally dissociate to the inner surface. Another model proposed has magainin peptides initially binding to the bilayer surface as α-helices at low peptide to phospholipid ratios and then inserting as transmembrane α-helices at higher peptide to phospholipid ratios.[552]

Using solution and solid-state NMR techniques, the structure of magainin and magainin analogues has been determined in aqueous trifluoroethanol,[553,554] SDS and DPC micelles[554,555] and phospholipid bilayers.[555–560] In general, the α-helical structure was found to exist in all of these environments. In solution the structure appears to be curved with the bend centred at residues Phe-12 and Gly-13.[554] A solid-state ^{15}N NMR study of magainin 2, a 23-residue magainin, incorporated into oriented lipid bilayers[557] and a solid-state ^{13}C NMR study using the REDOR technique of an analogue of magainin 2 (i.e. Ala replaces glutamic acid at position 19 in the amino acid sequence) incorporated into bilayers[560] found the α-helices to be lying parallel to the plane of the bilayer. However, the Ala-19 magainin 2 system exhibited both α-helical peptides and peptides in the β-sheet conformation while the magainin 2 study revealed only α-helical peptides. A recent NMR study of a 21-residue member of the magainin family (PGLa) incorporated into SDS and DPC micelles had an α-helical conformation between residues 6 and 21.[555] Solid-state ^{15}N NMR experiments of specifically labelled PGLa in oriented phospholipid bilayers showed that the axis of the

helix is oriented parallel to the plane of the bilayers.[555] The ^{15}N solid-state experiments on unoriented samples provided evidence that the amino terminal residues are very mobile and that the fluctuations of backbone sites decrease from Ala-6 towards the carboxy terminus.

Cecropins, positively charged antibacterial peptides found in the cecropia moth, and synthetic analogues form voltage-dependent ion channels in planar lipid membranes.[561] The voltage dependence of the conductance has been shown to be associated with a flexible hinge between the positively charged amphipatic N-terminal segment and the more hydrophobic C-terminal segment. The biological activity of cecropins has been associated with the aggregation of monomers to form pores in membranes. The primary structures of the three principal cecropins (i.e. cecropin A, B and D) contain 37, 35 and 36 residues, respectively. The solution conformation of cecropin A has been investigated using NOE distance restrained/simulated annealing.[562] The calculations indicated that there are two α-helical regions extending from residues 5–21 and from residues 24–37. The long axes of the two helices lie in two planes which are at an angle of 70–100° to each other. The conformation of an analogue of cecropin B in solution has been determined using NOE connectivities.[563] Two separate α-helices with one amphiphilic in the N-terminal domain (residues 5–21) and the other hydrophobic in the C-terminal domain (residues 25–35) with a hinge region between were found. The solution conformation of porcine cecropin P1 (31 amino acid residues) has been determined using NOE and coupling constraints with distance geometry calculations with further refinements by energy minimization and restrained molecular dynamics.[564] The conformation obtained is one of an α-helix of approximately seven turns along almost the entire length of the peptide. The solution structure of porcine cecropoin P1 is quite different from the structures of cecropin A and melittin and a hybrid between these two.[565] Whereas cecropin P1 shows a continuous amphipathic α-helix over nearly the whole length of the peptide, the other three peptides show structures with two helices and a bending hinge in between. In these bent two-helix structures one of the helices is amphipathic and the other is essentially hydrophobic. This would appear to suggest that a bent or hinged structure in itself might not be essential for the function. However, residues 20–21 of cecropin P1 might be a site where a bend could be initiated.

Pardaxin P-2 is a 33 amino acid peptide isolated from the mucosal secretion of the Pacific sole, *Pardachirus pavoninus*, that exhibits surfactant properties.[566] Pardaxin has been shown to interfere with ion transport in both epithelium[567] and nerve cells.[568] At concentration below 10^{-7} mmol l^{-1}, pardaxin forms voltage-dependent, ion-permeable channels in artificial liposomes.[569] The structure of pardaxin P2 in aqueous trifluoroethanol solution has been determined using the NOE distance restrained/molecular dynamics method.[570] This study showed that the peptide adopts an amphiphilic helix over residues 7–11, a bend at residues 12–13 and another helix over residues 14–26.

The dipeptide Ser-12–Pro-13 segment connecting the two helices exists as a bend or a hinge allowing the two helices to be oriented in an L-shape configuration. Pro-13 is a pivot point of the bend between the two helices. In aqueous solution pardaxin exists as a tetramer. However, it spontaneously assembles in membranes to form voltage-gated ion channels or pores.

3. PEPTIDE CHANNELS OF AUTHENTIC PROTEIN CHANNELS

Ligand-gated ion channels provide efficient communication between cells of the central nervous system, converting a chemical neurotransmitter signal released from one cell into an electrical signal that propagates along the target cell membrane. At the molecular biochemical level, the nicotinic acetylcholine receptor is one of the best characterized membrane proteins[571–574] and serves as a paradigm for a family of ligand-gated ion channels. The receptor recognizes and binds acetylcholine and transduces the binding into an increase in ion permeability across the membrane. The electrical changes associated with the ionic currents represent the primary signal transduction mechanism allied with fast synaptic responses. The ligand binding sites and the channel are part of the same multisubunit protein complex.

The nicotinic acetylcholine receptor[575] provided the first detailed description of fast synaptic transmission,[576] the first recording of single-ion channels[577,578] and has the most complete three-dimensional structure.[579–582] The structure of the membrane-spanning part of many ion-transporting proteins contains bundles of hydrophobic α-helical polypeptide segments that form a channel for ions. Although high-resolution structures of these channels are very difficult to obtain, models based upon bundles of α-helices have been developed, in particular for the acetylcholine receptor.[581,582] The nicotinic acetylcholine receptor from electric organs, for example, has four types of subunits ($\alpha_2\beta\gamma\delta$),[583] each glycosalated with apparent molecular weights of 40, 50, 60 and 65 kDa. Although high-resolution x-ray structural analysis has not been forthcoming, low-resolution analysis with membrane fragments in which the receptor spontaneously forms two-dimensional crystalline lattices have been used to obtain three-dimensional structures. The picture of the system obtained in this manner indicates that the five receptor subunits are arranged symmetrically about a central core that is wide at the extracellular domain and narrow in the region that traverses the membrane. A large part of the receptor is extracellular with the protein extending about 55 Å above the surface of the membrane. Each of the five subunits traverses the membrane in a linear manner that involves little intertwining of the subunits. The structure at 9 Å resolution, in both the open- and closed-channel forms, has been examined by electron microscopy of tubular crystals grown from *Torpedo* postsynaptic membranes.[584] Binding of acetylcholine to open the channel causes a localized disturbance in the extracellular domain and initiates small rotations of the

protein subunits, which trigger a change in configuration of α-helices lining the membrane-spanning pore. Solid-state NMR spectroscopy was used to obtain the ^{15}N chemical shifts of specifically labelled M2δ incorporated into lipid bilayers.[556] The chemical shift data were used to show that the helical segment was perpendicular to the plane of the bilayer.

The aqueous domains are large enough to permit rapid access of the ions to the membrane channel, but sufficiently constrained so that ion selectivity effects, as the result of charge interactions, are likely to be important. The nicotinic acetylcholine receptor channel is highly selective for cations. However, there is less specificity among the cations. The permeability sequence for monovalent cations, $Cs^+ > Rb^+ > K^+ > Na^+ > Li^+$ suggests weak interactions between the permeant ions and the channel wall. The transmembrane segments are referred to as M1, M2, M3 and M4. It is presently thought that five M2 helices, corresponding to one helix from each subunit, form the central ion-channel pore. Molecular dynamics simulations have been used to develop atomic models of M2 helix bundles forming the pore-lining domains of the channel.[585] It has been suggested that the M2 helices are tilted to form a truncated conical structure that is larger at the extracellular surface than at the cytoplasmic surface.[586–589]

It has been shown that a 23-mer peptide of the same sequence as the transmembrane segment of M2δ forms ion channels in lipid bilayers with single-channel properties that emulate those of the acetylcholine channels.[590–598] The magnetization inversion transfer (MIT) technique, previously described, has been used to observe the transport of $^{23}Na^+$ ions through the channel formed by bundles of the 23-mer incorporated into SDS micelles.[402]

The M2 protein from the influenza A virus has been shown to function as an ion channel.[599–602] The transmembrane segment of the M2 protein has been incorporated into DMPC lipid bilayers and studied by solid-state ^{15}N NMR.[603] Orientational constraints were obtained from the isotopically labelled peptide segment aligned between glass plates. The ^{15}N chemical shifts from single-site labelled samples constrain the molecular frame with respect to the magnetic field. When these constraints are applied to the peptide, modelled as a uniform δ-helix, the tilt of the helix with respect to the bilayer normal was found to be about 33°. The results of these experiments suggest that the packing of this tetrameric protein is in a left-handed, four-helix bundle.

Structural and functional studies of a synthetic peptide that mimics a proposed membrane inserting segment of a *Bacillus thuringiensis* delta-endotoxin have been conducted.[604] An NMR study of a methanol solution of a synthetic 31-mer peptide corresponding to the sequence of a putative pore-forming segment of the CrylA(c) toxin showed that the peptide exists as an α-helix. The peptide forms discrete, characterizable channels in planar lipid bilayers. It is possible that this helix is a component of the transmembrane pore formed by *Bacillus thuringiensis* delta-endotoxins *in vivo*.

Voltage-gated Na^+ channels occur in cells that can respond to stimuli by undergoing rapid changes in plasma membrane voltage. The Na^+ channels are opened by a small voltage change in some region of the plasma membrane which permits a large influx of Na^+ ions. This influx of Na^+ ions is responsible for much of the voltage change involved in the conduction of nerve impulses. Voltage-gated Na^+ channels are found in multiple, closely related forms in animal cells. For example, mammalian brain cells contain at least three different but closely related forms of the voltage-gated Na^+ channel. The voltage-gated Na^+ channel is a large, very complex membrane protein that consists of a 260 kDa α-subunit and smaller β-subunits. One important feature of the α-subunit sequences is the presence of four internal homologous repeats, I–IV, each consisting of approximately 250 amino acid residues. Each of these repeat domains contains six putative transmembrane α-helices, S1–S6. S1, S5 and S6 are composed of hydrophobic and neutral residues, while S2 and S3 include some charged amino acid residues. All S4 segments carry a net positive charge and are characterized by highly hydrophobic sequences. It has been proposed that S4 segments act as the proteins voltage sensor *in vivo*. Two shorter hydrophobic stretches between S5 and S6 of each repeat domain are involved in toxin binding and probably form the channel lining. The importance of Na^+ channels in cells is emphasized by the fact that many neurotoxins in naturally occurring venoms and poisons target the Na^+ channels in muscle and nerve. When bound, the neurotoxins lock the channels in a closed or open state.

The S4 peptide[605] and the IS2, IS4, IS34, IVS4 and Islink56 peptides[606] of the rat brain sodium channel have been synthesized and studied in aqueous trifluoroethanol and DPC micelles using the NOE distance restraint/simulated annealing technique. All of the peptides were found to have predominantly α-helical structures in both types of environment. There was some evidence for bending of the longer helices but no discernible evidence for a well-defined tertiary structure.[606]

Voltage-gated Ca^{2+} channels contribute to the generation of impulses in some nerve cells. In muscle cells, for example, a voltage induced by the arrival of a nerve impulse at the cell surface opens voltage-gated channels, releasing Ca^{2+} ions into the muscle cytoplasm. The resulting increase in Ca^{2+} ion concentration is the immediate trigger for muscle contraction. It has been shown that a 22-residue peptide based upon the sequence of one of the putative channel-lining α-helices of a membrane-bound calcium channel conducts divalent cations in a specific manner.[607] Proton NMR and CD studies of the peptide in an amphiphlic solvent indicate stable structures that have α-helical content.

A somewhat different approach has been shown to be useful in obtaining information about the topology of channels. This approach combines the complementary fit of toxin and channel with knowledge of the structure of the channel-blocking peptide toxins to map part of the topology of the channel.

The channel-blocking peptides become molecular calipers. The three-dimensional structure of many channel-blocking peptide toxins has been determined using the combination of NMR spectroscopy and molecular modelling.[608–646] The NMR-derived structures of a number of scorpion toxins have been used as calipers for probing the topology of K^+ channels.[647–649] An interesting extension of the use of toxin calipers has been described in which the low-resolution experimentally determined geometry parameters, such as that obtained from caliper experiments, can be incorporated as restraints within simulated annealing calculations to predict the structure of the pore of a channel and not just the helical conformation of one segment of a bundle that forms a pore.[650]

4. MINIMALLY DESIGNED SYNTHETIC PEPTIDE CHANNELS

A minimalist approach to peptide design has been used to investigate channel properties.[651,652] Minimally designed synthetic peptides are peptides composed of a limited number of types of hydrophobic and hydrophilic amino acids and bear no specific sequence relationship to naturally occurring channels, yet are designed to fold into amphipilic helices which cluster into a bundle motif.[4] The minimalist approach to the formation of a bundle of α-helices that form an ion-transporting channel requires that an α-helix peptide of at least 20 amino acid residues long, to span a 30 Å lipid bilayer, be used.[652] The α-helix should be sufficiently hydrophobic to be able to insert into a bilayer in a transmembrane orientation. Furthermore, the individual peptides should be able to pack together to produce a well-defined three-dimensional channel. On the basis of these criteria, the peptide, H_2N-(LeuSerSerLeuLeuSerLeu)$_3$-$CONH_2$, was synthesized and found to have ion-channel properties.[652] Serine was chosen as the pore-lining residue because its hydrophilic side-chain should serve to solvate mobile ions. Leucine was chosen for the remaining positions since it is hydrophobic and packs very well. The conformation of a similar synthetic peptide, CH_3CO-(LeuSerLeuLeuLeuSerLeu)$_3$Lys-NH_2, in aqueous trifluoroethanol has been determined from an NOE distance restrained/molecular dynamics study.[653] An α-helical conformation was found up to residue 17.

5. PROPERTY-DIRECTED SYNTHETIC CHANNELS

Another approach taken to form model channels is that of property-directed synthesis.[654] In property-directed synthesis, the principles of physical organic chemistry are applied both to understand the system and to design the target molecule. Again, the molecules of interest may bear *little structural* resemblance to the natural systems; however, it is their function that ones seeks

to mimic. Synthetic channel systems based upon cyclodextrin,[655] polymeric crown ethers,[656,657] bouquet-shaped crown ether and cyclodextrin[658] and self-assembling peptide nanotubes made from the cyclic peptide cyclo[-Trp-D-Leu)$_3$Gln-D-Leu-][659] have been investigated. A $^{23}Na^+$ NMR study, using the method previously described,[408] of a tris-crown ether channel system showed the transport of this model channel to be about 50% of that of gramicidin A.[654,660]

While NMR spectroscopy has provided much information about many aspects of channel structure and properties, many questions remain unanswered. With the advent of ultra-high magnetic field strengths and new techniques, such as TROSY,[661–663] which permits the NMR analysis of the structure, dynamics and interactions of proteins whose size is in the 100 kDa range and above, the future seems very bright for the application of NMR spectroscopy to the study of ion-transporting biological channels.

ACKNOWLEDGEMENTS

The author wishes to acknowledge the permission granted by Wadsworth Publishing Company for using material found in the introduction of this review. The National Science Foundation is thanked for Grant MCB-9313835.

REFERENCES

1. S. L. Wolfe, in *Molecular and Cellular Biology*, Wadsworth Publishing Company, Belmont, California, pp. 180–202, 1993.
2. M. Montal, *Chem. Engr. News*, 1998, **76**, 30.
3. D. A. Doyle, J. M. Cabral, R. A. Pfuetzner, A. Kuo, J. M. Gulbis, S. L. Cohen, B. T. Chait and R. MacKinnon, *Science*, 1998, **280**, 69.
4. M. Montal, *Current Opinion Struct. Biol.*, 1995, **5**, 501.
5. B. A. Wallace, *J. Struct. Biol.*, 1998, **121**, 123.
6. R. D. Hotchkiss and R. J. Dubos, *J. Biol. Chem.*, 1941, **141**, 155.
7. D. Bauer, R. Roskoski, H. Kleinkauf and F. Lipmann, *Biochemistry*, 1972, **11**, 3266.
8. R. Sarges and B. Witkop, *J. Am. Chem. Soc.*, 1965, **87**, 2011.
9. R. E. Koeppe, J. A. Paczkowski and W. L. Whaley, *Biochemistry*, 1985, **24**, 2822.
10. R. E. Koepe, R. A. Corder, O. S. Andersen, E. J. Narcessian, L. M. Peart and G. R. Waller, *Biophys. J.*, 1988, **53**, 328a.
11. L. P. Williams, E. J. Narcessian, O. S. Andersen and R. E. Koeppe, *Biophys. J.*, 1988, **3**, 329a.
12. L. P. Williams, E. J. Narcessian, O. S. Andersen, G. R. Waller, J. Taylor, J. R. Lazenby, J. F. Hinton and R. E. Koeppe, *Biochemistry*, 1992, **31**, 7311.
13. L. K. Ramachandran, *Biochemical Reviews*, 1975, **46**, 1.
14. J.-L. Mazet, R. E. Koeppe and O. S Andersen, *Biophys. J.*, 1984, **45**, 263.
15. E. W. B. Russell, L. B. Weiss, F. I. Navetta, R. E. Koeppe and O. S. Andersen, *Biophys. J.*, 1986, **49**, 673.

16. L. B. Weiss and R. E. Koeppe, *Intl. J. Peptide Res.*, 1985, **26**, 305.
17. R. E. Koeppe and O. S. Andersen, *Annu. Rev. Biophys. Bimol. Struct.*, 1996, **25**, 231.
18. E. Bamberg, K. Noda, E. Gross and P. Lauger, *Biochim. Biophys. Acta*, 1976, **419**, 223.
19. J. S. Morrow, W. R. Veatch and L. Stryer, *J. Mol. Biol.*, 1979, **132**, 733.
20. R. J. Bradley, K. U. Prasad and D. W. Urry, *Biochim. Biophys. Acta*, 1981, **649**, 281.
21. J.-L. Mazet and O. S. Andersen, *Ann. Rev. Physiol.*, 1984, **46**, 531.
22. F. Heitz, A. Heitz and Y. Trudelle, *Biophys. Chem.*, 1986, **24**, 149.
23. F. Heitz, C. Gavach, G. Spach and Y. Trudelle, *Biophys. Chem.*, 1986, **24**, 143.
24. J. T. Durkin, O. S. Andersen, E. R. Blout, F. Heitz and R. E. Koeppe, *Biophys. J.*, 1986, **49**, 118.
25. K. U. Prasad, S. Romanowski, C. M. Venkatachalam, T. L. Trapane and D. W. Urry, *Biochemistry*, 1986, **25**, 456.
26. S. B. Hladky and D. A. Haydon, *Curr. Top. Membr. Transp.*, 1984, **21**, 327.
27. Y. Trudelle and F. Heitz, *Int. J. Pept. Protein Res.*, 1987, **30**, 163.
28. N. Davion-Van Mau, P. Daumas, D. Lelievre, Y. Trudelle and F. Heitz, *Biophys. J.*, 1987, **51**, 843.
29. Y. Trudelle, P. Daumas, F. Heitz, C. Etchebest and A. Pullman, *FEBS Lett.*, 1987, **216**, 11.
30. J. A. Killian, K. N. J. Burger and B. De Kruiijff, *Biochim. Biophys. Acta*, 1987, **897**, 269.
31. M. D. Becker, R. E. Koeppe and O. S. Andersen, *Biophys. J.*, 1992, **62**, 25.
32. R. E. Koeppe and O. S. Andersen, in *Proteins: Structure and Function* (ed. G. J. L'Italien), pp. 623, Plenum Press, New York, 1987.
33. D. B. Sawyer, R. E. Koeppe and O. S. Andersen, *Biochemistry*, 1989, **28**, 6571.
34. J. T. Durkin, R. E. Koeppe and O. S. Andersen, *J. Mol. Biol.*, 1990, **211**, 221.
35. R. E. Koeppe, J.-L. Mazet and O. S. Andersen, *Biochemistry*, 1990, **29**, 512.
36. D. B. Sawyer, R. E. Koeppe and O. S. Andersen, *Biophys. J.*, 1990, **57**, 515.
37. A. M. O'Connell, R. E. Koeppe and O. S. Andersen, *Science*, 1990, **250**, 1256.
38. D. B. Sawyer, L. P. Williams, W. L. Whaley, R. E. Koeppe and O. S. Andersen, *Biophys. J.*, 1990, **58**, 1207.
39. M. D. Becker, D. V. Greathouse, R. E. Koeppe and O. S. Andersen, *Biochemistry*, 1991, **30**, 8830.
40. S. B. Hladky and D. A. Haydon, *Nature*, 1970, **225**, 451.
41. V. B. Meyers and D. A. Haydon, *Biochim. Biophys. Acta*, 1972, **274**, 313.
42. E. Bamberg, H. A. Kolb and P. Lauger, *The Structural Basis of Membrane Function*, Academic Press, New York, 1976.
43. E. Bamberg and P. Lauger, *Biochim. Biophys. Acta*, 1974, **367**, 127.
44. D. W. Urry, *International Review of Neurobiology* (eds J. R. Symthies and R. J. Bradley), vol. 21, Academic Press, New York, 1979.
45. E. Neher, *Biochim. Biophys. Acta*, 1975, **401**, 540.
46. J. Sandblom, G. Eisenman and E. Neher, *J. Membr. Biol.*, 1977, **31**, 383.
47. G. Eisenman, J. Sandblom and E. Neher, *Metal Ligand Interactions in Organic Chemistry and Biochemistry* (ed. B. Pullman), part 2, Reidel Publishing Co., Dordrecht, 1977.
48. H. J. Apell, E. Bamberg, H. Alpes and P. Lauger, *J. Membr. Biol.*, 1977, **31**, 171.
49. E. Bamberg and P. Lauger, *J. Membr. Biol.*, 1977, **35**, 351.
50. J. F. Hinton, J. Q. Fernandez, D. C. Shungu, W. L. Whaley, R. E. Koeppe and F. S. Millett, *Biophys. J.*, 1988, **54**, 527.
51. J. F. Hinton, J. Q. Fernandez, D. C. Shungu and F. S. Millett, 1988, *Biophys. J.*, 1988, **55**, 221.
52. E. Bamberg and P. Lauger, 1977, *J. Membr. Biol.*, 1977, **35**, 351.
53. D. W. Urry, T. L. Trapane, J. T. Walker and K. U. Prasad, *J. Biol. Chem.*, 1982, **257**, 6659.
54. L. V. Schangina, A. E. Grinfeldt and M. A. Lev, *Nature*, 1978, **272**, 243.
55. J. Procopio and O. S. Andersen, *Biophys. J.*, 1979, **25**, 8a.
56. O. S. Andersen, *10th Int. Biophys. Congr., Copenhagen*, p. 112 (abstr.) 1975.

57. E. Neher, *Biochim. Biophys. Acta*, 1975, **401**, 540.
58. J. Sandblom, G. Eisenman and E. Neher, *J. Membr. Biol.*, 1977, **31**, 383.
59. O. S. Andersen, in *Renal Function* (eds G. Giebisch and E. Purcell), p. 71, Josiah Macy Foundation, New York, 1978.
60. D. McBride and G. Szabbo, *Biophys. J.*, 1978, **21**, 25a.
61. P. A. Rosenberg and A. Finkelstein, 1978, *J. Gen. Physiol.*, **72**, 372.
62. P. A. Rosenberg and A. Finkelstein, 1978, *J. Gen. Physiol.*, **72**, 341.
63. D. G. Levitt, S. R. Elias and J. M. Hautman, 1978, *Biochim. Biophys. Acta*, **512**, 436.
64. A. Finkelstein and O. S. Andersen, 1981, *J. Membr. Biol.*, **59**, 155.
65. B. W. Urban, S. B. Hladky and D. A. Haydon, 1980, *Biochim. Biophys. Acta*, **602**, 331.
66. E. R. Decker and D. G. Levitt, 1983, *Biochim. Biophys. Acta*, **730**, 178.
67. P. M. Cowan and D. C. Hodgkin, 1953, *Proc. Roy. Soc. Ser. B*, **141**, 89.
68. D. W. Urry, *Proc. Natl Acad. Sci. (USA)*, 1971, **68**, 676.
69. W. R. Veatch, E. T. Fossel and E. R. Blout, *Biochemistry*, 1974, **13**, 5257.
70. W. R. Veatch and E. R. Blout, *Biochemistry*, 1974, **13**, 5261.
71. S. V. Sychev, L. I. Barsukov and V. T. Ivanov, *Eur. Biophys. J.*, 1993, **22**, 279.
72. A. S. Arseniev, V. F. Bystrov, V. T. Ivanov and Yu. A. Ovchinnikov, *FEBS Lett.*, 1984, **165**, 51.
73. A. S. Arseniev, I. L. Barsukov, E. N. Shepel, V. F. Bystrov and V. T. Ivanov, *Bioorgan. Khimia*, 1985, **11**, 5.
74. A. S. Arseniev, I. L. Barsukov and V. F. Bystrov, *FEBS Lett.*, 1985, **180**, 33.
75. I. L. Barsukov, A. S. Arseniev and V. F. Bystrov, *Bioorgan. Khimia*, 1987, **13**, 1501.
76. L. Braco, M. C. Bano, F. Chillaron and C. Abad, *Biophys. Chem.*, 1986, **25**, 297.
77. F. Heitz, A. Heitz and Y. Trudelle, *Biophys. Chem.*, 1986, **24**, 149.
78. J. A. Killian, K. U. Prasad, D. Hains and D. W. Urry, *Biochemistry*, 1988, **27**, 4848.
79. P. V. LoGrasso, F. Moll and T. A. Cross, *Biophys. J.*, 1988, **54**, 259.
80. D. B. Sawyer, R. E. Koeppe and O. S. Andersen, *Biophys. J.*, 1990, **57**, 515.
81. S. V. Sychev and V. T. Ivanov, Conformational states of gramicidin A in solution and in membranes, in *Membrane and Transport* (ed. A. N. Martonosi) Vol. 2, p. 301, Plenum Press, New York, 1982.
82. S. V. Sychev, N. A. Nevskaya, St. Jordanov, E. N. Shepel, A. I. Miroshnikov and V. T. Ivanov, *Bioorg. Chem.*, 1980, **9**, 121.
83. H. Tourniois, J. A. Killian, D. W. Urry, O. R. Bokking, J. de Gier and B. de Kruijff, *Biochim. Biophys. Acta*, 1987, **905**, 222.
84. M. Bouchard and M. Auger, *Biophys. J.*, 1993, **65**, 2484.
85. B. Roux, R. Bruschweiller and R. Ernst, 1990, *Eur. J. Biochem.*, **194**, 57.
86. A. S. Arseniev, I. L. Barsukov and V. F. Bystrov, *Chem. Pep. Proteins*, 1985, **3**, 2127.
87. S. M. Pascal and T. A. Cross, *J. Mol. Biol.*, 1992, **226**, 1101.
88. Z. Zhang, S. M. Pascal and T. A. Cross, *Biochemistry*, 1992, **31**, 8822.
89. K. J. Cox, C. Ho, J. V. Lombardi and C. D. Stubbs, *Biochemistry*, 1992, **31**, 1112.
90. N. V. Mau, B. Bonnet, A. Benayad and F. Heitz, *Eur. Biophys. J.*, 1994, **22**, 447.
91. J. T. Durkin, L. L. Providence, R. E. Koeppe and O. S. Andersen, *Biophys. J.*, 1992, **62**, 163.
92. N. Abdul-Manan and J. F. Hinton, *Biochemistry*, 1994, **33**, 6773.
93. J. A. Killian, *Biochim. Biophys. Acta*, 1992, **1113**, 391.
94. M. Engelike, H.-C. Klockmann and H. A. Diehl, *Spectrochim. Acta, Part A*, 1995, **51**, 1939.
95. S. Nayenova, A. G. Petrov and J. Yarwood, *Langmuir*, 1995, **11**, 3435.
96. S. F. Scarlata, *Biophys. J.*, 1988, **54**, 1149.
97. S. F. Scarlata, *Biochemistry*, 1991, **30**, 9853.
98. T. Henkel, S. Mittler, W. Pfeiffer, H. Rotzer, H.-J. Apell and W. Knoll, *Biochimie*, 1989, **71**, 89.
99. L. V. Schagina, K. Blasko, A. E. Grinfeldt, Y. E. Korchev and A. A. Lev, *Biochim. Biophys. Acta*, 1989, **978**, 145.

100. Z. Peng, N. Tjandra, V. Simplaceanu and C. Ho, *Biophys. J.*, 1989, **56**, 877.
101. Q. T. Teng, R. E. Koeppe and S. F. Scarlata, *Biochemistry*, 1991, **30**, 7984.
102. H. Takeuchi, Y. Nemoto and I. Harada, *Biochemistry*, 1990, **29**, 1572.
103. M. Morrow, *Biochim. Biophys. Acta*, 1990, **1023**, 197.
104. L. V. Schagina, Y. E. Korchev, A. E. Grinfeldt, A. A. Lev and K. Blasko, *Biochim. Biophys. Acta*, 1992, **1109**, 91.
105. H. Tournois, C. H. J. P. Fabrie, K. N. J. Burger, J. Mandersloot, P. Hilgers, H. van Dalen, J. de Gier and B. de Kruijff, *Biochemistry*, 1990, **29**, 8297.
106. M. R. Morrow, G. A. Simatos, R. Srinivasan, N. Grandal, L. Taylor and K. M. W. Keough, *Biochim. Biophys. Acta*, 1991, **1070**, 209.
107. G. Jyothi, C. K. Mitra and G. Krishnamoorthy, *Bioelectro. Bioenerg.*, 1991, **26**, 395.
108. A. Ring, *Biochim. Biophys. Acta*, 1996, **1278**, 147.
109. J. Mou, D. M. Czajkowsky and Z. Shao, *Biochemistry*, 1996, **35**, 3222.
110. J. M. Muller, G. van Ginkel and E. E. van Faassen, *Biochemistry*, 1996, **35**, 488.
111. A. Nelson, *Langmuir*, 1996, **12**, 2058.
112. D. C. J. Jaikaran, Z. Zhang and G. A. Woolley, *Biochim. Biophys. Acta*, 1995, **1234**, 133.
113. L. L. Providence, O. S. Andersen, D. V. Greathouse, R. E. Koeppe and R. Bittman, *Biochemistry*, 1995, **34**, 16404.
114. X. Chen and R. W. Cross, *Biochemistry*, 1995, **34**, 7356.
115. Y. G. Assaraf and M. J. Borgnia, *Eur. Biochem.*, 1994, **222**, 813.
116. T. C. B. Vogt, J. A. Killian and B. de Kruijff, *Biochim. Biophys. Acta*, 1994, **1193**, 55.
117. M. Ge and J. H. Freed, *Biophys. J.*, 1993, **65**, 2106.
118. A. Ring, *Biophys. J.*, 1992, **61**, 1306.
119. T. R. Bridal and D. Busath, *Biochim. Biophys. Acta*, 1992, **1107**, 31.
120. T. Mita and Y. Sairyo, *Biosci. Biotech. Biochem.*, 1992, **56**, 1971.
121. G. Schonknecht, G. Althoff and W. Junge, *J. Membr. Biol.*, 1992, **126**, 265.
122. B. A. Cornell and F. Separovic, *Eur. Biophys. J.*, 1988, **16**, 299.
123. D. W. Urry, M. M. Long, M. Jacobs and R. D. Harris, *Ann. N.Y. Acad. Sci.*, 1975, **264**, 203.
124. L. Masotti, A. Spisni and D. W. Urry, *Cell Biology*, 1980, **2**, 241.
125. B. A. Wallace, W. R. Veatch and E. R. Blout, *Biochemistry*, 1981, **20**, 5754.
126. D. C. Hodgkin, *Cold Spring Harbor Symp. Quant. Biol.*, 1949, **14**, 65.
127. R. L. M. Synge, *Cold Spring Harbor Symp. Quant. Biol.*, 1949, **14**, 191.
128. B. A. Wallace, *Biophys. J.*, 1986, **49**, 295.
129. R. E. Koeppe, K. O. Hodgson and L. Stryer, *J. Mol. Biol.*, 1978, **121**, 41.
130. R. E. Koeppe, J. M. Berg, K. O. Hodgson and L. Stryer, *Nature*, 1979, **279**, 723.
131. M. R. Kimball and B. A. Wallace, *Ann. N.Y. Acad. Sci.*, 1984, **435**, 551.
132. B. Hedman, K. O. Hodgson, J. R. Helliwell, R. Liddington and M. Z. Papiz, *Proc. Natl Acad. Sci. (USA)*, 1985, **82**, 7604.
133. B. A. Wallace, *Science*, 1988, **241**, 182.
134. D. Langs, *Science*, 1988, **241**, 188.
135. G. A. Olah, H. W. Haung, W. Liu and Y. Wu, *J. Mol. Biol.*, 1991, **218**, 847.
136. G. A. Olah, H. W. Huang, W. Liu and Y. Wu, *Chemtracts—Biochemistry and Molecular Biology*, **3**, 107 (1992).
137. D. A. Langs, *Biopolymers*, 1989, **28**, 259.
138. B. A. Wallace, W. A. Hendrickson and K. Ravikumar, *Acta Cryst.*, 1990, **B46**, 440.
139. D. A. Doyle and B. A. Wallace, *Current Trends in Polypeptide Structure and Synthesis*, 1994, 1043.
140. D. A. Doyle and B. A. Wallace, *Biophys. J.*, 1994, **66A**, 353.
141. D. A. Doyle and B. A. Wallace, *J. Mol. Biol.*, 1997, **266**, 963.
142. R. E. Koeppe and B. P. Schoenborn, *Biophys. J.*, 1984, **45**, 503.
143. K. He, S. J. Ludtke, Y. Wu and H. W. Haung, *Biophys. J.*, 1993, **64**, 157.
144. J. Katsaras, R. S. Prosser, R. H. Stinson and J. H. Davis, *Biophys. J.*, 1992, **61**, 827.

145. R. E. Koeppe and M. Kimura, *Biopolymers*, 1984, **23**, 23.
146. D. D. Busath, *Annu. Rev. Physiol.*, 1993, **55**, 473.
147. O. S. Andersen and R. E. Koeppe, *Physiol. Revs.*, 1992, **72**, S89.
148. D. Levitt, *Current Opinion in Cell Biology*, 1990, **2**, 689.
149. O. S. Andersen, D. B. Sawyer and R. E. Koeppe, Modulation of channel function by host bilayers, in *Biomembrane Structure and Function* (eds B. Baber and K. R. K. Easwaran) p. 227, Adenine Press, Schenectady, 1992.
150. S. Oiki, R. E. Koeppe and O. S. Andersen, Voltage-dependent gramicidin channels, in *Towards Molecular Biophysics of Ion Channels* (ed. M. Sokabe) Elsevier, Amsterdam, 1996.
151. D. W. Urry, K. U. Prasad and T. L. Trapane, *Proc. Natl Acad. Sci. (USA)*, 19182, **79**, 390.
152. D. C. Tosteson, T. E. Andreoli, M. Tiffenberg and P. Cook, *J. Gen. Physiol.*, 1968, **51**, 373.
153. D. C. Buster, J. F. Hinton and F. S. Millett, *Biophys. J.*, 1988, **53**, 145.
154. D. W. Urry, J. D. Goodall, J. D. Glickson and D. F. Meyers, *Proc. Natl Acad. Sci. (USA)*, 1971, **68**, 1907.
155. E. Bamberg and P. Lauger, *J. Membr. Biol.*, 1973, **11**, 177.
156. H. P. Zingshein and E. Neher, *Biophys. Chem.*, 1974, **2**, 197.
157. H. A. Kolb, P. Lauger and E. Bamberg, *J. Membr. Biol.*, 1975, **20**, 133.
158. W. R. Veatch, R. Mathies, M. Eisenberg and L. Stryer, *J. Mol. Biol.*, 1975, **99**, 75.
159. W. R. Veatch and L. Stryer, *J. Mol. Biol.*, 1977, **113**, 89.
160. M. C. Goodall, *Biochim. Biophys. Acta*, 1970, **219**, 471.
161. H.-J. Appel, E. Bamberg, H. Alpes and P. Lauger, *J. Membr. Biol.*, 1977, **31**, 171.
162. A. S. Cifu, R. E. Koeppe and O. S. Andersen, *Biophys. J.*, 1992, **61**, 189.
163. G. Schonecht, G. Althoff and W. Junge, *J. Membr. Biol.*, 1992, **126**, 265.
164. G. Stark, M. Strassle and Z. Takacz, *J. Membr. Biol.*, 1986, **89**, 23.
165. M. Strassle, G. Stark, W. Wilheim, P. Daumas, F. Heitz and R. Lazaro, *Biochim. Biophys. Acta*, 1989, **980**, 305.
166. V. F. Bystrov, Y. D. Gavilov, V. T. Ivanov and Y. A. Ovchinnikov, *Eur. J. Biochem.*, 1977, **8**, 63.
167. V. F. Bystrov, A. S. Arseniev, I. L. Barsukov, A. L. Lomize and M. M. Shemyakin, *Bull. Magn. Reson.*, 1986, **8**, 84.
168. A. S. Arseniev, I. L. Barsukov and V. F. Bystrov, in *Chemistry of Peptides and Proteins*, vol. 3, p. 127, Walter de Gruter Co., Berlin, 1986.
169. A. S. Arseniev, I. L. Barsukov, V. F. Bystrov and Y. A. Ovchinnikov, *Biol. Membr.*, 1986, **3**, 437.
170. A. L. Lomize, V. Yu. Orekhov and A. S. Arseniev, *Bioorg. Khimiya.*, 1992, **18**, 182.
171. A. G. Sobol and A. S. Arseniev, *Bioorg. Khimiya.*, 1988, **8**, 997.
172. A. L. Lomize, A. G. Sobol and A. S. Arseniev, *Bioorg. Khimiya.*, 1990, **16**, 179.
173. A. S. Arseniev, I. L. Barsukov, V. F. Bystrov and Y. A. Ovchinnikov, *Biol. Membr.*, 1986, **3**, 437.
174. I. L. Barsukov and A. S. Arseniev, *J. Magn. Reson.*, 1987, **73**, 148.
175. V. F. Bystrov, A. S. Arseniev, I. L. Barsukov, A. P. Golovanov and I. V. Maslennikov, *Gazz. Chim. Ital.*, 1990, **120**, 485.
176. N. Jing, K. U. Prasad and D. W. Urry, *Biophys. J.*, 1994, **66A**, 353.
177. L. K. Nicholson, F. Moll, T. E. Mixon, P. V. LoGrasso, J. C. Lay and T. A. Cross, *Biochemistry*, 1987, **26**, 6621.
178. T. A. Cross, *Biophys. J.*, 1986, **49**, 124.
179. R. Smith and B. A. Cornell, *Biophys. J.*, 1986, **49**, 117.
180. B. A. Cornell, F. Separovic, A. Baldassi and R. Smith, *Biophys. J.*, 1988, **53**, 67.
181. B. A. Cornell, L. E. Weir and F. Separovic, *Eur. J. Biochem.*, 1988, **16**, 113.
182. R. Smith, D. E. Thomas, F. Separovic, A. R. Atkins and B. A. Cornell, *Biophys. J.*, 1989, **56**, 307.

183. G. B. Fields, C. G. Fields, J. Petefish, H. E. Van Wart and T. A. Cross, *Proc. Natl Acad. Sci. USA*, 1988, **85**, 1384.
184. D. W. Urry, T. L. Trapane and K. U. Prasad, *Science*, 1983, **221**, 1064.
185. F. Moll and T. A. Cross, *Biophys. J.*, 1990, **57**, 351.
186. L. K. Nicholson, Q. Teng and T. A. Cross, *J. Mol. Biol.*, 1991, **218**, 621.
187. L. K. Nicholson and T. A. Cross, *Biochemistry*, 1989, **28**, 9379.
189. B. A. Cornell, *J. Bioenerg. Biomembr.*, 1987, **19**, 655.
190. N. D. Lazo, W. Hu and T. A. Cross, *J. Magn. Reson., Series B*, 1995, **107**, 43.
191. W. Mai, W. Hu, C. Wang and T. A. Cross, *Protein Science*, 1993, **2**, 532.
192. R. R. Katchem, W. Hu and T. A. Cross, *Science*, 1993, **261**, 1457.
193. A. W. Hing and J. Schaefer, *Biochemistry*, 1993, **32**, 7593.
194. R. Smith, D. E. Thomas, A. R. Atkins, F. Separovic and B. A. Cornell, *Biochim. Biophys. Acta*, 1990, **1026**, 161.
195. Q. Teng, L. K. Nicholson and T. A. Cross, *J. Mol. Biol.*, 1991, **218**, 607.
196. W. Hu., K.-C. Lee and T. A. Cross, *Biochemistry*, 1993, **32**, 7035.
197. K. P. Datema, K. P. Pauls and M. Bloom, *Biochemistry*, 1986, **25**, 3797.
198. J. A. Killian, M. J. Taylor and R. E. Koeppe, *Biochemistry*, 1992, **31**, 11283.
199. J. H. Davis, *Biochemistry*, 1988, **27**, 428.
200. R. S. Prosser, J. H. Davis, F. W. Dahlquist and M. A. Lindorfer, *Biochemistry*, 1991, **30**, 4687.
201. J. A. Killian, M. J. Taylor and R. E. Koeppe, *Biochemistry*, 1992, **31**, 11283.
202. W. Hu, N. D. Lazo and T. A. Cross, *Biochemistry*, 1995, **34**, 14138.
203. K.-C. Lee, S. Huo and T. A. Cross, *Biochemistry*, 1995, **34**, 857.
204. R. E. Koeppe, J. A. Killian and D. V. Greathouse, *Biophys. J.*, 1994, **66**, 14.
205. R. S. Prosser, S. I. Daleman and J. H. Davis, *Biophys. J.*, 1994, **66**, 1415.
206. K.-C. Lee, W. Hu and T. A. Cross, *Biophys. J.*, 1993, **65**, 1162.
207. A. W. Hing, S. P. Adams, D. F. Silbert and R. E. Norberg, *Biochemistry*, 1990, **29**, 4144.
208. R. E. Koeppe, T. C. B. Vogt, D. V. Greathouse, J. A. Killian and B. de Kruijff, *Biochemistry*, 1996, **35**, 3641.
209. P. M. MacDonald and J. Seelig, *Biochemistry*, 1988, **27**, 2357.
210. R. E. Koeppe, J. A. Killian and D. V. Greathouse, *Biophys. J.*, 1994, **66**, 14.
211. W. Hu., N. D. Lazo and T. A. Cross, *Biochemistry*, 1995, **34**, 14138.
212. W. Hu and T. A. Cross, *Biochemistry*, 1995, **34**, 14147.
213. C. L. North and T. A. Cross, *J. Magn. Reson., Series B*, 1993, **101**, 35.
214. C. L. North and T. A. Cross, *Biochemistry*, 1995, **34**, 5883.
215. M. Bouchard, J. H. Davis and M. Auger, *Biophys. J.*, 1995, **69**, 1917.
216. M. Bouchard, J. H. Davis and M. Auger, *Biophys. J.*, 1995, **69**, 1933.
217. E. Bamberg and K. Janko, *Biochim. Biophys. Acta*, 1977, **465**, 486.
218. G. Szabo and D. W. Urry, *Science*, 1979, **203**, 55.
219. E. Bamberg, H. J. Apell and H. Alpes, *Proc. Natl Acad. Sci. (USA)*, 1977, **74**, 2402.
220. R. J. Bradley, D. W. Urry, K. Okamoto and R. Rapaka, *Science*, 1978, **200**, 435.
221. H. J. Apell, E. Bamberg, H. Alpes and P. Lauger, *J. Membr. Biol.*, 1977, **3**, 171.
222. S. Weinstein, B. A. Wallace, E. R. Blout, J. S. Morrow and W. R. Veatch, *Proc. Natl Acad. Sci. (USA)*, 1979, **76**, 4230.
223. S. Weinstein, B. A. Wallace, J. S. Morrow and W. R. Veatch, *J. Mol. Biol.*, 1972, **143**, 1.
224. D. W. Urry, T. L. Trapane and K. U. Prasad, *Science*, 1983, **221**, 1064.
225. A. S. Arseniev, I. L. Barsukov, V. F. Bystrov, A. L. Lomize and Y. A. Ovchinnikov, *FEBS Lett.*, 1985, **186**, 168.
226. G. N. Ramachandran and R. Chandrasekharan, *Indian Chem. Biophys.*, 1972, **9**, 1.
227. B. Lotz, F. Colonna-Cesari, F. Heitz and G. Spach, *J. Mol. Biol.*, 1976, **106**, 915.
228. R. E. Koeppe and M. Kimura, *Biopolymers*, 1984, **23**, 23.
229. J. R. Elliot, D. Needham, J. P. Dilger and D. A. Haydon, *Biochim. Biophys. Acta*, 1983, **735**, 95.

230. D. W. Urry, J. T. Walker and T. L. Trapane, *J. Membr. Biol.*, 1982, **69**, 225.
231. J. K. Young, F. Mari, M. Xu, R. E. Humphreys, N. M. Clemente, J. M. Stattel, D. I. Nelson, I. Gambino and G. E. Wright, *J. Peptide. Res.*, 1997, **50**, 122.
232. J. Jarvet, J. Zdunek, P. Damberg and A. Graslund, *Biochemistry*, 1997, **36**, 8153.
233. K. J. Barnham, S. A. Monks, M. G. Hinds, A. A. Azad and R. S. Norton, *Biochemistry*, 1997, **36**, 5970.
234. E. Martinez, M. A. Jimenez, B. Segui-Real, J. Vandekerckhove and I. V. Sandoval, *J. Mol. Biol.*, 1997, **267**, 1124.
235. T. G. Fletcher and D. A. Keire, *Protein Sci.*, 1997, **6**, 666.
236. D. K. Chang, W. J. Chien and A. I. Arunkumar, *Biophys. J.*, 1997, **72**, 554.
237. M. Pellegrini, S. Mammi, E. Peggion and D. F. Mierke, *J. Med. Chem.*, 1997, **40**, 92.
238. J. P. Berlose, O. Conveert, D. Derossi, A. Brunissen and G. Chassaing, *Eur. J. Biochem.*, 1996, **242**, 372.
239. S. Morein, T. P. Trouard, J. B. Hauksson, L. Rilfors, B. Arvidson and G. Lindblom, *Eur. J. Biochem.*, 1996, **241**, 489.
240. K. H. Mayo, F. Fan, M. P. Beavers, A. Eckardt, P. Keane, W. J. Hoekstra and P. Andrade-Gordon, *Biochim. Biophys. Acta*, 1996, **1296**, 95.
241. G. Wang, G. K. Pierens, W. D. Treleaven, J. T. Sparrow and R. J. Cushley, *Biochemistry*, 1996, **35**, 10358.
242. G. Wang, W. D. Treleaven and R. J. Cushley, *Biochim. Biophys. Acta*, 1996, **1301**, 174.
243. D. A. Keire and T. G. Fletcher, *Biophys. J.*, 1996, **70**, 1716.
244. J. Sejbal, J. R. Cann, J. M. Stewart, L. Gera and G. Kotovych, *J. Med. Chem.*, 1996, **39**, 1281.
245. G. W. Buchko, W. D. Treleaven, S. J. Dunne, A. S. Tracey and R. J. Cushley, *J. Biol. Chem.*, 1996, **271**, 3039.
246. A. Bisello, S. Sala, A. Tonello, G. Signor, E. Melotto, S. Mammi and E. Peggion, *Int. J. Biol. Macromol.*, 1995, **17**, 273.
247. M. Chorev, M. Gurrath, V. Behar, S. Mammi, A. Tonello and E. Peggion, *Biopolymers*, 1995, **36**, 473.
248. V. Chupin, J. A. Killian, J. Breg, H. H. de Jongh, R. Boelens, R. Kaptein and B. de Kruijff, *Biochemistry*, 1995, **34**, 11617.
249. C. H. Papavoine, J. M. Jaelen, R. N. Konings, C. W. Hilbers and F. J. Van de Ven, *Eur. J. Biochem.*, 1995, **232**, 490.
250. I. E. Borissevitch, C. P. Borges, V. E. Yushmanov and M. Tabak, *Biochim. Biophys. Acta*, 1995, **1238**, 57.
251. L. V. Najbar, D. J. Craik, J. D. Wade, F. Lin and M. J. McLeish, *Biochim. Biophys. Acta*, 1995, **1250**, 163.
252. R. J. Mortishire-Smith, S. M. Pitzenberger, C. J. Burke, C. R. Middaugh, V. M. Garsky and R. G. Johnson, *Biochemistry*, 1995, **34**, 7603.
253. G. E. Gilbert and J. D. Baleja, *Biochemistry*, 1995, **34**, 3022.
254. V. E. Yushmanov, H. Imasato, J. R. Perussi and M. Tabak, *J. Magn. Reson. B.*, 1995, **106**, 236.
255. B. W. Koenig, L. D. Bergelson, K. Gawrisch, J. Ward and J. A. Ferretti, *Mol. Membr. Biol.*, 1995, **12**, 77.
256. J. R. Perussi, V. E. Yushmanov, S. C. Monte, H. Imasato and M. Tabak, *Physiol. Chem. Phys. Med. NMR*, 1995, **27**, 1.
257. C. H. Papavoine, R. N. Konings, C. W. Hilbers, F. J. van de Ven, *Biochemistry*, 1995, **33**, 12990.
258. R. Battistutta, A. Bisello, S. Mammi and E. Peggion, *Biopolymers*, 1994, **34**, 1535.
259. J. K. Young, C. Anklin and R. P. Hicks, *Biopolymers*, 1994, **34**, 1449.
260. M. J. McLeish, K. J. Nielsen, L. V. Najbar, J. D. Wade, F. Lin, M. B. Doughty and D. J. Craik, *Biochemistry*, 1994, **33**, 11174.

261. P. Amodeo, M. A. Morelli and A. Castiglione-Motta, *Biochemistry*, 1994, **33**, 10754.
262. J. C. Wilson, K. J. Nielsen, M. J. McLeish and D. J. Craik, *Biochemistry*, 1994, **33**, 6802.
263. S. Improta, A. Pastore, S. Mammi and E. Peggion, *Biopolymers*, 1994, **34**, 773.
264. J. C. Franklin, J. F. Ellena, S. Jayasinghe, L. P. Kelsh and D. S. Cafiso, *Biochemistry*, 1994, **33**, 4036.
265. B. M. Backlund, G. Wilkander, T. L. Peeters and A. Graslund, *Biochim. Biophys. Acta*, 1994, **1190**, 337.
266. V. Yu. Orekhov, K. V. Pervushin and A. S. Arseniev, *Eur. J. Biochem.*, 1994, **219**, 887.
267. K. V. Pervushin, V. Yu. Orekhov, A. I. Popov, L. Yu. Musina and A. S. Arseniev, *Eur. J. Biochem.*, 1994, **219**, 571.
268. V. E. Yushmanov, J. R. Perussi, H. Imasato and M. Tabak, *Biochim. Biophys. Acta*, 1994, **1189**, 74.
269. G. D. Henry and B. D. Sykes, *Methods Enzymol.*, 1994, **239**, 515.
270. M. Tessari, M. T. Foffani, S. Mammi and E. Peggion, *Biopolymers*, 1993, **33**, 1877.
271. F. J. van de Ven, J. W. van Os, J. M. Aelen, S. S. Wymenga, M. L. Remerowski, R. N. Konings and C. W. Hilbers, *Biochemistry*, 1993, **32**, 8322.
272. D. A. Kloosterman, T. A. Scahill and A. R. Friedman, *Pept. Res.*, 1993, **6**, 211.
273. K. Gawrisch, K. H. Han, L. D. Bergelson and J. A. Ferretti, *Biochemistry*, 1993, **32**, 3112.
274. M. J. McLeish, K. J. Nielsen, J. D. Wade and D. J. Craik, *FEBS Lett.*, 1993, **315**, 323.
275. W. H. Graham, E. D. Carter and R. P. Hicks, *Biopolymers*, 1992, **32**, 1755.
276. M. D. Bruch, J. Rizo and L. M. Gierasch, *Biopolymers*, 1992, **32**, 1741.
277. K. V. Pervushin, A. G. Sobol, L. Yu. Mushina, G. V. Abdulaeva and A. S. Areneien, *Mol. Biol. (Mosk)*, 1992, **26**, 1397.
278. M. Hayer-Hartl, H. Schagger, G. von Jagow and K. Beyer, *Eur. J. Biochem.*, 1992, **209**, 423.
279. M. D. Bruch and D. W. Hoyt, *Biochim. Biophys. Acta*, 1992, **1159**, 81.
280. K. V. Pervushin and A. S. Arseniev, *FEBS Lett.*, 1992, **308**, 190.
281. A. L. Lomize, K. V. Pervushin and A. S. Arseniev, *J. Biol. NMR*, 1992, **2**, 361.
282. R. P. Hicks, D. J. Beard and J. K. Young, *Biopolymers*, 1992, **32**, 85.
283. K. V. Pervushin, A. S. Arseniev, A. T. Kozhich and V. T. Ivanov, *J. Biomol. NMR*, 1991, **1**, 313.
284. A. Motta, A. Pastore, N. A. Goud and M. A. Castiglione-Morelli, *Biochemistry*, 1991, **30**, 10444.
285. G. Y. Xu and C. M. Deber, *Int. J. Pept. Protein Res.*, 1991, **37**, 528.
286. M. M. Snel, R. Kaptein and B. de Kruijff, *Biochemistry*, 1991, **30**, 3387.
287. E. Bairaktari, D. F. Mierke, S. Mammi and E. Peggion, *Biochemistry*, 1990, **29**, 10097.
288. E. Bairaktari, D. F. Mierke, S. Mammi and E. Peggion, *Biochemistry*, 1990, **29**, 10090.
289. D. Picone, A. D'Ursi, A. Motta, T. Tancredi and P. A. Temussi, *Eur. J. Biochem.*, 1990, **192**, 433.
290. G. D. Henry and B. D. Sykes, *Biochemistry*, 1990, **29**, 6303.
291. S. Mammi and E. Peggion, *Biochemistry*, 1990, **29**, 5265.
292. S. C. Lee, A. F. Russell and W. D. Laidig, *Int. J. Pept. Protein Res.*, 1990, **53**, 367.
293. L. Zetta, R. Consonni, A. De Marco, R. Longhi, E. Manera and G. Vecchio, *Biopolymers*, 1990, **30**, 899.
294. J. D. O'Neil and B. D. Sykes, *Biochemistry*, 1989, **28**, 6736.
295. E. T. Olejniczak, R. T. Gampe, T. W. Rockway and S. W. Fesik, *Biochemistry*, 1988, **27**, 7124.
296. A. B. Mandal, D. V. Ramesh and S. C. Dhar, *Eur. J. Biochem.*, 1987, **169**, 617.
297. K. H. Mayo, A. De Marco, E. Menegatti and R. Kaptein, *J. Biol. Chem.*, 1987, **262**, 14899.
298. L. Zetta and R. Kaptein, *Eur. J. Biochem.*, 1984, **145**, 181.
299. R. R. Ketchem, B. Roux and T. A. Cross, *Structure*, 1997, **5**, 1655.
300. A. D. Mackerell and M. Karplus, *Biophys. J.*, 1992, **61A**, 143.
301. T. Maruyama and H. Takeuchi, *Biochemistry*, 1997, **36**, 10993.

302. T. Maruyama and H. Takeuchi, *Biospectroscopy*, 1998, **4**, 171.
303. F. Tian, K. C. Lee and T. A. Cross, *Biochemistry*, 1996, **35**, 11959.
304. F. Separovic, K. Hayamizu, K. Smith and B. A. Cornell, *Chem. Phys. Lett.*, 1991, **181**, 157.
305. R. E. Koeppe, O. S. Andersen and A. K. Maddock, in *Twenty-First Jerusalem Symposium in Quantum Chemistry and Biochemistry on Transport Through Membranes: Carriers, Channels and Pumps*, D. Reidel Publishing Co., Holland, 1988.
306. W. R Veatch and L. Stryer, *J. Mol. Biol.*, 1977, **113**, 89.
307. F. Heitz, F. Spac and Y. Trudelle, *Biophys. J.*, 1982, **40**, 87.
308. J. S. Morrow, W. R. Veatch and L. Stryer, *J. Mol. Biol.*, 1979, **132**, 733.
309. D. G. Levitt, S. R. Elias and J. M. Hautman, *Biochim. Biophys. Acta*, 1978, **512**, 436.
310. J. Sandblom, G. Eisenman and J. V. Hagglund, *J. Membr. Biol.*, 1983, **71**, 61.
311. G. Eisenman and J. Sandblom, in *Physical Chemistry of Transmembrane Ion Motions* (ed. G. Spach), p. 329, Elsevier/North-Holland Biochemical Press, Amsterdam, 1983.
312. D. G. Levitt, *Biophys. J.*, 1982, **37**, 575.
313. P. Lauger, W. Stephan and E. Frehaland, *Biochim. Biophys. Acta*, 1980, **601**, 167.
314. E. Neher, J. Sandblom and G. Eisenman, *J. Membr. Biol.*, 1978, **40**, 97.
315. O. S. Andersen, *Ann. Rev. Physiol.*, 1984, **46**, 531.
316. R. Henze, E. Neher, T. L. Trapane and D. W. Urry, *J. Membr. Biol.*, 1982, **64**, 233.
317. P. Lauger, *Biochim. Biophys. Acta*, 1973, **311**, 423.
318. S. B. Hladky, B. W. Urban and R. W. Tsien, in *Membrane Transport Processes* (eds C. F. Steven and R. W. Tsien), vol. 3, Raven Press, New York, 1979.
319. B. W. Urban, S. B. Hladky and D. A. Haydon, *Fed. Proc.*, 1978, **37**, 2628.
320. J. Hagglund, B. Enos and G. Eisenman, *Brain Res. Bull.*, 1979, **4**, 154.
321. O. S. Andersen, E. W. Barrett and L. B. Weiss, *Biophys. J.*, 1981, **33**, 63.
322. G. Eisenman and J. Sandblom, *Biophys. J.*, 1984, **45**, 88.
323. G. Eisenman and R. Horn, *J. Membr. Biol.*, 1983, **76**, 197.
324. G. Eisenman, J. Sandblom and E. Neher, *Biophys. J.*, 1978, **22**, 307.
325. O. S. Andersen, *Biophys. J.*, 1983, **41**, 147.
326. J. A. Dani and D. G. Levitt, *Biophys. J.*, 1981, **35**, 485.
327. D. G. Levitt, *Biophys. J.*, 1978, **22**, 221.
328. O. S. Andersen, *J. Membr. Biol.*, 1981, **59**, 155.
329. G. Eisenman, J. Sandblom and E. Neher, *Biophys. J.*, 11978, **22**, 307.
330. D. G. Levitt, *Biophys. J.*, 1978, **22**, 2220.
331. F. J. Sigworth, D. W. Urry and K. U. Prasad, *Biophys. J.*, 1987, **52**, 1055.
332. A. Ring and J. Sandblom, *Biophys. J.*, 1988, **53**, 549.
333. V. V. Osipov, T. K. Rostovtseva and A. A. Lev, *Biol. Membr.*, 1988, **5**, 162.
334. D. G. Levitt and E. R. Decker, *Biophys. J.*, 1988, **53**, 33.
335. E. R. Decker and D. G. Levitt, *Biophys. J.*, 1988, **53**, 25.
336. D. W. Urry, N. Jing and K. U. Prasad, *Biochim. Biophys. Acta*, 1987, **902**, 137.
337. A. H. Hainsworth and S. B. Hladky, *Biophys. J.*, 1987, **52**, 109.
338. E. Jakobsson and S. W. Chiu, *Biophys. J.*, 1987, **52**, 33.
339. J. T. Durkin, O. S. Andersen, E. R. Blout and R. E. Koeppe, *Biophys. J.*, 1986, **49**, 118.
340. P. C. Jordan and I. S. Vayl, *Biochim. Biophys. Acta*, 1985, **818**, 416.
341. V. I. Prsechinik, M. N. Flerov and T. Hianik, *Gen. Physiol. Biophys.*, 1985, **4**, 53.
342. D. W. Urry, *Enzymes Biol. Membr.*, 1985, **1**, 229.
343. C. Etchebest and A. Pullman, *J. Biol. Struct. Dyn.*, 1985, **2**, 859.
344. F. Heitz, G. Spach, A. Heitz and Y. Trudelle, *Pept. Proc. Eur. Pept. Symp.*, 1984, **18**, 595.
345. S. B. Hladky and D. A. Haydon, *Curr. Top. Membr. Transp.*, 1984, **21**, 327.
346. C. M. Venkatachalam, S. Alnoso-Romannowski, K. U. Prasad and D. W. Urry, *Int. J. Quant. Chem. and Biol. Symp.*, 1984, **11**, 315.
347. D. B. Sawyer, L. P. Williams, W. L. Whaley, R. E. Koeppe and O. S. Andersen, *Biophys. J.*, 1990, **58**, 1207.

348. R. E. Koeppe, L. L. Providence, D. V. Greathouse, F. Heitz, Y. Trudelle, N. Purdie and O. S. Andersen, *Proteins: Structure, Function and Genetics*, 1991, **12**, 49.
349. M. D. Becker, R. E. Koeppe and O. S. Andersen, *Biophys. J.*, 1992, **62**, 25.
350. R. E. Koeppe, J. A. Killian, T. C. B. Vogt, B. de Kruijff, M. J. Taylor, G. L. Mattice and D. V. Greathose, *Biochemistry*, 1995, **34**, 9299.
351. G. L. Mattice, R. E. Koeppe, L. L. Providence and O. S. Andersen, *Biochemistry*, 1995, **34**, 6827.
352. V. Fonseca, L. Daumas, F. Ranjalahy-Rasoloarijao, F. Heitz, L. Lazaro, Y. Trudelle and O. S. Andersen, *Biochemistry*, 1992, **31**, 5340.
353. A.-A. Seoh and D. D. Busath, *Biophys. J.*, 1993, **65**, 1817.
354. R. E. Koeppe, D. V. Greathouse, A. Jude, G. Saberwal, L. L. Providence and O. S. Andersen, *J. Biol. Chem*, 1994, **269**, 12567.
355. S. Oiki, R. E. Koeppe and O. S. Andersen, *Biophys. J.*, 1994, **66**, 1823.
356. M. Jelokhani-Niaraki, H. Kodama, T. Ehara and M. Kondo, *J. Chem. Soc. Perkin Society*, 1995, **2**, 801.
357. M. D. Becker, D. V. Greathouse, R. E. Koeppe and O. S. Andersen, *Biochemistry*, 1991, **30**, 8830.
358. J. Heinemann and F. J. Sigworth, *Biophys. J.*, 1990, **57**, 499.
359. S. H. Tajima, K. Ono and N. Akaike, *Am. J. Physiol.*, 1996, **271**, C524.
360. S. B. Hladky and D. A. Haydon, *Biochim. Biophys. Acta*, 1972, **274**, 294.
361. D. W. Urry, in *Topics in Current Chemistry* (ed. F. L. Boschke), Springer-Verlag, Heidelberg, Germany, 1984.
362. S. S. Sung and P. C. Jordan, *Biophys. Chem.*, 1987, **27**, 1.
363. W. P. Grygiel and M. E. Starzak, *Biophysical Chemistry*, 1996, **60**, 39.
364. N. Jing and D. W. Urry, *Biochim. Biophys. Acta*, 1995, **1238**, 12.
365. J. F. Hinton, R. E. Koeppe, D. C. Shungu, W. L. Whaley, J. A. Paczkowski and F. S. Millett, *Biophys. J.*, 1986, **49**, 571.
366. J. F. Hinton, J. Q. Fernandez, D. C. Shungu, W. L. Whaley, R. E. Koeppe and F. S. Millett, *Biophys. J.*, 1988, **54**, 527.
367. D. W. Urry, A. Spisni and M. A. Kahled, *Biochem. Biophys. Res. Commun.*, 1979, **88**, 940.
368. A. Spisni, M. A. Khaled and D. W. Urry, *FEBS Lett.*, 1979, **102**, 321.
369. A. Pullman, *Q. Rev. Biophys.*, 1987, **20**, 173.
370. C. Etchebest and A. Pullman, *FEBS Lett.*, 1986, **204**, 261.
371. A. Pullman, *J. Biosci.*, 1986, **8**, 307.
372. C. Etchebest and A. Pullman, *J. Biomol. Struct. Dyn.*, 1986, **3**, 805.
373. C. Etchebest, A. Pullman and S. Ranganathan, *Biochim. Biophys. Acta*, 1985, **818**, 23.
374. C. Etchebest and A. Pullman, *J. Biomol. Struct. Dyn.*, 1985, **2**, 859.
375. K. S. Kim, D. P. Vercauteren, M. Welti, S. Chin and E. Clementi, *Biophys. J.*, 1985, **47**, 327.
376. K. S. Kim, H. S. Nguyen, P. K. Swaminathan and E. Clementi, *J. Phys. Chem.*, 1985, **89**, 2870.
377. K. S. Kim and E. Clementi, *J. Am. Chem. Soc.*, 1985, **107**, 5504.
378. D. W. Urry, *Bull. Magn. Reson.*, 1987, **9**, 109.
379. D. W. Urry, T. L. Trapane, C. M. Venkatachalam and K. U. Prasad, *J. Am. Chem. Soc.*, 1986, **108**, 1448.
380. D. W. Urry, T. L. Trapane and C. M. Vennkatachalam, *J. Membr. Biol.*, 1986, **89**, 107.
381. D. W. Urry, T. L. Trapane, R. A. Brown, C. M. Venkatachalam and K. U. Prasad, *J. Magn. Reson.*, 1985, **65**, 43.
382. H. Moni, *Biophys. J.*, 1985, **48**, 643.
383. D. W. Urry, T. L. Trapane, C. M. Venkatachalam and K. U. Prasad, *Can. J. Chem.*, 1985, **63**, 1976.
384. D. W. Urry, *NATO ASI* Ser. C, D. Reidel, Holland, 139, 1984.

385. D. W. Urry, T. L. Trapane, C. M. Venkatachalam and K. U. Prasad, *J. Phys. Chem.*, 1983, **87**, 2918.
386. C. M. Venkatachalam and D. W. Urry, *J. Magn. Reson.*, 1980, **41**, 313.
387. D. W. Urry, T. L. Trapane, J. T. Walker and K. U. Prasad, *J. Biol. Chem.*, 1982, **257**, 6659.
388. A. Cornelis and P. Laszlo, *Biochemistry*, 1979, **18**, 2004.
389. W. R. Veatch and J. T. Durkin, *J. Mol. Biol.*, 1980, **143**, 411.
390. R. E. Koeppe, J.-L. Mazet and O. S. Andersen, *Biochemistry*, 1990, **29**, 512.
391. B. A. Wallace, *Biophys. J.*, 1996, **71**, 163.
392. J. F. Hinton, *J. Magn. Reson. B.*, 1996, **112**, 26.
393. D. W. Urry, K. U. Prasad and T. L. Trapane, *Proc. Natl Acad. Sci. (USA)*, 1982, **79**, 390.
394. D. W. Urry, W. S. Alonso-Romanowski, C. M. Venkatachalam, R. J. Bradley and R. D. Harris, *J. Membr. Biol.*, 1984, **81**, 205.
395. F. Separovic, J. Gehrmann, T. Milne, B. A. Cornell, S. Y. Lin and R. Smith, *Biophys. J.*, 1994, **67**, 1495.
396. T. B. Woolf and B. Roux, *Biophys. J.*, 1997, **72**, 1930.
397. N. Jing, K. U. Prasad and D. W. Urry, *Biochim. Biophys. Acta*, 1995, **1238**, 1.
398. A. P. Golovanov, I. L. Barsukov, A. S. Arseniev, V. F. Bystrov, S. V. Sukhanov and L. I. Barsukov, *Biopolymers*, 1991, **31**, 425.
399. J. F. Hinton, J. Q. Fernandez, D. Shungu and F. S. Millett, *Biophys. J.*, 1989, **55**, 327.
400. J. F. Hinton, J. Q. Fernandez, D. Shungu, W. L. Whaley, R. E. Koeppe and F. S. Millett, *Biophys. J.*, 1988, **53**, 145.
401. J. F. Hinton, R. E. Koeppe, D. C. Shungu, W. L. Whaley, J. A. Paczkowski and F. S. Millett, *Biophys. J.*, 1986, **49**, 571.
402. J. F. Hinton, D. K. Newkirk and T. G. Fletcher, *J. Magn. Reson. B*, 1994, **105**, 11.
403. S. Forsen and R. A. Hoffman, *J. Chem. Phys.*, 1963, **39**, 2892.
404. S. Forsen and R. A. Hoffman, *J. Chem. Phys.*, 1964, **40**, 1189.
405. S. Forsen and R. A. Hoffman, *J. Chem. Phys.*, 1966, **45**, 2049.
406. J. R. Alger and R. G. Shulman, *Q. Rev. Biophys.*, 1984, **17**, 83.
407. J. R. Alger and J. H. Prestegard, *Biophys. J.*, 1979, **28**, 1.
408. F. G. Riddell, S. Arumugam and B. G. Cox, *J. Chem. Soc., Chem. Commun.*, 1989, 1987.
409. F. G. Riddell and S. Arumugam, *Biochim. Biophys. Acta*, 1988, **945**, 65.
410. F. G. Riddell and S. Arumugam, *Biochim. Biophys. Acta*, 1989, **984**, 6.
411. F. G. Riddell, S. Arumugam and A. Patel, *Inorg. Chem.*, 1990, **29**, 2398.
412. F. G. Riddell and M. K. Hayer, *Biochim. Biophys. Acta*, 1985, **817**, 313.
413. D. C. Buster, J. F. Hinton, F. S. Millett and D. C. Shungu, *Biophys. J.*, 1988, **53**, 145.
414. D. C. Shungu and R. W. Briggs, *J. Magn. Reson.*, 1988, **77**, 491.
415. D. C. Shungu, D. C. Buster and R. W. Briggs., *J. Magn. Reson.*, 1990, **89**, 102.
416. G. Robinson, P. W. Kuchel, B. E. Chapman, D. M. Doddrell and M. G. Irving, *J. Magn. Reson.*, 1987, **63**, 314.
417. R. K. Gupta and P. Gupta, *J. Magn. Reson.*, 1982, **47**, 344.
418. S. Chu, M. M. Pike, E. T. Fossel, T. W. Smith, J. A. Balschi and C. S. Springer, *J. Magn. Reson.*, 1984, **56**, 33.
419. M. M. Pike, S. R. Simon, J. A. Balschi and C. S. Springer, *Proc. Natl Acad. Sci. (USA)*, 1982, **79**, 810.
420. D. R. Muhandram and R. E. D. McClung, *J. Magn. Reson.*, 1987, **71**, 187.
421. J. F. Hinton, P. L. Easton, K. Newkirk and D. C. Shungu, *Biochim. Biophys. Acta*, 1993, **1146**, 191.
422. S. McKim and J. F. Hinton, *Biochim. Biophys. Acta*, 1994, **1193**, 186.
423. J. F. Hinton and A. M. Washburn-McCain, *J. Magn. Reson.*, 1997, **125**, 259.
424. P. Easton, J. F. Hinton and D. K. Newkirk, *Biophys. J.*, 1990, **57**, 63.
425. G. Jyothi, C. K. Mitra and G. Krishnamoorthy, *Bioelectro. Bioenerg.*, 1990, **24**, 297.
426. A. M. O'Connell, R. E. Koeppe and O. S. Andersen, *Science*, 1990, **250**, 1256.

427. J. T. Durkin, R. E. Koeppe and O. S. Andersen, *J. Mol. Biol.*, 1990, **211**, 221.
428. D. D. Busath and R. C. Waldbillig, *Biochim. Biophys. Acta*, 1983, **736**, 28.
429. D. Jones, E. Haydon and D. D. Busath, *Biochim. Biophys. Acta*, 1986, **861**, 62.
430. D. D. Busath and E. Haydon, *Biochim. Biophys. Acta*, 1988, **944**, 73.
431. S. McKim and J. F. Hinton, *Biochim. Biophys. Acta*, 1993, **1153**, 315.
432. C. J. Stankovic, S. H. Heinemann and S. L. Schreiber, *Biochim. Biophys. Acta*, 1991, **1061**, 163.
433. L. Kunz, U. Zeidler, S. H. Haegele, M. Przybylski and G. Stark, *Biochemistry*, 1995, **43**, 11895.
434. T. I. Rokitsksys, Y. N. Antonenko and E. Kotova, *FEBS*, 1993, **3**, 332.
435. M. Strassle and G. Stark, *Photochem. Photobiol.*, 1992, **55**, 461.
436. J. Sandblom and S. Theander, *Bioelectromagnetics*, 1991, **12**, 9.
437. S. Ranganathan, D. Kundu and M. V. Jaganadham, *Tetrahedron Letts.*, 1996, **37**, 5199.
438. T. B. Woolf, V. G. Malkin, O. L. Malkin, D. R. Salahub and B. Roux, *Chem. Phys. Letts.*, 1995, **239**, 186.
439. D. W. Deamer, *Biophys. J.*, 1996, **71**, 5.
440. R. Pomes and B. Roux, *Biophys. J.*, 1996, **71**, 19.
441. D. A. Sagnella, K. Laasonen and M. L. Klein, *Biophys. J.*, 1996, **71**, 11172.
442. S.-S. Sung and P. J. Jordan, *J. Theor. Biol.*, 1989, **140**, 369.
443. S.-W. Chiu, S. Subramanian, E. Jakobsson and J. A. McCammon, *Biophys. J.*, 1989, **56**, 253.
444. J. Aqvist and A. Warshel, *Comments Mol. Cell. Biophys.*, 1989, **6**, 91.
445. J. Wang and A. Pullman, *Biochim. Biophys. Acta*, 1990, **1024**, 10.
446. M. Oka, Y. Baba, A. K. Kagemoto and A. Nakajima, *Polymer J.*, 1990, **22**, 135.
447. P. Helfrich and E. Jakobsson, *Biophys. J.*, 1990, **57**, 1075.
448. P. Jordan, *Biophys. J.*, 1990, **58**, 1133.
449. J. Wang and A. Pullman, *Chem. Phys. Lipids*, 1991, **57**, 1.
450. T. B. Woolf and B. Roux, *Proteins: Structure, Function and Genetics*, 1996, **24**, 92.
451. S. Crouzy, T. B. Woolf and B. Roux, *Biophys. J.*, 1994, **67**, 1370.
452. T. B. Woolf and B. Roux, *Proc. Natl Acad. Sci. (USA)*, 1994, **91**, 11631.
453. B. Roux and M. Karplus, *Annu. Rev. Biophys. Biomol. Struct.*, 1994, **23**, 731.
454. M. Poxleitner, J. Seitz-Beywl and K. Heinzinger, *Z. Naturforsch.*, 1993, **48c**, 654.
455. B. Turano, M. Pear and D. D. Busath, *Biophys. J.*, 1992, **63**, 152.
456. S.-W. Chiu, E. Jakobsson, S. Subramanian and J. A. McCammon, *Biophys. J.*, 1991, **60**, 273.
457. M. Sancho and G. Martinez, *Biophys. J.*, 1991, **60**, 81.
458. H. Moni, *Biophys. J.*, 1991, **59**, 786.
459. S. Furois-Corbin and A. Pullman, *Biochim. Biophys. Acta*, 1986, **860**, 165.
460. S. Furois-Corbin and A. Pullman, *Biochim. Biophys. Acta*, 1989, **984**, 339.
461. S. Furois-Corbin and A. Pullman, *FEBS Lett.*, 1989, **252**, 63.
462. P. Jordan, in *Transport through Membranes: Carriers, Channels and Pumps* (eds A. Pullman, B. Pullman and J. Jortner), *The Jerusalem Symposium on Quantum Chemistry and Biochemistry*, vol. 21, Kluwer Academic Press, Dordrecht, 1998.
463. J. F. Hinton and A. M. Washburn, *Biophys. J.*, 1995, **69**, 435.
464. J. F. Hinton and A. M. Washburn-McCain, *J. Magn. Reson.*, 1997, **124**, 132.
465. C. K. Meyer and F. A. Reusser, *Experientia*, 1967, **23**, 85.
466. B. F. Gisin, S. Kobayashi, D. G. Davis and J. E. Hall, *Peptide Proc. Symp.* 1977, **5**, 215.
467. P. Mueller and D. O. Rudin, *Nature (London)*, 1968, **217**, 713.
468. G. Boheim, *J. Membr. Biol.*, 1974, **19**, 277.
469. D. Eisenberg, *Annu. Rev. Biochem.*, 1984, **53**, 595.
470. R. O. Fox and F. M. Richards, *Nature (London)*, 1982, **300**, 325.
471. V. Brumfeld and I. R. Miller, *Biochim. Biophys. Acta*, 1990, **1024**, 49.

472. H. Vogel, *Biochemistry*, 1987, **26**, 4562.
473. P. I. Harris and D. Chapman, *Biochim. Biophys. Acta*, 1988, **943**, 375.
474. U. P. Fringeli and M. Fringeli, *Pro. Natl Acad. Sci. (USA)*, 1979, **76**, 3852.
475. P. Ch. Rao, R. Nagaraj, C. N. R. Rao and P. Balaram, *Biochemistry*, 1980, **19**, 425.
476. L. P. Kelsh, J. F. Ellena and D. S. Cafisco, *Biochemistry*, 1992, **31**, 5136.
477. G. Esposito, J. A. Carver, J. Boyd and I. D. Campbell, *Biochemistry*, 1987, **26**, 1043.
478. U. Banerjee, R. P. Tsui, T. N. Balasubramanian, G. R. Marshall and S. I. Chan, *J. Mol. Biol.*, 1983, **165**, 757.
479. R. Nagaraj and P. Balaram, *Biochemistry*, 1981, **20**, 2828.
480. A. A. Yee and J. D. J. O'Neil, *Biochemistry*, 1992, **31**, 3135.
481. J. C. Franklin, J. F. Ellena, S. Jayasinche, L. P. Kelsh and D. S. Cafisco, *Biochemistry*, 1994, **33**, 4036.
482. L. Brachais, D. Davoust and G. Molle, *Int. J. Peptide Protein Res.*, 1995, **45**, 164.
483. A. Bax and D. G. Davis, *J. Magn. Reson.*, 1985, **63**, 207.
484. A. A. Bothner-By, R. L. Stephens, J. Lee, C. D. Warren and R. W. Jeanloz, *J. Am. Chem. Soc.*, 1984, **106**, 811.
485. K. Chandrasekhar, M. K. Das, A. Kumar and P. Balaram, *Int. J. Pept. Protein Res.*, 1988, **32**, 167.
486. J. E. Hall, I. Vodyanoy, T. M. Balasubramanian and G. R. Marshall, *Biophys. J.*, 1984, **45**, 233.
487. G. Boheim and H. A. Kolb, *J. Membr. Biol.*, 1978, **38**, 99.
488. G. Baumanand and P. Mueller, *J. Supramol. Struct.*, 1974, **2**, 538.
489. M. S. P. Sansom, *Eur. Biophys. J.*, 1993, **22**, 105.
490. G. A. Woolley and B. A. Wallace, *J. Membr. Biol.*, 1992, **129**, 109.
491. G. Boheim, S. Gelfert, G. Jung and G. Menestrina, in *Ion Transport through Membranes* (eds K. Yagi and B. Pullman), p. 131, Academic Press, Tokyo, 1987.
492. F. Fraternali, *Biopolymers*, 1990, **30**, 1083.
493. A. Pastore, T. S. Harvey, C. E. Dempsey and I. D. Campbell, *Eur. J. Biochem.*, 1989, **16**, 363.
494. L. Brachais, H. Duclohier, C. Meyer, D. Davoust and G. Molle, *Biopolymers*, 1995, **36**, 547.
495. S. Jayasinghe, M. Barranger-Mathys, J. F. Ellena, G. Franklin and D. S. Cafisco, *Biophys. J.*, 1998, **74**, 3023.
496. M. Barranger-Mathys and D. S. Cafisco, *Biochemistry*, 1996, **35**, 489.
497. C. L. North, M. Barranger-Mathys and D. S. Cafisco, *Biophys. J.*, 1995, **69**, 2392.
498. S. Rebuffat, H. Duclohier, C. Auvin-Guette, G. Molle, G. Spach and B. Bodo, *FEMS Microbiol. Immunol.*, 1992, **5**, 151.
499. S. Rebuffat, L. Conraux, M. Massias, C. Auvin-Guette and B. Bodo, *Int. J. Pept. Protein Res.*, 1993, **41**, 74.
500. S. Rebuffat, Y. Prigent, C. Auvin-Guette and B. Bodo, *Eur. J. Biochem.*, 1991, **201**, 661.
501. S. Wada, A. Iida, N. Akimoto, M. Kanai, Toyama and T. Fujita, *Chem. Pharm. Bull. (Tokyo)*, 1995, **43**, 910.
502. S. Fujita, S. Wada, A. Iida, T. Nishimura, M. Kanai and N. Toyama, *Chem. Pharm. Bull. (Tokyo)*, 1994, **42**, 489.
503. Y. Nagaoka, A. Iida and T. Fujita, *Chem. Pharm. Bull. (Tokyo)*, 1994, **42**, 1258.
504. I. L. Karle, M. Sukumar and P. Balaram, *Proc. Natl Acad. Sci. (USA)*, 1986, **83**, 9284.
505. G. J. Sharman, A. C. Try, D. H. Williams, A. M. Ainsworth, R. Beneyto, T. M. Gibson, C. McNicholas, D. V. Renno, N. Robinson, K. A. Wood and S. K. Wrigley, *Biochem. J.*, 1996, **320**, 723.
506. L. Zhu, Kemple, P. Yuan and F. G. Prendergast, *Biochemistry*, 1995, **34**, 13196.
507. C. E. Dempsey, *Biochim. Biophys. Acta*, 1990, **1031**, 143.
508. J. Cauldie, J. M. Hanson, F. D. Rumjanek, R. A. Shipolini and C. A. Vernon, *Eur. J. Biochem.*,

1976, **61**, 369.
509. J. F. Faucon, J. Dufourcq and C. Lussan, *FEBS Lett.*, 1979, **102**, 187.
510. J. C. Talbot, J. Dufourcq, J. de Bony, J.-F. Faucon and C. Lussan, *FEBS Lett.*, 1979, **102**, 191.
511. J. Lauterwein, L. R. Brown and K. Wüthrich, *Biochim. Biophys. Acta*, 1980, **622**, 219.
512. L. R. Brown, J. Lauterwein and K. Wüthrich, *Biochim. Biophys. Acta*, 1980, **622**, 231.
513. S. C. Quay and C. C. Condie, *Biochemistry*, 1983, **22**, 695.
514. C. R. Dawson, A. F. Drake, J. Helliwell and R. C. Hider, *Biochim. Biophys. Acta*, 1978, **510**, 75.
515. E. Knoppell, D. Eisenberg and W. Wickner, *Biochemistry*, 1979, **28**, 4177.
516. R. Bazzo, M. J. Tappin, A. Pastore, T. S. Harvey, J. A. Carver and I. D. Campbell, *Eur. J. Biochem.*, 1988, **173**, 139.
517. C. E. Dempsey, *Biochemistry*, 1988, **27**, 6893.
518. P. Buckley, A. S. Edison, M. D. Kemple and F. G. Prendergast, *J. Biomol. NMR*, 1993, **3**, 639.
519. C. E. Dempsey, R. Bazzo, T. S. Harvey, I. Syperek, G. Boheim and I. D. Campbell, *FEBS Lett.*, 1991, **281**, 240.
520. M. D. Kemple, P. Buckley, P. Yuan and F. G. Prendergast, *Biochemistry*, 1997, **36**, 678.
521. F. Inagaki, I. Shimada, K. Kawaguchi, M. Hirano, I. Terasawa, T. Ikura and N. Go, *Biochemistry*, 1989, **28**, 5985.
522. L. R. Brown and K. Wüthrich, *Biochim. Biophys. Acta*, 1981, **647**, 95.
523. L. R. Brown, W. Braun, A. Kumar and K. Wüthrich, *Biophys. J.*, 1982, **37**, 319.
524. J. Lauterwein, C. Bosch, L. R. Brown and K. Wüthrich, *Biochim. Biophys. Acta*, 1979, **556**, 244.
525. J. de Bony, J. Dufourcq and B. Clin, *Biochim. Biophys. Acta*, 1979, **552**, 531.
526. L. R. Brown, *Biochim. Biophys. Acta*, 1979, **557**, 135.
527. T. Ikura, N. Go and F. Inagaki, *Proteins*, 1991, **9**, 81.
528. A. Okada, K. Wakamatsu, T. Miyazawa and T. Higashijima, *Biochemistry*, 1994, **33**, 9438.
529. L. Zhu, M. D. Kemple, P. Yuan and F. C. Prendergast, *Biochemistry*, 1995, **34**, 13196.
530. P. Yuan, P. J. Fisher, F. G. Prendergast and M. D. Kemple, *Biophys. J.*, 1996, **70**, 2223.
531. T. C. Terwilliger, L. Weissman and D. Eisenberg, *Biophys. J.*, 1982, **37**, 353.
532. T. C. Terwilliger and D. Eisenberg, *J. Biol. Chem.*, 1982, **257**, 6010.
533. H. Tanaka, K. Matsunaga and H. Kawazura, *Biophys. J.*, 1992, **63**, 569.
534. G. R. Hunt, I. C. Jones and J. A. Veiro, *Biosci. Rep.*, 1984, **4**, 403.
535. T. Maurer, C. Lucke and H. Ruterjans, *Eur. J. Biochem.*, 1991, **196**, 135.
536. G. Beschiaschvili and H. D. Baeuerle, *Biochim. Biophys. Acta*, 1991, **1068**, 195.
537. M. Monette, M. R. Van Calsteren and M. Lafleur, *Biochim. Biophys. Acta*, 1993, **1149**, 319.
538. T. Pott and E. J. Dufourc, *Biophys. J.*, 1995, **68**, 965.
539. J. F. Faucon, J. M. Bonmatin, J. Dufourcq and E. J. Dufourc, *Biochim. Biophys. Acta*, 1995, **1234**, 235.
540. C. E. Dempsey and A. Watts, *Biochemistry*, 1987, **26**, 5803.
541. J. Dufourcq, J. F. Faucon, G. Foirche, J. L. Dasseux, M. LeMaire and T. Gulic-Krzywicki, *Biochim. Biophys. Acta*, 1986, **859**, 33.
542. E. J. Dufourcq, J. L. Faucon, G. Fourche, J. Dufourcq, T. Gulik-Krzywicki and M. LeMaire, *FEBS Lett.*, 1986, **201**, 205.
543. E. J. Dufourc, I. C. P. Smith and J. Dufourcq, *Biochemistry*, 1986, **25**, 6488.
544. C. E. Dempsey, G. Cryer and A. Watts, *FEBS Lett.*, 1987, **218**, 173.
545. C. E. Dempsey, M. Bitbol and A. Watts, *Biochemistry*, 1989, **28**, 6590.
546. E. J. Dufourc, J. M. Bonmatin and J. Dufourcq, *Biochimie*, 1989, **71**, 117.
547. H. C. Chen, J. H. Brown, J. L. Morell and C. M. Huang, *FEBS Lett.*, 1988, **236**, 462.
548. K. Matsuzaki, M. Harada, T. Handa, S. Funakoshi, N. Fujii, H. Yajima and K. Miyajima, *Biochim. Biophys. Acta*, 1989, **981**, 130.

549. D. Wade, A. Boman, B. Wahlin, C. M. Drain, D. Andreu, H. G. Boman and R. B. Merrifield, *Proc. Natl Acad. Sci. (USA)*, 1990, **87**, 4761.
550. R. A. Cruciana, J. L. Barker, S. R. Durell, G. Raghunathan, H. R. Guy, M. Zasloff and E. F. Stanley, *Eur. J. Pharmacol.*, 1992, **226**, 287.
551. K. Matsuzaki, O. Murase, N. Fujii and K. Miyajima, *Biochemistry*, 1995, **34**, 6521.
552. S. J. Ludtke, K. He, Y. Wu and H. W. Huang, *Biochim. Biophys. Acta*, 1994, **1190**, 181.
553. D. Marion, M. Zasloff and A. Bax, *FEBS Lett.*, 1988, **227**, 21.
554. J. Gesell, M. Zasloff and S. J. Opella, *J. Biomol. NMR*, 1997, **9**, 127.
555. B. Bechinger, M. Zasloff and S. J. Opella, *Biophys. J.*, 1998, **74**, 981.
556. B. Bechinger, Y. Kim, L. E. Chirlian, J. Gesell, J. M. Neumann, M. Montal, J. Tomich, M. Zasloff and S. J. Opella, *J. Biol. NMR*, 1991, **1**, 167.
557. B. Bechinger, M. Zasloff and S. J. Opells, *Protein Sci.*, 1993, **2**, 2077.
558. A. Ramamoorthy, F. M. Marassi, M. Zasloff and S. J. Opella, *J. Biomol. NMR*, 1995, **6**, 329.
559. B. Bechinger, L. M. Gierasch, M. Montal, M. Zasloff and S. J. Opella, *Solid State Nucl. Magn. Reson.*, 1996, **7**, 185.
560. D. J. Hirsh, J. Hammer, W. L. Maloy, J. Blazyk and J. Schaefer, *Biochemistry*, 1996, **335**, 12733.
561. B. Christensen, J. Fink, R. B. Merrifield and D. Mauzerall, *Proc. Natl Acad. Sci. (USA)*, 1988, **85**, 5072.
562. T. A. Holak, A. Engstrom, P. J. Kraulis, G. Lindberg, H. Bennich, T. A. Jones, A. M. Gronenborn and G. M. Clore, *Biochemistry*, 1988, **27**, 7620.
563. W. Xia, Q. Liu, J. Wu, Y. Xia, Y. Shi and X. Qu, *Biochim. Biophys. Acta*, 1998, **1384**, 299.
564. D. Sipos, M. Andersson and A. Ehrenberg, *Eur. J. Biochem.*, 1992, **209**, 163.
565. D. Sipos, K. Chandrasekhar, K. Arvidsson, A. Engstrom and A. Ehrenberg, *Eur. J. Biochem.*, 1991, **199**, 285.
566. S. A. Thompson, K. Tachibava, K. Nakanishi and I. Kubota, *Science*, 1986, **233**, 341.
567. N. Primor, *J. Exp. Biol.*, 1983, **105**, 83.
568. P. Renner, C. G. Caratsch, P. G. Waser, P. Lazarovici and N. Primor, *Neuroscience*, 1987, **23**, 319.
569. P. Lazarovici, N. Primor and L. M. Loew, *J. Biol. Chem.*, 1986, **261**, 16704.
570. M. G. Zagorski, D. G. Norman, C. J. Barrow, T. Iwashita, K. Tachibana and D. J. Patel, *Biochemistry*, 1991, **30**, 8009.
571. J. A. Dani and M. L. Mayer, *Curr. Opin. Neurobiol.*, 1995, **5**, 350.
572. H. A. Lester, *Annu. Rev. Biophys. Biomol. Struc.*, 1992, **21**, 267.
573. J. P. Changeux, *Trends Pharmacol. Sci.*, 1990, **11**, 485.
574. N. Unwin, *Neuron*, 1993, **10**, 31.
575. L. Sivilotti and D. Colquhoun, *Science*, 1995, **269**, 1681.
576. B. Hille, *Ionic Channels of Excitable Membranes*, Sinauer and Associates, Inc., Sunderland, MA, 1992.
577. E. Neher and B. Sakmann, *Nature*, 1976, **260**, 799.
578. D. Colquhoun and B. Sakmann, *J. Physiol. (London)*, 1985, **369**, 501.
579. N. Unwin, *J. Mol. Biol.*, 1993, **229**, 1101.
580. N. Unwin, *J. Mol. Biol.*, 1995, **373**, 37.
581. R. M. Stroud, M. P. McCarthy and M. Shuster, *Biochemistry*, 1990, **29**, 11009.
582. L. Pradier and M. G. McNamee, in *The Structure of Biological Membranes* (ed. P. Yeagle), p. 1047, CRC Press, Boca Raton, 1992.
583. F. Hucho, W. Oberthur and F. Lottspeich, *FEBS Lett.*, 1986, **205**, 137.
584. N. Unwin, *J. Struct. Biol.*, 1998, **121**, 181.
585. M. S. P. Sansom, C. Adcock and G. R. Smith, *J. Struct. Biol.*, 1998, **121**, 246.
586. S. Furois-Corbin and A. Pullman, *Biochim. Biophys. Acta*, 1986, **860**, 165.
587. S. Furois-Corbin and A. Pullman, *Biochim. Biophys. Acta*, 1989, **984**, 339.

588. S. Furois-Corbin and A. Pullman, *FEBS Lett.*, 1989, **252**, 63.
589. B. Sakmann, *Angew. Chem. Int. Ed. Engl.*, 1992, **31**, 830.
590. G. J. Kersh, J. M. Tomich and M. Montal, *Biochim. Biophys. Commun.*, 1989, **162**, 352.
591. S. Oiki, W. Danho and M. Montal, *Proc. Natl Acad. Sci. (USA)*, 1988, **85**, 8703.
592. S. Oiki, W. Danho and M. Montal, *Proc. Natl Acad. Sci. (USA)*, 1988, **85**, 2393.
593. S. Oiki, W. Danho and M. Montal, *Neuroscience*, 1987, **13**, 576.
594. S. Oiki, V. Madison and M. Montal, *Proteins: Structure, Function and Genetics*, 1990, **8**, 226.
595. J. P. Changeux, *Fida Neurosci. Award Lectures*, 1989, **4**, 21.
596. M. Oblatt-Montal, T. Iwamoto, J. M. Tomich and M. Montal, *FEBS Lett.*, 1993, **320**, 261.
597. G. Eisenman, A. Villarroel, M. Montal and O. Alvarez, in *Progress in Cell Research* (eds J. M. Ritchie, P. J. Magistrelli and L. Bolis), vol. 1, p. 195, Elsevier Science Publishers, Amsterdam, 1990.
598. E. von Kitzing, in *Modeling of Biomolecular Structures and Mechanisms* (ed. A. Pullman), p. 39, Kluwer Academic Publishers, Dordrecht, 1995.
599. C. Wang, K. Takeuchi, L. H. Pinto and R. A. Lamb, *J. Virol.*, 1993, **67**, 5585.
600. M. T. Tosteson, L. H. Pinto, L. J. Holsinger and R. A. Lamb, *J. Membr. Biol.*, 1994, **142**, 117.
601. L. H. Pinto, L. J. Holsinger and R. A. Lamb, *Cell*, 1992, **69**, 517.
602. L. J. Holsinger, M. A. Shaughnessy, A. Micko, L. H. Pinto and R. A. Lamb, *J. Virol.*, 1995, **69**, 1219.
603. F. A. Kovacs and T. A. Cross, *Biophys. J.*, 1997, **73**, 2511.
604. C. E. Cummings, G. Armstrong, T. C. Hodgman and D. J. Ellar, *Mol. Membr. Biol.*, 1994, **11**, 87.
605. D. Mulvey, G. F. King, R. M. Cooke, D. G. Doak, T. S. Harvey and I. D. Campbell, *FEBS Lett.*, 1989, **257**, 113.
606. D. G. Doak, D. Mulvey, K. Kawaguchi, J. Villalain and I. D. Campbell, *J. Mol. Biol.*, 1996, **258**, 672.
607. D. G. Reid, L. K. Maclachlan, C. J. Salter, M. J. Saunders, S. D. Jane, A. G. Lee, E. J. Tremeer and S. A. Salisbury, *Biochim. Biophys. Acta*, 1992, **1106**, 264.
608. J. M. Hill, P. F. Alewood and D. J. Craik, *Structure*, 1997, **5**, 571.
609. P. Sevilla, M. Bruix, J. Santoro, F. Gago, A. G. Garcia and M. Rico, *Biochem. Biophys. Res. Commun.*, 1993, **192**, 1238.
610. J. J. Skalicky, W. J. Metzler, D. J. Ciesla, A. Galdes and A. Pardi, *Protein. Sci.*, 1993, **2**, 1591.
611. P. K. Pallaghy, B. M. Duggan, M. W. Pennington and R. S. Norton, *J. Mol. Biol.*, 1993, **234**, 405.
612. M. J. Lew, J. P. Flinn, P. K. Pallaghy, R. Murphy, S. L. Whorlow, C. E. Wright, R. S. Norton and J. A. Angus, *J. Mol. Biol.*, 1997, **272**, 12014.
613. K. J. Nielsen, L. Thomas, R. J. Lewis, P. F. Alewood and D. J. Craik, *J. Mol. Biol.*, 1996, **263**, 297.
614. M. Raditsch, M. Geyer, H. R. Kalbitzer, W. Jahn, J. P. Ruppersberg and V. Witzemann, *Eur. J. Biochem.*, 1996, **240**, 416.
615. V. J. Basus, L. Hadasdi, J. Ramachandran and G. P. Miljanich, *FEBS Lett.*, 1995, **370**, 163.
616. T. Kohno, J. I. Kim, K. Kobayashi, Y. Kodera, T. Maeda and K. Sato, *Biochemistry*, 1995, **34**, 10256.
617. J. I. Kim, S. Konishi, H. Iwai, T. Kohno, H. Gouda, I. Shimada, K. Sato and Y. Arata, *J. Mol. Biol.*, 1995, **250**, 659.
618. S. Farr-Jones, G. P. Miljanich, L. Nadasdi, J. Ramachandran and V. J. Basus, *J. Mol. Biol.*, 1995, **248**, 106.
619. M. D. Reily, V. Thanabal and M. E. Adams, *J. Biomol. NMR*, *1995*, **5**, 122.
620. H. Yu, M. K. Rosen, N. A. Saccomano, D. Phillips, R. A. Volkmann and S. L. Schreiber, *Biochemistry*, 1993, **32**, 13123.

621. M. E. Adams, I. M. Mintz, M. D. Reily, V. Thanabal and B. P. Bean, *Mol. Pharmacol.*, 1993, **44**, 681.
622. W. Massefski, A. G. Redfield, D. R. Hare and C. Miler, *Science*, 1990, **249**, 521.
623. F. Bontems, C. Roumestand, P. Boyot, B. Gilquin, Y. Doljansky, A. Menez and F. Toma, *Eur. J. Biochem.*, 1991, **196**, 19.
624. F. Bontems, C. Roumestand, B. Gilquin, A. Menez and F. Toma, *Science*, 1991, **254**, 1521.
625. B. A. Johnson and E. E. Sugg, *Biochemistry*, 1992, **31**, 8151.
626. M. F. Fray, J. M. Lancelin, M. Hollecker and D. Marion, *Eur. J. Biochem.*, 1993, **211**, 813.
627. S. Meunier, J. M. Bernassau, J. M. Sabatier, M. F. Martin-Eauclaire, J. Van Rietschoten, C. Cambillau and H. Darbon, *Biochemistry*, 1993, **32**, 11969.
628. J. C. Martins, F. J. Van de Ven and F. A. Borremans, *J. Mol. Biol.*, 1995, **253**, 590.
629. M. Dauplais, B. Gilquin, L. D. Possani, G. Gurrola-Briones, C. Roumestand and A. Menez, *Biochemistry*, 1995, **34**, 16563.
630. T. R. Dyke, B. M. Duggan, M. W. Pennington, M. E. Byrnes, W. R. Ke and R. S. Norton, *Biochim. Biophys. Acta*, 1996, **1292**, 31.
631. V. A. Jaravine, D. E. Nolde, M. J. Reibarkh, Y. V. Korolkova, S. A. Kozlov, K. A. Pluzhnikov, E. V. Grishin and A. S. Arseniev, *Biochemistry*, 1997, **36**, 1223.
632. M. Delepierre, A. Prochnicka-Chalufour and L. D. Possani, *Biochemistry*, 1997, **36**, 2649.
633. T. C. Teneholz, R. S. Rogowski, J. H. Collins, M. P. Blaustein and D. J. Weber, *Biochemistry*, 1997, **36**, 2763.
634. E. Buisine, J. M. Wieruszeski, G. Lippens, D. Wouters, A. Tartar and P. Sautiere, *J. Pept. Res.*, 1997, **49**, 545.
635. E. Blanc, C. Lecomte, J. V. Rietschoten, J. M. Sabatier and H. Darbon, *Proteins*, 1997, **29**, 359.
636. E. Blanc, J. M. Sabatier, R. Kharrat, S. Meunier, M. el Ayeb, J. V. Rietschoten and H. Darbon, *Proteins*, 1997, **29**, 321.
637. K. Wakamatsu, D. Kohda, H. Hatanaka, J. M. Lancelin, Y. Ishida, M. Oya, H. Nakamura, F. Inagaki and K. Sato, *Biochemistry*, 1992, **31**, 12577.
638. F. Lebreton, M. Delepierre, A. N. Ramirez, C. Balderas and L. D. Possani, *Biochemistry*, 1994, **33**, 11135.
639. M. Chahine, L. Q. Chen, N. Fotouhi, R. Walsky, D. Fry, V. Santarelli, R. Horn and R. G. Kallen, *Receptors Channels*, 1995, **3**, 161.
640. D. O. Omecinsky, K. E. Holub, M. E. Adams and M. D. Reily, *Biochemistry*, 1996, **35**, 2836.
641. J. M. Hill, P. F. Alewood and D. J. Craik, *Biochemistry*, 1996, **35**, 8824.
642. C. Landon, P. Sodano, B. Cornet, J. M. Boumatin, C. Koneyan, H. Rochat, F. Vovelle and M. Ptak, *Proteins*, 1997, **28**, 360.
643. E. Blanc, O. Hassani, S. Meunier, P. Mansuelle, F. Sampieri, H. Rochat and H. Darbon, *Eur. J. Biochem.*, 1997, **247**, 1118.
644. J. I. Fletcher, B. E. Chapman, J. P. Mackay, M. E. Howden and G. F. King, *Structure*, 1977, **5**, 1525.
645. G. Lippens, J. Najib, S. J. Wodak and A. Tartar, *Biochemistry*, 1995, **34**, 13.
646. C. Landon, B. Cornet, J. M. Bonmatin, C. Kopeyan, H. Rochat, F. Vovelle and M. Ptak, *Eur. J. Biochem.*, 1966, **236**, 395.
647. A. M. Krezel, C. Kasibhatla, P. Hidalgo, R. MacKinnon and G. Wagner, *Protein Sci.*, 1995, **4**, 1478.
648. J. Aiyar, J. M. Withka, J. P. Rizzi, D. H. Singleton, G. C. Andrews, W. Lin, J. Boyd, D. C. Hanson, M. Simon and B. Dethlefs, *Neuron*, 1995, **15**, 1169.
649. S. R. Durell and H. R. Guy, *Neuropharmacology*, 1996, **35**, 761.
650. P.-K Yang, C.-Y. Lee and M.-J. Hwang, *Biophys. J.*, 1997, **72**, 2479.
651. W. F. DeGardo, Z. R. Wasserman and J. D. Lear, *Science*, 1989, **243**, 622.
652. K. S. Åkerfeldt, J. D. Lear, Z. R. Wasserman, L. A. Chung and W. F. DeGardo, *Acc. Chem. Res.*, 1993, **26**, 191.

653. G. Esposito, P. Dumy, V. Varma, M. Mutter and G. Bodenhausen, *Biopolymers*, 1997, **41**, 27.
654. G. W. Gokel, *Science Progress*, 1998, **81**, 153.
655. I. Tabushi, Y. Kuroda and K. Yokota, *Tetrahedron Lett.*, 1982, **23**, 4601.
656. U. F. Kragton, M. F. Roks and R. J. M. Nolte, *J. Chem. Soc., Chem. Commun.*, 1985, 1275.
657. T. M. Fyles, T. D. James and K. C. Kaye, *J. Am. Chem. Soc.*, 1993, **115**, 12315.
658. M. J. Pregel, L. Julien and J. M. Lehn, *Angew. Chem., Intl. Ed. Engl.*, 1992, **31**, 1637.
659. R. Ghadiri, J. R. Granja and L. K. Buehler, *Nature*, 1994, **369**, 301.
660. A. Nakano, Q. Xie, J. V. Mallen, L. Echegoyen and G. W. Gokel, *J. Am. Chem. Soc.*, 1990, **112**, 1287.
661. K. Pervushin, R. Riek, W. Gerhard and K. Wüthrich, *Proc. Natl Acad. Sci. (USA)*, 1997, **94**, 12366.
662. K. Pervushin, R. Riek, G. Wider and K. Wüthrich, *J. Am. Chem. Soc.*, 1998, **120**, 6394.
663. K. Wüthrich, *Nat. Struct. Biol.*, 1998, **5**, 492.

Applications of Heteronuclear X,Y-Correlation Spectroscopy in Organometallic and Organoelement Chemistry

DIETRICH GUDAT

Institut für Anorganische Chemie der Universität Bonn, Gerhard-Domagk-Strasse 1, D-53121 Bonn, Germany

1. INTRODUCTION

The unique power of NMR spectroscopy as a tool for structure elucidation in molecular systems is owing to the fact that it not only provides information on the chemically distinguishable atoms within a molecule and allows characterization of their environment by using the information available from the chemical shifts and perhaps relaxation parameters, but also elucidates the connectivity between the different atomic fragments. The source of this information is coupling interactions between the different nuclei which may either arise from direct dipole–dipole interactions or from indirect interactions which are transmitted via the electrons in chemical bonds. Dipolar couplings operate through space and may occur both inter- and intramolecularly, while indirect or *J*-couplings are strictly intramolecular. The analysis of *J*-coupling networks, which are frequently available from high-resolution NMR spectra of molecular systems in solution, allows

ANNUAL REPORTS ON NMR SPECTROSCOPY
VOLUME 38 ISBN 0-12-505338-X

characterization of the chemical bond pattern and thus provides an effective means for the (qualitative) elucidation of molecular constitutions.

An exceptionally ingenious method for the analysis of such coupling networks is multidimensional NMR. In particular, 2D shift correlated spectra[1,2] offer a means not only for the detection of couplings and the determination of their magnitudes, but also for mapping bond paths or interatomic distances, and thus allow direct visualization of molecular connectivities which are the basis of structure determination.[3] Since the recording of multidimensional NMR spectra with high resolution in more than one dimension is often time and resource consuming, in the last few years alternative strategies to collect the desired connectivity information were explored. One frequently used approach relies on a back-transformation of an n-dimensional experiment by replacing a hard excitation pulse by a frequency-selective "soft" pulse which excites only a single resonance, and then recording an $(n-1)$-dimensional spectrum with a fixed mixing time rather than acquiring an array of spectra with incremented mixing times.[4] In the case of a 2D experiment, this procedure boils down to measurement of a single 1D cross-section which contains only the connectivities of the selectively excited source nucleus. To obtain the whole information content of the 2D experiment, one needs to record a selective 1D spectrum for each chemically distinguishable nucleus. However, since the number of distinguishable heteronuclei in most organometallic and organoelement compounds is generally much smaller than the number of increments in a 2D experiment, this approach may result in substantial gains in instrument time and storage space as compared to recording a complete 2D matrix. In the extreme case, viz. for compounds with only one heteroatom, the whole information of a 2D spectrum is in principle available from a single 1D experiment, even if only "hard" (non-selective) excitation is employed.

Heteronuclear correlation spectroscopy between different nuclei offers, beside the structural information, the further advantage of measuring NMR parameters of nuclei with low gyromagnetic ratios γ at enhanced sensitivity. This enhancement is owing to the fact that the signal-to-noise ratio (S/N) of any NMR experiment involving information transfer between two nuclei depends on the gyromagnetic ratio of both the excited (γ_{exc}) and the detected nucleus (γ_{det}) and can, neglecting relaxation effects, be expressed by Eq. (1):[5]

$$S/N \propto \gamma_{exc} * \gamma_{det}^{3/2} \tag{1}$$

Thus, for an IS spin system with $\gamma_I > \gamma_S$, a correlation experiment with initial excitation of I and detection of S after a single coherence transfer brings a gain in sensitivity of the factor γ_I/γ_S with respect to a standard one-pulse experiment on the S nucleus. Further enhancement by an additional factor of $(\gamma_I/\gamma_S)^{1/2}$ can be obtained for an experiment starting with excitation of S and

detection of I after a coherence transfer in the reverse direction, while the highest efficient scheme would be one which starts and finishes with I magnetization and involves two coherence transfer steps, with a further gain in S/N of γ_I/γ_S. Two- and multidimensional experiments of this type have been called inverse or indirect NMR spectroscopy because the nucleus S is characterized indirectly through its satellites in the I spectrum.

1D and *n*D heteronuclear correlations involving either one or two coherence transfer steps between ^{1}H and heteronuclear spins ^{n}X have been widely applied for almost any spin-half nucleus.[3,5–8] Protons as source and/or receptor is particularly advantageous for several reasons: protons are available in a vast number of molecular systems, so that a wide variety of organic and biological as well as inorganic or organometallic samples can be studied; protons have, apart from the short-lived isotope ^{3}H, the largest gyromagnetic ratio of all nuclei, thus yielding the highest possible signal enhancement factors; protons have frequently shorter T_1 relaxation times, thus allowing to speed up experiments by using faster pulse repetition rates; and last but not least, these experiments can be carried out with the standard equipment of most commercial NMR spectrometers. Even though ^{1}H,^{n}X correlations are in principle also possible with quadrupolar nuclei ($I(^n\mathrm{X}) > \frac{1}{2}$), such experiments are frequently prevented by very high transversal relaxation rates $1/T_2$ of the quadrupole nucleus which are easily smaller than the magnitude of ^nJ(H,X) used for coherence transfer and lead to a quantitative decay of the correlation signal prior to acquisition.[5] However, correlation spectra have been successfully obtained in cases where the quadrupolar relaxation is ineffective due to small quadrupole moments (^{2}D, ^{6}Li) or small electric field gradient (highly symmetric molecules).[8]

In principle, heteronuclear correlation experiments are not confined to the combination ^{1}H,^{n}X, but any other nucleus can likewise be used as a source or receptor nucleus. The application of such ^{n}X,^{m}Y correlations can be desirable for many inorganic or organoelement compounds where the necessary through-bond communication between protons and heteronuclei is absent, either because protons are not present at all, or because $^nJ(^1\mathrm{H},^n\mathrm{X})$ couplings are vanishingly small and the long-range coherence transfer becomes very ineffective due to relaxation-induced magnetization losses. This situation occurs frequently in transition metal complexes or in compounds which require sterically bulky substituents for the reason of stabilization, where protons cover only the surface of a molecule and are separated by long bond paths from magnetically active heteronuclei. Last, but not least, ^{n}X,^{m}Y correlated spectroscopy can be considered an elegant experiment because it allows to detect directly the connectivity between magnetically active heteroatoms in the molecular skeleton.

Even if ^{n}X,^{m}Y correlation spectroscopy imposes no principle differences with respect to ^{1}H,^{m}Y correlations, its widespread use was until recently limited by hardware restrictions: recording of such spectra under additional ^{1}H

de-coupling requires three independent radio-frequency channels on both spectrometer and probe head, whereas the standard equipment contained only two channels which were reserved for ^{1}H and one ^{n}X nucleus. A change in this situation was triggered during the last years by the introduction of multidimensional ^{1}H, ^{13}C, ^{15}N or ^{1}H, ^{13}C, ^{31}P triple-resonance pulse schemes as key experiments for the structure determinations of proteins and nucleotides.[3] The booming interest in these studies led to a wider availability of spectrometers capable of triple-resonance experiments, and today these experiments can be carried out in many laboratories on a routine basis.

Acknowledging the increasing importance of $^{n}X,^{m}Y$ correlations in inorganic, organoelement and organometallic chemistry which is reflected, beside a large number of original publications, in the fact that certain aspects of this topic have attracted attention in several recent review articles,[7–14] we will focus in this chapter on a discussion of the currently employed techniques and their application for compound characterization in these fields. Only solution NMR will be considered, and apart from some basic examples, a general account on structure determination of biomolecules is considered beyond the scope of this article. The material is organized in four principal sections. Following this introduction, we will first discuss the methodological aspects of experiments which employ heteronuclear coherence transfer for measurement or assignment of chemical shifts, coupling constants, or relaxation times. This part will not be restricted to heteronuclear 2D- or 3D-shift correlation experiments, but includes also selective and non-selective 1D techniques designed in particular for the measurement of heteronuclear couplings and chemical shifts of low-γ nuclei, spin-echo experiments intended for multiplicity editing, and experiments with "passive" selection of satellite lines. The third section contains an overview on the application of these techniques in inorganic, organoelement and organometallic chemistry, and finally a short résumé will be given containing concluding remarks and some comments on future prospects.

2. METHODS

In contrast to biological applications, where $^{n}X,^{m}Y$ correlations are frequently executed as three-dimensional experiments with ^{1}H detection because of sensitivity reasons,[15] $^{n}X,^{m}Y$ correlation experiments on inorganic or organometallic systems are mostly performed by using two- or even one-dimensional techniques operating with direct detection of one heteronucleus. Considering that there is no general agreement about the nomenclature of $^{n}X,^{m}Y$ correlation spectroscopy, we will throughout this review use the following conventions: The term "$^{n}X,^{m}Y$" correlation is applied in a somewhat extended context, covering all one- and multidimensional experiments involving at least one direct coherence transfer between two different

heteronuclei. The detected nucleus is always written first; all other nuclei engaged in coherence transfer steps during the experiments follow, separated by commas (thus, the second nucleus represents in general the source nucleus in a 1D polarization transfer experiment, and the indirectly detected nucleus in a 2D experiment). Additional nuclei in { } are decoupled during a particular time period in the experiment. Notation of a nucleus in ( ) denotes that the corresponding satellite lines are selected passively, i.e. without applying pulses to this nucleus; experiments of this type are dubbed "pseudo" triple- or quadruple-resonance experiments.

2.1. Hardware considerations

Heteronuclear NMR experiments, which can be performed with the standard equipment of practically all modern spectrometers, require in general three separate radiofrequency (RF) channels for both spectrometer and probe head. The first two channels deliver the ^{1}H (for decoupling) and ^{n}X frequencies to the sample, and the third channel is commonly tuned to ^{2}D and operates the field frequency lock. In most standard probe heads, these three frequencies are delivered via two concentric coils.[16] The inner coil with the higher Q factor is generally used for detection, the outer one only for the application of pulses and decoupling. Two general designs are in use: in "normal" or forward probe heads, which are optimized for direct detection of X nuclei, the inner coil is a tuneable X coil and the outer coil is normally double tuned to ^{1}H and the lock frequency, while in "inverse" probe heads which are optimized for indirect detection of ^{n}X resonances via ^{1}H, this order is reversed.

Considering that, as other ^{n}X detected NMR experiments, $^{n}X,^{m}Y$ correlations are preferably recorded under proton decoupling, the experiments discussed in this review are generally triple-resonance experiments. The integration of an additional RF source in the spectrometer is straightforward and is as a consequence of the booming investigation of biological samples standard in most NMR spectrometers built in the last decade and has in many NMR laboratories been also adapted to older instruments. In contrast, the design of probe heads capable to deliver the additional radiofrequency of the Y nucleus to the sample requires some more thought. Several different architectures are in use, and the selection of a special one generally depends on the specific field of research.

The most simple design for a triple-resonance probe head contains two doubly tuned coils adjusted to the frequencies of ^{1}H, ^{2}D and two different heteronuclei (popular combinations include $^{13}C/^{15}N$, or $^{13}C/^{31}P$ which are useful in protein or nucleotide research). Since all frequencies in such a probe are fixed, it may easily be optimized and offers the most sensitive arrangement for the acquisition of $^{n}X,^{m}Y$ correlations. However, the drawback of this

architecture is obvious, since it is restricted to the special spin-triple once selected and may thus have only limited applicability for work in organometallic and organoelement chemistry.

An architecture which offers more variability is based essentially on a multinuclear probe head whose ^{1}H coil is triply tuned to deliver the additional ^{m}Y frequency and offers the possibility to perform triple-resonance experiments with a fixed nucleus ^{m}Y, but a choice of ^{n}X. The selection of the fixed channel depends on the intended usage; the most common options are ^{31}P and ^{13}C which offer widespread applicability in organometallic and coordination chemistry. For a good performance it is mandatory that RF interferences between the different channels are eliminated by appropriate filtering. Even if this arrangement is still less flexible than a probe head in which both ^{n}X and ^{m}Y are variable, it appears preferable because the presence of two tuneable broadband coils would probably lower sensitivity, and the handling would be rather difficult because of increased RF interference problems.

As standard multinuclear probe heads, variable triple-resonance probe heads may be constructed in either "forward" or "inverse" architecture. "Forward" probe heads are optimized for direct detection of X-nuclei via the tuneable inner coil and may yield similar performances as conventional broadband probes. As there, observation of nuclei assigned to the outer coil is only possible with reduced sensitivity, but this presents no problem for the acquisition of ^{1}H spectra, and for ^{m}Y nuclei of high receptivity such as ^{31}P, $^{m}Y\{^{1}H\}$ spectra and even $^{m}Y,^{n}X$ correlations can be acquired to our experience in acceptable time. In "inverse" probe heads, the inner coil is usually triply tuned to ^{1}H, ^{2}D and the additional heteronucleus ^{m}Y.[10] Although this architecture is certainly not the best choice for obtaining optimum sensitivity on the ^{m}Y channel, it can be easily used to measure $^{1}H,^{n}X$ and $^{n}X,^{m}Y$ correlations as ^{1}H detected 2D or 3D experiments, thus combining high flexibility with high sensitivity for the acquisition of heteronuclear NMR spectra of dilute samples. As in the case of conventional multinuclear probe heads, the tuning capability of the broadband X-coil covers normally not the whole range of heteronuclei; the standard range includes resonance frequencies from ^{31}P to ^{109}Ag (however, it was found that coils of this type can be tuned down to ^{183}W[17]), and for use with very low-γ nuclei (^{57}Fe, ^{103}Rh, ^{183}W, ^{187}Os) special probes with dedicated low-frequency coils are available.[18,19]

It should be mentioned that in cases where one of the heteronuclei is ^{19}F, ^{2}D or ^{6}Li, the use of designated triple-resonance probe heads for $^{n}X,^{m}Y$ correlations can be avoided, and standard equipment may be used. The resonance frequency of ^{19}F is far outside the range of other heteronuclei, but close to the ^{1}H frequency, so that ^{19}F, ^{n}X correlations can frequently be performed by detuning the proton coil of a standard multinuclear probe head.[20–22] Even if this procedure may result in longer pulses and some loss of sensitivity for experiments with ^{19}F detection, many experiments are still practicable due to the high receptivity of fluorine.[20,22] Of course, experiments with this set-up

have to be performed without proton decoupling, but this does not represent a severe restriction for investigation of many inorganic fluoro compounds or perfluorinated organyls where hydrogen atoms are absent anyway. For spectrometers which are unable to deliver pulses at the ^{19}F and ^{n}X frequencies at the same time, a workaround has been suggested in which one of the two radiofrequencies is taken from a different spectrometer console.[22]

The use of a specially designated triple resonance probe for ^{2}D,^{m}Y correlations may be avoided, since in principle pulses on deuterium can be transmitted through the lock channel of a standard multinuclear probe.[23,24] Due to the similarity of the resonance frequencies of ^{2}D and ^{6}Li, this set-up can also be used for ^{6}Li,^{m}Y correlations,[25–27] even without detuning the probe channel.[27] Naturally, since the lock channel is used for delivering pulses, these experiments must be performed either on spectrometers which offer an external lock facility (some ^{13}C,^{6}Li correlations with external ^{19}F lock were reported[25,28]), or in unlocked mode. Even if this might result in some degradation of the spectra, the field stability of modern superconducting magnets is usually sufficient to perform such experiments over a duration of several hours. As compared to the use of a dedicated triple-resonance probe, the use of the lock channel to transmit pulses results in considerably longer pulse widths (^{6}Li 90° pulse widths of several hundredths of a microsecond have been mentioned[27]).

2.2. Pulse sequences

(Pseudo)-^{n}X {^{m}Y}-INDOR and selective decoupling experiments

As early as 1971, McFarlane and co-workers used ^{19}F{^{31}P} and ^{19}F {^{183}W}-INDOR schemes for indirect recording of ^{31}P and ^{183}W chemical shifts of the reaction products of tungsten hexafluoride with trimethyl phosphite.[29] With the introduction of FT spectrometers, the INDOR technique became obsolete, but still a combination of selective decoupling and difference spectroscopy could be used to produce pseudo-INDOR spectra.[30] An alternative and less complicated approach turned out to be observation of the ^{n}X{^{1}H} signal of a scalar coupled ^{n}X,^{m}Y spin system under cw-decoupling in the ^{m}Y channel and stepping the decoupler frequency through the chemical shift range of interest until the collapse of the multiplet indicates that the decoupler is on resonance.[31–35] Naturally, the described procedure requires that the splitting due to $J(^{n}X,^{m}Y)$ in the ^{n}X spectrum must be resolved and directly observable, so that for rare ^{m}Y nuclei isotopic enrichment may be necessary. Today, this technique has been largely superseded by the more powerful inverse detected two-dimensional spectroscopy, even though some recent applications[34,35] indicate that this approach may still be useful for special reports.

Recording of a series of ^{n}X{^{1}H} spectra under selective decoupling of one

^{m}Y nucleus at a time may also be useful as a simple approach to assign individual heteronuclear couplings and thus determine intramolecular connectivities,[36,37] as long as the number of ^{m}Y resonances is small and their chemical shifts are known. If the decoupling power is further reduced to irradiate only a single line, or a part of a multiplet, this approach may even be applied to determine relative signs of heteronuclear ^{n}X,^{m}Y coupling constants.[36,38]

One-dimensional ^{n}X,^{m}Y pulse experiments

One-dimensional experiments involving direct heteronuclear ^{n}X,^{m}Y coherence transfer via scalar couplings can in principle be divided in two categories, depending if the excited nucleus or its coupling partner is used for signal detection. Experiments of the first type, which involve merely a modulation of the excited ^{n}X magnetization by heteronuclear couplings, are used for spectral editing purposes. Experiments in the second category proceed under net magnetization transfer and have been applied both for spectral editing, and for sensitivity enhancement in NMR spectroscopy of low-γ nuclei. Heteronuclear ^{n}X,^{m}Y magnetization transfer via dipolar interactions (heteronuclear NOE) has been studied in one case,[39] but a more widespread use of such experiments is discouraged by the general expectation that observable effects will be small to negligible, owing to low contributions of ^{n}X,^{m}Y dipolar interactions to the overall relaxation rate of most heteronuclei.

Experiments involving net heteronuclear magnetization transfer between two spin-half nuclei have been performed using standard INEPT[40] and DEPT[41,42] pulse schemes. DEPT sequences have been implemented as ^{n}X,^{m}Y double-resonance[43–46] or ^{n}X,^{m}Y{^{1}H} triple-resonance experiments[44,47] (Fig. 1(a)). While ^{n}X,^{1}H DEPT spectra are conventionally recorded under decoupling of the source nucleus ^{1}H during acquisition, ^{m}Y decoupling in bis-heteronuclear DEPT was restricted to a ^{13}C {^{19}F} experiment aimed at the generation of isotope-edited ^{13}C spectra for structural assignment purposes.[44]

^{n}X,^{m}Y INEPT experiments were preferably carried out without decoupling of ^{m}Y. This allows to omit a refocusing period and to detect the created antiphase magnetization directly after the mixing pulses. Whereas at first no proton decoupling was applied,[43,48–50] this was added later,[47] leading to the pulse scheme of Fig. 1(b). In addition to having a smaller number of pulses than a refocused INEPT, this sequence is also shorter, and thus less sensitive to relaxation-induced losses,[47] than both the refocused INEPT and DEPT.

Beside the standard implementation, two versions of soft ^{n}X,^{m}Y INEPT experiments with frequency selective excitation of source nuclei have been reported which may be useful as selective 1D analogues of 2D experiments.[51] In one case, selectivity was introduced by replacing the hard ^{m}Y pulses by

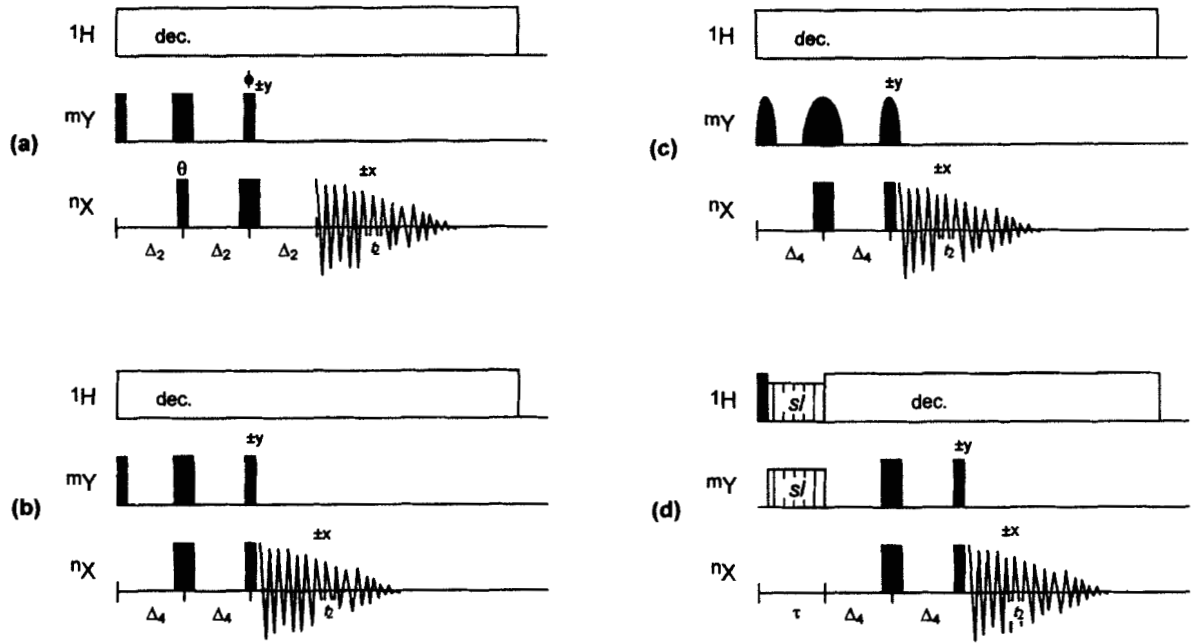

Fig. 1. Pulse sequences for 1D-^{n}X, ^{m}Y{^{1}H} polarization transfer experiments. If not stated otherwise, narrow and wide bars denote 90° and 180° hard pulses, narrow and wide ellipsoids 90° and 180° shaped pulses. Essential phase cycles for selection of the polarization transfer signal are given on top of the pulses, if no phase is indicated, pulses are applied along the x-axis; Δ_n denotes a fixed delay of length $(nJ(X,Y))^{-1}$. (a) UPT[54] (ϕ, $\theta \neq 90°$)/DEPT (ϕ, $\theta = 90°$), (b) unrefocused INEPT, (c) unrefocused selective INEPT with soft pulses, (d) INEPT with selective excitation via ^{1}H,^{m}Y cross-polarization; *sl* denote WALTZ-17 spinlock pulse trains which were applied for a period $\tau \sim (2J(^{1}H,Y))^{-1}$.[51]

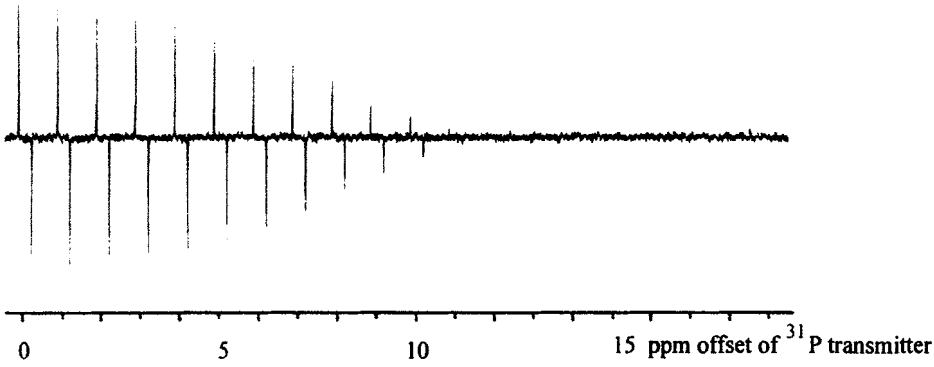

Fig. 2. ^{15}N signal of $P(NMe_2)_3$ (60% v/v in C_6D_6) obtained with the pulse sequence of Fig. 1(d) on a 300 MHz instrument. The transmitter was set on resonance for the first spectrum, and was shifted to higher field by 121.5 Hz (1 ppm) for each additional increment. Reprinted, with permission, from ref. 51. Copyright 1995 Academic Press.

shaped pulses (Fig. 1(c)). A comparison of different wave forms showed that the use of Q5 (90°) and Q3 (180°) quaternion pulses[52] yielded 25–30% higher signal-to-noise ratio than simple 90° and 180° gaussian pulses. Alternatively, selective excitation of ^{m}Y source nuclei was realized by replacing the excitation pulse of a hard INEPT experiment by a ^{1}H,^{m}Y cross-polarization sequence. The latter is a sandwich of a hard 90°(^{1}H) pulse followed by synchronized WALTZ-17 pulse trains which are simultaneously applied to ^{1}H and ^{m}Y during a mixing time τ and represent a heteronuclear spinlock (Fig. 1(d)). The method exploits the fact that the excitation bandwidth of such heteronuclear cross-polarization schemes in liquids is strongly limited due to its sensitivity to Hartmann–Hahn mismatch.[53] Even if this approach yields a lower selectivity than the application of shaped pulses, it is suited for band selective excitation of ^{n}X nuclei with a large chemical shift dispersion (Fig. 2).[51] An additional advantage is that, as a consequence of the initial ^{1}H,^{m}Y magnetization transfer step, an enhancement factor γ_H/γ_X (rather than γ_Y/γ_X as in a simple ^{n}X,^{m}Y polarization transfer experiment) is reached.

A number of ^{n}X, ^{m}Y coherence transfer experiments involving polarization transfer from or to quadrupolar nuclei were performed by using both INEPT and the universal polarization transfer (UPT) scheme[54] (Fig. 1(a)) which is a generalization of DEPT. The use of the INEPT method is unproblematic. It can be applied without modification for polarization transfer from any number of equivalent spin-half nuclei to a nucleus of arbitrary spin,[55] and a report on successful measurement of ^{13}C,^{2}D INEPT spectra also demonstrated its utilization for magnetization transfer from a quadrupolar to a spin-half nucleus.[23] Application of the UPT scheme requires appropriate adjustment of the variable pulses ϕ and θ to the spin and number of the

source and target nuclei, respectively. An expression for the calculation of optimum pulse angles has been derived theoretically[55] and its validity was experimentally verified for polarization transfer from ^{2}D to ^{13}C and ^{11}B, and from ^{11}B to ^{2}D.[56] It should be noted that the particular feature of DEPT between spin-half nuclei, i.e. the occurrence of undistorted multiplets in coupled spectra, is no longer conserved in UPT as soon as quadrupolar nuclei are involved. Thus, ^{13}C, ^{2}D UPT signals of CD_3 groups show up as 1:2:1 rather than the normal 1:1:1 triplets, and the ^{2}D, ^{11}B UPT signal of $[^{11}B]D_4^-$ appeared as a 1:2:2:1 rather than a 1:1:1:1 multiplet.[56]

One-dimensional $^{n}X,^{m}Y$ correlated experiments in which ^{n}X is both the excited and the detected nucleus have been performed with the purpose of detection of low abundant ^{n}Y satellites (isotope editing), or analysis of the number of ^{m}Y coupling partners of an individual ^{n}X nucleus. Isotope editing experiments were generally carried out with a one-dimensional version of the two-dimensional HMQC pulse scheme described in the next section.[57–59] Frequently less time consuming than a full two-dimensional experiment, the one-dimensional pulse scheme is particularly useful to extract low-intensity satellites obscured under the base of much more intense parent signals of ^{n}X nuclei coupled to magnetically inactive isotopes of Y, or to measure accurate coupling constants.[58,59]

Spin-echo spectroscopy which monitors the modulation of ^{n}X magnetization by $J(^{n}X,^{m}Y)$ couplings was employed for spectral editing of resonances of CD_n[60–62] and $C[^{6}Li]_n$[26] groups. The same methods as for $^{13}C,^{1}H$ spin systems were used, introducing amplitude modulation of the $^{13}C\{^{n}Y\}$ signal at the end of a 90° (^{13}C)-τ-180°(^{13}C)-τ sequence either by decoupling ^{n}Y during one half of the echo, or by applying a 180°(Y) pulse simultaneously to the 180° (^{13}C) pulse, and it was shown that for CY_n groups where Y is a spin-1 nucleus, the signal amplitudes are given by $I = I_0[1/3 + 2/3\cos(2\pi J(X,Y)\tau)]^n$.[62] Even if this confirms that for $\tau = (2\pi J)^{-1}$ a phase modulation of the ^{n}X signals depending on the number of coupled spin-1 nuclei occurs, the large reduction in signal intensities (XY_n spin systems with $n = 1, 2, 3, 4, 6$ give echo intensities of 33, 11, 3.7, 1.2 and 0.1% of the signal intensity in an $^{n}X\{^{m}Y\}$ spectrum) makes this experiment impractical for most applications.[9]

Two-dimensional $^{n}X,^{m}Y$ correlations

Having experienced a continuously increasing importance during the last years, two-dimensional experiments represent now the most widespread and most frequently employed methods for $^{n}X,^{m}Y$ shift correlation. Similar to one-dimensional experiments, both "direct" schemes which excite ^{m}Y and detect ^{n}X magnetization, and "inverse" schemes which start and end with ^{n}X magnetization, are in use. Most examples of $^{n}X,^{m}Y$ correlations reported so far involve cases where the indirectly observed ^{m}Y nucleus is a spin-half species, while the detected nucleus may be either spin-half or quadrupolar. In

these cases, the commonly employed pulse sequences for $^{1}H,^{n}X$ heteronuclear correlation were applied without change, while for indirect detection of quadrupolar nuclei in some cases modifications were proposed which will be discussed below.

Apart from a single example of a $^{13}C,^{6}Li$ HOESY experiment,[39] all reported $^{n}X,^{m}Y$ correlations were achieved via scalar couplings. Both techniques based on heteronuclear single quantum coherence transfer (HETCOR, INEPT, HSQC), and heteronuclear multiple quantum coherence transfer (DEPT, HMQC) were used. Cross-polarization schemes, which were shown to be a useful alternative for $^{1}H,^{n}X$ correlation spectroscopy,[63] have as yet not been applied for 2D $^{n}X,^{m}Y$ correlations; presumably, their use is discouraged by the limited excitation bandwidth achievable with this technique.[53] A detailed analysis of the basic pulse sequences is found elsewhere[3] and will not be repeated here. With few exceptions (mainly $^{19}F,^{m}Y$ experiments),[20–22] all pulse schemes were generally adapted to additional selective (cw)[19,64,65] or broadband ^{1}H decoupling[18,66] throughout the experiment, resulting in the familiar sequences shown in Fig. 3(a–c).

Phase cycles were in earlier implementations selected to produce magnitude mode spectra,[66] while more recent versions[6,27,67] use either TPPI or the States method to obtain phase-sensitive spectra. Coherence pathway selection by pulsed field gradients which is widely used in $^{1}H,^{n}X$ correlation spectroscopy[68–70] was applied but in a few exploratory cases.[13] With the exception of some $^{13}C,^{2}D$ or $^{6}Li,^{13}C$ HETCOR and $^{19}F,^{13}C$ HMQC experiments where noise[25] or composite pulse decoupling[71–74] of ^{13}C or ^{2}D was applied, decoupling of ^{n}Y during t_2 was generally omitted, whereas heteronuclear couplings in $F1$ are normally removed by a $180°(^{n}X)$ pulse during t_1 because of sensitivity reasons. Hence, the correlation signals appear as singlets in $F1$, but are split by $J(^{n}X,^{m}Y)$ in $F2$. Additional splitting in both dimensions may be present as a consequence of further couplings to passive spins,[18,19,75] or homonuclear couplings.[67] The conservation of the active coupling in $F2$ allows direct detection of the transferred antiphase magnetization immediately after the mixing pulse so that the refocusing delay prior to acquisition may be eliminated. This reduced length of the pulse sequence helps to minimize signal losses due to relaxation.[47] In combination with phase-sensitive processing, this approach offers further an easy way for distinction between active and passive couplings in a complex multiplet, thus helping spectral analysis when ^{m}Y is a rare nucleus and ^{m}Y satellites in ^{n}X spectra are not visible.[67]

In addition to some practical considerations which will be discussed in Section 2.3, the cases of spin systems with several magnetically equivalent ^{m}Y nuclei need some further consideration. In principle, both DEPT and HMQC pulse sequences are in their standard forms designed to detect magnetization of spin systems with a single indirectly detected ^{m}Y nucleus, which is perfectly suited for inverse observation of rare nuclei such as ^{13}C or ^{15}N. However, metal complexes may contain heteronuclei with high natural abundance such

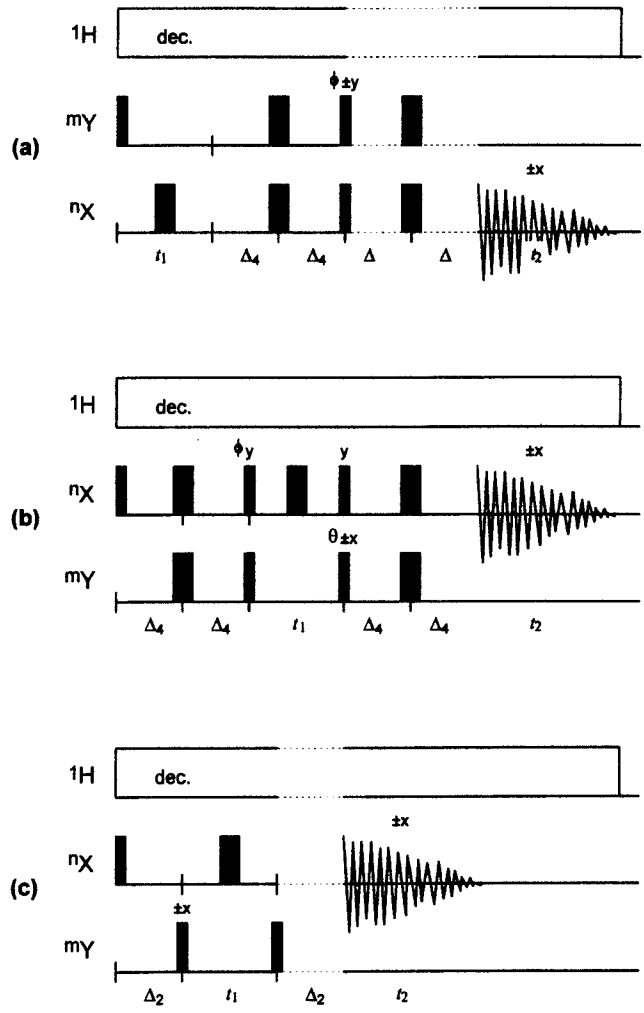

Fig. 3. Basic pulse sequences for 2D-^{n}X,^{m}Y{^{1}H} correlations. The same notation as in Fig. 1 is used. Minimum phase cycles for selection of correlation signals are given, more elaborate schemes for quadrature detection in *F*1 and phase-sensitive spectra may be applied following standard rules.[15] (a) HETCOR (without 180° pulses)/INEPT (with 180° pulses), the refocusing delays Δ are optional in both experiments; setting the mixing pulses θ to 45°/135° instead of 90° allows to determine coupling signs in ABX-type spectra.[67] (b), HSQC. (c), HMQC; the refocusing delay Δ_2 is optional.

as ^{103}Rh (100%), ^{195}Pt (33%), or ^{109}Ag (52%), and indirect observation of these nuclei may require to detect magnetization of species with more than one ^{m}Y spin (similar problems may arise with isotopically enriched samples[76]). A theoretical analysis of the HMQC experiment using the product

operator formalism was performed for I_2S_2 spin systems (I, S = spin-half nuclei), and it was shown that the standard pulse sequence yields the desired correlation spectra if fixed delay of $(4\,J(I,S))^{-1}$ instead of $(2\,J(I,S))^{-1}$ is used (see Fig. 3) and a modified phase cycle is applied.[77] Experimental verification of these results was reported for I_2S_2 spin systems with I nuclei having both spin-half[77] and spin-1.[76] Acquisition of HMQC spectra with omission of the 180°(^{n}X) refocusing pulse and a simplified two-step phase cycle was further used for simultaneous detection of isotopomers with different numbers of ^{m}Y nuclei.[78] Even if these spectra are not suitable for the determination of ^{m}Y chemical shifts, they contain helpful information related to the determination of the number of coupling nuclei and the evaluation of coupling constants.[77,78] The use of more complicated phase cycles for filtering of certain multiple quantum coherences to simplify larger spin systems was addressed, but not experimentally investigated.

Closely related to the measurement of HMQC spectra of I_nS_m spin systems is the indirect detection of quadrupolar nuclei. While the standard HMQC sequence of Fig. 3(c) proved feasible for indirect detection of spin-3/2 nuclei such as ^{11}B[79] and ^{61}Ni,[18] a theoretical analysis of the behaviour of spin systems with I(S) = 1 led to suggest a modified HMQC scheme (Fig. 4(a)) for systems with a single spin-1 S nucleus.[24] Deviations from the standard scheme include the use of a shorter defocusing delay $(4\,J(I,S))^{-1}$ and of an additional 90°(I) pulse prior to t_1. Application of the sequence was demonstrated for the case of a $^{13}C^2D$ spin system. In addition, it was shown that correlation spectra of I_nS_m spin systems with different numbers of spin-1 S-nuclei can be obtained with an HSQC sequence, albeit by paying the price that the correlation signals appear at twice their real chemical shift in $F1$.

Further modifications of the basic HMQC, HSQC or INEPT pulse sequences were developed for a number of special purposes. The performance of the HMQC sequence was improved by replacing the refocusing 180°(^{n}X) pulse by a 90°_x-240°_y-90°_x composite,[80] or by introducing an additional BIRD filter for better suppression of unwanted signals.[73,74] A low pass filter for the suppression of direct connectivities was applied to both ^{19}F,^{13}C and ^{31}P,^{13}C multiple bond correlation experiments.[73,74,81] A remedy of the problems of long repetition times in ^{n}X,^{m}Y correlations was found by replacing the excitation pulses of ^{n}X,^{m}Y HMQC and HETCOR sequences by ^{1}H,^{n}X[83,87] or ^{1}H,^{m}Y[84] INEPT excitation schemes, respectively, resulting in the pulse sequences shown in Fig. 4(b,c). Here, the use of ^{1}H rather than ^{n}X (or ^{m}Y) nuclei as polarization source allows not only to apply faster pulse repetition rates since $T_1(^1\mathrm{H})$ is generally much shorter than $T_1(^n\mathrm{X})$ or $T_1(^m\mathrm{Y})$, but yields also an additional signal enhancement by a factor of $\gamma_{^1\mathrm{H}}/\gamma_{^n\mathrm{X}}$ (or $\gamma_{^1\mathrm{H}}/\gamma_{^m\mathrm{Y}}$). Care must be taken in the choice of the delay Δ_2 in the INEPT–HMQC experiment (Fig. 4(b)) which must compromise between optimal ^{n}X,^{m}Y coherence transfer and optimal refocusing of ^{1}H,^{n}X magnetization vectors and depends thus on the magnitudes of both $J(^1\mathrm{H},^n\mathrm{X})$ and $J(^n\mathrm{X},^m\mathrm{Y})$. For ^{29}Si,^{13}C and ^{13}C,^{77}Se

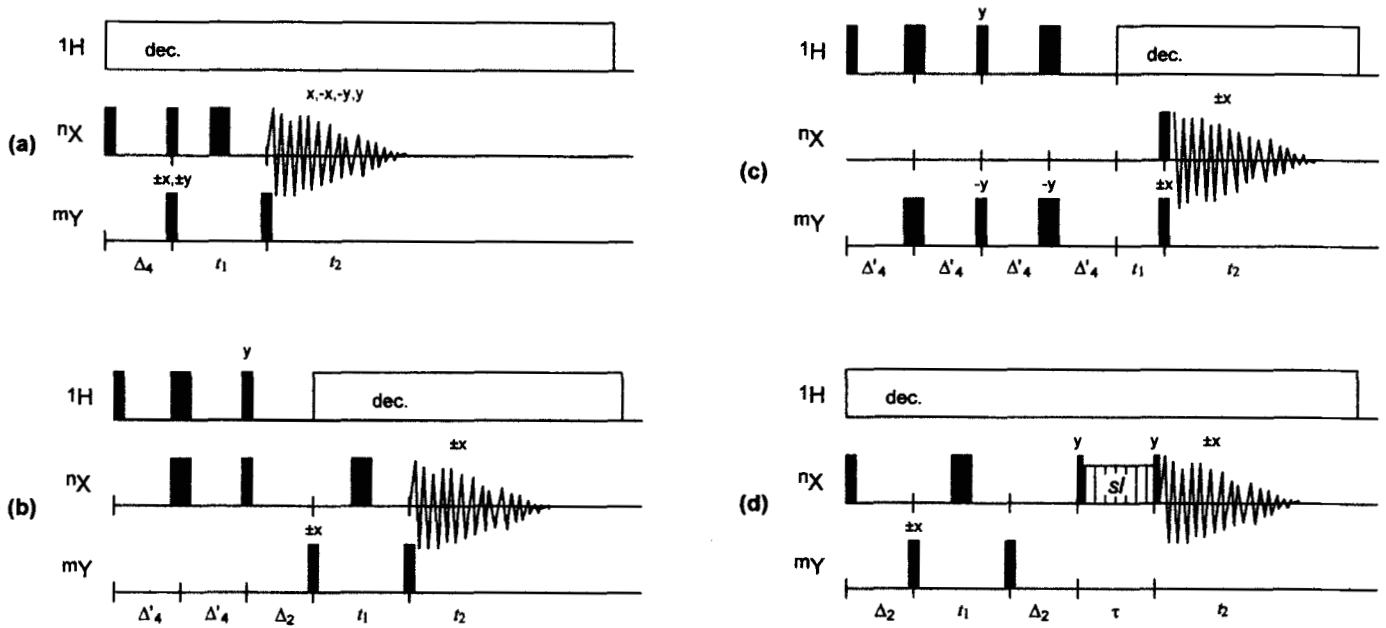

Fig. 4. Special pulse schemes for 2D-^{n}X,^{m}Y{^{1}H} correlations. The same notation as before is used; Δ'_n denotes a fixed delay of length $(nJ(^{1}\mathrm{H},\mathrm{Y}(\mathrm{X}))^{-1}$. (a) HMQC sequence for indirect detection of spin-1 nuclei.[79] (b) INEPT–HMQC.[83] (c) INEPT–HETCOR.[85] (d) HMQC–TOCSY; *sl* denotes an MLEV spinlock sequence of duration τ which is framed by trim pulses.[27]

correlations good results were obtained by adjusting this delay to $(2J(C,X))^{-1}$ and neglecting the incomplete refocusing of the ^{n}X magnetization after the INEPT transfer step.[82,85]

The $^{n}X,^{m}Y$ correlation techniques described so far do not allow to determine the number of magnetically equivalent detected ^{n}X nuclei. Such information is frequently of importance for structure elucidation; for example, it would permit to determine the number of phosphine ligands in a metal complex from a ^{31}P-detected phosphorus–metal shift correlation. A remedy to this problem has been found by recording fully coupled correlation spectra in which the number of X spins can be derived from the multiplet structure in $F1$. This is easily achieved in both HMQC and HSQC pulse schemes by omitting the refocusing 180° pulse during t_1, and various $^{n}X,^{m}Y$ correlations have been performed in this way.[77,78,86–89] For an interpretation of the results, however, it is important to remember that HMQC and HSQC give rise to different splitting patterns. In the HSQC experiment, all ^{n}X spins are longitudinal during t_1, and a group of n magnetically equivalent ^{n}X nuclei gives rise to an antiphase multiplet of $(n+1)$ lines with separation of $J(^{n}X,^{m}Y)$. For a multiplet with an odd number of lines the intensity of the central line is zero (see Fig. 5), and in particular an antiphase triplet with an intensity distribution of $1:0:-1$ ($1:0:1$ in magnitude mode) will appear as doublet with an apparent splitting of twice the value of $J(^{n}X,^{m}Y)$.[87] In contrast, in the HMQC case, a mixture of heteronuclear zero- and double-quantum coherences evolves during t_1 which requires that one of the n ^{n}X spins is transversal. Coupling evolves with the remaining $(n-1)$ spins, and the observed multiplet contains only n, rather than $(n+1)$, lines. Further, the evolution of ^{n}X chemical shifts during t_1 is no longer refocused, so that the signal position in the $F1$ domain corresponds no longer to the true ^{m}Y chemical shifts.

Two further modifications of pulse schemes for $^{n}X,^{m}Y$ correlation were introduced aiming at a special form of multiplicity editing, viz. the ring size determination in symmetric cyclic aggregates of type $(XY)_n$. Both methods were developed for the characterization of lithium organyls and amides, respectively, but they should also be applicable to other cyclic $(XY)_n$ systems. Both strategies rely on the fact that, even if each Y atom is regardless of the ring size coupled to two adjacent magnetically active X atoms and vice versa, higher oligomers ($n > 2$) differ from dimers in having additional remote X′ and Y′ nuclei (Fig. 6(a)), and detection of scalar interactions involving these chemically, but not magnetically, equivalent spins can be used for a

Fig. 5. Magnitude mode ^{31}P, ^{109}Ag HSQC spectra of $[Ag(cis\text{-}Ph_2PCH{=}CHPPh_2)_2]NO_3$ measured with (A) and without (B) 180° pulse during t_1. The coupling with four phosphorus atoms gives rise to a quintet splitting along $F1$ in (B) whose central line is missing because of the antiphase structure. Reproduced, with permission, from ref. 87.

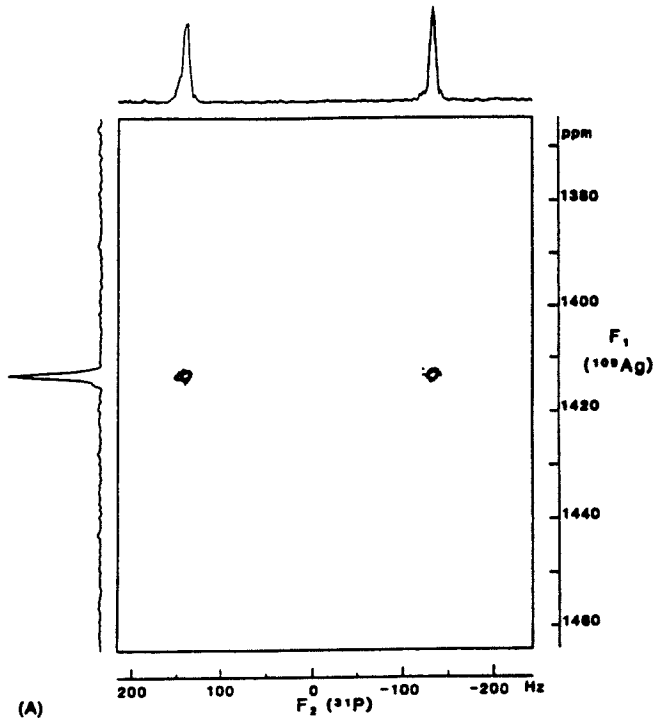
ppm
1380
1400
1420
1440
1460
F1
(109Ag)
200
100
0
-100
-200 Hz
F2 (31P)
(A)

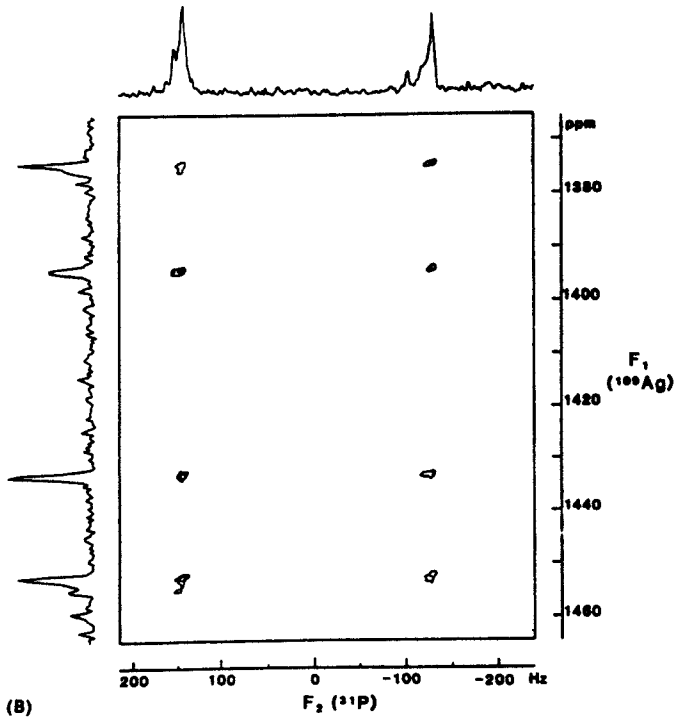
ppm
1380
1400
1420
1440
1460
F1
(109Ag)
200
100
0
-100
-200 Hz
F2 (31P)
(B)

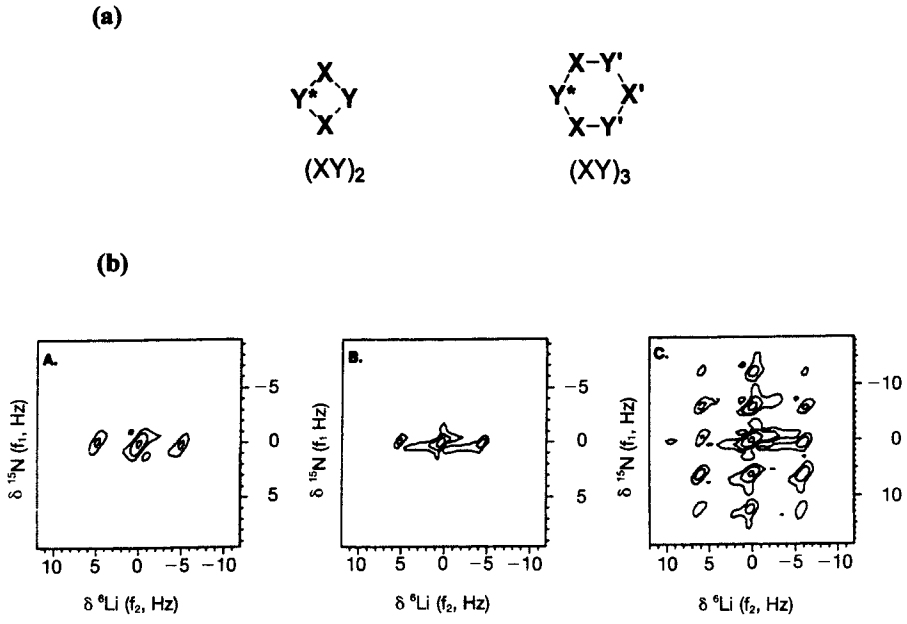

Fig. 6. (a) Schematic representation of the different topologies of dimeric and trimeric aggregates of lithium amides or lithium organyls. Seen from an observed Y* spin, the second Y spin in the dimer is magnetically equivalent while the trimer exhibits further magnetically inequivalent X′ and Y′ spins. (b) ^{6}Li-detected ^{15}N zero-quantum NMR spectra of (A) 0.15 M [^{6}Li,^{15}N]LDA in THF (−90°C), (B) 0.10 M [^{6}Li,^{15}N]LiTMP in 3:1 THF/pentane (−115°C) and (C) 0.25 M [^{6}Li,^{15}N]LiTMP in 3:1 THF/benzene (30°C). The splittings along $F1$ indicate the presence of dimers for (A) and (B), and of a higher oligomer for (C). Reproduced, with permission, from ref. 90. Copyright 1992 American Chemical Society.

discrimination between the different topologies. Gilchrist and Collum[90] suggested for this purpose an experiment which is based on indirect detection of homonuclear zero-quantum coherences of a (Y_1,Y_2) pair coupled to an observed X spin. The pulse scheme is a variation of the basic HSQC pulse scheme (Fig. 3(b)), and zero-quantum coherences were prepared by using a 90° phase shifted mixing pulse ϕ, and selected after evolution during t_1 by a four-phase cycle applied to the third "Y pulse θ. The basic idea is that the precession of the Y-zero-quantum coherence during t_1 is modulated by scalar coupling to X nuclei with an effective coupling constant $J_{eff} = \pm(J(Y_1,X) - J(Y_2,X)$.[91] This value vanishes for all X spins with equal couplings to both Y_1 and Y_2, while any spin X′ coupled to only one (but not both) atoms gives $J_{eff} = \pm J(Y_i,X')$. The zero-quantum line of a dimer, which contains no such nuclei, appears thus as a singlet in $F1$, while higher oligomers give rise to splittings whose multiplicity depends on the spin and the number of the remote X′ spins (Fig. 6(b)).

While the above method works only in cases where both ^{n}X and ^{m}Y are abundant spins, Bauer[27] suggested the HMQC–TOCSY pulse sequence of Fig. 4(d) which allows direct detection of magnetically inequivalent X and X′ nuclei of higher oligomers even in cases where ^{m}Y is a rare isotope. The pulse sequence works by first selecting the magnetization of ^{n}X nuclei adjacent to a magnetically active ^{m}Y spin by the HMQC part. In the case of a dimer, the additional mixing sequence leaves the spectrum unchanged, and the cross-peak appears as a multiplet showing the splitting due to $J(X,Y)$; for a higher oligomer, magnetization will be transferred to remote X′ nuclei whose resonances are not split by J-coupling and will therefore give rise to an additional singlet cross-peak.

In addition to the magnitudes of scalar couplings, also their signs are frequently a valuable source of information for the analysis and characterization of molecular structures. 2D-NMR techniques have developed into a versatile instrument to determine relative signs of individual couplings in larger spin systems, and numerous investigations of $^{n}X,^{m}Y$ correlations have addressed this issue. In the simplest case, viz. a system of three different, mutually coupled heteronuclei $^{n}X,^{m}Y,^{l}Z$, the sign information can be directly extracted from a two-dimensional $^{n}X,^{m}Y$ shift correlation obtained with any of the basic pulse sequences of Fig. 3. Since there is no changes in ^{l}Z spin states during the experiment, the $^{n}X,^{m}Y$ correlation signal consists of a superposition of subspectra which belong to the different ^{l}Z spin states and are split by the passive coupling constants $J(^{n}X,^{l}Z)$ in $F2$ and $J(^{n}Y,^{l}Z)$ in $F1$. The whole correlation signal reveals therefore an E.Cosy pattern (see Fig. 7) whose tilt (a positive/negative tilt indicates displacement of the subspectra parallel/perpendicular to the main diagonal of the correlation map, connecting the line appearing at highest field in $F2$ with the one at highest/lowest field in $F1$) characterizes the relative signs of the reduced coupling constants $K(^{n}X,^{l}Z)$ and $K(^{m}Y,^{l}Z)$. Using the definition $K(A,B) = 4\pi^2 J(A,B)\,(h\,\gamma_A\,\gamma_B)^{-1}$ gives then the relative signs of the J-couplings. Analysis of this type was frequently applied to $^{n}X,^{m}Y$ correlation spectra recorded without proton decoupling, thus using ^{1}H as the passive spin,[19,21,64,65,92] but also combinations comprising three different heteronuclei (e.g. $^{31}P,^{2}D,^{57}Fe$,[18] $^{31}P,^{19}F,^{57}Fe$,[19] $^{19}F,^{13}C,^{109}Ag$,[45] or $^{19}F,^{13}C,^{207}Pb$[75]) were studied. Decoupling of ^{m}Y during acquisition which may be desirable to achieve higher signal-to-noise ratios or a simplification of crowded spectra is possible, as the sign information is based on a comparison of passive couplings to a third nucleus.

A different case of heteronuclear three-spin system which occurs frequently if isotopes of high natural abundance such as ^{19}F, ^{31}P or ^{103}Rh are present, consists of two magnetically inequivalent homonuclear spins $^{m}Y_1,^{m}Y_2$ coupled to an ^{n}X spin. In this case, an $^{n}X,^{m}Y$ correlation experiment induces transitions of all three nuclei, and each $^{n}X,^{m}Y$ cross-signal shows additional lines due to transitions between the subspectra associated with the individual spin-states of the second Y nucleus. Bax and Freeman[93] were the

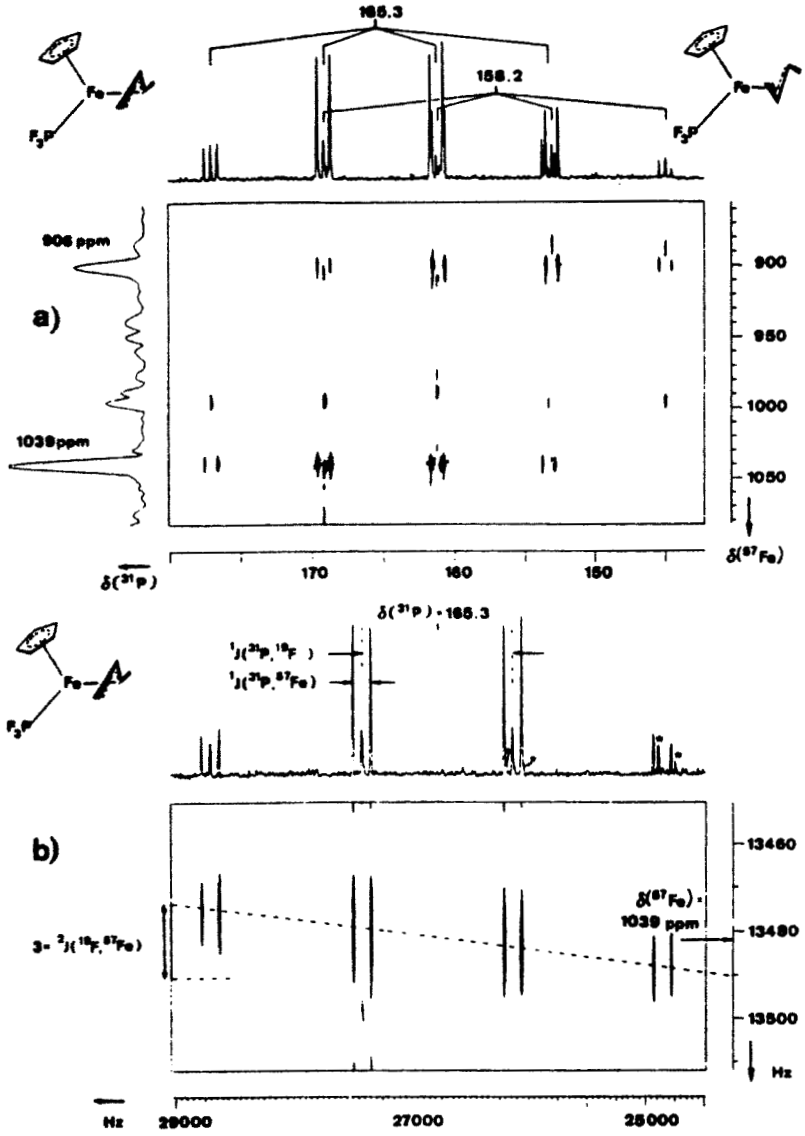

Fig. 7. Contour plot and expansion of a 2D-$^{31}P,^{57}Fe\{^1H\}$ correlation of *exo*- and *endo*-[η^5-Cp)(η^3-1-*syn*-methylallyl)(PF_3)]Fe. The tilt in the cross-signal of the major isomer (bottom) indicates that the passive couplings ^1J(P,F) in *F*2 and ^2J(Fe,F) in *F*1 are of opposite sign. Reproduced, with permission, from ref. 79. Copyright 1988 American Chemical Society.

first to show that the E.Cosy pattern which gives rise to the sign information is preserved in HETCOR spectra if mixing pulses θ with much smaller angles than 90° are applied. The use of this approach for ^{n}X,^{m}Y correlation experiments has been demonstrated recently for the analysis of relative signs of $J(^{31}P,^{15}N)$ and $J(^{31}P,^{13}C)$ couplings in phosphorus compounds.[67] An unrefocused 2D-INEPT sequence with a 45° mixing pulse was employed (Fig. 3(a)), and it was shown both by theoretical analysis using the product operator formalism, and by experiment, that the exchange in coherence orders induced by the two 180° pulses produces a reverse sense of the tilt in the correlation signal as compared to the Bax–Freeman experiment (Fig. 8). The same tilt as in the original experiment may be restored either by returning to the refocused INEPT scheme, or by applying a 135° instead of a 45° mixing pulse. Refocusing of the active heteronuclear coupling in $F1$ by a 180°(Y)-pulse during t_1, which is frequently applied for sensitivity reasons, leads to a simplification of the multiplet structure of the correlation signal, but has no effect on the sign determination, but ^{m}Y decoupling during t_2 which would lead to a collapse of both active and passive heteronuclear couplings in $F2$ must be avoided.

^{1}H detected ^{n}X,^{m}Y correlation experiments

Taking the idea of indirect detection to the extreme, the low sensitivity of many ^{n}X,^{m}Y correlation experiments could be for various organic and organometallic compounds remedied by recording the whole correlation spectrum indirectly as a ^{1}H-detected three-dimensional experiment. This approach was widely applied to investigation of biomolecules, and ^{1}H,^{13}C,^{15}N and ^{1}H,^{13}C,^{31}P correlation experiments have developed into valuable tools for structural studies of proteins and nucleotides.[3,94,95] The success of these techniques owes to the combination of high sensitivity, due to the high receptivity of ^{1}H, high power to simplify complicated spectra by three-dimensional signal dispersion, and high versatility, owing to the availability of rational methods to tailor experiments for selective extraction of desired and rejection of all other correlations. Today, a variety of multidimensional triple-resonance NMR experiments is known which were specially designed for the structure elucidation of different kinds of biomolecules. A detailed account of this topic is beyond the scope of this article, but the main aspects have been reviewed[3,94,95] and the interested reader is referred to these articles. Apart from studies on biopolymers, three-dimensional pulse schemes and their two-dimensional projections were also applied to characterize synthetic polymers and low-molecular-weight organophosphorus compounds, and the results demonstrate that these experiments may have considerable future potential as structural assignment tools in organic and organometallic chemistry.

So far, heteronuclear 3D correlation experiments in these fields were

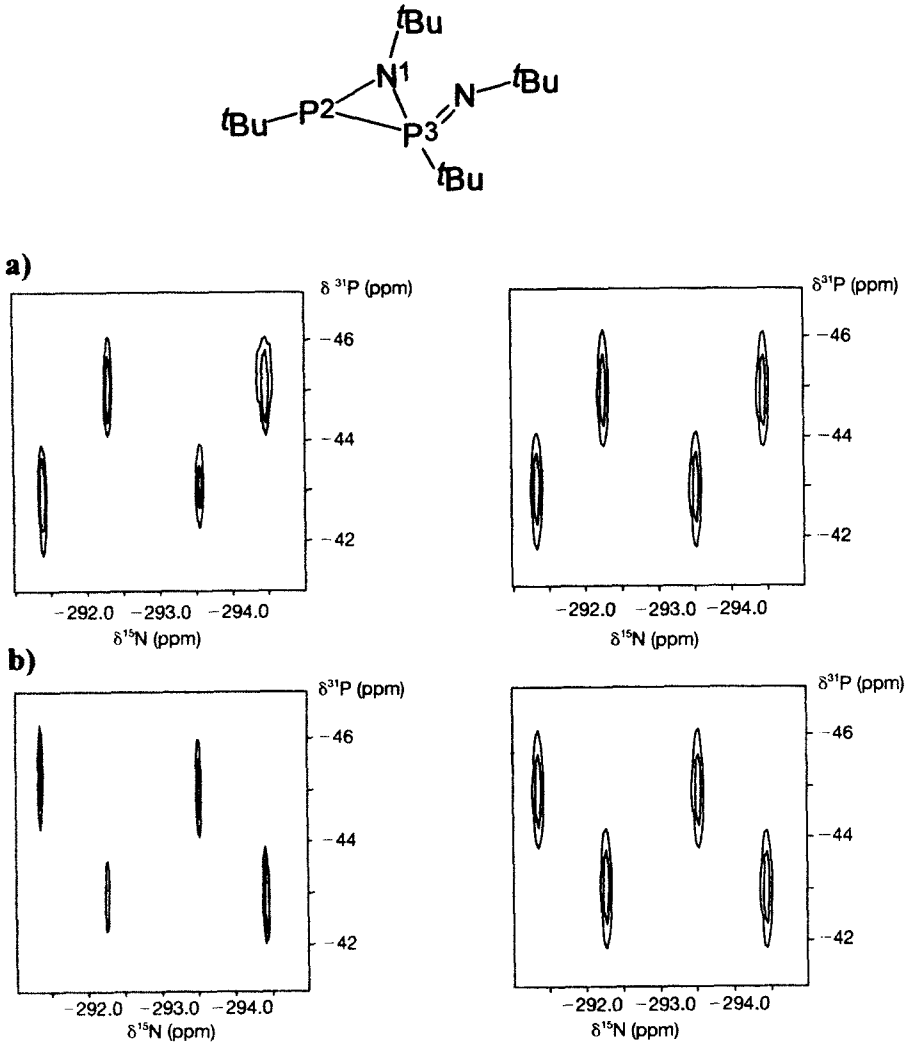

Fig. 8. Expansion of the P^2,N^1 correlation signal of the shown azadiphosphiridine in a 2D-^{15}N,^{31}P shift correlation obtained with (a) a HETCOR (Fig. 3(a), all 180° pulses and Δ omitted) and (b) an unrefocused INEPT pulse sequence (Fig. 3(a), only the last 180° pulses and Δ omitted), showing the influence of the pulse sequence on the sense of the cross-peak tilt. Experimental spectra are shown left and a spectral simulation (NMRSIM) right. The observed tilt indicates that the two passive couplings $^1J(P^2P^3)$ (in *F*2) and $^1J(P^3N^1)$ (in *F*1) are of like sign. Reproduced, with permission, from ref. 67.

carried out with the isotope combinations $^{1}H,^{13}C,^{31}P$, $^{1}H,^{13}C,^{19}F$ and $^{1}H,^{13}C,^{29}Si$, and using two cardinal types of pulse sequences based on the HNCO and HNCA[96,97] experiments which constitute standard schemes routinely employed for structure elucidation of peptides and proteins. However, whereas work on biomolecules is generally carried out with uniformly ^{13}C and ^{15}N labelled molecules, these studies were performed in natural abundance of isotopes, which required some adaptations of the experiments in order to improve the suppression of signals from isotopomers with magnetically inactive ^{12}C and ^{28}Si nuclei.

The first adaptation of an HNCA-type experiment for a $^{1}H,^{13}C,^{31}P$ correlation designated for the characterization of organophosphorus compounds was introduced by the group of Berger,[98] and a modified version for $^{1}H,^{13}C,^{19}F$ with an additional BIRD nulling sequence before the first excitation pulse was later described by the group of Rinaldi.[99,100] Using the product operator formalism, the basic principle of the pulse sequence (Fig. 9(a)) can be outlined as follows: the sequence starts with an INEPT transfer from ^{1}H to ^{13}C to generate antiphase magnetization $2H_zC_y$, followed by ^{13}C chemical shift evolution during t_1. The evolution of $^{31}P,^{13}C$ coupling during the following delay Δ_2 generates double antiphase magnetization $4H_zC_xP_z$ which is then transferred into three-spin coherence $4H_yC_xP_y$ by the simultaneous 90°(^{1}H) and 90°(^{31}P) pulses. ^{31}P chemical shifts evolve in t_2, and two 90° pulses on ^{1}H and ^{31}P restore a term $4H_zC_xP_z$ which refocuses during Δ_2 to give antiphase magnetization $2H_zC_y$. This is transferred by a reverse INEPT step to observable proton magnetization which is detected during t_3 under broadband GARP decoupling of ^{13}C.

The second approach to three-dimensional $^{1}H,^{13}C,^{31}P$ correlation via a transcribed HNCO pulse scheme (Fig. 9(b)) was first developed by Marino *et al.*[101] for the characterization of oligonucleotides. Modified versions were later reported by the Rinaldi group who dropped the originally used constant time evolution scheme, but incorporated composite pulsed field gradients for coherence selection,[102] and adapted the experiment further for $^{1}H,^{13}C,^{29}Si$ correlations.[103] The main difference to the above-mentioned experiment of Berger lies in the use of two consecutive INEPT and reverse INEPT steps to transfer the magnetization from protons via the intervening carbons to phosphorus and back, and the integration of ^{13}C chemical shift evolution into a constant delay τ_2 which also serves to refocus the $J(^{31}P,^{13}C)$ couplings, by shifting the last pair of 180° pulses on ^{13}C and ^{31}P within τ_2.

Both types of experiments detect magnetization arising from mutually coupled heteronuclear spin-triples. Even if the spectra can in principle be displayed in a 3D-cube representation (Fig. 10), the analysis of 2D slices or projections is often preferred for the interpretation. Important features can be derived as is demonstrated in the example shown in Fig. 10, e.g. from inspection of H,C planes taken at the chemical shift of an individual phosphorus atom, which give a two-dimensional H,C correlation of all signals

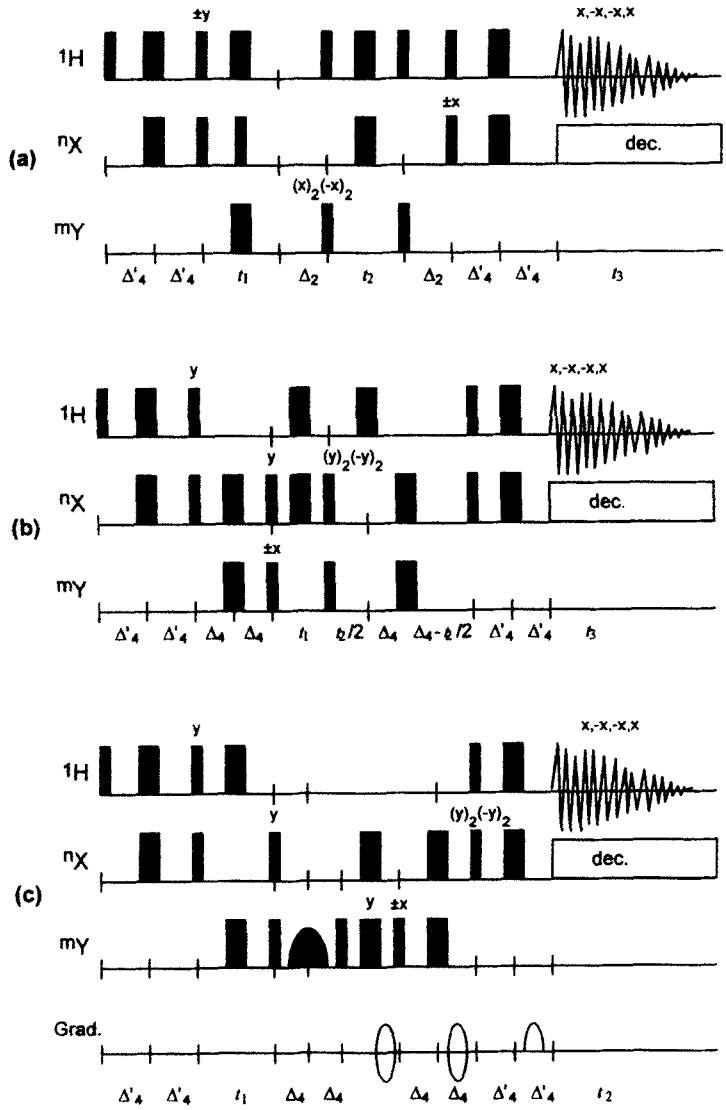

Fig. 9. Pulse sequences for 3D- and 2D-^{1}H,^{n}X,^{m}Y correlations. The same notation as in Fig. 1 is used. (a) HNCA-analogue 3D experiment.[98] (b) HNCO-analogue 3D experiment.[101] (c) gs-SELTRIP with a selective 180° gauss pulse; the gradient strength (for the case ^{1}H,^{13}C,^{31}P) is +/−25, −/+25, 22.7 for echo/antiecho selection.[104]

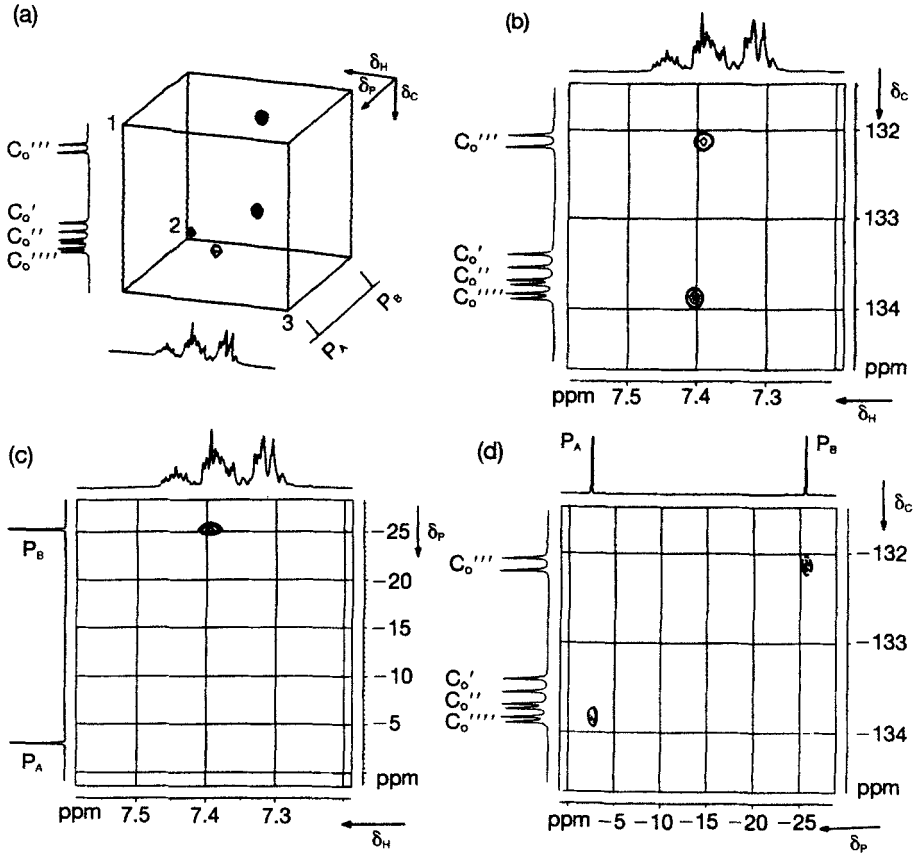

Fig. 10. Different representations of the 3D-^{1}H,^{13}C,^{31}P correlation of R-$Ph_2PCH_2CH(CH_3)PPh_2$ (R-prophos) obtained with the pulse sequence of Fig. 9(a): (a) 3D-cube representation. (b)–(d) 2D slices of (a) through the H,C plane at $\delta(P) = -25.2$ (b), through the H,P plane at $\delta(C) = 132.1$ (c), and through the C,P plane at $\delta(H) = 7.4$. Reproduced, with permission, from ref. 98. Copyright 1993 John Wiley & Sons.

coupled with this atom. Similar slices along the C,P plane reveal directly the corresponding C,P correlations.

Regarding the rather simple molecular structures of many organic or organometallic compounds, dispersion of resonances in three dimensions is generally not needed to obtain analysable spectra. Efforts have therefore been made to develop shortcuts which yield the connectivity information of a 3D spectrum while avoiding the long acquisition time of a complete data matrix. Wagner and Berger[104] suggested the gradient-enhanced gs-SELTRIP sequence for this purpose. The experiment is based on the replacement of the ^{31}P frequency domain in a ^{1}H,^{13}C,^{31}P correlation by a *selective* ^{13}C,^{31}P

coherence transfer step and allows essentially to measure a single C,H plane of the 3D cube at the position of the selected phosphorus nucleus. The pulse scheme (Fig. 9(c)), which replaced the older SELTRIP method[105] in which essentially all cross-peaks connected with a selected ^{31}P nucleus were destroyed, begins with a ^{1}H,^{13}C INEPT transfer, followed by ^{13}C chemical shift evolution during t_1. The magnetization of nuclei connected with a specific phosphorus atom is then extracted by a selective ^{13}C,^{31}P INEPT transfer and a ^{13}C,^{31}P double-quantum filter, and finally transferred back to the protons in two reverse INEPT steps. Pulsed field gradients have been applied for coherence selection, even though their use is not mandatory.

A 2D method aiming in particular at improvement of ^{1}H-detected measurement of $J(^{n}X,^{m}Y)$ couplings is J-scaled ^{1}H,^{n}X correlation spectroscopy. The method was introduced to measure $J(^{31}P,^{13}C)$ from the $F1$ domain of a ^{1}H,^{13}C HSQC spectrum even in cases of relatively low time-domain resolution.[106] Its crucial idea is the application of a scaling factor to the scalar couplings by insertion of a sequence of $(-\tau\text{-}180°(^{31}P,^{13}C)\text{-}\tau\text{-})$ spin-echoes before the t_1 period which allow evolution of heteronuclear couplings, but refocus ^{13}C chemical shifts, and thus introduce different effective evolution times for $\delta^{13}C$ and $J(^{31}P,^{13}C)$. Furthermore, the use of triple-resonance double-quantum/zero-quantum experiments for ^{1}H-detected measurement of $J(^{31}P,^{15}N)$and $J(^{15}N,^{15}N)$ has been suggested.[107]

Pseudo triple-resonance experiments for passive selection of ^{m}Y satellites

The techniques discussed so far rely essentially on the *active* selection of ^{n}X,^{m}Y coherences by the application of pulses to both heteronuclei. In addition, several researchers have also focused on methods which permit *passive* selection of ^{m}Y satellites in an ^{n}X spectrum without applying pulses on the ^{m}Y channel. Considering that the edited ^{n}X spectra are normally acquired either directly under proton decoupling, or via ^{1}H-detected inverse detection schemes, these techniques are essentially "pseudo" triple-resonance experiments. Their advantage is without doubt that they require only a single X-channel and are therefore easily performed on spectrometers without triple-resonance equipment. Limitations are, in addition to the unavailability of ^{m}Y chemical shifts, that the passive selection schemes may work only for spin systems with a single ^{m}X nucleus or rely on special relaxation properties, and are possibly not applicable to all samples of interest. Even if, in a rigorous sense, these experiments are no true X,Y correlations since they lack an ^{n}X,^{m}Y coherence transfer step, they have nonetheless proven to be versatile and powerful tools in the fields of organometallic and organoelement chemistry and are particularly suited to measure magnitudes and signs of J(X,Y) couplings between two rare heteronuclei in mononuclear organometallic complexes. In principle, passive selection of ^{m}Y satellite lines can be achieved by selective destruction of unwanted magnetization, or by

selective excitation. Techniques for suppression of unwanted magnetization by heteronuclear z-filters or jump and return (ψ-BIRD) sequences have been developed in particular by Wrackmeyer and Kupce.[108–110] Z-filtering was used in both 1D- and 2D-^{n}X,^{1}H(^{m}Y) polarization transfer experiments, and will be explained using the 2D-INEPT sequence[108] (Fig. 11(a)). The z-filter, which follows a standard refocused INEPT scheme whose X pulses are applied exactly at the frequency of the parent ^{n}X signal, starts with a delay of $(2J(\mathrm{X,Y}))^{-1}$ during which antiphase magnetization $2X_yY_z$ evolves under ^{1}H-decoupling. At the end of the delay, this term is aligned perpendicular to that of the parent signal, and is converted into longitudinal magnetization $2X_zY_z$ by a 90°(X) pulse of appropriate phase. The still transversal magnetization of the parent signal is now allowed to evolve into antiphase magnetization $2H_zX_x$ by switching off the decoupler for a period of $(2\,J(\mathrm{X,H}))^{-1}$. Switching on decoupling again removes now, in principle, the parent signal, while the stored longitudinal magnetization of the satellites is converted to observable antiphase magnetization by the final 90°(X) pulse and may be observed directly, or after refocusing.

The ψ-BIRD filter proved particularly useful for indirect measurement of J(X,Y) in ^{1}H,^{n}X(^{m}Y) HSQC experiments (Fig. 11(b)).[109] The filter corresponds to a ^{1}H jump-and-return pulse with the transmitter set on resonance to the signal to be suppressed, and the delay Δ_2 tuned to $(2\delta\Delta)^{-1}$ where $\delta\Delta$ is the separation of the parent line and the ^{m}Y satellites to be excited. The effect of this pulse sandwich is in essence to invert magnetization of protons on resonance (and at offsets $\pm 2n\,\delta\Delta$) and to return that of protons resonating at $\pm n\,\delta\Delta$ to the +z axis. The parent line is then eliminated by adjusting the delay T so that the first excitation pulse of the HSQC part is applied when nulling of the inverted magnetization occurs. A more elaborate version of a ψ-BIRD HMQC experiment involving additional ^{1}H,^{n}X spinlock and ^{n}X jump-and-return pulses for better artefact reduction was proposed as well.[112]

The conceptual elaboration of ψ-BIRD filtering, viz. selective excitation of desired satellite lines, was achieved by replacing the hard excitation pulse of a normal HMQC sequence by a bi-selective pulse designed for selective excitation at two frequencies (Fig. 11(c)).[111,112] Several proposed schemes differ in the utilization of either Dante[111] or binomial ($1\ \bar{3}\ 3\ \bar{1}$) sequences,[111,112] or a phase- and amplitude-modulated soft pulse which caused the least problems with unwanted excitation of signals outside the selected region, but required strong phase corrections in $F2$.[112] The use of binomial pulses was judged as best choice to measure couplings between rare spins on a routine basis. The application of this pulse scheme was also reported to measure $J(^{57}\mathrm{Fe},^{13}\mathrm{C})$ indirectly in a "pseudo quadruple-resonance" experiment via observation of ^{57}Fe satellites in a ^{31}P,^{13}C{^{1}H}(^{57}Fe) correlation.[112]

A further scheme designated specially for observation of ^{15}N satellites in ^{n}X spectra relies on the specific shortening of transverse relaxation times T_2 for ^{n}X nuclei adjacent to a quadrupolar ^{14}N nucleus by scalar relaxation of the

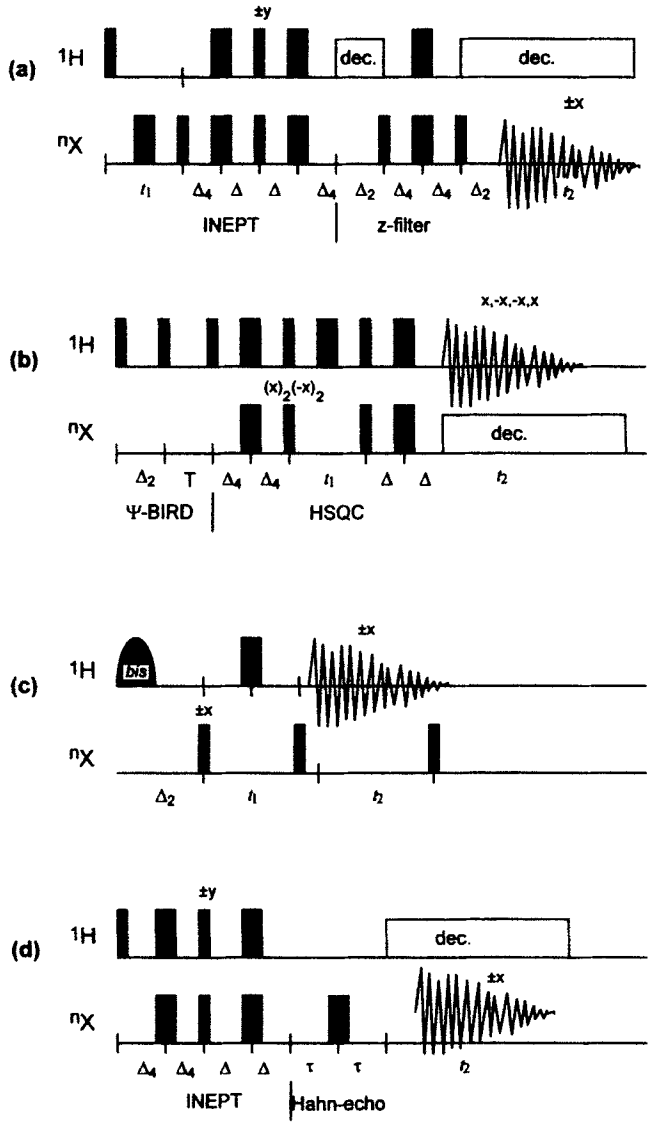

Fig. 11. Pulse sequences for pseudo triple-resonance experiments with passive selection of ^{m}Y satellites: (a) z-filtered 2D-^{n}X,^{1}H(^{m}Y) INEPT.[108] (b) Ψ-BIRD ^{1}H,^{n}X(^{m}Y) HMQC.[109] (c) ^{1}H,^{n}X(^{m}Y) HMQC experiment with biselective excitation pulse (*bis*); biselective excitation may be achieved with DANTE or Ψ-BIRD sequences, binomial pulses, or shaped pulses.[111,112] (d) ^{1}H,^{n}X(^{m}Y) HEED–INEPT.[113]

second kind. This effect can be exploited for relative enhancement of ^{15}N satellites in ^{n}X-detected NMR experiments by inserting a Hahn-echo pulse train $(\tau\text{-}180°(X)\text{-}\tau)_n$ between the last pulse and the beginning of the acquisition.[113] The transversal ^{n}X magnetization present at the beginning of this delay will decay with a rate proportional to $\exp(-2\tau/T_2^*)$ where $(\pi T_2^*)^{-1} = (\pi T_2)^{-1} \times \gamma\Delta B_0/2\pi$ and the last term denotes the magnetic field inhomogeneity in Hertz. The faster decay of magnetization of ^{14}N than of ^{15}N isotopomers will lead to a relative enhancement of the ^{15}N satellite intensity after the Hahn-echo by a factor of $R_w = T_2^*(X - {}^{15}N)/T_2^*(X - {}^{14}N)$.

Hahn-echo pulse trains have been implemented by the group of Wrackmeyer in conventional 1D- and 2D-polarization transfer schemes, the resulting pulse sequences being referred to as HEED-INEPT (cf. Fig. 11(d), HEED–DEPT, etc. (HEED = *H*ahn-*e*cho extend*ed*).[113] Even if HEED pulse sequences work best if the ^{n}X nuclei are coupled only to a single nitrogen and further quadrupolar nuclei are absent, satellites arising from ^{15}N isotopomers containing additional quadrupolar ^{14}N or $^{35/37}Cl$ nuclei have been observed in favourable cases.[114,115] It should be noted that by tuning the delay τ spectra with incomplete suppression of the parent line may be obtained which allow the determination of $^{14}N/^{15}N$ isotope shifts, and that in the case of very broad central lines a standard DEPT sequence may be long enough to grant suppression of the parent line even without application of a Hahn echo.[113]

Indirect measurement of relaxation times

Beside chemical shifts and coupling constants, spin–lattice relaxation times provide frequently another important source of information for structure elucidation, in particular for metal nuclei. In the same way as indirect detection allows effective chemical shift measurement for metal nuclei whose direct observation would be very time consuming or not feasible at all, it was also applied to relaxation time measurements.[19,116,117] Since most of the studied organometallic compounds contained only a single metal nucleus, the use of 1D sequences was preferred (however, analogous 2D schemes were applied to the characterization of peptides,[118–120] and ^{31}P and ^{19}F served beside ^{1}H as observed nucleus.

Three pulse schemes which were proposed for indirect T_1 measurements[117] and produce the same results as the inversion-recovery sequence are shown in Fig. 12. The first method is an inversion-recovery experiment on the insensitive ^{m}Y spin, with a subsequent DEPT transfer to the observed nucleus ^{n}X. Although successfully applied in model studies, the experiment suffers from the necessity of long relaxation delays and was considered to be too insensitive for application to ^{15}N and insensitive metal nuclei. Higher sensitivity can be achieved with double polarization transfer methods which start with ^{n}X magnetization. Two sequences were employed on the basis of double DEPT (Fig. 12(b)) or INEPT transfer (Fig. 12(c)). In order to remove effects of

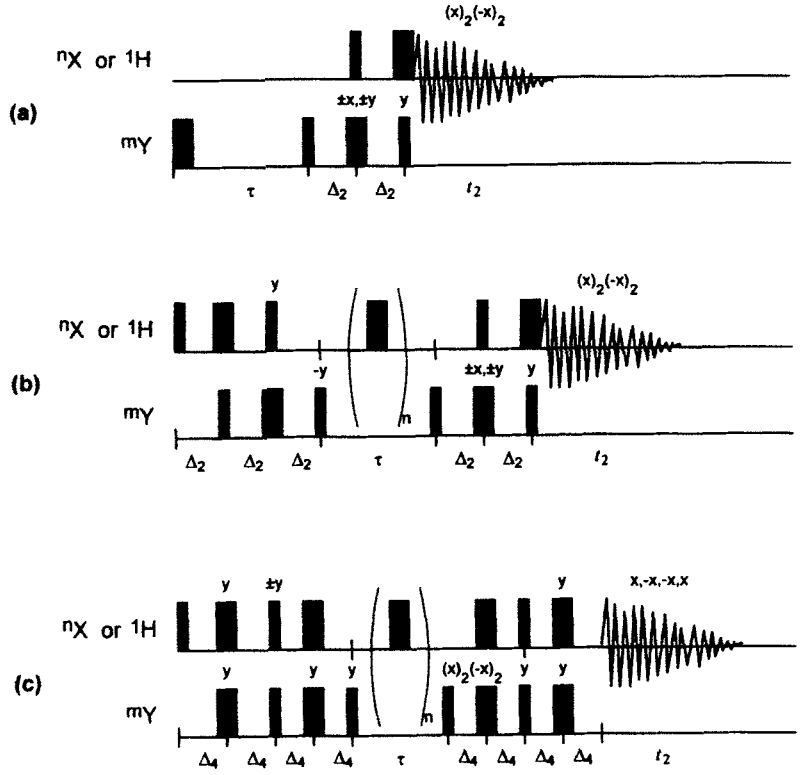

Fig. 12. Pulse sequences for indirect T_1 measurements:[112] (a) Inversion recovery with subsequent DEPT transfer. (b) Inversion recovery with double DEPT transfer and a series of 180°(X) pulses to suppress cross-relaxation effects. (c) Inversion recovery with double INEPT transfer.

cross-correlation between dipolar and CSA relaxation mechanisms, both schemes require application of 180°(X) pulses every 5 ms during the evolution delay τ. Even if DEPT is generally considered to be less sensitive to parameter missettings than INEPT, the INEPT scheme was found to be less susceptible to magnetization losses if T_2 relaxation times were short. The results obtained with both methods were found to be insensitive to variation of the repetition time between different scans.

2.3. Practical aspects

In principle, there is nothing uncommon in performing 1D- or 2D-^{n}X,^{n}Y correlation spectroscopy as compared to conventional ^{1}H,^{n}X heteronuclear

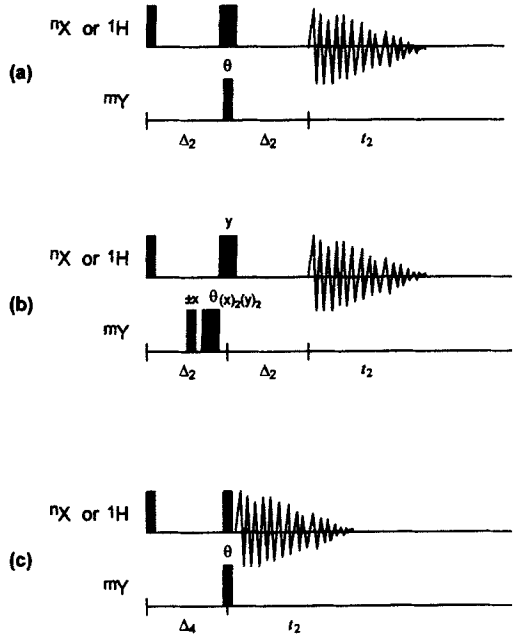

Fig. 13. Pulse sequences for indirect pulse calibration: (a) 90° pulses,[15] (b) 180° pulses,[15] (c) modified sequence for indirect calibration of 90° pulses on spin-1 nuclei.[24]

experiments. The practical aspects of these methods have been discussed in detail in the comprehensive works of Hull[16] and Berger *et al.*,[121] and the reader is referred to these works for the basic rules. In the following, we will focus on some additional aspects and complications which may arise specifically for correlations involving two heteronuclei.

Pulse calibration

Calibration of ^{m}Y decoupler pulses for ^{n}X{^{m}Y} experiments can be carried out by adapting the procedures for ^{1}H-detected ^{1}H,^{n}X correlations[15] to ^{n}X observation under ^{1}H decoupling. When the natural abundance of ^{m}Y is not exceedingly low, the spin-echo sequence shown in Fig. 13(a) which is essentially a refocused version of the two-pulse sequence of Bax[122] may be used. If ^{m}Y is a spin-half nucleus and $\Delta = (2\,J(\mathrm{X,Y}))^{-1}$, the intensity of the satellite lines is cancelled for $\theta(\mathrm{Y}) = 90°$, while shorter (longer) pulses give residual signals of the same (opposite) phase as the parent ^{n}X line. To achieve good results, the Y transmitter should be close to on-resonance, and the coupling should be large enough that the satellites are clearly observable. In cases of low abundant ^{m}Y nuclei, strong central signals can be suppressed by insertion

of an X-filter,[15] and for $^{m}Y = {}^{15}N$, a HEED pulse sequence may be applied.[123] Even if 180° pulses are generally assumed to be twice as long as 90° pulses, exact calibration for high-precision work can be performed with the sequence of Fig. 13(b),[15] once the 90° pulse is known. The same schemes may likewise be used for indirect calibration of pulses on spin-$n/2$ nuclei, but it must be borne in mind that for nuclei with integer spins the intensity of the central multiplet line remains unchanged.[24] Nulling of the complete signal upon application of an exact 90°(^{m}Y) pulse can be achieved for spin-one nuclei (e.g. ^{2}D, ^{6}Li) with the sequence shown in Fig. 13(c) if Δ_4 is set to $(4J(X,Y))^{-1}$.[24] Of course, X pulses calibrated by $^{1}H,^{n}X$ inverse methods can be used for $^{n}X,^{m}Y$ correlations, provided that the same hardware configuration is used for the X channel.

Chemical shift referencing

The position of an NMR signal is generally given as the chemical shift with respect to the absorption frequency of a reference substance according to Eq. (2):

$$\delta(\text{ppm}) = 10^6 \times (\nu_{obs} - \nu_{ref})/\nu_{ref} \tag{2}$$

In heteronuclear NMR work, the position of the reference line is generally derived from a separate measurement of an external standard sample under identical spectrometer conditions. However, the use of such a procedure may impose problems if the standard sample is chemically unstable or toxic, results are hard to reproduce because of strong temperature or concentration dependence of the signal position, or the acquisition of the reference spectrum is very time consuming, making frequent measurement of the standard impracticable. To avoid these problems, a calibration protocol on the basis of standard resonance frequencies Ξ[124] has been proposed. For a given nucleus X, $\Xi(X)$ corresponds to the resonance frequency of a standard sample in a magnetic field in which the TMS protons (under standard conditions) resonate at exactly 100 MHz (for some nuclei such as ^{103}Rh or ^{195}Pt an arbitrary frequency has been taken as reference because of problems with standard solutions). Once a reliable value of $\Xi(X)$ has been obtained, it can be used to compute chemical shifts according to Eq. (3) which was obtained by substituting $\nu_{obs} = \nu_{TMS} \times \Xi(X)/100$ in Eq. (2); here, ν_{TMS} denotes the measured absolute frequency of TMS in the sample.

$$\delta(X)(\text{ppm}) = 10^6 \times (\nu_{obs}/\nu_{TMS} \times 100/\Xi(X) - 1) \tag{3}$$

The value of ν_{TMS} is obtained either by measuring the frequency of the TMS line in the ^{1}H spectrum (if internal TMS is present), or by calculating its position from a secondary reference (e.g. residual ^{1}H signals of deuterated

Table 1. Standard reference frequencies Ξ [MHz]. Data from ref. 124 if not otherwise stated.

Nucleus	Ξ (MHz)	Shift of reference (ppm)	Reference compound
^{1}H	100.0000000	0.00	$SiMe_4$
^{10}B	10.743657	0.00	$BF_3{\cdot}OEt_2$
^{11}B	32.083971	0.00	
^{13}C	25.145004	0.00	$SiMe_4$
^{14}N	7.226455	0.00	$MeNO_2$
^{15}N	10.136767	0.00	
^{17}O	13.564269	569.0	Acetone
^{19}F	94.094003	0.00	$CFCl_3$
^{29}Si	19.867184	0.00	$SiMe_4$
^{31}P	40.480747	0.00	H_3PO_4 (85%)
^{53}Cr	5.642510	0.00	$[CrO_4]^{2-a}$
^{57}Fe	3.237798	0.00	$Fe(CO)_5$
^{59}Co	23.727118	0.00	$K_3[Co(CN)_6]$
^{77}Se	19.071523	0.00	Me_2Se
^{95}Mo	6.516926	0.00	$[MoO_4]^{2-}$aq., pH = 11[a]
^{103}Rh	3.16	0.00	rounded value
^{109}Ag	4.653623	0.00	Ag^+ aq., c→0
^{113}Cd	21.201887	0.00	$Cd(ClO_4)_2$ aq., 0.1 mol l^{-1}
^{119}Sn	37.290665	0.00	$SnMe_4$
^{125}Te	31.549802	0.00	$TeMe_2$
^{183}W	4.166388	0.00	$[WO_4]^{2-a}$
^{187}Os	2.282343	0.00	OsO_4 in $CDCl_3$
^{195}Pt	21.40	0.00	rounded value
^{199}Hg	17.870535	0.00	$Hg(ClO_4)_2$ 0.1 mol l^{-1} in 0.1 mol l^{-1} $HClO_4$
^{207}Pb	20.920597	0.00	$PbMe_4$

[a]Data from ref. 14.

solvents) of known chemical shift. Precise Ξ(X) values have been measured for various X nuclei, and the data are given in Table 1.

2.4. Comparison of experimental methods

With regard to the wealth of pulse schemes for $^{n}X,^{m}Y$ correlation, some consideration has to be put in the selection of the best-suited method for a certain application. In $^{1}H,^{n}X$ correlation spectroscopy, the high receptivity of protons makes inverse detection schemes generally the most effective protocol from the point of sensitivity. 2D experiments with ^{1}H detection are

now in most cases regarded as the method of choice for measuring both $J(^nX,^1H)$ and $\delta(^nX)$, while 1D schemes may serve as time-saving alternatives if only coupling constants are to be measured, or spectral editing is desired. In contrast, a quite different situation arises for $^nX,^mY$ correlations. In theory, detecting the nucleus with higher gyromagnetic ratio should still be favoured. However, signal enhancement is much smaller due to the lower factor of γ_X/γ_Y as compared to γ_H/γ_Y, and its effects may be overcompensated by other factors which may then limit the overall performance of an experiment. Important influences include details of the pulse sequence, T_1 and T_2 relaxation times of the involved nuclei, the required spectral width and resolution in both dimensions of a 2D experiment, the number of ^nX and ^nY nuclei, and last, but not least, the available hardware configuration. Even if at first glance the natural abundance of a nucleus should offer no arguments (the decisive factor for correlation spectroscopy is the product of abundances), the effectiveness of a pulse sequence to suppress unwanted signals is of high practical concern if the more abundant nucleus is to be detected. In the following discussion we will assume that the optimum hardware for each experiment is available, and neglect effects of instrument configuration.

Comparison of the performance of different $^nX,^mY$ correlation techniques, with a special focus on 2D methods, was the object of several investigations.[13,18,19,64,125] Of the 2D schemes with indirect detection, HMQC was found to yield better suppression of unwanted magnetization than HSQC which was attributed to the fewer number of pulses.[125] Further, HMQC was also found to be less sensitive to magnetization losses due to pulse imperfections[13,18,64,125] which may for example arise from pulse miscalibration, or from off-resonance effects. The latter was highlighted in ^{183}W NMR studies by Benn *et al.*[64] who demonstrated that the transfer amplitude of an INEPT step (which is also used in HSQC) decayed practically to zero when a transmitter offset of 10 kHz on the ^{183}W channel was used, whereas the HMQC technique permitted acquisition of spectra with spectral widths in $F1$ up to 50 kHz. That cross-peaks in HSQC spectra, unlike as in HMQC, are not broadened by additional homonuclear spin coupling may gain importance in systems with several strongly coupled nuclei, but should make no difference for the A_nX spin systems of many metal complexes, or for $^{13}C,^nY$ correlations where both nuclei are isotopically diluted. Polarization transfer schemes use in contrast to the indirect detection schemes only a single transfer step and may appear favourable if the heteronuclear magnetization transfer is ineffective because of the presence of a range of homo- and heteronuclear couplings,[10] and if a small γ_X/γ_Y ratio reduces further the advantage of indirect detection. Since the unrefocused HETCOR and the HMQC pulse sequences contain the same number of 90° and 180° pulses, both experiments can be expected to exhibit similar behaviour with respect to pulse offsets.

1D polarization transfer experiments can be a time-saving alternative to 2D protocols if only a few X nuclei, or even a single nucleus, are present, or if

only multiplicity editing is desired. Most 1D experiments are generally recorded with observation of the nucleus with the lower gyromagnetic ratio. The only exception has been the use of ^{13}C,^{2}D INEPT spectra for spectral editing; here, it was shown that despite the unfavourable enhancement factor of $\gamma_{^2D}/\gamma_{^{13}C} = 0.6$ similar signal-to-noise ratios as in one-pulse ^{13}C experiments were obtained owing to more favourable relaxation parameters of ^{2}D and additional ^{1}H,^{2}D NOE enhancement.[23]

With respect to relaxation, the best choice for an ^{n}X,^{m}Y correlation should be to use the nucleus with the shorter T_1 relaxation time as source nucleus, and to detect the one with the longer T_2 in order to minimize sensitivity losses associated with the detection of broad lines. Magnetization losses due to rapid T_2 relaxation during the pulse sequence can best be kept minimal by using the shortest available sequence. In order to comply with this need, 2D experiments are frequently set up with detection of antiphase magnetization immediately after the mixing pulse, thus avoiding an extra refocusing period,[18] while in 1D experiments the use of the shorter unrefocused INEPT scheme was shown to be preferable over DEPT.[47] For HMQC and HSQC schemes, different relaxation properties of single- and multiple-quantum coherences during t_1 might also be expected, although for most X,Y correlation these effects appear not predominant.[10]

In order to reduce the measuring time of a 2D experiment, the number of t_1 increments is normally kept as small as possible. To maintain sufficient resolution in the $F1$ dimension of an ^{n}X,^{m}Y correlation, it may thus appear preferable to detect the nucleus with the larger spectral width. Further, filtering of signals from outside the observation window is more easy in $F2$ than in $F1$, so that separation of a spectrum into different parts is more easily accomplished. Such an approach may be necessary for correlations involving ^{19}F or ^{31}P which exhibit both high resonance frequencies and large chemical shift ranges so that spectral regions can be too large to allow reasonably uniform 180° pulses. As a matter of curiosity it should be noted that in 2D ^{n}X,^{m}Y correlations obtained under such conditions, an ^{n}X nucleus outside the excited spectral region behaves as a heteronucleus, and correlation signals display E.Cosy patterns which allow sign determinations of couplings to this nucleus (cf. Fig. 15).

A special situation arises frequently in ^{n}X,^{m}Y correlations with a transition metal nucleus whose low receptivity enforces an indirect detection scheme, and the very large shift range of the metal must thus be covered in $F1$. In order to determine the chemical shift with sufficient accuracy in a short time, the measurement is normally carried out in two steps.[18] First, a rough estimate of $\delta(^{m}Y)$ is determined by acquiring a spectrum with a small number of t_1 increments and a large $F1$ spectral window. The Y-carrier frequency is then set near on-resonance, and the experiment repeated with a reduced spectral width, which allows to verify that the cross-peaks are not folded and affords $\delta(^{m}Y)$ with the desired accuracy.

In summary, two rules of thumb emerge for optimum conduction of ^{n}X,^{m}Y correlations: (i) indirect detection via the HMQC scheme is the method of choice if the ratio γ_X/γ_Y is high and/or large spectral widths in $F1$ have to be covered; (ii) in all other cases, relaxation and line width aspects turn the scale; 2D experiments are preferably performed by observing the nucleus with the narrower lines, with the use of HMQC, HSQC or polarization transfer schemes depending on the individual sample properties, and 1D-INEPT schemes may be competitive for systems with few ^{n}Y nuclei. The situation of case (i) is typically encountered for correlations between highly receptive nuclei as ^{19}F or ^{31}P and low-γ transition metals (^{57}Fe, ^{103}Rh, ^{109}Ag, ^{183}W, ^{187}Os). Case (ii) applies to correlations between ^{13}C and heteronuclei with comparable resonance frequencies (^{29}Si, ^{195}Pt, ^{199}Hg, ^{207}Pb), but also to borderline cases such as ^{31}P,^{13}C or ^{31}P,^{15}N where despite considerable enhancement factors ($\gamma_{^{31}P}/\gamma_{^{13}C}$ 1.61, $\gamma_{^{31}P}/\gamma_{^{14}N}$ 3.99), detection of the low-γ nucleus may under special circumstances be competitive with ^{31}P-detected experiments.[47]

3. APPLICATIONS OF X,Y CORRELATIONS

Heteronuclear ^{n}X,^{m}Y correlation spectroscopy has been put to use in the last years as tool for structure characterization in various fields of organometallic and organoelement chemistry, and its application is still growing. If one surveys the available literature on ^{n}X-detected ^{n}X,^{m}Y correlation spectroscopy, it emerges that, apart from a single study devoted to methodical aspects of polarization transfer between two quadrupolar species,[56] at least one of the four nuclei ^{6}Li, ^{13}C, ^{19}F and ^{31}P appears in all studied X,Y combinations, and a considerable amount of work involves cases where both nuclear species were chosen from this set. Quite obviously, this preference owes both to spectroscopic and chemical reasons. ^{19}F and, to some lesser extent, ^{31}P exhibit very high receptivities due to a combination of 100% natural abundance, the highest (with exception of the rarely used $^{203/205}$Tl) gyromagnetic ratio of all heteronuclei, and frequently shorter T_1 relaxation times than for other spin-half heteronuclei. Heteronuclear ^{19}F,^{m}Y or ^{31}P,^{m}Y correlations are thus readily acquired in a comparatively short time and offer large sensitivity gains over direct ^{m}Y spectroscopy. The easy accessibility and high analytical power of these methods were soon recognized and led to their widespread application in studies of phosphorus and fluorine compounds in various areas of organic or organometallic chemistry, including species which are of relevance in biological systems or in catalysis. In contrast, the ^{13}C nucleus offers far less favourable opportunities for NMR detection, but many organometallic or heterocyclic compounds possess molecular skeletons consisting of one or few heteroatoms embedded in a framework of carbon atoms. Since ^{13}C,^{m}Y correlations may detect directly the connectivities between the skeletal atoms,

they are expected to be extremely useful assignment tools, and have therefore been extensively developed in the last years. The use of correlation spectroscopy involving ^{6}Li was mainly triggered by the importance of lithiated species as reagents for organic and organometallic synthesis, and ^{6}Li,^{m}Y correlations have evolved today as a major source of structural information on organolithium reagents. Despite an unfavourable NMR receptivity due to rather low gyromagnetic ratio and long T_1 relaxation times, correlations with ^{6}Li are generally readily performed since isotopic enrichment of ^{6}Li is easily possible.

Beside the "true" ^{n}X,^{m}Y correlations, various studies devoted to the analysis of $J(^{n}X,^{m}Y)$ coupling information were performed by using pseudo triple-resonance techniques with passive selection of low abundant ^{m}Y satellite lines. Even though these methods give no access to ^{m}Y chemical shifts and are in most cases inappropriate to solve assignment problems if more than one ^{m}Y nucleus is present, their application has led to a substantial knowledge on systematic trends in couplings from ^{15}N and ^{13}C to other rare heteronuclei, which provides an important data base for future structural assignments. Most of the material has been reviewed,[114] but a short account on recent applications of these techniques will also be included in this section.

3.1. ^{19}F,^{m}Y correlations

Due to the high receptivity of ^{19}F, ^{19}F,^{m}Y correlation spectroscopy became available very early in the history of NMR spectroscopy. Using the INDOR technique on a cw-spectrometer, McFarlane and coworkers gave the first report whatsoever on the use of ^{n}X,^{m}Y correlated spectroscopy for indirect observation via ^{19}F of the ^{183}W resonances in complexes of the type $WF_{6-n}OR_n$ and WOF_4L.[29] Beside the first chemical shift determination for a low-γ transition metal, which was at that time not feasible by any other technique, further the indirect determination of $J(^{183}W,^{31}P)$, and the assignment of relative coupling signs, was reported.

Despite the high sensitivity gain achievable with ^{19}F detection, examples of correlations between ^{19}F and low-γ metals have remained scarce, presumably because of difficulties with the hardware set-up.[22] Still, Bourdonneau and Brevard demonstrated the application of ^{19}F,^{183}W HSQC and inverse ^{19}F,^{183}W DEPT experiments to measure $\delta(^{183}W)$ and $T_1(^{183}W)$ of a polytungstate.[20] A comparison of the indirect and direct T_1 (^{183}W) experiments showed that both methods yield the same results, but the indirect scheme used 1.3 instead of 72 h of instrument time. 1D- and 2D-^{109}Ag,^{19}F polarization transfer experiments were employed by the group of Eujen[45,46,92] for the characterization of CF_2H and CF_3 derivatives of silver(III). In combination with ^{13}C,^{19}F and ^{13}C,^{1}H correlations, these experiments aided in the analysis of the extremely complicated coupling patterns, and coupling sign determinations allowed to

conclude that all reduced couplings involving the metal are positive and no sign crossover occurs. A correlation between ^{19}F and a main group metal was reported for the pair $^{19}F,^{117}Sn$ (^{117}Sn was chosen because of apparative reasons instead of the more familiar ^{119}Sn)[126] and served to confirm the assignment of ^{19}F and $^{117/119}Sn$ signals of two conformers of a substituted difluorostannane.

Considerable more attention than correlations of ^{19}F with metal nuclei have received those with other nonmetals. Even though by far the most work in this area has been devoted to $^{19}F,^{13}C$ correlation spectroscopy of polyfluorinated carbon compounds, $^{15}N,^{19}F$ INEPT was used to record ^{15}N NMR spectra of perfluoropyridine and some perfluoroazines,[50] and the desire to determine relative signs for $^2J(^{207}Pb,^{19}F)$ and $^1J(^{207}Pb,^{13}C)$ inspired the use of 2D-$^{19}F,^{13}C$ correlations for the characterization of plumbanes $(CF_3)_nPbR_{4-n}$.[75] Interestingly, the results revealed that sign changes for $^1J(Pb,C)$ may be induced not only by different substituents, but also by a change of the solvent.

Investigations of fluorinated organic compounds by means of $^{13}C,^{19}F$ correlation were triggered by the intention to develop effective analytical methods for the identification and characterization of specifically fluorine-labelled metabolic products of pesticide or drug models. Giralt *et al.* studied the prospect of 1D-$^{13}C,^{19}F$ DEPT and INEPT via one- and two-bond couplings, and demonstrated the sensitivity-enhanced detection of the fluorinated carbon in a steroid by this method.[44] 2D-$^{13}C,^{19}F$ HETCOR experiments were employed together with $^{13}C,^1H$ correlations by Ribeiro *et al.*[21] to measure and assign heteronuclear couplings in the CF_3CH_n fragments of halothane and trifluoroethanol. Successful application of the methodology to an artificial compound mixture demonstrated further the potential for the analysis of complex blends of fluorinated products which are typical for metabolic studies.

Analysis of poly- and perfluorinated organic molecules is often hampered by the fact that for larger molecules the location and assignment of ^{19}F and ^{13}C resonances become uncertain, so that the carbon backbones of these molecules are frequently very poorly characterized.[74] In consideration of the large interest in applications of these compounds, several research groups set out to tackle the assignment problem by 2D-$^{13}C,^{19}F$ correlation techniques.[22,73,74,127] An efficient strategy for resonance assignment in linear perfluoroalkyl structures was developed in particular by Ribeiro[73,74] who showed that HMQC experiments are easily optimized for coherence transfer via $^1J(F,C)$ (average value ~275 Hz) or $^2J(F,C)$ (average value ~27–36 Hz), and that combination of both experiments allows to correlate a specific fluorine nucleus to the directly connected and the adjacent carbon atoms in a chain, respectively. Unlike the case of hydrocarbon molecules, where $^2J(C,H)$ and $^3J(C,H)$ are in the same range, cross-peaks via $^3J(F,C)$ (<1 Hz) are normally not detected, and no ambiguities between $^2J(F,C)$ and $^3J(F,C)$ connectivities arise.[73] It should be noted, however, that only partial

assignment of the spectra is feasible if incomplete sets of two bond connectivities are observed, presumably due to different magnitudes of ^2J(F,C) or destructive interference between various couplings.[74] For aromatic fluorine compounds where the resonances of adjacent ^{19}F nuclei can be identified on the basis of ^3J(F,F) couplings, the ^{13}C resonances have been assigned alone from ^{19}F,^{13}C HMQC spectra via ^1J(F,C).[22,127]

Rinaldi *et al.* introduced the use of ^{19}F,^{13}C correlations for the characterization of microstructures in fluoropolymers by demonstrating that highly dispersed 2D-^{19}F,^{13}C HMQC and HMBC spectra allowed the identification of different triads and pentads in a 1-chloro-1-fluoroethylene/isobutylene copolymer,[128] and 3D-^{1}H,^{13}C,^{19}F experiments permitted assignment of the tacticity in polymeric 1-chloro-1-fluoroethylene.[99,100] The latter experiment is interesting because it exploits the unique chemical shift dispersion of ^{19}F nuclei for the separation of resonances originating from different stereosequences, and then uses the cross-peak multiplicities in the ^{1}H,^{13}C slices of the 3D cube at each ^{19}F frequency for the assignment of the local stereochemistry, thus allowing to distinguish between mm, mr and rr triads (m = meso, r = racemic) (Fig. 14). Analysis of the occurrence of identical cross-peaks in more than one ^{19}F slice yields further information on the relative stereochemistry of adjacent diads and allows to assign ^{1}H and ^{13}C resonances of all possible tetrads in the polymer chain.

In a recent paper, Günther *et al.* demonstrated that ^{19}F,^{13}C correlation techniques are likewise applicable to the characterization of fluoro-substituted aromatics adsorbed on silica and alumina, thus highlighting the power of this method for studies of surface reactions which are of possible interest, e.g. in heterogeneous catalysis.[129]

3.2. ^{31}P,^{m}Y correlations

^{31}P,^{m}Y correlation experiments were initially inspired by the idea to exploit the high NMR sensitivity of ^{31}P for the detection of the resonances of low-γ transition metal nuclei, and still the major part of all activities in the general field of ^{n}X,^{m}Y correlations is dedicated to this purpose. The first ^{31}P,^{m}Y correlations were performed with $^{107/109}$Ag,[30,43] ^{183}W,[36,48] ^{57}Fe[48] and ^{103}Rh,[48] and the last two together with ^{187}Os[116] make up the main body of ^{31}P,^{m}Y correlations until today. Further metal nuclei which have been studied include the quadrupolar ^{61}Ni,[18] ^{195}Pt[78] and ^{199}Hg.[130] Whereas the first implementations of phosphorus–metal correlations used mainly ^{31}P-detected pseudo-INDOR[29,30] or metal detected polarization transfer schemes,[48] today the field has been taken over by 2D spectroscopy on the basis of ^{31}P-detected HMQC or HSQC pulse schemes.[13,18,87] The main incentives for correlation of ^{31}P with metal nuclei have been, beside the elucidation of chemical structures of metal complexes, attempts to use systematic studies of trends in transition metal

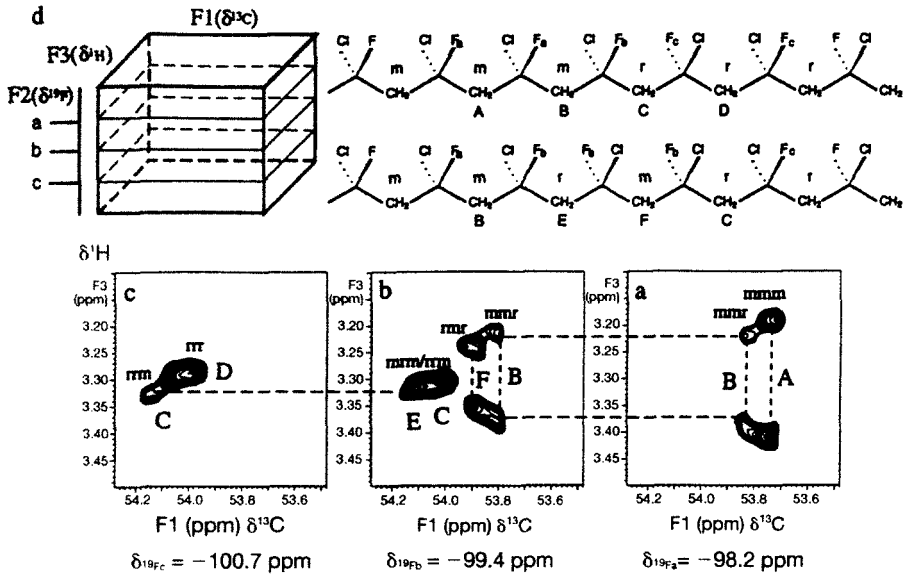

Fig. 14. 3D-^{1}H,^{13}C,^{19}F correlation of poly(1-chloro-1-fluoroethylene) with F_1F_3 slices at $\delta(^{19}F) = -98.2$ (a), -99.4 (b), -100.7 (c); (d) schematic illustration of the 3D spectrum with relative positions of the slices. Each slice in (a)–(c) displays two correlation signals representing the two CH_2 groups adjacent to a CF moiety. The polymer tacticity can be determined as follows:[100] the splitting of each signal reveals the stereochemistry of individual CFCl–CH_2–CFCl diads, the two protons at a methylene carbon being chemically inequivalent in meso (m) and chemically equivalent in racemic (r) diads. Consequently, the fluorine atoms can be assigned to rr (a), rm (b) or mm triads (c). The possible tetrad structures can be determined by looking for identical C–H cross-peaks in different ^{19}F slices; e.g. the A cross-peaks in (a) do not occur in the other two slices; therefore, the methylene group A shows only correlations with ^{19}F atoms in mm triads and must be centred in an mmm tetrad, etc. Reproduced, with permission, from ref. 100. Copyright 1996 American Chemical Society.

chemical shifts, phosphorus–metal couplings, or metal relaxation times to analyse differences in the electronic structures of the metal compounds. In some cases, also correlations between these NMR parameters and other chemical properties were found and used to obtain structure–reactivity relationships which may become very important in connection with the prediction of chemical reactivities.[19,35,131,132] A concise analysis of the origin of electronic effects on δ(M), J(M,P) and T_1(M) is complex, and a thorough discussion can be found elsewhere.[133–135] However, for understanding the basic ideas it is convenient to remember some approximative, but useful descriptions of the behaviour of the individual parameters. The metal chemical shifts are considered to be dominated by the variation of the Ramsey's

paramagnetic shielding term σ_p[136,137] which is for d-block metals commanded by the electrons in the metal d orbitals.[138,139] A frequently used approximation to σ_p is given in Eq. (4); here $\langle r \rangle$ denotes the mean radius of the valence d shell, ΔE is the average electronic excitation energy, and QN is the angular imbalance of charge.

$$\sigma_p = -\langle r^{-3} \rangle (\Delta E)^{-1} \Sigma_{QN} \tag{4}$$

Scalar couplings to metal nuclei are dominated by the Fermi contact term, and approximation on a similar level as for the chemical shifts leads to the expression in Eq. (5), with $^3\Delta E$ being the mean triplet excitation energy, $|S(0)|_X$ the s-electron density at the nucleus X, and π_{ML} the mutual polarizability of the orbital connecting the metal and the ligating atom L.[134]

$$^1J(M,L) \propto \gamma_M \gamma_L (^3\Delta E)^{-1} |S(0)|^2_M |S(0)|^2_L \pi_{ML} \tag{5}$$

Application of $^{31}P,^mM$ correlations to the structure elucidation of metal complexes

The use of the information from phosphorus–metal correlations as a structure assignment tool was the main issue in reports devoted to the study of silver complexes.[30,43,86–89,140] Colquhoun and McFarlane[30] were the first to demonstrate the prospect of 2D-$^{31}P,^mM$ correlations to determine the number of phosphite ligands in the complexes $[(PhO_3P)_nAg]^+$. Sadler *et al.*[43,86] applied both one-dimensional $^{109}Ag,^{31}P$ DEPT[43] and 2D $^{31}P,^{109}Ag$ HSQC to the characterization of tetrahedral silver complexes with various bidentate phosphine ligands and found that $^1J(^{109}Ag,^{31}P)$ values are readily obtained even in cases where ^{31}P spectra contain complicated higher-order multiplets which are difficult to interpret. Detection and analysis of dynamic equilibria by $^{31}P,^{109}Ag$ correlation were demonstrated in the case of the complexes $([Ag(d2pype)_2]_n^{n+}$ (d2pype = 1,2-bis-(di-2-pyridyl)phosphino)ethane); here, the analytic potential of $^{31}P,^{109}Ag$ correlations showed up not only in the detection of monomers, dimers and trimers, but in particular in the successful proof of different coordination modes for the d2pype ligands in individual oligomers.[89] Pregosin *et al.*[87] used 2D-$^{31}P,^{109}Ag$ correlation as crucial experiments in the identification of silver complexes which are presumed models for intermediates in the Au(I)-catalysed aldol condensation of aldehydes with isonitriles. $^{31}P,^{109}Ag$-HMQC spectra were further used by Gudat *et al.* to identify kinetically unstable complexes formed in the reaction of diazaphospholene ligands with silver triflate,[88] and to corroborate the structural assignment of silver complexes of a cationic bis-phosphonio-isophosphindolide (BPI) ligand;[140] in the latter case, the discrimination between complexes of composition $[(BPI)Ag(OTf)_2]$ and $[(BPI)Ag(OTf)(THF)]^+$ by their different ^{109}Ag chemical shifts is of particular interest as it demonstrates the use of

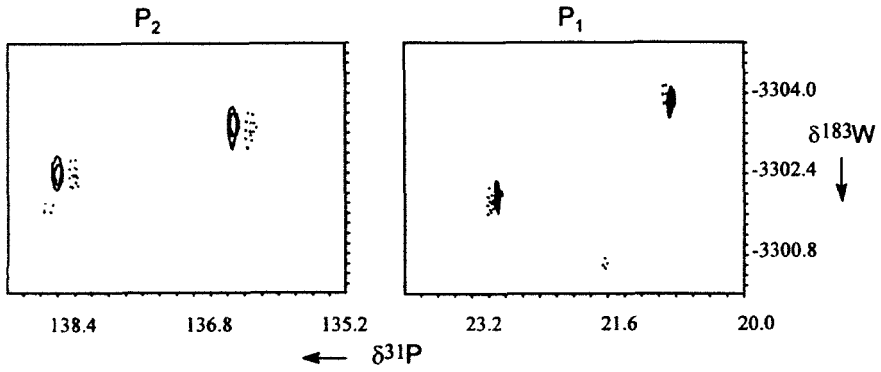

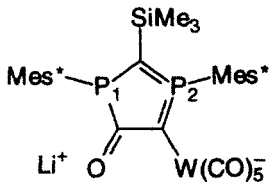

$\delta(P_1)$ 21.9, $^2J(W,P_1)$ 11.9 Hz
$\delta(P_2)$ 137.5, $^2J(W,P_2)$ 25.2 Hz
$^2J(P_1,P_2)$ 251.4 Hz

Fig. 15. $^{31}P,^{183}W$ correlation via long-range $^2J(W,P)$ and $^3J(W,P)$ couplings of the shown tungsten carbene complex (Mes* = 2,4,6-tri-*tert*-butylphenyl).[141] Both spectra were obtained with the HMQC pulse sequence of Fig. 3(c) using TPPI phase cycling to obtain a phase-sensitive spectrum, and with the ^{31}P transmitter set on-resonance to the signal of the observed P^1 and P^2 atoms, respectively. The $P^{1/2}$,W cross-peaks are split by the active $J(W,P^{1/2})$ and the passive $J(P^1,P^2)$ couplings in $F2$ and by the passive $J(W,P^{2/1})$ coupling in $F1$. The E.Cosy splitting owes to the fact that due to the large chemical shift difference between the ^{31}P signals ($\Delta\delta \approx 140$ ppm, corresponding to an offset of 14 kHz) the second phosphorus signal resonance lies outside the excited spectral region and behaves in essence as a heteronucleus. The identical tilt of the cross-peaks indicates like signs of $^2J(W,P)$ and $^3J(W,P)$.

indirect detection metal NMR to monitor the exchange of a spectroscopically "transparent" ligand.

Strategies for the use of $^{31}P,^{n}M$ correlations for structure elucidation of organometallic compounds of tungsten, iron or rhodium were outlined by Benn and coworkers[18,19,64,66] who demonstrated elegantly how the rich available information content can be utilized to extract coupling signs for both $^1J(M,P)$ and $^nJ(M,H)$ (cf. Fig. 7), and to assign resonances in complicated organometallic frameworks. The feasibility of $^{31}P,^{n}M$ correlations via long-range couplings is demonstrated by the $^{31}P,^{183}W$ HMQC spectrum of a tungsten carbene complex (Fig. 15) which yielded in addition to the value of $\delta(^{183}W)$ the confirmation of like coupling signs for $^2J(W,P)$ and $^3J(W,P)$.[141]

In regard of the importance of Rh-complexes as homogeneous catalysts, in particular 2D-$^{31}P,^{103}Rh$ correlation has been applied in several cases to the

structural characterization of complexes which have importance as model compounds in homogeneous catalysis. Lindner *et al.* determined $\delta(^{103}Rh)$ values for various complexes with hemilabile ether–phosphine ligands[142–145] and concluded that the results allow to distinguish between square-planar, square-pyramidal and octahedral metal coordination geometry.[143] Carlton characterized products and intermediates formed in the reaction of tris(phosphine)rhodium hydrides with carboxylic acids or thiols in the presence of pyridine.[146] As some of the intermediates were not isolable but may exist only in equilibrium mixtures in the presence of H_2, *in situ* methods are required for their characterization. The potential of $^{31}P,^{103}Rh$ correlation for this purpose is demonstrated in Fig. 16. To assist signal assignment, the spectrum was acquired without ^1H decoupling, thus enabling to identify the correlation peaks from hydride-containing products by means of the splitting due to $^1J(Rh,H)$ $^2J(P,H)$.

The benefit of $^{31}P,^mM$ correlation techniques in cases where direct observation of the metal is in principle feasible because of a sufficiently high γ-value was recently outlined for complexes of ^{195}Pt and ^{199}Hg. Ruegger and Moskau recorded a 2D $^{31}P,^{195}Pt$ correlation of a trinuclear platinum-phosphine cluster with a modified HMQC sequence and by using long-range couplings $^2J(Pt,P)$ for coherence transfer.[78] They demonstrated that, in contrast to 1D-^{31}P and ^{195}Pt spectra which show complicated patterns due to superposition of subspectra from isotopomers with zero to three magnetically active metals, the correlation maps are easily interpreted by using a small set of simple rules, and both magnitudes and signs of couplings (including the homonuclear $^2J(P,P)$) are readily available. Gudat *et al.*[130,147] obtained $^{31}P,^{199}Hg$ HMQC spectra of some mercury complexes via both $^1J(Hg,P)$ and $J(Hg,P)$ to support structural assignments and noted that avoiding the problems of very broad metal resonances by the indirect detection scheme allowed to obtain $\delta(^{199}Hg)$ in much shorter time as could be expected alone on the basis of gyromagnetic ratios.[147]

Application of $^{31}P,^mY$ indirect detection schemes to electronic structure correlations in metal complexes

In theory, proton-detected inverse spectroscopy can be considered the most sensitive method for measurement of transition metal chemical shifts and should be the method of choice for systematic investigations. Even if the higher sensitivity of ^1H- over ^{31}P-detected inverse spectroscopy has been experimentally confirmed for some examples,[17,19,66] ^{31}P-detection schemes may still be competitive or even advantageous in special circumstances: many organometallic and coordination compounds with phosphine ligands exhibit large $^1J(M,P)$ couplings and singlet resonances in the $^{31}P\{^1H\}$ spectra which helps to minimize relaxation losses since short defocusing delays can be used, and permits easy detection of the satellite lines. In contrast, ^1H-detection may

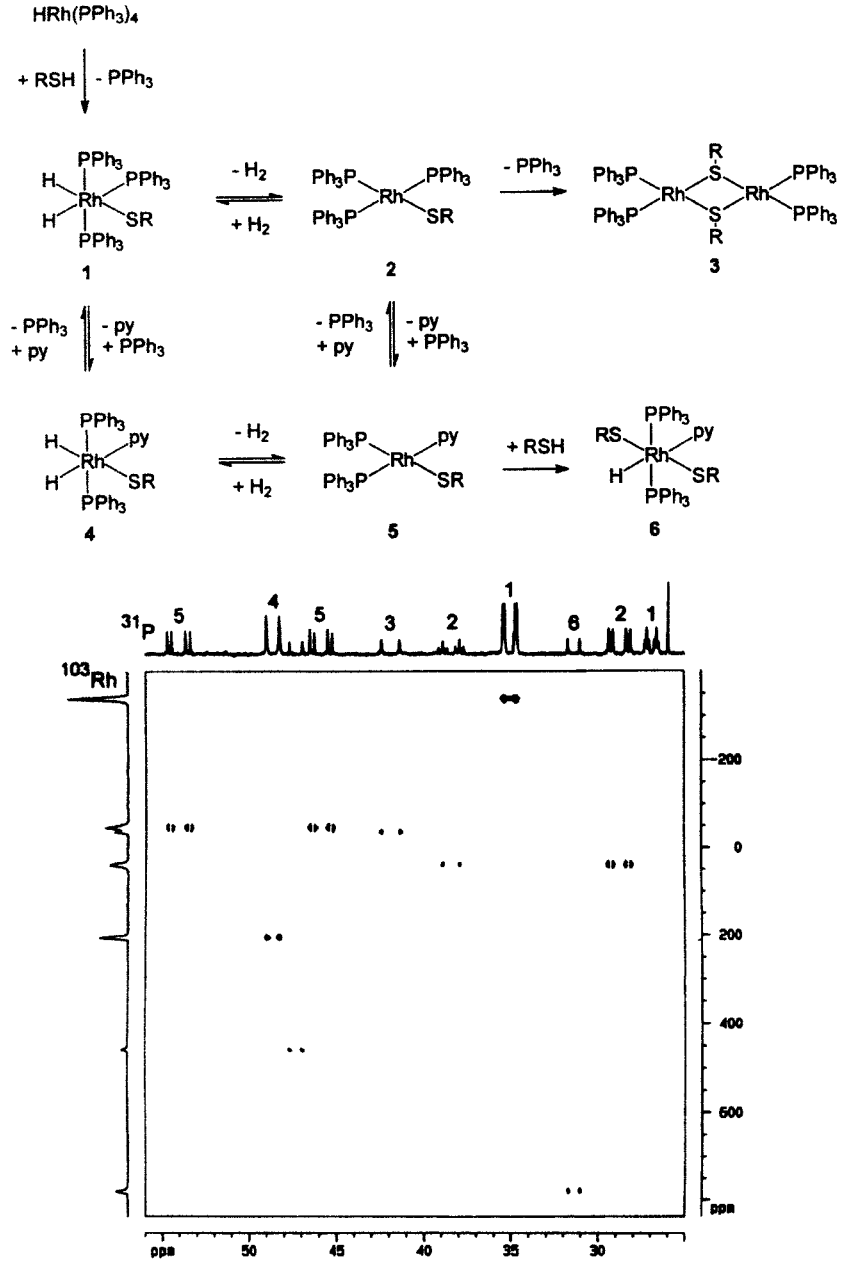

Fig. 16. $^{31}P,^{103}Rh$ HMQC spectrum of a reaction mixture of $[(PPh_3)_4(H)]Rh$ with cyclohexyl thiol showing the correlation signals of species 1–6. The spectrum was recorded without ^1H-decoupling to help identification of the correlation peaks from hydride-containing products by means of the splittings due to $^1J(Rh,H)$ and $^2J(P,H)$. Reproduced, with permission, from ref. 146. Copyright 1997, John Wiley & Sons.

require to use small long-range couplings for coherence transfer, resulting in severe relaxation losses, or M,H coupling may be absent at all; furthermore, proton resonances appear often as complicated multiplets, thus reducing the sensitivity advantage and making small M,H couplings hard to detect.[19,65] Consequently, ^{1}H- and ^{31}P-detected inverse spectroscopy have been used complementary to each other in some cases,[19,131,148,149] and today a considerable body of systematic studies of metal chemical shifts and phosphorus–metal couplings via ^{31}P,^{n}M-correlation in compounds with low-γ metals of group 6 (^{183}W), 8 (^{57}Fe,^{187}Os), 9 (^{103}Rh) and 10 (^{61}Ni) is known.

The first use of ^{31}P detection for a methodical investigation on metal shieldings was reported by McFarlane *et al.*[32,150] who studied $\delta(^{183}W)$ in complexes $LW(CO)_5$ and $L_2W(CO)_4$ where L is a phosphine or phosphite. They observed that the variation in $\delta(^{183}W)$ parallels that of $\delta(^{95}Mo)$ for the analogous molybdenum complexes, but is larger than there by a factor of 1.7. This was attributed to a larger influence of the electronic imbalance term, while the substituent-induced changes in δ(M) were explained by changes in the mean excitation energy ΔE induced by different ligand-metal back-donation. A similar parallelism between ^{1}K(M,P) in the two series of complexes was attributed to the smaller value of $|S(0)|^2$ for molybdenum. In a more recent investigation on alkenyl-carbyne tungsten complexes of the type $L_n(CO)_{3-n}W{\equiv}C{-}CH{=}C(CH_2)_m$ (L = phosphine, halide, MeCN), Lopéz-Ortiz *et al.*[17] concluded that the change in $\delta(^{183}W)$ induced by variation of L was dominated by electronic factors (higher ΔE with increasing π-bonding strength, and increase of $\langle r^{-3}\rangle$ with increasing charge, of L), while the influence of the different ring size of the cyclic $C(CH_2)_m$ fragment was attributed to both electronic and steric effects.

Detailed investigations on metal shieldings in organometallic iron and osmium complexes by means of ^{31}P,^{57}Fe(^{187}Os) HMQC schemes were performed by the groups of Benn and von Philipsborn. The structural types of studied complexes include cyclopentadienyls of the types $Cp^{\dagger}Fe(L)_2X$,[18,19] $Cp^{\dagger}Fe(L)_2R$,[18,19] $Cp^{\dagger}Os(L)_2R$,[19,65] $Cp^{\dagger}Fe(L)$(olefin)R,[19] $Cp^{\dagger}Fe(L')(L)R$,[148] diene complexes (diene)$Fe(CO)_2(L)$,[18,132] and arene complexes (arene)$Os(L)X_2$,[149] and (arene)Os(L')(L)I ($Cp^{\dagger}$ = (substituted) cyclopentadienyl, L = phosphine or phosphite, L' = non-phosphorus containing ligand, R = organyl, X = halogen). The general effects governing the variation in $\delta(^{57}Fe)$ and $\delta(^{187}Os)$ in all compounds can be summarized as follows: (i) substitution of directly bonded atoms (e.g. H vs. Cl, Br) induces large effects which are explained by assuming that with higher electronegativity of the ligand the radial term $\langle r^{-3}\rangle$ and the deshielding increases (normal halogen dependence); (ii) smaller changes following structural variation within the ligands L, L' were ascribed to an increase in the mean excitation energy ΔE which led to an increased metal shielding with higher π-acceptor power of the ligand; (iii) increasing size of the ligands produced further deshielding effects of lower or similar magnitude as the

electronic effects. The dominance of steric effects was proven for complexes $CpFe(L)(CO)COMe$[148] and $(cymene)Os(L)X_2$[149] by means of linear correlations betweeen δ(M) and Tolman's cone angles of the ligands L.

Interesting correlations between $\delta(^{57}Fe)$ and chemical properties were observed for complexes $CpFe(L)_2R$,[19] where the metal shifts show similar qualitative trends as thermal stabilities, cyclovoltammetric oxidation potentials, and reactivity towards ethylene insertion reactions, and for compounds $(L)Fe(CO)_2(\eta^4\text{-diene})$ where the thermodynamically more stable conformers with apical orientation of L with respect to the diene fragment exhibited substantially more shielded metal nuclei than the basal conformers.[132] A linear correlation between $\delta(^{57}Fe)$ and Taft's electronic parameter $\sigma^I(Y)$ allowed to rationalize substitution effects in the Cp ring of complexes $(C_5H_4Y)Fe(CO)(PPh_3)Me$.[148] For $Cp(Fe,Os)(PPh_3)_2X$, $\delta(^{57}Fe)$ and $\delta(^{187}Os)$ follow similar trends, but the osmium chemical shift range in these complexes seems to be somewhat surprisingly of similar size or even less than that of iron.[65]

A different class of iron compounds, viz. model haem complexes $(Por)Fe(PMe_3)(L')$ (Por = substituted porphyrins), were studied by Walker *et al.*[34,35] using a selective double-resonance technique in connection with isotopic enrichment of ^{57}Fe. The complexes display a linear correlation between $\delta^{57}Fe$ and $\delta^{31}P$ of the phosphine ligand, and the variation of iron chemical shifts could be explained in terms of electronic d–d transition energies.

In particular the groups of Elsevier and von Philipsborn applied $^{31}P,^{103}Rh$ HMQC spectroscopy to investigate metal shieldings in rhodium complexes. Most studies focused on square planar Rh(I) complexes of the type $[(L)_2Rh(L')_2]^+$ and $[(L)_4Rh]^+$,[151,152] $(L)_2(L')RhY$ and $(L)(L')_2RhY$,[153,154] (Y = H, organyl, halogen), octahedral rhodoximes $Rh(oxime)_2(R)(L)$,[155] and half-sandwich complexes $Cp^*Rh(L)Y_2$.[131,156] Even if it turned out that ^{103}Rh shifts are governed by the same factors as those of ^{57}Fe or ^{187}Os, it was suggested that electronic influences through the ΔE term are less important for square-planar Rh(I) complexes than for Rh(III) compounds, so that electronic influences which are transmitted through the $\langle r^{-3}\rangle$ term (e.g. different basicity of phosphines) and, in particular, steric effects dominate.[152] This is highlighted in the case of the complexes $(cod)Rh(L)Cl$[154] where regression analysis showed that 95% of the variability of ^{103}Rh chemical shifts could be accounted for by similar contributions from electronic and steric influences as were represented by Tolman's electronic parameter ν and cone angle θ. A correlation of $\delta(^{103}Rh)$ with the cone angles of the ligands L was also found for $Cp^*Rh(L)Cl_2$,[156] and $\delta(^{103}Rh)$ in alkyl rhodoximes (oxime)2Rh(L)R correlates with Taft's steric parameters for R.[155]

Two remarkable studies which correlate ^{103}Rh chemical shifts directly with chemical properties were reported by von Philipsborn *et al.* For chiral complexes (P-P*)Rh(enamide) where P-P* denotes an SS-dipamp or

SS-chiraphos ligand, they demonstrated that the metal in major diastereomer exhibits always the higher shielding. Analysis of this effect led to suggest that the enamide ligand in this diastereomer is a better electron donor and renders the complex less reactive towards H_2 addition, thus supporting the idea that the diastereoselectivity of this reaction, which is the basis for the application of such Rh catalysts in asymmetric hydrogenation, is electronically controlled.[153] More recently, they reported on a correlation between the rate of the PPh_3 assisted aryl migration in complexes Cp*Rh(CO)(I)(aryl) to give Cp*Rh(PPh_3)(C(O)aryl) with $\delta(^{103}Rh)$ of the products, which was interpreted by assuming an associative reaction mechanism with a late transition state.[131]

Cationic Rh(I) species with chelating phosphoraniminato-phosphines were further investigated by Cavell *et al.*,[157] who found it, however, impossible to establish any clear ligand effect on $\delta(^{103}Rh)$. Furthermore, the deshielding of compounds with five- as compared to six-membered chelate ring systems indicates a behaviour opposite to the results of previous studies.[152,154] A repeatedly noted feature of various types of Rh complexes is the absence of a clear relation between $\delta(^{103}Rh)$ and $^1J(Rh,P)$;[154,156] however, in some cases linear correlations between $\delta(^{103}Rh)$ and $\delta(^{31}P)$ of the ligands were mentioned.[152]

A single study of $\delta(^{61}Ni)$ in complexes $(R_3P)Ni(CO)_3$ by $^{31}P,^{61}Ni$ correlation revealed very small chemical shift differences ($\Delta\delta \sim 100$ ppm) as compared to the known chemical shift range of 2000 ppm for tetrahedral NiL_4 complexes which were not further interpreted.[18] Unlike as for spin-half metal nuclei, the sensitivity advantage of the HMQC scheme over a direct detection experiment was in in this case small since the sensitivity gain by $(\gamma_{^{31}P}/\gamma_{^{61}Ni})^3$ was essentially compensated by the longer relaxation time of ^{31}P as compared to the quadrupolar ^{61}Ni which enforced a lower pulse repetition rate for the 2D experiment.

$^{31}P,^mY$ correlations with nonmetals

Correlations between phosphorus and main group metals are unknown except the case of $^{31}P,^6Li$ which will be covered in Section 3.3, but several $^{31}P,^mY$ correlation experiments with nonmetals, predominantly ^{13}C and ^{15}N, have been performed. Apart from some studies where mainly techniques and strategies of 1D- and 2D-$^{31}P,^{13}C$ correlations were explored,[51,81,125] analytic applications of this technique focused on measurement of sign and magnitude of scalar couplings, and the determination of skeletal connectivities.

Grossmann *et al.* used 2D-$^{13}C,^{31}P$ HETCOR and DEPT spectra to analyse higher-order AA'X spin systems in the ^{13}C isotopomers of symmetrical bis-phosphonates with an RO_3P-C-C-PO_3R backbone.[158,159] Based on the known results of a product operator analysis,[160] it was shown that magnitudes and signs (relative to $^1J(P,C)$ which is positive) of $^3J(P,P)$ and $^2J(P,C)$ can be

reliably determined, even for strongly coupled spin systems. Both $^{13}C,^{31}P$ and $^{15}N,^{31}P$ correlations were employed by Gudat *et al.*[67] to specify skeletal connectivities and stereochemistry in the three-membered rings of azadiphosphiridines. Stereochemical assignments were derived from comparison of $^{2}J(P,C)$ couplings in a pair of diastereomers, by taking the constitution of one isomer, whose crystal structure was known, as reference, and appointing the other one by using the known dependence[161] of $^{2}J(P,C)$ on the dihedral angle between lone-pair axis and P–C bond. The required information on signs of $^{2}J(P,C)$ was obtained by recording $^{13}C,^{31}P$ INEPT spectra with 45° mixing pulses. Comparison of observed coupling patterns allowed to derive the conformations of other members of the series and shed light on the mechanism of the cycloaddition in which the heterocycles were formed.

A 3D-$^{1}H,^{13}C,^{31}P$ correlation (cf. Fig. 10) was used by Berger as the key tool to assign the ^{1}H, ^{13}C and ^{31}P NMR signals of R-prophos, $Ph_2PCH_2CH(Me)PPh_2$, which is an important chiral ligand in asymmetric catalysis.[98] Similar techniques have been shown useful for constitution analysis of oligonucleotides[101] and are now widely applied to the analysis of biological phosphorus compounds;[94,95] however, a detailed discussion of these applications is beyond the scope of this article. Rinaldi *et al.*[102] applied a gradient-enhanced 3D-shift correlation to identify chain-end structures in polystyrene materials which were obtained from phosphinyl-radical initiated polymerization of styrene. The experiment exploits the high dispersion of ^{31}P chemical shifts to distinguish between different topologies of the chain ends and works in much the same way as was described in Section 3.1 for the characterization of fluoropolymers by 3D-$^{1}H,^{19}F,^{13}C$ correlation. 1D-$^{13}C,^{31}P\{^{1}H\}$ INEPT was used for both sensitivity enhancement and signal selection in the characterization of thermolabile phosphavinylidene carbenoids $Mes^*P(=C(SiMe_3)_2)=C(X)\{Li(thf)_n\}$ and $Mes^*P=C(Cl)\{Li(thf)_n\}$.[162,163] Combination of phase cycle selection of the polarization transfer signal and presaturation of strong solvent signals permitted to measure $\delta(^{13}C)$, $J(P,C)$ and $J(C,Li)$ from singly ^{6}Li-labelled samples at natural abundance level of ^{13}C, and in non-deuterated solvents.

The first report on ^{31}P-enhanced ^{15}N NMR spectroscopy comprised the use of the ^{31}P-based INEPT sequence for the characterization of ^{15}N-enriched phosphine complexes of imido-gold compounds.[49] Later applications of ^{31}P, ^{15}N-INEPT focused on investigations of samples containing ^{15}N at natural abundance, and it was shown that in favourable cases achievable signal-to-noise ratios are comparable to those of ^{15}N, ^{1}H INEPT via $^{n}J(N,H)$ long-range couplings.[47] Consequently, the method was employed for the systematic measurement of ^{15}N parameters of various phosphorus nitrogen compounds with a single phosphorus atom (to render unambiguous assignment of couplings possible) and unusual coordination numbers or bonding situation, including iminophosphines RP=NR′,[47,164] bis-imino-phosphoranes $RP(=NR')_2$,[165] tris imido-metaphosphate ions $[P(NR)_3]^-$,[47] small

ring heterocycles,[166] and phosphazene derivatives.[167] Interpretation of the data by means of regression analysis and/or comparison with quantum chemical model calculations allowed to derive correlations between $\delta(^{15}N)$ or $^{1}J(P,N)$ with E/Z configuration of phosphorus nitrogen double bonds or with electronic properties of the substituents.[164,165]

2D-$^{31}P,^{15}N$ correlations based on both ^{31}P[58,59,168] or ^{15}N detection[67,165] were applied in several cases for the characterization of compounds with more complex molecular structures. Using $^{31}P,^{15}N\{^{1}H\}$ HMQC in combination with 1D-$^{15}N,^{31}P\{^{1}H\}$ INEPT permitted López-Ortiz *et al.*[58,59] for the first time to obtain a full complement of ^{15}N parameters of cyclotriphosphazenes at natural abundance of ^{15}N, including the assignment of signs and magnitude of both $^{1}J(P,N)$ and $^{3}J(P,N)$ couplings. The same methodology served also for successful measurement of ^{15}N NMR parameters of a linear polyphosphazene. Carlton[168] applied $^{31}P,^{15}N$ HMQC experiments to the characterization of azido complexes of rhodium and was able to distinguish between two different bonding modes of the azide ligand. The particular value of the indirect detection scheme for measurement of broadened ^{15}N resonances which arise from unresolved couplings to a quadrupolar nucleus such as ^{11}B is demonstrated in the example depicted in Fig. 17:[169] the 1D-$^{15}N,^{31}P$ INEPT spectrum of a borylated bis-imino-phosphorane displays only the resonance of the nitrogen in the arylimino fragment, while in the ^{31}P-detected 2D spectrum also the resonance of the borylimino group is clearly visible. 2D-$^{15}N,^{31}P\{^{1}H\}$ INEPT with 90° and 45° mixing pulses was used further to determine skeletal connectivities and measure $^{1,2}J(P,N)$ couplings in azadiphosphiridine and azatriphosphetidine heterocycles[67] and for a conformational analysis of a phosphino-substituted bis-iminophosphorane $(tBu_2)P–P(=NtBu)=NMes^*$.[165]

Correlations between ^{31}P and nonmetals other than ^{13}C or ^{15}N include each a single example of $^{31}P,^{17}O$ and $^{31}P,^{77}Se$ correlated spectroscopy. A 1D-$^{31}P,^{17}O$ HMQC experiment was used to identify the signal of ^{17}O-labelled orthophosphate beside unlabelled ADP in a phosphate mixture.[57] Despite the difficulties of correlation spectroscopy with rapidly relaxing quadrupole nuclei such as ^{17}O, such experiments may prove of value for nondestructive analysis and diagnostics in biological and medicinal research. 2D-$^{31}P,^{77}Se$ HMQC experiments were used for indirect detection of the ^{77}Se signals in a mixture of bis-seleno-phosphinates which were hard to observe directly due to dynamic exchange broadening.[170]

3.3. $^{13}C,^{m}Y$ correlations

The nearly ubiquitous occurrence of carbon in the molecular backbones of organometallic and organoelement compounds has inspired many studies on $^{13}C,^{m}Y$ correlations, and to date the diversity of correlation partners

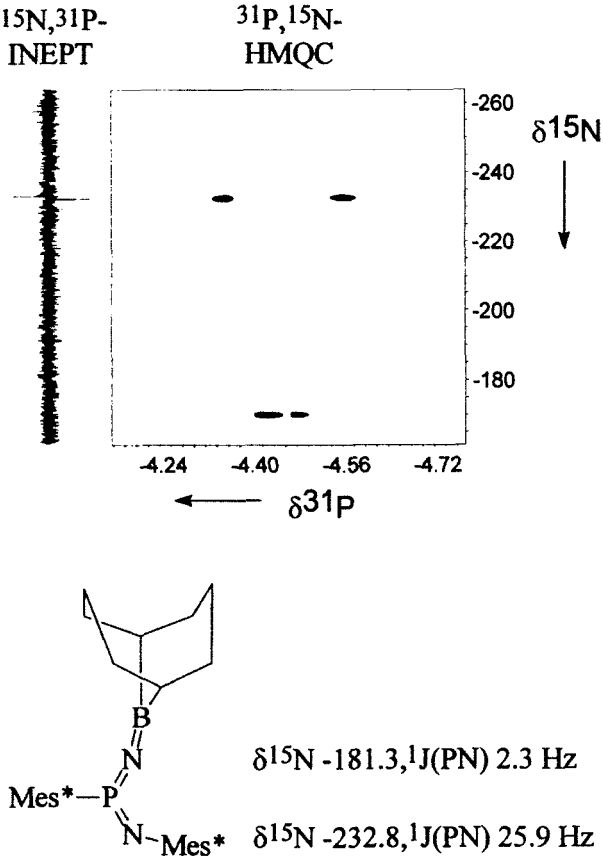

Fig. 17. 2D-^{31}P,^{15}N{^{1}H} HMQC and 1D-^{15}N,^{31}P{^{1}H} INEPT (shown as projection parallel to *F*1) spectra of Mes*P(=NMes*)=N(-9-BBN). Correlation of the phosphorus with both nitrogens is clearly visible in the 2D spectrum, whereas the INEPT spectrum fails to display the resonance of the nitrogen adjacent to the 9-BBN group which is broadened by coupling to the adjacent ^{11}B. Note the markedly different isotope shifts of both resonances. Data from ref. 169.

employed in these experiments is larger than for any other heteroelement. Owing to the less favourable NMR receptivity of ^{13}C as compared to ^{31}P or ^{19}F, ^{13}C,^{m}Y correlations have been in the first place used for the measurement of signs and magnitudes of scalar couplings and the determination of skeletal connectivities in the context of structure elucidation, even though indirect detection of insensitive transition metal nuclei via ^{13}C has also been reported in special cases. Since most ^{13}C,^{m}Y correlation methods were developed only very recently, many of them by pioneering work in the group of Berger,[10,12] analytical applications are relatively scarce, and in several cases the known

reports have been limited to a demonstration of the feasibility of the experiment and basic methodical studies; this holds e.g. for correlations between ^{13}C and $^{111/113}Cd$,[12] ^{125}Te,[10] ^{183}W,[12] and ^{195}Pt.[10] Applications of $^{19}F,^{13}C$ and $^{31}P,^{13}C$ correlations were already described in Sections 3.1 and 3.2, and the case of $^{13}C,^{6}Li$ will be covered in Section 3.4.

The first examples of correlations between ^{13}C and a second heteronucleus were reported during the 'eighties for the case $^{13}C,^{2}D$. Rinaldi *et al.*[23] suggested the use of $^{13}C\{^{2}D\}$ INEPT for spectral editing and resonance assignment in deuterated organic molecules. Günther *et al.* employed both one-dimensional *J*-modulated spin-echo techniques[60,61] and 2D-$^{13}C,^{2}D$ correlation spectroscopy[71,72] for the same purpose and gave several application examples to demonstrate the potential of these methods as an analytic tool in the context of deuterium-labelling studies which are of some interest in mechanistic organic and bioorganic chemistry.[72] In the late 'eighties, also $^{13}C,^{15}N$ HMQC pulse schemes were repeatedly applied to the structural characterization of ^{15}N-labelled peptides and proteins,[171–174] but these methods are now no longer in use and were replaced by ^{1}H-detected triple-resonance experiments which offer much higher sensitivity.[3]

The usefulness of $^{13}C,^{29}Si$ correlation in the analysis of silicon containing polymers was first demonstrated by Berger[82,83] who employed the INEPT–HMQC technique with an initial $^{1}H,^{29}Si$ INEPT transfer prior to a $^{29}Si,^{13}C$ HMQC element to separate overlapping ^{13}C signals from –$OSiMe_2O$– moieties in a polymeric silicone oil. More recently, Rinaldi *et al.* extended their approach of analysing polymer tacticity[99,102] to the characterization of a polysilabutane material by means of gradient-enhanced 3D-$^{1}H,^{13}C,^{29}Si$ spectroscopy.[103]

The group of Berger reported some further applications of 2D-$^{13}C,^{m}Y$ (INEPT)–HMQC and HETCOR experiments for structure elucidation of organometallic compounds, including correlations of ^{13}C with spin-half nuclei such as ^{77}Se,[85] ^{119}Sn,[175] ^{207}Pb,[176] ^{199}Hg,[177] and the quadrupolar isotope ^{11}B.[79] Correlations involving heavy spin-half nuclei (^{77}Se, ^{119}Sn, ^{199}Hg, ^{207}Pb) are characterized by the presence of many long-range couplings (scalar $J(^{13}C,^{207}Pb)$ couplings were observed across up to eight bonds[176]) and isotope effects[85,177] which yield a wealth of structural information and make these techniques valuable tools for unambiguous solution of even difficult spectral assignment problems.[85] In contrast, the information content of $^{13}C,^{11}B$ correlations can be limited by rapid relaxation of the quadrupolar ^{11}B, and even cross-peaks between directly connected $^{13}C,^{11}B$ pairs may be missing when the T_2 relaxation time of the latter is too short.[79]

Indirect observation of transition metal chemical shifts via ^{13}C was reported for the determination of $\delta(^{57}Fe)$ in a variety of ferrocenes and ferrocenyl carbenium ions,[31,178] as well as in a natural myoglobin carbonyl complex and two synthetic model compounds.[33] All measurements were made by selective double-resonance methods using either [^{57}Fe]-labelled[31,178] or

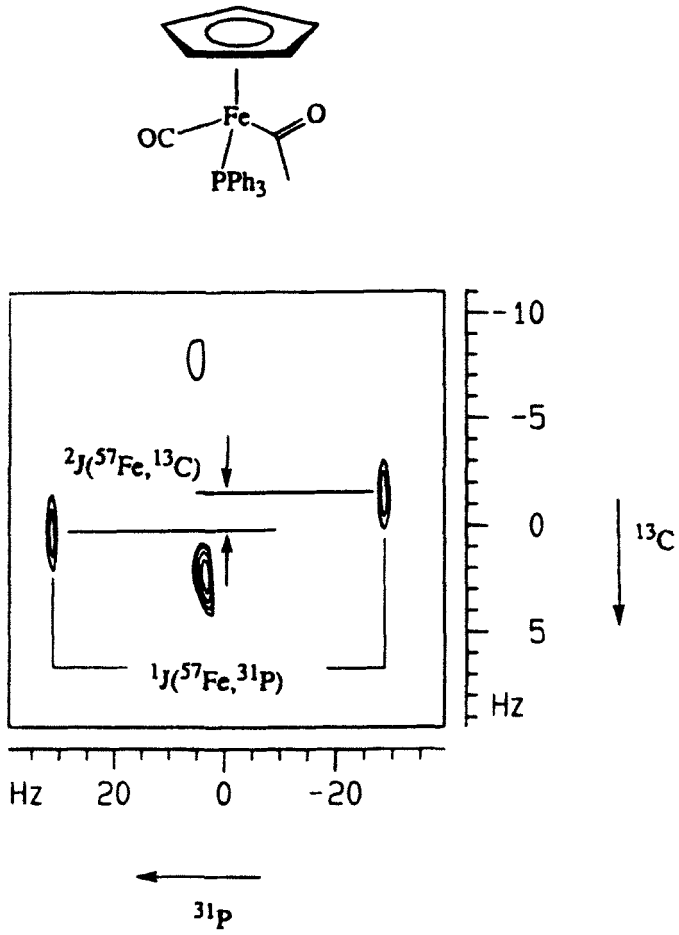

Fig. 18. $^{31}P,^{13}C\{^{1}H\}(^{57}Fe)$ HMQC spectrum of the complex $[(Cp)(PPh_3)(COCH_3)]Fe$ obtained with the bi-selective HMQC pulse sequence of Fig. 11(c) using a binomial excitation pulse. Reproduced, with permission, from ref. 112. Copyright 1996, John Wiley & Sons.

[$^{13}C,^{57}Fe$] doubly labelled samples.[33] In a more recent study, two-dimensional $^{31}P,^{13}C\{^{1}H\}$ and $^{1}H,^{57}Fe$ correlations with binomial excitation of ^{13}C satellites in the ^{31}P and ^{1}H spectra, respectively, were used to determine signs and magnitudes of $^{1}J(Fe,C)$ and $^{2}J(Fe,C)$ in some iron cyclopentadienyls at natural abundance of both elements (Fig. 18). Reported experiment times for these studies were in the order of some 12 h and the method was considered applicable to routine work, thus encouraging its future use for the characterization of different substrates and other metal nuclei than ^{57}Fe.[112]

3.4. ^{6}Li,^{m}Y correlations

The application of ^{6}Li,^{m}Y correlation techniques was inspired by the ambition for a concise structural characterization of lithium organyls and lithium amides which are eminently important as reagents in various fields of chemistry. These reagents are frequently formed by metallation (Li-H or Li-X exchange) reactions, and it is well known that their chemical reactivity is strongly affected by the formation of different aggregates and solvates. Hence, correlation experiments were set up to elucidate both the site of metallation in polyfunctional molecules, and the degree of association and the structures of the formed supramolecular aggregates. Even though of the two naturally occurring isotopes, ^{7}Li has both the higher abundance and the higher gyromagnetic ratio, and thus a better receptivity than ^{6}Li, the latter is much better suited for correlation spectroscopy because of its much smaller quadrupole moment. In fact, ^{6}Li behaves very much like a spin-half nucleus, allowing the separation of quadrupolar and dipole–dipole relaxation mechanisms (and thus the measurement of NOE to ^{6}Li),[9,11] and scalar couplings to ^{6}Li are despite the scaling by a factor $\gamma_{^{6}\mathrm{Li}}/\gamma_{^{7}\mathrm{Li}} = 0.38$ frequently better resolved, owing to substantially longer T_2 relaxation times. In order to improve the NMR receptivity, experiments involving ^{6}Li are routinely performed with uniformly ^{6}Li-labelled substances (>95% isotopic abundance), and even [^{6}Li,^{13}C] or [^{6}Li, ^{15}N] doubly labelled substrates have frequently been used. In some special cases, samples containing both ^{6}Li and ^{7}Li were employed.[11] In order to slow down chemical exchange, recording the spectra at low temperatures down to −120°C may be required.

The most used heteronuclear X,Y correlation technique for the characterization of lithium organyls seems to be 1D-^{1}H and 2D-^{6}Li,^{13}C HMQC experiments[25,28] which rely on ^{1}J(C,Li) couplings and allow the detection of directly connected ^{6}Li,^{13}C spin pairs. The two-dimensional version is particularly useful for the characterization of compounds containing several distinguishable different ^{6}Li sites and allowed to prove for the first time the existence of a dilithiated carbon atom carrying two different lithium atoms.[28]

Two ^{13}C,^{6}Li correlation experiments which were suggested in particular to determine the aggregate sizes of lithium organyls include detection of a $J(^{13}\mathrm{C},^{6}\mathrm{Li})$-modulated ^{13}C spin-echo created by a gated-decoupling ^{13}C{^{6}Li} sequence,[26] and the differentiation between cyclic organolithium dimers and trimers by means of ^{13}C,^{6}Li HMQC-TOCSY.[27] The ^{13}C spin-echo experiment relies on the fact that the observed ^{13}C,^{6}Li coupling in aggregates $(\mathrm{RLi})_n$ depends on the total number of metal nuclei and obeys the empirical formula[180,181] $J_{\mathrm{obs}} = C/n$ where C is an empirical constant (17 ± 2 Hz). The ^{13}C magnetization amplitude in a spin-echo spectrum can then be described as $M(t) = M_0\{1/3 + 2/3\cos[2\pi(C/n)\tau]\}^n$ where τ represents the echo time. The plot of this function (Fig. 19) reveals that refocusing of the magnetization

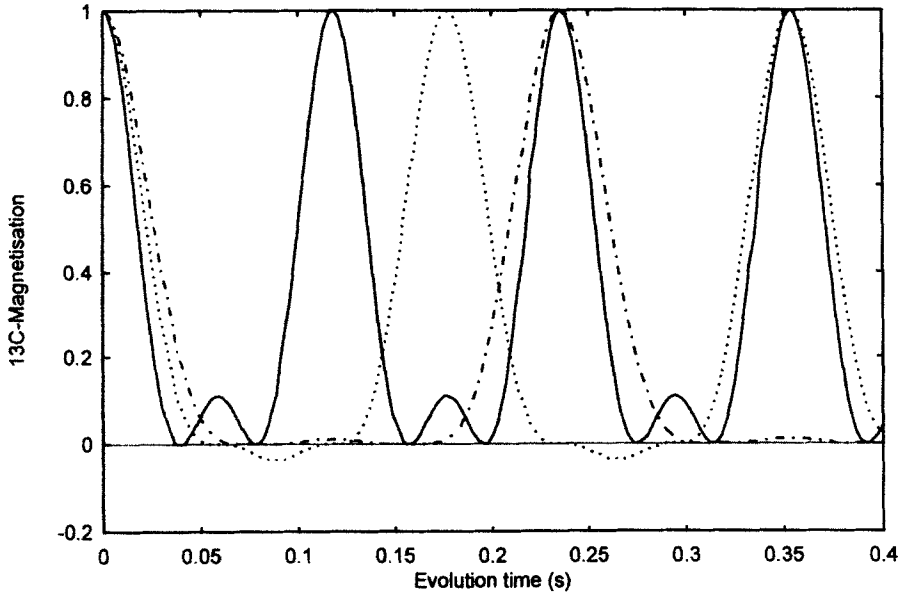

Fig. 19. Calculated intensities of $^{13}C\{^{6}Li\}$ multiplets of fluxional $(RLi)_n$ aggregates in ^{6}Li *J*-modulated spin-echo spectra as a function of evolution time for $n = 2$ (—), 3 (.....), 4 (–·–·–). Data from ref. 26.

occurs for each aggregate at a different echo time τ, so that evaluation of this time from a series of spin-echo experiments allows to determine the aggregation number n. The validity of this approach was experimentally verified for different aggregates $(Bu^{t}Li)_n$.[26] Despite the inherent limitations of both experiments (the spin-echo technique works only for fluxional aggregates, while HMQC–TOCSY cannot distinguish between trimers and higher aggregates with more than one "remote" lithium atom) they share the advantage of requiring no specific ^{13}C-labelling for their successful application.

A different approach to locate the metal in a lithium organyl, which exploits dipolar rather than scalar interactions, was presented by the group of Berger[39] who applied both 2D-$^{13}C,^{6}Li$ HOESY and 1D-$^{13}C\{^{6}Li\}$ difference spectroscopy to measure $^{13}C,^{6}Li$ heteronuclear Overhauser effects and demonstrated that the resulting data can be used for C–Li distance calculation. The major drawback of this technique is that the use of doubly $[^{6}Li,^{13}C]$-labelled samples is mandatory to ensure reliable measurement of very small NOE effects of some 1%.

Heteronuclear $^{6}Li,^{15}N$ correlations were employed extensively during the last years by the group of Collum for investigations on the solution structures of lithium amides. The experiments were generally performed with doubly $[^{6}Li,^{15}N]$-labelled samples, and by using both $^{6}Li,^{15}N$ HMQC and ^{6}Li-detected

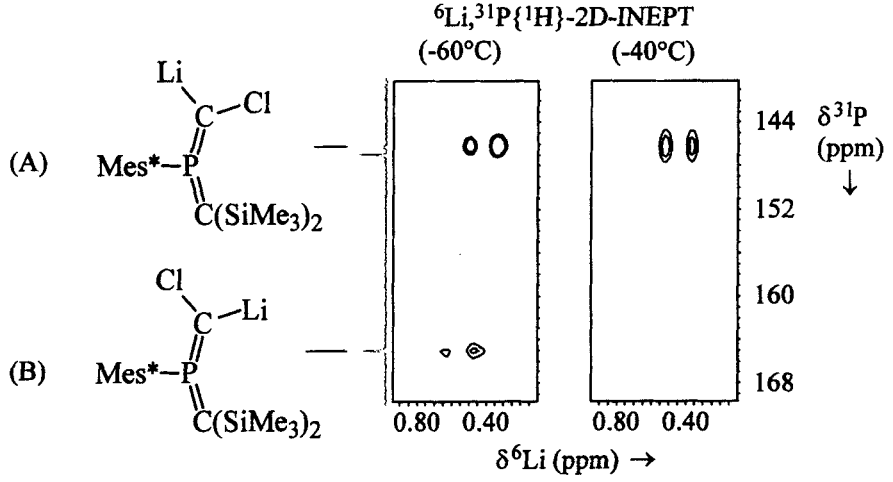

Fig. 20. 2D-^{6}Li,^{31}P{^{1}H} INEPT spectra of a mixture of stereoisomeric phosphavinylidene carbenoids at −40°C and −60°C.[163] The disappearance of the cross-peak for one isomer indicates that this species engages at the higher temperature in dynamic intermolecular exchange which leads to a loss of the spin–spin coupling.

^{15}N homonuclear zero-quantum spectroscopy.[76,90] The application of these methods gave a wealth of information on the structural complexity of etheral or hydrocarbon solutions of lithiated dialkyl amines[76,90,182] and lithiated hexamethyldisilazane,[183–185] as well as the formation of mixed aggregates of lithium amides with lithium halides and alkoxides,[76,90] amines,[182,186] hexamethylphosphoramide (HMPA),[183,187] or lithiated phenylacetonitrile.[188]

While ^{6}Li,^{13}C and ^{6}Li,^{15}N correlations have so far been successfully performed only with directly connected spin pairs, ^{6}Li,^{29}Si and ^{6}Li,^{31}P correlations were also shown to be applicable for long-range couplings. The group of Collum[183] introduced ^{31}P,^{6}Li HMQC spectroscopy for the characterization of lithium amide-HMPA adducts at temperatures below −115°C and demonstrated that cross-peaks which enabled an unambiguous signal assignment were even observable in cases where the splitting due to ^2J(P,Li) was not resolved in 1D spectra. Gudat *et al.*[162,163] used ^{6}Li,^{31}P HETCOR to determine $\delta(^6\text{Li})$ and ^2J(P,Li) in a mixture of isomeric phosphoranylidene carbenoids at −80°C. Monitoring of cross-peak intensities over a range of temperatures allowed further to establish a remarkable difference in the kinetic stability of the isomers (one isomer was kinetically stable, while the second one displayed intermolecular Li-exchange; see Fig. 20) which was suggested to be the reason for the previously observed[189] different reactivities. ^{6}Li,^{29}Si HMQC shift correlation was recently introduced by Günther[190] who used this method for the assignment of ^{6}Li and ^{29}Si resonances and the measurement of small (< 1 Hz) $^{2,3}J$(Si,Li) long-range couplings.

Finally, the ^{7}Li,^{6}Li correlation experiment, which has recently been performed for the first time by Günther,[11] is of interest as it allows to measure couplings between isochronous lithium nuclei and may open up new perspectives in the analysis of organolithium clusters.

3.5. Determination of ^{n}X,^{m}Y couplings by passive selection techniques

Pseudo triple-resonance experiments involving the passive selection of ^{m}Y satellite lines in 1D-^{n}X{^{1}H}(^{m}Y) or 2D-^{1}H,^{n}X(^{m}Y) spectra were introduced and massively applied by the group of Wrackmeyer. A main focus in these studies was the measurement of $^{1}J(^{15}\mathrm{N},^{m}\mathrm{Y})$ couplings via Hahn-echo extended (HEED) pulse schemes.[113] Both 1D (HEED–INEPT, HEED–DEPT) and 2D experiments (HEED–HETCOR) were applied, the former allowing to determine magnitudes of $^{1}J(^{15}\mathrm{N},^{m}\mathrm{Y})$ and ^{14}N/^{15}N induced isotope shifts on the ^{m}Y signals, while the latter yielded additional information on coupling signs. Even though HEED experiments work best if the ^{m}Y nucleus carries only a single nitrogen atom, they were also found applicable in special cases where the ^{m}Y nucleus was attached to more than one nitrogen,[114,115] and provided even an example for detection of doubly ^{15}N labelled isotopomers in natural abundance (Fig. 21).[115] The major body of these investigations was devoted to measurement of $^{1}J(^{31}\mathrm{P},^{15}\mathrm{N})$[113–115,191,192] and couplings between nitrogen and various group 14 elements (^{13}C, ^{29}Si, ^{119}Sn, ^{207}Pb).[113,193–195]

Recent applications of pseudo-triple- and -quadruple resonance techniques have in particular focused on the use of indirect detection schemes to measure heteronuclear couplings with increased sensitivity. The most versatile technique for this purpose proved to be ^{1}H,^{n}X(^{m}Y) or ^{31}P,^{n}X{^{1}H}(^{m}Y) HMQC experiments which use Ψ-BIRD or bi-selective pulses for selective excitation of transitions of ^{m}Y isotopomers and allow to determine both the magnitude of $J(^{n}\mathrm{X},^{m}\mathrm{Y})$ and its sign relative to $J(^{1}\mathrm{H}/^{31}\mathrm{P},^{m}\mathrm{X})$.[111,112,196] Experiments of this type are easily employed to spin systems where $J(^{1}\mathrm{H}/^{31}\mathrm{P},^{n}\mathrm{X}) \gg J(^{1}\mathrm{H}/^{31}\mathrm{P},^{m}\mathrm{Y})$ which is frequently the case if ^{m}Y is a ^{13}C nucleus which is directly bound to the detected ^{1}H or ^{31}P spin, and have been used in a number of cases to measure couplings between ^{13}C and rare spins such as ^{29}Si,[109,111] ^{57}Fe[112] or ^{187}Os.[196] A similar Ψ-BIRD-HSQC experiment has also been applied to the measurement of $^{1}J(^{29}\mathrm{Si},^{15}\mathrm{N})$ in NH-substituted azasilaboroles.[194]

4. CONCLUSIONS

The more widespread availability of spectrometers equipped with three RF channels together with general instrumentation improvements during the last years have made it feasible to run ^{n}X,^{m}Y correlation triple-resonance experiments on a routine basis. As is implied by the discussed examples, these

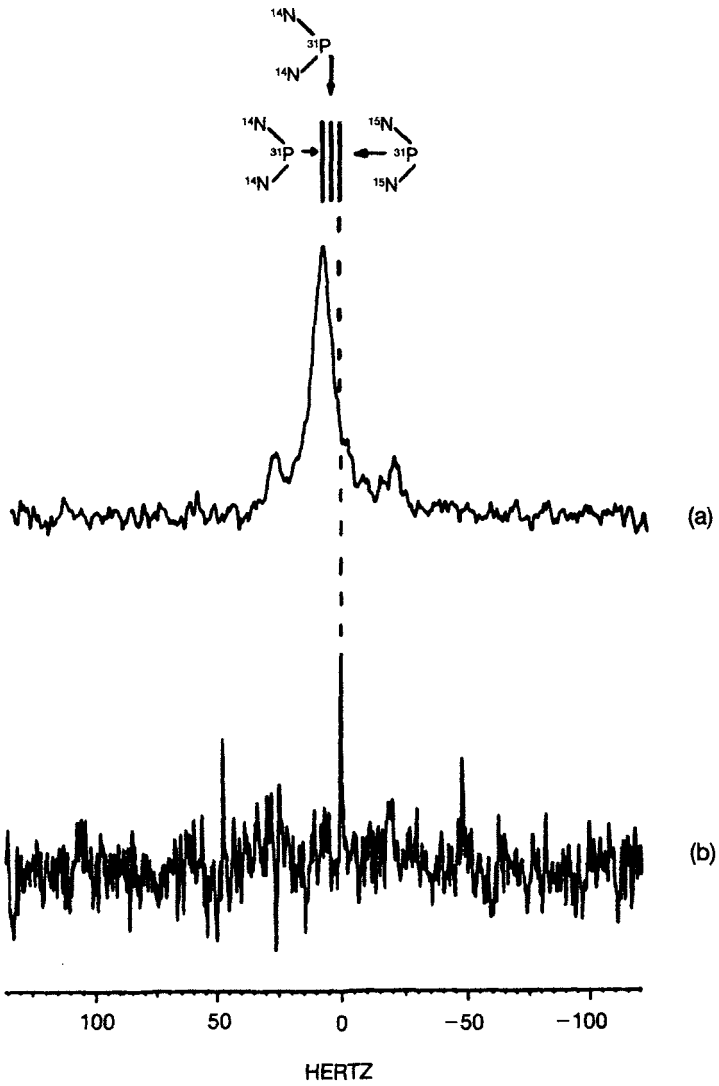

Fig. 21. 121.5 MHz $^{31}P,^{1}H(^{15}N)$ HEED–DEPT spectra of 2-*tert*-butyl-1,3-dimethyl-1.3.2-diazaphospholidine (~ 50% in C_6D_6) at natural abundance of ^{15}N; (a) 400 transients, Hahn-echo delay 0.1 s and (b) 4000 transients, Hahn-echo delay 0.2 s. The first spectrum displays the residual signal of the $[^{14}N]_2$ beside the $[^{14}N,^{15}N]$ isotopomer, the second one the signal of the $[^{15}N]_2$ isotopomer. Isotope shifts are marked and assigned at the top. Reproduced, with permission, from ref. 115. Copyright 1993, John Wiley & Sons.

techniques have found acceptance in various areas of organometallic and organoelement chemistry as an extremely valuable source of information, for several reasons. The possibilities of direct observation of heteroatom connectivities in molecular as well as supramolecular systems, and of rapid indirect measurement of chemical shifts of low-γ nuclei, have not only had a great impact on structure elucidation, but the information gained from such experiments provided also useful insight into reaction mechanisms and chemical behaviour of organic and inorganic compounds. This is in particular true for transition metal complexes, where measurement of chemical shifts and coupling constants involving the metal nucleus have been found to constitute sensitive probes for small distortions in the electronic structure, either of electronic or steric origin. In particular, the possibility to correlate transition metal chemical shifts with parameters related to chemical reactivity can be envisaged as a tool to derive exact structure–activity relationships which may help for example in the design of catalysts with higher efficiencies or selectivities, and may grant that the use of ^{n}X,^{m}Y correlations for indirect detection of transition metal nuclei will continue to receive considerable attention in the future. In the area of structure elucidation, ^{n}X,^{m}Y correlations will continue to have a great potential in particular for a more complete characterization of reaction intermediates which are thermally labile (e.g. carbenoids) or are merely present as components in dynamic solution equilibria, making *in situ* characterization directly in the equilibrium mixtures mandatory (e.g. lithium organyls and amides). In addition to providing "static" structural information, an increased use of variable temperature studies can be predicted to allow deeper insight into molecular dynamics and to aid in the identification of reaction mechanisms.

From a methodical point of view, most interesting aspects in future evolutions of ^{n}X,^{m}Y correlation experiments can be foreseen in an increased use of (pseudo) 3D experiments with ^{1}H detection for further improvements in sensitivity and resolving power, and the incorporation of pulsed field gradients, which are now a consolidated strategy for ^{1}H-detected inverse experiments. The latter aspect would be particularly interesting since the possibility to obtain very "clean" spectra with minimum artefacts should enable to extend the application of indirect detection metal NMR studies to lower concentration ranges, and improve indirect detection through very small coupling constants, thus further increasing the chemical applicability of these methods. A further foreseeable field of activity will be the implementation of *J*-cross polarization schemes which should in principle allow a magnetization transfer ^{1}H$\rightarrow{}^{n}$X$\rightarrow{}^{m}$Y in a single step[197] and are further known to give a superior performance to pulse-free precession methods in systems with slow chemical exchange,[198] although their general applicability may be somewhat limited owing to difficulties to cover the large excitation bandwidths which are required for some heteronuclei. A more widespread application of correlations via dipolar interactions (HOESY) would certainly

offer interesting prospects, although the low inherent sensitivity of such experiments will probably limit their application to specially selected examples. Still, also these methods could probably benefit from the implementation of indirect detection schemes which have been recently developed for observation of heteronuclear ^{1}H-^{n}X NOEs via ^{1}H.[199]

REFERENCES

1. J. Jeener, paper presented at the Ampère International Summer School, Basko Polje, 1971.
2. W. P. Aue, E. Bartholdi and R. R. Ernst, *J. Chem. Phys.*, 1976, **64**, 2229.
3. For a current review on methods and applications of 2D-NMR methods, see: *Two Dimensional NMR Spectroscopy. Applications for Chemists and Biochemists* (eds W. R. Croasmun and R. M. K. Carlson), 2nd edn, VCH Publishers, Weinheim, 1994.
4. H. Kessler, S. Mronga and G. Gemmecker, *Magn. Reson. Chem.*, 1991, **29**, 527.
5. R. R. Ernst, G. Bodenhausen and A. Wokaun, *Principles of Nuclear Magnetic Resonance in One and Two Dimensions*, Oxford University Press, Oxford, 1987.
6. R. Benn and A. Rufinska, *Angew. Chem.*, 1986, **98**, 851; *Angew. Chem. Int. Ed. Engl.*, 1986, **25**, 861.
7. B. E. Mann, *Ann. Rep. NMR Spectrosc.*, 1991, **24**, 141.
8. S. Berger, T. Fäcke and R. Wagner, *Magn. Reson. Chem.*, 1996, **34**, 4.
9. H. Günther, D. Moskau, P. Bast and D. Schmalz, *Angew. Chem.*, 1987, **99**, 1242; *Angew. Chem. Int. Ed. Engl.*, 1987, **26**, 1212.
10. T. Fäcke, R. Wagner and S. Berger, *Concepts Magn. Reson.*, 1994, **6**, 293.
11. H. Günther, in *Advanced Applications of NMR to Organometallic Chemistry* (eds M. Gielen, R. Willem and B. Wrackmeyer), pp. 247–290, Wiley & Sons, New York, 1996.
12. S. Berger, T. Fäcke and R. Wagner, in ref. 11, 29.
13. F. López-Ortiz and R. J. Carbajo, *Curr. Org. Chem.*, 1988, **2**, 97.
14. P. S. Pregosin (ed.), *Transition Metal Nuclear Magnetic Resonance*, Elsevier, Amsterdam, 1991.
15. C. Griesinger, H. Schwalbe, J. Schleucher and M. Sattler, in ref. 3, 457.
16. W. E. Hull, in ref. 3, 67.
17. L. Zhang, M. Pilar Gamasa, J. Gimeno, R. J. Carbajo, F. López-Ortiz, M. Lanfranchi and A. Tiripicchio, *Organometallics*, 1996, **15**, 4274.
18. R. Benn and A. Rufinska, *Magn. Reson. Chem.*, 1988, **26**, 895.
19. R. Benn, H. Brennecke, A. Frings, H. Lehmkuhl, G. Mehler, A. Rufinska and T. Wildt, *J. Am. Chem. Soc.* 1988, **110**, 5661.
20. M. Bourdonneau and C. Brevard, *Inorg. Chem.*, 1990, **29**, 3272.
21. A. A. Ribeiro and M. J. Glen, *J. Magn. Reson. Ser. A*, 1994, **107**, 158.
22. S. Berger, *J. Fluorine Chem.*, 1995, **72**, 117.
23. P. L. Rinaldi and N. J. Baldwin, *J. Am. Chem. Soc.*, 1982, **104**, 5791.
24. D. Nanz and W. von Philipsborn, *J. Magn. Reson.*, 1992, **100**, 243.
25. D. Moskau, F. Brauers, H. Günther and A. Maercker, *J. Am. Chem. Soc.*, 1987, **109**, 5532.
26. R. D. Thomas and D. H. Ellington, *Magn. Reson. Chem.*, 1989, **27**, 628.
27. W. Bauer, *J. Am. Chem. Soc.*, 1996, **118**, 5450.
28. H.-J. Gais, J. Vollhardt, H. Günther, D. Moskau, H. J. Lindner and S. Braun, *J. Am. Chem. Soc.*, 1988, **110**, 978.
29. W. McFarlane, A. M. Noble and J. M. Winfield, *J. Chem. Soc. A*, 1971, 948.
30. I. L. Colquhoun and W. McFarlane, *J. Chem. Soc. Chem. Commun.*, 1980, 145.
31. A. A. Koridze, P. V. Petrovskii, S. P. Gubin and E. I. Fedin, *J. Organomet. Chem.*, 1975, **93**, C26.

32. G. T. Andrews, I. J. Colquhoun, W. McFarlane and S. O. Grim, *J. Chem. Soc. Dalton Trans.*, 1982, 2353.
33. G. N. La Mar, C. M. Dellinger and S. S. Sankar, *Biochem. Biophys. Res. Commun.*, 1985, **128**, 628.
34. L. M. Mink, K. A. Christensen and F. A. Walker, *J. Am. Chem. Soc.*, 1992, **114**, 6930.
35. L. M. Mink, J. Reddy Polam, K. A. Christensen, M. A. Bruck and F. A. Walker, *J. Am. Chem. Soc.*, 1995, **117**, 9329.
36. I. J. Colquhoun, S. O. Grim, W. McFarlane, J. D. Mitchell and P. H. Smith, *Inorg. Chem.*, 1981, **20**, 2516.
37. T. Blum, M. P. Brown, B. T. Heaton, A. S. Hor, J. A. Iggo, J. S. Z. Sabounchei and A. K. Smith, *J. Chem. Soc. Dalton Trans.*, 1994, 513.
38. B. Wrackmeyer, K. Horchler v. Locquenghien, E. Kupce and A. Sebald, *Magn. Reson. Chem.*, 1993, **31**, 45.
39. S. Berger and F. Müller, *Chem. Ber.*, 1995, **128**, 799.
40. G. A. Morris and R. Freeman, *J. Am. Chem. Soc.*, 1979, **101**, 760.
41. D. M. Doddrell, D. T. Pegg and M. R. Bendall, *J. Magn. Reson.*, 1982, **48**, 323.
42. D. T. Pegg, D. M. Doddrell and M. R. Bendall, *J. Chem. Phys.*, 1982, **77**, 2745.
43. S. J. Berners Price, C. Brevard, A. Pagelot and P. J. Sadler, *Inorg. Chem.*, 1985, **24**, 4278.
44. M. Pons, M. Feliz and E. Giralt, *Tetrahedron Lett.*, 1985, **26**, 2817.
45. R. Eujen, B. Hoge and D. J. Brauer, *Inorg. Chem.*, 1997, **36**, 1464.
46. R. Eujen, B. Hoge and D. J. Brauer, *Inorg. Chem.*, 1997, **36**, 3160.
47. D. Gudat, *Magn. Reson. Chem.*, 1993, **31**, 925.
48. C. Brevard and R. Schimpf, *J. Magn. Reson.*, 1982, **47**, 528.
49. S. J. Berners Price, M. J. DiMartino, D. T. Hill, R. Kuroda, M. A. Mazid and P. J. Sadler, *Inorg. Chem.*, 1985, **24**, 3425.
50. A. Costa, M. Tato and R. S. Matthews, *Magn. Reson. Chem.*, 1986, **24**, 547.
51. D. Gudat, *J. Magn. Reson.*, 1995, **112A**, 246.
52. L. Emsley and G. Bodenhausen, *J. Magn. Reson.*, 1992, **97**, 135.
53. M. Ernst, C. Griesinger, R. R. Ernst and W. Bermel, *Mol. Phys.*, 1991, **74**, 219.
54. D. T. Pegg and M. R. Bendall, *J. Magn. Reson.*, 1983, **54**, 51.
55. D. T. Pegg and M. R. Bendall, *J. Magn. Reson.*, 1983, **55**, 51.
56. M. R. Bendall, D. T. Pegg, G. M. Tyburn and C. Brevard, *J. Magn. Reson.*, 1983, **55**, 322.
57. M. Tamura and Y. Harada, *J. Magn. Reson.*, 1995, **109B**, 97.
58. F. López-Ortiz, E. Peláez-Arango and P. Gómez-Elipe, *J. Magn. Reson. Ser. A*, 1996, **119**, 247.
59. E. Peláez-Arango, J. García-Alonso, G. Carriedo and F. López-Ortiz, *J. Magn. Reson. Ser. A*, 1996, **121**, 154.
60. J. R. Wesener and H. Günther, *Org. Magn. Reson.*, 1983, **21**, 433.
61. J. R. Wesener, P. Schmitt and H. Günther, *J. Am. Chem. Soc.*, 1984, **106**, 10.
62. M. R. Bendall, D. T. Pegg, J. R. Wesener and H. Günther, *J. Magn. Reson.*, 1984, **59**, 223.
63. M. G. Schwendinger, J. Quant, J. Schleucher, S. J. Glaser and C. Griesinger, *J. Magn. Reson. Ser. A*, 1994, **111**, 115, and cited refs.
64. R. Benn, H. Brennecke, J. Heck and A. Rufinska, *Inorg. Chem.*, 1987, **26**, 2826.
65. R. Benn, H. Brennecke, E. Joussen, H. Lehmkuhl and F. López Ortiz, *Organometallics*, 1990, **9**, 756.
66. R. Benn and C. Brevard, *J. Am. Chem. Soc.*, 1986, **108**, 5622.
67. D. Gudat, M. Link and G. Schröder, *Magn. Reson. Chem.*, 1995, **33**, 59.
68. T. J. Norwood, *Chem. Soc. Rev.*, 1994, 59.
69. J. Keeler, R. T. Cowes, A. L. Davis and E. D. Laue, *Meth. Enzym.*, 1994, **239**, 145.
70. W. Price, *Ann. Rep. NMR Spectrosc.*, 1996, **32**, 51.
71. J. R. Wesener, P. Schmitt and H. Günther, *Org. Magn. Reson.*, 1984, **22**, 468.
72. J. R. Wesener and H. Günther, *J. Am. Chem. Soc.*, 1985, **107**, 1537.

73. A. A. Ribeiro, *J. Fluorine Chem.*, 1997, **83**, 61.
74. A. A. Ribeiro, *Magn. Reson. Chem.*, 1997, **35**, 215.
75. R. Eujen and A. Patorra, *J. Organomet. Chem.*, 1992, **438**, 57.
76. J. H. Gilchrist, A. T. Harrison, D. J. Fuller and D. B. Collum, *Magn. Reson. Chem.*, 1992, **30**, 855.
77. D. Nanz and W. v. Philipsborn, *J. Magn. Reson.*, 1991, **92**, 560.
78. H. Ruegger and D. Moskau, *Magn. Reson. Chem.*, 1991, **29**, S11.
79. T. Fäcke and S. Berger, *Magn. Reson. Chem.*, 1994, **32**, 436.
80. E. S. Mooberry, B.-H. Oh and J. L. Markley, *J. Magn. Reson.*, 1989, **85**, 147.
81. L. D. Sims, L. R. Soltero and G. E. Martin, *Magn. Reson. Chem.*, 1989, **27**, 599.
82. S. Berger, *J. Magn. Reson. Ser. A*, 1993, **101**, 329.
83. P. Bast and S. Berger, *Bruker Rep.*, 1992, **91/92**, 20.
84. W. P. Niemczura, G. L. Helms, A. S. Chesnick, R. E. Moore and V. Bornemann, *J. Magn. Reson.*, 1989, **81**, 635.
85. T. Fäcke, R. Wagner and S. Berger, *J. Org. Chem.*, 1993, **58**, 5475.
86. S. J. Berners-Price, P. J. Sadler and C. Brevard, *Magn. Reson. Chem.*, 1990, **28**, 145.
87. F. Lianza, A. Macchioni, P. Pregosin and H. Rüegger, *Inorg. Chem.*, 1994, **33**, 4999.
88. D. Gudat, A. W. Holderberg, S. Kotila and M. Nieger, *Chem. Ber.*, 1996, **129**, 465.
89. S. J. Berners-Price, R. J. Boewn, P. J. Harvey, P. C. Healy and G. A. Koutsantonis, *J. Chem. Soc., Dalton Trans.*, 1998, 1743.
90. J. H. Gilchrist and D. B. Collum, *J. Am. Chem. Soc.*, 1992, **114**, 794.
91. O. W. Sørensen, G. W. Eich, M. H. Levitt, G. Bodenhausen and R. R. Ernst, *Prog. NMR Spectrosc.*, 1983, **16**, 163.
92. R. Eujen and B. Hoge, *Magn. Reson. Chem.*, 1997, **35**, 707.
93. A. Bax and R. Freeman, *J. Magn. Reson.*, 1981, **45**, 177.
94. G. Varani, F. Aboul-ela and F. H. T. Allain, *Prog. NMR Spectrosc.*, 1996, **29**, 51.
95. D. G. Gorenstein, in *Phosphorus-31 NMR Spectral Properties in Compound Characterization and Structural Analysis* (eds L. D. Quin and J. G. Verkade), p. 267, VCH Publishers, New York, 1994.
96. M. Ikura, L. E. Kay and A. Bax, *Biochemistry*, 1990, **29**, 4659.
97. L. E. Kay, M. Ikura, R. Tschudin and A. Bax, *J. Magn. Reson.*, 1990, **89**, 496.
98. S. Berger and P. Bast, *Magn. Reson. Chem.*, 1993, **31**, 1021.
99. L. Li and P. L. Rinaldi, *Macromol.*, 1996, **29**, 4808.
100. L. Li and P. L. Rinaldi, *Macromol.*, 1997, **30**, 520.
101. J. P. Marino, H. Schwalbe, C. Anklin, W. Bermel, D. M. Crothers and C. Griesinger, *J. Am. Chem. Soc.*, 1994, **116**, 6472.
102. T. Saito, R. E. Medsker, H. J. Harwood and P. L. Rinaldi, *J. Magn. Reson. Ser. A*, 1996, **120**, 125.
103. M. Chai, T. Saito, Z. Pi, C. Tessier and P. L. Rinaldi, *Macromolecules*, 1997, **30**, 1240.
104. R. Wagner and S. Berger, *J. Magn. Reson. Ser. A*, 1996, **120**, 258.
105. S. Berger, *J. Magn. Reson. Ser. A*, 1993, **105**, 95.
106. V. V. Krishnamurthy, *J. Magn. Reson. Ser. A*, 1995, **114**, 88.
107. G. Otting, B. A. Messerle and L. P. Soler, *J. Am. Chem. Soc.*, 1997, **119**, 5425.
108. E. Kupce and B. Wrackmeyer, *J. Magn. Reson.*, 1992, **99**, 338.
109. E. Kupce and B. Wrackmeyer, *J. Magn. Reson.*, 1992, **99**, 343.
110. E. Kupce and B. Wrackmeyer, *J. Magn. Reson.*, 1992, **100**, 401.
111. E. Kupce, E. Lukevics and B. Wrackmeyer, *Magn. Reson. Chem.*, 1994, **32**, 326.
112. E. J. Meier, W. Kozminski and W. v. Philipsborn, *Magn. Reson. Chem.*, 1996, **34**, 89.
113. E. Kupce and B. Wrackmeyer, *J. Magn. Reson.*, 1992, **97**, 568.
114. B. Wrackmeyer, C. Köhler and E. Kupce, *Magn. Reson. Chem.*, 1993, **31**, 769.
115. B. Wrackmeyer and G. Kehr, *J. Magn. Reson. Ser. A*, 1994, **107**, 106.
116. R. Benn, E. Joussen, H. Lehmkuhl, F. López Ortiz and A. Rufinska, *J. Am. Chem. Soc.*,

1989, **111**, 8754.
117. W. Kozminski and W. von Philipsborn, *J. Magn. Reson. Ser. A*, 1995, **116**, 262.
118. N. R. Nirmala and G. Wagner, *J. Am. Chem. Soc.*, 1988, **110**, 7557.
119. N. R. Nirmala and G. Wagner, *J. Magn. Reson.*, 1989, **82**, 659.
120. L. E. Kay, D. A. Torchia and A. Bax, *Biochem.*, 1989, **28**, 8972.
121. S. Braun, H.-O. Kalinowski and S. Berger, *150 and More Basic NMR Experiments*, Wiley-VCH, Weinheim, 1998.
122. A. Bax, *J. Magn. Reson.*, 1983, **52**, 76.
123. E. Kupce and B. Wrackmeyer, *J. Magn. Reson.*, 1991, **94**, 170.
124. J. Mason (ed.), *Multinuclear NMR*, pp. 7, 623–627, Plenum Press, New York, 1987.
125. P. Bast, S. Berger and H. Günther, *Magn. Reson. Chem.*, 1992, **30**, 587.
126. N. Pieper, C. Klaus-Mrestani, M. Schürmann and K. Jurkschat, *Organometallics*, 1997, **16**, 1043.
127. R. Willem, A. Bouhdid, M. Biesemans, J. C. Martins, D. de Vos, E. R. T. Tiekink and M. Gielen, *J. Organomet. Chem.*, 1996, **514**, 203.
128. L. Li, D. G. Ray, P. L. Rinaldi, H. Wang and H. J. Harwood, *Macromolecules*, 1996, **29**, 4706.
129. G. von Fircks, H. Hausmann, V. Francke and H. Günther, *J. Org. Chem.*, 1997, **62**, 5074.
130. D. Gudat, M. Nieger and M. Schrott, *Inorg. Chem.*, 1997, **36**, 1476.
131. V. Tedesco and W. von Philipsborn, *Organometallics*, 1995, **14**, 3600.
132. G. Hopp Rentsch, D. Nanz, I. Solana, R. Stefanova and W. v. Philipsborn, *Magn. Reson. Chem.*, 1996, **34**, 1036.
133. N. Juranic, *Coord. Chem. Rev.*, 1989, **96**, 253.
134. Ref. 124, p. 2.
135. J. Mason, *Polyhedron*, 1989, **8**, 1657.
136. N. F. Ramsey, *Phys. Rev.*, 1950, **77**, 567.
137. N. F. Ramsey, *Phys. Rev.*, 1950, **78**, 699.
138. K. Konda, N. Nakatsuiji and F. Yonezawa, *J. Am. Chem. Soc.*, 1984, **106**, 5888.
139. H. Nakatsuji and M. Sugimoto, *Inorg. Chem.*, 1990, **29**, 1221.
140. D. Gudat, M. Schrott, V. Bajorat, M. Nieger, S. Kotila and D. Stalke, *Chem. Ber.*, 1996, **129**, 337.
141. D. Gudat, A. Fuchs and E. Niecke, unpublished results.
142. E. Lindner, B. Keppeler, R. Fawzi and M. Steimann, *Chem. Ber.*, 1996, **129**, 1103.
143. E. Lindner, B. Keppeler, H. A. Mayer and K. Gierling, *J. Organomet. Chem.*, 1996, **515**, 139.
144. E. Lindner, B. Keppeler, H. A. Mayer, K. Gierling, R. Fawzi and M. Steimann, *J. Organomet. Chem.*, 1996, **526**, 175.
145. E. Lindner, K. Gierling, B. Keppeler and H. A. Mayer, *Organomet.*, 1997, **16**, 3531.
146. L. Carlton, *Magn. Reson. Chem.*, 1997, **35**, 153.
147. T. Baumgartner, B. Schinkels, D. Gudat, M. Nieger and E. Niecke, *J. Am. Chem. Soc.*, 1997, **119**, 12410.
148. E. J. M. Meier, W. Kozminski, A. Linden, P. Lustenberger and W. von Philipsborn, *Organometallics*, 1996, **15**, 2469.
149. A. G. Bell, W. Kozminski, A. Linden and W. von Philipsborn, *Organometallics*, 1996, **15**, 3124.
150. J. L. Bookham, W. McFarlane and I. J. Colquhoun, *J. Chem. Soc. Dalton Trans.*, 1988, 503.
151. C. J. Elsevier, J. M. Ernsting and W. G. J. de Lange, *J. Chem. Soc. Chem. Commun.*, 1989, 585.
152. J. M. Ernsting, C. J. Elsevier, W. G. J. de Lange and K. Timmer, *Magn. Reson. Chem.*, 1991, **29**, S118.
153. B. R. Bender, M. Koller, D. Nanz and W. von Philipsborn, *J. Am. Chem. Soc.*, 1993, **115**, 5889.

154. C. J. Elsevier, B. Kowall and H. Kragten, *Inorg. Chem.*, 1995, **34**, 4836.
155. F. Asaro, G. Costa, R. Dreos, G. Pellizer and W. von Philipsborn, *J. Organomet. Chem.*, 1996, **513**, 193.
156. V. Tedesco and W. v. Philipsborn, *Magn. Reson. Chem.*, 1996, **34**, 373.
157. D. J. Law, G. Bigam and R. G. Cavell, *Can. J Chem.*, 1995, **73**, 635.
158. H. Beckmann, G. Grossmann and G. Ohms, *Magn. Reson. Chem.*, 1992, **30**, 860.
159. H. Beckmann, G. Grossmann and G. Ohms, *Magn. Reson. Chem.*, 1995, **33**, 160.
160. L. E. Kay and R. E. D. McClung, *J. Magn. Reson.*, 1988, **77**, 258.
161. V. M. S. Gil and W. von Philipsborn, *Magn. Reson. Chem.*, 1989, **27**, 409.
162. O. Schmidt, D. Gudat, M. Nieger, E. Niecke and W. W. Schoeller, *J. Am. Chem. Soc.*, 1999, **121**, 519.
163. T. Baumgartner, T. Schiffer, D. Gudat, M. Nieger and E. Niecke, *J. Am. Chem. Soc.*, 1999, in press.
164. D. Gudat and E. Niecke, *Fresenius J. Anal. Chem.*, 1997, **357**, 482.
165. D. Gudat, E. Niecke, A. Ruban and V. von der Gönna, *Magn. Reson. Chem.*, 1996, **34**, 799.
166. R. Streubel, S. Priemer, F. Ruthe, P. G. Jones and D. Gudat, *Eur. J. Inorg. Chem.*, 1998, 575.
167. F. López-Ortiz, E. Peláez-Arango, B. Tejerina, E. Pérez-Carreño and S. García-Granda, *J. Am. Chem. Soc.*, 1995, **117**, 9972.
168. L. Carlton and R. Weber, *Magn. Reson. Chem.*, 1997, **35**, 817.
169. D. Gudat and M. Larbig, unpublished results.
170. D. Gudat and M. Schrott, *Phosphorus, Sulfur, and Silicon*, 1996, **111**, 13.
171. W. M. Westler, B. J. Stockman, J. L. Markley, Y. Hosoya, Y. Miyake and M. Kainosho, *J. Am. Chem. Soc.*, 1988, **110**, 6256.
172. J. R. Garbow, D. P. Weitekamp and A. Pines, *Chem. Phys. Lett.*, 1982, **93**, 504.
173. A. Bax and S. Subramanian, *J. Magn. Reson.*, 1986, **67**, 565.
174. R. E. Moore, V. Bornemann, W. P. Niemczura, J. M. Gregson, J.-L. Chem, T. R. Norton, G. M. L. Patterson and G. L. Helms, *J. Am. Chem. Soc.*, 1989, **111**, 6128.
175. S. Berger and T. N. Mitchell, *Organometallics*, 1992, **11**, 3481.
176. T. Fäcke and S. Berger, *Main Group Met. Chem.*, 1994, **17**, 463.
177. T. Fäcke and S. Berger, *J. Organomet. Chem.*, 1994, **471**, 35.
178. A. A. Koridze, N. M. Astakhova and P. V. Petrovskii, *J. Organomet. Chem.*, 1983, **254**, 345.
179. D. Hüls, H. Günther, G. van Koten, P. Wijkens and J. T. B. H. Jastrzebski, *Angew. Chem.*, 1997, **109**, 2743; *Angew. Chem. Int. Ed. Engl.*, 1997, **36**, 2629.
180. W. Bauer, W. R. Winchester and P. v. R. Schleyer, *Organometallics*, 1987, **6**, 2371.
181. W. Bauer, M. Feiel, G. Muller and P. v. R. Schleyer, *J. Am. Chem. Soc.*, 1988, **110**, 6033.
182. J. F. Remenar, B. L. Lucht, D. Kruglyak, F. E. Romesberg, J. H. Gilchrist and D. B. Collum, *J. Org. Chem.*, 1997, **62**, 5748.
183. F. E. Romesberg, M. P. Bernstein, J. H. Gilchrist, A. T. Harrison, D. J. Fuller and D. B. Collum, *J. Am. Chem. Soc.*, 1993, **115**, 3475.
184. B. L. Lucht and D. B. Collum, *J. Am. Chem. Soc.*, 1995, **117**, 9863.
185. B. L. Lucht and D. B. Collum, *J. Am. Chem. Soc.*, 1996, **118**, 2217.
186. B. L. Lucht and D. B. Collum, *J. Am. Chem. Soc.*, 1996, **118**, 3529.
187. F. E. Romesberg and D. B. Collum, *J. Am. Chem. Soc.*, 1994, **116**, 9198.
188. P. R. Carlier, B. L. Lucht and D. B. Collum, *J. Am. Chem. Soc.*, 1994, **116**, 11 602.
189. E. Niecke, P. Becker, M. Nieger, D. Stalke and W. W. Schoeller, *Angew. Chem.*, 1995, **107**, 2012; *Angew. Chem. Int. Ed. Engl.*, 1995, **34**, 1849.
190. B. Böhler and H. Günther, *Tetrahedr. Lett.*, 1996, **37**, 8723.
191. B. Wrackmeyer and C. Köhler, *Magn. Reson. Chem.*, 1993, **31**, 573.
192. B. Wrackmeyer, E. Kupce and A. Schmidpeter, *Magn. Reson. Chem.*, 1991, **29**, 1045.
193. E. Kupce and B. Wrackmeyer, *Magn. Reson. Chem.*, 1991, **29**, 351.

194. B. Wrackmeyer, E. Kupce, R. Köster and G. Seidel, *Magn. Reson. Chem.*, 1995, **33**, 812.
195. B. Wrackmeyer, B. Schwarze and W. Milius. *J. Organomet. Chem.*, 1995, **489**, 201.
196. A. Gisler, M. Schaade, E. J. M. Meier, A. Linden and W. von Philipsborn, *J. Organomet. Chem.*, 1997, **545**, 315.
197. A. Majmudar and E. R. P. Zuiderweg, *J. Magn. Reson. Ser. A*, 1995, **113**, 19.
198. V. V. Krishnan and M. Rance, *J. Magn. Reson. Ser. A*, 1995, **116**, 97.
199. W. Bauer, *Magn. Reson. Chem.*, 1996, **34**, 532.

Application of ^{119}Sn NMR Parameters

BERND WRACKMEYER

Laboratorium für Anorganische Chemie der Universität Bayreuth, D-95440 Bayreuth, Germany

1. INTRODUCTION

The element tin possesses a large number of isotopes of which three (^{115}Sn, ^{117}Sn, ^{119}Sn) are magnetically active spin-1/2 nuclei (see Table 1). The natural abundance of ^{117}Sn and ^{119}Sn is fairly high, and their NMR receptivity is sufficient (~20 times better as compared to the popular ^{13}C nucleus) in order to obtain most ^{119}Sn NMR spectra (and also ^{117}Sn NMR spectra, if desired) within reasonable time both in solution and in the solid state. Although there are reports on ^{115}Sn NMR,[1] these measurements are much more time-consuming and applications are of limited value. The ever increasing performance of modern NMR spectrometers makes ^{119}Sn NMR an extremely valuable routine tool in all fields of tin chemistry. Furthermore, many more sophisticated NMR techniques, typical of improving the information from NMR measurements of spin-1/2 nuclei, have already been applied or can be applied if necessary.[2] In the last two decades, the progress in ^{119}Sn NMR has

ANNUAL REPORTS ON NMR SPECTROSCOPY
VOLUME 38 ISBN 0-12-505338-X

Table 1. NMR poperties of the magnetically active isotopes ^{115}Sn, ^{117}Sn and ^{119}Sn.

Isotope	Natural abundance (%)	Magnetic moment (μ/μ_N)	Magnetogyric ratio γ^a (10^{-7} rad T^{-1} s^{-1})	NMR frequency (Ξ, Hz)[a,b]	Relative receptivity $D(^{13}C)^c$
^{115}Sn	0.35	−1.582	−8.014	32 718 780	0.7
^{117}Sn	7.61	−1.723	−9.589	35 632 295	19.5
^{119}Sn	8.58	−1.803	−10.0318	37 290 665	25.2

[a]Values taken from J. Mason (ed.) *Multinuclear NMR*, p. 627, Plenum Press, New York, 1987.
[b]For neat tetramethyltin, Me_4Sn; Ξ values refer to the field strength for which the $^1H(Me_4Si)$ frequency is exact at 100.000 000 MHz.
[c]Relative to the ^{13}C nucleus; see R. K. Harris in *NMR and the Periodic Table* (eds R. K. Harris and B. E. Mann), p. 4, Academic Press, London, 1978.

been the subject of several reviews.[2–7] The flood of NMR data, produced in the last decade, also includes such a great amount of ^{119}Sn NMR data that the present review cannot aim for a complete assessment (sometimes it is rather difficult to extract data, e.g. if species are not properly identified in the text and tables,[280] or if just an approximate range of $\delta^{119}Sn$ is given.[306,313,376,401] It is intended to provide representative examples, showing the development in using and applying ^{119}Sn NMR parameters in various areas, excluding paramagnetic compounds, alloys and inorganic solids. The literature is covered and selected for the period from 1985 to the beginning of 1998. Data for compounds from previous reviews will be reported only if they are relevant for the understanding and classification of new data.

2. EXPERIMENTAL

2.1. Referencing

It is most convenient, using modern NMR spectrometers, to define a fixed frequency as the reference for chemical shifts δ of those nuclei where an internal reference cannot be generally applied. These frequencies are given in Table 1, referring to samples of neat tetramethyltin, Me_4Sn. By multiplying these frequencies with the appropriate factor, depending on the $^1H(Me_4Si)$ frequency of the individual NMR spectrometer, the exact reference frequency is provided and it is not necessary to handle Me_4Sn as a chemical. This procedure[8] guarantees precise reproduction of δSn data and, since there is no primary isotope effect (*vide infra*), the δ values are the same for all three tin isotopes. The use of other referencing techniques, some of which are still proposed in various text books, should be discouraged.

2.2. Techniques for observing ^{119}Sn resonances

As a result of relatively high sensitivity to the NMR experiment (Table 1) ^{119}Sn resonance signals can be observed in most cases directly using the PFT technique. If ^{1}H decoupling is required, it may prove necessary to use inverse gated ^{1}H decoupling in order to suppress the NOE (maximum NOE $\eta_{max} = -1.34$) which may partially or completely cancel the ^{119}Sn NMR signal. Frequently, there is a significant dependence of the position of the ^{119}Sn NMR signal on temperature gradients in the sample. Therefore, the ^{1}H decoupling power should be carefully adjusted, and a constant temperature is required to ensure that the line width of the ^{119}Sn NMR signal is not controlled by experimental conditions.

If the approximate magnitude of coupling constants $^{1}J(^{119}\text{Sn},^{1}\text{H})$ is known, polarization transfer pulse sequences such as INEPT[9,162] or DEPT[10] can be successfully applied in order to enhance the sensitivity of the NMR experiments. These techniques, if applied correctly with optimized setting of the spectrometer, normally give ^{119}Sn NMR signals for which the line widths are mainly governed by natural transverse relaxation processes (see Figs 1 and 2).

Indirect detection of ^{119}Sn NMR signals, in general by ^{1}H NMR, using various types of techniques[2] (HMQC, HMBC, HSQC), provides a powerful alternative to direct observation of ^{119}Sn resonances. These experiments may be further improved by the application of pulsed field gradients.[2,154] One major advantage of indirect detection is the dramatic increase in sensitivity: a gain by $[\gamma(^{1}\text{H})/\gamma(^{119}\text{Sn})]^{3/2} = 4.4$, when compared with the INEPT experiment, and by $[\gamma(^{1}\text{H})/\gamma(^{119}\text{Sn})]^{5/2} = 11.8$, when compared with normal detection. Furthermore, ^{119}Sn NMR signals may be severely broadened, e.g. by partially relaxed scalar coupling of ^{119}Sn with a quadrupolar nucleus, whereas the relevant ^{1}H NMR signals remain sharp. Therefore, broad ^{119}Sn NMR signals are very easy to record by ^{1}H detection.[11] A typical example is shown in Fig. 3.

In the solid state, high-resolution ^{119}Sn NMR spectra[12] can be readily obtained, in most cases, by using CP/MAS techniques, based on an optimized contact time (see Fig. 4) or by using variable contact times. Owing to the high NMR sensitivity, even single-pulse techniques[12b] will provide meaningful ^{119}Sn NMR spectra within reasonable time.

3. NUCLEAR SPIN RELAXATION

Various relaxation mechanisms (DD = dipole–dipole; SC = scalar; SR = spin–rotation; CSA = chemical shift anisotropy) have been shown to contribute to ^{119}Sn nuclear spin relaxation. In axially symmetrical organotin compounds, ^{119}Sn nuclear spin relaxation is governed mainly by the

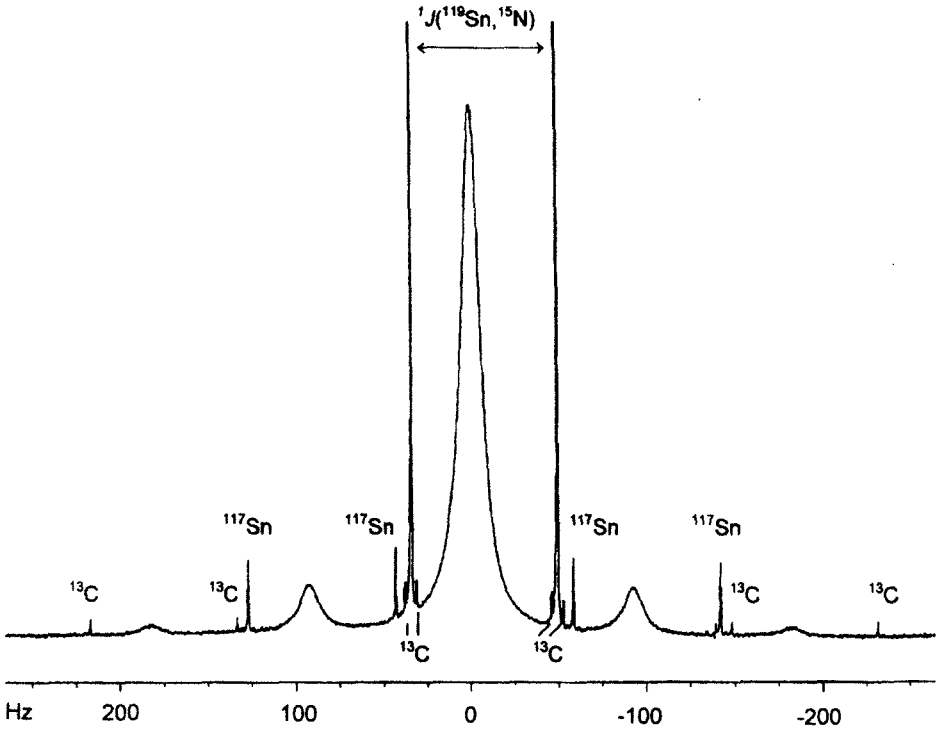

Fig. 1. 186.5 MHz ^{119}Sn NMR spectra (recorded by the refocused INEPT pulse sequence with CPD ^{1}H decoupling) of tris(trimethyl)stannylamine in, $(Me_3Sn)_3N$, toluene, labelled partially (~13%) with ^{15}N (sample by courtesy of W. Storch, M. Vosteen, University of Munich). The broad lines originate from the ^{119}Sn–^{14}N and ^{119}Sn–^{14}N–^{117}Sn isotopomers. All sharp lines arise from the ^{119}Sn–^{15}N and ^{119}Sn–^{15}N–^{117}Sn isotopomers. Note the isotope induced chemical shift $^{1}\Delta^{14/15}N(^{119}Sn) = -38.4$ ppb and the resolved ^{13}C satellites of the sharp lines due to $^{3}J(^{119}Sn,N,Sn,^{13}C)$ in the isotopomers containing ^{15}N.

spin–rotation mechanism, at least at moderate field strength (2.11–5.97 T). The more frequent use of NMR spectrometers working at very high field strength has the consequence that CSA may become the dominant relaxation mechanism for ^{119}Sn nuclei in surroundings of low local symmetry.[48] This may cause significant additional broadening of ^{119}Sn NMR signals (i.e. short T_2^{CSA} values), since the efficiency of this relaxation mechanism increases with B_0^2. It was found that CSA relaxation of ^{119}Sn is already dominant at moderate field strength for two-coordinate tin nuclei in bis(amino)stannylenes.[13] Nevertheless, for organotin compounds at low temperature or in the case of large molecules, dipole–dipole relaxation may become dominant, which means that the NOE has to be taken into account (*vide supra*).

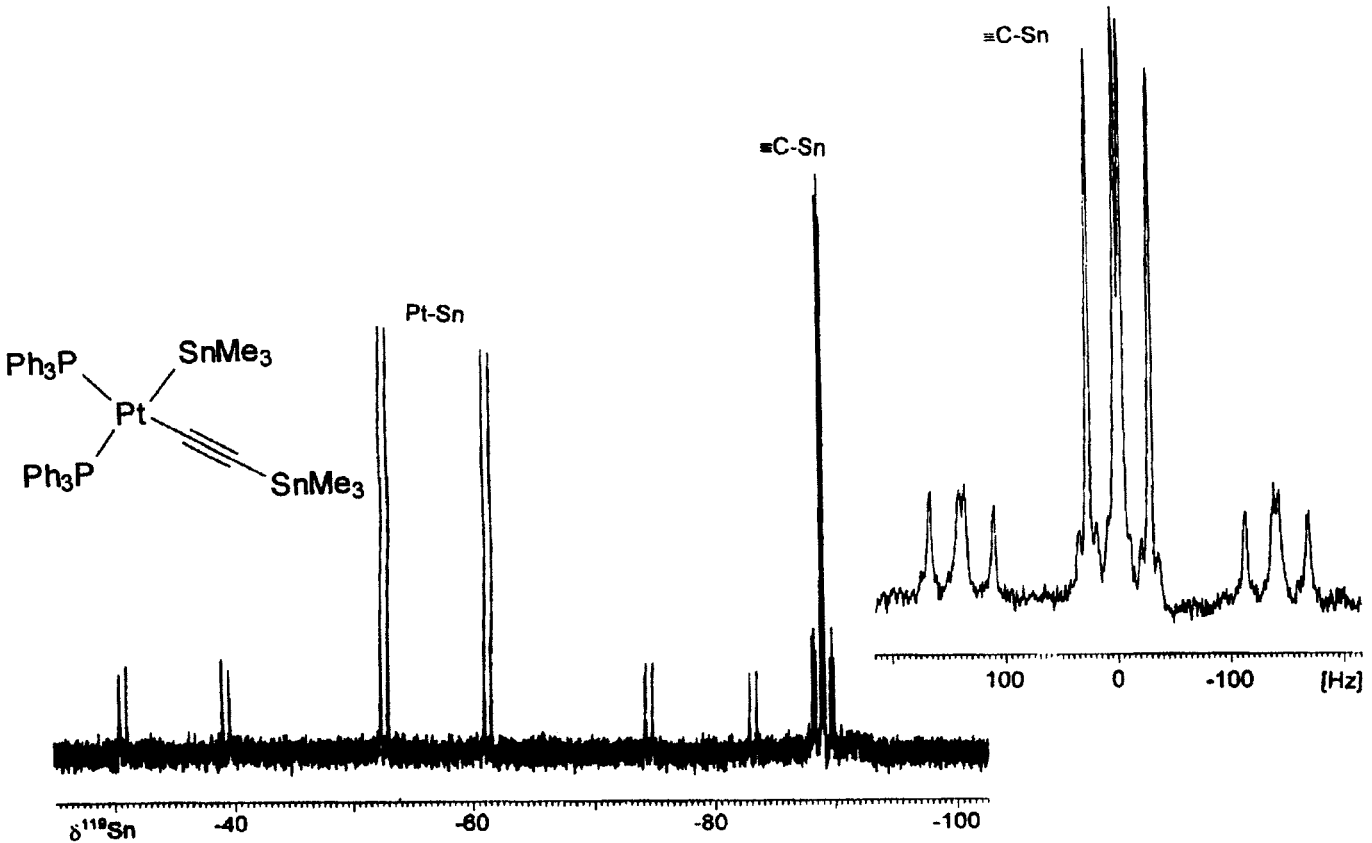

Fig. 2. 186.5 MHz ^{119}Sn NMR spectrum (recorded by the refocused INEPT pulse sequence with CPD ^{1}H decoupling) of *cis*-[Pt(PPh$_3$)$_2$(SnMe$_3$)C≡C-SnMe$_3$].[79] The expected splitting of the central ^{119}Sn resonance signals is observed due to ^{119}Sn–^{31}P coupling, together with the ^{195}Pt satellites. The expanded region of the ^{119}Sn(C≡) resonance also shows $^{117/119}$Sn satellites due to ^{4}J(Sn,Sn) which is not resolved at the bottom of the broader ^{119}Sn(Pt) resonance. (Reproduced, with permission, from Ref. 79.)

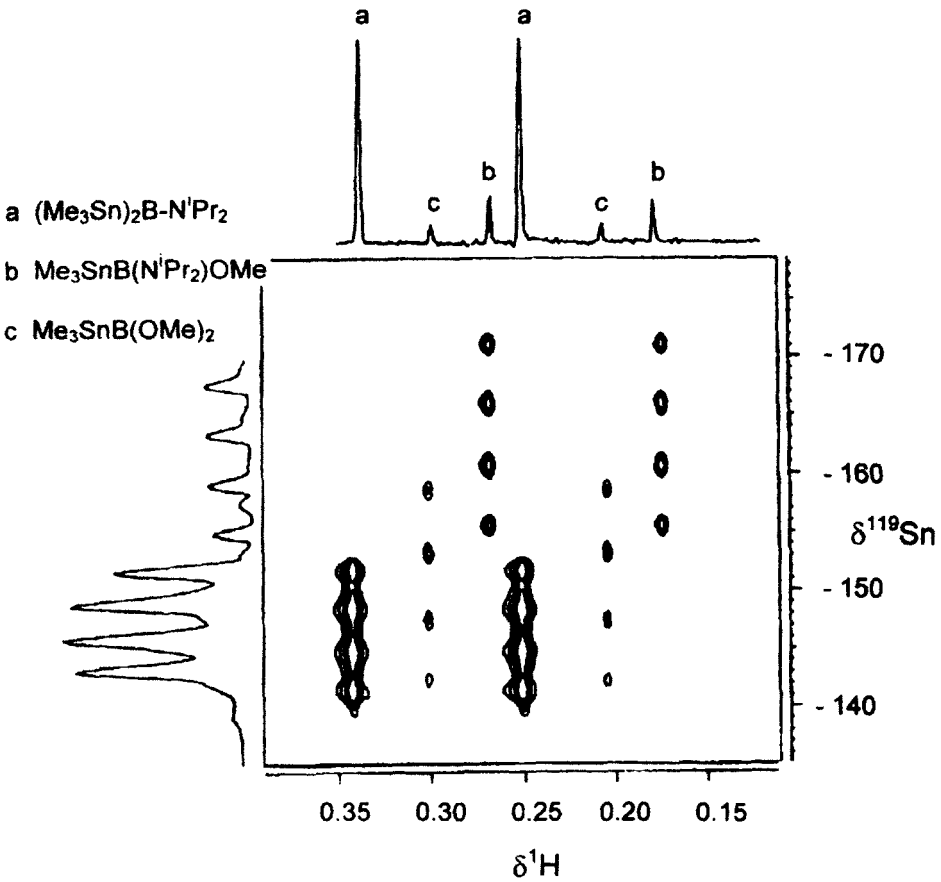

Fig. 3. Contour plot of the 2D 500.13 MHz ^{1}H detected $^{1}H/^{119}Sn$ shift correlation of a sample containing three types of tin–boron compounds.[11] The F_1 projection shows the ^{119}Sn NMR spectrum with its broad lines as a result of $^{1}J(^{119}Sn,^{11}B)$ ~1000 Hz. The overlapping ^{119}Sn resonances are nicely resolved in the contour plot, and the unstable species $Me_3SnB(OMe)_2$ can be identified. (Reproduced, with permission, from Ref. 11.)

The observation of indirect nuclear ^{119}Sn-X spin–spin coupling either in the ^{119}Sn or in the X NMR spectrum may be affected by fast relaxation either of the ^{119}Sn or of the X nucleus (see Fig. 1 for X = ^{14}N with rather fast ^{14}N nuclear spin relaxation,[14] Fig. 3 for X = ^{11}B with moderately fast ^{11}B nuclear spin relaxation,[11] Figs 5 and 6 for X = ^{13}C[15] and ^{29}Si,[13] respectively, with moderately fast ^{119}Sn nuclear spin relaxation[15]). The line shape of $^{117/119}Sn$ satellites in X NMR spectra, recorded at very high field, indicates isotropic or anisotropic surroundings of the tin nuclei.[13,15] For crystalline solids, these properties can be readily verified by solid-state ^{119}Sn NMR spectra.[15]

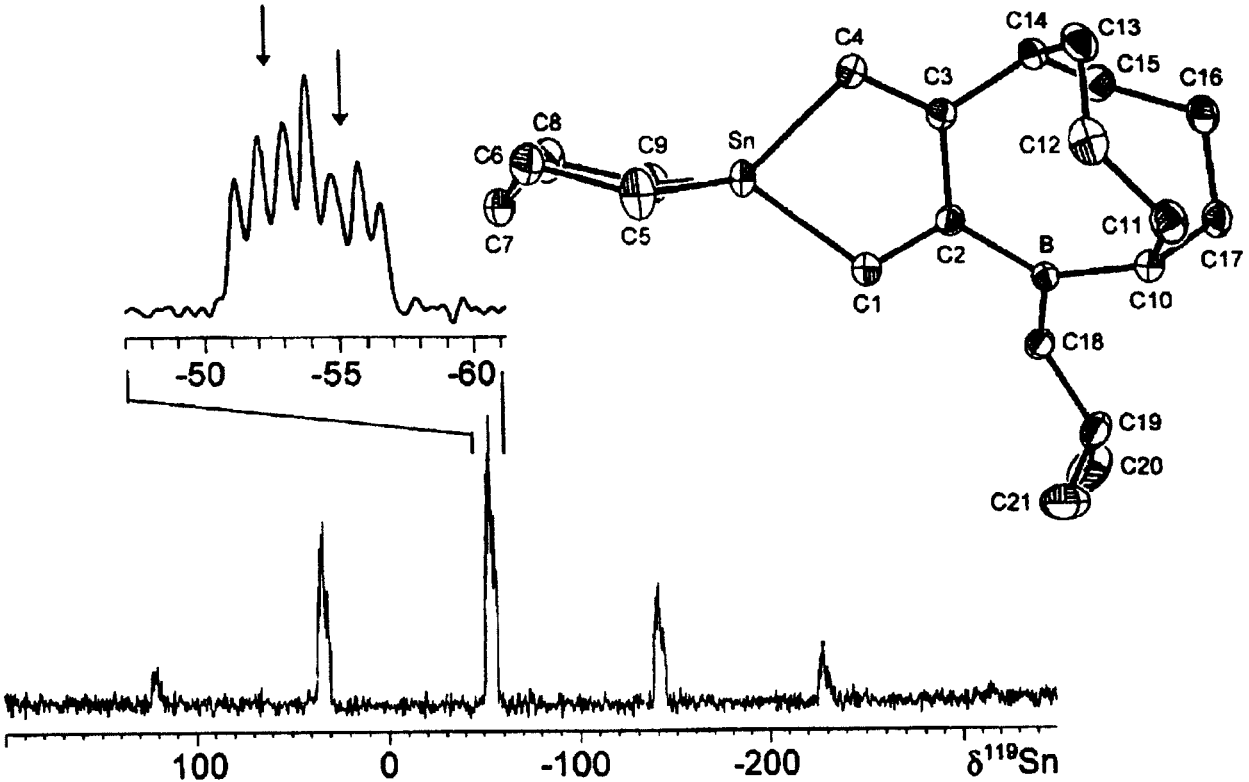

Fig. 4. 111.9 MHz solid-state ^{119}Sn CP/MAS NMR spectrum (recycle delay 5 s; contact time 1 ms) of a stannole derivative,[422] showing two signals with resolved scalar ^{119}Sn–^{11}B coupling across three bonds (68 and 65 ± 5 Hz). The x-ray structural analysis revealed the presence of only one isomer in the unit cell. The solid-state ^{119}Sn (and also ^{213}C NMR) CP/MAS NMR spectra of the macroscopic sample indicates the presence of two slightly different isomers (not present in solution!). (Reproduced, with permission, from Ref. 422.)

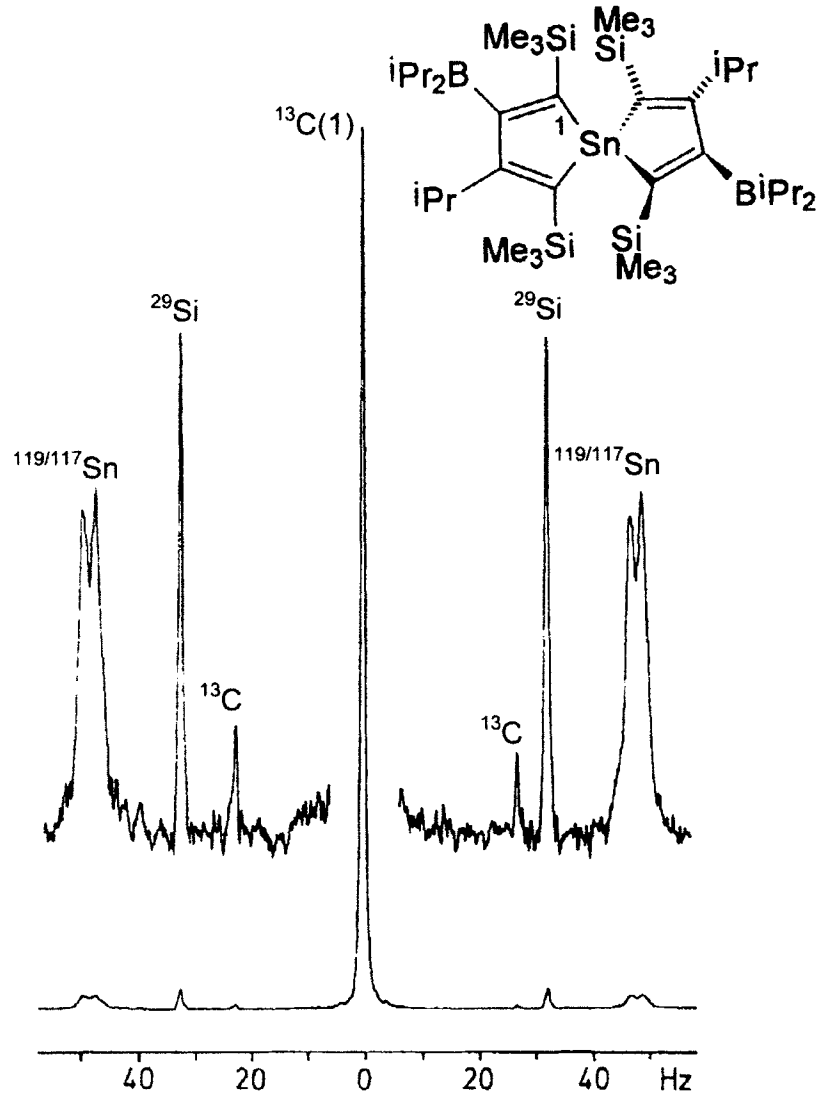

Fig. 5. 75.5 MHz ^{13}C NMR spectrum of the spiro-compound with the given formula (shown is the $^{13}C(1)$ NMR signal with satellites, recorded by using the refocused INEPT pulse sequence based on $^{3}J(^{13}C,Si,C,^{1}H)$ ~3.3 Hz).[15] The $^{117/119}Sn$ satellites are broadened (note the sharp ^{29}Si and ^{13}C satellites) as a result of fast ^{119}Sn nuclear spin relaxation owing to chemical shift anisotropy $\Delta\sigma \approx 725$ ppm, determined from the side-band pattern of the 111.9 MHz ^{119}Sn CP/MAS NMR spectrum. (Reproduced, with permission, from Ref. 15.)

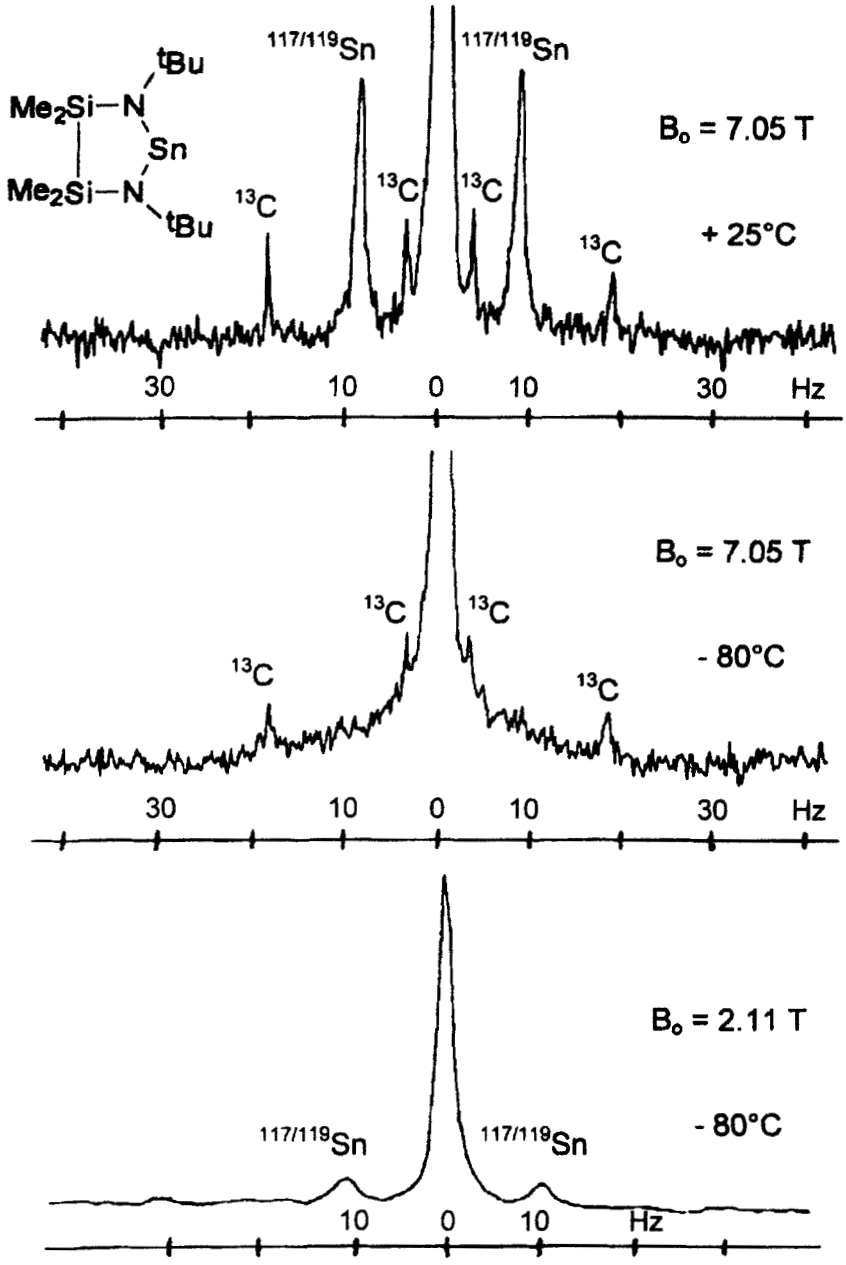

Fig. 6. ^{29}Si NMR spectra (refocused INEPT) of cyclic bis(amino)stannylene recorded at different temperatures and different field strengths. The chemical shift does not change appreciably, however, the $^{117/119}$Sn satellites [due to $^{2}J(\mathrm{Sn},^{29}\mathrm{Si}) = 21.2$ Hz] disappear owing to increasingly fast CSA relaxation of the $^{117/119}$Sn nuclei at low temperature and high field strength. (Reproduced, with permission, from Ref. 13.)

4. CHEMICAL SHIFTS δ^{119}Sn

4.1. General

^{119}Sn chemical shifts cover a range of approximately 6500 ppm, from ~ > 4000 to −2500 with δ^{119}Sn for Me_4Sn at zero. The general concept behind chemical shifts has already been outlined in previous reviews.[3–6] It appears that calculations of nuclear shielding of tin are going to be feasible.[16] The prerequisite is an absolute scale of magnetic shielding for ^{119}Sn, and this has been proposed on the basis of relaxation studies on a series of spherical molecules such as SnH_4, $SnMe_4$ and $SnCl_4$.[54] If the development in theory continues (there is little doubt about this), the impact on ^{119}Sn NMR would become extremely valuable. The isotropic δ^{119}Sn values measured in solution is also obtained for solids. If these data agree, and other direct structural information is available, the prominent structural features are the same both in solution and in the solid state. Frequently, one observes shifts of the ^{119}Sn nuclei to low frequency in the solid state as compared to solutions. This can be explained if the tin atom can expand its coordination sphere, and interactions which are fairly weak in solution become stronger in the solid state.[17–20,291,320,331] However, in the solid state, additional information is provided on the tensor components of nuclear shielding which, in favourable cases, can be used to discuss the bonding situation, as has been shown in the example of the dimeric stannylene **1**.[21]

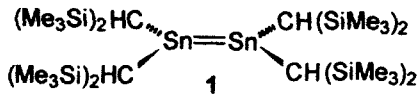

1

4.2. Patterns of ^{119}Sn chemical shifts

Coordination number of tin and electronic structure

Most tin compounds contain tin in the formal oxidation state +2 or +4. In both series of compounds the increase in the coordination number is related to a significant increase in ^{119}Sn nuclear shielding. This pattern has been noted in the early days of ^{119}Sn NMR, and nowadays we have a vast number of examples fitting into this picture. There are also numerous examples where changes in the δ^{119}Sn values, either induced by temperature[22,23] or by slight modification of the steric requirements of substituents,[22,23] reflect more or less weak interactions between the tin atoms and potential donor sites (intra- or intermolecular).

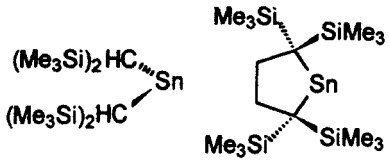

2 **3** **4**

δ^{119}Sn (Ar = 2,4,6-$(CF_3)_3C_6H_2$) +723 [26a]

δ^{119}Sn +2315 +2323 (Ar = 2,4,6-$[(Me_3Si)_2CH]_3C_6H_2$) +2208 [26e]

In the case of tin(II) compounds, the lowest ^{119}Sn nuclear shielding is observed for monomeric stannylenes, such as **2**[21,24] (the monomer of **1**) at high temperature in solution, or for relatesd compounds such as **3**[25] (which is also a monomer in the solid state) or **4**[26] (which exists for Ar = 2,4,6-$(CF_3)_3C_6H_2$ in two modifications in the solid state, one of which has extremely weak Sn···Sn interactions[153]). One can assume Sn···F interactions in the CF_3-substituted compound, since the ^{119}Sn nuclear shielding in the derivative without CF_3 groups is much more typical of monomeric diorganostannylenes. However, the monomeric stannylene Ar_2Sn with Ar = 2,4,6-Bu^t_3-C_6H_2 has been reported to give two ^{119}Sn resonances[26d] (δ^{119}Sn 961, 1105) at rather high field, and no explanation had been offered.

The shielding of ^{119}Sn in monomeric bis(amino)stannylenes[17,27,28] such as **5–7** is increased when compared with **2–4**, but it is still fairly low. The shielding difference between these stannylenes can be explained by considering the relative energies of electrons in the Sn–C and Sn–N σ bonds. In the bis(amino)stannylenes, this energy is lower and, therefore, the energy difference between ground states and relevant excited states is larger, which causes a smaller contribution to the paramagnetic shielding term in the tin amides **5–7** than in the diorganostannylenes **2–4**. This trend is amplified if one amino group is replaced by OAr (Ar = 2,6-Bu^t_2-4-Me-C_6H_2):$(Me_3Si)_2$N-Sn-OAr with δ^{119}Sn = 277.[51]

The molecular structure of **5** shows that the planes of the $N(SiMe_3)_2$ groups are twisted by almost 90° against the SnN_2 plane.[29] This should also apply to the N(^{t}Bu)$SiMe_3$ group in **6** in contrast to the situation in **7**. However, the δ^{119}Sn values of **6** and **7** lie in the same range. Therefore, potential SnN(pp)π bonding must play a minor role and does not contribute to the increase in ^{119}Sn nuclear shielding in the amides **5–7** with respect to **2–4**, although, in principle, the heterocyclic structure of **7** would be ideal for this type of interaction. It is also evident from the ^{119}Sn chemical shifts of transition metal complexes of bis(amino)stannylenes,[36,116] that the engagement of the lone pair of electrons at the tin atom in M–Sn bonds does not induce a dramatic shift of the ^{119}Sn

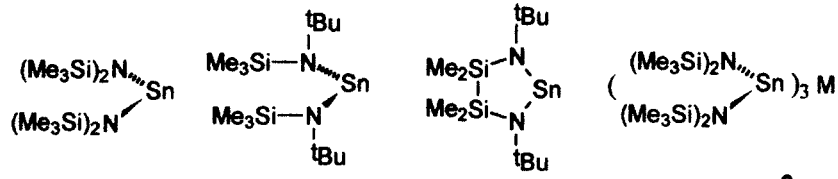

5 **6** **7** **8**

δ^{119}Sn	+776 [273]	+850 [273]	+759 [273]	+815 [36] (M = Pt)
				+885 [36] M = Pd

NMR signal (compare the δ^{119}Sn values of **5** and **8**). Thus, paramagnetic effects as the result of B_0 induced charge circulation involving the formally unoccupied Sn-p_z orbital arises mainly from Sn–C or Sn–N bonds and to a minor extent from the lone pair of electrons at the tin atom. This explains that the dimerization of stannylenes causes a marked increase in ^{119}Sn nuclear shielding since the Sn-p_z orbital is now used in donor–acceptor interaction.[17]

The search for element–element multiple bonds for heavy elements has produced numerous unexpected novel compounds. For example, the attempt to form an Si=Sn bond has led to heteroleptic silylstannylenes **9** and **10**.[156] However, there are examples in which multiple bonding was firmly established. In the case of tin, the discussion of multiple bonding is of particular interest since the tin atoms tend to avoid a classical double bond like a C=C bond, as exemplified in the case of **1**. Thus, δ^{119}Sn data may contribute to this discussion, as shown for **11**[164] and **12**[155] (compare also δ^{119}Sn = 932 for the stannadiyl Ar-Sn-C(PPh_3)-C(O)-Ar with Ar = 2,4,6-$(CF_3)_3C_6H_2$).[176] The relatively high ^{119}Sn magnetic shielding in **12**, as compared to **11**, points towards a greater contribution of the zwitterionic structure, in which the aromatic cyclopropenylium cation is retained.

Another extreme bonding situation in tin(II) compounds is encountered in stannocenes, in which the tin atom has a formal coordination number of 10 and the highest ^{119}Sn nuclear shielding is realized. Relevant examples are the compounds **13–16** for which the molecular structures have been determined in the solid state, and the ^{119}Sn NMR spectra have been measured both in the solid state and in solution.

There is little difference between the δ^{119}Sn values for **13–16** in solution and in the solid state, indicating comparable structures in both phases. The crystal structure of **13**[33] reveals that there are two different molecules in the unit cell with bond angles centroid–Sn–centroid 143.7° and 148.0°. This is reflected by the solid-state ^{119}Sn CP/MAS spectrum (see Fig. 7) which shows markedly different side band patterns for the ^{119}Sn resonances of the two tin sites.[30] In the case of **14**[31] the centroid–Sn–centroid bond angles are almost identical

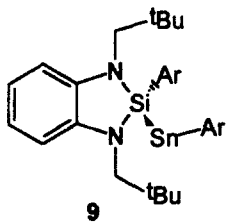

9

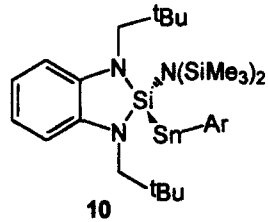

10

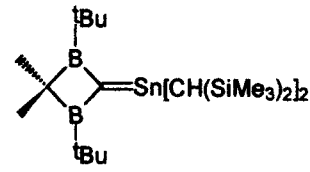

11

Ar = 2,6-$(Me_2N)_2C_6H_3$

δ^{119}Sn	+412	+621	+835.0

$^1J(^{119}Sn,^{29}Si)$ = 749 Hz

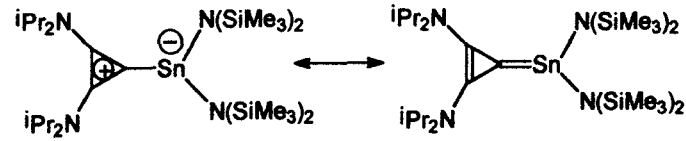

12

δ^{119}Sn - 44.7

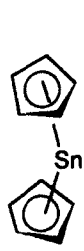

13

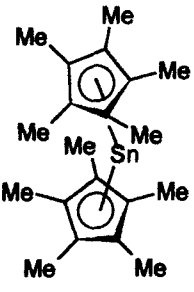

14

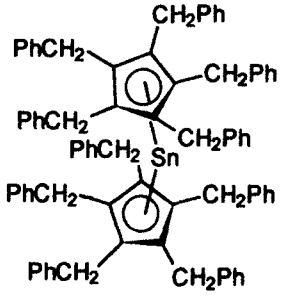

15

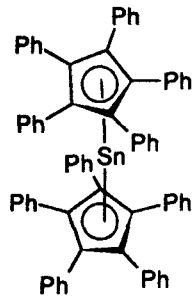

16

δ^{119}Sn			
-2199 [30]	-2129 [30]	-2188 [32]	-- (solution)
-2162.8 [30]	-2136.6 [31]	-2288 [32]	-2215 [32] (solid-state)
-2224.4 [30]	-2140.2 [31]		

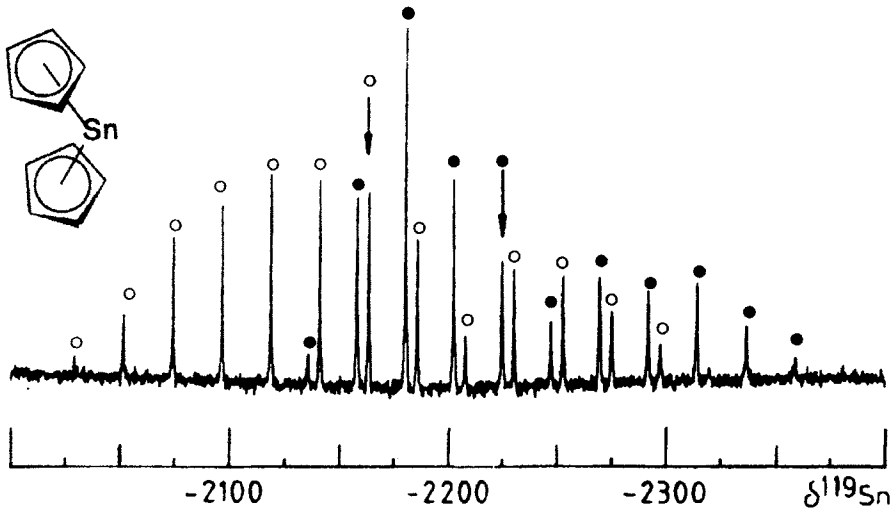

Fig. 7. 111.9 MHz ^{119}Sn CP/MAS NMR spectrum of solid dicyclopentadienyltin,[30] showing the two different tin sites in agreement with the x-ray stuctural analysis.[33] Note the completely different side-band patterns for the two ^{119}Sn NMR signals (isotropic shifts are indicated by arrows). (Reproduced, with permission, from Ref. 30.)

(143.8°, 144.6°),[34] but the ^{119}Sn CP/MAS NMR spectrum clearly distinguishes the two different sites, this time with very similar side-band patterns. It should be noted that the solid-state ^{13}C CP/MAS NMR of **13** and **14** did not show the presence of different molecules in the unit cell.[30,31] As expected from the results of the crystal structure determination of **15**,[35] only a single ^{119}Sn site is observed,[32] whereas the ^{119}Sn CP/MAS spectrum of **16** shows several central lines, very close to each other, indicating polymorphism for the bulk sample of **16**.[32] Decaisopropylstannocene, $(\eta^5\text{-Pr}^i_5C_5)_2Sn$, has been shown to exist as two diastereomers; although the ^{119}Sn NMR spectrum in solution was not reported, the solid-state ^{119}Sn NMR gave a signal at $\delta - 2362$ which was interpreted to represent two different tin sites.[53] The δ^{119}Sn value (−2100) of bis(1,3-di-*tert*-butyl-cyclopentadienyl)tin also indicates η^5-coordinated ligands.[434] Interestingly, removal of one of the cyclopentadienyl rings gives an ionic compound $[\eta^5\text{-}2,5\text{-Bu}^t_2\text{-}C_5H_3]Sn^+[BF_4]^-$ in which the ^{119}Sn nuclear shielding is again rather high (δ^{119}Sn −2337.7).[434]

There are examples where the cyclopentadienyl groups in **13** are replaced by comparable η^5-bonded ligands. The δ^{119}Sn values prove that the electronic structure does not change significantly (see **17**).[151] Although, on a first glance, **18** seems to belong to the same class of compounds (structural data are very similar for **13–18**), the δ^{119}Sn value of **18** is completely different.[152] The explanation is straightforward: **18** is a tin(IV) compound.

Tin(IV) compounds can be obtained with the coordination numbers 4, 5, 6,

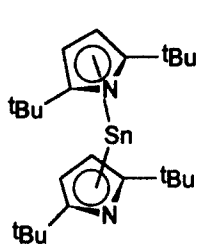

17

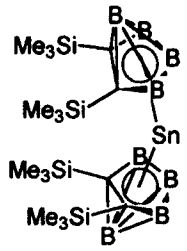

18

δ^{119}Sn -1889.0 -139.2

and in some cases >6. There are extensive compilations of δ^{119}Sn data available,[4] and in the last decade numerous further new examples of each class of compounds have been studied by ^{119}Sn NMR. The existence of a new class of organotin(IV) compounds has been firmly established. These are zwitterionic species in which a formally positively charged tin atom is coordinated by one (**19**) or two alkynyl groups (**20**) which are part of alkynylborate fragments.[37] These reactive compounds can be stabilized by intramolecular N-Sn (**21**) or O-Sn coordination.[37d] Cyclic bis(amino)organotin cations, stabilized by side-on coordination of the C≡C bond to the tin atom, have also been described.[187] The existence of three-coordinate tin cations in solution has been claimed on the basis of δ^{119}Sn data, but final evidence is still missing.[188]

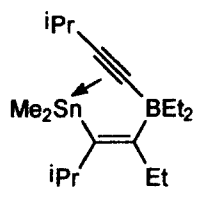

19

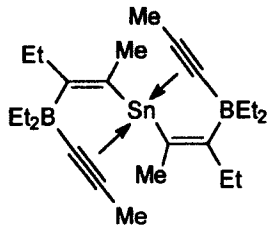

20

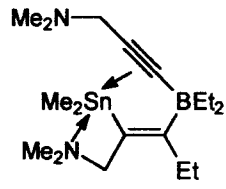

21

δ^{119}Sn [37] +215.4 +165.6 +127.7

Substituent effects and effects of cyclic structures

The influence of various substituents on δ^{119}Sn of tetra-coordinate tin(IV) compounds has been shown in previous reviews.[3–6] The larger data set available today confirms the trends which have been outlined. There are also many new examples which confirm and document the influence of the bond

Table 2. ^{119}Sn NMR parameters of some organotin hydrides.

Compound	$\delta^{119}Sn$	$^1J(^{119}Sn,^1H)$	$J(^{119}Sn,^{13}C)$	Ref.
Me_3SnH	−104.5	1744	352	4
Bu^n_3SnH	−91.4	1604.4		4
Ph_3SnH	−164.5	1935.8		4
$C_8H_{12}Sn(H)Me$[b]	−134.5, 142.1	1720		
$(PhCMe_2CH_2)_3SnH$[c]	−153.2	n.r.	343.3	95
$(PhCMe_2CH_2)_2$[(−)menthyl]SnH	−137.2			
$Me(PhCMe_2CH_2)$[(−)menthyl]SnH	−114.0, −117.2			
$(CF_3)_3SnH$	−309.8	2798	912	96
$Bu^n_2Sn(Cl)H$	−18.3	2178	451	98
$Bu^n_2Sn(Cl)H\text{-}OP(NMe_2)_3$	−139.3	2389	547	98
$Fe(C_5H_4\text{-}SnMe_2H)_2$	−102.4	1824	371.8 (Me) 514.4 (C-1)	35
Me_2SnH_2	−225.0	1797	–	4
$Bu^n_2SnH_2$	−202.4	1669	[c]	227
$He^n_2SnH_2$	−202.6	1667	n.r.	227
$Oct^n_2SnH_2$	−203.7	1597.2	n.r.	227
Ph_2SnH_2	−234.0	1928		4
$(CH_2{=}CH\text{-}CH_2)_2CH_2CH_2SnMeH_2$	−227.3	1744		94
$C_8H_{12}SnH_2$[b]	−256.3	1815		94
$(CF_3)_2SnH_2$	−303.1	2536	777	96
$Fe(C_5H_4\text{-}SnMeH_2)_2$	−210.5	1876	387 (Me) 546.6 (C-1)	35
$MeSnH_3$	−346.0	1852		4
$PhSnH_3$	−320.0	1920		4
$H_2C{=}CH\text{-}SnH_3$	−361			111
$H_2C{=}C{=}CH\text{-}SnH_3$	−338.4	2010.3	488.0	112
$HC{\equiv}C\text{-}SnH_3$	−320.6	2242.4	517.2	112
CF_3SnH_3	−351.6	2207	653	96
$Fe(C_5H_4\text{-}SnH_3)_2$	−330.7	1947	583.2	35

[a]See ref. 4 for a more extensive compilation; n.r. means not reported.

[b]$C_8H_{12}Sn$ =

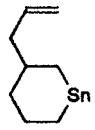

[c]Coupling data are wrong.

angle at the tin atom on $\delta^{119}Sn$ values: ^{119}Sn nuclear deshielding is typical of five-membered rings when compared with non-cyclic structures or larger rings. There are still insufficient data in order to assess the influence of four- or three-membered rings with certainty, although it appears that relatively high ^{119}Sn nuclear shielding is frequently observed in the case of three-membered rings.[424]

Various new organotin hydrides have been prepared and their ^{119}Sn NMR parameters are given in Table 2. All data are found in the expected range.

There is a steadily increasing number of tetraorganotin compounds for which δ^{119}Sn values are now routinely measured. A selection of these data is given in Table 3. ^{119}Sn NMR spectra, recorded by inverse gated ^{1}H decoupling, enables one to determine quantitatively the diastereoisomeric composition of diastereomeric tertraorganotin compounds.[337]

Pentaalkyl(aryl) tin ate complexes such as **22–24**, potential intermediates in lithium–tin exchange reactions, were detected by NMR spectroscopy.[167,168]

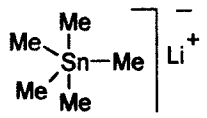

22

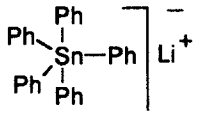

23

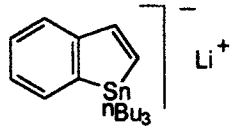

24

δ^{119}Sn	-277.0 [167]	-303.0 [167]	-44.0 [168]

Data for some new tin haiides are compiled in Table 4. Intramolecular coordination is frequently observed if suitable donor sites are available.[286,293,312,316,327,330,331,341,361,364,368,395,441] Surprisingly (see for example the Sn..Cl..Sn bridge in an anionic chloro complex),[278] 1,1′-bis(trichlorostannyl)ferrocene **25** (δ^{119}Sn −23.2), for which the crystal structure has been determined,[38] does not possess appreciable intra- or intermolecular Sn..Cl..Sn interactions, neither in the solid state nor in solution.[38] Organotin halides, in general, react as Lewis acids with numerous Lewis bases in solution, forming either strong or weak adducts.[281,293,295,324,338,349,351,352,367,375,389,392,410] The rate of *cis/trans* isomerization of octahedral dimethylsulfide adducts of $SnCl_4$ has been determined by ^{119}Sn NMR, using magnetization transfer.[371]

Table 5 contains selected δ^{119}Sn values of tin(IV) compounds with a Sn–chalcogen bond. Dialkylstannylene acetals, derived from various carbohydrates, are shown by ^{119}Sn NMR to exist mainly as dimers in solution,[336,398] but there are also trimers, tetramers and polymers, as found by ^{119}Sn solid-state NMR studies.[318,320] In the case of suitably tailored diole derivatives, intramolecular coordination can also be observed.[384] The complex products arising from the hydrolysis of butyltin alkoxides have been studied by ^{119}Sn NMR in the liquid and solid state[355] (see also the hydrolysis of $BuSnCl_3$).[298,347] If salicylaldehydethiosemicarbazone is treated with $(Me_2SnO)_n$ a product with coordination number 5 is formed in which oxygen and sulfur occupy the axial positions and the amide function is not involved in coordination to tin, as shown by x-ray structural analysis (δ^{119}Sn −104.7).[339] There is an enormous amount of data for organotin carboxylates (most of them are biologically active) which could not all be implemented in Table 5.[199,209,232,246,251,256,285,303,304,308,309,314,315,317,322,326,332,334,359,388,396,409,436] Fascinating

Table 3. ^{119}Sn NMR parameters of some tetraorganotin compounds.[a]

Compound	$\delta^{119}Sn$	$^{1}J(^{119}Sn,^{13}C)$	$^{2}J(^{119}Sn,^{13}C)$	$^{3}J(^{119}Sn,^{13}C)$	Ref.
Me_4Sn	0	336.6	–	–	4, 45
Et_4Sn	1.4	320.0	23.0	–	4, 135
Pr^n_4Sn	−16.8	316.0	30.0	51.0	4, 135
Pr^i_4Sn	−43.9	308.5	15.0	–	4, 45
Bu^n_4Sn	−11.5	314.0	20.0	52.0	4, 135
$(H_2C{=}CHCH_2)_4Sn$	−47.9	264.9	48.3	51.3	4, 135
$(PhCH_2)_4Sn$	−35.8	258.8	37.8	23.6	367
Ph_4Sn	−128.8	531.1	35.5	53.1	100
$(p\text{-}CF_3\text{-}C_6H_4)_4Sn$	−132.3	535.0	39.4	53.7	103
$(CH_2{=}CH)_4Sn$	−157.4	519.3	<4		4, 135
$(HC{\equiv}C)_4Sn$	−356.3	1176.2			45, 99
$(MeC{\equiv}C)_4Sn$	−345.4	1167.7	242.5	20.1	101
$(Bu^tC{\equiv}C)_4Sn$	−338.1	1148.4	223.8	16.2	101
$(Me_3SiC{\equiv}C)_4Sn$	−384.9	1036.0	171.9	18.6 (^{29}Si)	101
$(CF_3)_4Sn$	−350.4	1001.0	542 (^{19}F)		212
$(ICH_2)_4Sn$	−50.2	398.5			158
(benzoxazolyl-2-$SCH_2)_4Sn$	−82.4				118
$[2\text{-}Me_2Si\text{-}(4\text{-}Bu^t\text{-}C_5H_3)_2]_2Sn$	−45.3	90.0	103 (^{1}H)		423
$Me_3SnCH_2CH_2SnMe_3$	−0.2	309.0 (Me) 356.0 (CH_2)	37.8	1117 (^{117}Sn)	102
$CH_2[Sn(Me_2)(CH_2)_2]_2$	22.4	309.5 (Me) 350.0 (CH_2) 240.9 (CSn_2)	24.9 284.5 (^{119}Sn)		323
$Me_2C[Sn(Me_2)(CH_2)_2]_2$	27.3	277.0 (Me) 326.0 (CH_2) 326.0 (CSn_2)	20.0 (CH_2) 20.1 (Me) 36.6 (^{119}Sn)		323
$(Me_3Sn)_3C\text{-}CH_3$	44.6	306.6 (Me) 178.0 (C)	26.2 234.0 (^{117}Sn)		102

1-Me_3Sn-adamantane	−6.5	n.r.	12.2	48.8	104
1,4-$(Me_3Sn)_2$-bicyclo[2.2.2]octane	−5.0 ($CDCl_3$)	297.0 (Me) 478.0 (C)	5.9	52.7	166
(Z)-Me_3Sn-CH_2CH=$CHCH_2$-$SnMe_3$	−3.3	317.4 (Me) 310.8 (CH_2)	<2	51.6	131
1,1-$(Me_3Sn)_2$-cyclopentadiene	9.8	347.7 (Me) 193.9 (C-1)	9.1 n.r. (^{117}Sn)	24.7	159
$(C_6H_5CH_2)_3Sn$-C_5H_5	−20	266.1 (CH_2) 9.8 (C_5H_5)	39.1	25.6	136
$Ph_2Sn(CH_2)_{16}SnPh_2$	−72.0	n.r.	n.r.	n.r.	245
$Me_2Sn(CH_2I)_2$	14.4	380.6 (Me) 317.2 (CH_2)			158
$MeN[(CH_2)_3]_2SnMe_2$	−28.5	377.7 (Me) 418.3 (CH_2)	21.2	21.9	253
$[Me_3SnCH_2CH_2CH_2N(Me)CH_2]_2$	0.7	320.0 (Me) 362.0			364
$MeSn(CH_2I)_3$	−6.4	411.4 (Me) 354.0 (CH_2)			158
Me_3Sn-C(O)Ph	−80.0	n.r.	n.r.	n.r.	160
2-Me_3Sn-cyclohexanol[i]	−2.4	302.0 (Me) 400.0 (C-2)	25.0 (C-1) 16.0 (C-3)	60.0 (C-4) 46.0 (C-6)	124
3-Me_3Sn-cyclohexanol[c]	0.6	310.0 (Me) 400 (C-3)	17.0 (C-2) 20.0 (C-4)	80.0 (C-1) 71.0 (C-5)	124
1-Me_3Sn-2-C(O)Me-tetralin[h]	1.0	320.4 (Me) 333.1 (C-1)	n.r.	12.7 (CO)	141
2-Me_3Sn-3-C(O)Me-indene[h]	−0.5	335.7 (Me) 385.3 (C-2)	n.r.	22.9 (CO)	140
$Me_3SnCH_2N(Me)CH_2CH_2NMe_2$	−23.3	301.8 (Me) 410.6 (CH_2)		30.0 (NMe) 41.1 (NCH_2)	402
$N(CH_2CH_2CH_2)_3SnMe$	−14.4	170.9 (Me) 405.4 (CH_2)	23.3	26.0	368

Table 3.—*Continued*

Compound	$\delta^{119}Sn$	$^{1}J(^{119}Sn,^{13}C)$	$^{2}J(^{119}Sn,^{13}C)$	$^{3}J(^{119}Sn,^{13}C)$	Ref.
2-Me_3Sn-CH_2-pyridine	8.6	333.0 (Me) 276.3 (CH_2)	40.9	21.3	134
$(Me_3Sn)_2CHC(Et)_2B(OMe)Et$	1.7	302.1 (Me) 316.9 (CH)			40
$Me_2Sn(CH_2InMe_2)_2$	−0.7	n.r.			158
$Me_3SnCH(Me)CH_2P(O)Ph_2$	15.2	n.r.	n.r.	147.9 (^{31}P)	204
Ph_3Sn-C(S)SCH_2Ph	−191.0	n.r.	n.r.	13.6 (CH_2)	244
Ph_3Sn-$CH_2CH_2CH_2$C(S)SMe	−101.8	384 (CH_2)	18.1 (CH_2)	70.1 (CH_2)	244
Ph_3Sn-CH_2S-2-benzthiazolyl	−121.1	344.2			118
$PhBu_2SnCH_2CH_2CN$	−41.0	n.r.	n.r.	n.r.	342
Ph_3Sn-$CH_2CH_2CH_2NMe_2$	−102.2	487.0 (Ph) 400.0 (CH_2)	38.0 (Ph) 20.0 (CH_2)	63.0 (CH_2)	105
$(Me_3Sn$-$C_5H_4)_2Fe$	−4.2	357.8 (Me) 492.5 (C-1)	51.8	40.3	122
$(Et_3Sn$-$C_5H_4)_2Fe$	−9.6	353.5 (Et)	23.9 (Et)		123
$[(Ph_3Sn$-$C_6H_5)FeCp]^+$	−132.2				138
$(Me_3Sn)_2C_2Co_2(CO)_6$	15.0	328.0	33.3		110
MeC≡C-$Sn[C_2MeCo_2(CO)_6]_3$	−172.2	814.1 (C≡) 565.5 (C)	149.8 (≡C) 23.3 (C)	14.4 (MeC≡) <5 (MeC)	147
Me_3Sn-2,4,6-$(CF_3)_3C_6H_2$	−0.1	375.0 (Me)	6.4		106
$(Me_3Si)_3CSnMe_2$-CN	−58.0	n.r.	n.r.	n.r.	259
2-Me_3Sn-pyridine	−52.9	346.6 (Me) 605.5 (C=)	37.1	93.2	113
2-Me_3Sn-pyridine-BEt_3	−30.4	369.8 500.0 (C=)	66.4	35.0	271
2-Me_3Sn-thiazole	−32.6	373.8 (Me) 461.5 (C=)		68.6	115
5-Me_3Sn-1,2,4-triazole	−48.1	380.0 (Me) 450.8 (C=)		61.0	115

bis[3-(2-pyridyl)-2-thienyl-*C*,*N*]-$SnPh_2(CN_{Sn} = 6)^j$	−245.5	794.9 (Ph)	43.2 (Ph)	58.6	242
(E)-Me_3Sn^1-$CH_2CH{=}CH$-Sn^2Me_3	−8.3 (Sn^1) −39.8 (Sn^2)	284.8 (CH_2) 485.7 (C=)	n.r.		143
Me_3Sn^1-CH_2-C≡C-Sn^2Me_3	0.8 (Sn^1) −75.8 (Sn^2)	339.5 (Me^1) 404.4 (Me^2) 276.6 (CH_2) 532.2 (C≡)	53.4 (Sn^1) 113.5 (Sn^2)	37.2 (Sn^1) 11.4 (Sn^2)	108
(E,E)-$Me_2Sn(CH_2CH{=}CHMe)_2$	−12.6				197
(E,Z)-$Me_2Sn(CH_2CH{=}CHMe)_2$	−9.6				
(Z,Z)-$Me_2Sn(CH_2CH{=}CHMe)_2$	−6.8				
$Me_3Sn(Br)C{=}CMe_2$	−20.5	n.r.	n.r.	28 (*cis*, *trans*)	157
(E)-Me_3Sn-CH=CH-CH-$SnMe_3$	−52.3	337.0 (Me) 409.0 (C=)	n.r.	1013.0 (^{119}Sn)	139
(Z)-$Me_3SnCH{=}CH$-$SnMe_3$	−60.6	340.0 (Me) 496.1 (C=)	n.r.	491.0 (^{119}Sn)	139
$Me_3Sn(Me_3Si)C{=}CMe_2$	−50.4		73.2 (^{29}Si)		121
(E)-Me_3Sn-CH=CHPh	−31.0	355.5 (Me) 451.7 (C=)	13.8	69.9	107
(Z)-Me_3Sn-CH=CHPh	−49.7	355.3 (Me) 431.8 (C=)	6.3	32.0	107
1-MeC(O)-2-Bu^n_3Sn-1,4-cyclohexadiene	−57.7				137
$(Me_3Sn)_2C{=}C(NEt_2)CH_2OMe$	−44.9	333.1 (Me) 324.8, 352.8	603.9 (^{119}Sn)	72.1, 28.3	120
(Z)-$Bu^n_3Sn^1$-CH=C(CH_2S-*p*-tolyl)-$^2SnBu^n_3$	−54.1 (Sn^1) −65.8 (Sn^2)	410.1 (CH=) 409.6 (C=)	65.8 (Sn^2) 38.1 (Sn^1)	97.3 256 (^{117}Sn)	127
(Z)-Me_3Sn^1-CH=C(Et)-$^2SnMe_3$	−62.5 (Sn^1) −50.2 (Sn^2)	323.7 (^{1}Me) 340.1 (^{2}Me) 498.0 (CH=) 516.1 (C=)	78.5 (CH=) 34.3 (C=) 73.6 (CH_2)	101.9 (Sn^1) 432.3 (^{119}Sn)	129
$CH[Me_2Si(Me_3Sn)C{=}C(Et)]_3B$	−58.3	306.2 (Me) 302.0 (C=)	39.5 92.7 (^{29}Si)	98.9	150

Table 3.—*Continued*

Compound	δ^{119}Sn	$^1J(^{119}Sn,^{13}C)$	$^2J(^{119}Sn,^{13}C)$	$^3J(^{119}Sn,^{13}C)$	Ref.
(E)-Me_3Sn-CH=C(Et)-B(Et)-N-pyrrol[g]	−53.0	343.0 (Me) 482.0 (C=)	–	87.5 (CH_2)	148
(E)-Me_2B(Fc)C=C(Me)-$SnMe_3$[b,e]	−48.3	322.9 (Me) 508.1 (C=)	60.0 (Me-C=) 79.5 (=CB)	103.8 (C-1)	145
(E)-Bu^n_3SnCH=CH-B(N^iPr_2)$_2$	−55.5	n.r.	n.r.		109
[(E)-Me_3Sn(Me)C=C(Et)BEt_2-NH_2]$^-Na^+$ in THF (CN_{Sn} = 5)	−175.6 (−50°C)	450.0 (Me) 861.9 (C=)		136.2	161
(Z)-1-(2-Ph_3Sn-CH=CH)-cyclohexanol[f]	−155.5	540.0 (Ph) 583.0 (C=)	38.0 (Ph) 4.0 (=C)	51.0 (Ph) 39.0 (COH)	126, 163
2,5-$(Me_3Si)_2$-3-Et_2B-4-Et-stannacyclopentadiene[d]	133.5	259.1 (Me) 194.2 (C-2) 260.4 (C-5)	94.8 (C-4) 97.4, 98.2 (^{29}Si)	92.2 (CH_2) 9.0, 11.7 (Me)	180
[$Pr^iB(C(Pr^i)$=C(Me)]$_2$Sn	−201.3	n.r.	53.7 (Me)	69.5 (CH)	190
$(Me_3Sn)_2C$=C=CH_2	−9.6	348.2 (Me) 261.7 (C=)	30.5	60.6	119
$(Me_3Sn^1)_2C$=C=C(Et)-C($Sn^2Me_3)_2$-BEt_2	−11.5 (Sn^1) −3.3 (Sn^2)	324.2 (^{1}Me) 313.5 (^{2}Me) 294.2 (C=) 153.0 (CSn^2)			146
Me_3Sn-C≡C-CH_2OSnMe_3	−70.4 135.3 (SnO)	404.9 (Me) 454.5 (C≡)	86.7	9.4	165
PhP(C≡C-$SnMe_3)_2$	−63.0	402.6 (Me) 368.1 (C≡)	56.9	16.6 (^{31}P)	262
Me_3Sn-C≡C-$SiMe_2$-C≡C-Bu^t	−74.8	402.2 (Me) 391.8 (C≡)	63.2	11.7 (^{29}Si)	144
Me_3Sn-C≡C-$SiMe_2$-C≡C-$SiMe_2$-C≡C-$SnMe_3$	−74.5	402.7 (Me) 379.9 (C≡)	60.7	11.4 (^{29}Si)	130
Me_3Sn-C≡C-C≡C-$PbMe_3$	−61.8	404.7 (Me) 405.2 (C≡)	90.3	19.2	125

trans-[Pt(PEt_3)$_2$(C≡C-$SnMe_3$)$_2$]	−93.7	392.5 (Me) 552.5 (C≡)	111.0	237.2 (^{195}Pt)	117
cis-[Pt(dppe)(C≡C-$SnMe_3$)$_2$]	−85.3	396.0 (Me)		250.0 (^{195}Pt)	117
$Me_2Sn(C{\equiv}C(CH_2)_4C{\equiv}C)_2SnMe_2$	−158.0	499.7 (Me) 628.2	129.7	11.4	267
$Me_2Sn(C{\equiv}C\text{-}PMe_2)_2$	−150.8	495.4 (Me) 555.2 (C≡)	94.3	12.5 (^{31}P)	262
$MeSn(C{\equiv}CMe)_3$	−250.4	617.1 (Me) 873.9 (C≡)	184.2	16.2	128
$MeSn(C{\equiv}C\text{-}Bu^t)_3$	−273.4	612.5 (Me) 864.3 (C≡)	171.1	14.2	128
$Me(C{\equiv}C\text{-}SiMe_3)_3$	−273.4 −279.7 (solid)	603.8 (Me) 760.3 (C≡)	126.8	15.3 (^{29}Si)	128

[a]See ref. 4 for further data; n.r. means not reported.
[b]Fc = $C_5H_4FeC_5H_5$ (ferrocenyl).
[c]See also ref. 149; see ref. 333 for solution- and solid-state ^{119}Sn NMR data of C-stannylated carbohydrate derivatives.
[d]See also ref. 181.
[e]See also ref. 193 for further stannyl-, boryl-substituted alkenes.
[f]See also ref. 220.
[g]See also ref. 270 for similar compounds.
[h]See ref. 363 for an x-ray structural analysis 1-Me_3Sn-2-C(O)Me-1,4-cyclohexadiene.
[i]See ref. 345 for x-ray structural analysis and NMR data of [Z]-2-Me-3-Ph_3Sn-3-pentene-2-ol.
[j]See also ref. 406 for further data on similar compounds.

Table 4. ^{119}Sn NMR parameters of compounds with tin–halogen bonds.

Compound	$\delta^{119}Sn$	$^1J(^{119}Sn,^{13}C)$	$^2J(^{119}Sn,^{13}C)$	$^3J(^{119}Sn,^{13}C)$	Ref.
$(PhMe_2Si)_3CSnMe_2F$	124.5	2374 (^{19}F)			240
$(Me_3Si)_3CSnPh_2F$	−40.8	2463 (^{19}F)			240
$N[CH_2CH_2N(Me)]_3SnF$	−261.6	2920 (^{19}F)	16.4	26.8	331
	−274.0 (solid)	3000 (^{19}F)			
$[SnF_3]^-$	−700	n.r.			372
$[SnF_6]^{2-}$	−803	1625 (^{19}F)			214
$[PhSnF_5]^{2-}$	−692	1180 (d, ^{19}F)			214
		2430 (^{19}F)			
$[Ph_2SnF_3]^-$	−402	2310 (d, ^{19}F)			214
		2250 (t, ^{19}F)			
$[Ph_3SnF_2]^-$ $[NBu_4]^+$	−345.9	2010 (^{19}F)			349
	−339	1958 (^{19}F)			290
$[Bu^n_2(F)Sn]_2O$	−156	1766 (^{19}F)			
		795 (^{19}F)			
$Ph_3SnF\text{-}OP(NMe_2)_3$	−272.0	2040 (^{19}F)			349
Me_3SnCl ($CDCl_3$, 33 mol%)	165.7	379.0[a]			213
($CDCl_3$, 15 mol%)	171.2				
(acetone, 30.5 mol%)	119.8				
$Me_3SnCl + Cl^-$ ($CDCl_3$, −60°C)	101.3				301
Pr^i_3SnCl (neat)	100.4	n.r.			407
Np_3SnCl ($CDCl_3$)	122.8	n.r.			407
cy_3SnCl	+82.0 (solid)				366
$MeSnCl_3$	6.0	n.r.			255
$Bu^n(Me)SnCl_2$	132.1	391.2 (Bu)	n.r.	102.4	344
$Bu^n_2SnCl_2$ ($CDCl_3$)	126.3	419.9	36.6	85.4	385
Bu^nSnCl_3 ($CDCl_3$)	6.1	645.0	40.0	120.0	352
Bu^nSnCl_3 (DMSO)	−457.1	n.r.	71.6	210.3	352
$PhCH_2SnCl_3$ ($CDCl_3$)	−31.3	623.5	106.9	71.5	367
$PhCH_2SnCl_3$ (DMSO)	−492.2	1125.4	123.3	80.6	367

$PhSnCl_3$	−65.0	n.r.	n.r.	n.r.	255
2,6-$(MeO)_2$-C_6H_3-CH_2SnCl_3	−344.0	n.r.	n.r.	n.r.	327
Cl-$Sn(CH_2CH_2CH_2SnMe_2Cl)_3$	137.6 (Cl-Sn) 162.3 ($SnMe_2$)	350.0 (Me)			225
$N(CH_2CH_2CH_2)_3SnCl$	19.5	476.6	28.9	38.5	368
$(Me_3Si)_3CSnMe_2$-Cl	133.8	n.r.	n.r.	n.r.	259
$(PhMe_2Si)_3CSnMe_2$-Cl	115.9	377 (Me)			240
$[Me_2Sn(Cl)CH_2CH_2]_2P(O)Ph$	60.5	460.7 (Me) 472.3 (CH_2)	17.9	67.1 (^{31}P)	
$MeSn(Bpz_4)Cl_2$[d,f]	−473.6				294
$(H_2C{=}CH)_3Sn$-Cl	−52.8 ($CDCl_3$) −215.5 (DMSO)	587.2 778.1			
$Cl_2Sn(CH_2)_{16}SnCl_2$[e]	56.7	n.r.	n.r.	n.r.	245
$[Cl_2SnCH_2CH_2CH_2N(Me)CH_2]_2$	−176.5	957.0	55.0 78.1 (NCH_2)		364
$(H_2C{=}CH)_2SnCl_2$	−30.2 ($CDCl_3$) −394.1 (DMSO)	750.7 1469.7			200
$(PhCH_2)_3Sn$-Cl	51.3	293.0	42.7	31.8	248
$(Me_5C_5)Sn$-Cl	993				210
$(CF_3)_3Sn$-Cl	−255.8	1179	636 (^{19}F)		212
$(CF_3)_2SnCl_2$	−179.1	1498	773 (^{19}F)		212
CF_3SnCl_3	−141.5	2055	966 (^{19}F)		212
$H_2C{=}C[C(O)OEt]$-$SnCl_3$[e]	−152.7				217
Me_2SnCl_2-bipyridine	−267.0 (solid)				351
Ph_2SnCl_2-bipyridine	−383.0 (solid)				351
$[Ph_2SnCl_3]^-$	−250				214
$[Ph_2SnCl_4]^{2-}$	−425				214
$(Bu^tOSnCl)_2$	270.8				207
$(Bu^n_2SnCl)_2O$	−139.8	n.r.	73.2 (^{117}Sn)		374
Cl_2Sn(maltolate)$_2$	−465.5				221
$[HB(3\text{-}Bu^t\text{-}5\text{-}Mepz)_3]SnCl$[d,f]	−577.9				329
$(Bu^t_2P$-$SnCl)_2$	507	1432 (t, ^{31}P)			233

Table 4.—*Continued*

Compound	δ^{119}Sn	$^{1}J(^{119}Sn,^{13}C)$	$^{2}J(^{119}Sn,^{13}C)$	$^{3}J(^{119}Sn,^{13}C)$	Ref.
$N[CH_2CH_2N(Me)]_3SnCl$	−180.2 −192 (solid)		9.1	23.1	331
$[CH_2(CH_2CMe_2)NSnCl]_2$	192.2, 1770				206
$(Et_2N)_2SnCl_2$	−100.1				185
$CH_2[CH_2N(Bu^t)]_2SnCl_2$	−163.0 −164.0 (solid)				185
$[(Me_3Si)_2N]_2SnCl_2$	−143.8				185
$PhSn(dpa)Cl_2$[b]	−445				215
$Me_2SnCl_2[p\text{-}NH_2C_6H_4C(O)Me]$	26.8	610.8	n.r.	n.r.	257
$MeSnCl_3\text{-}OPBu^n_3$[g]	−265 (−90°C)	n.r.	230 (^{31}P)		255
$SnCl_4$	−150 ± 2	–	–	–	4
$acacSnCl_2$	−640				403
$PhCH_2OC(Me)HC(O)Et\text{-}SnCl_4$	−542.1	n.r.	n.r.	n.r.	252
$(ClMe_2Sn)_3N$	83.5	492.0 66.4 (^{15}N)	38.0 (^{117}Sn)		361
$Sn(NEt_2)_4\text{-}SnCl_4$	−200.6 (SnN) −517.5 (SnCl)			188 (^{2}J(Sn,Sn)	185
$[SnX_3]^-$	−26 (Cl), 142 (Br), 362 (I)				288
$[SnX_6]^{2-}$	−732 (Cl) −2070 (Br) −916 (CN)				425
$[SnCl(H_2O)_5]^{3+}$[i]	−620				195
$[SnCl_2(H_2O)_4]^{2+}$[i]	−623, −625				195
$[SnCl_3(H_2O)_3]^{+}$[i]	−631, −635				195
Pr^i_3SnBr (neat)	115.5	n.r.			407
Np_3SnBr (CCl_4)	79.5	n.r.			407
cy_3SnBr ($CDCl_3$)	79.2 (94 solid)				366
Me(Ph)(1-adamantyl)Sn-Br	56.1				216
$Bu^n_2SnBr_2$ (neat)	89.7	391.8	34.2	85.4	385

$(\eta^1\text{-}Me_5C_5)_2SnBr_2$	−58.5				
$BuSnBr_3$ ($CDCl_3$)	−114.7	590.6	56.8	117.8	352
$BuSnBr_3$ (DMSO)	−604.1	n.r.	69.7	218.9	352
$(BrMe_2Sn)_3N$	66.6	485.0	45.0 (^{117}Sn)		361
$(PhCH_2)_3Sn\text{-}I$	−19.1	273.4	43.0	31.7	248
Ph_2(1-adamantyl)Sn-I	−61.0				216
$Bu^n_2SnI_2$ (neat)	−56.1	347.9	33	83.6	385
$(IMe_2Sn)_3N$	24.9	447.0	67.0 (^{117}Sn)		361

[a]See ref. 4 for more data; n.r. means not reported.
[b]dpa = di-2-pyridylketone-2-aminobenzoylhydrazone (x-ray structural analysis).
[c]Halogen (Cl/Br) exchange in allyltin trihalides studied by 2D EXSY.
[d]pz = pyrazolyl.
[e]See also refs 250, 323.
[f]See ref. 340 for the molecular structure of $[HB(pz)_3]_2Sn$, ref. 302 for further ^{119}Sn NMR data; refs 274, 387 for ^{119}Sn NMR data of organotin(IV) polypyrazolylborates.
[g]See ref. 392 for NMR data of complexes of Ph_2SnCl_2 with tri-n-octylphospane oxide.
[h]See ref. 379 for $^1J(^{119}Sn,^{13}C)$ in 22 different solvents.
[i]See also ref. 412 for similar results.

Table 5. ^{119}Sn NMR parameters of compounds with tin–chalcogen bonds.

Compound	δ^{119}Sn	$^1J(^{119}Sn,^{13}C)$	$^2J(^{119}Sn,^{13}C)$	Ref.
$Sn(OSO_2F)_2$	−1534 (solid)			311
Me_3SnOEt	136.8			343
Me_3SnOPh	151.0			343
$N(CH_2CH_2CH_2)_3SnOH$	−16.9	502.0	25.9	368
Me_3Sn-O-$SiMe_3$	121.0	407.7		198
$Pr^i_3Sn(OPr^i)_3$	−217.9 (−364.2 solid)	866.3	41.9	19
$Bu^n_3SnOPr^i$	92.1	363.8	19.5	332
Bu^n_3Sn-OBu^t	71.7	363.8	18.4	332
Bu^n_3Sn-OPh	119.1	353.6	19.9	201
cy_3Sn-OH	1.5	n.r.	n.r.	249
$(cy_3Sn)_2O$	−7.9			408
cy_3Sn-oxinate[f]	−57.6			408
$(Bu^tO)_2Sn$	644.4			207
$[2,4,6\text{-}Pr^i_3\text{-}C_6H_2]_2Sn(OEt_2)CR_2$ R_2 = fluorenylidene	288.0			319
Me_3Sn-*m*-Me-*trans*-cinnamate	129.0	402.0		359
Me_3Sn-O-C(O)-O-$SnMe_3$	123.5, −62.2 solid state			199
Bu^n_3Sn-OC(O)Me	103.8	360.1	18.5	332
Bu^n_3Sn-OC(O)CCl_3	171.8	337.5	20.9	332
Bu^i_3Sn-OC(O)-$OSnMe_3$ solid state	101.7 86.5, −75.1, −96.4	356.0		199
Me_3Sn-OSO_2Me ($CDCl_3$)	75.5	456.0		357
Me_3Sn-OSO_2Me (DMSO)	16.9	517.8		357
Me_3Sn-OC(O)N(benzoyl)-R	142.4 (D,L-Ala)	405.9		246
Bu^n_3Sn-$OC(O)CH_2OPh$	130.9	352.2	20.8	254
Bu^n_3Sn-OC(O)-N(acetyl)-R[d]	116.4 (D,L-Ala)	361.3	22.0	209
Ph_3Sn-OC(O)Ph	−114.3	n.r.	n.r.	251
Bu^n_2Sn (*p*-MeO-*trans*-cinnamate)$_2$	−154.6	n.r.	n.r.	256
$(Ph_3SnO)_2SO$	−49.7	n.r.	n.r.	268
Ph_3Sn-oxinate[f]	−190.1 (−213.2, solid)			291, 381
cy_2Sn(glycylglycinate)	−175.9	553		326
Me_3Sn-O-ReO_3	91.8	480.7		365
$Bu^t_2Sn(OCH_2)_2$	−225 (−225 solid)	n.r.	n.r.	277
$Bu^t_2SnOCH_2CH_2S$	−25 (0.45 M) 52 (0.02 M) (−96, −101 solid)	n.r.	n.r.	277
$[Ph_3Sn\text{-}O\text{-}C(CF_3)_2CHSPh]^-$	−227.9	–	–	335
$Sn(OPr^i)_4$ ($CDCl_3$)	−596			403
$Sn(OBu^n)_4$ ($CDCl_3$)	−583, −616, −629.6			403
$Sn(OBu^t)_4$	−373			403
$[(hmp)_3Sn]^+X^-$ (X = Cl, Br)[b]	−457.6			328
$[I\text{-}Sn(OPr^i)_9Ti_2]_2$	−111.5, −191.6			208
$\{[(Me_3Si)_2N]_2Sn\ (\mu\text{-}O_2)\}_2$	−268			235
$Bu^n_3SnSBu^n$	74.1	330.7	21.2	332
$Bu^n_3SnSBu^t$	50.4	330.8	20.8	332

Table 5.—*Continued*

Compound	δ^{119}Sn	$^1J(^{119}Sn,^{13}C)$	$^2J(^{119}Sn,^{13}C)$	Ref.
Bu^n_3SnSPh	84.1(79.5,[305] 82.6[299])	326.4	21.4	201
Bu^n_3Sn-2-S-naphthol	82.2			305
Me_3Sn-SC(S)NMe_2	25.0	n.r.	n.r.	258
$Me_2Sn[SC(S)NMe_2]_2$	−338	n.r.	n.r.	258
Me_3SnSFc^c	91.3	348.9	15.7	39
$(Bu^n_3Sn)_2S$	81.6	n.r.	205 (^{117}Sn)	249
$(cy_3Sn)_2S$	22.6	322	13.0	348
$(H_2C{=}CH)_3Sn$-SBu^n	−73.8	539.0	not found	218
$Me_2Sn(SCH_2CH_2S)$	193.0 (66.9 solid)	372.0, 445.0 (solid)		20f
$Bu^t_2Sn(SCH_2)_2$	171 (171 solid)	n.r.	n.r.	277
Me_2Sn(2-S-pyridine)$_2$	−124.0	598.0	n.r.	346
$Me_2Sn[S_2P(OCMe_2)_2]$ (solid)	−257.1			282
cy_2Sn(2-S-pyridine)$_2$	−160.5	543.0	27.0	325
$Ph_3Sn[S_2P(OPh)_2]$	−75.5, −128.0, −268.5	n.r.		211
$(Bu^t_2SnS)_2$	124.0	363	114 (^{117}Sn)	283
$[(p\text{-tolyl})_2SnS]_3$	21.0		193.2 (^{117}Sn)	243
$[(4\text{-F-}C_6H_4)_2SnS]_3$	22.9		200.2 (^{117}Sn)	243
$\{Ph_2Ga[\mu\text{-Ssncy}_3]\}_2$	43.1, 22.6			348
$(p\text{-}tolylSn)_4S_6$	86.4		260.7 (^{117}Sn)	243
$(C_6F_5Sn)_4S_6$	46.4		290.0	243
$(SCH_2CH_2S)_2Sn$	277.0 (241.0 solid)			20f
$Sn(SPh)_4$	49.5			238
$Sn(S\text{-Fc})_4$	−32.1	–	12.0	39
$[ClMe_2SnSN{=}S{=}N]^-$	26	543		276
$Sn(SCH_2CH_2)_2PPh$	−113.6	1270 (^{31}P)		383
Me_3Sn-Se-Fc^c	53.6	333.2 977.6 (^{77}Se)	19.3	39
$fc(SnMe_2)_2Se^e$	28.1	364.1 491.1 1133 (^{77}Se)	60.5 204.8 (^{117}Sn)	266
$(Bu^t_2SnSe)_2$	51.2	333 923 (^{77}Se)	17 (^{117}Sn)	283
Ar(Ar′)Sn(SeSe)	−406 (broad)	n.r.		424
Ar(Ar′)Sn=Se	440, −556	n.r.		424
$Sn(SePh)_4$	−132.7	1584 (^{77}Se)		238
$Sn(Se\text{-Fc})_4^c$	−218.3	1700 (^{77}Se)	11.9	39
$[SnSe_3]^{2-}$	−264.3	2951 (^{77}Se)		239
$[SnSe_4]^{4-}$	−476.6	1363 (^{77}Se)		239
$[Sn_2Se_6]^{4-}$	−499.0	2014, 873 (^{77}Se)		360
$[Sn_2Se_7]^{4-}$	−338.0	2045, 1306, 1130 (^{77}Se)		360
$[Sn_4Se_{10}]^{4-}$	−350.1	2274, 1536 (^{77}Se)	342 (^{117}Sn)	353
$[Sn(Se_4)_3]^{4-}$	−723	not observed		296

Table 5.—*Continued*

Compound	δ^{119}Sn	$^1J(^{119}Sn,^{13}C)$	$^2J(^{119}Sn,^{13}C)$	Ref.
$\{[Me_3Si)_2N]_2Sn(\mu\text{-Se})\}_2$	−382.6	1128(^{77}Se)	790 (^{117}Sn)	310
$Me_3Sn\text{-Te-Fc}^c$	−42.9	312.6 2654.5(^{125}Te)	16.6	39
$(Bu^t_2SnTe)_2$	−125.2	289 2117(^{125}Te)	29 (^{117}Sn)	283
$Sn(TePh)_4$	−570.5	3379(^{125}Te)		238
$[SnTe_3]^{2-}$	−1170.1	4535(^{125}Te)		239
$[SnTe_4]^{4-}$	−1823.6	2851(^{125}Te)		239
$[Sn_2Te_6]^{4-}$	−1675.0	3998, 1633 (^{125}Te)		360
$[Sn_2Te_7]^{4-}$	−1344.9	4023, 2902, 2319(^{125}Te)		360
$\{[Me_3Si)_2N]_2Sn(\mu\text{-Te})\}_2$	−988.8	2700(^{125}Te)	569 (^{117}Sn)	310

[a]See ref. 4 for more data; n.r. means not reported.
[b]Hhmp = 3-hydroxy-2-methyl-pyridin-4-one.
[c]Fc = C_5H_4FeCp(1-ferrocenyl).
[d]See also refs 232, 314, 315, 334 for further data.
[e]fc = 1,1′-ferrocenediyl.
[f]See refs 373, 378 for further NMR data on triorganotin quinolates.

examples are the drum and ladder organooxotin carboxylates[404,405] and similar compounds derived from phosphorus containing acids.[400] Further interesting examples are tungstostannate(II) heteropolyanions.[399] The trimeric dimethyltin chalcogenides have been studied by solid-state CP/MAS ^{119}Sn NMR,[369] and the Sn–Sn couplings have been determined by using the INADEQUATE pulse sequence also in the solid state[307] (see also solution-state NMR data).[380] The compound **26**[39] provides another instructive example for the application of solid-state NMR: the ^{119}Sn CP/MAS NMR

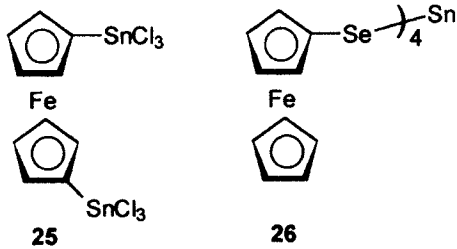

25 **26**

δ^{119}Sn -23.2 [38] -218.3 (solid: -233) [39]

δ^{77}Se + 80.6 (solid: 49.1,106.7,113.1,120.0)[39]

spectrum shows only one signal (slightly shifted by 15 ppm to lower frequency as compared to solutions of **26**), whereas the ^{77}Se CP/MAS NMR spectrum shows four different selenium sites for the four selenium atoms, covering a range of ~70 ppm, the average being close to δ^{77}Se for solutions.

Numerous dynamic problems can be studied in an elegant way by using 2D ^{119}Sn NMR exchange spectroscopy, as shown in an early study of this type for the fluxional heterocyclic compound $CH_2[(Ph)Sn(SCH_2CH_2)_2NMe]_2$.[377] The neighbourhood of the tin atom to an oxonium (**27**)[17,40] or ammonium-type (**28**)[41] oxygen or nitrogen atom causes a marked deshielding of the ^{119}Sn nucleus.

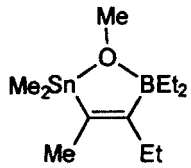

27

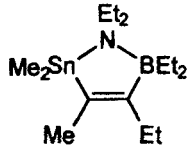

28

δ^{119}Sn	174.5	124.1

Many tin–nitrogen and tin–phosphorus compounds have been investigated by ^{119}Sn NMR. Relevant data are summarized in Tables 6 and 7 (see also Ref. 41b,437). Rearrangements can be studied very often most conveniently by ^{119}Sn NMR, as shown for the **29** to **31**.[189] These examples also serve for demonstrating the usefulness of a multinuclear approach, looking at the relevant ^{11}B and ^{14}N NMR data which are also readily recorded from reaction solutions.

There are many examples of compounds with Sn–Si, Sn–Ge, Sn–Sn and Sn–Pb bonds which have been prepared in the last decade, and the majority has been characterized by ^{119}Sn NMR (Table 8). More examples became also available for compounds with Sn–B, Sn–Li and even Sn–K (in the solid state) bonds (Table 8).

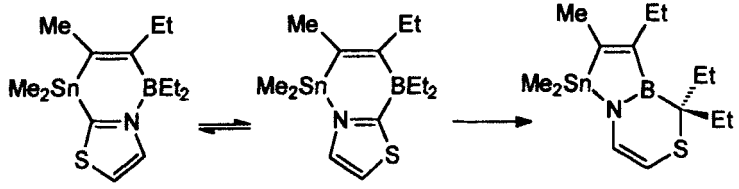

	29	**30**	**31**
δ^{119}Sn	-106.5	15.2	77.3
δ^{11}B	2.5	-9.6	40.6
δ^{14}N	-92.0	-147.0	-244.0

Table 6. ^{119}Sn NMR parameters of compounds with tin–nitrogen bonds.

Compound	δ^{119}Sn	$^1J(^{119}Sn,^{13}C)$	$^1J(^{119}Sn,^{15}N)$	Other	Ref.
$Bu^t_3Sn\text{-}NH_2$	−27.9		113.3	16.5 ^2J(Sn,H)	219
$Me_3Sn\text{-}NH\text{-}SnBu^t_3$	74.5 (SnMe) −15.7 ($SnBu^t$)	n.r.	n.r.		219
$(Bu^t_3Sn)_2NH$	−16.1	n.r.	138.5	35.0 ^2J(Sn,H)	219
$Me_3SnNHSiBu^t_2F$	67.1	n.r.	n.r.	19.2 $^3J(^{119}Sn,^{19}F)$	362
$(Me_3Sn)_3N$[a]					
$(Me_3Sn)_2NC(O)Me$ solid state	40.7, 126.6 0.3, −19.4	389.6	n.r.		356
$(Me_3Sn)_2NSiBu^t_2F$	51.7, 77.8	n.r.	n.r.	36.7, 100.3 ($^3J(^{119}Sn,^{19}F)$)	362
$Me_3Sn\text{-}N(Bu^t)\text{-}S\text{-}N(Et)BEt_2$	74.0	385.3	7.6		231
$Me_2Sn\text{-}N(Bu^t)BMeN(Bu^t)CH_2$	67.8	337.1 (Me)	n.r.		247
$[(Me_3Sn)_4M(CN)_6]_n$ (solid-state)[e]	−88, −118 (Co) −108, 46 (Fe) −97, 32 (Ru)		≈127 (^{14}N)		297
$Me_2(Et_2N)Sn\text{-}C{\equiv}CMe$	−38.7	480.2 (Me) 560.3 (C≡)	24.9		186
$(Et_2N)_2Sn(C{\equiv}CMe)_2$	−176.9	1009.6	146.8		186
$CH_2[CH_2N(Bu^t)]_2Sn(C{\equiv}CMe)_2$	−265.4	1009.3	100.1		186
cy_3SnNCS	−3.2	n.r.	136 (^{14}N)		391
$Me_3Sn(NSN)SnMe_3$	40.5	n.r.			182
$Sn[(NSN)Bu^t]_4$ (solid state)	−624.0	–	n.r.		272

$Me_2Si[N(Bu^t)]_2$-Sn[N(Et)SN(Et)]$_2$	−146.3	–	4.2 (SnNSi) 20.1 (SnNS)		237
$Me_2Si[N(Bu^t)]_2Sn[N(Bu^t)]_2Se$	−128.4	–	24.3 (SnNSi) 101.8 (SnNSe)		260
$[(Me_3Si)_2N]_2Sn{=}NAr$[c]	−3.5	–	n.r.		175
$S[CH_2CH_2N(Bu^t)]_2Sn$	77.6				226
$[Me_3Si(C_8H_{14}B)N]_2Sn$[d]	791.5	–	234 (^{14}N)		269
$Ph_2Sn(CH_2)_3$-CN_4 (DMSO)[f]	−224.3				289
$N[CH_2CH_2N(Me)]_3Sn$-C≡CPh	−173.9		n.r.	135.9 $^2J(^{119}SnC{\equiv}^{13}C)$	331
	−172 (solid)	785.5			
$[Sn(NCS)_6]^{2-}$[g]	−842		150 (^{14}N)		370

[a] See refs 4, 430 for more data; n.r. means not reported.

[b] Application of the Ψ-BIRD pulse sequence: ref. 184; application of z-filtered polarization transfer: ref. 183.

[c] Ar = 2,6-^{i}Pr$_2$-C$_6$H$_3$.

[d] $C_8H_{14}B$ = 9-borabicyclo[3.3.1]nonyl.

[e] See ref. 321 for 2D exchange MAS ^{13}C NMR.

[f]

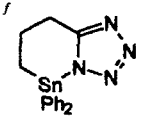

[g] See ref. 386 for ^{119}Sn NMR data in the system $SnBr_4$–KSCN–MeOH.

Table 7. ^{119}Sn NMR parameters of compounds with tin–phosphorus and tin–arsenic bonds.[a]

Compound	δ^{119}Sn	$^1J(^{119}Sn,^{31}P)$	Other	Ref.
$Bu^t_3Sn\text{-}PH_2$	32.2	626-		284
$Bu^t_3Sn\text{-}PHBu^t$	15.1	897		284
$Bu^t_3Sn\text{-}PHSiMe_3$	25.6	855	37.5 (^{29}Si)	219
$Bu^t_3Sn\text{-}P(SiMe_3)_2$	30.7	1028	27.9 (^{29}Si)	219
$(Bu^t_2SnPH)_3$[b]	55.2	1048	357 (^{119}Sn)	219
$(Bu^t_2SnPMe)_2$	−30.5	1030.8		300
$Bu^t_2Sn(PH_2)_2$	74.9	672.6		300
$Bu^t_2Sn[P(SiMe_3)_2]_2$	96.7	1030.4		300
Me_3SnPcy_2	−19.0	644		393
Me_3SnPPh_2	6.0	569		393
Et_3SnPPh_2	7.0	635		393
$Bu^n_3SnPPh_2$	−8.0	525		393
fc($SnMe_2$)PPh[c]	1.3	735.4	365.4 (^{117}Sn)	265
$Me_2Sn(PPh_2)_2$	−2.0	768		279
$Me_2Sn(Cl)PPh_2$	−99	718		279
$Ph_3Sn\text{-}Pcy_2$	−109.0	784		393
Ph_3SnPPh_2	−125.0	702		393
$^{(1)}P(SnPh_2)_3P_3^{(2)}$[d]	235.7	1069.6(1) 1294.5(2)	n.r. (^2J)(^{117}Sn)	428
$(Pr^i_3SiPSn)_6$	n.r.	708		390
$[(Me_2P)_3C]_2Sn$	−258.0	776	102 (^3J)(^{31}P)	62, 234
$(2,4,6\text{-}Pr^i_3\text{-}C_6H_2)_2Sn{=}PAr$[e]	499.5	2208		427
$[(Me_3Si)_2CH]_2Sn{=}PAr$[e]	658.3	2295		426
$\{[Ar_2(F)Si]_2P\}_2Sn$[f]	1551	1682		177
$Ph_2SnCl_2\text{-}PhPcy_2$	−296	710		279
$(Me_3Sn)_3As$	6.2		288.8 (^{13}C)	275
$(Me_3Sn)_2AsBu^t$	−21.2		281.1 (^{13}C)	275
$Me_3SnAsBu^t_2$	−48.8		257.4 (^{13}C)	275
$(Me_3Sn)_3As\text{-}Co(CO)_2NO$	31.7		303.3 (^{13}C)	275
$(Me_3Sn)_3As\text{-}Fe(CO)(NO)_2$	37.8		308.4 (^{13}C)	275

[a] See ref. 4 for more data; n.r. means not reported.
[b] See ref. 292 for the x-ray structural analysis of the dimer $(Bu^t_2SnPH)_2$.
[c] fc = 1,1′-ferrocenediyl.
[d] See ref. 429 for data of five-membered P_4Sn heterocycles.
[e] Ar = 2,4,6-$Bu^t_3C_6H_2$.
[f] Ar = 2,4,6-Pr^i_3-C_6H_2.

A wealth of new ^{119}Sn NMR data has become available for transition metal complexes with M–Sn bonds (Table 9; see also Fig. 2). Many of these complexes possess a rigid structure as compared to the NMR time scale. Others are fluxional, and ^{119}Sn NMR parameters can be used to understand the dynamic processes. An example is the iron complex *cis*-$[Fe(CO)_4(SnMe_3)_2]$, in which the magnitude of the geminal coupling constant $^2J(^{119}Sn,^{117}Sn)$ does not change under slow or fast exchange conditions. This

indicates that the tin atoms do not change their mutual positions in the fluxional process. Another example is shown by the ^{31}P NMR spectrum in Fig. 8 for a bis(stannyl)bis(triphenylphosphane)platinum complex. At room temperature the $Pt(PPh_3)_2$ fragment rotates about an axis which passes through the middle of a line connecting the two tin atoms. At low temperature, this process is slow and the expected pattern emerges for the satellites corresponding to $^2J(^{117/119}Sn,^{31}P)_{trans}$ and $^2J(^{117/119}Sn,^{31}P)_{cis}$.

Tin compounds with a formal oxidation state <+2

The tin nuclei in Zintl anions of the type $[Sn_5]^{2-}$, $[Sn_9]^{4-}$ and others such as $[Sn_8Tl]^{5-}$ and $[Sn_{9-n}Pb_n]^{4-}$ are highly shielded (δ^{119}Sn values range from around −1100 to around −1900).[4,59]

The least shielded ^{119}Sn nuclei so far were found in transition metal complexes which contain trigonally planar coordinated tin atoms in the formal oxidation state ±0 (**32**)[49] or −2 (**33**).[50] This deshielding is related to the presence of an energetically low-lying π^* LUMO available for B_0-induced charge circulation by which the paramagnetic contribution to magnetic shielding increases.

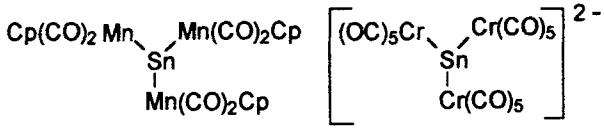

32 **33**

δ^{119}Sn 3301.0 3924.0

4.3. Isotope-induced ^{119}Sn chemical shifts

There are no primary isotope shifts for the magnetically active tin nuclei.[42] However, secondary isotope effects may be quite large and can be readily detected. Tri-*n*butyl tritide has been prepared; the $^1\Delta^{1/3}H(^{119}Sn)$ value was determined as −2.7 ppm, whereas $^1\Delta^{1/2}H(^{119}Sn)$ is −1.8 ppm.[191] In stannane $SnH_{4-n}D_n$, the $^1\Delta^{1/2}H(^{119}Sn)$ values are ~−0.403 ppm/D.[192] The effect of the substitution of ^{1}H against deuterium can be used to verify intramolecular (weak) associative bonding to tin, e.g. in an RO(H)-Sn group.[43] Numerous data have been collected for $^1\Delta^{12/13}C(^{119}Sn)$.[44,45,58,119] These data (Table 10) show that the expected shifts of the ^{119}Sn NMR signals to lower frequency for the heavy isotopomer are not observed in all cases. In addition to vibrational effects, responsible for isotope-induced chemical shifts, there is also a strong

Table 8. ^{119}Sn NMR parameters of compounds with tin–silicon, –germanium, –tin, lead, –boron, calcium, –lithium and –potassium bonds.

Compound	$\delta^{119}Sn$	$^1J(^{119}Sn,^{13}C)$	$^1J(^{119}Sn,M)$	Ref.
$Me_2Sn[Si(SiMe_3)_3]_2$	−175.1	n.r.	n.r.	236
$Cl_2Sn[Si(SiMe_3)_3]_2$	648.1	–	n.r.	236
$Ph_2Si(SnPh_3)$	−167	413	515 (^{29}Si)	241
			724 (^2J(Sn,Sn)	
$Ph_2Ge(SnPh_3)_2$	−147	419	725 (^2J(Sn,Sn)	241
$(Me_3Sn)_4Ge$	−25.2	258.1	37.5 (^{73}Ge)	133
$CH_2(SnMe_2SnMe_2)_2CH_2$	−78.5	4245 (^{119}Sn)		435
$(Me_2Sn)_6$[g]	−241.4	n.r.	1176 (^{117}Sn)	229
$(Me_2Sn)_n$ $(n>6)$	−231	n.r.	938.3 (^{117}Sn)	228
$(Et_2Sn)_n$ $(n>6)$	−173.6	n.r.	145.3 (^{117}Sn)	228
$(Bu^n_2Sn)_5$	−201.2	n.r.	476 (^{117}Sn)	230
$(Bu^n_2Sn)_6$	−202.4	n.r.	462 (^{117}Sn)	
$(Bu^n_2Sn)_5$[f]	−200.9	n.r.	466.6 (^{117}Sn)	227
$(Bu^n_2Sn)_6$[f]	−202.1	n.r.	n.r.	
$(Bu^t_2Sn)_4$ (100°C)	99.0	n.r.	1195	382
$(Am^t_2Sn)_4$	101	n.r.	1339	382
$[N(CH_2CCH_2CH_2)_3Sn]_2$	−77.4	237.8	1338 (^{117}Sn)	368
$[MeSn(CH_2CH_2CH_2)_2NMe]_2$	−101.9	162	4060 (^{117}Sn)	431
$\{Me_2Si[N(Bu^t)]_2Sn\}_2C_2(CMe_2CH_2)_2S$	155.0	n.r.	3723	432
$\{Me_2Si[N(Bu^t)]_2Sn\}_2$-$\mu$-$Se(NBu^t)_2$	−116.0	–	13 865 (^{117}Sn)	260
$\Delta^{1,8}$-9,10-$(R_2Sn)_2$bicyclo-[6.2.0]decane[b,c]	56.5	n.r.	2436 (^{117}Sn)	173
2,2,4,4,5,5-Ar_6-pentastanna-[1,1,1]propellane[d]	356.0 (Sn-2,4,5)	n.r.	4159 (^{119}Sn)	172
	−1751 (Sn-1,3)			
$fc(SnMe_2)_2$[h]	−45.3	227.0 (Me)	5274 (^{117}Sn)	264
		338.9 (C-1)		
$fc(SnMe_2)_3$[h]	−102.5 (C-Sn)	244.7 (Me)	2875 (^{117}Sn)	263
	−249.3 (-Sn-)	185.0 (Me)	537.2 (^2J(Sn,Sn)	
		362.9 (C-1)		

$(p\text{-Tol})_3Sn\text{-}Pb(p\text{-Tol})_3$	−59.6	n.r.	3640 (^{207}Pb)	433
2,3-μ-$Me_3Sn\text{-}B_5H_8$[e]	n.r.	343.0	n.r.	196
2,3-μ-$Ph_3Sn\text{-}B_5H_8$[e]	−98.3	n.r.	n.r.	196
1-$Ph_3Sn\text{-}B_5H_8$[e]	−89.2	n.r.	1117 (^{11}B)	196
2-$Ph_3Sn\text{-}B_5H_8$[e]	−87.5	n.r.	1061 (^{11}B)	196
1-$Ph_2(Cl)Sn\text{-}B_5H_8$[e]	72.1	n.r.	1272 (^{11}B)	196
Me_3Sn-carb[d]	−117.1	256.0	944 (^{11}B)	171
Ph_3Sn-carb[d]	−137.8	392.0	926 (^{11}B)	171
Cl_3Sn-carb[d]	44.0	–	1400 (^{11}B)	171
Br_3Sn-carb[d]	−96.1	–	1255	171
closo-1-Sn-2,4-$(SiMe_3)_2$-2,4-$C_2B_4H_8$	−533.1 (broad)	n.r.		350
$SnC_2Me_2B_9H_9$	−379			210
$[Sn(C_2Me_2B_9H_9)_2]^{2-}$	449			210
$[ClSnC_2Me_2B_9H_9]^-$	224			210
$(Me_3Sn)_2Ca$/THF	−203.3	106.3	n.r.	178
$[(Me_3Sn)_3Sn]_2Ca$/THF	−100.8 ($SnMe_3$)	116.1	5806 (^{119}Sn)	178
	−1071.5 (Sn)		873.0 (^2J)	
Bu^n_3SnLi/Et_2O	−155	–	402.5 (^7Li)	169
Ph_3SnLi/benzene			412.0 (^7Li)	170
$(Bu^tCH_2)_3SnK$	−221; −211 (solid)	n.r.	289 (^{39}K)	179

[a] See ref. 4 for more data; n.r. means not reported.
[b] R = $CH(SiMe_3)_2$.
[c] See also ref. 202.
[d] Ar = 2,6-diethylphenyl.
[d] carb = 1,2,3,4,5-pentaalkyl-2,3,4,5-tetracarba-*nido*-hexaborane(6)-6-yl (alkyl = Me, Et).
[e] For a review, see ref. 222; for other diphenyltin derivatives see ref. 354.
[f] The satellite patterns have not been correctly interpreted before;[229] the assignment of pentameric or hexameric cyclic structures should also be considered in the light of other results; see ref. 228.
[g] These data have been reported for the cyclic pentamer; however, the intensity patterns of ^{117}Sn satellites (2:2:1) correspond to the hexamer.
[h] fc = 1,1'-ferrocenediyl.

Table 9. ^{119}Sn NMR parameters of compounds with a transition metal–tin bond.

Compound	δ^{119}Sn	[$J(^{119}$Sn,M)] {$^2J(^{119}$Sn,^{117}Sn)}	$J(^{119}$Sn,^{13}C)	$J(^{119}$Sn,^{31}P)	Ref.
$[Me_3Sn\text{-}Ti(CO)_6]^-$	35.0	–	94.0 (^2J)	–	55
$[chex_3Sn\text{-}Ti(CO)_6]^-$	25.2	–	82.0 (^2J)	–	55
$[Ph_3Sn\text{-}Ti(CO)_6]^-$	23.5	–	97.0 (^2J)	–	55
$[(Me_3Sn)_2Zr(CO)_5]^{2-}$	16.4	–	49.0 (^2J)	–	56
$[(Me_3Sn)_4Zr(CO)_4]^{2-}$	49.5	–	92.0 (^2J)	–	56
$[(Ph_3Sn)_4Zr(CO)_4]^{2-}$	337.0	{1100}	100.0 (^2J)	–	90
$[(Ph_3Sn)_4Hf(CO)_4]^{2-}$	301.0	–	93.0 (^2J)	–	90
$Cp_2Zr[Sn(CHSiMe_3)_2]_2$	+1677.6	{630.0}	–	–	57
$[Cl_3Sn\text{-}V(Cp)(CO)_3]^-$	n.r.	[920.0]	–	–	60
$[Cl_3Sn\text{-}Mo(CNBu^t)_3\text{-}(PMe_3)_3]SnCl_3$	−136.8 (SnMo) −71.8	–	–	224.0	61
$[Cl_3Sn\text{-}W(CNBu^t)_3\text{-}(PMe_3)_3]^+[SnCl_3]^-$	83.1 (SnW) −65.3	–	–	260.0	61
$[(Me_2P)_2CSiMe_3]Sn\text{-}MoCp(CO)_3$	474.7	–	–	1263.0	62
closo-$Ph_3Sn\text{-}WC_2B_9H_{11}(CO)_3$	−23.3	[262]	–	–	91
$[(Ph_2P)_2CPPh_2]Sn\text{-}WCp(CO)_3$	329.3			1331.0, 146.0	62
(8-Me_2N-1-naphthyl-*C*,*N*)$_2$Sn-W(CO)$_5$	220.0 (−60°C) 267.0 (50°C)	[976.0]	125.3 (^1J)	–	63
$[[(OC)_5W\text{-}Sn(Cl)\text{-}Fe(CO)_4]_2]^{2-}$	453.0	n.r.	–	–	64
(2-Me_2NCH_2-1-C_6H_4)$_2$Sn-W(CO)$_5$[j]	195.4	[892]	182.0 (^1J)	–	88
(2-Ph_2PCH_2-1-C_6H_4)$_2$Sn-W(CO)$_5$	−7.5	[894.0]	179.0 (^1J)	443.0	81
$Ph_3Sn\text{-}Mn(H)Cp'(CO)_2$	58.6	136.0 (J(Sn,H))	–	–	65
$(Ph_3Sn)_2MnCp'(CO)_2$	61.1	–	–	–	65
$Ph_3Sn\text{-}Mn(Bu^t\text{-}DAB)(CO)_3$	+12.2[b]	–	–	–	66
$Ph_3Sn\text{-}Re(Bu^t\text{-}DAB)(CO)_3$	−18.4[b]	–	–	–	66
$Ph_3Sn\text{-}Re(CO)_4C(Ph)OEt$	−88[c]		319.8 (^1J)		87
$Ph_3Sn\text{-}Re(CO)_4C(OEt)NPr^i_2$	−133[c]	–			67

$(Me_3Sn)_2Fe(CO)_4$	80.4	{349.8}	274.4 (^1J)	–	68
$(Me_3Sn)_2Fe(CO)_3CS$	78.5	{332.3}	282.3 (^1J)	–	68
$(Me_2ClSn)_2Fe(CO)_4$	258.5	{302.0}	–	–	69
$[Me_2SnFe(CO)_4]_2$	87.8	[64.0] {1798}	86.0, 48.0 28.0 (^2J)	–	69
$\{Me_2Sn[Fe(CO)_4]_2\}_2Sn$	123.8 (Me_2Sn) 287.7 (Sn)	{1580}	–	–	69
$Me_2Sn[Fe(CO)_4]_2Sn\text{-}[Fe(CO)_4]_2$	101.5 (Me_2Sn) 953.0 (Sn)	{1710}	–	–	69
$Sn[Fe(CO)_4]_4$	1532.0	[36.0]	42.0 (^2J)	–	69
$Me_3Sn\text{-}FeCp(CO)_2$	144.1	[42.7]	–	–	69
$Me_3Sn\text{-}FeCp'(CO)_2$	141.7	–	–	–	70
$Me_3Sn\text{-}FeCp'(CO)P(OMe)_3$	119.5	–	–	479.2	70
$Me_3Sn\text{-}FeCp'(CO)PMePh_2$	100.6	–	–	376.0	70
$Me_3Sn\text{-}FeCp'(CO)PPh_3$	88.9	–	–	357.3	70
$Me_3Sn\text{-}FeCp'(CO)PBz_3$	80.5	–	–	363.8	70
$Ph_2Sn\text{-}Fe(CO)_3PhPPh_2CH_2CH_2^-$	137.5	–	–	75.0	71
$[(OC)_2CpFe\text{-}Sn(Cl)]_2$	689.6	2981 (^1J(Sn,Sn)	–	–	72
$Sn[FeCp(CO)_2]_2$	889.9	–	95 (^2J)	–	72
$Ar(ArCMe_2CH_2)SnFe(CO)_4$[j]	888.8				114
$Ar(ArCMe_2CH_2)SnNi(CO)_3$[j]	955.8				114
$(OEP)Rh\text{-}SnBu_3$[k]	118.3	[314.2]	n.r.		358
$(OEP)Rh\text{-}SnPh_3$[k]	−121.6	[412.9]	n.r.		358
$RhH(\mu\text{-}HSnBu_3)_2(PPh_3)_2$	−11.7	[102.9]			92
$RhH(\mu\text{-}HSnPh_3)_2(PPh_3)_2$	−58.4	[148.5]		17.5 (^2J)	92
$[Rh(H)(SnCl_3)_5]^{3-}$[d]	77.8 (ax) −13.7 (eq)	[532, ax] [596, eq]	–	–	73
$[Rh(SnCl_3)_3Cl_3]^{3-}$	−370.0	[732] {3023}	–	–	74
$[Rh(SnCl_3)_5Cl]^{3-}$	−117.5	[558] {1843}	–	–	74
$RhSnCl_3(NBD)bda$[i]	251.0	[615]			93
$[Ir(H)(SnCl_3)_5]^{3-}$	−185.6 (ax) −318.8 (eq)	[e]	–		73

Table 9.—*Continued*

Compound	δ^{119}Sn	[$J(^{119}Sn,M)$] {$^2J(^{119}Sn,^{117}Sn)$}	$J(^{119}Sn,^{13}C)$	$J(^{119}Sn,^{31}P)$	Ref.
$IrH_2(SnCl_3)(PPh_3)_3$	−274	–	–	232.0	
$Ir_2(\mu\text{-pz})(\mu\text{-SBu}^t)(\mu\text{-}SnCl_2)\text{-}(CO)_2[P(OMe)_3]_2$	−388.6	–	–	222.0	75
		799.0		144.0	
$Pd_2(\mu\text{-Cl})_2(SnCl_3)_2[P(o\text{-tolyl})_3]_2$	−239.0 (*trans*)	799.1 (^4J(Sn,Sn)	–	195.0	84
	−229 (*cis*)	120.0 (^4J(Sn,Sn)		174.0	
cis-$(Me_3Sn)_2Pt(PPh_3)_2$	−16.5	[8532.0]	–	652.3[f]	79
					80
$fcSnMe_2Pt(PPh_3)_2SnMe_2$[g]	−27.5	[9056.0]	–	+206.0 (*cis*)	78
				−1574.5 (*trans*)	79
cis-$Me_3Sn(Me_3SnC{\equiv}C)Pt\text{-}(PPh_3)_2$	−57.5 (SnPt)	[8140]	–	111.0 (*cis*)	79
	−88.9 (SnC≡)	278.8 (^3J(Pt,Sn))		1606 (*trans*)	
trans-$[Pt(PEt_3)_2(Me)SnCl_3]$	140.0	[6620]	–	242.0	82
trans-$[Pt(PEt_3)_2(COPh)SnCl_3]$	87.0	[2376]	–	275.0	82
$\{Pt[CH_2C(Me)CH_2](SnCl_3)_3\}^{3-}$	−33.0	[12 140] {3006}	51.0 (^2J)	–	76
$[etpPt\text{-}SnCl_3]^{-}$[h]	−144.0	[15 077]	–	190.0 (*cis*)	86
				2044.0 (*trans*)	
trans-$[PtCl(SnCl_3)_2CO]$	17.0	[18 628] {46 118}	86.0 (^2J)	–	85
$Pt(\eta^3\text{-}C_4H_7)(CO)SnCl_3$	76.9	[29 287]			89

cis-$[PtCl_2(SnCl_3)_{2'}]^{2-}$	−375	[27 627] {2936}			223
cis-$[PtBr_2(SnBr_3)_2]^{2-}$	−422.2	[25 720] {1675}			223
$[Pt(SnCl_3)_5]^{2-}$	−126.4	[15 791] {6057}	–	–	77
$[Pt(SnBr_3)_5]^{2-}$	−234.3	[14 852] {6266}	–	–	77

[a]See ref. 4 for a more extensive compilation; n.r. means not reported.
[b]Bu^t-DAB = di-*tert*-butyl-1,4-diaza-1,3-butadiene.
[c]Recalculated with respect to Me_4Sn; reported relative to neat $SnCl_4$.
[d2]$^2J(^{119}Sn,^{117}Sn)$ (eq-eq, trans) = 25 506 Hz; $^2J(^{119}Sn,^{117}Sn)$ (eq eq, cis) = 1975 Hz; $^2J(^{119}Sn,^{117}Sn)$ (ax-eq) = 1762 Hz.
[e2]$^2J(^{119}Sn,^{117}Sn)$ (eq-eq, trans) = 21 094 Hz; $^2J(^{119}Sn,^{117}Sn)$ (eq eq, cis) = 1820 Hz; $^2J(^{119}Sn,^{117}Sn)$ (ax-eq) = 1388 Hz.
[f]Mean value; at lower temperature coupling constants $^2J(^{119}Sn,^{31}P)_{cis}$ and $^2J(^{119}Sn,^{31}P)_{trans}$ of opposite sign are observed.
[g]1,3-Distanna-2-platina-[3]ferrocenophane.
[h]etp = tris(2-diphenylphosphanoethyl)phosphane.
[i]NBD = norbornadiene; bda = PhN=C(Me)C(Me)=NPh.
[j]Ar = 2,4,6-Bu^t_3-C_6H_2.
[l]See also ref. 174: $(2\text{-}Me_2NCH_2C_6H_4)_2Sn$ $\delta^{119}Sn$ 127.0 (−40°C, in THF; $h_{1/2}$ = 100 Hz); $(2\text{-}Me_2N\text{-}C_6H_4)_2Sn\text{-}Co(Cp)(C_2H_4)$ $\delta^{119}Sn$ 121 (−40°C, in THF; $h_{1/2}$ = 1100 Hz).
[k]OEP = 2,3,7,8,12,13,17,18-octaethylporphyrinato ligand.

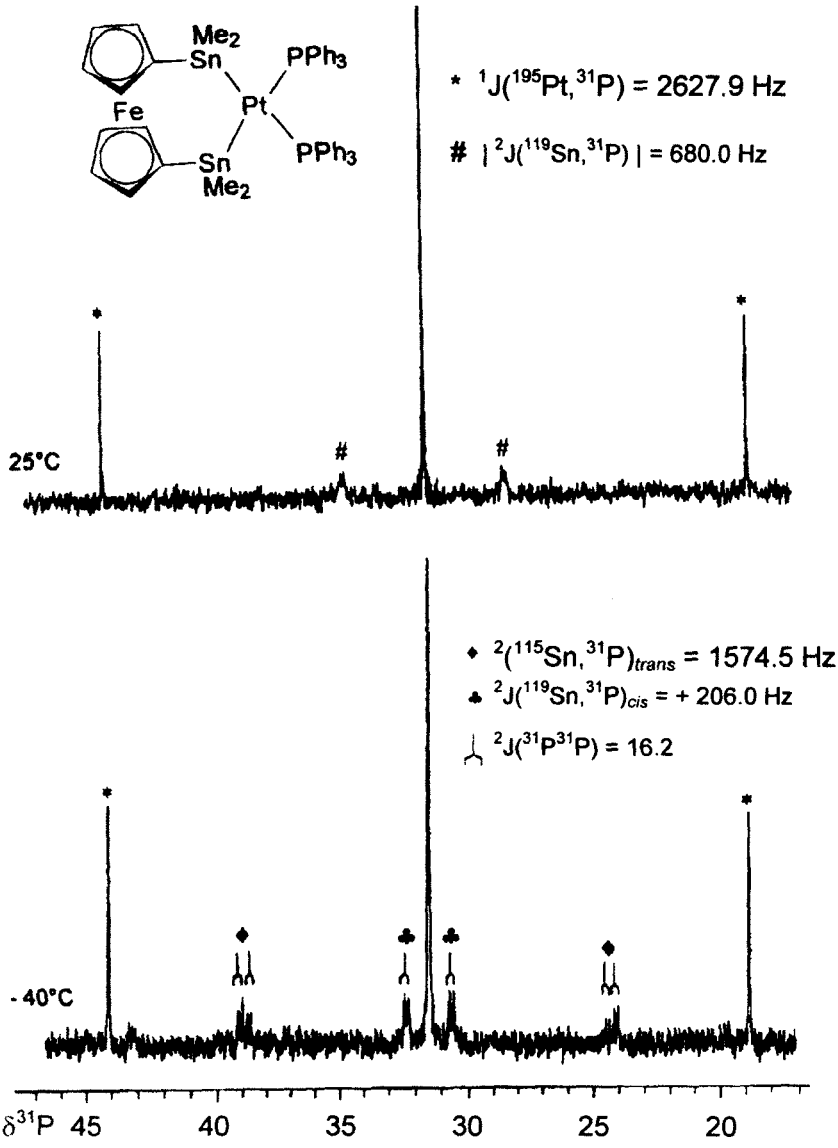

Fig. 8. 101.3 MHz $^{31}P\{^{1}H\}$ NMR spectra of the bis(stannyl)platinum complex shown.[79] At room temperature, there is fast exchange of the two phosphorus sites; the $^{117/119}Sn$ satellites indicate averaged coupling to ^{31}P. At −40°C this exchange is slow, revealing the different coupling constants $^{2}J(^{119}Sn,^{31}P)$ of opposite sign, and also the coupling constant $^{2}J(^{31}P,^{31}P)$. (Reproduced, with permission, from Ref. 79.)

Table 10. Isotope-induced chemical shifts $^1\Delta^{12/13}C(^{119}Sn)$.[a]

Compound	$^1\Delta^{12/13}C(^{119}Sn)$ (ppb)	$^1J(^{119}Sn,^{13}C)$ (Hz)	Ref.
Me_4Sn	−18	336.6	44
Et_4Sn	−20	320.0	44
Pr^i_4Sn	−23	308.5	44
Me_3SnBu^t	−19 (Me), ±2 (Bu^t)	294.0 (Me), 436.6 (Bu^t)	44
Bu^n_3SnMe	−21 (Me), −19 (Bu^n)	285.9 (Me), 329.8 (Bu^n)	44
$Me_3SnCH_2N(Me)CH_2CH_2NMe_2$	−10 (Me), −10 (CH_2)	300.6 (Me), 410.5 (CH_2)	402
$(Me_3Sn)_4C$	−16 (Me), −24 (C)	316.3 (Me), 108.3	133
$(Me_3Sn)_4Ge$	−21 (Me)	258.1 (Me)	133
$Me_3SnCH{=}CH_2$	−13 (Me), −25 (C=)	353.5 (Me), 450.9 (C=)	44
$Me_2Sn(CH{=}CH_2)_2$	−10 (Me), −20 (C=)	369.4 (Me), 466.8 (C=)	44
6-Me_3Sn-bicyclo[3.2.1]-octa-2,6-diene	−12 (Me), −15 (C-6)	348.5 (Me), 456.7 (C-6)	45
$(Me_3Sn)_2C{=}C{=}CH_2$	−9.0 (Me), −31.8 (C=)	348.2 (Me), 261.7 (C=)	119
$Me_3Sn\text{-}C{\equiv}C\text{-}H$	±2 (Me), −59 (C≡)	410.3 (Me), 414.8 (C≡)	44
Bu^t_3 Sn-C≡C-H	+3.8 (C), −61.8 (C≡)	371.4 (C), 207.6 (C≡)	58
$Me_2Sn(C{\equiv}CH)_2$	+16 (Me), −27 (C≡)	503.0 (Me), 576.2 (C≡)	44
$MeSn(C{\equiv}CH)_3$	+25 (Me), −9 (C≡)	630.9 (Me), 833.0 (C≡)	44
$Sn(C{\equiv}CH)_4$	+9	1176.2	45
Me_3SnH	−15	349.5	45
Me_2SnH_2	−3	485.1	45
$Me_3Sn\text{-}O\text{-}SnMe_3$	+12	396.3	132
$Me_3Sn\text{-}NEt_2$	±2	381.0	45
$Me_2Sn(NEt_2)_2$	+3	469.7	45
$MeSn(NEt_2)_3$	+25	592.4	45

[a]A negative sign of $^1\Delta^{12/13}C(^{119}Sn)$ indicates a shift of the heavy isotopomer to lower frequency with respect to the lighter isotopomer.

Table 11. Isotope induced chemical shifts $^1\Delta^{14/15}N(^{119}Sn)$.[a]

Compound	$^1\Delta^{14/15}N(^{119}Sn)$ (ppb)	$^1J(^{119}Sn,^{15}N)$ (Hz)	Ref.
$(Me_3Sn)_2N$-Ph	−44.4	−41.4	14
$(Me_3Sn)_3N$	−38.4	−83.7	14
$(Me_3Sn)_2N$-$SiMe_3$[b]	−42.0	−59.0	132
Me_3Sn-$N(SiMe_3)_2$	−49.0	−52.5	132
$(Me_3Sn)_2N$-BC_8H_{14}[c]	−42.6	−31.9	14
1-Me_3Sn-pyrrole[d]	−38	−37.2	52
1-Me_3Sn-2,5-Me_2-pyrrole	−46	−25.7	52
1-Me_3Sn-indole	−50.8	−45.3	142
1-Me_3Sn-2-Me-indole	−52.5	−40.4	142
8-Me_3Sn-carbazole	−56.6	−48.1	142
1-Et_3Sn-pyrrole	−48	−66.5	142
1-Bu^t_3Sn-pyrrole	−59.5	−99.9	142
$(Me_3Sn)_2N$-NMe_2	−37	−45.5	52
2-[$Me_3Sn(Me_3Si)N$]-pyridine	−55	8.9	134
2-[$Me_3Sn(Me_3Si)N$]-3-Me-pyridine	−40.6	24.9	134
2,6-[$Me_3Sn(Me_3Si)N]_2$-pyridine	−41.0	14.3	134

[a]A negative sign of $^1\Delta^{14/15}N(^{119}Sn)$ indicates a shift of the heavy isotopomer to lower frequency with respect to the lighter isotopomer.
[b]$^2J(^{119}Sn,^{29}Si)$ = 8.4 Hz; $^1J(^{29}Si,^{15}N)$ = 6.7 Hz; $^1\Delta^{14/15}N(^{29}Si)$ = −9.4 ppb.
[c]BC_8H_{14} = 9-borabicyclo[3.3.1]nonyl.
[d]See ref. 261 for a bicyclic N-pyrrolyl tin compound: $^1\Delta^{14/15}N(^{119}Sn)$ = −58.0.

contribution arising from electronic effects.[46] The latter effects will become increasingly important and noticeably for heavy nuclei.

Previously it was necessary to use ^{15}N labelled samples in order to determine isotope shifts $^1\Delta^{14/15}N(X)$. By the application HEED extended pulse sequences,[52] it proved possible to determine these parameters for numerous compounds in the natural abundance of ^{15}N (0.37%). Table 11 lists a number of these data and an example for the application of the HEED INEPT pulse sequence is shown in Fig. 9.

5. INDIRECT NUCLEAR SPIN–SPIN COUPLING CONSTANTS $^nJ(^{119}Sn,X)$

5.1. General

A recent review has summarized important aspects concerning coupling constants $^nJ(^{119}Sn,X)$.[7] The advances in NMR instrumentation allow in many cases to determine the signs of these coupling constants [note that $\gamma(^{119}Sn) < 0$; therefore, the signs of $J(^{119}Sn,X)$ and of the reduced coupling constant $K(^{119}Sn,X)$ are opposite if $\gamma(X) > 0$], and the techniques have been

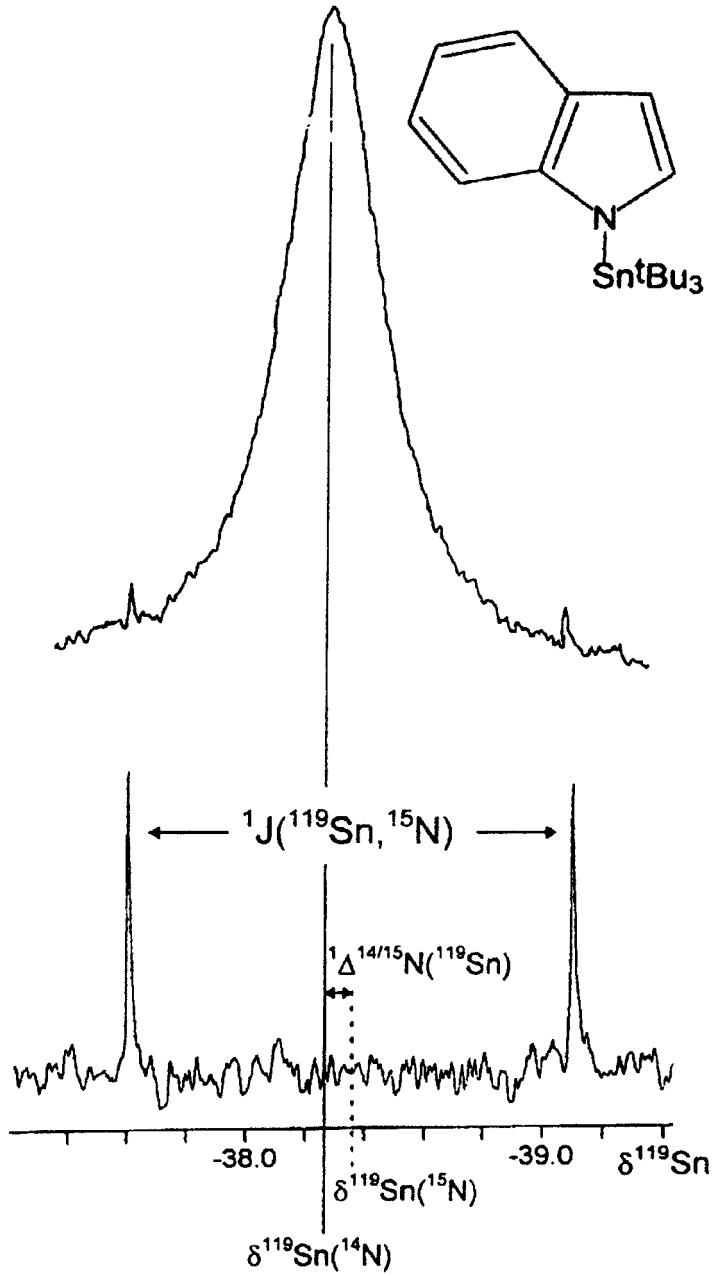

Fig. 9. 186.5 MHz ^{119}Sn NMR spectra of N-indolyl-tri-*tert*-butylstannane,[142] recorded by using the HEED INEPT technique,[52] with Hahn echo delays of 0.008 s (upper trace) and 0.2 s (lower trace) for suppression of the signal due to the ^{119}Sn–^{14}N isotopomer. The isotope-induced shift. $^1\Delta^{14/15}N(^{119}Sn) = -80.5$ ppb can be readily and accurately determined. (Reproduced, with permission, from Ref. 142.)

described.[7] Numerous coupling constants are already listed in Tables 2–11, and previous reviews[2–7] also contain compilations of coupling constants. Therefore, this section will deal mainly with some results which have been published in the years 1996, 1997 and in part 1998.

5.2. One-bond couplings, $^1J(^{119}Sn,X)$

All reduced coupling constants $^1K(^{119}Sn,^{13}C)$ in tetraorganotin and in most organotin(IV) compounds are positive ($^1J(^{119}Sn,^{13}C<0$), exceptions are triorganotin lithium derivatives.[413] In contrast, the sign of $^1K(^{119}Sn,^{13}C)$ is negative in organotin(II) compounds.[273] A roughly linear correlation exists for numerous values $^1J(^{119}Sn,^{13}C)$ and $^1J(^{207}Pb,^{13}C)$ for comparable compounds.[414] The magnitude of $^1J(^{119}Sn,^{13}C)$ has been related to the bond angle C–Sn–C(Θ) ($|^1J(^{119}Sn,^{13}C)| = 10.7(\pm0.5)\Theta - 778(\pm64)$ for Me_2Sn[397] and $|^1J(^{119}Sn,^{13}C)| = 9.99(\pm0.73)\Theta - 746(\pm100)$ for Bu^n_2Sn compounds).[385,394]

In silylstannanes, the sign of $^1K(^{119}Sn,^{29}Si)$ is positive.[417] Recently, a positive sign of $^1K(^{119}Sn,^{73}Ge)$ in $(Me_3Sn)_4Ge$ has been determined.[133]

In the case of polystannanes, a sign inversion of $^1J(^{119}Sn,^{119}Sn)$ from positive ($^1K>0$) to negative ($^1K<0$) has been proposed if the Sn–Sn bond length exceeds 285 pm.[401] Examples for negative reduced coupling constants $^1K(^{207}Pb,^{119}Sn)$ have been reported.[415]

	$Me_3Sn–PbMe_3$	$Me_3Sn–PbEt_3$	$Me_3Sn–Pb^iPr_3$	$Me_3Sn–Pb^tBu_3$
$^1J(^{207}Pb,^{119}Sn)$	−3570[416]	−1398[415]	+303[415]	+1637[415]

There are many new data $^1J(^{119}Sn,^{15}N)$ (Table 11) confirming the trends established previously.[4,415] For a given amino group RR'N in aminotin(IV) compounds the sign of $^1J(^{119}Sn,^{15}N)$ may change readily, depending on the nature of the other substituents at the tin atom. In the case of aminotin(II) compounds a negative sign of $^1J(^{119}Sn,^{15}N)$ (^1K also <0, since $\gamma(^{15}N)<0$) can be safely assumed as the result of negative contributions to the Fermi contact term arising from the presence of the lone pairs of electrons at the tin and nitrogen atoms.[418]

The sign of $^1K(^{119}Sn,^{31}P)$ is negative in all tin–phosphorus compounds (dominant influence of the lone pair of electron at the phosphorus atom), except of phosphane adducts of tin(IV) halides. Even in transition metal complexes of stannylphosphanes[419] or in borane complexes of stannylphosphanes[41b] the coupling sign does not change, although the phosphorus lone pair of electrons is engaged.

A negative sign of $^1K(^{119}Sn,^{77}Se)$ and $^1K(^{125}Te,^{119}Sn)$ is likely for all tin–selenium and tin–tellurium compounds, and this can also be assumed for

$^1K(^{119}Sn,^{19}F)$. In contrast, it appears from the data available so far that all $^1K(^{119}Sn,M)$ (M = transition metal nuclei) possess a positive sign.

5.3. Two-bond (geminal) coupling, $^2J(^{119}Sn,X)$

If X = ^{1}H, the majority of data concerns organotin compounds with coupling across a carbon atom. For intervening aliphatic carbon atoms the sign of $^2J(^{119}Sn,^1H)$ is positive ($^2K(^{119}Sn,^1H) < 0$) with few exceptions,[413] whereas an intervening olefinic carbon atom induces a negative sign of $^2J(^{119}Sn,^1H)$. For methyltin compounds, a relationship between the magnitude of $|^2J(^{119}Sn,^1H)|$ and the Me–Sn–Me angle Θ has been proposed ($\Theta = 0.016\ |^2J(^{119}Sn,^1H)| - 1.32\ [^2J(^{119}Sn,^1H)]^2 + 133.4$). The analogous behaviour to ^{1}H, in principle, is found for $^2J(^{119}Sn,^{13}C)$, although the magnitude of this coupling constant is less predictable. Therefore, it is recommended to determine the sign of this coupling constant in order to discuss these data in a proper way. This is also true for most nuclei other than ^{1}H or ^{13}C. The most convenient techniques for the determination of coupling signs involving ^{119}Sn have been reviewed.[7] An example for the determination of the sign of $^2J(Sn,Sn)$ is shown in Fig. 10. The data $^2J(^{119}Sn,^{119}Sn)$ have attracted interest with respect to correlations with structural features, namely the bond angle Sn–E–Sn.[287,421] However, only few determinations of coupling signs have been carried out and, therefore, these relationships should be used with great care.

5.4. Three-bond (vicinal) coupling, $^3J(^{119}Sn,X)$

The well-known Karplus-type dependence of the magnitude of vicinal coupling constants on the respective dihedral angle is also evident for numerous tin compounds and values $^3J(^{119}Sn,X)$ (X = ^{1}H,^{11}B,^{13}C) have been widely exploited in this respect.[4,5,7] So far all signs determined for $^3K(^{119}Sn,X)$ are positive, with very few exceptions. If X is a quadrupolar nucleus such as ^{11}B, differential broadening of the ^{119}Sn NMR signals (as a result of partially relaxed scalar ^{119}Sn–^{11}B coupling, can be used to compare the relative magnitudes of $|^3J(^{119}Sn,^{11}B)|$.[4,6]

5.5. Long-range coupling, $^nJ(^{119}Sn,X)$ with $n > 3$

Coupling between ^{119}Sn and other nuclei X across four or more bonds is often observed. However, these data are still of limited value with respect to diagnostic conclusions regarding the bonding situation. As expected, such long-range couplings are fairly large and easy to observe if a π system and/or a metal is involved. Thus, in most benzyltin compounds (see Tables 2–5) it

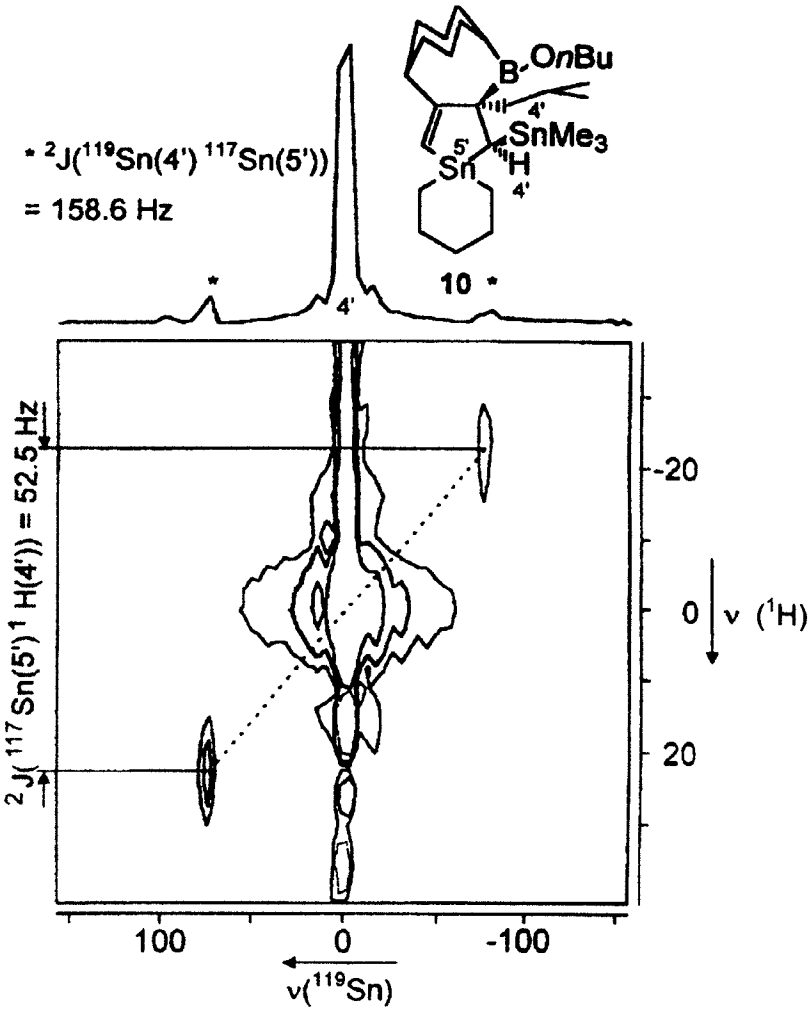

Fig. 10. Contour plot of the 111.9 MHz 2D ^{119}Sn/^{1}H shift correlation ($Me_3{}^{119}Sn$ and ^{1}H(4') signals are shown) of a trimethyltin-substituted stannolene derivative,[422] typical for comparing the signs of coupling constants as indicated. The positive tilt of the relevant cross-peaks (dotted line) proves that the signs of $^2K(^{119}Sn,^{117}Sn)$ and $^2K(^{117}Sn,^1H)$ are alike. Since the sign of the latter ^2K is known to be negative, it follows the sign of the former ^2K is also negative. (Reproduced, with permission, from Ref. 422.)

is possible to measure $^5J(^{119}Sn,^{13}C)$. The same is true for 2-picolyltin derivatives.[134] Numerous allenyltin compounds have been studied and various types of long-range couplings $^nJ(^{119}Sn,^1H)$, $^nJ(^{119}Sn,^{13}C)$ and $^nJ(^{119}Sn,^{119}Sn)$ (n = 4,5) have been determined, including the sign.[146] A collection of

values ^{n}J(Sn,Sn) with $n > 3$ is given by Mitchell and Nettelbeck.[143] In the bis(alkynyl)platinum complex **34**,[117] $^{6}J(^{119}Sn,^{117}Sn) = 25$ Hz is readily resolved.

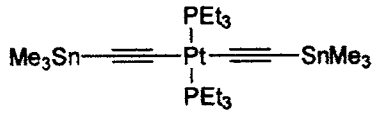

34

Considering the increasing quality of NMR spectra, such long range coupling constants $^{n}J(^{119}Sn,X)$ ($n > 3$) can become valuable tools for assignment techniques and for improvement of NMR experiments. This becomes already evident for X = ^{1}H, as shown in a recent review.[2] Knowing the magnitude of $^{n}J(^{119}Sn,^{1}H)$ various selective 1D and 2D polarization transfer experiments become feasible.

6. CONCLUSIONS

The impact of ^{119}Sn NMR parameters, determined either by ^{119}Sn NMR or in the NMR spectra of other nuclei, on tin chemistry is remarkable. Our understanding of tin chemical shifts, coupling constants and nuclear spin relaxation with respect to physical principles is growing. At the same time, the application of more or less sophisticated NMR techniques enables one to monitor reactions, identify unstable intermediates, discover their relevance for mechanistic implications, assign structural features, investigate intra- and intermolecular dynamic processes, or to compare structures in the solid and liquid state. Clearly, ^{119}Sn NMR parameters, in addition to those of the more common nuclei, e.g. ^{1}H, ^{13}C or ^{31}P, add to our attempts at a more complete description of the bonding situation. It must be emphasized that the great potential of modern NMR spectrometers can be exploited in particular by a multinuclear approach in order to obtain a large self-consistent set of NMR data. This also includes isotope induced chemical shifts and long-range coupling constants which have been neglected in the past.

ACKNOWLEDGEMENT

Support of this work by the Deutsche Forschungsgemeinschaft, Fonds der Chemischen Industrie und Volkswagen-stiftung is gratefully acknowledged.

REFERENCES

1. J. C. Meurice, M. Vallier, M. Ratier, J.-G. Duboudin and M. J. Petraud, *J. Chem. Soc. Perkin Trans. 2*, 1996, 1331.

2. F. Kayser, M. Biesemans, M. Gielen and R. Willem, in *Physical Organometallic Chemistry – Advanced Applications of NMR to Organometallic Chemistry*, Vol. 1 (eds M. Gielen, R. Willem and B. Wrackmeyer), pp. 45–86, Wiley, London, 1996.
3. P. J. Smith and A. P. Tupciauskas, *Annu. Rep. NMR Spectrosc.*, 1978, **8**, 291.
4. B. Wrackmeyer, *Annu. Rep. NMR Spectrosc.*, 1985, **16**, 73.
5. J. D. Kennedy and W. McFarlane, in *Multinuclear NMR* (ed. J. Mason), pp. 305–333, Plenum Press, New York, 1987.
6. B. Wrackmeyer, in *Encyclopedia of NMR*, Vol. 4 (eds R. K. Harris and D. M. Grant), pp. 2538–2548, Wiley, London, 1996.
7. B. Wrackmeyer, in *Physical Organometallic Chemistry – Advanced Applications of NMR to Organometallic Chemistry*, Vol. 1 (eds. M. Gielen, R. Willem and B. Wrackmeyer), pp. 87–122, Wiley, London, 1996.
8. W. McFarlane, *Proc. R. Soc. Lond.*, 1968, **A306**, 185.
9. (a) G. A. Morris and R. Freeman, *J. Am. Chem. Soc.*, 1979, **101**, 760. (b) G. A. Morris, *J. Am. Chem. Soc.*, 1980, **102**, 428. (c) G. A. Morris, *J. Magn. Reson.*, 1980, **41**, 185. (d) D. P. Burum and R. R. Ernst, *J. Magn. Reson.*, 1980, **39**, 163.
10. (a) D. T. Pegg, D. M. Doddrell, W. M. Brooks and M. R. Bendall, *J. Magn. Reson.*, 1981. **44**, 32. (b) D. T. Pegg, D. M. Doddrell and M. R. Bendall, *J. Chem. Phys.*, 1982, **77**, 2745.
11. B. Wrackmeyer, E. Kupce and J. Kümmerlen, *Magn. Reson. Chem.*, 1982, **30**, 403.
12. (a) A. Sebald, in *Physical Organometallic Chemistry – Advanced Applications of NMR to Organometallic Chemistry*, Vol. 1 (eds M. Gielen, R. Willem and B. Wrackmeyer), pp. 123–157, Wiley, London, 1996. (b) A. Sebald, in *Solid-State NMR II – NMR-Basic Principles and Progress*, Vol. 31 (eds P. Diehl, E. Fluck, H. Günther, R. Kosfeld and J. Seelig), pp. 91–131, Springer, Berlin, 1994.
13. B. Wrackmeyer, C. Stader, K. Horchier, H. Zhou and D. Schlosser, *Inorg. Chim. Acta*, 1990, **176**, 205.
14. B. Wrackmeyer, J. Weidinger, H. Nöth, W. Storch, T. Seifert and M. Vosteen, *Z. Naturforsch., Teil B*, in press.
15. B. Wrackmeyer, G. Kehr and R. Boese, *Chem. Ber.*, 1992, **125**, 643.
16. A. C. de Dios, *Magn. Reson. Chem.*, 1996, **34**, 773, and literature cited.
17. B. Wrackmeyer, K. Wagner, A. Sebald, L. H. Merwin and R. Boese, *Magn. Reson. Chem.*, 1991, **29**, S3–10.
18. D. L. Roger, M. F. Huff, S. J. Knox, R. J. Adam, D. C. Apperley and R. K. Harris, *Inorg. Chem.*, 1993, **32**, 4472.
19. H. Reuter and D. Schröder, *J. Organomet. Chem.*, 1993, **451**, 83.
20. (a) R. A. Komoroski, R. G. Parker and A. M. Mazany, *J. Magn. Reson.*, 1987, **73**, 389. (b) P. A. Bates, M. B. Hursthouse, A. G. Davies and S. D. Slater, *J. Organomet. Chem.*, 1987, **325**, 129. (c) T. P. Lockhart, J. C. Calabrese and F. Davidson, *Organometallics*, 1987, **6**, 2479. (d) T. P. Lockhart, *Organometallics*, 1988, **7**, 1438. (e) K. C. Molloy, *Inorg. Chim. Acta*, 1988, **141**, 151. (f) A. G. Davies, S. D. Slater, D. C. Povey and G. W. Smith, *J. Organomet. Chem.*, 1988, **352**, 283.
21. K. W. Zilm, G. A. Lawless, R. M. Merrill, J. M. Miller and G. G. Webb, *J. Am. Chem. Soc.*, 1987, **109**, 7236.
22. J. Holecek, K. Handlir, V. Cerny, M. Nadvornik and A. Lycka, *Polyhedron*, 1987, **5**, 1037.
23. J. D. Kennedy, W. McFarlane, P. J. Smith, R. F. M. White and L. Smith, *J. Chem. Soc. Perkin Trans. 2*, 1973, 242.
24. S. Masamune, Y. Eriyama and T. Kawase, *Angew. Chem.*, 1987, **99**, 601; *Angew. Chem. Int. Ed. Engl.*, 1987, **26**, 584.
25. M. Kiru, R. Yauchibara, R. Hirano, C. Kabuto and H. Sajurai, *J. Am. Chem. Soc.*, 1991, **113**, 7185.
26. (a) H. Grützmacher, H. Pritzkow and F. T. Edelmann, *Organometallics*, 1991, **10**, 23. (b) S. Masamune and L. R. Sita, *J. Am. Chem. Soc.*, 1985, **107**, 6390. (c) M. Weidenbruch, A.

Schäfer, H. Kilian, S. Pohl, W. Saak and H. Marsmann, *Chem. Ber.*, 1992, **125**, 563. (d) M. Weidenbruch, J. Schaefke, A. Schäfer, K. Peters and H.-G. von Schnering, *Angew. Chem.*, 1994, **106**, 1938; *Angew. Chem. Int. Ed. Engl.*, 1994, **33**, 1846. (e) N. Tokitoh, M. Saito and R. Okazaki, *J. Am. Chem. Soc.*, 1993, **115**, 2065.

27. (a) K. Horchler, C. Stader and B. Wrackmeyer, *Inorg. Chim. Acta*, 1986, **117**, L39. (b) C. Stader and B. Wrackmeyer, *J. Magn. Reson.*, 1987, **72**, 544. (c) C. Stader and B. Wrackmeyer, *Z. Naturforsch., Teil B*, 1987, **42**, 1515. (d) C. Stader, B. Wrackmeyer and D. Schiosser, *Z. Naturforsch., Teil B*, 1988, **43**, 707. (e) B. Wrackmeyer, C. Stader and K. Horchler, *J. Magn. Reson.*, 1989, **83**, 601. (f) B. Wrackmeyer, K. Horchler and H. Zhou, *Spectrochim. Acta*, 1990, **46A**, 809.
28. H. Braunschweig, P. B. Hitchcock, M. F. Lappert and L. J. M. Pierssens, *Angew. Chem.*, 1994, **106**, 1243; *Angew. Chem. Int. Ed. Engl.*, 1994, **33**, 1156.
29. T. Fjeldberg, H. Hope, M. F. Lappert, P. P. Power and A. J. Thomas, *J. Chem. Soc. Chem. Commun.*, 1983, 639.
30. B. Wrackmeyer, E. Kupce, G. Kehr and A. Sebald, *Magn. Reson Chem.*, 1992, **30**, 964.
31. B. Wrackmeyer, A. Sebald and L. H. Merwin, *Magn. Reson. Chem.*, 1991, **29**, 260.
32. C. Janiak, H. Schumann, C. Stader, B. Wrackmeyer and J. J. Zuckerman, *Chem. Ber.*, 1988, **121**, 1745.
33. J. L. Atwood, W. Hunter, A. H. Cowley, R. A. Jones and C. A. Stewart, *J. Chem. Soc. Chem. Commun.*, 1981, 925.
34. P. Jutzi, F. Kohl, P. Hofmann, C. Krüger and Y.-H. Tsay, *Chem. Ber.*, 1980, **113**, 757.
35. H. Schumann, C. Janiak, E. Hahn, C. Kolax, J. Loebel, M. D. Rausch, J. J. Zuckerman and M. J. Heeg, *Chem. Ber.*, 1986, **119**, 2656.
36. (a) T. A. K. Al-Allaf, C. Eaborn, P. B. Hitchcock, M. F. Lappert and A. Pidcock, *J. Chem. Soc. Chem. Commun.*, 1985, 548. (b) P. B. Hitchcock, M. F. Lappert and M. C. Misra, *J. Chem. Soc. Chem. Commun.*, 1985, 863.
37. (a) B. Wrackmeyer, G. Kehr and R. Boese, *Angew. Chem.*, 1991, **103**, 1374; *Angew. Chem. Int. Ed. Engl.*, 1991, **30**, 1370. (b) B. Wrackmeyer, *Coord. Chem. Rev.*, 1995, **145**, 125. (c) B. Wrackmeyer, S. Kundler and R. Boese, *Chem. Ber.*, 1993, **126**, 1361. (d) B. Wrackmeyer, S. Kundler, W. Milius and R. Boese, *Chem. Ber.*, 1994, **127**, 333. (e) B. Wrackmeyer, G. Kehr, A. Sebald and J. Kümmerlen, *Chem. Ber.*, 1992, **125**, 1597. (f) R. Köster, G. Seidel, I. Klopp, C. Krüger, G. Kehr, J. Süß and B. Wrackmeyer, *Chem. Ber.*, 1993, **126**, 1385. (g) B. Wrackmeyer, K. Horchler von Locquenghien and S. Kundler, *J. Organomet. Chem.*, 1995, **503**, 289.
38. M. Herberhold, W. Milius, U. Steffl, K. Vitzithum, B. Wrackmeyer, R. H. Herber, M. Fontani and P. Zanello, *Eur. J. Inorg. Chem.*, 1999, **145**.
39. M. Herberhold, M. Hübner and B. Wrackmeyer, *Z. Naturforsch., Teil B*, 1993, **48**, 940.
40. B. Wrackmeyer and K. Wagner, *Chem. Ber.*, 1991, **124**, 503.
41. (a) S. Kerschl and B. Wrackmeyer, *Z. Naturforsch., Teil B*, 1985, **40**, 845. (b) B. Wrackmeyer, S. Kerschl and H. E. Maisel, *Main Group Met. Chem.*, 1998, **21**, 89.
42. H. C. E. McFarlane, W. McFarlane and C. Turner, *Mol. Phys.*, 1979, **37**, 1639.
43. F. Kayser, M. Biesemans, A. Delmotte, R. Hendrix, P. Malschaert, I. Verbruggen, B. Mahieu, R. Willem and M. Gielen, *Bull. Soc. Chim. Belg.*, 1994, **103**, 273.
44. S. Kerschl, A. Sebald and B. Wrackmeyer, *Magn. Reson. Chem.*, 1985, **23**, 514.
45. N. Hertkorn and F. H. Köhler, *J. Organomet Chem.*, 1988, **355**, 19.
46. C. J. Jameson, in *Isotopes in the Physical and Biomedical Sciences*, Vol. 2 (eds E. Buncel and J. R. Jones), pp. 1–54, and references cited therein, Elsevier, New York, 1991.
47. S. Chapelle and P. Granger, *J. Magn. Reson.*, 1988, **76**, 1.
48. T. B. Grindley, R. D. Curtis, R. Thangarasa and R. E. Wasylishen, *Can. J. Chem.*, 1990, **68**, 2102.
49. B. Schiemenz, G. Huttner, L. Zolnai, P. Kircher and T. Diercks, *Chem. Ber.*, 1995, **128**, 187.

50. P. Kircher, G. Huttner and K. Heinze, *J. Organomet. Chem.*, 1998, **562**, 217.
51. H. Braunschweig, R. W. Chorley, P. B. Hitchcock and M. F. Lappert, *J. Chem. Soc. Chem. Commun.*, 1992, 1311.
52. E. Kupce and B. Wrackmeyer, *J. Magn. Reson.*, 1992, **97**, 568.
53. H. Sitzmann, R. Boese and P. Stellberg, *Z. Anorg. Allg. Chem.*, 1996, **622**, 751.
54. A. Lacksonen and R. E. Wasylishen, *J. Am. Chem. Soc.*, 1995, **117**, 392.
55. J. E. Ellis and P. Yuen, *Inorg. Chem.*, 1993, **32**, 4998.
56. J. E. Ellis, P. Yuen and M. Jang, *J. Organomet. Chem.*, 1996, **507**, 283.
57. W. E. Piers, R. M. Whittal, G. Ferguson, J. F. Gallagher, R. D. J. Froese, H. J. Stronks and P. H. Krygsman, *Organometallics*, 1992, **11**, 4015.
58. E. Liepins, I. Birgele, E. Lukevics, E. G. Bogoradovsky and V. S. Zavgorodny, *J. Organomet. Chem.*, 1990, **390**, 139.
59. W. L. Wilson, R. W. Rudolph, L. L. Lohr, R. C. Taylor and P. Pyykkö, *Inorg. Chem.*, 1986, **25**, 1535.
60. M. Hoch and D. Rehder, *J. Organomet. Chem.*, 1985, **288**, C25.
61. M. J. Fernandez-Trujillo, M. Jimenez-Tenerio, M. C. Puerta and D. L. Hughes, *J. Organomet. Chem.*, 1989, **377**, 241.
62. H. H. Karsch and A. Appelt, *J. Organomet. Chem.*, 1986, **312**, C6.
63. J. T. B. H. Jastrzebski, P. A. van der Schaaf, J. Boersma, G. van Koten, D. Heijdenrijk, K. Goubitz and D. J. A. de Ritter, *J. Organomet. Chem.*, 1989, **367**, 55.
64. A. L. Balch, M. M. Olmstead and D. P. Oram, *Inorg. Chem.*, 1988, **27**, 4309.
65. U. Schubert, E. Kunz, B. Harkers, J. Willnecker and J. Meyer, *J. Am. Chem. Soc.*, 1989, **111**, 2572.
66. R. R. Andrea, W. G. J. de Lange, D. J. Stufkens and A. Oskam, *Inorg. Chim. Acta*, 1988, **149**, 77.
67. A. C. Fillippou, E. O. Fischer and H. G. Alt, *J. Organomet. Chem.*, 1987, **330**, 325.
68. W. Petz, B. Wrackmeyer and W. Storch, *Chem. Ber.*, 1989, **122**, 2261.
69. B. Wrackmeyer, B. Distler and M. Herberhold, *Z. Naturforsch., Teil B*, 1992, **47**, 1749.
70. L. Carlton, G. Pattrick and N. J. Coville, *Inorg. Chim. Acta*, 1989, **160**, 65.
71. U. Schubert and S. Grubert, *Organometallics*, 1996, **15**, 4707.
72. Z. Duan, D. Lei and M. J. Hamdensmith, *Polyhedron*, 1991, **10**, 2105.
73. T. Yamakawa, S. Shinoda, Y. Saito, H. Moriyama and P. S. Pregosin, *Magn. Reson. Chem.*, 1985, **23**, 202.
74. K. R. Koch and J. M. Wyrley-Birch, *Inorg. Chim. Acta*, 1985, **102**, L5.
75. M. T. Pinillos, A. Elduque, J. A. Lopez, F. J. Lahoz, L. A. Oro and B. E. Mann, *J. Chem. Soc. Dalton Trans.*, **1992**, 2389.
76. C. Ammann, P. S. Pregosin, H. Rüegger, M. Grassi and A. Musco, *Magn. Reson. Chem.*, 1989, **27**, 355.
77. K. R. Koch, *Magn. Reson. Chem.*, 1992, **30**, 158.
78. M. Herberhold, M. Herberhold, U. Steffl, W. Milius and B. Wrackmeyer, *Angew. Chem.*, 1997, **107**, 1545; *Angew. Chem. Int. Ed. Engl.*, 1997, **36**, 1510.
79. Max Herberhold, Udo Steffi, Wolfgang Milius and Bernd Wrackmeyer, *Chem. Eur. J.*, 1998, **4**, 1027.
80. Y. Obora, Y. Tsuji, K. Nishiyama, M. Ebihara and T. Kawamura, *J. Am. Chem. Soc.*, 1996, **118**, 10922.
81. K. Jurkschat, H.-B. Abicht, A. Tzschach and B. Mahieu, *J. Organomet. Chem.*, 1986, **309**, C47.
82. A. Albinati, U. von Gunten, P. S. Pregosin and H. J. Ruegg, *J. Organomet. Chem.*, 1985, **295**, 239.
83. M. Kretschmer, P. S. Pregosin, A. Albinati and A. Tognis, *J. Organomet. Chem.*, 1985, **281**, 365.
84. C. Arz, I. R. Herbert and P. S. Pregosin, *Organomet Chem.*, 1986, **308**, 373.

85. I. R. Herbert, P. S. Pregosin and H. Ruegger, *Inorg. Chim. Acta*, 1986, **112**, 29.
86. P. Brüggeller, *Z. Naturforsch., Teil B*, 1986, **41**, 1561.
87. A. C. Fillippou, E. O. Fischer, G. Müller and H. G. Alt, *J. Organomet. Chem.*, 1987, **329**, 223.
88. H. P. Abicht, K. Jurkschat, A. Tzschach, K. Peters, E.-M. Peters and H. G. von Schnering, *J. Organomet. Chem.*, 1987, **326**, 357.
89. M. Grassi, S. V. Meille, A. Musco, R. Pontellini and A. Sironi, *J. Chem. Soc. Dalton Trans.*, 1989, 615.
90. J. E. Ellis, K.-M. Chi, A.-J. DiMaio, S. R. Frerichs, J. R. Stenzel, A. L. Rheingold and B. S. Haggerty, *Angew. Chem.*, 1991, **103**, 196; *Angew. Chem. Int. Ed. Engl.*, 1991, **30**, 194.
91. J. Kim, Y. Do, Y. S. Sohn, C. B. Knobler and M. F. Hawthorne, *J. Organomet. Chem.*, 1991, **418**, C1.
92. L. Carlton and R. Weber, *Inorg. Chem.*, 1993, **32**, 4169.
93. L. Fidalgo, M. A. Garralda, R. Hernandez and L. Ibarlucea, *Inorg. Chim. Acta*, 1993, **207**, 121.
94. F. Krech and K. Issleib, *Z. Anorg. Allg. Chem.*, 1989, **557**, 143.
95. A. B. Chopa, A. E. Zuniga and J. C. Podesta, *J. Chem. Res. (S)*, 1989, 234.
96. R. Eujen, N. Jahn and U. Thurmann, *J. Organomet. Chem.*, 1992, **434**, 159.
97. J. C. Podesta, A. B. Chopa, G. E. Radivoy and C. A. Vitale, *J. Organomet. Chem.*, 1995, **494**, 11.
98. T. Kawakami, T. Sugimoto, A. Baba, H. Matsuda and N. Sonoda, *J. Org. Chem.*, 1995, **60**, 2677.
99. B. Wrackmeyer, *Z. Naturforsch. Teil B*, 1982, **37**, 1524.
100. I. Wharf, *Inorg. Chim. Acta*, 1989, **159**, 41.
101. B. Wrackmeyer, G. Kehr, D. Wettinger and W. Milius, *Main Group Met. Chem.*, 1993, **16**, 433.
102. T. N. Mitchell, W. Reimann and C. Nettelbeck, *Organometallics*, 1985, **4**, 1044.
103. B. King, H. Eckert, D. Z. Denney and R. H. Herber, *Inorg. Chim. Acta*, 1986, **122**, 45.
104. W. Adcock and C. I. Clark, *J. Org. Chem.*, 1993, **58**, 7341.
105. D. Dakternieks, G. Dyson, K. Jurkschat, R. Tozer and E. R. T. Tiekink, *J. Organomet. Chem.*, 1993, **458**, 29.
106. A. Vij, R. L. Kirchmeier, R. D. Willett and J. M. Shreeve, *Inorg. Chem.*, 1994, **33**, 5456.
107. J. C. Cochran, H. K. Phillips, S. Tom, A. R. Hurd and B. S. Bronk, *Organometallics*, 1994, **13**, 947.
108. B. Wrackmeyer, G. Kehr and J. Süß, *Main Group Met. Chem.*, 1995, **18**, 127.
109. F. Lhermite and B. Carboni, *Synlett*, **1996**, 377.
110. P. Galow, A. Sebald and B. Wrackmeyer, *J. Organomet. Chem.*, 1983, **259**, 253.
111. T. Janati, J.-C. Guillemin and M. Soufiaoui, *J. Organomet. Chem.*, 1995, **486**, 57.
112. L. Lasalle, T. Janati and J.-C. Guillemin, *J. Chem. Soc. Chem. Commun.*, 1995, 699.
113. B. Wrackmeyer, H. E. Maisel and H. Zhou, *Main Group Met. Chem.*, 1993, **16**, 475.
114. M. Weidenbruch, A. Stilter, K. Peters and H. G. von Schnering, *Chem. Ber.*, 1996, **129**, 1565.
115. I. I. Padilla-Martinez, M. de Jesus Rosalez-Hoz, R. Contreras, S. Kerschl and B. Wrackmeyer, *Chem. Ber.*, 1994, **127**, 343.
116. W. Petz, *Chem. Rev.*, 1986, **86**, 1019.
117. B. Wrackmeyer, K. Horchler von Locquenghien, E. Kupce and A. Sebald, *Magn. Reson. Chem.*, 1993, **31**, 45.
118. K. C. Molloy and P. C. Waterfield, *J. Organomet. Chem.*, 1992, **424**, 281.
119. E. Liepins, I. Birgele, E. Lukevics, E. T. Bogoradovsky and V. S. Zavgorodny, *J. Organomet. Chem.*, 1991, **402**, 43.
120. E. Kupce, B. Wrackmeyer and E. Lukevics, *Magn. Reson. Chem.*, 1991, **29**, 444.
121. T. N. Mitchell, *Magn. Reson. Chem.*, 1986, **24**, 1019.
122. F. H. Köhler, W. A. Geike and N. Hertkorn, *J. Organomet. Chem.*, 1987, **334**, 359.

123. C. Krüger, K.-H. Thiele and M. Dargatz, *Z. Anorg. Allg. Chem.*, 1989, **569**, 97.
124. A. Ricci, M. Taddei and G. Seconi, *J. Organomet. Chem.*, 1986, **306**, 23.
125. B. Wrackmeyer and K. Horchler, *J. Magn. Reson.*, 1990, **90**, 569.
126. F. F. Xin, S. X. Lin, F. Y. Jie, H. Pan, B. Mahieu, M. Gielen, F. Kayser and R. Willem, *Z. Anorg. Allg. Chem.*, 1994, **620**, 1006.
127. M. P. Lambert, M. Ratier, J.-G. Duboudin and M. Petraud, *J. Organomet. Chem.*, 1994, **467**, 181.
128. B. Wrackmeyer, G. Kehr and D. Wettinger, *Inorg. Chim. Acta*, 1994, **220**, 161.
129. B. Wrackmeyer and K. Wagner, *Chem. Ber.*, 1989, **122**, 857.
130. B. Wrackmeyer, G. Kehr, J. Süß and E. Molla, *J. Organomet. Chem.*, 1998, **562**, 207.
131. N. Hertkorn and F. H. Köhler, *Z. Naturforsch., Teil B*, 1988, **43**, 1405.
132. B. Wrackmeyer, unpublished results.
133. B. Wrackmeyer and P. Bernatowicz, *Magn. Reson. Chem.*, 1999, in press.
134. B. Wrackmeyer, G. Kehr, H. Zhou and S. Ali, *Magn. Reson. Chem.*, 1996, **34**, 921.
135. B. E. Mann and B. F. Taylor, *^{13}C NMR Data of Organometailic Compounds*, Academic Press, London, 1981.
136. K. Jacob, M. Glanz, J. Holecek and A. Lycka, *Z. Anorg. Allg. Chem.*, 1990, **581**, 33.
137. B. Jousseaume and P. Villeneuve, *Tetrahedron*, 1989, **45**, 1145.
138. C. S. Frampton, K. G. Ofori-Okai, R. M. G. Roberts and J. Silver, *J. Organomet. Chem.*, 1986, **307**, 231.
139. T. N. Mitchell, A. Amamria, H. Killing and D. Rutschow, *J. Organomet. Chem.*, 1986, **304**, 257.
140. A. D. Ayala, N. Giagante, J. C. Podesta and W. P. Neumann, *J. Organomet. Chem.*, 1988, **340**, 317.
141. J. C. Podesta, A. D. Ayala, A. B. Chopa and N. N. Giagante, *J. Organomet. Chem.*, 1989, **364**, 39.
142. B. Wrackmeyer, G. Kehr, H. E. Maisel and H. Zhou, *Magn. Reson. Chem.*, 1998, **36**, 39.
143. T. N. Mitchell and C. Nettelbeck, *Magn. Reson. Chem.*, 1987, **25**, 879.
144. B. Wrackmeyer, G. Kehr and J. Süß, *Chem. Ber.*, 1993, **126**, 2221.
145. B. Wrackmeyer, U. Dörfler, W. Milius and M. Herberhold, *Z. Naturforsch., Teil B*, 1996, **51**, 851.
146. B. Wrackmeyer, U. Dörfler, G. Kehr, H. E. Maisel and W. Milius, *J. Organomet. Chem.*, 1996, **524**, 169.
147. B. Wrackmeyer, H. E. Maisel, G. Kehr and H. Nöth, *J. Organomet. Chem.*, 1997, **532**, 201.
148. B. Wrackmeyer, H. E. Maisel, B. Schwarze, W. Milius and R. Köster, *J. Organomet. Chem.*, 1997, **541**, 97.
149. M. Ochiai, S. Iwaki, T. Ukita, Y. Matsuura, M. Shiro and Y. Nagao, *J. Am. Chem. Soc.*, 1988, **110**, 4606.
150. B. Wrackmeyer, D. Wettinger and W. Milius, *J. Chem. Soc. Chem. Commun.*, 1995, 399.
151. N. Kuhn, G. Henkel and S. Stubenrauch, *J. Chem. Soc. Chem. Commun.*, 1992, 760.
152. L. Jia, H. Zhong and N. S. Hosmane, *Organometallics*, 1992, **11**, 2957.
153. U. Lay, H. Pritzkow and H. Grützmacher, *J. Chem. Soc. Chem. Commun.*, 1992, 260.
154. T. Parella, *Magn. Reson. Chem.*, 1998, **36**, 467.
155. H. Schumann, M. Glanz, F. Girgsdies, F. E. Hahn, M. Tamm and A. Grzegorewski, *Angew. Chem.*, 1997, **109**, 2328; *Angew. Chem. Int. Ed. Engl.*, 1997, **36**, 2232.
156. C. Drost, B. Gehrhus, P. B. Hitchcock and M. F. Lappert, *J. Chem. Soc. Chem. Commun.*, 1997, 1845.
157. T. N. Mitchell and W. Reimann, *Organometallics*, 1986, **5**, 1991.
158. H. Schumann, R. Mohtachemi and M. Schwichtenberg, *Z. Naturforsch, Teil B*, 1988, **43**, 1510.
159. J. Blümel and F. H. Köhler, *J. Organomet. Chem.*, 1988, **340**, 303.

160. A. Capperucci, A. Degl'Innocenti, C. Faggi, G. Reginato, A. Ricci, P. Dembech and G. Seconi, *J. Org. Chem.*, 1989, **54**, 2966.
161. R. Köster, G. Seidel, B. Wrackmeyer, K. Horchler and D. Schlosser. *Angew. Chem.*, 1989, **101**, 945; *Angew. Chem. Int. Ed. Engl.*, 1989, **28**, 918.
162. V. Gouron, B. Jousseaume, M. Ratier, J.-C. Lartigue and M. Petraud, *Magn. Reson. Chem.*, 1990, **28**, 755.
163. F. Fu, H. Li, D. Zhu, O. Fang, H. Pan, E. R. T. Tiekink, F. Kayser, M. Biesemans, I. Verbruggen, R. Willem and M. Gielen, *J. Organomet. Chem.*, 1995, **490**, 163.
164. H. Meyer, G. Baum, W. Massa, S. Berger and A. Berndt, *Angew. Chem.*, 1987, **99**, 559; *Angew. Chem. Int. Ed. Engl.*, 1987, **26**, 546.
165. B. Wrackmeyer, G. Guldner and S. T. Abu-Orabi, *Tetrahedron*, 1989, **45**, 1119.
166. W. Adcock, H. Gangodawila, G. B. Kok, V. S. Iyer, W. Kitching, G. M. Drew and D. Young, *Organometallics*, 1987, **6**, 156.
167. H. J. Reich and N. H. Phillips, *J. Am. Chem. Soc.*, 1986, **108**, 2102.
168. A. Maercker, H. Bodenstedt and L. Bransdma, *Angew. Chem.*, 1992, **104**, 1387; *Angew. Chem. Int. Ed. Engl.*, 1992, **31**, 1339.
169. H. J. Reich, J. P. Borst and R. R. Dykstra, *Organometallics*, 1994, **13**, 1.
170. D. Reed, D. Stalke and D. S. Wright, *Angew. Chem.*, 1991, **103**, 1539; *Angew. Chem. Int. Ed. Engl.*, 1991, **30**, 1459.
171. B. Wrackmeyer and A. Glöckle, *Main Group Met. Chem.*, 1997, **20**, 181.
172. L. R. Sita and R. D. Bickerstaff, *J. Am. Chem. Soc.*, 1989, **111**, 6454.
173. L. R. Sita, I. Kinoshita and S. P. Lee, *Organometallics*, 1990, **9**, 1644.
174. K. Angermund, K. Jones, C. Krüger, J. L. Latten and Y.-H. Tsay, *J. Organomet. Chem.*, 1989, **353**, 17.
175. (a) G. Ossig, A. Meller, R. Freitag and R. Herbst-Irmer, *J. Chem. Soc. Chem. Commun.*, 1993, 497. (b) G. Ossig, A. Meller, S. Freitag, R. Herbst-Irmer and G. M. Sheldrick, *Chem. Ber.*, 1993, **126**, 2247.
176. H. Grützmacher, W. Deck, H. Pritzkow and M. Sander, *Angew. Chem.*, 1994, **106**, 467; *Angew. Chem. Int. Ed. Engl.*, 1994, **33**, 456.
177. M. Drieß, R. Janoschek, H. Pritzkow and U. Winkler, *Angew. Chem.*, 1995, **107**, 1746; *Angew. Chem. Int. Ed. Engl.*, 1995, **34**, 1614.
178. M. Westerhausen, *Angew. Chem.*, 1994, **106**, 1585; *Angew. Chem. Int. Ed. Engl.*, 1994, **33**, 1493.
179. P. B. Hitchcock, M. F. Lappert, G. A. Lawless and B. Royo, *J. Chem. Soc. Chem. Commun.*, 1993, 554.
180. B. Wrackmeyer, *J. Organomet. Chem.*, 1989, **364**, 331.
181. S. Kerschl and B. Wrackmeyer, *J. Organomet. Chem.*, 1988, **338**, 195.
182. M. Herberhold, S. Gerstmann and B. Wrackmeyer, *Phosphorus, Sulfur, Silicon*, 1992, **66**, 273.
183. E. Kupce and B. Wrackmeyer, *J. Magn. Reson.*, 1992, **99**, 338.
184. E. Kupce and B. Wrackmeyer, *J. Magn. Reson.*, 1992, **99**, 343.
185. B. Wrackmeyer, G. Kehr, H. Zhou and S. Ali, *Inorg. Chim. Acta*, 1992, **197**, 129.
186. B. Wrackmeyer, G. Kehr, H. Zhou and S. Ali, *Main Group Met. Chem.*, 1992, **15**, 89.
187. B. Wrackmeyer, G. Kehr, H. Zhou and S. Ali, *Inorg. Chim. Acta*, 1994, **216**, 51.
188. J. B. Lambert and B. Kuhlmann, *J. Chem. Soc. Chem. Commun.*, 1992, 931.
189. B. Wrackmeyer, S. Kerschl, H. E. Maisel and W. Milius, *J. Organomet. Chem.*, 1995, **490**, 197.
190. B. Wrackmeyer and G. Kehr, *Polyhedron*, 1991, **10**, 1497.
191. D. K. Jaiswal, H. Andres, H. Morimoto and P. G. Williams, *J. Chem. Soc. Chem. Commun.*, 1993, 907.
192. K. L. Leighton and R. E. Wasylishen, *Can. J. Chem.*, 1987, **65**, 1469.
193. B. Wrackmeyer and S. T. Abu-Orabi, *Chem. Ber.*, 1987, **120**, 1603.

194. K. Handlir, J. Holecek, M. Nadvornik, S. M. Teleb and A. Lycka, *Inorg. Chim. Acta*, 1988, **150**, 287.
195. M. J. Taylor and J. M. Coddington, *Polyhedron*, 1992, **11**, 1531.
196. D. K. Srivastava, N. P. Rath and L. Barton, *Organometallics*, 1992, **11**, 2263.
197. T. Carofiglio, D. Marton and F. Lenzmann, *Anal. Chim. Acta*, 1993, **281**, 119.
198. B. Wrackmeyer, U. Klaus and W. Milius, *Chem. Ber.*, 1995, **128**, 679.
199. J. Kümmerlen, A. Sebald and H. Reuter, *J. Organomet. Chem.*, 1992, **427**, 309.
200. J. Holecek, K. Handlir, M. Nadvornik, S. M. Teleb and A. Lycka, *J. Organomet. Chem.*, 1988, **339**, 61.
201. A. Lyska, J. Holecek and K. Handlir, *Collect. Czech. Chem. Commun.*, 1989, **54**, 2386.
202. L. R. Sita and R. D. Bickerstaff, *Phosphorus, Sulfur, Silicon*, 1989, **41**, 31.
203. M. Dargatz, H. Hartung, E. Kleinpeter, B. Rensch, D. Schollmeyer and H. Weichmann, *J. Organomet. Chem.*, 1989, **361**, 43.
204. T. N. Mitchell and H.-J. Belt, *J. Organomet. Chem.*, 1989, **368**, 167.
205. V. K. Jain, V. B. Mokal and P. Sandor, *Magn. Reson. Chem.*, 1992, **30**, 1158.
206. R. W. Chorley, P. B. Hitchcock, B. S. Jolly, M. F. Lappert and G. A. Lawless, *J. Chem. Soc. Chem. Commun.*, 1991, 1302.
207. Chr. Zybill and G. Müller, *Z. Naturforsch, Teil B*, 1988, **43**, 45.
208. M. Veith, S. Mathur and V. Hoch, *J. Chem. Soc. Dalton Trans.*, **1996**, 2485.
209. J. Klein, F. Thunecke and R. Borsdorf, *Monatsh. Chem.*, 1992, **123**, 801.
210. P. Jutzi, D. Wegener, H.-G. Stammler, A. Karaulov and M. B. Hursthouse, *Inorg. Chim. Acta*, 1992, **198**, 369.
211. A. A. S. Elkhaldy, R. K. Mehrotra and G. Srivastava, *Synth. React. Inorg. Met.-Org. Chem.*, 1992, **22**, 997.
212. R. Eujen and U. Thurmann, *J. Organomet. Chem.*, 1992, **433**, 63.
213. S. E. Johnson and C. B. Knobler, *Organometallics*, 1992, **11**, 3684.
214. D. Dakternieks and H. Zhu, *Organometallics*, 1992, **11**, 3820.
215. S. Ianelli, M. Orcesi, C. Pelizzi, G. Pelizzi and G. Predieri, *J. Organomet. Chem.*, 1993, **451**, 59.
216. M. T. Ahmet, A. Houlton, C. S. Frampton, J. R. Miller, R. M. G. Roberts, J. Silver and B. Yavari, *J. Chem. Soc. Dalton Trans.*, 1993, 3085.
217. I. Pianet, E. Fouquet, M. Pereyre, M. Gielen, F. Kayser, M. Biesemans and R. Willem, *Magn. Reson. Chem.*, 1994, **32**, 617.
218. K. Handlir, A. Lycka, J. Holecek, M. Nadvornik, V. Pejchal and A. Sebald, *Collect. Czech. Chem. Commun.*, 1994, **59**, 885.
219. A. Dörr, D. Gudat, D. Hänssgen, H. Hens and E. Stahlhut, *Bull. Soc. Chim. Fr.*, 1994, **131**, 674.
220. F. Kayser, M. Biesemans, A. Delmotte, I. Verbruggen, I. de Borger, M. Gielen, R. Willem and E. R. T. Tiekink, *Organometallics*, 1994, **13**, 4026.
221. R. Littger, N. Metzler, H. Nöth and M. Wagner, *Chem. Ber.*, 1994, **127**, 1901.
222. L. Barton, H. Fang, D. K. Srivastava, T. A. Schweitzer and N. P. Rath, *Appl. Organomet. Chem.*, 1996, **10**, 183.
223. J. H. Nelson, W. L. Wilson, L. W. Cary, N. W. Alcock, H. J. Clase, G. S. Jas, L. Ramsey-Tassin and J. W. Kenney, III, *Inorg. Chem.*, 1996, **35**, 883.
224. P. Jutzi and K.-H. Schwartzen, *Chem. Ber.*, 1989, **122**, 287.
225. N. A. Chaniotakis, K. Jurkschat and A. Rühlemann, *Anal. Chim. Acta*, 1993, **282**, 345.
226. A. Tzschach, M. Scheer and K. Jurkschat, *Z. Anorg. Allg. Chem.*, 1984, **515**, 147.
227. T. Imori, V. Lu, H. Cai and T. D. Tilley, *J. Am. Chem. Soc.*, 1995, **117**, 9031.
228. B. Wrackmeyer and U. Klaus, *J. Organomet. Chem.*, 1996, **520**, 211.
229. B. Watta, W. P. Neumann and J. Sauer, *Organometallics*, 1985, **4**, 1954.
230. B. Jousseaume, N. Noiret, M. Pereyre, A. Saux and J.-M. Frances, *Organometallics*, 1994, **13**, 1034.

231. B. Wrackmeyer, U. Klaus and W. Milius, *Inorg. Chim. Acta*, 1996, **250**, 327.
232. G. K. Sandhu, G. Kaur, J. Holecek and A. Lycka, *J. Organomet. Chem.*, 1988, **345**, 51.
233. A. H. Cowley, D. M. Giolando, R. A. Jones, C. M. Nunn, J. M. Power and W. W. du Mont, *Polyhedron*, 1988, **7**, 1317.
234. H. H. Karsch, A. Appelt and G. Müller, *Organometallics*, 1986, **5**, 1664.
235. R. W. Chorley, P. B. Hitchcock and M. F. Lappert, *J. Chem. Soc. Chem. Commun.*, 1992, 525.
236. S. P. Mallela and R. A. Geanangel, *Inorg. Chem.*, 1990, **29**, 3525.
237. M. Herberhold, C. Köhler, W. Milius and B. Wrackmeyer, *Z. Naturforsch., Teil B*, 1995, **50**, 1811.
238. P. A. W. Dean and R. V. S. Srivastava, *Inorg. Chim. Acta*, 1985, **105**, 1.
239. R. C. Burns, L. A. Devereux, P. Granger and G. J. Schrobilgen, *Inorg. Chem.*, 1985, **24**, 2615.
240. S. S. Al-Juaid, S. M. Dhaher, C. Eaborn, P. B. Hitchcock and J. D. Smith, *J. Organomet. Chem.*, 1987, **325**, 117.
241. S. Adams and M. Dräger, *J. Organomet. Chem.*, 1987, **323**, 11.
242. V. G. K. Das, L.-K. Mun, C. Wei and T. C. W. Mak, *Organometallics*, 1987, **6**, 10.
243. H. Berwe and A. Haas, *Chem. Ber.*, 1987, **120**, 1175.
244. U. Kunze and R. Tischer, *Chem. Ber.*, 1987, **120**, 1099.
245. M. Newcomb, A. M. Madonik, M. T. Blanda and J. K. Judice, *Organometallics*, 1987, **6**, 145.
246. G. K. Sandhu, G. Kaur, J. Holecek and A. Lycka, *J. Organomet. Chem.*, 1987, **332**, 75.
247. G. Schmid, D. Vehreschild-Yzermann and R. Boese, *J. Organomet. Chem.*, 1987, **326**, 307.
248. A. Lycka, J. Jirman, A. Kolonicny and J. Holecek, *J. Organomet. Chem.*, 1987, **333**, 305.
249. S. J. Blunden and R. Hill, *J. Organomet. Chem.*, 1987, **333**, 317.
250. M. Newcomb, J. H. Horner and M. T. Blanda, *J. Am. Chem. Soc.*, 1987, **109**, 7478.
251. K. C. Molloy, S. J. Blunden and R. Hill, *J. Chem. Soc. Dalton Trans.*, **1988**, 1259.
252. M. T. Reetz, K. Harms and W. Reif, *Tetrahedron Lett.*, 1988, **29**, 5881.
253. K. Jurkschat, J. Schilling, C. Mügge, A. Tzschach, J. Meunier-Piret, M. de Maerssche, M. Gielen and R. Willem, *Organometallics*, 1988, **7**, 38.
254. J. Holecek, K. Handlir, A. Lycka, T. K. Chattopadhyay, B. Majee and A. K. Kumar, *Collect. Czech. Chem. Commun.*, 1986, **51**, 1100.
255. R. Colton and D. Dakternieks, *Inorg. Chim. Acta*, 1988, **143**, 151.
256. H. K. Sharma, S. Iata, K. K. Sharma, K. C. Molloy and P. C. Waterfield, *J. Organomet. Chem.*, 1988, **353**, 9.
257. A. S. Kothiwal, A. Singh, A. K. Rai and R. C. Megrotra, *Ind. J. Chem.*, 1988, **27A**, 507.
258. O.-S. Jung and Y. S. Sohn, *Bull. Korean Chem. Soc.*, 1988, **9**, 365.
259. S. M. Dhaher, C. Eaborn and J. D. Smith, *J. Organomet. Chem.*, 1988, **355**, 33.
260. B. Wrackmeyer, C. Köhler, W. Milius and M. Herberhold, *Z. Anorg. Allg. Chem.*, 1995, **621**, 1625.
261. B. Wrackmeyer, I. Ordung and B. Schwarze, *J. Organomet. Chem.*, 1997, **532**, 71.
262. B. Wrackmeyer, S. Kundler and A. Ariza-Castolo, *Phosphorus, Sulfur, Silicon*, 1994, **91**, 229.
263. M. Herberhold, U. Steffl, W. Milius and B. Wrackmeyer, *Z. Anorg. Allg. Chem.*, 1998, **624**, 386.
264. M. Herberhold, U. Steffl, W. Milius and B. Wrackmeyer, *Angew. Chem.*, 1996, **108**, 1927; *Angew. Chem. Int. Ed. Engl.*, 1996, **35**, 1803.
265. M. Herberhold, U. Steffl and B. Wrackmeyer, *Z. Naturforsch., Teil B*, 1998, in press.
266. M. Herberhold, U. Steffi, W. Milius and B. Wrackmeyer, *J. Organomet. Chem.*, 1997, **533**, 109.
267. B. Wrackmeyer, G. Kehr and D. Wettinger, *Main Group Met. Chem.*, 1997, **20**, 573.
268. M. Herberhold, S. Gerstmann, W. Milius and B. Wrackmeyer, *Z. Naturforsch., Teil B*, 1997, **52**, 1278.

269. B. Wrackmeyer and J. Weidinger, *Z. Naturforsch., Teil B*, 1997, **52**, 947.
270. B. Wrackmeyer, B. Schwarze and W. Milius, *J. Organomet. Chem.*, 1997, **545–546**, 297.
271. B. Wrackmeyer, H. E. Maisel and W. Milius, *Z. Naturforsch., Teil B*, 1995, **50**, 809.
272. M. Herberhold, S. Gerstmann and B. Wrackmeyer, *Z. Naturforsch., Teil B*, 1998, **53**, 573.
273. B. Wrackmeyer, in *Unkonventionelle Wechselwirkungen in der Chemie metallischer Elemente*, (ed. B. Krebs), pp. 111–124, VCH, Weinheim, 1992.
274. G. G. Lobbia, F. Bonati, P. Cecchi, A. Cingolani and A. Lorenzotti, *J. Organomet. Chem.*, 1989, **378**, 139.
275. H. Schumann and K.-H. Köhricht, *J. Organomet. Chem.*, 1989, **373**, 307.
276. T. Chivers, J. Fait and K. J. Schmidt, *Inorg. Chem.*, 1989, **28**, 3018.
277. P. A. Bates, M. B. Hursthouse, A. G. Davies and S. D. Slater, *J. Organomet. Chem.*, 1989, **363**, 45.
278. K. Jurkschat, H. G. Kuivila, S. Liu and J. A. Zubieta, *Organometallics*, 1989, **8**, 2755.
279. D. Dakternieks and C. L. Rolls, *Inorg. Chim. Acta*, 1989, **161**, 105.
280. S. J. Blunden and R. Hill, *J. Organomet. Chem.*, 1989, **371**, 145.
281. K. Jurkschat, F. Hesselbarth, M. Dargatz, J. Lehmann, E. Kleinpeter and A. Tzschach, *J. Organomet. Chem.*, 1990, **388**, 259.
282. F. Huber, A. K. Saxena and R. K. A. Sebald, *J. Organomet. Chem.*, 1989, **368**, 130.
283. H. Puff, G. Bertram, B. Ebeling, M. Franken, R. Gattermayer, R. Hundt, W. Schuh and R. Zimmer, *J. Organomet. Chem.*, 1989, **379**, 235.
284. D. Hännsgen, H. Aldenhoven and M. Nieger, *J. Organomet. Chem.*, 1989, **367**, 47.
285. F. Huber, B. Mundus-Glowacki and H. Preut, *J. Organomet. Chem.*, 1989, **365**, 111.
286. J. T. B. H. Jastrzebski, P. A. van der Schaaf, J. Boersma and G. van Koten, *Organometallics*, 1989, **8**, 1373.
287. T. P. Lockhart, H. Puff, W. Schuh, H. Reuter and T. N. Mitchell, *J. Organomet. Chem.*, 1989, **366**, 61.
288. J. Coddington and M. J. Taylor, *J. Chem. Soc. Dalton Trans.*, **1989**, 2223.
289. M. F. Mahon, K. C. Malloy and P. C. Waterfield. *J. Organomet. Chem.*, 1989, **361**, C5.
290. M. Gingras, T. H. Chan and D. N. Harpp, *J. Org. Chem.*, 1990, **55**, 2078.
291. A. Lycka, J. Holecek, B. Schneider, J. Straka, *J. Organomet. Chem.*, 1990, **389**, 29.
292. D. Hännsgen, H. Aldenhoven and M. Nieger, *Chem. Ber.*, 1990, **123**, 1837.
293. J. Holecek, A. Lycka, K. Handlir and M. Nadvornik, *Coll. Czech. Chem. Commun.*, 1990, **55**, 1193.
294. G. G. Lobbia, F. Bonati, P. Cecchi and D. Leonesi, *J. Organomet. Chem.*, 1990, **391**, 155.
295. T. A. K. Al-Alaf and M. A. M. Al-Tayy, *J. Organomet. Chem.*, 1990, **391**, 37.
296. S.-P. Huang, S. Dhingra and M. G. Kanitzidis, *Polyhedron*, 1990, **9**, 1389.
297. D. C. Apperly, N. A. Davies, R. K. Harris, A. K. Brimah, S. Eller and R. D. Fischer, *Organometallics*, 1990, **9**, 2672.
298. S. J. Blunden and R. Hill, *Inorg. Chim. Acta*, 1990, **177**, 219.
299. F. Thunecke, D. Schulze and R. Borsdorf, *Z. Chem.*, 1990, **30**, 444.
300. D. Hännsgen and H. Aldenhoven, *Chem. Ber.*, 1990, **123**, 1833.
301. S. E. Johnson, K. Polborn and H. Nöth, *Inorg. Chem.*, 1991, **30**, 1410.
302. D. L. Reger, S. J. Knox, M. F. Huff, A. L. Rheingold and B. S. Haggerty, *Inorg. Chem.*, 1991, **30**, 1754.
303. J. Holecek, A. Lycka, M. Nadvornik and K. Handlir, *Collect. Czech. Chem. Commun.*, 1991, **56**, 1908.
304. S. J. Blunden, R. Hill and S. E. Sutton, *Appl. Organomet. Chem.*, 1991, **5**, 159.
305. E. Rafii, M. Ngassoum, R. Faure, L. Lena and J. Metzger, *Fuel*, 1991, **70**, 132.
306. R. S. Deeb and D. H. Peyton, *J. Biol. Chem.*, 1991, **266**, 3728.
307. I. D. Gay, C. H. W. Jones and R. D. Sharma, *J. Magn. Reson.*, 1991, **91**, 186.
308. M. Boualam, R. Willemi M. Biesemans and M. Gielen, *Appl. Organomet. Chem.*, 1991, **5**, 497.

309. Q.-L. Xie, Z.-Q. Yang, D.-K. Zhang and J.-T. Wang, *Chin. J. Chem.*, 1991, **9**, 327.
310. P. B. Hitchcock, H. A. Jasim, M. F. Lappert, W.-P. Leung, A. K. Rai and R. E. Taylor, *Polyhedron*, 1991, **10**, 1203.
311. D. C. Adams, T. Birchall, R. Gaggiani, R. L. Gillespie and J. E. Vekris, *Can. J. Chem.*, 1991, **69**, 2122.
312. J. T. B. H. Jastrzebski, D. M. Grove, J. Boersma and G. van Koten, *Magn. Reson. Chem.*, 1991, **29**, S25.
313. A. Vij, S. Singh and R. D. Verma, *J. Fluorine Chem.*, 1992, **58**, 43.
314. B. Bundus-Glowacki, F. Huber, H. Preut, G. Ruisi and R. Barbieri, *Appl. Organomet. Chem.*, 1992, **6**, 83.
315. M. Vornefeld, F. Huber, H. Preut, G. Ruisi and R. Barbieri, *Appl. Organomet. Chem.*, 1992, **6**, 75.
316. J. T. B. H. Jastrzebski, P. A. van der Schaaf, J. Boersma and G. van Koten, *Organometallics*, 1992, **11**, 1521.
317. J. H. Webgrovius and M. F. Garbauskas, *Organometallics*, 1992, **11**, 1334.
318. T. B. Grindley, R. Thangarasa, P. K. Bakshi and T. L. Cameron, *Can. J. Chem.*, 1992, **70**, 197.
319. G. Anselme, H. Ranaivonjatovo, J. Escudie, C. Couret and J. Satge, *Organometallics*, 1992, **11**, 2748.
320. T. B. Grindley, R. E. Wasylishen, R. Thangarasa, W. P. Power and R. D. Curtis, *Can. J. Chem.*, 1992, **70**, 205.
321. D. C. Apperly, N. A. Davies, R. K. Harris, S. Eller, P. Schwarz and R. D. Fischer, *J. Chem. Soc. Chem. Commun.*, **1992**, 740.
322. M. Gielen, M. Boualam, A. Meriem, B. Mahieur, M. Biesemans and R. Willem, *Heteroatom Chem.*, 1992, **3**, 449.
323. D. Farah, K. Swami and H. G. Kuivila, *J. Organomet. Chem.*, 1992, **429**, 311.
324. T. S. B. Baul and A. Lycka, *Polyhedron*, 1992, **11**, 2423.
325. M. Boualam, J. Meunier-Piret, M. Biesemans, R. Willem and M. Gielen, *Inorg. Chim. Acta*, 1992, **198–200**, 249.
326. F. Huber, M. Vornefeld, H. Preut, E. v. Angerer and G. Ruisi, *Appl. Organomet. Chem.*, 1992, **6**, 597.
327. S. Dostal, S. J. Stoudt, P. Fanwick, W. F. Sereatan, B. Kahr and J. E. Jackson, *Organometallics*, 1993, **12**, 2284.
328. C. I. F. Denekamp, D. F. Evans, J. Parr and J. D. Woollins, *J. Chem. Soc. Dalton Trans.*, 1993, 1489.
329. D. L. Reger, S. S. Mason, J. Takats, X. W. Zhang, A. L. Rheingold and B. S. Haggerty, *Inorg. Chem.*, 1993, **32**, 4345.
330. C. Kober, J. Kroner and W. Storch, *Angew. Chem.*, 1993, **105**, 1693; *Angew. Chem. Int. Ed. Engl.*, 1993, **32**, 1608.
331. W. Plass and J. G. Verkade, *Inorg. Chem.*, 1993, **32**, 5153.
332. J. Klein, F. Thunecke and R. Borsdorf, *Fresenius J. Anal. Chem.*, 1993, **346**, 789.
333. L. A. Burnett, S. M. S. V. Doidge-Harrison, S. J. Garden, R. A. Howie, O. J. Taylor and J. L. Wardell, *J. Chem. Soc. Dalton Trans.*, **1993**, 1621.
334. F. Huber, M. Vornefeld, G. Ruisi and R. Barbieri, *Appl. Organomet. Chem.*, 1993, **7**, 243.
335. T. Kawashima, N. Iwama and R. Okazaki, *J. Am. Chem. Soc.*, 1993, **115**, 2507.
336. X. Kong and T. B. Grindley, *Can. J. Chem.*, 1994, **72**, 2405.
337. J. Klein, S. Neels and R. Borsdorf, *J. Chem. Soc. Perkin Trans. 2*, **1994**, 2523.
338. J. McManus, D. Cunningham and M. J. Hynes, *J. Organomet. Chem.*, 1994, **468**, 87.
339. J. S. Casas, A. Sanchez, J. Sordo, A. Vazquez-Lopez, E. E. Castellano, J. Zukerman-Schpector, M. C. Rodriguez-Arguelles and U. Russo, *Inorg. Chim. Acta*, 1994, **216**, 169.
340. D. L. Reger and Y. Ding, *Polyhedron*, 1994, **13**, 869.
341. U. Kolb, M. Beuter and M. Dräger, *Inorg. Chem.*, 1994, **33**, 4522.

342. S. J. Blunden, M. F. Mahon, K. C. Molloy and P. C. Waterfield, *J. Chem. Soc. Dalton Trans.*, 1994, 2135.
343. M.-C. Ye and J. G. Verkade, *Energy & Fuels*, 1994, **8**, 172.
344. S. S. Sharma, S. Gupta and A. K. Narula, *Ind. J. Chem.*, 1994, **33A**, 1119.
345. R. Willem, A. Delmotte, I. De Borger, M. Biesemans, M. Gielen and F. Kayser, *J. Organomet. Chem.*, 1994, **480**, 255.
346. R. Schmiedgen, F. Huber, H. Preut, G. Ruisi and R. Barbieri, *Appl. Organomet. Chem.*, 1994, **8**, 397.
347. D. Dakternieks, H. Zhu, E. R. T. Tiekink and R. Colton, *J. Organomet. Chem.*, 1995, **476**, 33.
348. S. U. Ghazi, M. J. Heeg and J. P. Oliver, *Inorg. Chem.*, 1994, **33**, 4517.
349. M. Jang and A. F. Janzen, *J. Fluorine Chem.*, 1994, **66**, 129.
350. N. S. Hosmane, L. Jia, H. Zhang and J. A. Maguire, *Organometallics*, 1994, **13**, 1411.
351. N. A. Davies, K. B. Dillon, R. K. Harris, G. F. Hewitson and L. Toms, *Polyhedron*, 1994, **13**, 19.
352. V. Pejchal, J. Holecek, M. Nadvornik and A. Lycka, *Collect. Czech. Chem. Commun.*, 1995, **60**, 1492.
353. J. Campbell, D. P. DiCiommo, H. P. A. Mercier, A. M. Pirani, G. J. Schrobilgen and M. Willuhn, *Inorg. Chem.*, 1995, **34**, 6265.
354. H. Fang, D. Zhao, N. P. Rath, L. Brammer and L. Barton, *Organometallics*, 1995, **14**, 1700.
355. F. Banse, F. Ribot, T. J. Maquet and C. Sanchez, *Inorg. Chem.*, 1995, **34**, 6371.
356. S. Geetha, M. Ye and J. G. Verkade, *Inorg. Chem.*, 1995, **34**, 6158.
357. R. Kapoor, V. Sood and P. Kaboor, *Polyhedron*, 1995, **14**, 489.
358. T. Mizutani, T. Uesaka and H. Ogoshi, *Organometallics*, 1995, **14**, 341.
359. M. Danush, S. Ali, M. Mazhar, A. Badshah, M. I. Choudhary, H. G. Alt and G. Kehr, *Polyhedron*, 1995, **14**, 3115.
360. J. Campbell, L. A. Devereux, M. Gerken, H. P. A. Mercier, A. M. Pirani and G. J. Schrobilgen, *Inorg. Chem.*, 1995, **35**, 2945.
361. A. Appel, C. Kober, C. Neumann, H. Nöth, M. Schmidt and W. Storch, *Chem. Ber.*, 1996, **129**, 175.
362. D. Stalke, U. Klingebiel and G. M. Sheldrick, *J. Organomet. Chem.*, 1988, **341**, 119.
363. B. Jousseaume, P. Villeneuve, M. Dräger, S. Roller and J. M. Chezeau, *J. Organomet. Chem.*, 1988, **349**, C1.
364. K. Jurkschat, J. Kalbitz, M. Dargatz, E. Kleinpeter and A. Tzschach, *J. Organomet. Chem.*, 1988, **347**, 41.
365. W. A. Herrmann, J. G. Kuchler, J. K. Felixberger, E. Herdtweck and W. Wagner, *Angew. Chem.*, 1988, **100**, 420; *Angew. Chem. Int. Ed. Engl.*, 1988, **27**, 394.
366. R. K. Hrris, A. Sebald, D. Furlani and G. Tagliavini, *Organometallics*, 1988, **7**, 388.
367. J. Holecek, A. Lycka, K. Handlir and M. Nadvornik, *Collect. Czech Chem. Commun.*, 1988, **53**, 571.
368. C. Mügge, H. Pepermans, M. Gielen, R. Willem, A. Tzschach and K. Jurkschat, *Z. Anorg. Alig. Chem.*, 1988, **567**, 122.
369. I. D. Gay, R. W. H. Jones and R. D. Sharma, *J. Magn. Reson.*, 1989, **84**, 501.
370. S. J. Blunden, P. A. Cussack and D. G. Gillies, *J. Magn. Reson.*, 1984, **60**, 114.
371. C. T. G. Knight and A. E. Merbach, *J. Am. Chem. Soc.*, 1984, **106**, 804.
372. T. Birchall and G. Denes, *Can. J. Chem.*, 1984, **62**, 591.
373. A. Lycka, E. Holecek, M. Nadvornik and K. Handlir, *J. Organomet. Chem.*, 1985, **280**, 323.
374. T. Yano, K. Nakashima, J. Otera and R. Okawara, *Organometallics*, 1985, **4**, 1501.
375. C. T. Aitken and M. Onyszchuk, *J. Organomet. Chem.*, 1985, **295**, 149.
376. R. J. Rao, B. S. Saraswat, G. Srivastava and R. C. Mehrotra, *Ind. J. Chem.*, 1985, **25**, 76.
377. (a) C. Wynants, G. van Binst, C. Mügge, K. Jurkschat, A. Tzschach, H. Pepermans, M. Gielen

and R. Willem, *Organometallics*, 1985, **4**, 1906. (b) F. Kayser, M. Biesemans, F. Fu, H. Pan, M. Gielen, R. Willem, *J. Organomet. Chem.*, 1995, **486**, 263.
378. V. K. Jain, J. Mason, B. S. Saraswat and R. C. Mehrotra, *Polyhedron*, 1985, **4**, 2089.
379. R. M. Davidson, H. G. Grant and D. O'Smith, *Spectrochim. Acta*, 1985, **41A**, 581.
380. C. H. W. Jones, R. D. Sharma and S. P. Taneja, *Can. J. Chem.*, 1986, **64**, 980.
381. J. Holecek, A. Lycka and R. Wagener, *Collect. Czech. Chem. Commun.*, 1986, **51**, 2116.
382. H. Puff, C. Bach, W. Schuh and R. Zimmer, *J. Organomet. Chem.*, 1986, **312**, 313.
383. U. Baumeister, H. Hartung, K. Jurkschat and A. Tzschach, *J. Organomet. Chem.*, 1986, **304**, 107.
384. C. Picard, P. Tisnes and L. Casaux, *J. Organomet. Chem.*, 1986, **315**, 277.
385. J. Holecek, M. Nadvornik, K. Handlir and A. Lycka, *J. Organomet. Chem.*, 1986, **315**, 299.
386. S. J. Blunden, P. A. Cussack and D. G. Gillies, *Magn. Reson. Chem.*, 1986, **24**, 921.
387. S. K. Lee and B. K. Nicholson, *J. Organomet. Chem.*, 1986, **309**, 257.
388. K. C. Molloy, K. Quill, S. J. Blunden and R. Hill, *Polyhedron*, 1986, **5**, 959.
389. A. Saxena, F. Huber, L. Pellerito, A. Girasolo and G. C. Stocco, *Inorg. Chim. Acta*, 1986, **125**, 197.
390. M. Driess, S. Martin, K. Merz, V. Pintchouk, H. Pritzkow, H. Grützmacher and M. Kaupp, *Angew. Chem.*, 1997, **109**, 1982; *Angew. Chem. Int. Ed. Engl.*, 1997, **36**.
391. K. C. Molloy, K. Quill, S. J. Blunden and R. Hill, *J. Chem. Soc. Dalton Trans.*, 1986, 875.
392. A. Lycka and J. Holecek, *Inorg. Chim. Acta*, 1986, **122**, 15.
393. D. Dakternieks, B. F. Hoskins and C. L. Rolls, *Aust. J. Chem.*, 1986, **39**, 1221.
394. J. Holecek and A. Lycka, *Inorg. Chim. Acta*, 1986, **118**, L15.
395. J. T. B. H. Jastrzebski, G. van Koten, C. T. Knaap, A. M. M. Scheurs, J. Kroon and A. L. Spek, *Organometallics*, 1986, **5**, 1551.
396. S. Dietzel, K. Jurkschat, A. Tzschach and A. Zschunke, *Z. Anorg. Allg. Chem.*, 1986, **537**, 163.
397. T. P. Lockhart and W. F. Manders, *J. Am. Chem. Soc.*, 1987, **109**, 7015.
398. C. Luchinat and S. Roelens, *J. Org. Chem.*, 1987, **52**, 4444.
399. G. S. Chorghade and M. T. Pope, *J. Am. Chem. Soc.*, 1987, **109**, 5134.
400. K. C. K. Swami, R. O. Day and R. R. Holmes, *J. Am. Chem. Soc.*, 1987, **109**, 5546.
401. S. Adams and M. Dräger, *Angew. Chem.*, 1987, **99**, 1280; *Angew. Chem. Int. Ed. Engl.*, 1987, **26**, 1255.
402. F. H. Köhler, N. Hertkorn and J. Blumel, *Chem. Ber.*, 1987, **120**, 2081.
403. C. D. Chandler, G. D. Fallon, A. J. Koplick and B. O. West, *Aust. J. Chem.*, 1987, **40**, 1427.
404. R. R. Holmes, C. G. Schmid, V. Chandrasekhar, R. O. Day and J. M. Holmes, *J. Am. Chem. Soc.*, 1987, **109**, 1408.
405. V. Chandrasekhar, C. G. Schmid, S. D. Burton, J. M. Holmes, R. O. Day and R. R. Holmes, *Inorg. Chem.*, 1987, **26**, 1050.
406. V. G. K. Das, L. K. Mun, C. Wie, S. J. Blunden and T. C. W. Mak, *J. Organomet. Chem.*, 1987, **322**, 163.
407. J. M. Fukuto, D. A. Newman and F. R. Jensen, *Organometallics*, 1987, **6**, 415.
408. S. J. Blunden, B. N. Patel, P. J. Smith and B. Sugavanam, *Appl. Organomet. Chem.*, 1987, **1**, 241.
409. L. R. Sherman, M. J. Coyer and F. Huber, *Appl. Organomet Chem.*, 1987, **1**, 355.
410. C. H. Yoder, D. Mokrynka, S. M. Coley, J. C. Otter, R. E. Haines, A. Grushow, L. J. Ansel, J. W. Hovick, J. Mikus, M. A. Shermak and J. N. Spencer, *Organometallics*, 1987, **6**, 1679.
411. O.-S. Jung, J. H. Jeong and Y. S. Sohn, *Polyhedron*, 1989, **8**, 1413.
412. X.-A. Mao, X.-Z. You and A.-B. Dai, *Inorg. Chim. Acta*, 1989, **156**, 177.
413. J. D. Kennedy and W. McFarlane, *J. Chem. Soc. Chem. Commun.*, **1974**, 983.
414. B. Wrackmeyer and K. Horchler, *Magn. Reson. Chem.*, 1990, **28**, 56.
415. M. Herberhold, V. Tröbs and B. Wrackmeyer, *J. Organomet. Chem.*, 1997, **541**, 391.
416. J. D. Kennedy, W. McFarlane and B. Wrackmeyer, *Inorg. Chem.*, 1976, **15**, 1299.

417. J. D. Kennedy, W. McFarlane, G. S. Pyne and B. Wrackmeyer, *J. Chem. Soc. Dalton Trans.*, 1975, 386.
418. V. M. S. Gil and W. von Philipsborn, *Magn. Reson. Chem.*, 1989, **27**, 409.
419. W. McFarlane and D. S. Rycroft, *J. Chem. Soc. Dalton Trans.*, **1974**, 1977.
420. T. P. Lockhart and W. F. Manders, *Inorg. Chem.*, 1986, **25**, 892.
421. T. P. Lockhart, W. F. Manders and F. E. Brinckman, *J. Organomet. Chem.*, 1985, **286**, 153.
422. B. Wrackmeyer, U. Klaus, W. Milius, E. Klaus and T. Schaller, *J. Organomet. Chem.*, 1996, **517**, 235.
423. M. Hüttendorfer, F. Schaper and H. H. Brintzinger, *Angew. Chem.*, 1998, **110**, 2378; *Angew. Chem. Int. Ed. Engl.*, 1998, **37**, 2268.
424. M. Saito, N. Tokitoh and R. Okazaki, *J. Am. Chem. Soc.*, 1997, **115**, 11 124.
425. K. B. Dillon and A. Marshall, *J. Chem. Soc. Dalton Trans.*, **1987**, 315.
426. C. Couret, J. Escudie, J. Satge, A. Rabarinirina and J. D. Andriamizaka, *J. Am. Chem. Soc.*, 1985, **107**, 8281.
427. H. Ranaivonjatovo, J. Escudie, C. Couret and J. Satge, *J. Chem. Soc. Chem. Commun.*, **1992**, 1047.
428. G. Heckmann, H. Binder and D. Bongett, *Magn. Reson. Chem.*, 1998, **36**, 250.
429. D. Bongert, H. D. Hausen, W. Schwarz, G. Heckmann and H. Binder, *Z. Anorg. Allg. Chem.*, 1996, **622**, 1167.
430. B. Wrackmeyer and E. Kupce, ^{15}N NMR of Silicon, Germanium, Tin and Lead-Nitrogen Compounds, in *Topics of Physical Organometallic Chemistry*, Vol. 4 (ed. M. Gielen), pp. 289–352, Freund Publishing House, Tel Aviv, 1992.
431. K. Jurkschat, A. Tzschach, C. Mügge, J. Piret.Meunier, M. van Meerssche, G. van Binst, C. Wynants, M. Gielen and R. Willem, *Organometallics*, 1988, **7**, 593.
432. A. Krebs, A. Jacobsen-Bauer, E. Haupt, M. Veith and V. Huch, *Angew. Chem.*, 1989, **101**, 640.
433. C. Schneider and M. Dräger, *J. Organomet. Chem.*, 1991, **415**, 349.
434. P. Jutzi and R. Dickbreder, *J. Organomet. Chem.*, 1989, **373**, 301.
435. T. N. Mitchell, R. Faust, B. Fabisch and R. Wickenkamp, *Magn. Reson. Chem.*, 1990, **28**, 82.
436. B. D. James, S. Gioskos, S. Chandra, R. J. Magee and J. D. Cashion, *J. Organomet. Chem.*, 1992, **436**, 155.
437. D. Hänssgen, T. Oster, M. Nieger, *J. Organomet. Chem.*, 1996, **526**, 59.

Copper-63 NMR Spectroscopy

JOHN MALITO

Department of Chemistry, Cork Institute of Technology, Rossa Avenue, Bishopstown, Cork, Ireland

ABBREVIATIONS

AcO	acetate
Alk	alkyl group
Ar	aryl group
Bu	butyl group
Bu^t	tertiary butyl group
depe	1,2-*bis*(diethylphosphino)ethane
dmpe	1,2-*bis*(dimethylphosphino)ethane
dppe	1,2-*bis*(diphenylphosphino)ethane
dppm	*bis*(diphenylphosphino)methane
dppp	1,3-*bis*(diphenylphosphino)propane
Et	ethyl group
HB(3,5-R_1, $R_2Pz)_3$	hydrotris(3,5-disubstituted-1-pyrazolyl)borate
Me	methyl group
Ph	phenyl group
Pr	propyl group
Pr^i	isopropyl group

ANNUAL REPORTS ON NMR SPECTROSCOPY
VOLUME 38 ISBN 0-12-505338-X

py	pyridine
R	organic group
tol	tolyl group

1. COPPER-63 NMR

1.1. Introductory remarks

There are several good texts and other reference sources for technical and/or more detailed information related to multinuclear nuclear magnetic resonance,[1–8] but it will be seen that, in general, NMR studies of transition metal nuclei can provide direct information about the metal centre in different physical and chemical environments. Of particular importance are the chemical shift (δ, ppm) which can give some indication of the electronic environment about the metal nucleus; the linewidth (or width at half height, $\Delta\upsilon_{1/2}$, Hz) which can inform about the degree of symmetry of the electric field at the nucleus; and finally, the coupling constants (^nJ, Hz), which, if resolvable, can help to delineate molecular structure and, possibly, intramolecular bonding. For a given nucleus, there are a few nucleus-specific factors which must be considered: resonant frequency and inherent sensitivity, which are ultimately related because they each depend on the magnetogyric ratio (γ, rad T^{-1} s^{-1}); natural abundance, and the nuclear spin, I.

Nuclei with $I = 1/2$ have their positive charge distributed symmetrically within the nucleus, and so, in the first approximation, may be regarded as uniformly charged spheres. When this electric charge is spinning it creates a magnetic field, but because of the prevailing high symmetry, only a simple magnetic dipole positioned along the spin axis can arise. For cases where $I > 1/2$, however, the nuclear charge is distributed nonuniformly. This means the distribution of charge is no longer spherical but ellipsoidal (either flattened or prolate), and since the charge density is uneven, there will be a gradient of charge (or an electric field gradient, EFG) within the nucleus. This, then, is the origin of a quadrupole, and the nucleus will possess a distinct electric quadrupole, moment (Q, m^2) because the quadrupole can interact with any EFG arising from the electric charge distribution within the molecule. This interaction, in turn, provides a means by which the nucleus can exchange energy with the molecule, thereby leading to certain profound NMR effects. A uniform spherical orbital, however, produces zero EFG.

In general, the quadrupole mechanism is a highly effective means of relaxation. The sign of Q relates to the distribution of charge around the nucleus while its magnitude depends upon several factors. Thus, observed relaxation times can vary over a wide range of values. The effects of the quadrupole relaxation mechanism on NMR lineshapes and linewidths have already been treated in appreciative detail.[9–11] A very recent theoretical

study of relaxation times for spin $I = 3/2$ nuclei in the quadrupole nutation NMR experiment has confirmed that they are inversely proportional to the linewidths of the quadrupole nutation NMR spectra.[12] In the end, a useful generalization is that, if the relaxation is fast, then the spectral lines will be broad.[13] Therefore, the relaxation times, T_1 and T_2, for spin–lattice and spin–spin relaxations respectively, can be of very crucial importance as parameters in the NMR study of quadrupolar nuclei.

1.2. Background and parameters

Typically, quadrupole relaxation increases rapidly in effectiveness as Q increases, but it also depends upon the interaction of the electric quadrupole moment with the local EFG. For a fixed value of Q, this interaction is essentially geometry dependent for molecules and other structures, and it can be reduced by the minimalization of the EFG. The latter may be accomplished by situating the quadrupolar nucleus in a cubic environment (of either T_d or O_h symmetry). This will lead to slower relaxation rates and, therefore, narrower spectral lines with resolvable spin–spin coupling, if the latter applies.

Thus, in the case of quadrupolar nuclei like copper, nuclei of free ions and of atoms at the centres of strictly regular tetrahedral molecules formed from a single type of ligand will all possess near-zero electric field gradients. On the other hand, the same quadrupolar nuclei situated in lower symmetry environments, including distorted tetrahedra even when all the ligands are the same, will have much shorter relaxation times. Such distortions, often due to steric effects, are important contributors to electric field gradients. It should be noted that within this context, lone pair electrons are treated as ligands.

Of the 11 isotopes (including nuclear isotopes) of copper, ranging in mass from 58 to 68, two are NMR active, ^{63}Cu and ^{65}Cu, each having spin $I = 3/2$. Their receptivities, or relative sensitivities, relative to either ^{1}H or ^{13}C, are quite similar, as are their quadrupole moments (see Table 1), and they have been described as medium-strength magnetic nuclei.[3] Although the heavier ^{65}Cu has the more favourable Q value, ^{63}Cu is the significantly more naturally abundant isotope. Thus, the latter is usually the isotope of choice for copper NMR spectroscopy. Nonetheless, ^{63}Cu and ^{65}Cu NMR data are often both measured and/or reported in the same study. It might be noted here that exact natural abundance values reported for copper isotopes can be slightly variable either normally, or due to commercial separation.

2. SOLUTION-STATE STUDIES

Although originally the chemical shift reference standards were powdered CuCl, or $K_3[Cu(CN)_4]$ in D_2O,[3] all $^{63,65}Cu$ chemical shifts are now routinely

Table 1. Some key properties of NMR-active copper isotopes.

Property	^{63}Cu	^{65}Cu
Resonance frequency (MHz)	106.02[a]	113.52[a]
	26.505[b]	28.394[b]
Spin	3/2	3/2
Natural abundance (%)	69.09	30.91
Relative sensitivity (^1H = 1.00)	0.0931	0.114
Absolute sensitivity (^1H = 1.00)[c]	0.0643	0.0352
Receptivity (^{13}C = 1.00)	365	201
Quadrupole moment, $Q/10^{-28}$ m^2	−0.211[d]	−0.195[d]
Magnetogyric ratio, $\gamma(\times 10^7 \text{rad T}^{-1}\text{s}^{-1})$	7.0965	7.6018

[a] ^1H resonance frequency = 400 MHz.
[b] ^1H resonance frequency = 100 MHz.
[c] Product of relative sensitivity and natural abundance.
[d] Other values have been given: −0.15 and −0.14[1,3], and −0.16 and −0.15[2], for ^{63}Cu and ^{65}Cu respectively.

reported relative to an external solution of $[Cu(NCMe)_4]X$ (X = BF_4^-, PF_6^- or ClO_4^-) in MeCN (usually 0.1 mmol l^{-1}) at ambient temperatures (≈ 300K). The NMR signal for this solution is assigned a resonance position of exactly 0.00 ppm, and resonances downfield of this signal are given positive chemical shift values. The linewidth for the reference standard, at ambient temperatures, is in the region of 400 Hz. (Alternative reference solutions, or variations, are noted wherever relevant in this review.) Typically, chemical shifts and line-widths which can be measured, are measured to an accuracy of ± 1 ppm and ± 10 Hz respectively. It might be noted that for qualitative discussions, solution-state chemical shifts for quadrupolar nuclei can be rationalized on the basis of a simplified Ramsey expression; in which instance, the electronic and steric properties of ligands signify highly.[14] In any case, discussion of NMR signals for quadrupolar nuclei is often as concerned with linewidths and/or lineshapes as it is with chemical shifts.

Although the natural abundance receptivities for $^{63,65}Cu$ make them each readily more detectable than some other commonly studied nuclei, like ^{35}Cl, prior to 1970 copper resonances were almost exclusively observed only for solid-state samples (*vide infra*). Very few solution studies were carried out, and this was in part due to the poor solubilities (in common solvents) normally displayed by most copper complexes of the T_d symmetry initially required for NMR measurements. Another problem, however, is that four-coordinate species, which normally at least approach cubic symmetry, tend spontaneously to undergo equilibria exchange processes with species of lower symmetry.[15] The presence of co-existent species of different coordination number and/or symmetry will broaden the NMR signals, often beyond reasonable limits of detection. It is quite common therefore for the ligand also

to be used as the solvent in order to achieve saturated solutions, to overcome ligand competition for limited coordination sites, and also to circumvent the known concentration dependence of ^{63}Cu resonances.[15]

Although the two principal oxidation states for copper, Cu(I) and Cu(II), are more or less equally common, solution-state NMR is really only feasible for complexes of the diamagnetic cuprous centre. The two short general review articles which precede the present review, and cover $^{63,65}Cu$ NMR results for both solution- and solid-state systems, will verify this.[16,17]

2.1. Inorganic compounds

Most likely the earliest solution work reported was a study of linewidth measurements of the ^{63}Cu resonance signal in concentrated hydrochloric acid solution containing cuprous and cupric chloride.[18,19] These studies afforded reasonable calculations for the bimolecular rate constant for the equilibrium electron-exchange process (Eq. 1):

$$Cu^{2+} + Cu^{+} = Cu^{+} + Cu^{2+} \tag{1}$$

Other early work involved measurements of a 1.0 mmol l^{-1} solution of $K_3[Cu(CN)_4]$ in D_2O,[20] and for aqueous solutions of Cu(I) cyanides in the presence of excess alkali cyanide. The species $[Cu(CN)_4]^{3-}$ was found to resonate at a frequency 820 ppm higher than that for the powdered CuCl employed as the external reference.[21] In the latter study, signals were only detected when $CN^- : Cu > 4$, and as this ratio was increased the observed linewidths were seen to decrease. The authors concluded that the predominant species in solution, $[Cu(CN)_4]^{3-}$, retains its T_d symmetry and that other lower symmetry species, like $[Cu(CN)_3]^{2-}$ or $[Cu_2(CN)_6]^{4-}$, make little or no contribution to the NMR linewidths. The *in situ* formation of mixed complexes of the type, $[Cu(CN)_3L]^{(2+n)-}$ ($L = Cl^-$, Br^-, I^-, SCN^-, NH_3, $(NH_2)_2CO$ or $(NH_2)_2CS$) (see Eq. 2a) led to significant line broadening, as optimum linewidths as low as 85 Hz were broadened to as high as 5000 Hz. On the basis of the linewidth measurements, it was suggested that the equilibrium constant (Eq. 2b) for the substitution reaction:

$$[Cu(CN)_4]^{3-} + L^{n-} = [Cu(CN)_3L]^{(2+n)-} + CN^- \tag{2a}$$

$$K = \frac{[Cu(CN)_3L]^{(2+n)-}\,[CN^-]}{[Cu(CN)_4]^{3-}\,[L^{n-}]} \tag{2b}$$

increases according to the order, $L = (NH_2)_2CS > SCN^- > I^- \approx NH_3 > Br^- > Cl^- \approx (NH_2)_2CO$.

The above, in conjunction with the earlier observation that CuBr absorbs at

a position 57 ppm to lower frequency of solid CuCl,[22] indicated an inverse halogen dependence, or that δ^{63}Cu is more shielded as $Cl^- > Br^- > [CN]^-$, even though CuI had been observed to absorb 10 ppm to higher frequency of CuCl. The discrepancy was initially ascribed to inherent errors incurred upon dealing with very broad lines.

A solution study of ^{63}Cu NMR signals for several tetrahedrally coordinated Cu(I) complexes as a function of temperature, solvent and counteranion revealed strong dependencies of linewidths and chemical shifts,[23] ultimately ascribed to exchange processes with species of lower symmetry. The concentration dependence of copper NMR spectra was further investigated for mixed crystal systems of $[(CH_3NH_3)_2Cu(Cl_{4-x}Br_x)_4]$ in aqueous solution.[24,25] NMR lines are distinguishable for all species (i.e. $x = 0$–4), but chemical shifts and linewidths are concentration dependent.[25] By comparing the relative intensities of the lines observed for any given sample, composition ratios of the various complexes present in the sample could be determined.[24]

Copper-63 spectra recorded for $[Cu(NCMe)_4]X$ ($X = ClO_4^-$, BF_4^- or PF_6^-) and $[Cu(py)_4]X$ ($X = ClO_4^-$ or BF_4^-) in MeCN at different temperatures and concentrations[15] showed broadening of the spectral lines, concomitant with changes in the chemical shifts, upon lowering of temperature. This indicates equilibria of the higher-symmetry four-coordinate species with at least one other complex of lower symmetry. Preferential solvation of Cu^+ by pyridine over acetonitrile in MeCN/py solvent mixtures was clearly demonstrated.[15] Solvation of $[Cu(NCMe)_4][ClO_4]$[26] and $[Cu(NCPh)_4][ClO_4]$[27] in mixed-solvent systems containing acetonitrile or benzonitrile along with water,[26] propionitrile,[26,27] butyronitrile,[26,27] or valeronitrile[26,27] present as co-solvents, as well as $P(OR)_3$ (R = Me, Et, Bu),[27] was also compared by ^{63}Cu NMR. In the case of the mixed nitrile systems, linewidths and chemical shifts increased almost linearly with increasing co-solvent concentration, indicating no preferential solvation of Cu(I). The authors discuss their results in detail, taking into consideration coupling of the copper nucleus with the nitrile ^{14}N nucleus, differing solvent viscosities, ion-pair influence and the Sternheimer antishielding factor.[28]

For a series of complexes of the type, $[CuL_4][ClO_4]$ (L = NCR, py, RCN, ArCN or CN^-), the ^{63}Cu NMR spectra each show only one signal at ambient temperatures under an applied field of 52.92 MHz (4.7 T).[29] These signals (see Table 2) each correspond to a unique four-coordinate species, and for the entire series, downfield shifting occurs as NCR < py < CN^- ~ RNC < ArNC, in agreement with the commonly suggested order for increasing ligand π-acceptor capabilities. Sharp ^{63}Cu lines were also observed at room temperature, in spite of C_3 symmetry, for a series of Cu(I) species having the general structure, $[CuL_3L']$. These carbonyl complexes, $[L^{R1,R2}Cu(CO)]$, contain substituted hydrotris(pyrazolyl)borate ligands, where R1 and R2 in L are substituents at the 3- and 5-positions of the pyrazole ring respectively.[30] NMR signals were observed over the shift range, 580–730 ppm, and complexes with

R1, R2 = Me, Me; Pr^i, Pr^i; Bu^t, Me; and Bu^t, Pr^i were observed at lower field than those with aromatic derivatives, R1, R2 = Ph, Pr^i and Ph, Ph (see Table 2). Overall, the chemical shifts reflect the relative electron density at the copper centre, and correlate well with CO stretching vibrations. That is, δ^{63}Cu moves to lower field as υ(CO) increases. Previous attempts to observe trigonal geometries were either unsuccessful[31,32] or gave spectra with very broad lines.[33]

Copper NMR spectra have also been recorded for complexes containing group 15 ligands with donor atoms other than nitrogen. Coupling between ^{63}Cu and ^{31}P was first observed for the tetrahedral complex, $[Cu\{P(OMe)_3\}_4]^+$, formed from CuI dissolved in $P(OMe)_3$.[34] Although linewidths for the quintet observed are on the order of 200 Hz, the quite large ^1J (^{63}Cu–^{31}P) value of 1210 ± 10 Hz is an unequivocal one. The same authors found that the temperature dependence for the central line was 0.055 ppm K^{-1}, 1–2 orders of magnitude less than those for ^{59}Co, ^{103}Rh or ^{195}Pt. This is as expected because the d^{10} ion has no ligand–field transitions to affect the paramagnetic term of the Ramsey expression. Other early examples include the phosphites, phosphonites and phosphinites, $[Cu\{P(OR)_{3-n}R'_n\}]^+$ (n = 0–2)[31,35] and ^{65}Cu NMR for $[Cu(Ph_2PCH_2CH_2PEt_2)_2]Cl$ in CD_2Cl_2 ($\Delta\upsilon_{1/2}$ = 5000 Hz).[36]

More recent studies have reported chemical shifts for $[Cu(dmpe)_2]_2[BF_4]_2$, for which variable temperature ^{63}Cu NMR indicated no dimer–monomer rapid equilibrium, suggesting that the dimer remains intact in solution,[37] for complexes of the types $[CuL_4][BF_4]$ and $[Cu(L\text{-}L)_2][BF_4]$ (L = PMe_3, $AsMe_3$, $SbMe_3$, $SbEt_3$, $SbPh_3$; L-L = $Me_2Sb(CH_2)_3SbMe_2$, $Ph_2Sb(CH_2)_3SbPh_2$),[38] and for $[CuL_4]Y$ (L = PMe_3, PMe_2Ph, $PMePh_2$, PPh_3, PPh_2H, $PPhH_2$, $AsMe_3$, $AsMe_2Ph$, $AsMePh_2$, $AsPh_3$, $SbMe_3$, $SbEt_3$ or $SbPh_3$; L-L = $Me_2P(CH_2)_2PMe_2$, o-$C_6H_4(PMe_2)_2$, $Ph_2P(CH_2)_nPPh_2$ (n = 1–4), *cis*-$Ph_2PCH{=}CHPPh_2$, o-$C_6H_4(PPh_2)_2$, o-$C_6H_4(AsMe_2)_2$, *cis*-$Ph_2AsCH{=}CHAsPh_2$, o-$C_6H_4(SbMe_2)_2$; Y = PF_6^- of BF_4^-).[39]

Quite detailed multinuclear (including ^{63}Cu) and variable temperature NMR studies have been reported for the Group 16 donor atom complexes, $[Cu(R_2E)_4]$ $[O_3SCF_3]$ and $[Cu\{RE(CH_2)_nER\}_2][PF_6]$ (R = Me or Ph; E = S, Se or Te; n = 2 or 3).[40] Homoleptic Cu(I) complexes of the type $[Cu\{(o\text{-}C_6H_4(EMe)_2\}_2]$ $[PF_6]$ (E = S, Se or Te) were also characterized by several methods including ^{63}Cu NMR and x-ray crystallography which showed them to be of trigonal geometry.[41] Only the E = Te species (see Fig. 1) exhibited a ^{63}Cu resonance over the temperature range 180–300K (see Table 2).

2.2. Organometallic compounds

The study of purely organometallic compounds using ^{63}Cu NMR has been extremely limited. However, because copper metal and/or ions can activate organic molecules, an *in situ* copper-63 NMR study was undertaken to

Table 2. Solution-state ^{63}Cu NMR data for some selected Cu(I) complexes.[a]

Compound	Solvent	δ ^{63}Cu (ppm)	$\Delta\nu_{1/2}$ (Hz)	Ref.
$[Cu(NCMe)_4][ClO_4]$	MeCN	0.0	500	29
		0.0	480	27
$[Cu(NCMe)_4][PF_6]$	MeCN	0.0	400	33
		0.0	540	16
$[Cu(NCMe)_4][BF_4]$	MeCN	0.0	8570	42
$[Cu(C_2H_5CN)_4][ClO_4]$	C_2H_5CN	13[b]	950	29
$[Cu(4\text{-Me-py})_4][ClO_4]$	4-Me-py	100[b]	2440	29
$[Cu(3\text{-Me-py})_4][ClO_4]$	3-Me-py	108[b]	2830	29
$[Cu(py)_4][ClO_4]$	py	110[b]	1100	29
		111[b]	1560	27
$[Cu(CN)_4][ClO_4]$	H_2O	499[b]	940	29
$[Cu(C_4H_9NC)_4][ClO_4]$	C_4H_9NC	451[b]	4000	29
$[Cu(C_6H_{11}NC)_4][ClO_4]$	$C_6H_{11}NC$	468[b]	880	29
$[Cu(4\text{-}CH_3C_6H_4NC)_4][ClO_4]$	$4\text{-}CH_3C_6H_4NC$	547[b]	320	29
$[Cu(C_6H_5NC)_4][ClO_4]$	C_6H_5NC	549[b]	300	29
		–	690	27
$[Cu(4\text{-}ClC_6H_4NC)_4][ClO_4]$	CH_2Cl_2	553[b]	230	29
$L^{Me,Me}CuCO$[f]	toluene	716	110	30
$L^{Pr^i,Pr^i}CuCO$[f]	toluene	730	205	30
$L^{Bu^t,Me}CuCO$[f]	toluene	700	70	30
$L^{Bu^t,Pr^i}CuCO$[f]	toluene	703	75	30
$L^{Ph,Pr^i}CuCO$[f]	toluene	603	2900	30
$L^{Ph,Ph}CuCO$[f]	toluene	585	4200	30
$[Cu(^{13}CO)O\text{-}Bu^t]_4$	C_6D_6	49		33
$[Cu(P(OMe)_3)_4][ClO_4]$	PhCN	82.6[b,g]	130	27
$[Cu(P(OMe)_3)_4][BF_4]$	MeCN	82	166	31
$[Cu(P(OEt)_3)_4][BF_4]$	MeCN	86[e]	137	42
$[Cu(P(OEt)_3)_4][ClO_4]$	PhCN	90.7[b,h]	150	27
	MeCN	88	137	31
$[Cu(P(OBu)_3)_4][ClO_4]$	PhCN	91.3[b,i]	350	27
$[Cu(PMe_3)_4][BF_4]$	CH_2Cl_2/CD_2Cl_2[k]	286[j]	–	38
$[Cu(PMe_3)_4][PF_6]$	CH_2Cl_2/CD_2Cl_2[k]	287[l]	–	39
$[Cu(PMe_2Ph)_4][ClO_4]$	MeCN	247	2750	31
$[Cu(PMe_2Ph)_4][PF_6]$	CH_2Cl_2/CD_2Cl_2[k]	265[m]	–	39
$[Cu(PMePh_2)_4][BF_4]$	CH_2Cl_2/CD_2Cl_2[k]	192	6300[n]	39
$[Cu(PPh_2H)_4][PF_6]$	CH_2Cl_2/CD_2Cl_2[k]	234[o]	–	39
$[Cu(PPhH_2)_4][PF_6]$	CH_2Cl_2/CD_2Cl_2[k]	250[p]	–	39
$[Cu(dmpe)_2][PF_6]$	CH_2Cl_2/CD_2Cl_2[k]	194[q]	–	39
$[Cu(dppe)_2][PF_6]$	CH_2Cl_2/CD_2Cl_2[k]	150	3000	39
$[Cu(dppp)_2][PF_6]$	CH_2Cl_2/CD_2Cl_2[k]	231	~4000	39
$[Cu(Ph_2PCH{=}CHPPh_2)_2][PF_6]$	CH_2Cl_2/CD_2Cl_2[k]	126	3000	39
$[Cu\{o\text{-}C_6H_4(PMe_2)_2\}_2][PF_6]$	CH_2Cl_2/CD_2Cl_2[k]	210[p]	–	39
$[Cu(dmpe)_2]_2[BF_4]_2$	CD_3OD/CD_2Cl_2[c]	186.7[d]	–	37
$[Cu(AsMe_3)_4][BF_4]$	CH_2Cl_2/CD_2Cl_2[k]	20	6000	38
$[Cu(AsMe_3)_4][PF_6]$	CH_2Cl_2/CD_2Cl_2[k]	20	700	39
$[Cu(AsMe_2Ph)_4][PF_6]$	CH_2Cl_2/CD_2Cl_2[k]	−17	1500	39
$[Cu(AsMePh_2)_4][PF_6]$	CH_2Cl_2/CD_2Cl_2[k]	−62	1200	39

Table 2. *(continued)*

Compound	Solvent	δ ^{63}Cu (ppm)	$\Delta\upsilon_{1/2}$ (Hz)	Ref.
$[Cu(AsPh_3)_4][PF_6]$	CH_2Cl_2/CD_2Cl_2[k]	−153	4000	39
$[Cu(Ph_2AsCH{=}CHAsPh_2)_2][PF_6]$	CH_2Cl_2/CD_2Cl_2[k]	−148	–	39
$[Cu\{o\text{-}C_6H_4(AsMe_2)_2\}_2][PF_6]$	CH_2Cl_2/CD_2Cl_2[k]	−63	1600	39
$[Cu(SbMe_3)_4][BF_4]$	CH_2Cl_2/CD_2Cl_2[k]	−6	180	38
$[Cu(SbEt_3)_4][BF_4]$	CH_2Cl_2/CD_2Cl_2[k]	1	680	38
$[Cu(SbPh_3)_4][BF_4]$	CH_2Cl_2/CD_2Cl_2[k]	−249	250	38
$[Cu(SbPh_3)_4][PF_6]$	CH_2Cl_2/CD_2Cl_2[k]	−245	160	39
$[Cu(Me_2Sb(CH_2)_3SbMe_2)_2][BF_4]$	CH_2Cl_2/CD_2Cl_2[k]	−167	390	38
$[Cu(Ph_2Sb(CH_2)_3SbPh_2)_2][BF_4]$	CH_2Cl_2/CD_2Cl_2[k]	−197	1250	38
$[Cu\{o\text{-}C_6H_4(SbMe_2)_2\}_2][PF_6]$	CH_2Cl_2/CD_2Cl_2[k]	−179	700	39
$[Cu\{o\text{-}C_6H_4(TeMe)_2\}_2][PF_6]$	CH_2Cl_2/CD_2Cl_2[k]	−109	4500	41
$[Cu(Me_2S)_4][O_3SCF_3]$	$Me_2CO/(CD_3)_2CO$[k]	80	2500	40
$[Cu(Me_2Se)_4][O_3SCF_3]$	$Me_2CO/(CD_3)_2CO$[k]	−56	1500	40
$[Cu(Me_2Te)_4][O_3SCF_3]$	$Me_2CO/(CD_3)_2CO$[k]	−56	600	40
$[Cu(Ph_2Te)_4][O_3SCF_3]$	$Me_2CO/(CD_3)_2CO$[k]	−153	3400	40
$[Cu\{MeS(CH_2)_3SMe\}_2][PF_6]$	$MeCN/CD_3CN$[k]	75	1000	40
$[Cu\{MeSe(CH_2)_3SeMe\}_2][PF_6]$	$MeCN/CD_3CN$[k]	21	1500	40
$[Cu\{PhSe(CH_2)_3SePh\}_2][PF_6]$	$MeCN/CD_3CN$[k]	18	1500	40
$[Cu\{MeTe(CH_2)_3TeMe\}_2][PF_6]$	$MeCN/CD_3CN$[k]	21	1500	40
$[Cu\{PhTe(CH_2)_3TePh\}_2][PF_6]$	CH_2Cl_2/CD_2Cl_2[k]	−36[r]	6000	40

[a] Measured for saturated solutions at ambient temperatures (~283–300K) relative to 0.1 mmol l^{-1} $[Cu(NCMe)_4][ClO_4]$ in MeCN unless otherwise noted.
[b] Shifts are relative to a 0.05 mmol l^{-1} $[Cu(NCMe)_4][ClO_4]$ in MeCN.
[c] 50 : 50 solvent mixture.
[d] 1 : 4 : 6 : 4 : 1 quintet, $^1J(^{63}Cu\text{–}^{31}P) = 800 \pm 10$ Hz.
[e] $^1J(^{63}Cu\text{–}^{31}P) = 1208$ Hz.
[f] L = hydrotris(pyrazoyl)borate substituted in the 3- and 5-positions of the pyrazolyl ring.
[g] $^1J(^{63}Cu\text{–}^{31}P) = 1220$ Hz.
[h] $^1J(^{63}Cu\text{–}^{31}P) = 1211$ Hz.
[i] $^1J(^{63}Cu\text{–}^{31}P) = 1215$ Hz.
[j] $^1J(^{63}Cu\text{–}^{31}P) = 790$ Hz; $^1J(^{65}Cu\text{–}^{31}P) = 830$ Hz.
[k] 95 : 5 solvent mixture.
[l] $^1J(^{63}Cu\text{–}^{31}P) = 796$ Hz; from ^{31}P NMR spectrum, $^1J(^{65}Cu\text{–}^{31}P) = 830$ Hz.
[m] $^1J(^{63}Cu\text{–}^{31}P) = 785$ Hz.
[n] At 183K.
[o] Ill-defined coupling, $^1J(^{63}Cu\text{–}^{31}P) \approx 750$ Hz.
[p] $^1J(^{63}Cu\text{–}^{31}P) = 800$ Hz.
[q] $^1J(^{63}Cu\text{–}^{31}P) = 805$ Hz.
[r] At 273K.

investigate the interaction between the Cu nucleus in $[Cu(NCMe)_4][BF_4]$ and some 2-bromoarylazo molecules in acetonitrile solution.[42] Specifically, the authors were interested in the copper-assisted nucleophilic substitution of aryl halides by cyanide and dialkylphosphonate, intermediate species of which they had not been able to isolate. The spectra observed were single lines with

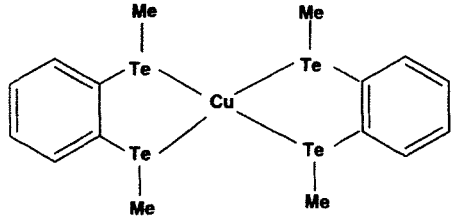

Fig. 1. Skeletal structure for $[Cu\{o\text{-}C_6H_4(TeMe)_2\}_2]^+$ which has been shown by X-ray crystallography[41] to adopt a *meso* configuration, but one that deviates significantly from ideal tetrahedral geometry.

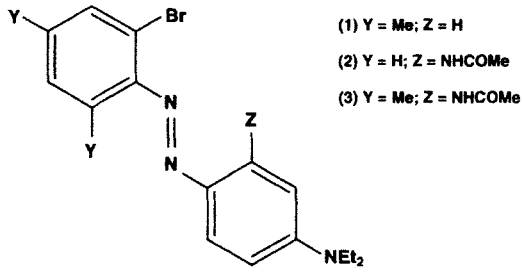

Fig. 2. The skeletal structure for some substituted diarylazo ligands.

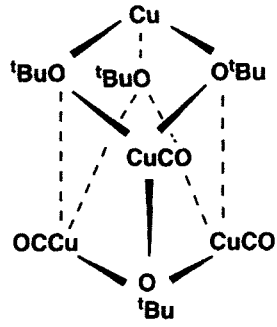

Fig. 3. Idealized structure for $[Cu(CO)O\text{-}Bu^t]_4$. X-ray data indicate trigonally distorted tetrahedral geometry.[33]

$\Delta\nu_{1/2}$ values on the order of 9600 Hz, and chemical shifts of 12, 17 and 18 ppm for reactions with ligands 1, 2 and 3 respectively (see Fig. 2). No reaction was observed to occur with either benzene or N,N-diethylaniline on the basis of NMR tube experiments.

Carbonylation of planar $[CuO\text{-}Bu^t]_4$ yields $[Cu(CO)O\text{-}Bu^t]_4$ which is shown by x-ray crystallography to have a Cu_4O_4 core of cubane form, with each copper exhibiting a trigonally distorted tetrahedral geometry (see Fig. 3). The

^{63}Cu NMR spectrum, probably the first ever observed for a copper complex lacking rigorous T_d symmetry, for a sample of the carbonylation product prepared with 99% ^{13}C-enriched CO shows a single broad and unstructured resonance at ambient temperatures. At 60°C, however, there is an upfield shift, from 49 to 40.2 ppm, and the relaxation rate is sufficiently slowed to allow resolution of a doublet with ^1J (^{63}Cu–^{13}C) = 800 Hz, indicating that the tetramer dissolves without fragmenting or otherwise breaking down even at relatively high temperatures.[33]

3. SOLID-STATE STUDIES

Solid-state NMR has proven very useful in the study of copper-based materials, and although there have not yet been any review articles dealing specifically with solid-state copper NMR, there have been several detailed reviews of the technique in general for quadrupolar nuclei.[43–46] Furthermore, a very recent paper[47] describes a newer and more efficient way of performing numerical calculations of the dynamics of nuclear spin systems in magic-angle spinning (MAS) NMR experiments based on time domain integration. A more general, yet very comprehensive, treatment of MAS NMR appeared several years ago.[48]

3.1. Nuclear quadrupole resonance

Closely related to the NMR of quadrupolar nuclei, and often included within the same studies, are both the Knight shift and nuclear quadrupole resonance spectroscopy, NQR. The latter technique does not necessarily require an external magnet, although it is based on the measurement of transitions between allowed orientations of the quadrupole upon application of appropriate amounts of energy. That is, individual nuclear orientations constitute different energy levels, and active nuclei can interact with the electric field gradients which are already present in the molecule. NQR spectroscopy is especially useful for structural, bonding and EFG studies. For example, electric field gradients at ^{63}Cu in Cu_2O and CuO were measured as a function of pressure by using the NQR frequency.[49] The authors suggest that similar measurements, at easily accessible pressures, can be made for high Tc superconductors (*vide infra*). Other NQR studies of some relevance to topics in this review include an outline of broadband excitation sequences for NQR spectroscopy for $I = 3/2$ nuclei,[50] an effective multinuclear investigation of cation diffusion in $CuGaBr_4$,[51] and the calculation of ^{63}Cu NQR frequencies in $CuGeO_3$[52] which might be compared to an in-depth ^{63,65}Cu NMR study carried out for the same compound.[53]

NQR spectroscopy has proven very useful in studies of lower than cubic

symmetry coordination species which cannot be observed in the solution state. Species such as $[CuX\{P(C_6H_4\text{-}oMeO)_3\}]_2$ (X = Cl or Br),[54] $[Cu_2X_2(PPh_3)_3]$ (X = Cl, Br or I),[55,56] $[\{CuX(PPh_3)\}_4] \cdot 2CHCl_3$ (X = Br or I)[56] and $[L_3Cu_2X_2]$ (L = $P(C_6H_4\text{-}oMeO)_3$ or P(*p*-tolyl)$_3$; X = Cl or Br)[57] have been studied in this way. Some ^{63}Cu NQR data have also been reported for systems containing substituted pyridines[58–60] and thiones.[61] Very recently ^{63}Cu NQR spectra were also reported for five three-coordinate Cu(I) complexes containing isocyanide ligands.[62] Based upon the comparison of the spectra of these isocyanide complexes to those for others of similar geometry, the authors determined that partial coupling constants for isocyanide ligands are much higher than those for any other ligands thus far studied. They suggest that the order for donor atom partial field gradients for terminal ligands is: $C > N > Cl > P \approx S \approx Br > I > O$.

3.2. Inorganic and organometallic compounds

The earliest solid-state studies included ^{63,65}Cu NMR measurements for $K_3[Cu(CN)_4]$[63] and for CuX (X = Cl, Br, I).[64–66] The ^{63}Cu chemical shifts measured for these Cu(I) salts, and the trends observed, were later found to be in contradiction to expectations based on theoretical calculations of ionicity,[67] and the authors in this case rationalized the apparent aberration by taking into account the differing π-bonding abilities of the halides. Another study to determine the same chemical shifts, but in terms of ionic radii and electronegativities, and by CP/MAS ^{63,65}Cu at 294K took into account: (i) nearest-neighbour interactions; (ii) next-nearest-neighbour interactions; (iii) isolation effects; and (iv) covalency effects.[68] In this particular study, negative temperature effects were observed for static samples, and were interpreted in terms of lattice vibrations, lattice expansion and cation motion.

Spin lattice measurements for ^{63}Cu and ^{65}Cu were made over the temperature range, 78–300K, for cuprous halides having the zinc blende structure.[69,70] Ratios determined for the T_1 values for the two isotopes were found to be in good agreement with the inverse squares of their respective quadrupole moments. Continuous-wave NMR measurements in the temperature range, 77–600K, of CuCl, CuI and $CuRh_2Se_4$ were used to determine the ratio $^{63}\gamma/^{65}\gamma = 0.9335232(6)$.[71]

An investigation of the effects of different spinning rates on ^{63,65}Cu NMR for the cuprous halides[72,73] showed that with faster spinning the isotropic peak positions shifted towards lower frequencies, and that these shifts occur in the order, $X = Cl^- < Br^- < I^-$. Furthermore, complementary ^{79}Br and ^{127}I NMR spectra showed that the shifts due to changes in spinning rates for the halogen signals are of comparable magnitudes but in opposite directions. Overall, magnitudes for the spinning-induced shifts were found to be proportional to the square of the spinning rate, but also to the strength of

the magnetic field. It was proposed that these shifts may have their origin in the Lorentz force acting on Cu^+ ions being forced to move in a strong magnetic field.[73]

Mixed $[CuBr_xI_{4-x}]$ crystals have also been examined by solid-state NMR,[74] and the broad spectra observed appear to correspond with overlapping peaks of $[CuBr_4]$, $[CuBr_3I]$, $[CuBr_2I_2]$, $[CuBrI_3]$ and $[CuI_4]$. The various symmetries (T_d, C_1, C_{2v} and C_{3v}) are invoked to explain the range observed for the quadrupolar coupling tensors. Signals in the core–shell-type crystal, however, were sharp and obtained over a range of chemical shifts between limits set by those for CuI and CuBr. Copper-63 NMR spectra recorded for dimeric $[Cu(AcO)_2]_2 \cdot H_2O$ over a temperature range of 20–60°C[75,76] afforded one of the first observations of indirect nuclear spin coupling as a quartet with spacings of 9.6 G was observed. An electric quadrupole coupling tensor of 117 MHz and asymmetry parameter of 2.8% were also calculated.

The NMR data for tetragonal single crystals of $[CuAlX_4]$ (X = Cl, Br) were found to be consistent with data from x-ray powder diffraction and other structural measurements.[77] The quadrupole coupling constants were determined to be 0.89 and 0.35 MHz for the chloro- and bromo-species respectively. Observed temperature-dependent behaviour of linewidths and lineshapes confirmed a suspected diffusion of the Cu^+ ion. The activation energies measured for the diffusion process were 48.5 and 46.4 kJ mol^{-1} for the chloro- and bromo-species respectively. Diffusion of Cu^+ was also found to affect the T_1 values for both the ^{35}Cl and ^{81}Br NQR signals. Related systems which had been studied earlier include $[CuCsCl_3]$,[78] $[Cu_2HgI_4]$[79] and $[CuInX_2]$ (X = S, Se, Te).[80]

Copper-63 NMR/NQR spectra for CuS, from 4.2K up to ambient temperatures, show two distinct lines based on the abrupt change in the spectrum at 55K. This is ascribed to a structural phase transition for both the powder and the oriented CuS.[81] A more recent study of powdered samples at temperatures as low as 1.5K under a magnetic field of 6.5 T revealed more detail.[82] An intense resonance with satellites was observed at all temperatures up to the ambient. This peak consisted of two resonance lines above 60K and four lines below 50K. The splittings observed correspond to crystal distortions below 55K. The central peaks with satellites were assigned to the metallic Cu(1) and Cu(2) in the crystal structure of CuS, for which spin–lattice relaxation times of 4 ms and 55 ms, respectively, were measured at 15K. The authors suggest that the anomalously short T_1 for Cu(1) is indicative of the metallic character in the plane formed by Cu(1)–S bonds.

Finally, ^{31}P CP/MAS spectra for $[CuS_2CPh(PPh_3)_2]$, $[\{CuS_2C\text{-}Ptol\}_4(PPh_3)_2]$, $[\{CuS_2C\text{-}Ph\}_4(PPh_3)_2]$, $[CuS_2C\text{-}Ph(dppm)]_2$, and $[CuO_2C\text{-}Ph(dppm)]_2$, consisting of distorted quartets due to the magnetically non-equivalent P atoms, have allowed for the approximation of spin–spin coupling values for ^{63}Cu with ^{31}P,[83] indicative of the covalency of the dithiocarboxylate–Cu bonding. Spacing distortions, related to a number of molecular and structural parameters, were

employed to estimate the ^{63}Cu quadrupole coupling constant which was found to be smaller for the higher-symmetry species.[83]

3.3. Pure metal

Knight shifts have been measured for ^{63}Cu and ^{65}Cu in metallic copper.[84,85] NMR techniques have been used for the determination of electric field gradients in relation to point defects in metallic copper.[86] Copper-65 NMR and ^{65}Cu–^{27}Al spin-echo, double-resonance measurements from Cu-exchanged ZSM-5 catalysts have shown the presence of Cu^+ cations. Upon heating, auto-reduction of Cu^{2+} to Cu^+ was observed, with further reduction to the metal upon exposure to CO at high temperatures.[87] Copper NMR was used to investigate the nanostructure of .../Cu/CO/Cu... layers which had been prepared by different methods.[88]

Spectra have been measured for small copper particles (< 50 Å) at low temperatures (< 1.5K) and high magnetic field (13 T) as part of a study of the size-dependent electronic structure of small solids.[89] The linewidths observed are very large (100–700 kHz) and may have a magnetic origin intimately connected with the particle size distribution. The linewidths also appear to correlate with T_2 values, which become larger as the particle size diminishes. Other trends in NMR line shapes for nanoparticles of various metals, including copper, have also been analysed.[90] The different electronic environments seen by each magnetic nucleus produces a distribution of Knight shifts of the NMR frequencies such that an inhomogeneously broadened lineshape results. The latter are ultimately appreciated on the basis of some simple LCAO models. Copper-63 linewidth measurements were also used to investigate adsorbed states of hydrogen on Cu surfaces in fine copper powder.[91] The results indicate that the adsorbed states in the powder are the same as in the bulk metal.

3.4. Alloys and other metallic compounds

Spin–lattice relaxation has been studied by ^{63}Cu NMR for dilute Cu–Mn and Cu–Cr alloys at temperatures of 0.32–20K[92] while the NMR lines in deformed Cu alloys with Si, Al and Ga were investigated as a function of plastic deformation.[93] Variations in ^{63}Cu Knight shifts in Cu–Zn alloys have been reported.[94] Spectra from NMR experiments performed on binary Cu–Au ordered alloys and martensitic ternary Au–Cu–Zn alloys in order to study crystallographic Cu sites microscopically[95] have revealed different distributions of Cu atoms that change appreciably with Cu content.

The ^{63}Cu nuclear relaxation rates in Cu–Mn and Cu–Au fine particles of mean diameter 60 Å have been measured, and rate suppression, due to level

quantization of conduction electrons, is eliminated by spin-orbit scattering from Mn impurities but not from Au impurities.[96] For the Cu layers of Fe/Cu multilayers, the existence and distribution of an induced spin polarization of the conduction electrons in the Cu layers are indicated. Fine structure associated with the spin-echo signals of ^{63,65}Cu nuclei shows that the spin polarization and an associated field oscillate in sign.[97]

Copper NMR was used to gauge the quality of [Ni/Cu][98–100] and [Co/Cu][99] superlattices synthesized by the ion sputtering method. The authors noted that the shapes of the spectra vary noticeably with the change in angle between the interface planes and the external field. This is a unique feature of superlattice systems, not observed in bulk metals, and which can offer information on the electronic states in the copper layers. A study of $CuAl_2$ by ^{27}Al and ^{63,65}Cu NMR investigated quadrupole and anisotropic shift interactions between 3 and 40 MHz.[101]

3.5. Other materials

A copper NMR study using the spin-echo technique has been used to look at Cu–Mn–Fe spin glasses.[102] A combination of ^{63,65}Cu and ^{91}Zr NMR measurements for the metallic glass $Zr_xCu_{1-x}CO$ ($0.38 \leq x \leq 0.72$), in conjunction with magnetic determinations, has shown that the d-electron density of states increases with increasing value of x.[103] Temperature and compositional dependences of T_1 and T_2 in ^{63}Cu NMR were determined and then used to investigate the possible atomic diffusion of copper in glassy Cu–As–Se.[104] Below 300K a weak temperature dependence was observed for T_1, and for temperatures higher than 300K, sharp declines were observed for both T_1 and T_2, suggesting that the relaxation processes at higher temperatures are dominated by an inhomogeneous diffusion of copper atoms. The authors were able to fit the magnetization recovery curves to an equation for a well-defined stretched exponential.

Some ^{63}Cu NMR studies have been carried out for the organic conductors $(DMe\text{-}DCNQI)_2Cu$, $(DMeO\text{-}DCNQI)_2Cu$, $(DBr\text{-}DCNQI)_2Cu$ and partially deuterated $(DMe\text{-}DCNQI\text{-}d_2[1, 1:0])_2Cu$.[105–107] The results show that the metallic and insulating states each possess similar electronic and magnetic properties. A systematic measurement of $(1/T_1)$ for ^{63}Cu failed to identify any specific effect of d-electron correlations near the metal–insulator (Cu-I) boundary.

4. SUPERCONDUCTING MATERIALS

Copper NMR and NQR have been employed extensively over the past five years in the study of superconducting cuprates and related materials. In fact,

all that can be really presented here is a brief overview to supply leading references to the most recent literature.

In simplest terms, then, superconductivity can occur in many metals, alloys and intermetallic compounds. If these substances are cooled below a certain transition temperature, Tc, their electrical resistances vanish. Typically, the transition temperature is close to absolute zero, but the system, $HgBa_2Ca_2Cu_3O_{8+d}$, has Tc = 133K, which, to date, appears to be the highest observed transition temperature. ^{63}Cu NMR studies of spin-lattice relaxation, $(1/T_1)$, were carried out in order to investigate this phenomenon.[108,109] Several other NMR studies have also been reported for this material[110] and the related material, $HgBa_2CuO_{4+d}$.[111–113] For copper-based superconductors in general, there have been a number of relevant, physical, theoretical and/or application studies[114–117] and several reviews specifically for the ^{63,65}Cu NMR/NQR of high Tc superconductors.[118–124] One review[125] covers similar ground for cuprates ranging from the antiferromagnetic to the superconducting states. Other reviews have covered the use of copper NMR in conjunction with other techniques like neutron scattering[126] and microwave absorption.[127]

An important family of cuprate superconductors is the YBCO family. NMR/NQR studies of $YBa_2Cu_3O_{7-x}$[128,129] and $YBa_2Cu_4O_8$[130,131] with emphases on different aspects have been reviewed, as has the charge differentiation of inequivalent copper sites of $YBa_2Cu_3O_y$ $(6.0 \leq y \leq 6.91)$ by NMR/NQR.[132] More recently there has been a review of NMR/NQR spectra and spin–lattice relaxation measurements for crystals of this material, as well as other YBCO-type superconductors.[133] The reviewers have attempted to derive some insights into the correlation and spin dynamics of Cu^{2+} ions, and the microscopic mechanisms of high-Tc superconductors. Another report which appeared at about the same time was devoted solely to NQR experiments.[134] A review for ^{63}Cu/^{17}O NMR studies of $YBa_2Cu_3O_7$ and $YBa_2Cu_3O_{6.63}$ revealed some temperature-dependent antiferromagnetic Cu spin correlations and a spin gap behaviour in the reduced oxygen material.[135] Each of these phenomena now appears to be a general property for many high-Tc cuprates. Other multinuclear NMR/NQR investigations, particularly of $YBa_2Cu_3O_7$ and $YBa_2Cu_4O_8$, have also been reviewed,[136] with emphases on EFG temperature and pressure dependencies, Tc enhancement by Ca doping, and Knight shifts for Cu and O nuclei.

Copper NQR has demonstrated that in the family $Y_{1-x}Ca_xBa_2Cu_3O_6$, superconductors are highly two-dimensional and quite different in electronic structures from the $YBa_2Cu_3O_{6+x}$ family.[137] A more recent NQR study of $YBa_2Cu_3O_{6.95}$, before and after electron irradiation at 2.76 MeV, as well as after annealing at several temperatures up to 440K, has indicated a decrease in Tc from 91.8K to 89.5K after irradiation.[138] The results are explained in terms of a displacement of the O(4) atoms in the Cu–O chains that results in a modification of the Cu(2) atoms in the plane. Recovery of the radiation damage sets in during annealing at 300K but is incomplete at 440K.

Within the last three years there has been a large number of other reports of NQR[139–141] and NMR/NQR studies of YBCO systems,[142–151] and other copper-based systems like $Sr_{14}Cu_{24}O_{41}$,[152–154] $Sr_{14-x}Ca_xCu_{24}O_{41}$,[155–157] $La_{2-x}Sr_xCuO_4$,[158–163] $La_2Cu_{1-x}Zn_xO_4$[164] and $Tl_2Ba_2Ca_2Cu_3O_{10}$,[165–168] but to go into more detail here would be well outside the scope of the present review.

5. CONCLUDING REMARKS

Solution-state copper NMR studies have been relatively limited in number, but it is clear that the copper species being investigated must be of high enough symmetry to slow down relaxation rates sufficiently to allow enough narrowing of the NMR lines for observation. Of the Cu(I) species observed, most with pseudo-tetrahedral but some with trigonal geometry, trends for the ^{63}Cu resonances appear to be a deshielding and a line broadening with increasing π-acceptor capability of ligand (see Table 2). For a homologous series, ligand substituent effects (steric and electronic) on metal–ligand bonding can be inferred from the ^{63}Cu NMR spectra, via analysis of either chemical shift or linewidth values. The overall range of ^{63}Cu chemical shifts, of $\sim$ 980 ppm (see Fig. 4), is indicative of satisfactory sensitivity to the metal–ligand bonding in spite of the closed d-shell system.

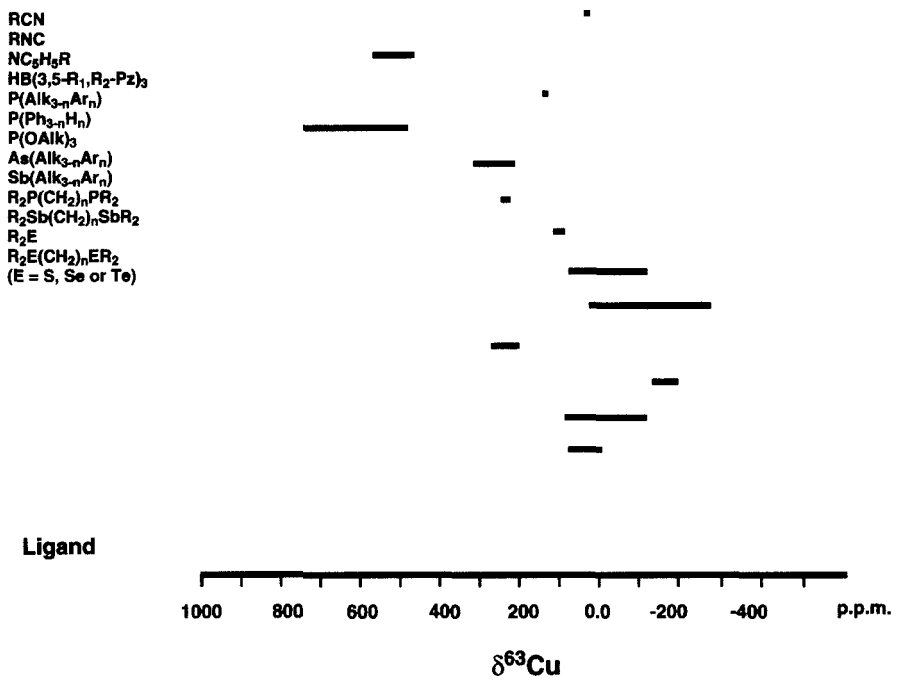

Fig. 4. The ^{63}Cu chemical shift range by ligand type.

In general, for solution studies, copper NMR seems to be of use primarily as a supporting technique. This is less true for the case of solid-state samples, where both Cu(I) and Cu(II) species can be observed, in conjunction with measurements of Knight shifts, copper NQR and/or NMR/NQR spectroscopy of some of the other nuclei present in the system. The vast majority of copper NMR reports over the last five years have dealt with solid-state studies of copper materials, especially those materials recognized as superconductors.

REFERENCES

1. F. A. Bovey, *Nuclear Magnetic Resonance Spectroscopy.* Academic Press, New York, 1969.
2. E. D. Becker, *High Resolution NMR: Theory and Applications.* Academic Press, London and New York, 1969.
3. R. K. Harris and B. E. Mann, *NMR and the Periodic Table.* Academic Press, London and New York, 1978.
4. C. Brevard and P. Granger, *Handbook of Higher Resolution Multinuclear NMR.* Wiley, New York, 1981.
5. P. Laszlo (ed.), *NMR of Newly Accessible Nuclei.* Academic Press, London and New York, 1983.
6. W. Kemp, *NMR in Chemistry: A Multinuclear Introduction.* MacMillan Education Ltd, London, 1986.
7. J. Mason (ed.), *Multinuclear NMR.* Plenum Press, New York, 1987.
8. B. E. Mann, in *Specialist Periodical Reports: Spectroscopic Properties of Inorganic and Organometallic Compounds.* Volume 23, pp. 1–170, Royal Society of Chemistry, London, 1990.
9. J. Bacon, R. J. Gillespie and J. W. Quail, *Can. J. Chem.*, 1963, **41**, 3063.
10. E. M. Menger and W. S. Veeman, *J. Magn. Reson.*, 1982, **46**, 257.
11. P. Granger, in *Transition Metal NMR* (ed. P. S. Pregosin), Elsevier, Amsterdam, 1991.
12. S. Bahceli and J. Klinowski, *Solid State Nucl. Magn. Reson.*, 1993, **2**, 269.
13. F. W. Wehrli, *Annu. Rep. NMR Spectrosc.*, 1979, **9**, 125.
14. J. Malito, *Annu. Rep. NMR Spectrosc.*, 1997, **33**, 151.
15. U. Ochsenbein and C. W. Schlaepfer, *Helv. Chim. Acta*, 1980, **63**, 1926.
16. O. Lutz, H. Oehler and P. Kroneck, *Z. Phys. A.*, 1978, **288**, 17.
17. H. A. Alloul, *J. Appl. Phys.*, 1991, **69**, 4513.
18. H. M. McConnell and H. E. Weaver, *J. Chem. Phys.*, 1956, **25**, 307.
19. H. M. McConnell and S. B. Berger, *J. Chem. Phys.*, 1957, **27**, 230.
20. P. D. Ellis, H. C. Walsh and C. S. Peters, *J. Magn. Reson.*, 1973, **11**, 426.
21. Y. Yamamoto, H. Haraguchi and S. Fujiwara, *J. Phys. Chem.*, 1970, **74**, 4369.
22. B. D. Guenther and R. A. Hultsch, *J. Magn. Reson.*, 1968, **1**, 609.
23. P. Kroneck, J. Kodweiss, O. Lutz, A. Nolle and D. Zepf, *Z. Naturforsch., A*, 1982, **37A**, 186.
24. Y. Suzuki, H. Kubo and K. Hirakawa, *Kyushu Daigaku Kogaku Shuho*, 1982, **55**, 351 (CA: 98: 118275v).
25. H. Kubo, T. Akitomi, Y. Suzuki, K. Tsuru and N. Uryu, *J. Magn. Magn. Mater.*, 1983, **31**, 711.
26. D. S. Gill, L. Rodehüser and J.-J. Delpuech, *J. Chem. Soc., Faraday Trans.*, 1990, **86**, 2847.
27. D. S. Gill, L. Rodehüser, P. Rubini and J.-J. Delpuech, *J. Chem. Soc., Faraday Trans.*, 1995, **91**, 2307.

28. R. M. Sternheimer, *Phys. Rev.*, 1950, **80**, 102.
29. S. Kitagawa and M. Munakata, *Inorg. Chem.*, 1984, **23**, 4388.
30. S. Imai, K. Fujisawa, T. Kobayashi, N. Shirasawa, H. Fujii, T. Yoshimura, N. Kitajima and Y. Moro-oka, *Inorg. Chem.*, 1998, **37**, 3066.
31. P. Kroneck, O. Lutz, A. Nolle and H. Oehler, *Z. Naturforsch.*, 1980, **35A**, 221.
32. S. Kitagawa, M. Munakata and M. Sasaki, *Inorg. Chim. Acta*, 1986, **120**, 77.
33. R. L. Geerts, J. C. Huffman, K. Folting, T. H. Lemmen and K. G. Caulton, *J. Am. Chem. Soc.*, 1983, **195**, 3503.
34. W. McFarlane and D. S. Rycroft, *J. Magn. Reson.*, 1976, **24**, 95.
35. O. Lutz, H. Oehler and P. Kroneck, *Z. Naturforsch.*, 1978, **33A**, 1021.
36. S. J. B. Price, C. Brevard. A. Pagelot and P. J. Sadler, *Inorg. Chem.*, 1986, **24**, 596.
37. B. Mohr, E. E. Brooks, N. Rath and E. Deutsch, *Inorg. Chem.*, 1991, **39**, 4541.
38. A. Hetherington, W. Levason and M. D. Spicer, *Polyhedron*, 1990, **9**, 1609.
39. J. R. Black, W. Levason, M. D. Spicer and M. Webster, *J. Chem. Soc. Dalton Trans.*, 1993, 3129.
40. J. R. Black and W. Levason, *J. Chem. Soc. Dalton Trans.*, 1994, 3225.
41. J. R. Black, N. R. Champness, W. Levason and G. Reid, *Inorg. Chem.*, 1996, **35**, 1820.
42. J. A. Connor and R. J. Kennedy, *Polyhedron*, 1988, **7**, 161.
43. F. Tautelle, *Nato ASI Ser., Ser. C.*, 1990, **322**, 293.
44. J. Haase and H. Pfeifer, *J. Magn. Reson.*, 1990, **86**, 217.
45. R. A. Wind, *Pract. Spectrosc.*, 1991, **11**, 53.
46. J. L. Dye, A. S. Ellaboudy and J. Kim, *Pract. Spectrosc.*, 1991, **11**, 217.
47. T. Charpentier, C. Fermon and J. Virlett, *J. Magn. Reson.*, 1998, **132**, 181.
48. C. A. Fyfe, *Solid State NMR for Chemists*, CFC Press, Guelph, 1983.
49. R. G. Graham, P. C. Riedi and B. M. Wanklyn, *J. Phys.: Condens. Matter*, 1991, **3**, 135.
50. A. Ramamoorthy and P. T. Narasimhan, *Mol. Phys.*, 1991, **73**, 207.
51. Y. Tomita, K. Yamada, H. Ohki and T. Okuda, *Bull. Chem. Soc. Jpn.*, 1997, **70**, 2405.
52. E. I. Yurieva and V. A. Gubanov, *J. Struct. Chem.*, 1997, **38**, 34.
53. Y. Fagot-Revurat, M. Horvatic, C. Berthier, J. P. Boucher, P. Segransan, G. Dhalenne and A. Revcolevschi, *Phys. Rev. B: Condens. Matter*, 1997, **55**, 2964.
54. S. Ramaprabhu, N. Amstutz, E. A. C. Lucken and G. Bernardinelli, *J. Chem. Soc., Dalton Trans.*, 1993, 871.
55. H. Negita, M. Hiura, K. Yamada and T. Okuda, *J. Mol. Struct.*, 1980, **58**, 205.
56. T. Okuda, M. Hiura, K. Yamada and H. Negita, *Chem. Lett.*, 1977, 367.
57. S. Ramaprabhu, N. Amstutz, E. A. C. Lucken and G. Bernadinelli, *Z. Naturforsch., A: Phys. Sci.*, 1998, **53**, 625.
58. A. Habiyakare, E. A. C. Lucken and G. Bernardinelli, *J. Chem. Soc., Dalton Trans.*, 1992, 2591.
59. A. Habiyakare and E. A. C. Lucken, *J. Mol. Struct.*, 1989, **213**, 231.
60. A. Habiyakare and E. A. C. Lucken, *Z. Naturforsch., Teil A*, 1990, **45**, 224.
61. S. Ramaprabhu and E. A. C. Lucken, *Z. Naturforsch., Teil A*, 1992, **47**, 125.
62. F. Khajenouri, S. Motallebi and E. A. C. Lucken, *Z. Naturforsch., A: Phys. Sci.*, 1998, **53**, 599.
63. G. Becker, *Z. Phys.*, 1951, **130**, 415.
64. S. Domngang and J. Wucher, *C.R. Acad. Sci. Paris, Ser. B*, 1969, **268**, 1608.
65. P. K. Burkert and H. P. Fritz, *Z. Naturforsch.*, 1968, **B23**, 1312.
66. P. K. Burkert and H. P. Fritz, *Z. Naturforsch.*, 1969, **B24**, 253.
67. R. W. Mebs, G. C. Carter, B. J. Evans and L. H. Bennett, *Solid State Commun.*, 1972, **10**, 769.
68. S. Hayashi and K. Hayamizu, *J. Phys. Chem. Solids*, 1992, **53**, 239.
69. E. R. Andrew, W. S. Hinshaw and R. S. Tiffen, *J. Phys. (C)*, 1973, **6**, 2217.
70. E. R. Andrew, W. S. Hinshaw and R. S. Tiffen, *Phys. Lett. (A)*, 1973, **43**, 113.

71. P. R. Locher, *Phys. Rev. B*, 1974, **10**, 801.
72. S. Hayashi and K. Hagamizu, *Chem. Lett.*, 1989, 1419.
73. S. Hayashi and K. Hayamizu, *J. Chem. Phys.*, 1990, **92**, 2818.
74. K. Endo, K. Yamamoto and K. Deguchi, *J. Phys. Chem. Solids*, 1993, **54**, 15.
75. A. Kawamori, R. Takagi and G. Soda, *Mol. Phys.*, 1973, **25**, 489.
76. A. Kawamori and G. Soda, *Mol. Phys.*, 1975, **29**, 1085.
77. K. Yamada, Y. Tomita and T. Okuda, *J. Mol. Struct.*, 1995, **345**, 219.
78. H. Kubo, I. Yahara and K. Hirakawa, *J. Phys. Soc. Jpn.*, 1976, **40**, 591.
79. K. D. Becker and G. W. Herzog, *Ber. Bunsenges. Phys. Chem.*, 1974, **78**, 45 (CA: 80: 139096f).
80. K. D. Becker and S. Wagner, *Phys. Rev. B: Condens. Matter*, 1983, **27**, 5240.
81. Y. Itoh, A. Hayashi, H. Yamagata, M. Matsumura, K. Koga and Y. Ueda, *J. Phys. Soc. Jpn.*, 1996, **65**, 1953.
82. S. Saito, H. Kishi, K. Nie, H. Nakamaru, F. Wagatsuma and T. Shinohara, *Phys. Rev. B: Condens. Matter*, 1997, **55**, 14527.
83. F. Asaro, A. Camus, R. Gobetto, A. C. Olivieri and G. Pellizer, *Solid State Nucl. Magn. Reson.*, 1997, **8**, 81.
84. E. R. Andrew, J. L. Carolan and P. J. Randall, *Phys. Lett., A*, 1971, **35**, 435.
85. E. R. Andrew, J. L. Carolan and P. J. Randall, *Chem. Phys. Lett.*, 1971, **11**, 298.
86. C. Minier and M. Minier, *Point Defects Defect Interact. Met.* [Proc. Yamada Conf.], 5th, 1981 (pub. 1982), **27–32**, 76.
87. S. Hu, J. A. Reimer and A. T. Bell, *J. Phys. Chem. B*, 1997, **101**, 1869.
88. P. Panissod and C. Meny, *J. Magn. Mater*, 1993, **126**, 16.
89. D. P. Tunstall, P. P. Edwards, J. Todd and M. J. Williams, *J. Phys.: Condens. Matter*, 1994, **6**, 1791.
90. H. M. Pastawski and J. A. Gascon, *Phys. Rev. B: Condens. Matter*, 1997, **56**, 4887.
91. T. Ito and T. Kadowaki, *Jpn. J. Appl. Phys.*, 1975, **14**, 1673.
92. H. Alloul and P. Bernier, *J. Phys. F*, 1974, **4**, 870.
93. G. Serfozo and K. Tompa, *Hung. Acad. Sci., Cent. Res. Inst. Phys.*, KFKI 1976, KFKI-76-38 (CA: 85: 114268d).
94. B. Li and Y. Wang, *Phys. Rev. B: Condens. Matter*, 1993, **47**, 16582.
95. T. Shinohara, T. Tadaki, S. Yamaguchi, S. Saito, F. Azuma and K. Shimizu, *Shindo Gijutsu Kenkyu Kaishi*, 1996, **35**, 72 (CA: 127: 124853r).
96. H. Goto, S. Katsumoto and S. Kobayashi, *J. Phys. Soc. Jpn.*, 1993, **62**, 1439.
97. Q. Y. Jin, Y. B. Xu, M. R. Zhai, C. Hu, M. Lu, Q. S. Bie, Y. Zhai, G. L. Dunifer, R. Naik and M. Ahmad, *Phys. Rev. Lett.*, 1994, **72**, 768.
98. A. Goto, H. Yasuoka, H. Yamamoto and T. Shinjo, *J. Magn. Magn. Mater.*, 1993, **124**, 285.
99. A. Goto, H. Yasuoka, K. Takanashi, K. Saito and H. Fujimori, *J. Magn. Magn. Mater.*, 1993, **126**, 358.
100. A. Goto, H. Yasuoka, H. Yamamoto and S. Teruya, *J. Phys. Soc. Jpn.*, 1993, **62**, 2129.
101. D. R. Torgeson and R. G. Barnes, *J. Chem. Phys.*, 1975, **62**, 3968.
102. C. Schlosser and H. Broemer, *Hyperfine Interact.*, 1983, **16**, 669.
103. H. J. Eifert, B. Elschner and K. H. J. Buschow, *Phys. Rev. B: Condens. Matter*, 1982, **25**, 7441.
104. Z. M. Saleh, G. A. Williams and P. C. Taylor, *J. Non-Cryst. Solids*, 1991, **137–138**, 1047.
105. K. Ishida, Y. Kitaoka, H. Masuda, K. Asayama, T. Takahashi, K. Kanoda, A. Kobayashi, R. Kato and H. Kobayashi, *Physica B (Amsterdam)*, 1993, **186–188**, 1059.
106. K. Ishida, Y. Kitaoka, H. Masda, K. Asayama, T. Takahashi, A. Kobayashi, R. Kato and H. Kobayashi, *Synth. Met.*, 1995, **71**, 1915.
107. K. Ishida, Y. Kitaoka, H. Masuda, K. Asayama, T. Takahashi, A. Kobayashi, R. Kato and H. Kobayashi, *J. Phys. Soc. Jpn.*, 1995, **64**, 2970.

108. K. Magishi, Y. Kitaoka, G.-Q. Zheng, K. Asayama, K. Tokiwa, A. Iyo and H. Ihara, *Phys. Rev. B: Condens. Matter*, 1996, **53**, R8906.
109. K. Magishi, G.-Q. Zheng, Y. Kitaoka, K. Asayama, K. Tokiwa, A. Iyo and H. Ihara, *Physica C (Amsterdam)*, 1996, **263**, 375.
110. M.-H. Julien, M. Horvatic, C. Berthier and P. Segransan, *J. Low. Temp. Phys.*, 1996, **105**, 371.
111. M. Baenitz, M. Heinze, W. Hoffmann, K. Luders and E. V. Antipov, *Adv. Supercond. IX, Proc. 9th Int. Symp.*, Volume 1, 107 (eds S. Nakajima and M. Masato), Springer, Tokyo, 1997.
112. A. A. Gippius, E. V. Antipov, W. Hoffmann and K. Lueders, *Physica C (Amsterdam)*, 1997, **276**, 57.
113. Y. Itoh, T. Machi, S. Adachi, A. Fukuoka, K. Tanabe and H. Yasuoka, *J. Phys. Soc. Jpn.*, 1998, **67**, 312.
114. B. S. Shastry, *Phys. Rev. Lett.*, 1989, **63**, 1288.
115. R. Akis, C. Jiang and J. P. Carbotte, *Physica C (Amsterdam)*, 1991, **176**, 485.
116. A. Karkin, V. Verkhovskii, V. Voronin, B. Goshchitskii and A. Mirmelstein, *Stud. High Temp. Supercond.*, 1997, **22**, 79.
117. I. Kupcic, S. Barisic and E. Tutis, *Phys. Rev. B: Condens. Matter Mater. Phys.*, 1998, **57**, 8590.
118. Y. Kitaoka, K. Ishida, K. Fujiwara, Y. Kohori, K. Asayama, H. Katayama-Yoshida, Y. Okabe and T. Takahashi, *Springer Ser. Mater. Sci.*, 1989, **11**, 148.
119. C. Y. Huang, *Prog. High Temp. Supercond.*, 1989, **12**, 116.
120. S. G. Sankar, H. S. Lessure and S. Simizu, *Ferroelectrics*, 1990, **102**, 337.
121. Y. Kitaoka, *NSMF News*, 1992, **33**, 2 (CA: 118: 91612v).
122. Y. Kitaoka, K. Ishida, S. Ohsugi, K. Fujiwara and G.-Q. Zheng, *Appl. Magn. Reson.*, 1992, **3**, 549.
123. K. Asayama, Y. Kitaoka, G.-Q. Zheng, K. Ishida and S. Ohsugi, *Osaka Daigaku Chodendo Erekutoronikusu Kenkyu Senta Hokoku*, 1993, **2**, 58 (CA:120: 285985f).
124. K. Asayama, Y. Kitaoka, G.-Q. Zheng, K. Ishida and K. Magishi, *Physica B (Amsterdam)*, 1996, **223–224**, 478.
125. P. Carretta and A. Rigamonti, *High Temp. Supercond., Proc. GNSM Sch., 1994* (pub. 1996), 493 (ed. M. Acquarone).
126. H. Monien, *Proc. Workshop Phase Sep. Cuprate Supercond.*, 1992, 232, World Sci., Singapore (eds K. A. Mueller and G. Benedek).
127. M. Mehring, M. Baehr, P. Gergen, J. Gross, C. Kessler and N. Winzek, *Proc. Workshop Phase Sep. Cuprate Supercond.*, 1992, 62, World Sci., Singapore (eds K. A. Mueller and G. Benedek).
128. G. V. S. Rao, Y. U. V. Raju and R. Srinivasan, *Prog. High Temp. Supercond.*, 1988, **7**, 42.
129. R. E. Walstedt and W. W. Warren, Jr, *Springer Ser. Mater. Sci.*, 1989, **11**, 137.
130. R. L. Corey, N. J. Curro, K. O'Hara, T. Imai, C. P. Slichter, K. Yoshimura, M. Katoh and K. Kosuge, *Phys. Rev. B: Condens. Matter*, 1996, **53**, 5907.
131. D. Brinkmann, *Z. Naturforsch., A: Phys. Sci.*, 1988, **53**, 488.
132. H. Yasuoka, *Springer Ser. Mater. Sci.*, 1989, **11**, 156.
133. F. Borsa, P. Carretta, M. Corti and A. Rigamonti, *Appl. Magn. Reson.*, 1992, **3**, 509.
134. K. Kume, *Appl. Magn. Reson.*, 1992, **3**, 745.
135. M. Takigawa, *Appl. Magn. Reson.*, 1992, **3**, 495.
136. D. Brinkmann, *Appl. Magn. Reson.*, 1992, **3**, 483.
137. A. J. Vega, M. K. Crawford, E. M. McCarron and W. E. Farneth, *Physica C (Amsterdam)*, 1989, **162–164**, 165.
138. M. Kieninger, G. Majer, A. Seeger and F. Dworschak, *Z. Naturforsch., A: Phys. Sci.*, 1994, **49**, 391.

139. Y. Tokunaga, K. Ishida, Y. Kitaoka and K. Asayama, *Physica C (Amsterdam)*, 1997, **282–287**, 1351.
140. M. Kato, H. Kato, T. Ohmura, M. Nakanishi, T. Miyano, K. Yoshimura, M. Kakihana and K. Kosuge, *Adv. Supercond. IX, Proc. 9th Int. Symp.*, Volume 1, 387 (eds S. Nakajima and M. Murakami), Springer, Tokyo, 1997.
141. T. Machi, M. Kosuge, N. Koshizuka and H. Yasuoka, *Adv. Supercond. IX, Proc. 9th Int. Symp.*, Volume 1, 111 (eds S. Nakajima and M. Murakami), Springer, Tokyo, 1997.
142. S. P. Klein, R.-P. Wang, A. W. Sleight and W. W. Warren, Jr, *Phys. Rev. B: Condens. Matter*, 1997, **56**, 6335.
143. A. Suter, M. Mali, J. Roos, D. Brinkmann and J. Karpinski, *Physica C (Amsterdam)*, 1997, **282–287**, 1345.
144. T. Auler, M. Horvatic, J. A. Gillet, C. Berthier, Y. Berthier, P. Segransan and J. Y. Henry, *Phys. Rev. B: Condens. Matter*, 1997, **56**, 11294.
145. A. Ananyev, A. Gerashenko, K. Mikhalev, Yu. Zhdanov, S. Verkhovskii, Eu. Medvedev and B. Goshchitskii, *Physica C (Amsterdam)*, 1997, **282–287**, 1337.
146. H. Niki, K. Tamaki, K. Kano, T. Shinohara, S. Tomiyoshi, M. Omori and T. Kajitana, *J. Phys. Soc. Jpn.*, 1997, **66**, 3655.
147. A. Suter, M. Mali, J. Roos, D. Brinkmann, J. Karpinski and E. Kaldis, *Phys. Rev. B: Condens. Matter*, 1997, **56**, 5542.
148. B. Grevin, Y. Berthier, I. Monot, J. Wang and F. Weiss, *Physica C (Amsterdam)*, 1997, **289**, 77.
149. P. Huesser, S. Schafroth, E. Stoll, H. U. Suter and P. F. Meier, *Helv. Phys. Acta*, 1997, **70**, 25.
150. H. Niki, K. Kano, M. Takase, K. Majikina, K. Yagasaki, T. Shinohara, M. Omori, S. Tomiyoshi and E. Akiba, *Z. Naturforsch., A: Phys. Sci.*, 1998, **53**, 518.
151. B. Grevin, Y. Berthier, I. Monot, J. Wang and F. Weiss, *Eur. Phys. J.: Appl. Phys.*, 1998, **1**, 279.
152. P. Carretta, S. Aldrovandi, R. Sala, P. Ghigna and A. Lascialfari, *Phys. Rev. B: Condens. Matter*, 1997, **56**, 14587.
153. T. Imai, K. R. Thurber, K. M. Shen, A. W. Hunt and F. C. Chou, *Phys. Rev. Lett.*, 1998, **81**, 220.
154. M. Takigawa, N. Motoyama, H. Eisaki and S. Uchida, *Phys. Rev. B: Condens. Matter Mater. Phys.*, 1998, **57**, 1124.
155. K. Magishi, S. Matsumoto, K. Ishida, Y. Kitaoka, K. Asayama, M. Uehara, T. Nagata and J. Akimitsu, *Physica C (Amsterdam)*, 1997, **282**, 1115.
156. K. Kumagai, S. Tsuji, K. Maki, M. Kato and Y. Koike, *Physica C (Amsterdam)*, 1997, **282–287**, 1343.
157. K. Magishi, S. Matsumoto, Y. Kitaoka, K. Ishida, K. Asayama, M. Uehara, T. Nagata and J. Akimitsu, *Phys. Rev. B: Condens. Matter Mater. Phys.*, 1998, **57**, 11533.
158. T. Imai, C. P. Slichter, K. Yoshimura, M. Katoh, K. Kosuge, J. L. Cobb and J. T. Market, *Physica C (Amsterdam)*, 1994, **235–240**, 1627.
159. Y.-Q. Song, A. P. Reyes, X. P. Tang, W. P. Halpern and D. Hinks, *J. Phys. Chem. Solids*, 1995, **56**, 1939.
160. T. Goto, K. Chiba, M. Mori, T. Suzuki, K. Seki and T. Fukase, *J. Phys. Soc. Jpn.*, 1997, **66**, 2870.
161. S. Fujiyama, Y. Itoh, H. Yasuoka and Y. Ueda, *J. Phys. Soc. Jpn.*, 1997, **66**, 2864.
162. K. Ishida, T. Tanaka, H. Yamanaka, T. Mito, Y. Tokunaga, K. Yoshida, K. Yamazoe, S. Ohsugi, Y. Kitaoka and K. Asayama, *Physica C (Amsterdam)*, 1997, **282–287**, 1367.
163. S. Ohsugi, Y. Kitaoka and K. Asayama, *Physica C (Amsterdam)*, 1997, **282–287**, 1373.
164. P. Carretta, A. Rigamonti and R. Sala, *Phys. Rev. B: Condens. Matter*, 1997, **55**, 3734.
165. Yu. Piskunov, A. Geraschenko, K. Mikhalev, Yu. Zhdanov, S. Verkhovskii, A. Yakubovskii, A. Trokiner and P. V. Bellot, *Physica C (Amsterdam)*, 1997, **282–287**, 1361.

166. A. Gerashenko, K. Mikhalev, S. Verkhovskii, Yu. Piskunov and A. Yakubovskii, *Physica C (Amsterdam)*, 1997, **282–287**, 1347.
167. G.-Q. Zheng, H. Wakabayashi, Y. Kitaoka, K. Asayama, K. Hamada, H. Yamauchi and S. Tanaka, *J. Phys. Soc. Jpn.*, 1997, **66**, 1880.
168. V. F. Masterov, F. S. Nasredinov, N. P. Seregin and P. P. Seregin, *Phys. Status Solidi B*, 1998, **207**, 223.

Water Signal Suppression in NMR Spectroscopy

WILLIAM S. PRICE

Water Research Institute, Sengen 2-1-6, Tsukuba, Ibaraki 305-0047, Japan

The area of solvent suppression has a long history and is an indispensable part of almost every NMR experiment conducted in a solvent containing nuclei of the type to be detected. This chapter provides a general coverage of solvent suppression methods in NMR with special attention to the enormous developments in the past decade that have occurred due to the

ANNUAL REPORTS ON NMR SPECTROSCOPY
VOLUME 38 ISBN 0-12-505338-X

widespread usage of magnetic field gradients and shaped RF pulses. The general considerations and instrumental complications associated with the presence of a large signal are first discussed. The complications resulting from the radiation damping and demagnetizing fields are considered in some detail since their effects are becoming more manifest with the increasingly higher field strengths available. The methods of solvent suppression are then covered including their application to multidimensional experiments. Brief coverage is also given to suppression in imaging experiments, experiments involving high-molecular-weight compounds and also ^{17}O NMR.

1. INTRODUCTION

Perhaps the most common and unavoidable problem in solution-state NMR results from the necessity of dissolving the solute in a solvent which contains nuclei of the type to be observed. Even though it is the solute that is the focus of the experiment it is the solvent, which is generally present at a far higher concentration, that composes most of the NMR signal. For example, in a protein sample the water concentration is about 55 M (i.e. 110 M protons) whilst the protein concentration is normally in the millimolar range. In this chapter we use solvent and water interchangeably since many of the methods were developed with water being the solvent in question (we stress, however, that the methods discussed in this chapter are not restricted only to water). The need for solvent suppression pervades almost all areas of NMR including protein and nucleic acid studies,[1–3] imaging and organic chemistry. Liquid chromatography (LC) NMR[4,5] has particularly severe suppression requirements since there is typically more than one solvent resonance (together with corresponding ^{13}C satellites) and the flow of the mobile phase means that the spins within the RF coil are constantly being replenished by fresh spins and the solvent resonances change frequencies during an experiment due to the solvent gradients used.[4,6]

Due to the way in which NMR signals are detected, a large solvent resonance causes complications. To avoid saturation of the receiver by the (unsuppressed) solvent resonance, the gain must be set very small which may result in the solute signal being too small to be digitized (note analogue-to-digital converters (ADC) are typically 12 or 16 bit) thereby precluding its observation (see Fig. 1). Thus, the solvent peak must be suppressed to a level adequate to ensure proper digitization of the solute signal. However, the large residual solvent peak still distorts the baseline and so generally the suppression needs to be much better than that required for the ADC. Typically a suppression of at least two orders of magnitude is required and for good spectra with only 1 mM of solute, suppression factors of the order of 10^3 to 10^5 may be required. In fortunate cases it may be possible to use an inert solvent

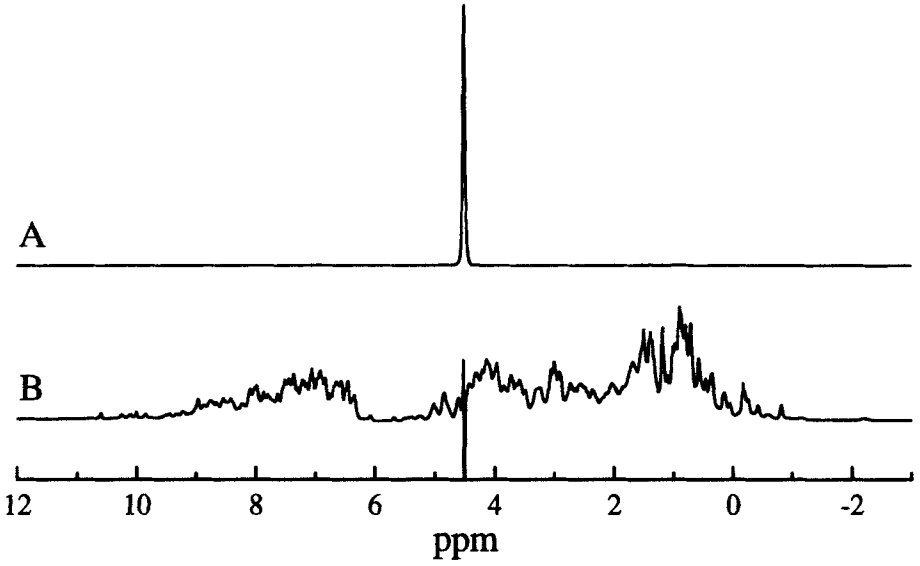

Fig. 1. ^{1}H NMR spectra of a lysozyme solution (10 mM in 10:90 ^2H_2O:H_2O, pH 3.7) (A) without water suppression and (B) with the water resonance suppressed using the Water-PRESS sequence (see p. 305). Both spectra were acquired at 310 K at 300 MHz and in both cases a $\pi/2$ observe pulse was used. To avoid saturation of the analogue-to-digital converter the receiver gain used in acquiring spectrum (A) was 28 dB less than that used in acquiring spectrum (B). (From Price *et al.*[112])

(e.g. $^2H^2O$ in the case of ^{1}H NMR), but solvent substitution can be both expensive and tedious as well as hindering/preventing the observation of exchangeable residues. In many cases, such as *in vivo* studies, it is completely impossible. Also due to chemical reasons (i.e. solubility and aggregation) the range of allowable solute concentration is strictly limited. This is particularly true in the case of macromolecules where the onset of aggregation can occur in the millimolar range (e.g. Price *et al.*[7]).

Solvent suppression is a very difficult problem because it is not generally possible to manipulate the solvent resonance independently of the solute resonances in the frequency domain. Deeper reflection reveals a myriad of associated complications that derive from either chemical, physical or instrumental origins. For example, how to observe signals that resonate close or under the water resonance (e.g. protein α-protons) and resonances of nuclei that exchange with the solvent without being affected by the solvent suppression and problems resulting from the presence of large signals (e.g. radiation damping (RD) and demagnetization field effects). Instrumental limitations[8–10] including the inhomogeneity of the static magnetic (i.e. B_0) and radio frequency (i.e. B_1) fields and the imperfection of selective pulses (frequency selectivity and pure phase), can diminish both the selectivity and degree of

suppression. Thus, in theory while some suppression methods should work very well, in practice they go nowhere near their theoretical predictions. Hence in the present chapter although we discuss the pitfalls of different methods we try not to be too judgemental since the success of a particular method depends on the spectrometer RF capabilities, probe sensitivity, sample and field strength. Thus, what will work well in one instance may fail dismally in another.

There exist a vast number of suppression methods, and comprehensive reviews covering the earlier development and applications of solvent suppression of a general nature[8,9,11–14] and also related to *in vivo* NMR[8,13,15] can be found elsewhere. Solvent suppression techniques are intricately linked with the progress in both theoretical and technical aspects of many of the subdisciplines in NMR from signal-processing to shaped excitation pulses and more efficient gradient coils. In the last decade the rapid progress in these fields has resulted in suppression techniques undergoing a renaissance, accordingly in this review particular attention will be given to developments in the last decade, although earlier methods will be briefly covered to put these later developments into context. For example, in protein studies it is now commonplace to observe all of the spectra required for structural studies in water instead of having to go through the tedious process of solvent exchange. Working in water has the advantage that water can be used as a magnetization reservoir affording the possibility of performing experiments such as the reverse detection of ^{15}N in ^{15}N labelled molecules.

Many of the limitations of the different approaches to solvent suppression, especially on modern spectrometers, result from the "side-effects" of performing NMR in the presence of an intense signal. In this chapter we will pay special attention to the effects of radiation damping and the demagnetization field since these effects are more troublesome with modern sensitive spectrometers and higher magnetic field strengths. Consequently, before presenting any of the methods of solvent suppression, we review in Section 2 the complications arising from NMR in the presence of concentrated samples. In Section 3 the basic pulse sequence methods of suppressing solvents are discussed with greater emphasis placed on more recent developments. Further reductions of the solvent signal can then be performed using postprocessing, and these techniques are also considered in this section. Suppression of radiation damping effects is considered in Section 4. Finally, the use of solvent suppression in multidimensional experiments is discussed in Section 5. Some attention is given to suppression in *in vivo* and imaging studies in Section 6. Finally in Section 7 solvent suppression in the presence of high-molecular-weight solutes and suppression of ^{17}O is briefly discussed. As all encompassing as this review might endeavour to be, it is not possible in the space of one chapter to give more than a scant overview of the current *status quo*. We stress that most of what shall be discussed below is equally applicable to any strong (i.e. concentrated) solvent resulting in an intense signal.

2. COMPLICATIONS DUE TO LARGE RESONANCES

2.1. Introduction

In this section we state more clearly why we want to suppress and/or control the behaviour of the solvent resonance beyond the naïve viewpoint of solvent suppression merely for allowing adequate digitization of the solute signals. In the last five or so years in particular, it has more generally been realized that the behaviour of small signals and large signals differs for two reasons: (i) radiation damping and (ii) the effects of the demagnetizing field (sometimes called a "dipolar field" or "bulk susceptibility effect"). Consequently, a (theoretically sound) suppression method might fail miserably in practice since the solvent effectively sees a different pulse sequence than the solute. Both of these two rather different "collective" effects, which both originate from strong net magnetization, cause the magnetic field during a pulse sequence to become time-dependent. This not only decreases the efficiency of solvent suppression sequences but can also generate artifacts. Sobol *et al.*[16] have noted that radiation damping and demagnetization field effects have serious consequences for difference-type experiments as are commonly employed for studying macromolecular hydration. They noted that in spite of its small magnitude, the radiation damping field may affect nuclei resonating as much as 2 or 3 kHz away from the solvent signal. Such disturbances can be of the order of 1% of the equilibrium nuclear spin magnetization; the corresponding signals may become visible when using difference techniques.

The radiation damping field, which points in a direction perpendicular to both B_0 and the magnetization vector,[17] acts as a torque on the magnetization thereby greatly affecting the apparent relaxation properties (see Fig. 2); whereas the demagnetizing field is parallel to the z direction[18,19] which results in the addition of a very weak field to the externally applied field.

In the absence of collective effects, the Bloch and Redfield equations are linear differential equations for the components of the average spin magnetization and the reduced density operator of the spins in one molecule, respectively. However, the presence of an additional magnetic field (i.e. demagnetizing field and/or radiation damping) which depends explicitly on the average state of the molecules makes these equations nonlinear.[20] Both of these additional magnetic fields can result in insidious artifacts that can be easily confused with multiple-quantum effects in multidimensional experiments,[20–31] such as multiple-quantum-like harmonic peaks along the F_1 dimension in COSY spectra of liquid water. Possible mechanisms for these peaks have included classical radiation damping fields,[27–29] quantized radiation damping fields,[21–23] intermolecular dipole–dipole interactions[24] and demagnetizing field effects.[20,24,32,33] As this area is still somewhat controversial with much continuing research and discussion aimed at clarifying which artifacts result from which of the effects and what theoretical framework

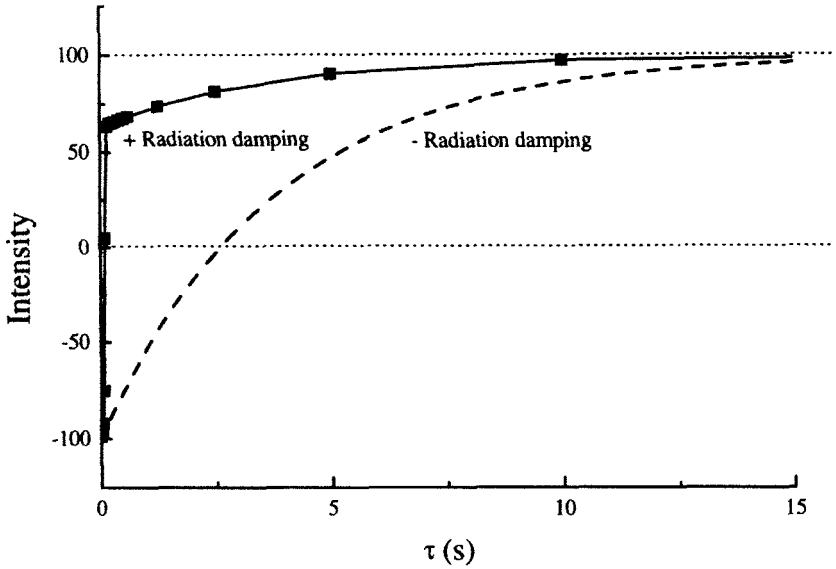

Fig. 2. Radiation damping effects on water longitudinal relaxation versus the τ delay in an inversion recovery sequence (i.e. π-τ-$\pi/2$-Acq.) in a lysozyme sample (10 mM in 10:90 ^2H_2O:H_2O, pH 3.7) at room temperature at 300 MHz using a 5 mM inverse probe. In the absence of radiation damping (---) the water has a relaxation time of about 3.8 s. Radiation damping significantly enhances the effective longitudinal relaxation of the water (—) and the recovery is clearly nonexponential with the null-point of the signal occurring before 0.1 s (i.e. T_1 ~140 ms). (From Price *et al.*[112])

should be used in describing them, we will not consider it further except for noting that as far as the present chapter is concerned, it is important that both the radiation damping and demagnetizing field effects be accounted for in order to achieve good suppression.[34–38] We consider in more detail the characteristics of the radiation damping and demagnetizing fields in the following two subsections.

2.2. Radiation damping

Radiation damping effects have been known since very early times in NMR[39–41] and have recently been reviewed.[17,42] Radiation damping results from the nonlinear coupling between the RF coil and the transverse magnetization.[17,30,40,41,43,44] The precessing spin magnetization generates an oscillating current in the receiver coil which in turn generates an oscillating magnetic field which tends to rotate the magnetization back to its equilibrium position without changing the length of the magnetization vector (even

though this is implied by the term "damping"). However, the transverse magnetization does decay and so it is conceptually easy to realize that it can have a significant line-broadening effect. The effect of radiation damping can be characterized by a time constant (in CGS units)[40,41,45]

$$T_{RD}^{-1} = 2\pi\gamma\eta QM_0 \tag{1}$$

where γ is the gyromagnetic ratio of the spins, η is the filling factor of the probe, $Q = \omega L/R$ is the quality factor of the probe (where ω, L and R are the resonance frequency, inductance and resistance of the coil, respectively) and M_0 is the equilibrium magnetization per unit volume. Importantly, radiation damping depends on the total transverse magnetization and is insensitive to the exact spatial distribution of this magnetization in the sample. Radiation damping is an intrinsic phenomenon in all NMR experiments, but its effects are much more prevalent in modern spectrometers with their larger static fields and more sensitive probes especially probes with superconducting RF coils with their extremely large Q values. Radiation damping effects are observable for water concentrations less than 1 mM on a modern 500 MHz spectrometer.[46] Mao and Ye[47] have pointed out that the radiation damping time can be determined by measuring the line-width of a $\pi/2$-excited resonance by using the following formula,

$$\nu_{1/2} = 0.8384/(\pi T_{RD}) \tag{2}$$

The nutation induced by an applied RF pulse has a constant angular velocity,

$$(d\theta/dt)_{\text{rf pulse}} = \gamma\mathbf{B}_1 \tag{3}$$

where θ is the angle between the magnetization and the $\mathbf{B}_0$ field. However, the nutation induced by radiation damping is not a constant and is given by

$$(d\theta/dt)_{RD} = -\sin\theta/T_{RD} \tag{4}$$

It might be reasoned from Eq. (4) that even if the solvent resonance was perfectly inverted there would be no radiation damping. However, it has been shown that radiation damping can be initiated in magnetization stored along the $-z$-axis by residual RF leakage and even thermal noise from the RF coil.[48]

As is evident from Eq. (1), the radiation damping effect is particularly severe for large solvent peaks and can make the solvent return to equilibrium many times faster than the intrinsic longitudinal relaxation time (see Fig. 2). Thus, the effects of radiation damping are a major source of difficulties in manipulating solvent magnetization and need to be considered in the

design and application of solvent suppression schemes, the design of soft pulses and of course whole pulse sequences.[8,20,45,49,50] Suppression sequences which involve periods in which the water magnetization is perpendicular to the static field are the worst affected. Further, radiation damping effects may vary considerably at different stages of an RF phase cycle[51] thereby adding further complexity to the problem. Magnetization that has been spatially encoded has no net transverse magnetic moment and is thus not subject to radiation damping. Hence, B_0 or B_1 gradients can be used to purge transverse magnetization thereby eliminating and/or delaying the onset of radiation damping.

Neglecting relaxation, the envelope of a strongly radiation-damped free induction decay (FID) is given by a hyperbolic secant function,[47]

$$S(t) = M_0 \exp(i\Delta\omega t)\mathrm{sech}\{t/T_{RD} - \ln[\tan(\theta_0/2)]\} \quad (5)$$

where $\Delta\omega$ is the chemical shift offset and θ_0 is the initial angle of the magnetization with respect to $\mathbf{B}_0$. Thus, if $\theta_0 \leq \pi/2$, the FID simply decays but if $\theta_0 \geq \pi/2$ the FID must first reach a maximum before decaying and the phase cannot be adjusted to obtain a pure absorption lineshape (see Fig. 3).[47,52] This effect has been elegantly explained by Mao and Ye[17] (see Fig. 4). In the absence of radiation damping the magnetization will return to equilibrium by simple decay, however, in the presence of radiation damping, the magnetization will return to equilibrium by tracing out the surface of the Bloch sphere.

Given the effects on the FID, it is less than surprising that radiation damping hampers the determination of spin–lattice relaxation times using the inversion recovery sequence,[53–55] spin–spin relaxation time determination,[56] and also has large effects on lineshapes and intensities.[46,47,57–59] Consequently, an FID from nuclear spins subject to radiation damping is a poor guide for magnetic homogeneity adjustment. Radiation damping during the evolution period (t_1) and mixing times of 2D experiments such as NOESY and ROESY results in broadening of the water cross-peaks along F_1.[60]

Fig. 3. The effects of radiation damping on an FID acquired after a single pulse and the corresponding Fourier transformed spectrum. The FIDs were simulated using Eq. (5) with 2048 points, T_{RD} = 50 ms and a spectral width of 400 Hz. The flip angles (i.e. θ_0) were (A) $\pi/4$, (B) $\pi/2$, (C) $3\pi/4$ and (D) 0.99 π. For $\theta_0 \leq \pi/2$ the FID and spectra appear normal with the FID simply decaying. However, as $\theta_0 > \pi/2$ the situation changes dramatically with the FID first "growing" before it decays and it is no longer possible to phase the spectrum into a totally absorption lineshape. As θ_0 approaches π (FID and spectrum D) the situation becomes particularly severe. Such lineshapes are commonly observed when trying to calibrate RF pulse lengths by determining the π pulse length using strong signals.

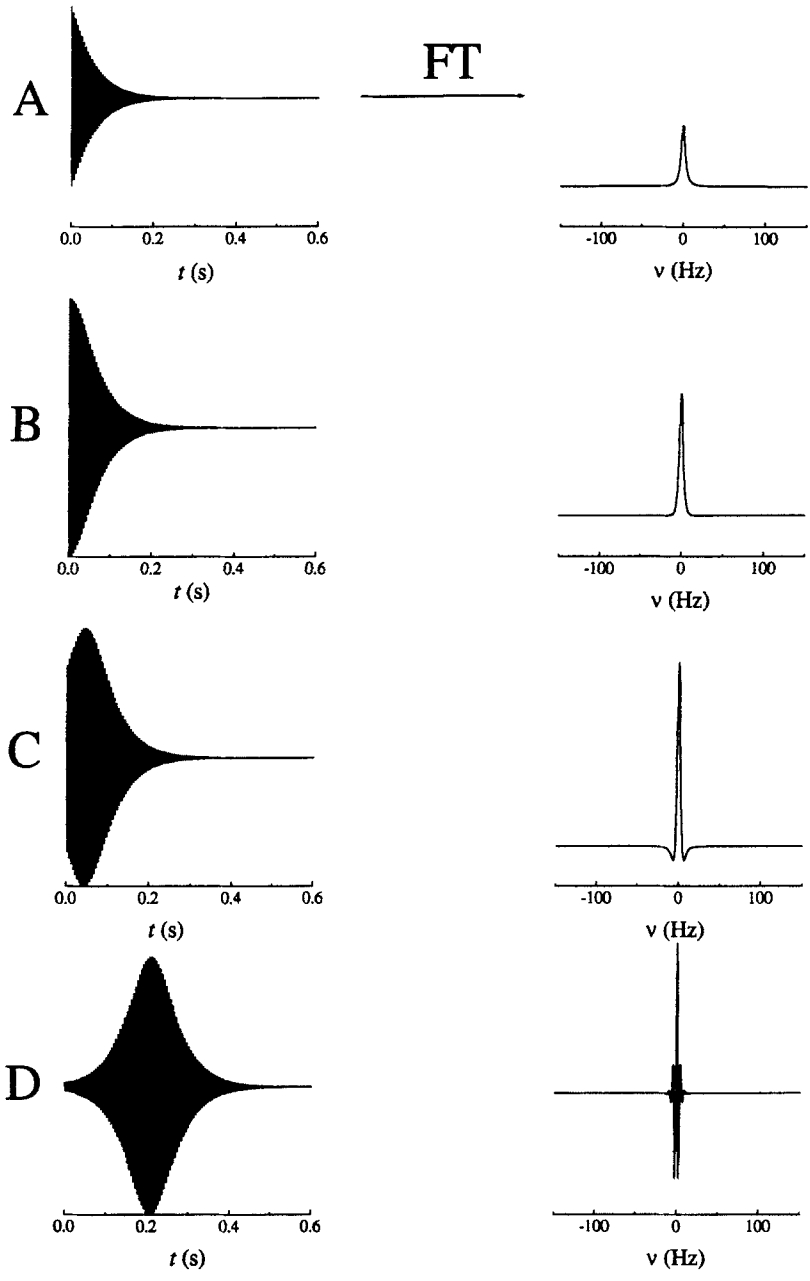
A
FT
0.0
0.2
0.4
0.6
t (s)
-100
0
100
ν (Hz)
B
0.0
0.2
0.4
0.6
t (s)
-100
0
100
ν (Hz)
C
0.0
0.2
0.4
0.6
t (s)
-100
0
100
ν (Hz)
D
0.0
0.2
0.4
0.6
t (s)
-100
0
100
ν (Hz)

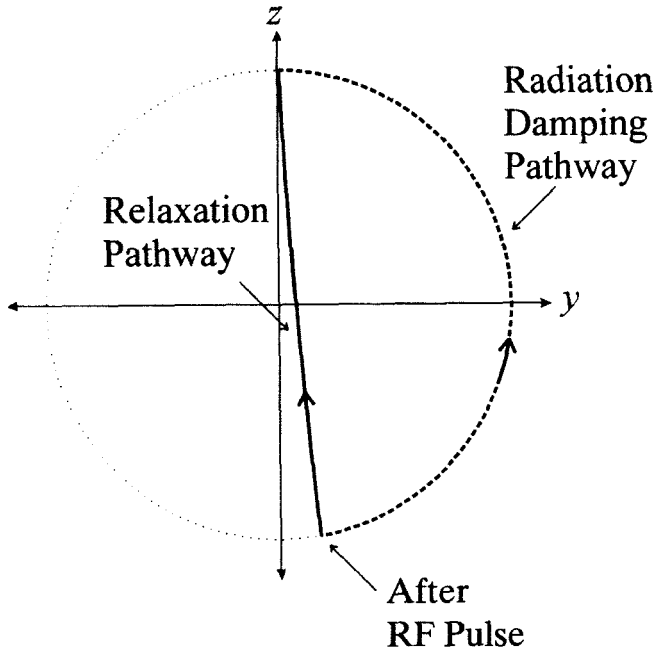

Fig. 4. An RF pulse initially rotates the magnetization away from the z-axis (i.e. thermal equilibrium) by, in this example, an angle of about 170°. In the absence of radiation damping effects the magnetization follows the normal relaxation pathway (—) back to the thermal equilibrium. However, in the presence of radiation damping, the magnetization retains its coherence and returns to the equilibrium position on the surface of the Bloch sphere (----). (After Mao *et al.*[53])

2.3. Demagnetization field effects

The equilibrium proton (or other highly abundant species) magnetization in water at room temperature directly generates a field. This can result in nonlinear behaviour and, in fact, was first observed in solid ^{3}He[61] and later for liquid ^{3}He.[62] Depending on whether the bulk magnetization of the water is oriented parallel or anti-parallel to the main field, the solute signals can be shifted by 1 Hz.[63] This contribution is sufficient to shift slightly the NMR frequencies of other species in the sample including those of other isotopes. Thus, this effect can be changed nearly instantaneously with RF pulses. This effect can be a local effect or through the entire sample and depends strongly on the shape of the sample and the spatial distribution of the spin magnetization and is further complicated by the use of magnetic and RF gradients since these introduce a spatial modulation of the magnetization. We also emphasize that whenever radiation damping effects are strong so are the demagnetiza-

tion field effects.[17] In fact, in a long cylindrical sample with uniform magnetization, the maximum radiation damping field is of the order of the maximum dipolar field multiplied by ηQ.[20]

The magnitude of the dipolar coupling between two spins has an angular dependence of

$$3\cos^2\theta - 1 \tag{6}$$

where θ is the angle between the interspin vector and $\mathbf{B}_0$. For a spin pair separated by a short distance R, molecular diffusion will rapidly average this to zero. However, for more distant spin pairs the average is incomplete as the interspin vector will not sample all possible angles. While the couplings diminish at R^{-3}, the number of spins at a distance R from a given spin is proportional to R^2, so the net couplings between (distant) spins can still be significant. Ordinarily the orientation of the magnetization vector is uniform throughout the sample and so averaging over all spins at a distance R makes the net magnetic field vanish. However, the situation changes if magnetization direction is made anisotropic through, for example, the application of gradient pulses. In such a case the long-range couplings might not be completely averaged. The classical demagnetizing field is embodied in the collectivity of these couplings.

The demagnetizing field can cause a number of puzzling effects, most of which have recently been carefully reviewed by Levitt[19] including multiple spin-echoes in liquids.[61,62,64–68] The magnitude of the demagnetizing field is 5×10^{-9} of B_0 or less and yet this small field can produce a second echo of the order of 40% of the size of the main echo.[65] It is emphasized that large field strengths are not necessary for the observation of such effects; they were predicted to occur for water with a field strength of only 1 T[61] and have certainly been observed at a frequency of only 90 MHz.[66] Thus these effects are relevant to nearly all modern spectrometers. The demagnetizing field effect has been implicated as the cause of unusual phase behaviour in ^{3}H NOESY experiments.[69]

These effects on NMR can either be described by a classical treatment of the demagnetization field or by a macroscopic quantum treatment which removes several important simplifications such as the concept of the molecular spin system and the rejection of the high-temperature approximation.[24,26,70,71] However, Levitt[19] has noted that only the classical treatment produces quantitative agreement with experiment.

A means of minimizing the effects of the demagnetizing field can be found from inspection of Eq. (6). If pulsed field gradients (PFGs) are applied at the magic angle (54.7°, i.e. magic angle gradients or MAGs) with respect to the main magnetic field the demagnetizing field effects disappear (or are at least reduced).[25,34–36,38] MAGs inhibit the conversion of solvent antiphase magnetization present at the beginning of the acquisition period to in-phase magnetization and hence to observable signal.[26,64,72]

3. SUPPRESSION METHODS

3.1. Introduction

A suppression method must appeal to some NMR accessible difference between the solvent and the solute. The most obvious basis for discrimination lies in a difference in chemical shift and, with increasing field strength, this becomes a better basis for discrimination. However, the chemical shift fails as a basis for discrimination when the solute resonances of interest are too near or even under the water resonance (e.g. protein α-protons) or because good shimming is impossible (e.g. a magnetically heterogeneous sample). In such cases differences in relaxation time (i.e. T_1 or T_2), translational diffusion (D) or that water has no heteronuclear couplings may be used as the basis of the suppression method – these discriminants have the advantage of not requiring good lineshape. Many methods of suppression have become possible only with the advent of magnetic gradients and selective RF pulses, and some pertinent aspects with regard to solvent are considered in the following subsection. In the broadest sense, suppression methods can be classified either as pulse sequence methods or hardware/postprocessing methods. Hardware suppression methods, although being inflexible, have the advantage of not requiring any user intervention after being set up. Software-based postprocessing schemes can be used in addition to pulse sequence suppression methods to enhance further the degree of suppression. These methods are reviewed in the section on Postprocessing and selective detection-based methods (p. 325).

Many pulse sequence suppression schemes exist and these can be loosely classified into three broad classes: (i) saturation based, (ii) magnetization destruction based, and (iii) methods avoiding solvent saturation. An ideal method would suppress the solvent only with no other effect on the spectrum. In reality this is never the case. For example, some suppression sequences which involve frequency-selective excitation result in frequency-dependent artifacts such as phase shifts and amplitude responses. Sometimes the applicability of a suppression method depends on the sample. For example, in addition to creating artifacts, caution must be taken when using suppression methods that involve saturation since cross-relaxation can result in significant signal loss, especially with large molecules.

Suppression sequences are normally used in combination with some form of measurement pulse sequence which could be a multidimensional sequence (e.g. a NOESY sequence). This may change the requirements (less restrictive or more restrictive) of the suppression method. Suppression in multidimensional experiments is considered in Section 5. Suppression techniques, as we have noted above, are influenced/restricted by instrumental limitations and the sample itself and we note that simply by confining the sample to a smaller volume, for example through the use of susceptibility matched microtubes,

many of the problems (e.g. B_0 and B_1 homogeneity) are reduced. It is difficult to decide on a bench mark to enable easy comparisons of performance. Guéron and Plateau[9] have proposed the use of a standard sample. They emphasize that artifacts due to the suppression sequence are perhaps more important than the degree of residual solvent signal. Comparisons of binomial-type sequences,[12] gradient-based sequences[14] and with respect to use in magic-angle sample spinning of various unsonicated biological membranes and lipid suspensions[73] and for use in biofluid studies[74] have been presented in the literature.

3.2. Gradients and shaped RF pulses

Gradients

Due to the great strides in gradient generation technology, most recent spectrometers are capable of generating highly constant gradients suitable for solvent suppression that have fast rise and fall times and rapidly decaying residual gradients.[75] Gradients provide the basis of new and/or more efficient means of water suppression and can effect suppression through either (i) coherence selection, (ii) differential diffusion between solvent and solute or (iii) by destruction of the magnetization after it has been selectively excited. We also note that their ability to provide spatial encoding and spatially selective excitation has particular relevance for suppression in *in vivo* studies.

All of the gradient-based methods can be understood from the Larmor equation and thus for a spin at location $\mathbf{r}$ after the application of a gradient pulse $\mathbf{g}$ of duration δ, the phase ϕ will be given by

$$\phi(\mathbf{r}) = n\gamma\delta\mathbf{g}\cdot\mathbf{r} \tag{7}$$

where n is the order of the coherence. Thus, the gradient pulse results in a strong positionally dependent phase shift and the magnitude of the shift is larger for higher coherence orders. The gradient is generally only directed along z although on more sophisticated machines it may be possible to generate the gradients along any of the x, y or z axes or linear combinations of these. For example, for generating a magic angle gradient with respect to $\mathbf{B}_0$ (i.e. $\theta = 54.74° = \cos(\sqrt{g_x^2 + g_y^2 + g_z^2})^{-1}$).

Shaped pulses

The selectivity of a rectangular RF pulse can be increased merely by lengthening the pulse and using a reduced power; however, this approach is limited as it results in a sinc function-shaped excitation profile. Also, to achieve the desired selectivity, the pulse duration will eventually become too long and solute and solvent relaxation effects may become significant during the pulse. Hence in attempts to keep the pulses short while retaining

selectivity, increasingly sophisticated shaped pulses have been developed including some that allow multifrequency irradiation with only a single transmitter such as shifted laminar pulses (SLP).[76] The exact magnetization excitation pattern resulting from an RF pulse can, in general, be calculated from the Bloch equations. However, the reverse problem of how to find the form of the time-domain RF excitation needed to achieve the desired frequency domain is not straightforward due to the nonlinearity of the Bloch equations. Recently there have been a number of reviews on shaped pulses, selective excitation and design techniques.[77–79] The choice of the selective excitation pulse depends on the required excitation profile and the phase requirements of the excited magnetization and this can be particularly difficult in *in vivo* applications due to the greater B_1 inhomogeneity. Accurate flip angles in the presence of B_1 inhomogeneity can be obtained using adiabatic RF pulses.[80] Importantly, whenever the selectively excited magnetization is to be subsequently destructed by a gradient pulse, the phase requirement is removed.[15,81]

3.3. Saturation-based methods

Discrimination by chemical shift

Presaturation and spin-locking-based methods. The notion behind presaturation suppression techniques[82] is to selectively saturate the solvent signal before the excitation of the spins of interest and subsequent acquisition of their signals. The simplest variant of this type of sequence is where a soft pulse of constant amplitude (i.e. cw irradiation) is applied at the solvent frequency for a period of the order of the solvent T_1 to "presaturate" the solvent (see Fig. 5A). Often there is a residual baseline hump and some improvement can be had by combining the presaturation method with volume selection, since the volume selection filters out signal from parts of the sample where B_0 or B_1 is less homogeneous. A widely used means of doing this is to combine presaturation with a 1D NOESY sequence. This sequence corresponds to the first increment of a 2D NOESY experiment with the mixing time set to some very short value (see Fig. 5B). The NOESY sequence gives better signal suppression mainly due to the volume selection resulting from the phase cycling of the pulses.[83] Apart from the NOESY sequence, many volume selection sequences exist, for example the sequence $90^\circ_x 90^\circ_y 90^\circ_{-x} 90^\circ_{-y}$[84] is equivalent to 90°_y. Volume selection as part of suppression schemes has also been proposed using the GROPE-16 sequence[85] and composite refocusing pulses.[86] Neuhaus *et al.*[83] have proposed a variation termed FLIPSY (*FLIP*-angle adjustable one-dimensional NOE*SY*) sequence which combines presaturation with a low angled pulse for excitation and two π pulses (see Fig. 5C). The volume selection is achieved by application of the EXORCYCLE

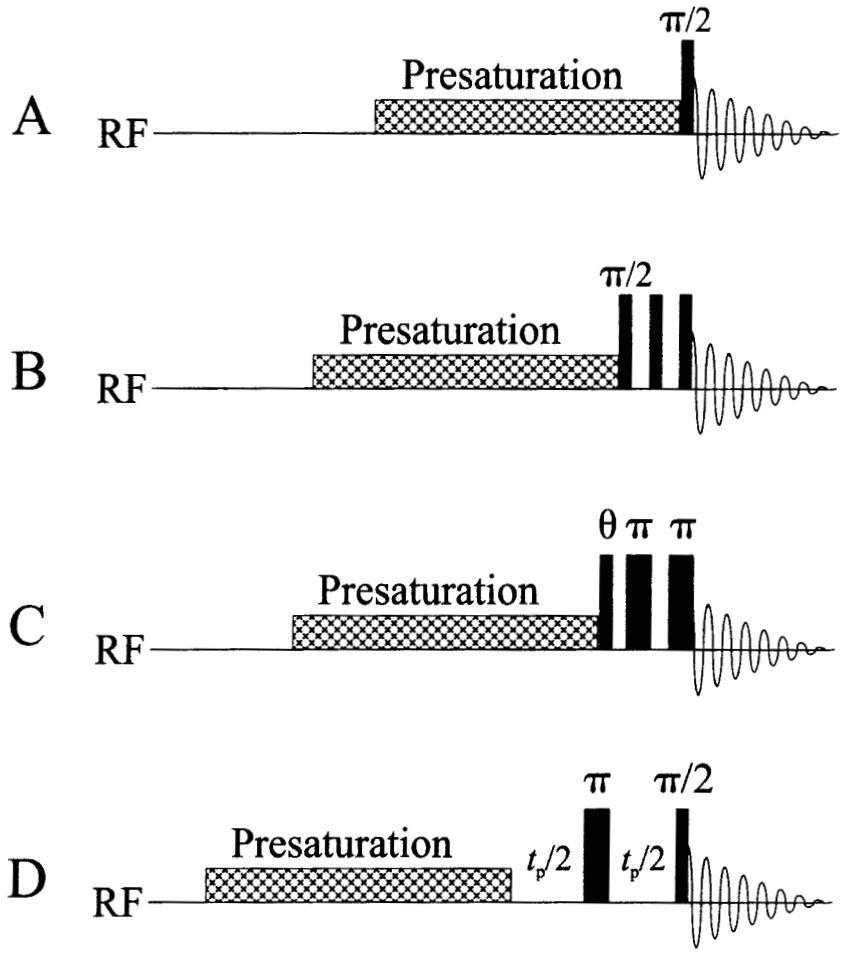

Fig. 5. Various presaturation-based suppression sequences: (A) presaturation, (B) 1D NOESY, (C) FLIPSY and (D) SCUBA. The phase cycling for the 1D NOESY and FLIPSY sequences can be found elsewhere.[83] The π pulse in the SCUBA sequence can be replaced with a composite π pulse to ensure more complete inversion.

phase cycle[87] to one or both of the π pulses. An important difference is that with FLIPSY, unlike the 1D NOESY experiment, the excitation pulse angle can be varied.

Presaturation may result in significant bleaching out of the resonances near the solvent frequency (e.g. protein $C^{\alpha}H$ protons if irradiating at the water frequency) in the resulting spectrum (see Fig. 6). The saturation can also be spread to labile protons via chemical exchange and, especially in macro-

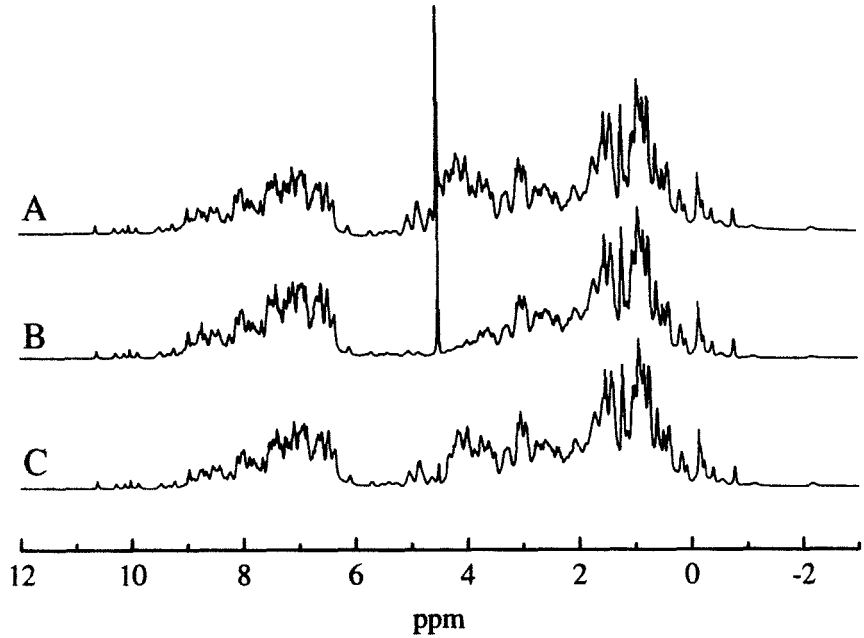

Fig. 6. Comparison of the (A) Water-PRESS, (B) WATERGATE and (C) presaturation methods on a lysozyme sample (10 mM in 90:10 ^2H_2O:H_2O, pH 3.7). All three spectra were acquired at 310 K at 300 MHz and under the same conditions as far as possible (e.g. receiver gain and number of scans). In acquiring spectrum (C), an inversion delay (D_{NP}) of 2.58 s was used with a series of 0.5 ms z-gradient pulses with an intensity of about 1 G cm^{-1}. It can be clearly seen that the intensities of the protein $C^{\alpha}H$ protons near the water frequency (~ 4.5 ppm) are greatly attenuated in (A) and nearly absent in (B) compared to those in (C). (From Price *et al.*[111])

molecules, by propagating through the spin system by cross-relaxation (i.e. spin-diffusion; see Section 7.1). The bleaching and saturation transfer effects can be reduced by making the presaturation frequency range more selective and/or using a lower-powered presaturation pulse. The degree of attenuation of labile protons depends on the proton–water exchange rate.[88] The exchange rate may be able to be minimized by judicious choice of pH.[89] One way of recovering these resonances especially in the case of large macromolecules (i.e. for which $T_2 \ll T_1$) is by using the SCUBA (*s*timulated *c*ross-peaks *u*nder *b*leached *a*lphas) method[90] (see Fig. 5D) in which a short delay, t_p, is placed after the presaturation pulse to allow the resonances (e.g. $C^{\alpha}H$) to equilibrate with their neighbours through dipolar cross-relaxation. A composite π pulse in the middle of t_p prevents recovery of the water.

In spin-locking-based methods[91,92] the inhomogeneity of the RF field is used to dephase the water magnetization that is not aligned along the

spin-lock (SL) axis. Hence, the effectiveness of the suppression increases with the RF strength. High-power spin-lock pulses of 1 to 2 ms duration are sufficient nearly to complete average magnetization in the plane orthogonal to the spin-lock axis. If a pair of orthogonal spin-lock pulses is separated by a delay τ for free precession (e.g. SL_y–τ–SL_x), only the magnetization at the carrier frequency and at multiples of $1/(2\tau)$ is suppressed. The excitation profile is described by

$$\sin(2\pi\tau\nu) \tag{8}$$

where ν is the offset from the carrier frequency. Consequently, if there is no interpulse delay (i.e. $\tau = 0$), then all magnetization is suppressed. To avoid echo effects SL pulses of different length are generally used.[93–95] Sodano and Delepierre[96] have recently reported short-hard pulse and SL pulse combinations that gave very good suppression and have binomial-like (see Binomial sequences, p. 322) frequency responses. They presented examples of NOESY spectra of a 0.25 mM DNA sample in 90% H_2O acquired using these suppression schemes.

No matter how strong the RF pulse is and how long it is applied for, it is difficult to suppress the solvent peak by more than a factor of 10^3.[97] This mainly results from the long RF irradiation with fixed phase making some of the solvent magnetization align along the direction of the RF field (i.e. spin-locking).[98] Taking this as a basis, Mao and Ye[97,99] have proposed the phase-shift presaturation technique in which the RF phase is shifted by $\pi/2$ during the cw irradiation. This results in the spin-locked magnetization being forced to nutate and be dephased by the RF inhomogeneity. With suitable phase-cycling, they have achieved suppressions of the order of 10^5–10^6 using this method.[97]

Discrimination by relaxation time

Since the solvent is typically a much smaller molecule than the solute (e.g. a protein), its relaxation time is generally much longer than that of the solute and this difference can be exploited. However, as the difference in relaxation time between the solvent and the solute becomes smaller, there is a significant loss of signal of the resonances of interest when relaxation differences are used as the basis of suppression. Importantly, relaxation-based suppression sequences result in flat baseline responses throughout the entire spectrum.

WATR, WEFT and Water-PRESS. If the transverse relaxation of the water is faster than the spins of interest, suppression can be achieved using the CPMG-based WATR (*w*ater *a*ttenuation by T_2 *r*elaxation) method.[100,101] The T_2 relaxation time of the water can be selectively decreased through the

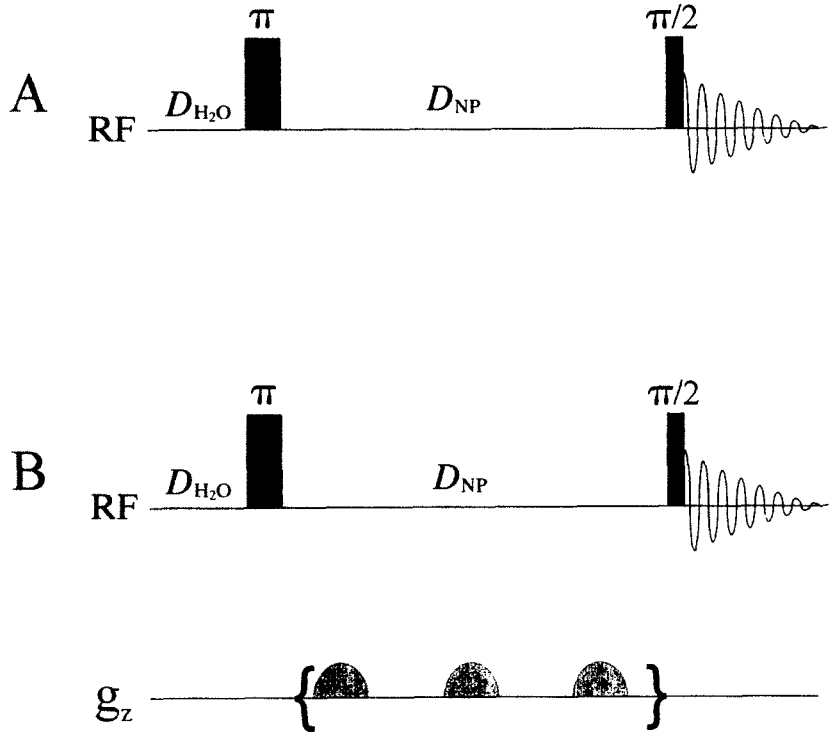

Fig. 7. (A) The WEFT sequence; in this sequence the π pulse is applied to rotate all of the magnetization (i.e. both solute and solvent) to the $-z$-axis. A delay (D_{NP}) of sufficient length is used to allow the water magnetization to relax to the origin ($D_{NP} = \ln(2)T_1^{H_2O}$) whilst during the same period, by virtue of faster longitudinal relaxation, the solute resonances have reached thermal equilibrium. An excitation pulse (represented here as a $\pi/2$ pulse) is then applied and an almost water-free spectrum is acquired. However, in the presence of radiation damping the water quickly returns nonexponentially to the equilibrium position at a similar rate to the solute nuclei (see Fig. 2). However, if during D_{NP} a series of n very weak and evenly spaced gradient pulses are applied so as to inhibit the effects of radiation damping, the water relaxes according to its natural spin–lattice relaxation rate. This is the basis of the Water-PRESS sequence (B). An example of a spectrum obtained with Water-PRESS is shown in Fig. 1B and Fig. 6.

addition of molecules that promote exchange such as urea,[101] by addition of transition metal complexes[102] or through the use of ^{17}O-enriched water.[103]

An elegant suppression technique is to use the difference in relaxation time between the water, $T_1^{H_2O}$, and the solute, T_1^{Sol}, in an inversion recovery experiment to suppress the water resonance (also known by the acronym WEFT, *w*ater *e*liminated *f*ourier *t*ransform spectrum)[104,105] and variations on this approach.[106–108] In this method (see Fig. 7A) the $\pi/2$ pulse is applied at a

time D_{NP} after the π pulse which corresponds to the null point of the water signal (i.e. $D_{NP} = \ln(2)T_1^{H_2O}$). Providing that $T_1^{H_2O} \gg T_1^{Sol}$ the solute magnetization will be acquired with nearly full intensity whilst that of the water will be greatly suppressed. WEFT-based techniques are particularly attractive for protein studies as they provide one of the best opportunities for observing solute resonances close to the water resonance.[109] Mirau[110] has presented a method which is a combination of the WATR and WEFT techniques which uses selective pulses. If the solvent has a shorter T_1 than the solute, some suppression may be had by preceding the sequence with an inversion recovery sequence.

While the intrinsic longitudinal relaxation time of water is nearly an order of magnitude longer than that of most protein resonances, the effects of radiation damping, especially at higher magnetic fields and with sensitive probes, dominate the effects of the inherent relaxation mechanisms of the water protons (see Fig. 2). This results in the water resonance having a very similar effective relaxation time to that of the protein resonances. Consequently the efficiency of the WEFT method is not only compromised but the intensity of the solute resonances is distorted by differential relaxation as the protein resonances do not have sufficient time to reach thermal equilibrium while maintaining the conditions necessary for the nulling of the H_2O signal. A recent variant of WEFT termed *w*ater-*pres*equence *s*uppression (Water-PRESS, see Fig. 7B) uses magnetic field gradient pulses to inhibit the initiation of radiation damping by dephasing any net transverse magnetization (see Section 4.2).[111,112] In Fig. 1 an aqueous solution of lysozyme is used to demonstrate water suppression obtained using the Water-PRESS subunit. Water-PRESS is compared with presaturation and WATERGATE (see WATERGATE and related sequences, p. 314) in Fig. 6.

An obvious criticism of WEFT-based sequences from a practical viewpoint is the (long) delays needed to achieve the null-point. However, it is unnecessary to wait for full solvent relaxation between scans as in reality only the difference in the relaxation time between the solvent and solute is important. Thus, we can show that the delay required for water relaxation (i.e. the recycle delay), D_{H_2O}, is given by[112]

$$D_{H_2O} = \ln\left(\frac{\cos(\theta)\exp\left(-\frac{D_{NP}}{T_1^{H_2O}}\right)}{1 + (\cos(\theta) - 1)\exp\left(-\frac{D_{NP}}{T_1^{H_2O}}\right)}\right) T_1^{H_2O} \qquad (9)$$

where θ is the flip angle of the excitation pulse and $T_1^{H_2O}$ is in reality only an effective relaxation time due to the effects of radiation damping. An example of a spectrum of lysozyme acquired with the water in the steady state regime is given in Fig. 8.

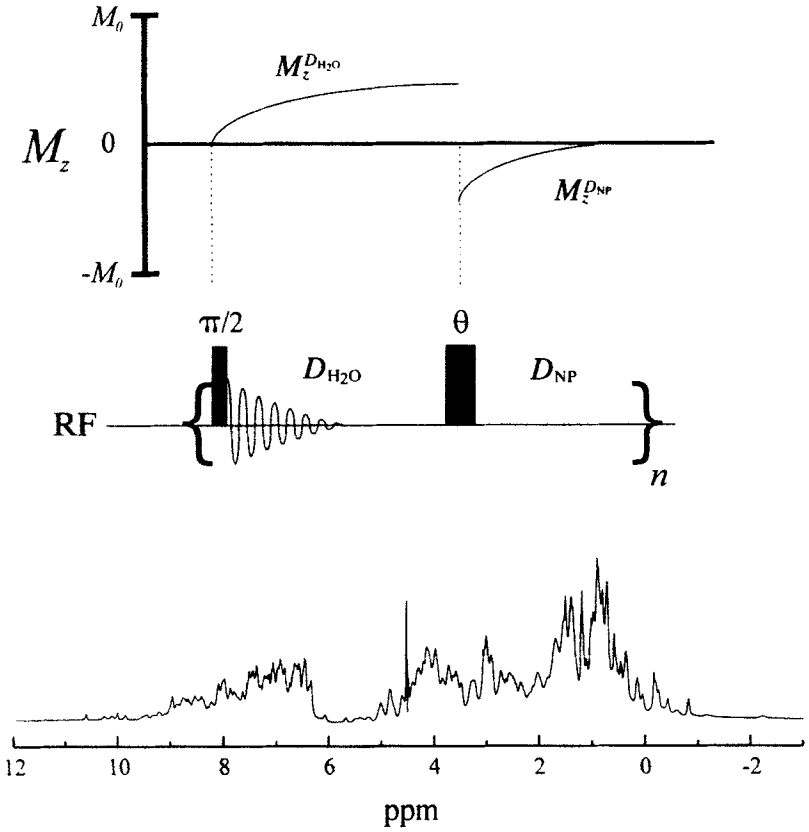

Fig. 8. Water-PRESS sequence under steady-state conditions. The change in the longitudinal magnetization of the water protons when $D_{H_2O} \ll 5 \times T_1^{H_2O}$ is schematically shown in (A). We have chosen to present the sequence in this order to make it more obvious that the acquisition time is part of D_{H_2O}. As before (e.g. Fig. 7B) there is a series of z-gradient pulses applied during D_{NP} (not shown). The sequence is shown contained in brackets with a subscript n (integer) to emphasize the repetition of the sequence which in combination with $D_{H_2O} \ll 5 \times T_1^{H_2O}$ maintains the water in a steady state. The spectrum of lysozyme (10 mM in 90:10 ^2H_2O:H_2O, pH 3.7) shown in (B) was obtained at 310 K and at 300 MHz with D_{H_2O} = 2.3 s (note this includes the acquisition time of 0.8 s) and D_{NP} = 1.363 s. Because the Water-PRESS sequence was run in the steady state the effects of radiation damping are largely eliminated throughout the entire sequence including the acquisition time and the only remaining evidence of the water (including a contribution from the transmitter spike) is the small narrow spike at ~ 4.5 ppm.

3.4. Magnetization destruction-based methods

Randomization

In the randomization approach, a selective RF pulse is used to excite the solvent signal to become a transverse coherence. This transverse coherence is then dephased by a gradient pulse (see Fig. 9A). After the randomization of the solvent magnetization, a hard $\pi/2$ pulse may then be used as the final excitation pulse, thus resulting in uniform excitation with minimal phase distortion.[113–116] More recently this approach has "acquired" the acronym RAW (i.e. *r*andomization *a*pproach to *w*ater suppression).[117] In the imaging literature it is referred to as CHESS.[118] The randomization technique is both frequency and lineshape independent. Conversely, excellent lineshape and phase coherence of the selective pulse are not prerequisites to obtaining solvent suppression. The method, with appropriate frequency selective pulses, has the possibility of suppressing multiple solvent peaks.

Assuming that the gradient used is oriented in the z direction, then from Eq. (7) the phase randomization attenuates the transverse magnetization in a homogeneous sample by a factor f, given by[15,119]

$$f = \left(\frac{1}{z_2 - z_1} \int_{z_1}^{z_2} e^{-i\phi_z} \, dz \right)^{-1} \tag{10}$$

where z_1 and z_2 are the volume element dimensions in the gradient direction and the phase at position z, ϕ_z, is given by analogy to Eq. (7). It is important to realize that the phase randomization occurs in the plane perpendicular to the gradient and that the phase only appears random when integrated over the sample volume. Magnetization oriented in the direction of the gradient is unaffected by the gradient pulse. When gradient pulses are used to effect phase randomization they are sometimes referred to as "crusher" or "homospoil" gradients. The efficiency of the randomization also depends on the local static field homogeneity. Hopkins *et al.*[120] have noted that for simple sample geometries, maximum signal attenuation occurs when the gradient is directed along the body diagonal of the detectable sample, since this corresponds to the maximum length along the gradient and results in a gradual increase in sample volume with distance in the gradient direction. Hence the best results should be obtained for B_0 gradients by simultaneous applications of z, and x and/or y gradients.

Apart from the gradient itself, the degree of suppression is related to the efficiency of excitation by the selective pulse and thus the choice of selective pulse is important with, for example, hyperbolic secant pulses perform better than sinc pulses.[115] If the solvent T_1 is very short and on the order of the time for the dephasing procedure, then some (unwanted) z-magnetization will be re-established prior to the excitation pulse. One method of circumventing this

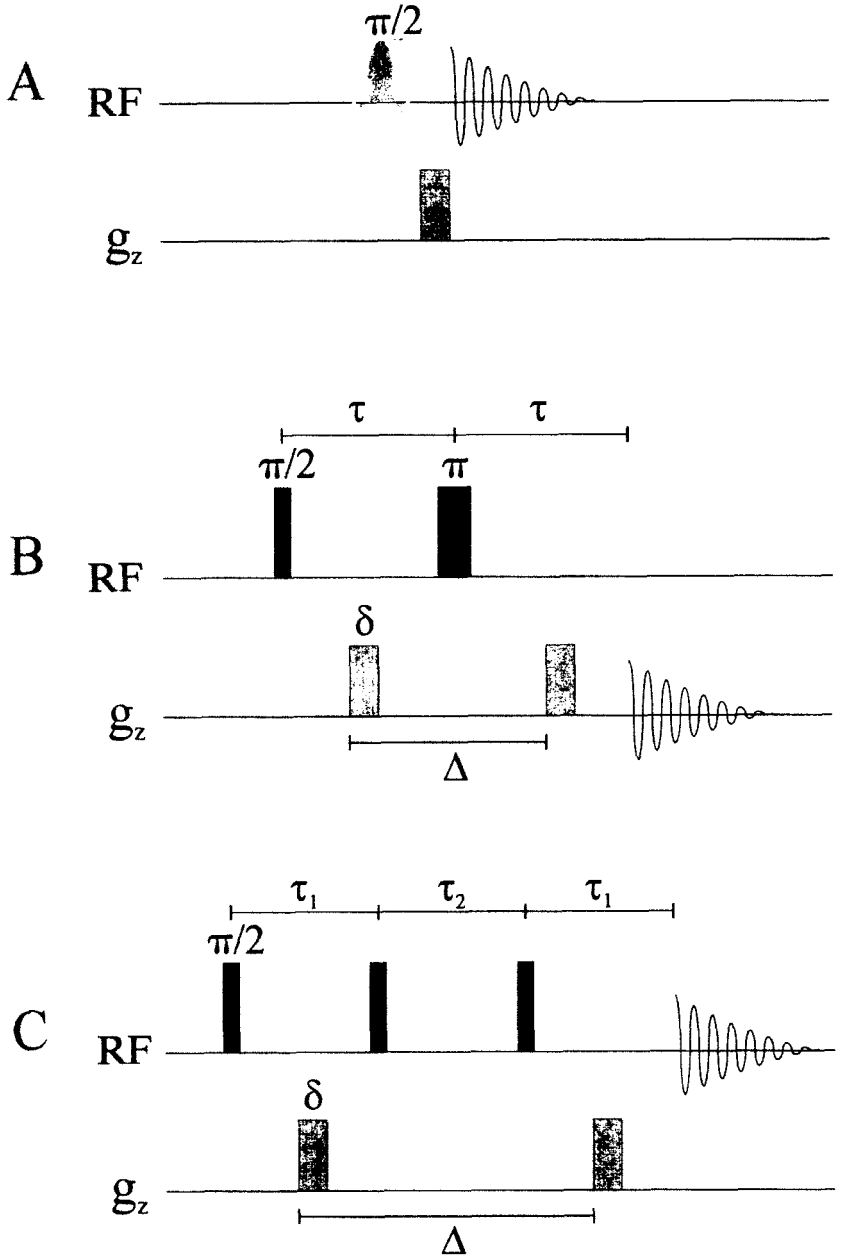

Fig. 9. (A) Selective excitation and destruction of magnetization using a magnetic field gradient pulse. PGSE sequences used for diffusional attenuation of the solvent signal, based on the Hahn spin-echo sequence (B) and the stimulated-echo sequence (C). In the Hahn spin-echo sequence the magnetization is always subject to spin–spin relaxation. However, in the stimulated-echo sequence the delays can be set such that Δ is mainly contained in τ_2 where the relaxation is longitudinal and thus this sequence is preferable for large solute molecules since the condition $T_2 \ll T_1$ usually holds.

problem is to follow the dephasing gradient by a weak gradient to broaden the solvent signal to 100–200 Hz. A noise pulse is then applied and thus, following gradient collapse, the remaining solvent magnetization is randomized and no coherence is read by the final excitation pulse.[115] Another more efficient variation is to use a selective (i.e. shaped) pulse with a flip angle slightly larger than $\pi/2$ to account for this relaxation so that the solvent magnetization becomes null at the time of acquisition.[121] Nevertheless, a 1 RF pulse/gradient pulse combination is extremely sensitive to any missetting of the $\pi/2$ pulse. The solvent suppression can be improved by using further applications of the selective RF pulse/gradient combination before the excitation pulse.[116] However, it is necessary to take precautions to avoid gradient recalled echoes such as halving the gradient strengths in subsequent RF pulse/gradient episodes[6] or using different gradient directions.

A combination of the SCUBA (see Discrimination by chemical shift, p. 302) and randomization approaches has also been reported under the name RAWSCUBA.[117] In this sequence the solvent resonance is first randomized by a selective $\pi/2$ pulse and gradient pulse combination and then the SCUBA sequence is applied (i.e. $t_p/2$–composite π–$t_p/2$) and a final gradient pulse in the opposite direction to the first to dephase the water further.

Mobility-based (diffusion) filters. In many instances, the solute is a much larger molecule than the solvent. Since (roughly) $D \propto \mathrm{MW}^{-1/3}$ the solute diffusion coefficient is often much less than that of the solvent. For example, the diffusion coefficient of proteins is typically at least an order of magnitude below that of water.[75] This difference in diffusion coefficients as pointed out by Stilbs[122] can be used as the basis of a solvent suppression method. This is now commonly referred to by the acronym DRYCLEAN (*d*iffusion-*r*educed water signals in spectroscopy of molecules moving *s*lower th*an* water) method.[13,123] The DRYCLEAN method is merely the application of the pulse-gradient spin-echo (PGSE) diffusion sequences (see Figs 9B and 9C).[75,123] For a single diffusing species the signal is given by[124,125]

$$S(g) = S(0)\exp(-2\pi/T_2)\exp(-\gamma^2 g^2 D\delta^2(\Delta - \delta/3)) \tag{11}$$

where $S(0)$ is the signal in the absence of gradient pulses, Δ is the separation between the gradient pulses and the echo time is given by 2τ. It is possible to normalize out the relaxation attenuation and thereby define the attenuation of the spin-echo signal giving the well-known Stejskal and Tanner relation,[124,125]

$$E = \frac{S(g)}{S(0)} = \exp(-\gamma^2 g^2 D\delta^2(\Delta - \delta/3)) \tag{12}$$

When the difference in diffusion coefficients is very large between the solute

and the solvent, the experimental parameters can be chosen such that there is very little attenuation of the solute resonances but almost complete suppression of the solvent resonance. Thus, we can think of the PGSE approach to suppression as being a diffusion or molecular weight filter of the signals. From Eq. (12) it can be shown that, neglecting relaxation effects, the relative attenuation of the solvent and the solute is given by,

$$\frac{\ln(E_{\text{solvent}})}{\ln(E_{\text{solute}})} = \frac{D_{\text{solvent}}}{D_{\text{solute}}} \tag{13}$$

However, as the molecular weight of the solute increases, so does generally its transverse relaxation rate so that unless strong gradients are available which enable the δ, Δ and consequently τ delays to be kept short, the loss of signal due to spin–spin relaxation becomes more pronounced. Additionally, the diffusional loss in intensity of exchangeable protons, whose effective diffusion coefficient contains a contribution from the solvent, will be affected more than nonexchangeable protons. Further, any echo-based system such as DRYCLEAN will result in unequal losses of the protein resonances according to the T_2 relaxation rates of the individual spins and complications due to J-modulation.

To minimize signal loss due to spin–spin relaxation, it is often preferable with larger solute molecules to use a stimulated-echo-based sequence (see Fig. 9C) in lieu of the Hahn spin-echo sequence, for which the attenuation equation is given by

$$S(g) = \frac{S(0)}{2}\exp(-2\tau_1/T_2)\exp(-\tau_2/T_1)\exp(-\gamma^2 g^2 D\delta^2(\Delta - \delta/3)) \tag{14}$$

and the delays τ_1 and τ_2 are defined in Fig. 9C. After normalization, the equation describing the signal attenuation is again given by Eq. (12). Larger solute molecules have $T_2 \ll T_1$ and the inherent loss of a factor of two in signal (see Eq. (14)) is often more than compensated by the reduced relaxation-related signal loss since the magnetization is subject to longitudinal relaxation for the majority of the sequence (i.e. during τ_2). A further consequence of keeping the magnetization transverse for a shorter period of time is the reduction in J-modulation effects.

So long as there is a significant difference in the relative diffusion coefficients, large suppression factors are easily obtained and the method produces a flat baseline with no phase errors. Further, the method allows signals under the water resonance and exchangeable resonances to be observed and it does not depend on the lineshape of the resonances. Diffusion filters also afford the possibility of suppressing multiple solvents simultaneously (i.e. all of the rapidly diffusing species) as demonstrated in a NOESY sequence by Pontsingl and Otting.[126] This is a very important point since it provides a simple way of

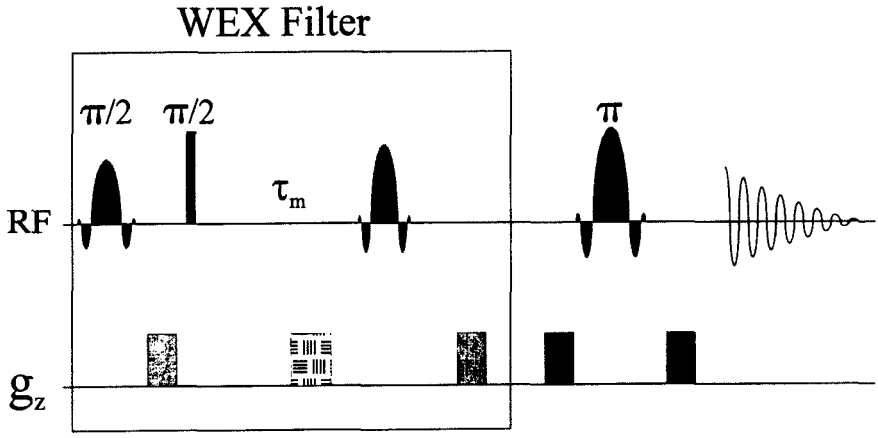

Fig. 10. WEX filter[128] combined with WATERGATE suppression. The first $\pi/2$ pulse in the WEX filter is selective to the water, the second is nonselective and the third can be either hard or, as shown, selective on the NH protons. τ_m defines the mixing period. The grey gradient pulses are used for coherence selection, the mottled gradient pulse is a crusher gradient and the two gradient pulses for the WATERGATE subunit are coloured black. Ideally three orthogonal directions would be used for the different gradient pulses.

removing small-molecular-weight contaminants and buffer resonances from NMR spectra.

Diffusion filtering techniques also allow the separation of intermolecular from intramolecular water–protein NOEs in 1D NOE difference experiments.[127] Mori *et al.*[128] have developed the WEX filter (see Fig. 10) which is based on a stimulated-echo diffusion sequence (see Fig. 9C). The filter only allows through those signals that result from exchanged water. The nonexchanged water can then be selectively suppressed with, for example, WATERGATE (see below), leaving only those resonances that result from the exchange of the water. This exchange filter provides efficient water suppression, single-scan gradient-coherence selection and clear definition of the mixing time in the pulse sequence.

Diffusion-based methods such as DRYCLEAN are also applicable to cases where the solute of interest, although not having an inherently small diffusion coefficient, has an effectively small diffusion coefficient by virtue of its environment (i.e. restricted diffusion such that would occur if the solute were in the intracellular matrix). For example, the intracellular solutes of perfusing cells were able to be selectively observed whilst the extracellular water and solutes in the surrounding medium were suppressed using the stimulated-echo sequence.[129] In a later work Potter *et al.*[130] used the same idea to suppress extracellular water in bacterial suspensions in porous media.

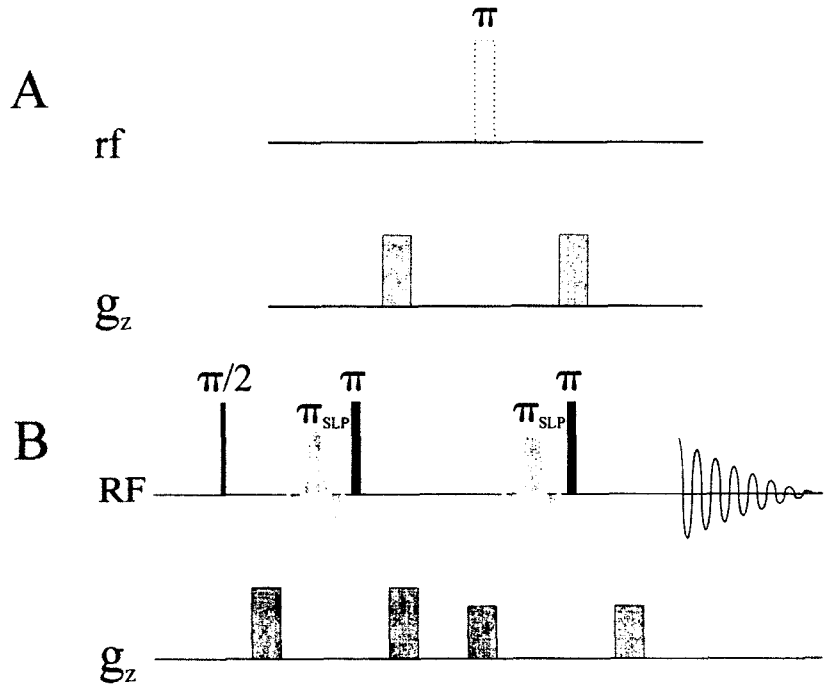

Fig. 11. (A) A conceptual diagram of the WATERGATE subunit, the π RF pulse is some type of selective π pulse. (B) Multiple solvent suppression using the double-pulsed field gradient echo.[140] The selective π pulses are SLP pulses to enable multiple solvent suppression. To avoid breakthrough of undesired coherences, different values for the gradients are used in the first and second echo. The phase cycling is given elsewhere.[140]

WATERGATE and related sequences. The WATERGATE (*water* suppression by *gra*dient *t*ailored *e*xcitation) sequence[131–133] is like a PGSE diffusion sequence except that it uses a selective π pulse which (ideally) affects only the solute resonances and has zero intensity at the water frequency (see Fig. 11A). Thus solute resonances are refocused whilst the water resonance is destroyed by the two gradient pulses. However, magnetization aligned along the z- or $-z$-axis is unaffected by the sequence. The selective π pulse can take a number of forms: (i) it can be a hard π_x pulse sandwiched by two soft $\pi/2_{-x}$ pulses (applied at the water frequency) which gives zero net rotation of the water[131] with the selectivity being determined by the length of the $\pi/2$ pulses, (ii) a sophisticated shaped π pulse or (iii) a binomial π pulse, for example 3α-τ-9α-τ-19α-τ-19α-τ-9α-τ-3α (i.e. a "3-9-19" sequence where $\alpha = \pi/26$).[132] When the phases of the pulses are set as x, x, x, $-x$, $-x$, $-x$ the binomial π sequence produces zero net excitation on resonance and at offsets,

$$\Delta\nu_{zero} = n/\tau, \text{ for } n = 0, 1, 2 \ldots \quad (15)$$

and if the phases of the pulses are set as x, $-x$, x, x, $-x$, x the binomial π sequence produces off-resonance suppression at offsets,

$$\Delta\nu_{\text{zero}} = (2n + 1)/2\tau, \text{ for } n = 0, 1, 2 \ldots .. \quad (16)$$

The use of the binomial sequence in WATERGATE has the advantage of being more insensitive to errors in pulse amplitudes and phases. However, the excitation profile is no longer uniform with a broad excitation region around the water and at the ends of the spectrum. Although achieving high levels of suppression, resonances close to the water resonance are also significantly suppressed since the π pulse is not totally selective (see Fig. 6). Recently a modified WATERGATE sequence with reduced suppression bandwidths has also been developed.[134] Interestingly, radiation damping effects can actually make the half-width suppression profile narrower in WATERGATE when using a high-proton concentration water sample.[134] This is due to the effects of radiation damping providing an efficient decay mechanism for the transverse magnetization.[58] If the transmitter is set to the water frequency, there is no radiation damping and the highest degree of suppression is obtained. The degree of suppression is reduced as the transmitter is moved away from the water frequency.

Providing the echo interval in WATERGATE is kept short to minimize J-modulation, T_2 relaxation and molecular diffusion effects (i.e. note the similarity with the Hahn spin-echo-based PGSE sequence in Fig. 9B), the desired resonances are retained in the spectrum with near-full intensity while the water peak should be suppressed by a factor of at least 10^4. Scalar coupling evolution can be refocused if the π pulse in the WATERGATE sequence excites only some of the solute resonances but not the scalar coupled partners (for example amide resonances).[128]

In one-dimensional usage, a $\pi/2$ nonselective excitation pulse can be applied before the WATERGATE sequence. In cases where it is desired to observe exchangeable protons, a selective $\pi/2_{-x}$ pulse (selective of the water resonance, for example an EBURP2 pulse[135]) can precede the nonselective $\pi/2$ pulse. WATERGATE can be incorporated into two- and higher-dimensional experiments (see Section 5).

Dalvit *et al.*[136] have recently presented a modified version of the WATERGATE sequence that they have termed "MULTIGATE" which can be used to suppress multiple solvent signals. In this modified sequence, the two selective $\pi/2$ pulses of the WATERGATE sequence are replaced with two selective $\pi/2$ SLP. These pulses excite two or more solvent signals. Shaka *et al.*[137,138] have proposed a *d*ouble gradient *p*ulsed *f*ield *g*radient *s*pin-*e*cho (DPFGSE) method which is sometimes referred to as "excitation sculpting" (see Fig. 11B), which is in effect a double-echo version of the WATERGATE sequence and is very tolerant of miscalibrated pulses and gradient strengths. Although the double-echo approach allows for better suppression and phase

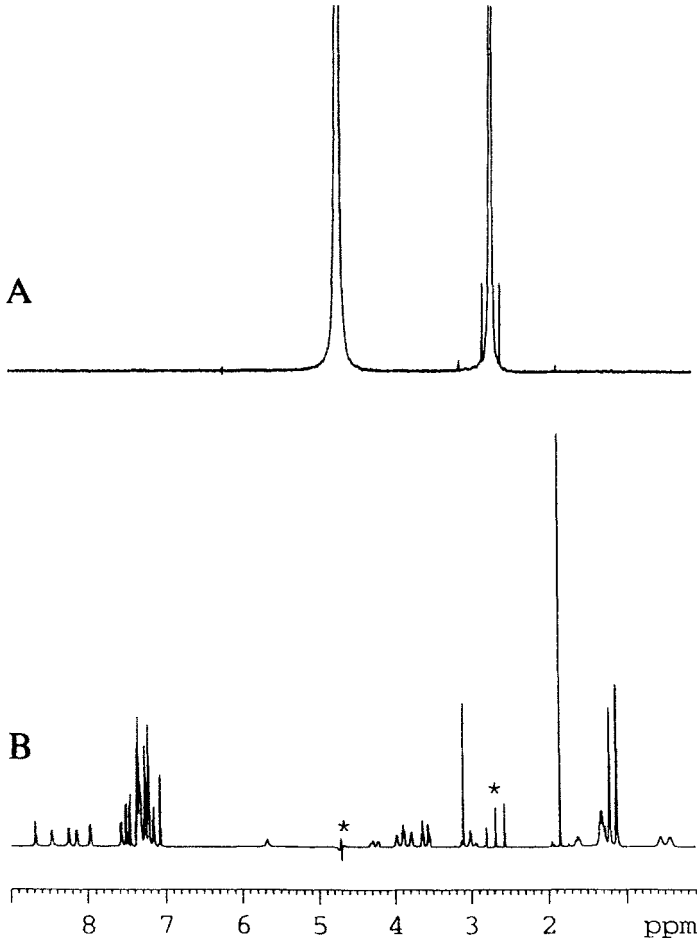

Fig. 12. Example of multiple suppression. (A) Reference spectrum of 4 mM Sandostatin® at pH 7.6 in 250 μl H_2O, 250 μl h_6-DMSO (50 μl ^2H_2O). (B) Spectrum recorded with the pulse sequence given in Fig. 11B using 16 scans. The length of the π_{SLP} pulses was 2.9 ms. The asterisks denote residual solvent signal. (From Dalvit[140] with permission.)

properties, the suppression profile is somewhat broader and the sequence takes twice as long. Parella *et al.*[139] have demonstrated that a simple variant of the double gradient echo sequence[137] using rectangular-shaped selective π pulses can be used to effect multiple solvent suppression. In a related work, Dalvit[140] has presented another modified DPFGSE sequence incorporating SLP pulses,[76] based on soft rectangular strongly truncated Gaussian pulses, which can be used to affect solvent at multiple frequencies (see Fig. 11B). The SLP pulses contain as many modulations as the number of solvent signals to

be suppressed (see Fig. 12). We note that to achieve good multiple suppression, some degree of sequence optimization is required.

Mescher *et al.*[141] have proposed the MEGA sequence which is related to both the WATERGATE and DPFGSE sequences, with the additional advantage that signals outside the suppression band are refocused with a single pulse, whereas in the DPFGSE sequence more time is required as the signals of interest must experience at least two refocusing pulses. MEGA, like DPFGSE, is less susceptible to flip angle errors of the selective pulses than WATERGATE.[141] However, while DPFGSE generates constant magnetization phase, MEGA yields uniform magnetization phase only when a constant rotation axis is provided by the pulse used to refocus the spins of interest.

WET. WET (*w*ater suppression *e*nhanced through T_1 effects)[6,142] was originally proposed for use in localized spectroscopy where T_1 and B_1 inhomogeneity can be a problem.[119] It uses a series of four frequency-selective RF pulses each followed by a gradient pulse. If simultaneous ^{13}C decoupling is applied at the time of the frequency selective pulses, ^{13}C satellites of solvent resonances (e.g. CH_3OH and CD_3CN) are also suppressed – this can be especially useful in applications such as LC NMR. The four-element pattern is optimized to create a highly effective solvent suppression pulse sequence element (see Fig. 13). WET is capable of solvent suppression factors in excess of 10^4 in a single scan. The use of multi-frequency shifted laminar SEDUCE pulses[76,143] results in WET being capable of suppressing multiple solvent resonances. WET self compensates for miscalibrated pulse widths/poorly tuned probes and flowing samples. By changing the angles of the selective pulses the WET subunit can be made T_1 in addition to B_1 insensitive. It suppresses in less than 100 ms and can be used under both stopped flow and flowing conditions. Although WET is a solvent saturation technique, due to its short time scale like WATERGATE, resonances undergoing slow or medium exchange will still be observable. Smallcombe *et al.*[6] have presented and demonstrated a variety of 2D and pulsed field gradient sequences incorporating the WET suppression subunit.

Coherence selection

The use of heteronuclear and homonuclear coherence selection as a means of solvent suppression has been reviewed in some detail in the literature already.[12,13,15] Thus, we will only note some of the salient features. As noted above, water (i.e. $^1H_2{}^{18}O$) has no heteronuclear couplings and this can often be exploited as a means of suppression using pulse sequence editing procedures such that only those species that contain such couplings are detected. Generally, the proton detection of heteronuclei (coupled) containing compounds (i.e. indirect detection) can be classified into spin-echo or polarization transfer and multiple-quantum methods. Since some of these are in effect

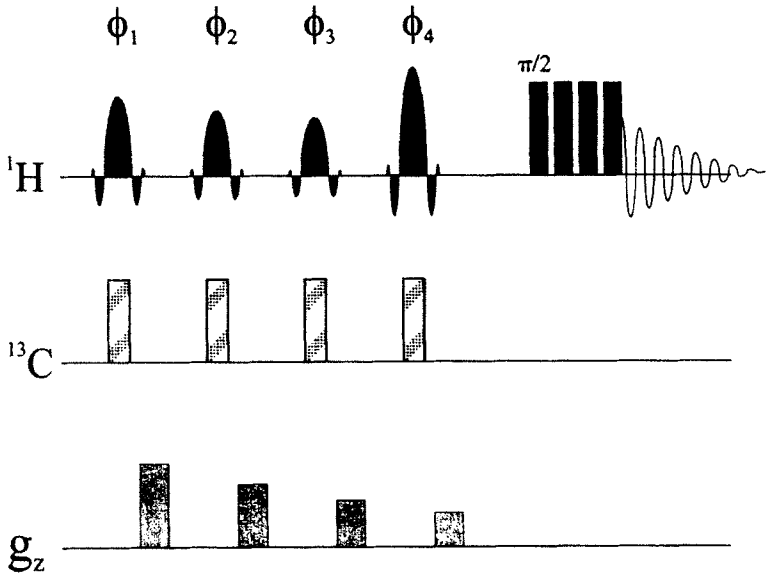

Fig. 13. The WET sequence modified for use with 1D LC NMR.[6] The four SEDUCE RF pulses are $98.2°_x$, $80.0°_y$, $75.0°_y$ and $152.2°_y$ for B_1-insensitive WET. Other angles are used in the case of B_1- and T_1-insensitive WET. The gradient pulses are each 2 ms long with amplitudes of 32, 16, 8 and 4 G cm^{-1}, respectively. There is a delay of 2 ms between each gradient pulse and the next RF pulse. Carbon decoupling with a field strength of 100 Hz is applied during the ^{1}H-selective pulses. Instead of a single (hard) $\pi/2$ excitation pulse, a volume selective composite hard $\pi/2$ pulse scheme[84] (i.e. $90°_x 90°_y 90°_{-x} 90°_{-y}$) can be used which affords a flatter baseline.

difference techniques, it must be remembered that the signals must first be acquired before they can be subtracted so that digitization by the ADC can still be a limiting factor. For example, with an AX spin system the following spin-echo sequence shown in Fig. 14A could be used. In the absence of the heteronuclear π pulse, both the proton chemical shifts and the components of the multiplets will be refocused at $t = 2\tau$ (note $\tau = (2J)^{-1}$). However, in the presence of the heteronuclear π pulse, only the chemical shifts will be refocused and the multiplets will have opposite sign. Hence subtraction of the two experiments eliminates uncoupled spins. Bulsing and Doddrell[144] have considered the potential of reverse polarization transfer experiments for solvent suppression.

Once a heteronuclear correlation is established, the water resonance can be saturated since it is not involved in the correlation.[145] The heteronuclear magnetization transfer sequence can be designed so that at some point the heteronuclear correlation is oriented along z and the water magnetization is transverse. A z-gradient pulse can then be used to purge the water magnetiza-

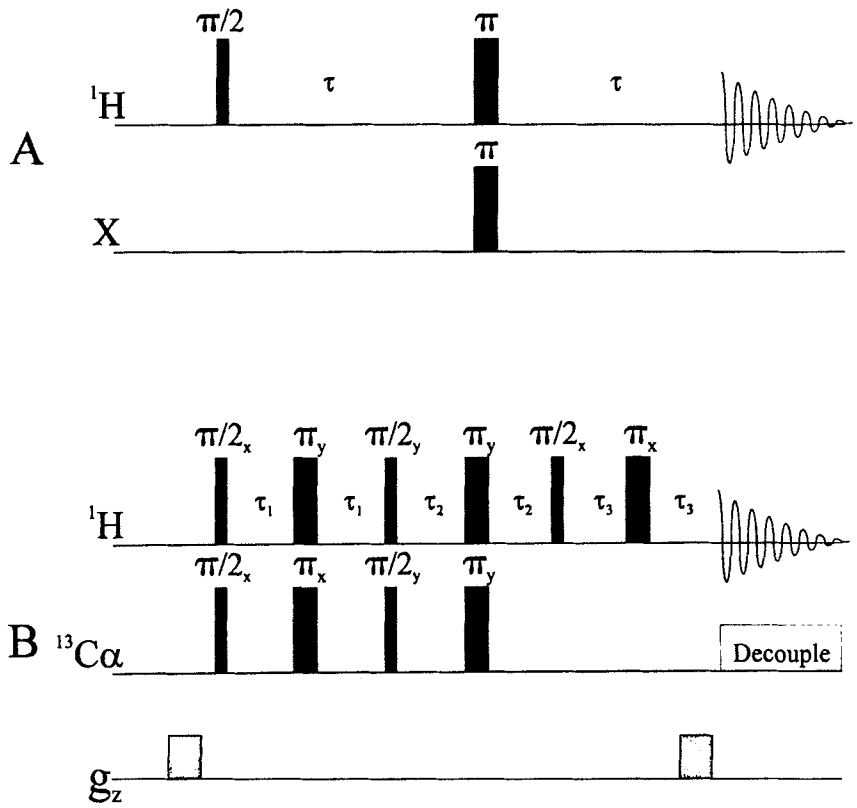

Fig. 14. (A) A spin-echo sequence for water suppression based on heteronuclear editing. $\tau = (2J)^{-1}$ and the heteronuclear π pulse is applied only in alternating experiments and the experiments are subtracted. (B) A water suppression module based on heteronuclear-coherence selection which results in full sensitivity.[150]

tion (see above). Since the water has no J-coupling this aligning of the water magnetization can be accomplished without the need for any frequency selective pulses.[146,147] However, homonuclear polarization transfer or any homonuclear sequence with $n = 0, \pm 1$ cannot be achieved without chemical-shift selective pulses, and additional means of suppression must be employed.[15]

The efficiency of various editing sequences has been greatly improved with the advent of PFGs as they allow the selection to be performed in one step (i.e. not as a difference experiment).[148,149] Starting from Eq. (7) and considering all of the applications of the gradient pulses in a sequence, we have

$$\sum_i \phi_i(\mathbf{r}) = 0 \tag{17}$$

where the subscript i denotes the different periods of the pulse sequence. Thus, in the general case only those coherences are observed for which the cumulative phase factor is zero, and a particular coherence transfer pathway can be selected according to the ratios of the gradient pulses used. Hence, if, for example, the pulse sequence is designed to detect only double-quantum coherence, then the water resonance will be unrefocused (i.e. it is dephased) at the end of the sequence, this then is a means of water suppression. A disadvantage of water suppression with gradient-based heteronuclear-coherence selection is that in general for the same experimental time they give lower signal-to-noise than their phase-cycled counterparts (this is not the case when the gradients are used as purge pulses). Also diffusional losses are often a problem when using gradients for coherence selection. Dötsch *et al.*[150] have presented a heteronuclear-coherence-based suppression scheme which results in both a normal amplitude modulated signal and full sensitivity (see Fig. 14B).

Gradient selection is also commonly used in homonuclear experiments like multiple-quantum COSY experiments, although it has been shown that coherence selection alone with a single gradient is insufficient to fully remove the H_2O signal from a multiple-quantum filtered COSY.[116] More recently Van Zijl *et al.* have shown that the use of MAGs provides superior suppression in a DQF COSY.[34] Similarly, Dalvit and Böhlen[151] have used coherence selection in 2D ^{1}H diffusion-weighted phase-sensitive PFG DQ experiments to effect solvent suppression. Although this can be done using only z-gradients they found that the use of MAGs gave more efficient suppression.

B_1 gradient-based suppression methods

Although less commonly used than B_0 gradients, water suppression is also possible using B_1 gradients. In fact, from geometry considerations[120,152] transverse gradients across a cylindrical sample, as is normally the case when using B_1 gradients, give more complete cancellation of magnetization than longitudinal gradients. Canet and co-workers[152] have developed the DEBOG (*D*ANTE *e*limination by *B*-*o*ne *g*radient) sequence in which a DANTE train of B_1 gradient pulses is used to suppress water selectively. The sequence may be written as

$$[(\alpha)_{g_1} - \tau]_n \tag{18}$$

where $(\alpha)_{g_1}$ is an RF gradient pulse of "mean" flip angle α (note that since the B_1 field is a gradient, α is the flip angle corresponding to the centre of the sample) and τ is the precession interval which governs the selectivity. The suppression results from the selective purge (defocusing) process. A negative point of this method is the total duration of the train which may require up to several hundreds of cycles if α is small; such a duration can also result in the

(unintentional) suppression of protons that exchange with water. Recently, Brondeau *et al.*[153] proposed a remedy to this in which $(\alpha)_{g_1}$ is replaced by $(2\pi)_{g_1}$. A $(2\pi)_{g_1}$ pulse has more efficient defocusing properties and thereby allows the number of cycles (i.e. n in Eq. (18)) to be reduced by an order of magnitude.

A water suppression technique based on the formation of B_1 gradient spin-echoes or B_1 gradient recalled echoes (i.e. rotary echoes) has been developed by Maas and Cory.[154] Their technique is reasonably insensitive to artifacts such as J-modulation, off-resonance excitation, radiation damping and chemical shift evolution, and will allow the observation of exchangeable protons. The method is in effect the B_1 gradient analogue of the WATERGATE sequence (see Mobility-based filters, p. 311). However, it differs from the B_0 gradient WATERGATE sequence in that the magnetization to be observed rotates in a plane perpendicular to the applied RF field and the relaxation is given by an effective T_1 defined by

$$\frac{1}{T_{1\text{eff}}} = \frac{1}{2}\left(\frac{1}{T_1} + \frac{1}{T_2}\right) \tag{19}$$

whereas in the WATERGATE sequence the relaxation of the observed spins depends on T_2.

3.5. Methods avoiding solvent saturation

Jump-and-return sequences

The jump-and-return (JR) pulse sequence[155] consists of two hard $\pi/2$ pulses that are opposite in phase, at the solvent frequency. The first $\pi/2$ pulse brings, in the rotating frame, all of the spins to the $+y$ direction, then during a subsequent delay τ the water protons remain directed along $+y$ whilst the other spins rotate in the plane by $\omega\tau$, where ω is the frequency offset from the water (i.e. pulse) frequency. The second $\pi/2$ pulse is then applied to bring all of the spins into the z–x plane, thus the amplitude response is $\sin \omega\tau$. τ is chosen so that

$$\omega_{\text{max}} = \pi/2\tau \tag{20}$$

where ω_{max} is the frequency of the spins of interest. Hence the phase is constant across the entire spectrum apart for the step of π at the solvent frequency. Water suppression is effected since the water magnetization is directed along $+z$. The JR sequence is thus equivalent to a single rotation of $\omega\tau$ around y, irrespective of the initial orientation of the magnetization. Providing that $\pi/2$ pulses are used, the JR sequence does not cause a linear

phase shift. If the pulses are not exactly $\pi/2$, whilst the suppression will be unaffected, there will be a slight linear phase shift. For pulses longer than $\pi/2$, the JR sequence produces a phase shift corresponding to a negative delay which leads to a spin-echo.[156] JR is the shortest known sequence since the spins of interest precess by only $\pi/2$ during the τ delay. Since for spins of interest, a τ value will be chosen such that the rotation angle is approximately $\pi/2$, JR can easily be incorporated into many pulse sequences involving $\pi/2$ pulses by replacing each pulse with a JR pulse sequence. Although JR sequences are almost free from phase problems, the amplitude response is still a problem. This can be corrected to some extent by multiplying the spectrum by $1/\sin \omega\tau$; however, although the resonances near the solvent frequency will be corrected in amplitude, the noise will not be scaled evenly.

Stonehouse *et al.*[51] have presented a modified jump-and-return sequence $\pi/2_x$-τ-$\pi/2_y$-gradient, which may be repeated n times. If $n \geq 2$ both the x and y magnetization will be dephased and thus the sequence is less sensitive to the initial orientation of the magnetization. To avoid gradient recalled echoes, however, the gradient strength or length should be changed in each repeat of the sequence. Sklenář and Bax[157] proposed the 1–1 echo (jump return and echo, JRE), $\pi/2_x$-τ-$\pi/2_{-x}$-Δ-$\pi/2_\phi$-2τ-$\pi/2_{-\phi}$-Δ- where the two $\pi/2$-τ-$\pi/2$ elements perform as $\pi/2$ and π pulses, respectively. That is, the sequence acts as a sort of spin-echo sequence. The excitation profile is given by $\sin^3(\omega\tau)$. Addition of PFG pulses to the 1–1 echo sequence during the Δ delays improves the refocusing and the degree of suppression by a factor greater than 50.

The jump-and-return type and binomial sequences (see below) result in offset-dependent signal amplitudes. If the sequence is started from full relaxation, this dependence can be corrected for relatively easily. However, such sequences are often run under partially T_1 saturated conditions. Consequently, this causes an offset dependence of the degree of saturation which affects the effective excitation profile. This has implications for the use of such sequences for their efficiency in solvent suppression, quantitative measurements and T_1 measurements by progressive saturation. Hsu and Gregory[158] have examined this effect for the JR and JRE sequences. In particular, they show that when using a short repetition time for the JR sequence it might be advantageous to place the solvent resonance at $\omega\tau = \pm \pi$ rather than 0, since the saturation effect gives a broader null at $\pm \pi$. Clearly similar concerns apply to any suppression scheme which uses offset-dependent excitation.

Binomial sequences

In binomial composite pulse sequences the amplitudes of the pulses are proportional to the binomial coefficients of $n + 1$ square pulses separated by equal interpulse delays, τ.[159,160] These sequences provide broad regions of near-zero excitation at the solvent frequency while the solute resonances are

rotated by $\pi/2$. There are two possible series using these coefficients each with characteristics profiles. Series of hard pulses with constant phase (e.g. 1–1, 1–2–1, etc.) have a

$$\cos^n(\pi\nu\tau) \tag{21}$$

while series with a π phase shift for successive pulses (i.e., 1–$\bar{1}$, 1–$\bar{2}$–1, etc.) give the profile

$$\sin^n(\pi\nu\tau) \tag{22}$$

Clearly these alternating series are related to JR. For the constant phase experiments the transmitter is placed on the resonances of interest whereas for the alternating series it is placed on the solvent. Alternating sequences are more commonly used.

We consider the 1–1 sequence as an example. The two pulses may be thought of as two delta functions of opposite sign at $-\tau$ and 0 (i.e. the beginning of signal acquisition), respectively. The Fourier transform of this sequence is

$$2e^{-i\omega\tau/2}\cos(\omega\tau/2) \tag{23}$$

Hence maximum amplitude occurs when $\omega\tau = 0$ and zero when $\omega\tau = \pi$ with the phase varying from 0 to $\pi/2$. Since only hard pulses are used, all of the spectrum is equally excited; however, there is a linear phase shift of the excitation spectrum. The amplitude modulation can be corrected for; however, it results in the noise being unevenly scaled.[8]

Modified binomial sequences in which a binomial sequence is inserted between a $-\pi$ and a $+\pi$ pulse have been developed[156,161] that significantly reduce the phase shift. The phase behaviour of the binomial sequences can also be improved using true binomials with a total flip angle of $3\pi/2$.[162–164] Morris *et al.*[165] considered computer optimization to improve the amplitude response of binomial sequences. More complex hard pulse sequences have also been developed such as NERO[166] and others.[167] However, as these sequences become more complicated so does their experimental setup, for example the accurate determination of the pulse lengths required by these sequences which are generally not multiples of $\pi/2$.

Inglis *et al.*[168] have presented a BIR-4 (B_1-*i*nsensitive *r*otations; a composite adiabatic pulse)-based version of the binomial pulse sequence, $1\bar{2}1$,[169] that provides excellent water suppression with a symmetric response profile about the on-resonance frequency. The sequence has particular relevance to *in vivo* applications due to its B_1 insensitivity.

Shaped pulses

Symmetrically shifted pulses have been proposed as a means of solvent suppression.[170] Symmetrically shifted pulses are symmetrically shifted laminar pulses[76] that contain equal numbers of rectangular pulse components of the same phase at ± an offset frequency. The basis of the symmetrically shifted pulse family is the SS pulse which is conceptually equivalent to applying simultaneous $\pi/2$ rectangular pulses with two separate, but in-phase, transmitters at ± offset frequency from the water. On a practical basis an SS pulse is obtained by a complete 2π cosine modulation of a single transmitter (see Fig. 15). An S pulse is half of an SS pulse (i.e. a half-cycle π pulse) which results in a narrower null and a 180° phase inversion at the transmitter frequency. They are also the soft, continuous equivalent of binomial sequences.[170] The SS and S pulses have broader excitation maxima than the sinusoidal profile of the JR sequence. The method has maximal excitation at an offset frequency of $\pm\ \omega$ with second-order U-shaped water suppression. The excitation profile is related to the maximum amplitude modulation and can be determined by numerical evaluation of the Bloch equations. Hence a new pulse shape must be used for each excitation window. The SS pulses give better water suppression than the JR sequence, but at the expense of poorer excitation of resonances closer to the water. Also, there is no phase inversion at zero frequency. The S pulse gives better excitation near the water frequency but with less water suppression.

McCoy *et al.*[171] have proposed a method termed "ERASER" based on self-refocused and hard rectangular pulses. The scheme does not generate phase roll. Moy *et al.*[89] have demonstrated the use of frequency shifted, self-refocused "top hat" pulses[135] to observe amide resonances, that they termed "selective-excitation-corrected spectroscopy" (SelECSy). This method, although not providing exceptional water suppression, overcomes the dynamic range problem and produces uniform amide proton excitation

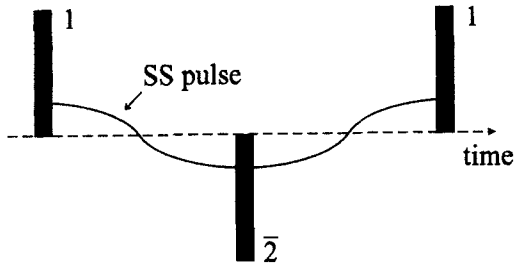

Fig. 15. SS pulse[170] showing the similarity to the binomial 1–2̄–1 pulse sequence. An S pulse is half of the SS pulse.

with no saturation transfer or spin-diffusion effects. However, the method requires more time than conventional techniques such as presaturation.

Liu *et al.*[172] have developed shaped self-refocusing $\pi/2$ RF pulses with a duration of 1–3 ms that provide a flat null (i.e. a "notch") at a narrow band (several hundred hertz) of resonance frequencies with uniform excitation and minimum phase distortion at the other frequencies ($\pm$ 5000 Hz).

Flip-back

Although, as we will see below, flip-back pulses have most application in multidimensional experiments they are nevertheless a (weak) form of suppression. Various flip-back techniques[173–177] have been proposed to align the water along the z-axis. A simple example of a flip-back method is the use of a selective $\pi/2_{-x}$ prior to a $\pi/2_x$ read pulse in a NOESY sequence. This avoids saturation of the water and allows the pulse sequence to be more quickly cycled since it can be done only by taking the solute relaxation time into account. This flip-back sequence provides only very limited suppression and requires the water magnetization to be longitudinal prior to the application of the flip-back pulse. Shaped pulses[178,179] and even radiation damping[180,181] can be used to flip the water back. As a means of water suppression, the flip-back method is extremely sensitive to missettings, and optimization is tedious.[182]

3.6. Postprocessing and selective detection-based methods

As noted in the previous sections, pulse sequence approaches are incapable of totally removing the water resonance. This section considers the various postprocessing schemes that can be invoked to provide and/or further reduce the water signal. A major difficulty with postprocessing is that the residual water peak cannot be described by an analytic function, mainly because its shape reflects the pulse sequence suppression method used and also because of magnetic inhomogeneity. Further, these correction schemes themselves may introduce different forms of artifacts, for example, changing the peak areas and phases of peaks lying on the tails of the water resonance making it difficult to quantify accurately peaks of interest in the spectrum. Postprocessing schemes are often computationally intensive, but with increasingly faster computers, this is becoming less of a limitation to both their general usage and further development. Sophisticated postprocessing schemes are increasingly used to minimize artifacts in *in vivo* and multidimensional spectra.

Postprocessing schemes generally require some degree of prior knowledge about the solvent resonance, for example the frequency and lineshape of the resonance. Perhaps the simplest approach is to use hardware frequency

filters.[183–185] Using software procedures, the solvent suppression generally takes the form of a bandpass filter or by subtracting a synthetic solvent peak. These procedures are performed either in the time or frequency domains.

In multidimensional spectra the phase of the residual water resonance does not have a constant relationship with the peaks of interest, and thus it is generally better to apply postprocessing methods in the time domain instead of in the frequency domain.[186] This also allows the use of non-iterative fitting procedures such as singular value decomposition (SVD)-type methods.[187] Further, since it is the largest peak in the spectrum that contributes most to baseline and phase difficulties, for example, a rolling baseline may result from linear phase correction on the solvent line, there is some benefit in subtracting the residual solvent peak in the time-domain prior to Fourier transformation.[8] Still it should be recalled that any method which works on frequency for discrimination will have the effect of removing signals close to the water frequency. We note that de Beer *et al.*[188] have recently considered the use of various signal postprocessing schemes for removing unwanted background features (e.g. water) from the perspective of quantitative imaging.

Time-domain methods. Amongst the time-domain methods, Marion and co-workers[189] have described the use of a convolution filter in the time domain. In their method a low-frequency component, $L(n)$, of the FID, $S(n)$, is calculated by

$$L(n) = \left[\sum_{k=-K}^{k=K} f(k)S(n+k)\right] \Big/ A \tag{24}$$

with

$$A = \sum_{k=-K}^{k=K} f(k) \tag{25}$$

where n is the number of the data point and $2K+1$ is the width of the convolution window. The shape of the convolution window, $f(k)$, is typically chosen to be Gaussian, i.e.

$$f(k) = \exp(-4k^2/K^2) \tag{26}$$

or sine-bell shaped, i.e.

$$f(k) = \cos(k\pi/(2K+2)) \tag{27}$$

The averaging of the neighbouring time-domain data points in Eq. (24) is equivalent to convolution with a rectangular function. The width of the rectangle corresponds to the number of points that are averaged. The

generated low-frequency component data, $L(n)$, is then subtracted from the original signal, $S(n)$, prior to Fourier transformation. In a related work, Friedrichs *et al.*[190] used a low-frequency convolution filter to remove selectively the diagonal peaks from COSY spectra. Kuroda *et al.*[191] have proposed a similar but less selective technique than that of Marion *et al.*,[189] based on Fourier transforming the derivative of the FID. A problem with the method of Marion *et al.*[189] is that to calculate the first few points of the convolution filter, knowledge of the signal prior to $t_2 = 0$ is required. In an attempt to get around this problem, Marion and co-workers used linear extrapolation to generate the initial time points. However, small errors in the first few points led to an imperfect convolution filter and consequently small baseline distortions. Since the frequency response of the convolution is known, the amplitudes of resonances affected by the filter can be corrected after Fourier transformation. Linear prediction methods have been used for dealing with the initial data point problem.[192–194] Waltho and Cavanagh[186] have pointed out that it is preferable to use a spin-echo and thereby to record these "negative-time" points experimentally. However, the use of an echo has two drawbacks: it introduces J-modulation and T_2 relaxation problems. Sodano and Delepierre[195] proposed the use of a shifted-time-domain-data convolution difference to circumvent the problem of the first few points of the FID. In their approach they discarded the first K points of the averaged FID. An example of their approach applied to a NOESY spectrum is shown in Fig. 16. They noted that since the major part of the FID originates from the solvent signal which is on resonance, shifting the time-domain data changes only the amplitude but not its phase. Interestingly, although these time-domain convolution methods are very successful, their actions do not have a strong theoretical basis since the convolution theorem does not apply.[189,196] Craven and Waltho[196] have presented an approximate theorem that allows many of the features of these time-domain convolution filters for solvent suppression to be understood.

Singular value decomposition (SVD)-type methods[187,197–200] represent a very promising area of "black box" methods (i.e. requiring little or no prior knowledge) for suppressing unwanted strong resonances (e.g. water or lipid). SVD-type techniques are able to provide a good fit to the water resonance, including the tails. This is then subtracted from the original signal. Since these methods are computationally expensive, various modifications have been developed such as HSVD (where the H stands for Hankel)[187] and a faster HSVD method which uses the Lanczos algorithm HLSVD.[201] The applicability of SVD-type methods for removing the (strong) lipid and water resonances in spectroscopic magnetic resonance imaging (MRSI) data sets has also been investigated.[198,199,202,203] Recently, Vanhamme *et al.*[204] have presented a method termed HLR in which the SVD is replaced by a more efficient low-rank algorithm. While being as accurate as HSVD, it is much less demanding computationally.

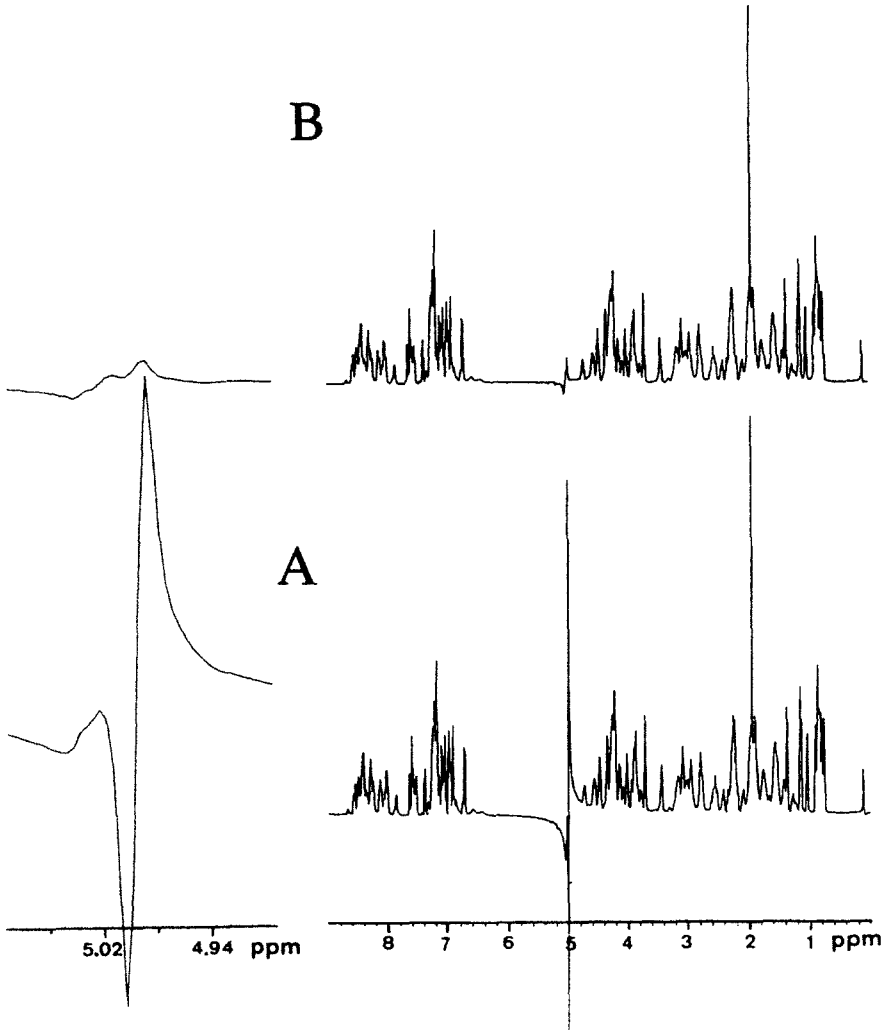

Fig. 16. (A) The first increment of a NOESY spectrum of a 3 mM sample of a 26 amino acid peptide from the hepatitis B envelope protein recorded in 90% H_2O at 273 K on a 500 MHz spectrometer. (B) Same as (A) but after applying the shifted time-domain convolution difference filter. (From Sodano and Delepierre[195] with permission.)

Mitschang *et al.*[205] proposed the use of a Karhunen–Loéve transformation to the time-domain signal and the undesired signals are removed on the basis of their intensity. They demonstrated its effectiveness in 3D TOCSY–NOESY experiments. Smallcombe[170] fitted a low-frequency filtered (i.e. ± 300 Hz) FID to an *n*th-order polynomial. This was then subtracted from the FID to

remove the residual water peak. Cross[206] has proposed the use of a tangent high-pass Butterworth filter. His method is computationally simple and has a narrow stop band in the frequency domain and minimal distortion for passband frequencies. Leclerc[207] has proposed a method based on a time-domain analysis of the FID using total-least-squares analysis to identify and subsequently subtract the water-peak components. Zhu *et al.*[208,209] have presented an alternative simpler SVD approach in which a Toeplitz matrix is formed from the FID and the corresponding solvent-suppressed FID is then constructed by removing the largest singular value of the Toeplitz matrix. They note that when other resonances are close to the solvent peak there is a residual solvent peak left after application of their method although the tail of the peak is removed and the baseline is much flatter. Recently, Barache *et al.*[210] have outlined the use of continuous wavelet transforms to suppress large spectral lines.

Frequency-domain methods

Tsang *et al.*[211] proposed a simple frequency-domain procedure in which the spectrum is first phased so that the target signal is absorptive. The solvent signal is then eliminated and the imaginary data necessary for rephasing the spectrum is generated using a Hilbert transform. Pelczer[212] has used a similar approach to remove the diagonal from COSY spectra. Adler and Wagner[213] have proposed a simple method in which they assume that the distortion stems from a dispersive (i.e. residual water) signal at the carrier frequency. They then apply a dispersive term to a polynomial baseline correction routine to fit directly the dispersive lineshape. In another approach, Deriche and Hu[214] assumed that the shoulders of the residual water peak can be described by a broad Lorentzian baseline. A Lorentzian is fitted using a nonlinear least-squares method and subtracted from the spectrum to effect suppression.

The recent development of oversampling combined with digital signal processing[215,216] improves dynamic range performance resulting in reduced noise. Also, there is scope for providing very sharp cutoff filters without introducing baseline distortion and to remove aliasing artifacts from solvent resonances.

4. SUPPRESSION OF RADIATION DAMPING

There are many methods for suppressing radiation damping and these can be roughly divided into hardware and pulse sequence approaches. We stress that these methods generally suppress only radiation damping and that the demagnetizing field effects will be suppressed only if the magnetization is also suppressed. Since radiation damping can have adverse effects on

pulse sequence performance, it is generally desirable to suppress its effects throughout the entire sequence.

4.1. Hardware methods

From Eq. (1), it can be reasoned that for a tuned resonant circuit the simplest way of reducing radiation damping is simply to detune the probe;[41] however, this is generally an impractical solution. It has also been noted that there is no radiation damping in an open, series-resonant circuit.[156] Later, Picard *et al.*[217] demonstrated this approach using a preamplifier presenting a high input reflection coefficient and a coaxial cable of suitable length. Although this method is easily implemented and maintains a high signal-to-noise ratio, it does require a separate circuit for transmission and the preamplifier must be noise matched to the impedance presented by the overcoupled probe.

More sophisticated solutions that require complicated electronics such as selective current feedback have been developed.[218–220] Such approaches are based on creating a magnetization-dependent field in the sample which exactly compensates for the radiation damping field. Practically, this approach consists of the following operations. First, the total signal is detected in the receiver coil. This signal is then transposed to low frequency by demodulation with the carrier frequency and filtered to retain only a limited region about the solvent frequency. After reverting back to the correct frequency, this signal is then fed back to the probe via the decoupling channel.[219,220] Abergel *et al.*[219] have investigated the possibility of using this form of radiation-damping compensation in a time-shared mode and thereby enabling compensation during acquisition. We note that commercial radiation damping compensation units have now become available.

Q-switching probes[221,222] have also been developed in which the Q factor of the radiofrequency coil is high only during pulses and signal acquisition and low elsewhere (see Fig. 17), thereby suppressing radiation damping (i.e. see Eq. (1)). Such probes are able to switch between the two Q levels in less than 2 μs.[221] It has been noted that the control of radiation damping and the use of Q-switching probes will have increasingly important roles to play in NMR experiments designed to detect intermolecular cross-peaks between water and protein where the otherwise broad water signal would obscure the observation of the cross-peaks.[221,223]

4.2. Pulse sequence methods

In considering the pulse sequence methods for suppressing radiation damping, it is important to realize that in reality M_0 in Eq. (1) should really be

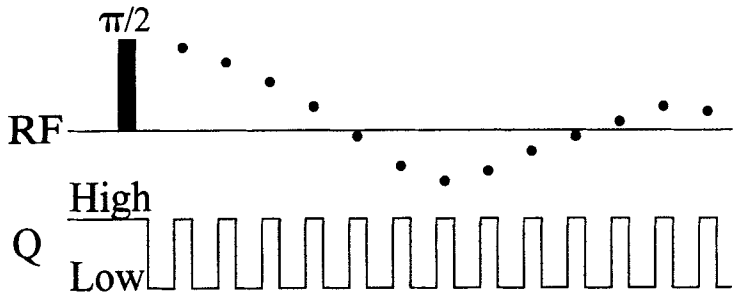

Fig. 17. Q-switching for suppressing radiation damping during acquisition.[221,222] The Q of the probe is switched high only during the data point acquisition and low during the dwell times.

replaced by M.[17] Thus as the magnetization becomes smaller, either by saturation or relaxation, so does the radiation damping effect. Many pulse sequence methods for suppressing radiation damping have been presented and the majority of these involve the use of gradients. Although, as has recently been noted,[17,98] perhaps the simplest and most effective way to stop radiation damping is to use presaturation since as the magnetization is gradually saturated, the radiation damping becomes smaller. Further, when using presaturation as the basis of water suppression, radiation damping is not a problem since the strength of the presaturating field is generally much greater than the radiation damping field.[45] Presaturation, however, is not a good solution if it is the behaviour of the solvent resonance or resonances underneath the solvent resonance that you wish to observe.

Instead of saturating the magnetization that causes radiation damping, another obvious alternative is simply to dephase the magnetization using a gradient pulse. Sklenář has proposed the use of weak alternating z-gradient pulses during the evolution and mixing periods as a means for suppressing the effects of radiation damping (see Fig. 18A),[224] the idea being that the gradient pulses prevent any net magnetization being present in the transverse plane but the magnetization is refocused before the next RF pulse. Very weak gradient pulses are required to minimize signal losses due to translational diffusion. Dalvit and Böhlen[225] have demonstrated that radiation damping can be suppressed in the preparation period of 2D and 3D DQ experiments by the addition of two very weak gradients of equal sign and intensity in the DQ excitation period. In a somewhat related work, except that it is designed to prevent radiation damping during acquisition, Zhang and Gorenstein have proposed the idea of interleaving pairs of opposed z-gradient pulses between the acquisition of FID data points (see Fig. 18B).[226] In this method the z-gradient dephases (and rephases) the magnetization between the acquisi-

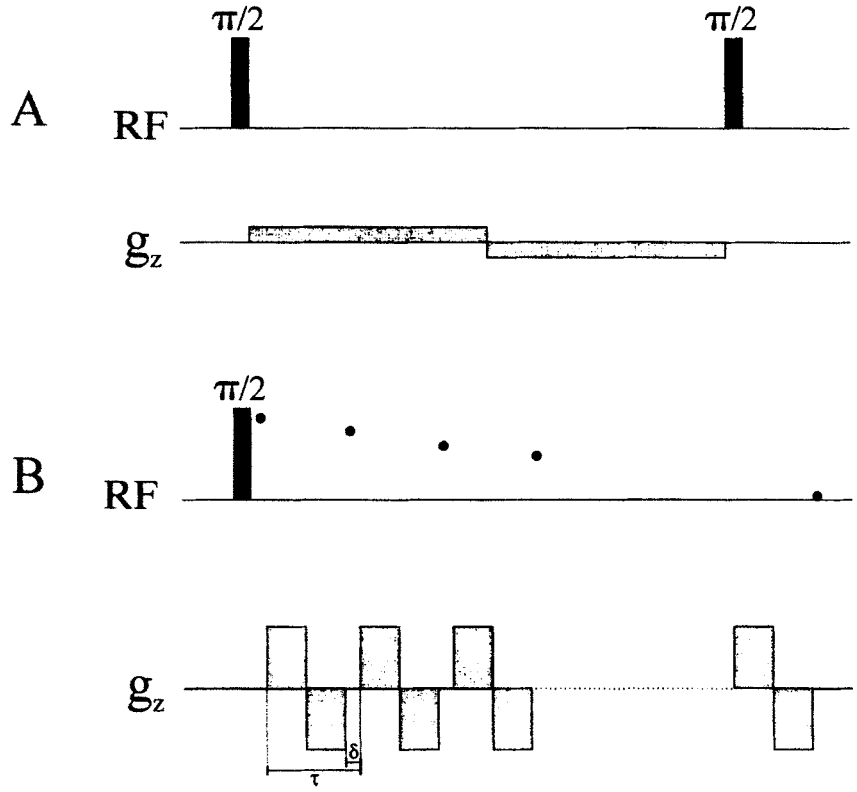

Fig. 18. Pulse sequence methods for controlling radiation damping. (A) Gradient recalled echoes in the evolution period.[224] The bipolar gradient pulse uses only very weak z-gradients (~0.2 G cm^{-1}). (B) Bipolar gradient pulses between the acquisition of data points in the FID.[226]

tion of the data points. To do this the requirement

$$\frac{\gamma g_z l_z}{2\pi} \gg T_{RD}^{-1} \tag{28}$$

where l_z is the length of the sample, must be met such that the magnetization is dephased before there is substantial precession. The alternating gradient pulses result in some line broadening which can be reduced by keeping the time between subsequent pairs of alternating gradient pulses (denoted by τ in Fig. 18B) small. However, if there are too many refocusings of the magnetization, the signal will be more affected by radiation damping.

Otting and Liepinsh[223] presented a technique for efficient and selective excitation of the water resonance, "Q-switched selective pulses", in which the

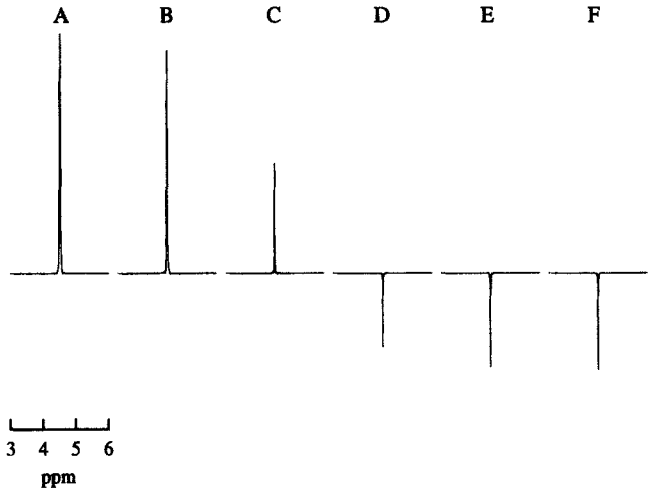

Fig. 19. An example of the use of the Water-PRESS pulse sequence to control the effective water relaxation rate of the water resonance in a lysozyme solution (10 mM in 10:90 ^2H_2O:H_2O, pH 3.7) acquired at 310 K at 300 MHz. In this experiment D_{H_2O} was set to 20 s and D_{NP} was set to 2 s. The number of homospoil pulses (0.5 ms, half sine with a maximum strength of 1 G cm^{-1}) used in acquiring the spectra were (A) 1, (B) 21, (C) 31, (D) 41, (E) 51 and (F) 61. As can be clearly seen, after the interval between homospoil pulses is decreased to about 40 ms (i.e. spectrum E) there is no further increase in the effective water relaxation time. Since the effect of radiation damping is diminished with increasing number of gradient pulses the line width of the water signal decreases. (From Price *et al.*[112])

water is excited by a shaped pulse (e.g. Gaussian) represented as a series of short pulse elements with DANTE-like zero-amplitude elements between the pulse elements. The Q factor of the probe used is switchable[221] and is only set high during the pulse elements, thus controlling the effects of radiation damping. In a related fashion, Böckmann and Guittet[227] have proposed the WANTED (*w*ater-selective D*ANTE* using gra*d*ients) sequence for efficient and selective excitation of the water resonance in which gradient echoes are applied between the single pulses of a DANTE train to suppress the radiation damping. They presented NOESY, ROESY and NOESY–HSQC experiments modified to contain the sequence.

Another way of suppressing radiation is to inhibit its initiation as can be understood by considering Eq. (4). As noted in the section on randomization (p. 309), a gradient has no effect on magnetization that is collinear with it. Consequently, a z-gradient pulse will not eliminate radiation damping completely, but while it is being applied it will prevent its onset as it dephases any transverse magnetization as in the Water-PRESS sequence.[111,112] Thus, the Water-PRESS subunit can be used to change the effective water relaxation

time from the minimum determined by the effects of radiation damping up to the time given by the true T_1 (i.e. unaffected by radiation damping) by changing the ratio [number of gradient pulses]:[duration of D_{NP}] as shown in Fig. 19.

The various methods considered in this section allow the suppression of radiation damping in most parts of pulse sequences.

5. SUPPRESSION IN MULTIDIMENSIONAL NMR

5.1. Introduction

Pulse sequence suppression methods can be classified into "preparation methods" or "read pulse methods". Presaturation, which would be classified as a preparation method, is still the most commonly used technique for suppression in multidimensional NMR. Read pulse methods are those that are selective for the water and they can be used as a replacement for the last pulse of a single or multidimensional experiment. Generally the transmitter must be set at the water resonance frequency although there are exceptions, for example using frequency shifted shaped pulses[89] (see Shaped pulses, p. 324) or WATERGATE with off-resonance suppression[132] (see WATERGATE and related sequences, p. 314). These off-resonance methods allow selective manipulation of the water resonance while keeping the transmitter offset in the region of interest. Off-resonance approaches are generally of value only if a part of the spectrum, upfield or downfield of the water, is to be observed.

In applying suppression methods to multidimensional sequences, it is important to consider what preconditions the suppression scheme makes on the water magnetization. For example, multidimensional sequences are generally run with a recycle delay less than sufficient to allow the water magnetization to relax back to equilibrium before the start of the next scan. Thus the water is always at least partially saturated but the theory behind most suppression methods assumes that the water magnetization starts from thermal equilibrium in each instance. We note in particular that spin-lock, WATERGATE and diffusion filters can be used to suppress the water irrespective of whether the solvent magnetization is at equilibrium.

Another complication is that the phase cycling, for example the t_1-dependent phase cycling necessary for quadrature detection in the indirectly detected dimensions,[49,228] may result in the water having a different orientation on each scan. If WATERGATE is used for suppression and recalling that magnetization aligned along the z or $-z$-axis is unaffected by the WATERGATE sequence, the degree of water suppression will change with each successive scan. This situation will be further complicated by the effects of radiation damping during the evolution period. In severe cases the ADC might be

overloaded on some scans whilst, in less severe cases, the imbalance in the water suppression efficiency over the TPPI cycle will result in a t_1 modulation of the baseline resulting in antidiagonal spectral artifacts.[229] For example, in a conventional TOCSY experiment the state of the water prior to the WATERGATE sequence is not so well defined. However, in the WATERGATE–NOESY the modulation of the water resonance is generally not a problem, since with the assistance of radiation damping the water resonance is likely to reach equilibrium during the mixing time for each t_1 increment.[51]

Many multidimensional experiments are inherently designed to remove solvent signals, for example multiple-quantum filtered experiments, and even the gradients used for providing quadrature detection have the added advantage of also producing diffusion-based attenuation of the water signal.[193] Also since the interest is the cross-peaks which are generally well separated from the water signal, it might appear that the requirements for water suppression in multidimensional experiments are less stringent than for one-dimensional experiments. However, many homonuclear multidimensional experiments, for example NOESY studies of peptide hydration, are adversely affected by the residual solvent peaks. Not only does the residual water resonance cover some of the cross-peaks involving α-protons but also the poorly averaged random behaviour of water signals results in a random baseline variation in each 1D spectrum obtained by Fourier transformation with respect to t_2 prior to Fourier transform in the t_1 dimension in the case of a two-dimensional experiment. This gives rise to stripes along the F_2 axis spreading from the F_2 position of the water and results in the experiment having an artificially poor signal-to-noise ratio.[213,230] These streaks generally have a dispersive character and are difficult/impossible to remove by conventional baseline correction routines such as polynomial fits, which in any case are hampered, especially in the case of protein spectra, by there being very little "free" baseline that can be used as a reference. Thus, in multidimensional experiments, there is a great need to improve both the solvent suppression using better pulse sequence suppression methods and also better postprocessing methods.

Commonly in multidimensional sequences, more than one type of suppression method is used. For example, presaturation might be used before the start of the sequence and if at some point during the sequence the magnetization of interest is (or can be) aligned along the z-axis, gradient purge pulses can be used to improve solvent suppression (see Randomization, p. 309) and reduce artifacts by destroying transverse magnetization.

The number of multidimensional sequences using some form of solvent suppression is almost without bound. Consequently, we have limited the examples drawn from multidimensional sequences to some (randomly) chosen examples of the flip-back method and suppression in COSY, TOCSY, NOESY and ROESY sequences. A final subsection gives two examples of suppression in multidimensional sequences using B_1 gradients.

5.2. Flip-back

The importance of not saturating water in multidimensional NMR experiments has recently been discussed by Grzesiek and Bax.[173] Importantly, the large molar excess of slowly relaxing water provides a reservoir of nuclear spin magnetization and it can be used in measuring water–protein NOEs or for rapidly restoring the magnetization of exchangeable protons to thermal equilibrium. This can provide greater sensitivity in many experiments[174–176,228,231,232] including ROESY[233] and *J*-modulated HMQC and 3D HNHA sequences,[176] ^{1}H–^{15}N HSQC, ^{15}N-$\{^{1}H\}$ NOE and water–protein NOE difference constant time ^{1}H–^{13}C HSQC experiments.[173] However, due to the fast repetition times (with respect to the water T_1) in multidimensional sequences, methods that scramble the magnetization result in the water being maintained in a partially saturated state.[173,234] This results in significantly reduced signal intensities of exchanging amide protons and carbon-attached protons.[173]

Mori *et al.*[234] have noted that selective pulses such as those used in flip-back pulses in WATERGATE flip-back ^{1}H–^{15}N HSQC[173] can introduce frequency losses due to imperfect frequency responses. They have proposed a fast HSQC sequence (FHSQC, see Fig. 20) that avoids the use of soft pulses. In their sequence the dephasing by the first *z*-filter gradient is refocused by the second *z*-filter. The phase of the second polarization transfer pulse is changed so that the water is aligned along the $+z$-axis and is thereby made insensitive to the effects of the WATERGATE sequence. Although the sequence has

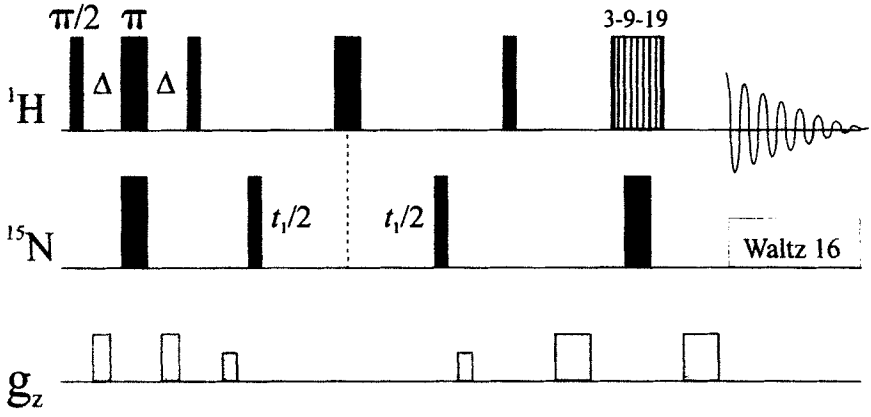

Fig. 20. A fast flip-back WATERGATE HSQC (FHSQC) that avoids water saturation and radiation damping.[234] The WATERGATE subunit uses a 3–9–19 pulse. Details of the phase cycling, delays and gradient strengths can be found elsewhere.[234]

potential for diffusional losses, this turns out not to be a problem since only very small gradients are used and for the protons of interest, single-quantum ^{15}N evolution occurs which, by virtue of its low γ, is in any case rather insensitive to the effects of the gradient pulses.

5.3. COSY and TOCSY

By prefixing the Water-PRESS subunit to the beginning of a COSY sequence, excellent water suppression can be obtained. In Fig. 21 the amide regions of COSY spectra of lysozyme acquired using presaturation and Water-PRESS are compared. Since Water-PRESS does not bleach out the α-protons under the water resonance, there are numerous amide cross-peaks close to the water frequency that are only visible in the COSY acquired using Water-PRESS.

John *et al.*[116] used two gradient randomization episodes to produce water suppression before a phase-sensitive gradient-enhanced DQF–COSY. Trimble and Bernstein[179] have applied WATERGATE in multiple-quantum filtered COSY experiments. WATERGATE can also be combined with flip-back pulses to take the residual water magnetization back to the z-axis. Dhalluin *et al.*[235] have proposed an improved WATERGATE TOCSY experiment with minimal water saturation. Fulton *et al.*[229] have presented a WATERGATE TOCSY with flip-back experiment (see Fig. 22) that provides apparently better reduction of radiation-damping effects than the sequence by Dhalluin *et al.*[235] Xu *et al.*[236] have demonstrated that DPFGSE combined with selective 1D homonuclear transfer experiments (i.e. SELCOSY, SELRELAY, SELTOCSY) provides water suppression on a par with presaturation. Callihan *et al.*[182] have presented a TOCSY sequence using excitation sculpting (i.e. DPFGSE) for improved solvent suppression and no baseline distortion (see Fig. 23).

It has been found that the use of MAGs for coherence selection in a gradient-enhanced multiple-quantum magic angle DQF gradient COSY results in much better suppression of the water signal.[34,38] This is probably due to the reduction in demagnetizing field effects through the use of the MAGs.[225]

5.4. NOESY and ROESY

Many different ways of effecting water suppression in the NOESY sequence have been implemented, for example, presaturation, jump and return, 1–$\bar{1}$–echo,[237] WATERGATE,[131,177] SS pulses[170] and excitation sculpting.[182] The basic NOESY sequence using presaturation and two variations using WATERGATE are illustrated in Fig. 24. In the basic NOESY sequence (Fig.

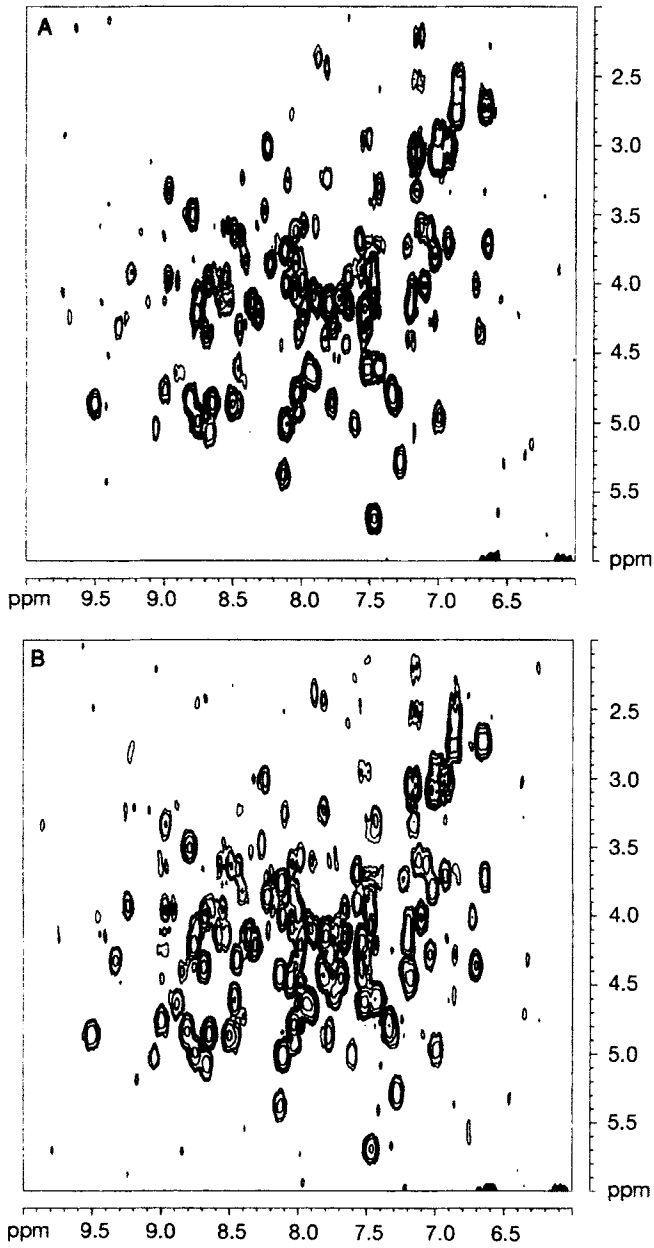

Fig. 21. Amide regions of COSY spectra of the lysozyme solution acquired using (A) presaturation of the water resonance prior to the COSY sequence and (B) the Water-PRESS sequence prefixed to the COSY sequence. The water resonance was at 4.51 ppm. The effects of presaturation on the resonances near and under the water resonance are clearly seen by the absence/diminution of the cross-peaks having α-proton resonances around 4.5 ppm.

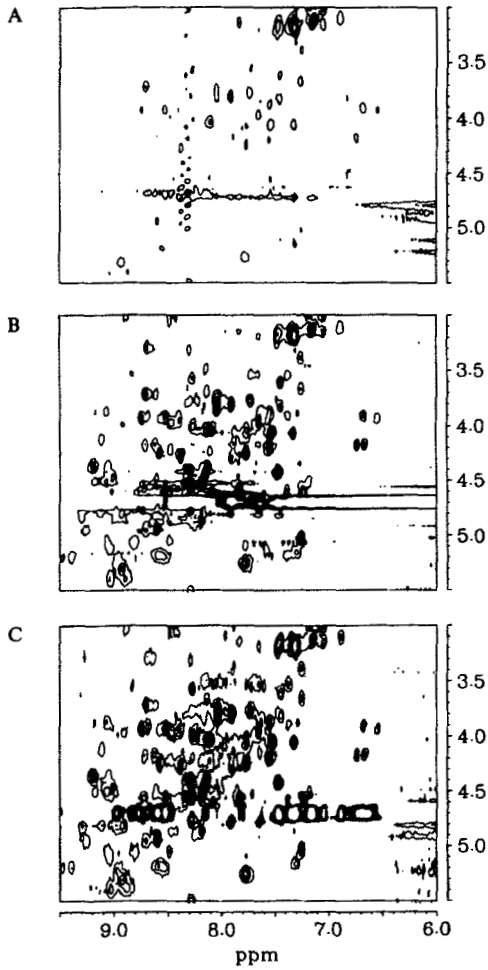

Fig. 22. Fingerprint regions of 2D TOCSY spectra of angiotensin (0.7 mM in 90:10 ^2H_2O:H_2O, pH 7.0) at 298 K acquired at 500 MHz. (A) TOCSY with presaturation, (B) basic TOCSY–WATERGATE and (C) flip-back TOCSY–WATERGATE. There is considerable bleaching of cross-peaks near the water frequency in (A). Spectrum (B) is cleaner with some cross-peaks visible at the water frequency. The flip-back TOCSY–WATERGATE (C) has improved suppression with increased intensity of many of the cross-peaks. (From Fulton *et al.*[229] with permission.)

24A), presaturation during the relaxation delay and mixing time result in the water being suppressed to near zero at the beginning of acquisition. In the WATERGATE NOESY[131] (Fig. 24B), all of the suppression is produced by the WATERGATE subunit just prior to acquisition. Hence, for most of the NOESY sequence, there is a large water signal which is susceptible to the

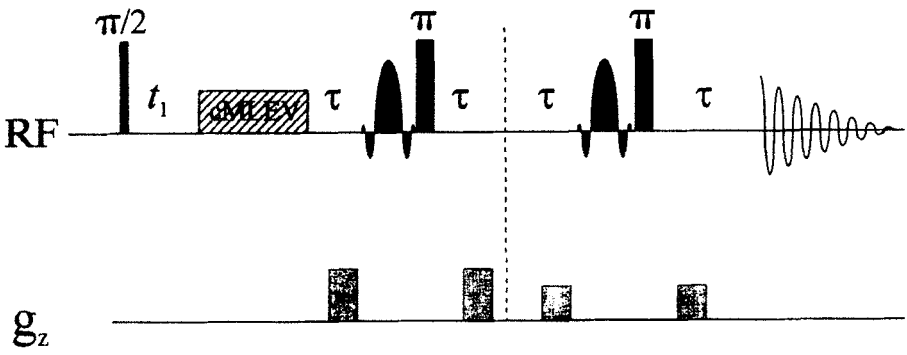

Fig. 23. Excitation-sculpting TOCSY sequence.[182] The shaped pulses have SEDUCE profiles.

effects of radiation damping. Consequently, especially for longer mixing times the water is often fully returned to the equilibrium $+z$ direction. In the general case, however, there is insufficient time to allow full relaxation and consequently the water is almost always semisaturated. In the flip-back WATERGATE NOESY sequence[177] (Fig. 24C) the third $\pi/2$ pulse (i.e. the final pulse) of the actual NOESY part of the sequence is preceded by a water-selective $\pi/2$ pulse of the opposite phase. In theory this will result in the water magnetization still being directed along $+z$ after the third pulse; it will thus be unaffected by the WATERGATE sequence and thus the magnetization will not have any transverse component during acquisition. In practice this approach is not perfect, otherwise the WATERGATE subunit would be redundant. Implicit in this sequence is the idea that the radiation damping brings the water magnetization to a totally reproducible state at the end of the mixing period; however, for short mixing times this may not be true. Nevertheless, it is reported that the addition of the water flip-back pulse significantly increases the intensities involving NH and/or α protons while allowing the use of conveniently short recycle delays.[177]

Amplifying the effects of radiation damping can provide important signal enhancement (see Fig. 25). Also the increased RD can be used as a water flip-back pulse resulting in considerably improved water suppression (see Fig. 26). Further, since the lineshape in the indirectly detected domains is that of the bulk water, the cross-peaks will be significantly broadened.[60,224] Otting[95] has discussed the use of solvent suppression in NOESY experiments performed to detect intermolecular NOEs with water. In an earlier work he demonstrated that if radiation damping was suppressed during the evolution period by defocusing the magnetization before and after the period with a pair of spin-lock pulses (which act as B_1 gradient pulses) and by suppressing radiation damping in the mixing time using B_0 gradients, significantly nar-

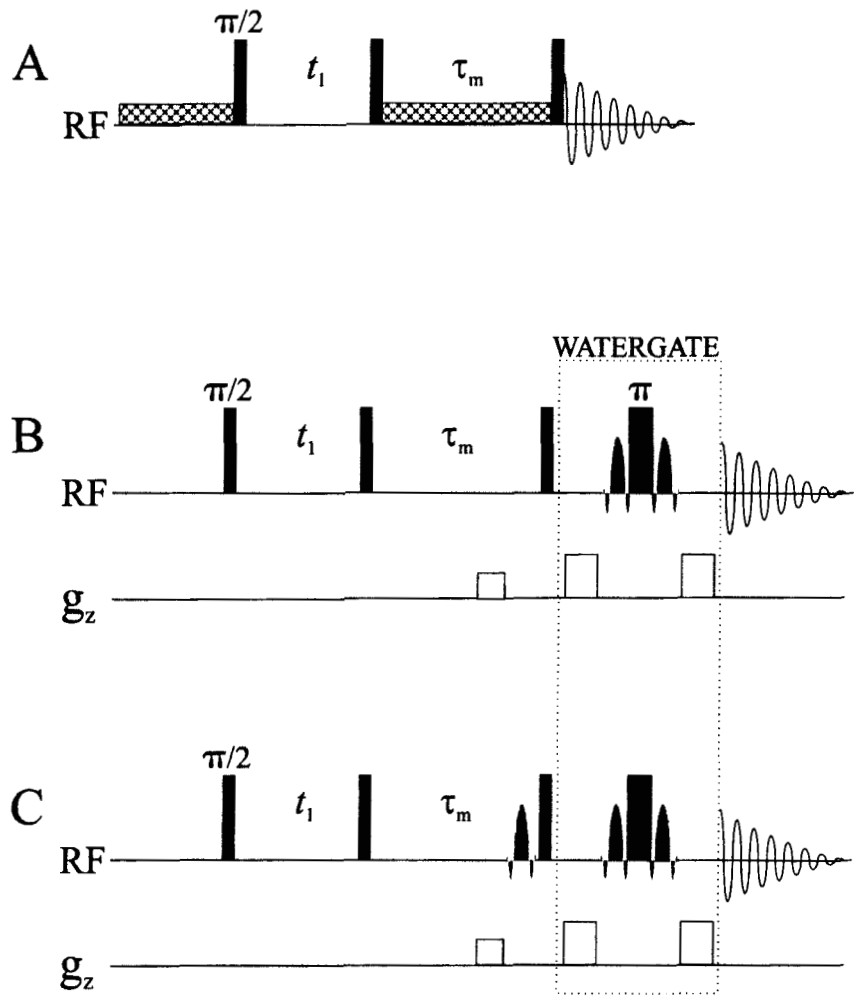

Fig. 24. Various NOESY–water suppression combinations. (A) NOESY using presaturation in the relaxation delay and mixing times, (B) WATERGATE NOESY[131] and (C) the water flip-back WATERGATE NOESY.[177]

rower cross-peaks were obtained.[60] He also presented a modified ROESY sequence that suppresses the effects of radiation damping.

Radiation effects and a need to achieve F_1 frequency discrimination can lead to reduced water suppression in jump-and-return NOESY experiments especially at short mixing times.[51] Stonehouse *et al.*[51] therefore modified the original sequence to include gradient pulses to achieve a constant water suppression for all phases and t_1 increments.

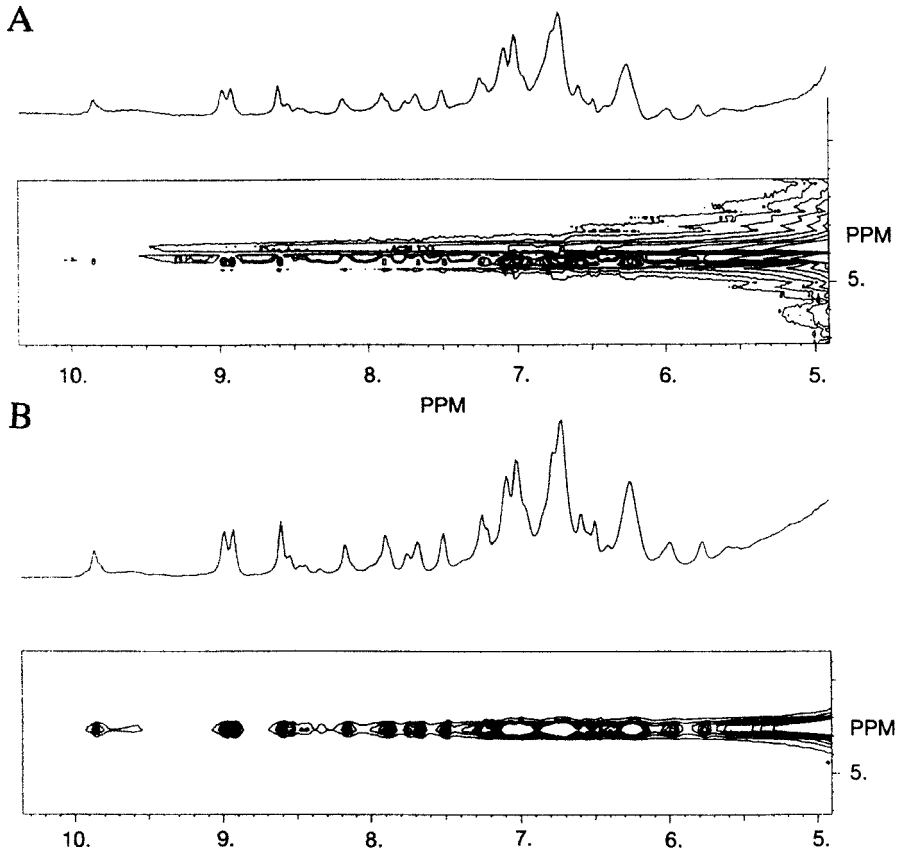

Fig. 25. Water exchanging-protons region (i.e. at the water frequency) of a 2D NOESY difference experiment of 3 mmol l^{-1} BPTI at 279 K (mixing time = 90 ms) without (A) and with (B) amplification of RD. The amplification of the RD affords important signal enhancement. (From Abergel *et al.*[250] with permission.)

5.5. B_1-based suppression

COSY experiments using B_1 gradient-based water suppression have been presented.[238–240] In a later work Brondeau *et al.*[153] have successfully combined B_1 gradient suppression (i.e. their DEBOG sequence; see B_1 gradient-based suppression methods, p. 320) with a NOESY sequence, which they termed NOESY–DEBOG (see Fig. 27),

$$\begin{aligned}&(\text{DEBOG} - \text{I})_{\varphi 1}(\pi/2)\varphi_2 - t_1 - (\pi/2)\varphi_3 - t_m \\ &\quad - (\text{DEBOG} - \text{II})_{\varphi 4}(\pi/2)\varphi_5(\text{Acq} - t_2)_{\varphi_n}\end{aligned} \tag{29}$$

A

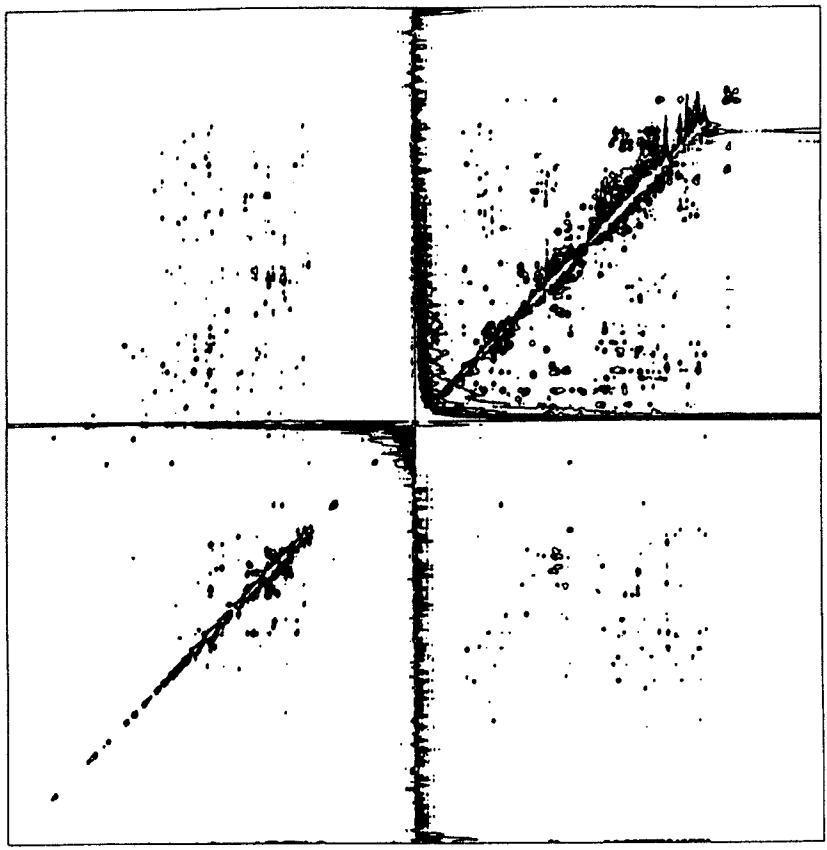

Fig. 26. Two-dimensional NOESY experiment (conditions as for Fig. 25), without (A) and with (B) RD amplification used as a water "flip-back" pulse. The spectrum in (B) has noticeably better water suppression due to the complete alignment of the water magnetization along the $+z$ axis at the end of the detection period. (From Abergel *et al.*[250] with permission.)

the phase cycling can be found in their paper. The first DEBOG episode using a single-turn gradient coil before the first $\pi/2$ pulse largely suppresses the water; however, some water magnetization recovers during t_m. This water magnetization is then suppressed using a second DEBOG episode but using a conventional saddle coil (i.e. so that the B_1 gradient is in a different direction).

B

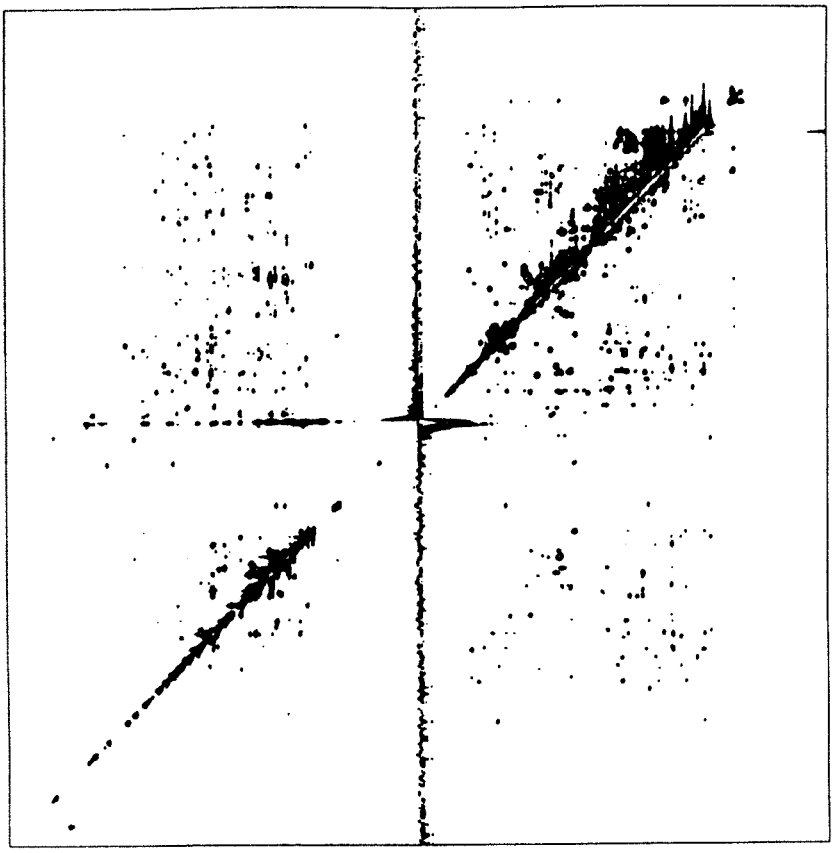

Fig. 26B.

6. IMAGING AND *IN VIVO* EXPERIMENTS

In imaging and *in vivo* studies, it is often necessary to suppress water and fat (triglycerides). It is outside the scope of this chapter to delve deeply into suppression in imaging and *in vivo* experiments and so we will only stress the most salient points. Interested readers are referred to the reviews by Guéron *et al.*[8] and Van Zijl and Moonen.[13,15]

Imaging especially of *in vivo* system brings new complications. For example, heat deposition limits when working with living animals may limit the types of suppression techniques used (i.e. spin-lock) and sample movement mediates against the use of diffusion-based suppression due to their sensitivity to motion. Conversely, the use of gradients over phase cycling for coherence selection is particularly advantageous in *in vivo* studies where motion (e.g. whole sample motion or blood flow) can be a problem.[15] Even using

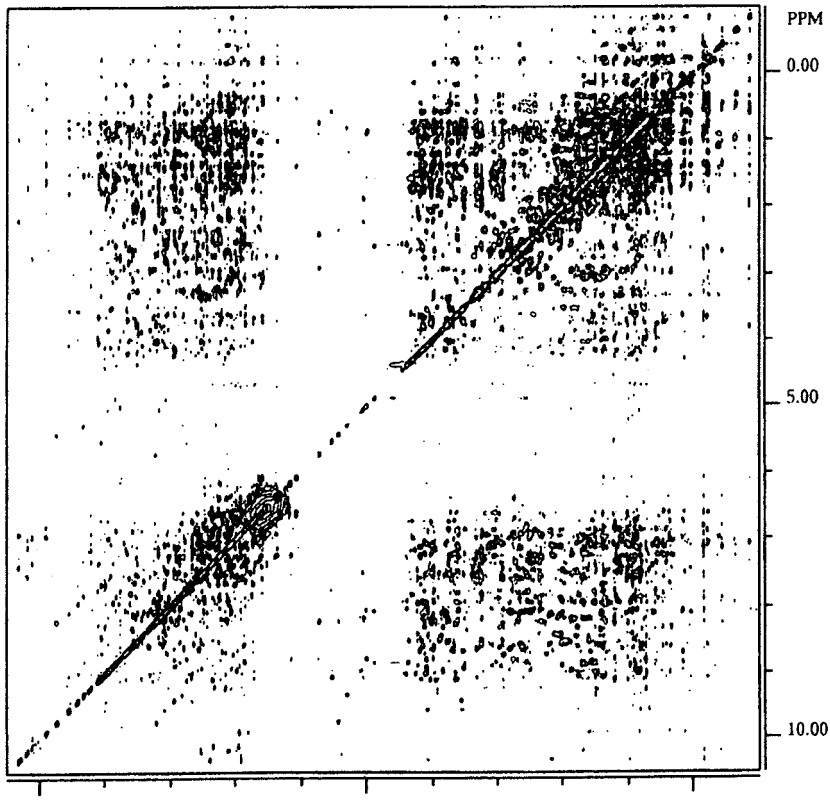

Fig. 27. The NOESY–DEBOG experiment for a 2 mM solution of lysozyme. The time domain data processing includes the convolution scheme of Marion *et al.*[189] (From Brondeau *et al.*[153] with permission.)

single-scan suppression with gradients, motion is still a problem as it results in a phase shift. The possibilities for suppression are further limited by both B_0 and B_1, generally being more inhomogeneous than in high-resolution NMR. As a consequence of the B_0 inhomogeneity, the water chemical shift range in some biological samples can be several ppm which precludes the use of chemical-shift-based suppression techniques. Further, due to susceptibility differences over the sensitive volume combined with B_0 inhomogeneity, water in some regions will have resonance frequencies similar to that of the metabolites of interest in the region being examined. Moonen and Van Zijl[15] note two consequences of this: first, frequency-based water suppression may work in a well-shimmed area but not over the entire volume encompassed by the RF coils and second, frequency-based water suppression is only applicable when high-quality localization is possible. A more detailed coverage of localization techniques can be found in the review by Moonen and Van

Zijl[15] and elsewhere.[241] We also note that T_1-based suppression schemes can be compromised by the inherent T_1 variations and more T_1-independent methods have been developed.[242] T_2-based schemes can be advantageous in biological systems since in addition to removing the water peak they can be used to remove broad resonances and the J-modulation patterns can be used for selecting certain molecules (e.g. lactate).

The inhomogeneity in B_1, especially when using surface coils, can lead to a spatially dependent population of desired and undesired coherence pathways. Field gradient pulses in combination with shaped RF pulses lead to spatially selective excitation or refocusing and, in such cases, localization can be viewed as a type of coherence pathway selection. The inherent B_1 gradients resulting from the inhomogeneous RF fields of surface coils have also been used for water suppression in *in vivo* experiments.[243]

Postprocessing suppression methods (see Postprocessing and selective detection-based methods, p. 325) have particular relevance to imaging since insufficient apodization and truncation can result in "ringing" over a large portion of the spectrum. This is often the case in spectroscopic imaging using multiple spin-echoes.[15]

The suppression methods that can be used to effect fat suppression (mainly triglycerides) are more limited than water since triglycerides have many resonances which thus precludes the use of frequency-based methods. However, three features of fat resonances can be used for suppression purposes:[15] (i) the fat resonances have short T_1 values, (ii) the triglycerides have some natural localization and so careful volume selection (or outer volume suppression) will provide some suppression and (iii) the coupling patterns in triglycerides.

7. MISCELLANEOUS

7.1. High-molecular-weight solutes

Solvent suppression in samples with very large macromolecules (i.e. MW $\gg$ 10 000) such as immunoglobulins presents special difficulties due to the unfortunate combination of short relaxation times and high susceptibility to spin-diffusion.[244,245] Spin-diffusion causes rapid propagation of the effects of the continuous irradiation used for suppression throughout the entire spectrum. Thus, the irradiation at the water frequency can result in a severe loss of intensity of the protein resonances. Further, the short T_2 relaxation times of the resonances[245] severely limit the available suppression methods, especially those involving echoes or (time-consuming) frequency-selective pulses. Spectra of IgG (MW ~ 150 000) acquired using presaturation and the Water-PRESS sequence are shown in Fig. 28. It can be clearly seen that presaturation results in larger signal losses than Water-PRESS.

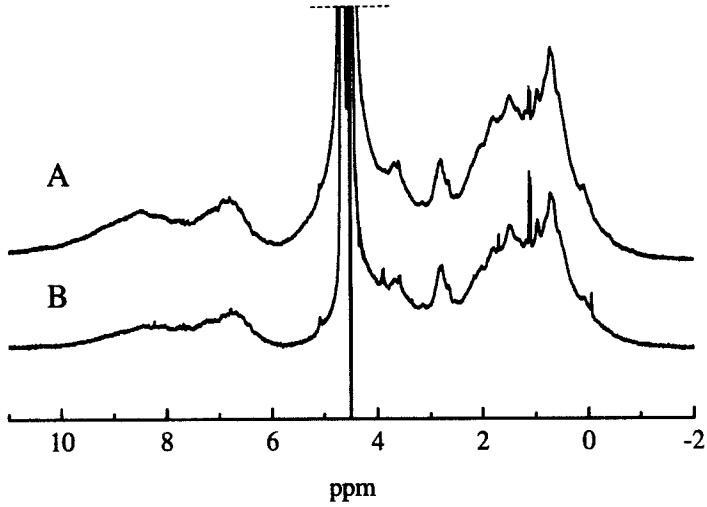

Fig. 28. One-dimensional ^{1}H spectra of IgG solution (10 mg of protein in 0.4 ml of H_2O:$^{2}H_2O$ 90:10, pH 6.9) acquired using (A) the Water-PRESS method and (B) presaturation. Both spectra were acquired using a recycle delay of 20 s, the same receiver gain and averaging 160 transients. Spectrum (B) was acquired using 1.5 s of presaturation (included as part of the recycle delay) at a field strength of ~35 Hz at the water frequency. Many of the resonances in the spectrum acquired with presaturation have lost more intensity due to the effects of spin-diffusion. (From Price *et al.*[112])

7.2. Suppression of ^{17}O NMR signals

Perhaps surprisingly, solvent suppression can also be required even when the observed nucleus is not ^{1}H. In fact, in ^{17}O NMR of aqueous solutions the intense water resonance hinders the observation of nearby resonances such as alcohols and ethers.[246,247] A partial, expensive and troublesome solution is to use ^{17}O-depleted water which provides about a thirty-fold reduction of the water intensity. However, this solution fails if it exchanges with the solute oxygens. Lauterwein and Gerothanassis have developed a steady-state pulse sequence[248] comprising rapid pulsing with subsequent DC shift and zero-filling of the FID to achieve a water suppression factor of 100. However, because of the short acquisition time the residual solvent resonance is strongly broadened. They were able to achieve a suppression factor of about 1000 using the $1\text{–}\bar{3}\text{–}3\text{–}\bar{1}$ sequence.[159,169] WEFT and presaturation were both found to be suitable for observing resonances close to the water signal. Importantly, they found that it was also possible to combine the WEFT technique with techniques for reducing acoustic ringing[249] (see Fig. 29).

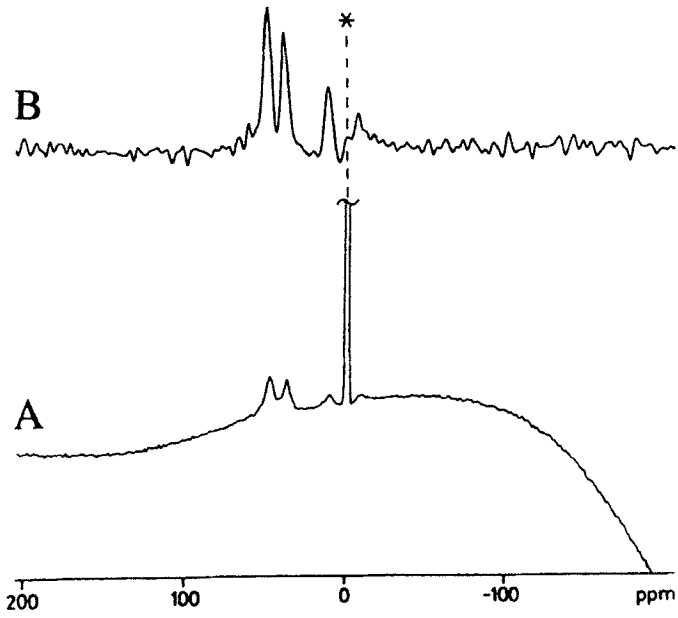

Fig. 29. A ^{17}O NMR spectrum of 0.5 mM D-glucose in H_2O at 353 K recorded at 48.8 MHz. (A) Reference spectrum acquired using $\pi/2$ pulses. The baseline is distorted due to acoustic ringing effects. (B) Combination of the inversion-recovery technique with the RIDE sequence for acoustic ringing elimination. The asterisk denotes the water resonance. (From Schulte and Lauterwein[249] with permission.)

8. CONCLUDING REMARKS

The ideal suppression scheme would be (i) take no time, (ii) only affect the solvent resonance(s) leaving the solute resonances unchanged and (iii) be experimentally simple to set up and not interact or have bearing on the rest of the pulse sequence. No suppression scheme exists that meets all of these criteria and a judicious choice of suppression technique will thus have an enormous bearing on the success of the experiment being attempted. In practice, the choice of suppression scheme depends on the characteristics of the sample, the solvent and the spectrometer as well, and perhaps more importantly, the experiment being attempted and the information desired and the time available. The development of suppression techniques is still one of the most active areas of research in NMR and the performance will be enhanced in unison with developments with shaped RF pulses and stronger high-performance magnetic field gradients especially on high-resolution probes. These developments will also be spurred on by the need to develop efficient suppression schemes suitable for use in applications such as

LC NMR and structural NMR studies of higher-molecular-weight proteins with their concomitant problems of short T_2 and susceptibility to spin-diffusion.

REFERENCES

1. W. S. Price, G. L. Mendz and R. E. Martenson, *Biochemistry*, 1988, **27**, 8990.
2. S. Nonin, J.-L. Leroy and M. Guéron, *Nucleic Acids Research*, 1996, **24**, 586.
3. A. Kettani, M. Guéron and J.-L. Leroy, *J. Am. Chem. Soc.*, 1997, **119**, 1108.
4. S. A. Korhammer and A. Bernreuther, *Fresenius J. Anal. Chem.*, 1996, **354**, 131.
5. P. A. Keifer, *Drug Discovery Today*, 1997, **2**, 468.
6. S. H. Smallcombe, S. L. Patt and P. A. Keifer, *J. Magn. Reson.*, 1995, **A117**, 295.
7. W. S. Price, M. Nara and Y. Arata, *Biophys. Chem.*, 1997, **65**, 179.
8. M. Guéron, P. Plateau and M. Decorps, *Prog. NMR Spec.*, 1991, **23**, 135.
9. M. Guéron and P. Plateau, *Encyclopedia of Nuclear Magnetic Resonance* (eds D. M. Grant and R. K. Harris), pp. 4931–4942, Wiley, New York, 1996.
10. B. C. Gerstein and C. R. Dybowski, *Transient Techniques in NMR of Solids*, p. 175, Academic Press, New York, 1985.
11. P. J. Hore, *Methods Enzymol.*, 1989, **176**, 64.
12. J. E. Meier and A. G. Marshall, *Biological Magnetic Resonance* (eds L. J. Berliner and J. Reuben), pp. 199–240, Plenum Press, New York, 1990.
13. P. C. M. Van Zijl and C. T. W. Moonen, *NMR Basic Princ. Progr.*, 1992, **26**, 67.
14. A. S. Altieri, K. E. Miller and R. A. Byrd, *Magnetic Resonance Review*, 1996, **17**, 27.
15. C. T. W. Moonen and P. C. M. Van Zijl, *Encyclopedia of Nuclear Magnetic Resonance* (eds D. M. Grant and R. K. Harris), pp. 4943–4955, Wiley, New York, 1996.
16. A. G. Sobol, G. Wider, H. Iwai and K. Wüthrich, *J. Magn. Reson.*, 1998, **130**, 262.
17. X.-A. Mao and C.-H. Ye, *Concepts Magn. Reson.*, 1997, **9**, 173.
18. M. P. Augustine and K. W. Zilm, *J. Magn. Reson.*, 1996, **A123**, 145.
19. M. H. Levitt, *Concepts Magn. Reson.*, 1996, **8**, 77.
20. A. Vlassenbroek, J. Jeener and P. Broekaert, *J. Chem. Phys.*, 1995, **103**, 5886.
21. M. A. McCoy and W. S. Warren, *J. Chem. Phys.*, 1990, **93**, 858.
22. D. Abergel, M. A. Delsuc and J.-Y. Lallemand, *J. Chem. Phys.*, 1992, **92**, 1657.
23. W. S. Warren, Q. He, M. McCoy and F. C. Spano, *J. Chem. Phys.*, 1992, **96**, 1659.
24. Q. He, W. Richter, S. Vathyam and W. S. Warren, *J. Chem. Phys.*, 1993, **98**, 6779.
25. W. S. Warren, W. Richter, A. H. Andreotti and B. T. Farmer, II, *Science*, 1993, **262**, 2005.
26. W. Richter, S. Lee, W. S. Warren and Q. He, *Science*, 1995, **267**, 654.
27. G. E. Ball, G. J. Bowden, T. H. Heseltine, M. J. Prandolini and W. Bermel, *Chem. Phys. Lett.*, 1996, **261**, 421.
28. J.-H. Chen, X.-A. Mao and C.-H. Ye, *J. Magn. Reson.*, 1996, **A123**, 126.
29. X.-A. Mao, J. Guo and J.-H. Chen, *J. Phys.*, 1996, **D29**, 1595.
30. W. S. Warren and W. Richter, *Encyclopedia of Nuclear Magnetic Resonance* (eds D. M. Grant and R. K. Harris), pp. 1417–1423, Wiley, New York, 1996.
31. J.-H. Chen and X.-A. Mao, *Chem. Phys. Lett.*, 1997, **274**, 549.
32. G. J. Bowden, T. Heseltine and M. J. Prandolini, *Chem. Phys. Lett.*, 1995, **233**, 639.
33. A. Vlassenbroek, J. Jeener and P. Broekaert, *J. Magn. Reson.*, 1996, **A118**, 234.
34. P. C. M. Van Zijl, M. O. Johnson, S. Mori and R. E. Hurd, *J. Magn. Reson.*, 1995, **A113**, 265.
35. C. Dalvit and J.-M. Böhlen, *J. Magn. Reson.*, 1996, **B111**, 76.
36. C. Dalvit and J. M. Böhlen, *J. Magn. Reson.*, 1996, **B113**, 195.
37. C. Dalvit and J. M. Böhlen, *Magn. Reson. Chem.*, 1996, **34**, 829.

38. D. L. Mattiello, W. S. Warren, L. Mueller and B. T. Farmer, II, *J. Am. Chem. Soc.*, 1996, **118**, 3253.
39. G. Suryan, *Curr. Sci.*, 1949, **6**, 203.
40. N. Bloembergen and R. V. Pound, *Phys. Rev.*, 1954, **95**, 8.
41. A. Abragam, *The Principles of Nuclear Magnetism*, Clarendon Press, Oxford, 1961.
42. V. V. Krishnan, *Curr. Sci.*, 1998, **74**, 1049.
43. D. Abergel and J.-Y. Lallemand, *J. Magn. Reson.*, 1994, **A110**, 45.
44. E. L. Hahn, *Concepts Magn. Reson.*, 1997, **9**, 65.
45. W. S. Warren, S. L. Hammes and L. J. Bates, *J. Chem. Phys.*, 1989, **91**, 5895.
46. X.-A. Mao, J. Guo and C.-H. Ye, *Chem. Phys. Lett.*, 1994, **218**, 249.
47. X.-A. Mao and C.-H. Ye, *J. Chem. Phys.*, 1993, **99**, 7455.
48. A. Sodickson, W. E. Maas and D. G. Cory, *J. Magn. Reson.*, 1996, **B110**, 298.
49. Ad. Bax, V. Sklenár, G. M. Clore and A. M. Gronenborn, *J. Am. Chem. Soc.*, 1987, **109**, 6511.
50. N. Birlirakis, R. Cerdan and E. Guittet, *J. Biomol. NMR*, 1996, **8**, 487.
51. J. Stonehouse, G. L. Shaw and J. Keeler, *J. Biomol. NMR*, 1994, **4**, 799.
52. J. Guo and X.-A. Mao, *Phys. Rev.*, 1994, **B50**, 13461.
53. X.-A. Mao, J. Guo and C.-H. Ye, *Chem. Phys. Lett.*, 1994, **222**, 417.
54. D.-H. Wu and C. S. Johnson, Jr, *J. Magn. Reson.*, 1994, **110**, 113.
55. J.-H. Chen, X.-A. Mao and C.-H. Ye, *J. Magn. Reson.*, 1997, **124**, 490.
56. X. Mao, J. Guo and C. Ye, *Chem. Phys. Lett.*, 1994, **227**, 65.
57. X.-A. Mao, D.-H. Wu and C.-H. Ye, *Chem. Phys. Lett.*, 1993, **204**, 123.
58. X.-A. Mao, J. Guo and C.-H. Ye, *Phys. Rev.*, 1994, **B49**, 15 702.
59. H. Barjat, G. P. Chadwick, G. A. Morris and A. G. Swanson, *J. Magn. Reson.*, 1995, **A117**, 109.
60. G. Otting, *J. Magn. Reson.*, 1994, **B103**, 288.
61. G. Deville, M. Bernier and J. M. Delrieux, *Phys. Rev.*, 1979, **B19**, 5666.
62. D. Einzel, G. Eska, Y. Hirayoshi, T. Kopp and P. Wölfle, *Phys. Rev. Lett.*, 1984, **53**, 2312.
63. H. T. Edzes, *J. Magn. Reson.*, 1990, **86**, 293.
64. R. Bowtell, R. M. Bowley and P. Glover, *J. Magn. Reson.*, 1990, **88**, 643.
65. A. S. Bedford, R. Bowtell and R. M. Bowley, *J. Magn. Reson.*, 1991, **93**, 516.
66. H. Körber, E. Dormann and G. Eska, *J. Magn. Reson.*, 1991, **93**, 589.
67. R. P. O. Jones, G. A. Morris and J. C. Waterton, *J. Magn. Reson.*, 1992, **98**, 115.
68. R. Bowtell and P. Robyr, *Phys. Rev. Lett.*, 1996.
69. M. G. Kubinec, A. S. Culf, Ho. Cho, D. C. Lee, J. Burkham, H. Morimoto, P. G. Williams and D. E. Wemmer, *J. Biomol. NMR*, 1996, **7**, 236.
70. J. Jeener, A. Vlassenbroek and P. Broekaert, *J. Chem. Phys.*, 1995, **103**, 1309.
71. P. Broekaert, A. Vlassenbroek, J. Jeener, G. Lippens and J.-M. Wieruszeski, *J. Magn. Reson.*, 1996, **A120**, 97.
72. S. Lee, S. Richter, S. Vathyam and W. S. Warren, *J. Chem. Phys.*, 1996, **105**, 874.
73. D. E. Warschawski and P. F. Devaux, *J. Magn. Reson.*, 1995, **B106**, 76.
74. B. Wright, D. Greatbanks, J. Taberner and I. D. Wilson, *Pharm. Sci.*, 1995, **1**, 197.
75. W. S. Price, *Annual Reports on NMR Spectroscopy* (ed. G. A. Webb), pp. 51–142, Academic Press, London, 1996.
76. S. L. Patt, *J. Magn. Reson.*, 1991, **96**, 94.
77. W. S. Warren and M. S. Silver, *Adv. Magn. Reson.*, 1988, **12**, 247.
78. A. A. Maudsley and G. B. Matson, *Encyclopedia of Nuclear Magnetic Resonance* (eds D. M. Grant and R. K. Harris), pp. 4210–4218, Wiley, New York, 1996.
79. P. G. Morris, *Encyclopedia of Nuclear Magnetic Resonance* (eds D. M. Grant and R. K. Harris), pp. 1390–1396, Wiley, New York, 1996.
80. M. S. Silver, R. I. Joseph and D. I. Hoult, *J. Magn. Reson.*, 1984, **59**, 347.
81. M. Garwood and K. Ugurbil, *NMR Basic Princ. Progr.*, 1992, **26**, 109.
82. D. I. Hoult, *J. Magn. Reson.*, 1976, **21**, 337.

83. D. Neuhaus, M. I. Ismail and C.-W. Chung, *J. Magn. Reson.*, 1996, **A118**, 256.
84. Ad. Bax, *J. Magn. Reson.*, 1985, **65**, 142.
85. M. G. Zagorski, *J. Magn. Reson.*, 1991, **91**, 141.
86. S.-I. Tate and F. Inagaki, *J. Magn. Reson.*, 1992, **96**, 635.
87. G. Bodenhausen, R. Freeman and D. L. Turner, *J. Magn. Reson.*, 1977, **27**, 511.
88. Y.-C. Li and G. T. Montelione, *J. Magn. Reson.*, 1993, **B101**, 315.
89. F. J. Moy, H. A. Scheraga, S. L. Patt and G. T. Montelione, *J. Magn. Reson.*, 1992, **98**, 451.
90. S. C. Brown, P. L. Weber and L. Mueller, *J. Magn. Reson.*, 1988, **77**, 166.
91. Z. Starcuk, L. Pucek, R. Fiala and Z. Starcuk, Jr, *J. Magn. Reson.*, 1988, **80**, 344.
92. B. A. Messerle, G. Wider, G. Otting, C. Weber and K. Wüthrich, *J. Magn. Reson.*, 1989, **85**, 608.
93. G. Otting, E. Liepinsh, B. T. Farmer, II and K. Wüthrich, *J. Biomol. NMR*, 1991, **1**, 209.
94. G. Otting, E. Liepinsh and K. Wüthrich, *J. Am. Chem Soc.*, 1992, **114**, 7093.
95. G. Otting, *Prog. NMR Spec.*, 1997, **31**, 259.
96. P. Sodano and M. Delepierre, *J. Biomol. NMR*, 1993, **3**, 471.
97. X. Mao and C. Ye, *Sci. China*, 1997, **C40**, 345.
98. X.-A. Mao and J.-H. Chen, *Chem. Phys.*, 1996, **202**, 57.
99. X.-A. Mao and C.-H. Ye, *Chem. Phys. Lett.*, 1994, **227**, 645.
100. D. L. Rabenstein and A. A. Isab, *J. Magn. Reson.*, 1979, **36**, 281.
101. D. L. Rabenstein, S. Fan and T. T. Nakashima, *J. Magn. Reson.*, 1985, **64**, 541.
102. R. G. Bryant and T. M. Eads, *J. Magn. Reson.*, 1985, **64**, 312.
103. M. L. Magnuson and B. M. Fung, *J. Magn. Reson.*, 1992, **99**, 301.
104. F. W. Benz, J. Feeney and G. C. K. Roberts, *J. Magn. Reson.*, 1972, **8**, 114.
105. S. L. Patt and B. D. Sykes, *J. Chem. Phys.*, 1972, **56**, 3182.
106. R. K. Gupta, *J. Magn. Reson.*, 1976, **24**, 461.
107. C. A. G. Haasnoot, *J. Magn. Reson.*, 1983, **52**, 153.
108. T. Inubushi and E. D. Becker, *J. Magn. Reson.*, 1983, **51**, 128.
109. R. Freeman, *A Handbook of Nuclear Magnetic Resonance*, Longman, Harlow, 1988.
110. P. A. Mirau, *J. Magn. Reson.*, 1987, **73**, 122.
111. W. S. Price and Y. Arata, *J. Magn. Reson.*, 1996, **B112**, 190.
112. W. S. Price, K. Hayamizu and Y. Arata, *J. Magn. Reson.*, 1997, **126**, 256.
113. D. M. Doddrell, G. J. Galloway, W. M. Brooks, J. Field, J. M. Bulsing, M. G. Irving and H. Baddeley, *J. Magn. Reson.*, 1986, **70**, 176.
114. I. M. Brereton, J. Field, L. N. Moxon, M. G. Irving and D. M. Doddrell, *Magn. Reson. Med.*, 1989, **9**, 118.
115. I. M. Brereton, G. J. Galloway, J. Field, M. F. Marshman and D. M. Doddrell, *J. Magn. Reson.*, 1989, **81**, 411.
116. B. K. John, D. Plant, P. Webb and R. E. Hurd, *J. Magn. Reson.*, 1992, **98**, 200.
117. A. S. Altieri and R. A. Byrd, *J. Magn. Reson.*, 1995, **B107**, 260.
118. A. Haase, J. Frahm, W. Hänicke and D. Matthei, *Phys. Med. Biol.*, 1985, **30**, 341.
119. C. T. W. Moonen, G. S. Sobering, P. C. M. Van Zijl, J. Gillen, M. von Kienlin and A. Bizzi, *J. Magn. Reson.*, 1992, **98**, 556.
120. J. A. Hopkins, J. B. Grutzner and D. Canet, *J. Magn. Reson.*, 1995, **A114**, 98.
121. C. T. W. Moonen and P. C. M. Van Zijl, *J. Magn. Reson.*, 1990, **88**, 28.
122. P. Stilbs, *Prog. NMR Spec.*, 1987, **19**, 1.
123. P. C. M. Van Zijl and C. T. W. Moonen, *J. Magn. Reson.*, 1990, **87**, 18.
124. W. S. Price, *Concepts Magn. Reson.*, 1997, **9**, 299.
125. E. O. Stejskal, *J. Chem. Phys.*, 1965, **43**, 3597.
126. H. Pontsingl and G. Otting, *J. Biomol. NMR*, 1997, **9**, 441.
127. G. Wider, R. Riek and K. Wüthrich, *J. Am. Chem Soc.*, 1996, **118**, 11629.
128. S. Mori, M. O. Johnson, J. M. Berg and P. C. M. Van Zijl, *J. Am. Chem. Soc.*, 1994, **116**, 11982.

129. P. C. M. Van Zijl, C. T. W. Moonen, P. Faustino, J. Pekar, O. Kaplan and J. S. Cohen, *Proc. Natl. Acad. Sci. USA*, 1991, **88**, 3228.
130. K. Potter, R. L. Kleinberg, F. J. Brockman and E. W. McFarland, *J. Magn. Reson.*, 1996, **B113**, 9.
131. M. Piotto, V. Saudek and V. Sklenář, *J. Biomol. NMR*, 1992, **2**, 661.
132. V. Sklenář, M. Piotto, R. Leppik and V. Saudek, *J. Magn. Reson.*, 1993, **A102**, 241.
133. V. Saudek, M. Piotto and V. Sklenář, *Bruker Report*, 1994, 6.
134. M. Liu, X.-A. Mao, C. Ye, He. Huang, J. K. Nicholson and J. C. Lindon, *J. Magn. Reson.*, 1998, **132**, 125.
135. H. Geen and R. Freeman, *J. Magn. Reson.*, 1991, **93**, 93.
136. C. Dalvit, S. Y. Ko and J. M. Böhlen, *J. Magn. Reson.*, 1996, **B110**, 124.
137. T.-L. Hwang and A. J. Shaka, *J. Magn. Reson.*, 1995, **A112**, 275.
138. K. Stott, J. Stonehouse, J. Keeler, T.-L. Hwang and A. J. Shaka, *J. Am. Chem. Soc.*, 1995, **117**, 4199.
139. T. Parella, P. Adell, F. Sánchez-Ferrando and A. Virgili, *Magn. Reson. Chem.*, 1998, **36**, 245.
140. C. Dalvit, *J. Biomol. NMR*, 1998, **11**, 437.
141. M. Mescher, A. Tannus, M. O. Johnson and M. Garwood, *J. Magn. Reson.*, 1996, **A123**, 226.
142. R. J. Ogg, P. B. Kingsley and J. S. Taylor, *J. Magn. Reson.*, 1994, **B104**, 1.
143. M. A. McCoy and L. Mueller, *J. Am. Chem. Soc.*, 1992, **114**, 2108.
144. J. M. Bulsing and D. M. Doddrell, *J. Magn. Reson.*, 1986, **68**, 52.
145. G. Otting and K. Wüthrich, *J. Magn. Reson.*, 1988, **76**, 569.
146. Ad. Bax and S. S. Pochapsky, *J. Magn. Reson.*, 1992, **99**, 638.
147. G. Wider and K. Wüthrich, *J. Magn. Reson.*, 1993, **B102**, 239.
148. J. Ruiz-Cabello, G. W. Vuister, C. T. W. Moonen, P. van Gelderen, J. S. Cohen and P. C. M. Van Zijl, *J. Magn. Reson.*, 1992, **100**, 282.
149. J. R. Tolman and J. H. Prestegard, *Concepts Magn. Reson.*, 1995, **7**, 247.
150. V. Dötsch, R. E. Oswald and G. Wagner, *J. Magn. Reson.*, 1995, **108**, 285.
151. C. Dalvit and J. M. Böhlen, *NMR Biomed.*, 1997, **10**, 285.
152. D. Canet, J. Brondeau, E. Mischler and F. Humbert, *J. Magn. Reson.*, 1993, **A105**, 239.
153. J. Brondeau, P. Mutzenhardt, J.-M. Tyburn and D. Canet, *J. Magn. Reson.*, 1995, **B109**, 310.
154. W. E. Maas and D. G. Cory, *J. Magn. Reson.*, 1994, **A106**, 256.
155. P. Plateau and M. Guéron, *J. Am. Chem. Soc.*, 1982, **104**, 7310.
156. M. Guéron, P. Plateau, A. Kettani and M. Decorps, *J. Magn. Reson.*, 1992, **96**, 541.
157. V. Sklenář and Ad. Bax, *J. Magn. Reson.*, 1987, **74**, 469.
158. A. C. Hsu and C. D. Gregory, *J. Magn. Reson.*, 1998, **131**, 46.
159. P. J. Hore, *J. Magn. Reson.*, 1983, **55**, 283.
160. D. L. Turner, *J. Magn. Reson.*, 1983, **54**, 146.
161. G. J. Galloway, L. J. Haseler, M. F. Marshman, D. H. Williams and D. M. Doddrell, *J. Magn. Reson.*, 1987, **74**, 184.
162. K. Takagoshi, S. Tsuda and K. Hikichi, *J. Magn. Reson.*, 1989, **85**, 198.
163. K. Takagoshi, S. Tsuda and K. Hikichi, *J. Magn. Reson.*, 1990, **89**, 399.
164. L. Pucek and V. Sklenář, *J. Magn. Reson.*, 1990, **86**, 376.
165. G. A. Morris, A. C. T. Silveston and J. C. Waterton, *J. Magn. Reson.*, 1989, **82**, 97.
166. M. H. Levitt, *J. Chem. Phys.*, 1988, **88**, 3481.
167. A. L. Davis and S. Wimperis, *J. Magn. Reson.*, 1989, **84**, 620.
168. B. A. Inglis, K. D. Sales and S. C. R. Williams, *J. Magn. Reson.*, 1994, **105**, 61.
169. P. J. Hore, *J. Magn. Reson.*, 1983, **54**, 539.
170. S. H. Smallcombe, *J. Am. Chem. Soc.*, 1993, **115**, 4776.
171. M. A. McCoy, F. Loaiza, K. Valentine and W. S. Warren, *J. Magn. Reson.*, 1988, **80**, 155.

172. H. Liu, K. Weisz and T. L. James, *J. Magn. Reson.*, 1993, **A105**, 184.
173. S. Grzesiek and Ad. Bax, *J. Am. Chem. Soc.*, 1993, **115**, 12593.
174. S. Grzesiek and Ad. Bax, *J. Biomol. NMR*, 1993, **3**, 627.
175. W. Jahnke and H. Kessler, *J. Biomol. NMR*, 1994, **4**, 735.
176. H. Kuboniwa, S. Grzesiek, F. Delaglio and Ad. Bax, *J. Biomol. NMR*, 1994, **4**, 871.
177. G. Lippens, C. Dhalluin and J.-M. Wieruszeski, *J. Biomol. NMR*, 1995, **5**, 327.
178. V. Sklenář, R. Tschudin and Ad. Bax, *J. Magn. Reson.*, 1987, **75**, 352.
179. L. A. Trimble and M. A. Bernstein, *J. Magn. Reson.*, 1994, **B105**, 67.
180. A. Böckmann, F. Penin and E. Guittet, *FEBS Lett.*, 1996, **383**, 191.
181. S. Talluri and G. Wagner, *J. Magn. Reson.*, 1996, **B112**, 200.
182. D. Callihan, J. West, S. Kumar, B. I. Schweitzer and T. M. Logan, *J. Magn. Reson.*, 1996, **B112**, 82.
183. T. E. Skinner, J. Pruski and P.-M. L. Robataille, *J. Magn. Reson.*, 1992, **98**, 604.
184. O. Gonen and G. Johnson, *J. Magn. Reson.*, 1993, **B102**, 98.
185. A. G. Redfield and S. D. Kunz, *J. Magn. Reson.*, 1998, **130**, 111.
186. J. P. Waltho and J. Cavanagh, *J. Magn. Reson.*, 1993, **A103**, 338.
187. H. Barkhuijsen, R. de Beer and D. van Ormondt, *J. Magn. Reson.*, 1987, **73**, 553.
188. R. de Beer, A. van den Boogaart, E. Cady, D. Graveron-Demilly, A. Knijn, K. W. Langenberger, J. C. Lindon, A. Ohlhoff, H. Serrai and M. Wylezinska-Arridge, *Eurospin Annual 1995–1996* (eds F. Podo, W. M. M. Bovée, J. D. de Certaines, O. Henriksen, M. O. Leach and D. Leibfritz), pp. 341–365, Istituto Superiore Di Sanità, Rome, 1996.
189. D. Marion, M. Ikura and Ad. Bax, *J. Magn. Reson.*, 1989, **84**, 425.
190. M. S. Friedrichs, W. J. Metzler and L. Mueller, *J. Magn. Reson.*, 1991, **95**, 178.
191. Y. Kuroda, A. Wada, T. Yamazaki and K. Nagayama, *J. Magn. Reson.*, 1990, **88**, 141.
192. J. J. Led and H. Gesmar, *Chem. Rev.*, 1991, **91**, 1413.
193. M. von Kienlin, C. T. W. Moonen, A. van der Toorn and P. C. M. Van Zijl, *J. Magn. Reson.*, 1991, **93**, 423.
194. F. Ni, *J. Magn. Reson.*, 1992, **99**, 391.
195. P. Sodano and M. Delepierre, *J. Magn. Reson.*, 1993, **A104**, 88.
196. C. J. Craven and J. P. Waltho, *J. Magn. Reson.*, 1995, **B106**, 40.
197. H. Barkhuijsen, R. de Beer, W. M. M. Bovée and D. van Ormondt, *J. Magn. Reson.*, 1985, **61**, 465.
198. R. de Beer and D. van Ormondt, *NMR Basic Princ. Progr.*, 1992, **26**, 201.
199. R. de Beer and D. van Ormondt, *Appl. Magn. Reson.*, 1994, **6**, 379.
200. A. van den Boogaart, D. van Ormondt, W. W. F. Pijnappel, R. de Beer and M. Ala-Korpela, *Mathematics in Signal Processing III* (ed. J. G. McWhirter), pp. 175–195, Clarendon Press, Oxford, 1994.
201. W. W. F. Pijnappel, A. van den Boogaart, R. de Beer and D. van Ormondt, *J. Magn. Reson.*, 1992, **97**, 122.
202. R. de Beer, A. van den Boogaart, D. van Ormondt, W. W. F. Pijnappel, J. A. den Hollander, A. J. H. Marien and P. R. Luyten, *NMR Biomed.*, 1992, **5**, 171.
203. R. de Beer, F. Michels, D. van Ormondt, B. P. O. van Tongeren, P. R. Luyten and H. van Vroonhoven, *Magn. Reson. Imaging*, 1993, **11**, 1019.
204. L. Vanhamme, R. D. Fierro, S. Van Huffel and R. de Beer, *J. Magn. Reson.*, 1998, **132**, 197.
205. L. Mitschang, C. Cieslar, T. A. Holak and H. Oschkinat, *J. Magn. Reson.*, 1991, **92**, 208.
206. K. J. Cross, *J. Magn. Reson.*, 1993, **A101**, 220.
207. J. H. J. Leclerc, *J. Magn. Reson.*, 1994, **B103**, 64.
208. G. Zhu, D. Smith and Y. Hua, *J. Magn. Reson.*, 1997, **124**, 286.
209. G. Zhu, W. Y. Choy, G. Song and B. C. Sanctuary, *J. Magn. Reson.*, 1998, **132**, 176.
210. D. Barache, J.-P. Antoine and J.-M. Dereppe, *J. Magn. Reson.*, 1997, **128**, 1.
211. P. Tsang, P. E. Wright and M. Rance, *J. Magn. Reson.*, 1990, **88**, 210.
212. I. Pelczer, *J. Am. Chem. Soc.*, 1991, **113**, 3211.

213. M. Adler and G. Wagner, *J. Magn. Reson.*, 1991, **91**, 450.
214. M. Deriche and X. Hu, *J. Magn. Reson.*, 1993, **A101**, 229.
215. G. Wider, *J. Magn. Reson.*, 1990, **89**, 406.
216. M. E. Rosen, *J. Magn. Reson.*, 1994, **A107**, 119.
217. L. Picard, M. von Kienlin and M. Décorps, *J. Magn. Reson.*, 1995, **A117**, 262.
218. P. Broekaert and J. Jeener, *J. Magn. Reson.*, 1995, **A113**, 60.
219. D. Abergel, C. Carlotti, A. Louis-Joseph and J.-Y. Lallemand, *J. Magn. Reson.*, 1995, **B109**, 218.
220. A. Louis-Joseph, D. Abergel and J.-Y. Lallemand, *J. Biomol. NMR*, 1995, **5**, 212.
221. C. Anklin, M. Rindlisbacher, G. Otting and F. H. Laukien, *J. Magn. Reson.*, 1995, **B106**, 199.
222. W. E. Maas, F. H. Laukien and D. G. Cory, *J. Magn. Reson.*, 1995, **A113**, 274.
223. G. Otting and E. Liepinsh, *J. Magn. Reson.*, 1995, **B107**, 192.
224. V. Sklenář, *J. Magn. Reson.*, 1995, **A114**, 132.
225. C. Dalvit and J. M. Böhlen, *J. Magn. Reson.*, 1997, **126**, 149.
226. S. Zhang and D. G. Gorenstein, *J. Magn. Reson.*, 1996, **A118**, 291.
227. A. Böckmann and E. Guittet, *J. Biomol. NMR*, 1996, **8**, 87.
228. J. Stonehouse, G. L. Shaw, J. Keeler and E. D. Laue, *J. Magn. Reson.*, 1994, **A107**, 178.
229. D. B. Fulton, R. Hrabal and F. Ni, *J. Biomol. NMR*, 1996, **8**, 213.
230. S. Kristensen, M. D. Sørenson, H. Gesmar and J. J. Led, *J. Magn. Reson.*, 1996, **B112**, 193.
231. L. E. Kay, G.-Y. Xu and T. Yamazaki, *J. Magn. Reson.*, 1994, **A109**, 129.
232. J. Stonehouse, R. T. Clowes, G. L. Shaw, J. Keeler and E. D. Laue, *J. Biomol. NMR*, 1995, **5**, 226.
233. D. B. Fulton and F. Ni, *J. Magn. Reson.*, 1997, **129**, 93.
234. S. Mori, C. Abeygunawardana, M. O. Johnson and P. C. M. Van Zijl, *J. Magn. Reson.*, 1995, **B108**, 94.
235. C. Dhalluin, J.-M. Wieruszeski and G. Lippens, *J. Magn. Reson.*, 1996, **B111**, 168.
236. G. Xu and J. S. Evans, *J. Magn. Reson.*, 1996, **B111**, 183.
237. P. R. Blake and M. F. Summers, *J. Magn. Reson.*, 1990, **86**, 622.
238. J. Brondeau, D. Boudot, P. Mutzenhardt and D. Canet, *J. Magn. Reson.*, 1992, **100**, 611.
239. D. G. Cory, F. H. Laukien and W. E. Maas, *J. Magn. Reson.*, 1993, **A105**, 223.
240. P. Mutzenhardt, J. Brondeau and D. Canet, *J. Magn. Reson.*, 1994, **A108**, 110.
241. W. S. Price, *Annual Reports on NMR Spectroscopy* (ed. G. A. Webb), pp. 139–216, Academic Press, London, 1998.
242. J. Star-Lack, S. J. Nelson, J. Kurhanewicz, L. R. Huang and D. B. Vigneron, *Magn. Reson. Med.*, 1997, **38**, 311.
243. P. Blondet, M. Decorps, J. P. Albrand, A. L. Benard and C. Remy, *J. Magn. Reson.*, 1986, **69**, 403.
244. A. Kalk and H. J. C. Berendsen, *J. Magn. Reson.*, 1976, **24**, 343.
245. P. Tsang and M. Rance, *J. Magn. Reson.*, 1996, **B111**, 135.
246. I. P. Gerothanassis, J. Lauterwein and N. Sheppard, *J. Magn. Reson.*, 1982, **48**, 431.
247. J. Lauterwein, J. Schulte, M. Schumacher and M. Cerny, *Magn. Reson. Chem.*, 1992, **30**, 312.
248. J. Lauterwein and I. P. Gerothanassis, *J. Magn. Reson.*, 1983, **51**, 153.
249. J. Schulte and J. Lauterwein, *J. Magn. Reson.*, 1993, **A101**, 95.
250. D. Abergel, A. Louis-Joseph and J.-Y. Lallemand, *J. Biomol. NMR*, 1996, **8**, 15.

Variable Temperature ^{1}H MAS NMR: A Powerful Tool for the Investigation of Dynamic Properties of Acidic Protons in Zeolites and Heteropoly Compounds

TOSHIHIDE BABA and YOSHIO ONO

Department of Chemical Engineering, Tokyo Institute of Technology, Ookayama, Meguro-ku, Tokyo 152-8552, Japan

ANNUAL REPORTS ON NMR SPECTROSCOPY
VOLUME 38 ISBN 0-12-505338-X

The dynamic nature of the protons in zeolites such as H-ZSM-5, metallosilicates molecular sieves and heteropoly compounds was examined by temperature dependence of ^1H MAS NMR in the range of 298 and 473K. The temperature-dependent lineshape of ^1H MAS NMR spectra of acidic protons in zeolites showed the first and unambiguous evidence for proton migration in zeolite structure. The dynamic property of protons was a more sensitive measure for the activity of protons than the static parameters such as NMR chemical shift and IR band position of OH bonds.

The temperature-dependent ^1H MAS NMR also revealed the mobility of protons in heteropoly compounds ($H_3PW_{12}O_{40}$, $Ag_3PW_{12}O_{40}$ and palladium metal loaded on $H_3PW_{12}O_{40}$). This method gave the information of the dynamical process between protons and hydrogen molecules in the gas phase.

The variable temperature ^1H MAS NMR is a very useful technique for understanding dynamic properties of protons in solid acids. The dynamic property is an important factor influencing the catalytic activity of a solid acid catalyst.

1. INTRODUCTION

Knowledge of heterogeneous catalyst structure and composition is crucial to an understanding of the factors that affect the catalyst activity and selectivity. Such information plays an important role to determine the catalytically active sites and to investigate their properties. Moreover, the study of catalytic reaction mechanism and kinetics provides a basis for understanding the relationships between catalytic structure and catalyst activity and selectivity. Among the techniques that can be used for characterization of heterogeneous catalysts, solid-state NMR using magic-angle spinning (MAS NMR) has become a successful tool to provide information about structure and dynamics.[1] For example, ^{29}Si MAS NMR spectra can be used to probe the local Si^{4+} and Al^{3+} distributions in zeolite lattices. A particularly useful feature of the spectra is that the SiO_2/Al_2O_3 ratio of the lattice can be calculated directly.[2]

In this report, we describe the temperature-dependent ^1H MAS NMR of acidic protons zeolites[3–6] and heteropoly compounds[7–9] in order to examine the dynamic properties of their protons. We will show that the variable

temperature ^{1}H MAS NMR is a very useful technique for understanding dynamic properties of protons in solid acids and that the dynamic property is an important factor to have the influence on the catalytic activities of protons.

2. ZEOLITES

2.1. Structure

Zeolites molecular sieves are porous inorganic crystals built from TO_4 tetrahedra.[10,11] In zeolites, T represents silicon or aluminium atom. The overall composition of zeolites is given by the formula as follows:

$$1/m\, M^{m+}[(SiO_2)_n AlO_2^-](H_2O)_z$$

where n denotes the Si/Al ratio ($SiO_2/Al_2O_3 = 2n$) and z is the number of H_2O molecules adsorbed on the zeolite. The negative charge of the zeolite framework $(SiO_2)_n AlO_2^-$ is compensated by exchangeable cations M^{m+} ($m = 1$, 2 or 3) as, e.g. Na^+, Mg^{2+} or La^{3+}. Al–O–Al pairs cannot be formed in the zeolites framework (Loewenstein's rule[12]), i.e. the first T-coordination sphere of an Al atom is completely occupied by Si atoms.

Zeolites are crystalline alumino silicates with a highly ordered crystalline structure. Cavities of a definitive size are formed in three-dimensional network composed of SiO_4 and AlO_4 tetrahedra. The lattice contains cavities of varying diameters, depending on the type of zeolites. A distinction is made between large-, medium- and small-pore zeolites.

In this report, proton-exchanged mordenite, MCM-22 and ZSM-5 zeolites are used. They are denoted as H-mordenite, H-MCM-22 and H-ZSM-5, respectively. Mordenite has a one-dimensional system bonded by 12-oxygen rings, with crosslinks bonded by eight-oxygen rings. The pore size is 0.65×0.70 nm. MCM-22 contains two independent channel systems with 10- and 12-oxygen rings and a large super cage ($0.71 \times 0.71 \times 1.82$ nm).[13] The medium-pore ZSM-5 zeolite consists of intersecting channel formed by 10-oxygen rings of 0.54 nm mean diameter. The unit cell of ZSM-5 is built from four-channel intersection and exhibits 96 T atoms and 192 oxygen atoms.

Silicon and aluminium atoms in a framework of zeolite can be substituted to some extent by other elements like B and Ga.[14,15] In ZSM-5 zeolites, B and Ga can be incorporated into the zeolite skeleton instead of Al. These metallosilicates molecular sieves are denoted as B-ZSM-5 and Ga-ZSM-5 in this report. Moreover, a part of Al atoms in ZSM-5 zeolite lattice can be also replaced by B atoms. This metallosilicate molecular sieve is denoted as [B-Al]-ZSM-5.

2.2. Surface hydroxyl groups in zeolites

The charge compensating cations M^{m+} (see above) may be exchanged by NH_4^+ ions. A thermal treatment at temperature higher than ~600K leads to the removal of NH_3 and consequently to the formation of structural hydroxyl groups as follows:

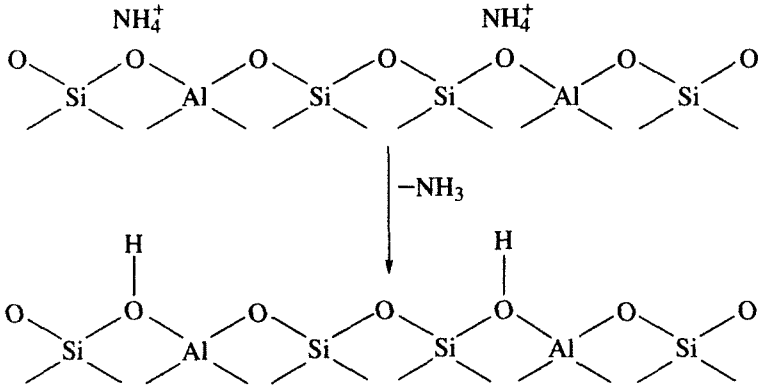

(1)

which are called bridging OH groups. Formally, the charge-compensating cations M^{m+} have been exchanged by H^+ ions but it has to be mentioned that the bridging hydroxyl groups do not exhibit a purely ionic bond character. Further, zeolites may exhibit other types of surface hydroxyl groups as, for example, terminal Si-OH groups at the outer surface of the crystallites, and Si-OH groups on the lattice defect.

2.3. Acidic properties of hydroxyl groups

Brönsted acid sites

Zeolites are widely used as solid acid catalysts for a number of organic transformations, such as the cracking of n-paraffins which are catalysed by Brönsted acid sites.[16–19] In the case of zeolites, the so-called bridging hydroxyl groups in the ≡Si–OH–Al≡ configuration as shown in Eq. (1) are known to act as Brönsted acid sites and they are responsible for the ability of zeolites to catalyse the reactions. Therefore, the characterization of acidic properties of solid acids is of great importance in discussing the catalytic properties of solid acids.

Typical test reactions often used for the characterization of zeolites are the cracking of n-hexane[20,21] and disproportionation of ethylbenzene.[22] The catalytic activity of a zeolite is determined by the concentration of protons and the acid strength.

Acid strength

In the case of zeolites, the acid strength is theoretically correlated with Sanderson electron negativity,[23,24] topological densities,[25] bond length and angles of Al-O-Si unit[26,27] and deprotonation energy.[27,28] The detailed discussion of these theoretical approaches was reviewed by Dwyer[29] and Rabo and Gajda.[30]

Experimentally, the acid strength has been estimated by various methods such as temperature programmed desorption (TPD) of probe molecules such as NH_3,[31,32] microcalorimetry of adsorption of base molecules such as NH_3,[33–35] the shift of OH stretching vibrations[36] and the test reactions.[37]

Pfeifer and co-workers demonstrated that the chemical shift value in ^{1}H MAS NMR spectrum of acidic zeolite was a suitable measure of the acid strength, since it reflects the electron density at the protons.[38–42] In general, protons with higher chemical-shift values are considered to be more electron deficient and more acidic as far as they are not hydrogen.[43–48] Furthermore, the chemical shift values of protons are correlated with other measures of the acid strength. Thus, the chemical shift values due to bridging OH groups are correlated with the wave numbers of the infrared spectra of OH groups[49–55] and their deprotonation energy.[50] They are also correlated well with Sanderson's intermediate electronegativity of the lattice of zeolites.[51,52] In general, the protons with higher acid strength are expected to be more active as a solid acid.

The interaction of probe molecules with acidic OH groups is also studied,[53–61] even though the detail is not described in this report. Moreover, the spinning sidebands analysis in ^{1}H MAS NMR offers the information on the distance between the bridging OH groups and aluminium ions in the zeolite framework.[62,63]

3. WHY VARIABLE TEMPERATURE ^{1}H MAS NMR?

IR spectroscopy has been mainly used to characterize the properties of acidic OH groups in zeolites. As mentioned above, the wave numbers of OH stretching vibrations measured at room temperature were related with their chemical shift values of ^{1}H MAS NMR.

The concept of "acid site" is based on the idea that protons are fixed at definite position. Thus, the measures of the acid strength, which are described so far, are basically based on the static properties of OH groups. However, the solid acid catalysed reactions are often carried out at higher temperatures than room temperature. In general, the catalysts undergo structural and chemical change under reaction conditions. Therefore, the characterization of properties of zeolites at high temperatures is more desirable.

At higher temperatures, there is a high possibility that protons in zeolites

are mobile and not fixed at the specific "sites". The concept of "crystal liquid" was proposed by Barthomeuf.[64] It is important to know whether the protons are delocalized or not in solid acid catalysts, in order to understand the catalytic activities of zeolites. That is, the activity of mobile protons may be different from that of fixed protons on the acid sites.

IR spectroscopy has been applied to characterize the bridging OH groups of zeolites. Several authors reported that the integrated intensity of the OH bands in H-Y zeolites decreased at elevated temperature.[65–67] For example, the intensity became half when the temperature was raised from room temperature to 743K.[65] The authors interpreted this intensity decrease in terms of proton mobility. However, there is an experimental problem for quantitative investigation in IR method. The emission from a sample becomes more intense at higher temperatures and it tends to cause the saturation of the detector.[68]

Since NMR is more a successful tool to investigate the dynamic process on the surface as compared with other tools such as IR, we used ^{1}H MAS NMR to characterize the dynamic properties of protons in zeolites and heteropoly compounds.

It has been established that the mobility of protons can be estimated by the detailed analysis of NMR lineshape.[69] Brunner described theoretical model for the lineshape of ^{1}H MAS NMR as a function of correlation time when proton mobility is a decisive factor for the residual linewidth.[70]

4. DYNAMIC PROPERTY OF PROTONS IN ZEOLITES

4.1. Broadline NMR

The dynamic properties of protons are rarely discussed compared with static properties. Relaxation and line width studies with broadline NMR have been employed to investigate the proton mobility.[71–75] According to Mestdagh *et al.*,[71] the temperature dependence of the second moment and the spin–lattice relaxation time due to the protons of H-Y zeolites could be ascribed to proton motion involving jumps on the lattice oxygen atom. Freude *et al.*[73] have applied an instationary pulse technique in addition to stationary wideline ^{1}H NMR measurements to investigate the mobility or residence time of the protons in A-, X- and Y-type zeolites. At 473K, the proton jump frequency (i.e. inverse mean life time on the lattice oxygen atoms) was estimated to be $3 \times 10^4\ s^{-1}$ for the Y zeolites. Freude and Pfeifer[75] measured the correlation times of the OH groups of Y-type zeolites and the corresponding activation energies, which ranged from 26 to 41 kJ mol^{-1}. In their study, however, acidic protons could not be distinguished from silanol protons; only the average behaviour of the two types of protons (the bridging hydroxyl groups and terminal Si-OH groups) was observed.

4.2. Variable temperature ^{1}H MAS NMR: change of central lineshape by thermal motion

It has been established that the mobility of protons can be estimated by the detailed analysis of NMR lineshape.[69,70] Fenzke *et al.* theoretically treated the influence of isotropic thermal motion upon MAS NMR for spin $I = 1/2$. When the broadening results from an inhomogeneous magnetic dipolar interaction, the lineshape is expressed by Lorentzian line with line width given by the following equation.

$$v^{MAS} = (M_2^{IS}/3\pi)\{2\tau_c/[1+(\omega\tau_c)^2] + \tau_c/[1 + (2\omega\tau_c)^2]\} \quad (2)$$

where ω (rad s^{-1}) is the spinning rate of the sample ($\omega = 2\pi\nu_r$), M_2^{IS} (s^{-2}) is the second moment for the central line, and τ_c (s) is the correlation time. ν_r is the spinning frequency.

The linewidth of ^{1}H MAS NMR spectrum expressed by Eq. (2) exhibits a maximum as a function of correlation time at $(\omega\tau_c) \approx 0.8$, and a simple decrease of the value of v^{MAS} both at smaller (line narrowing caused by thermal motion) and at larger (line narrowing caused by MAS) values of the correlation time. Thus, the linewidth increases and though a maximum, it decreases upon decreasing the correlation time, τ_c. The spinning sidebands exhibit a larger linewidth than the central line and disappear upon decreasing the correlation time. They demonstrated these features by simulating the lineshape of MAS NMR spectra as a function of correlation time.

Brunner described a theoretical model for the lineshape of ^{1}H MAS NMR as a function of correlation time when proton mobility is a decisive factor for the residual linewidth.[70] Sarv *et al.* have recently reported the study on the mobility of acidic protons of various zeolites including H-ZSM-5 by the measurements of ^{1}H MAS NMR spectra at high temperature up to 660 K.[76] The linewidth of the peak attributed to acidic protons narrowed and the intensity of their spinning sidebands gradually disappeared upon raising the temperature. Sarv *et al.* analysed the temperature dependence of the second moments of the spinning sidebands, which is caused by dipolar interaction between acidic protons and the neighbouring aluminium nucleus, and estimated the activation energy of proton mobility.[76]

5. SAMPLE PREPARATION AND ^{1}H MAS NMR MEASUREMENTS OF ZEOLITES

NH_4^+-exchanged zeolites (0.50 g) was packed in a glass tube with side arms, each of which was connected to a glass capsule used for ^{1}H MAS NMR measurements. The view of glass apparatus was shown in Fig. 1. The most important characteristic of the home-made glass apparatus is that the sample

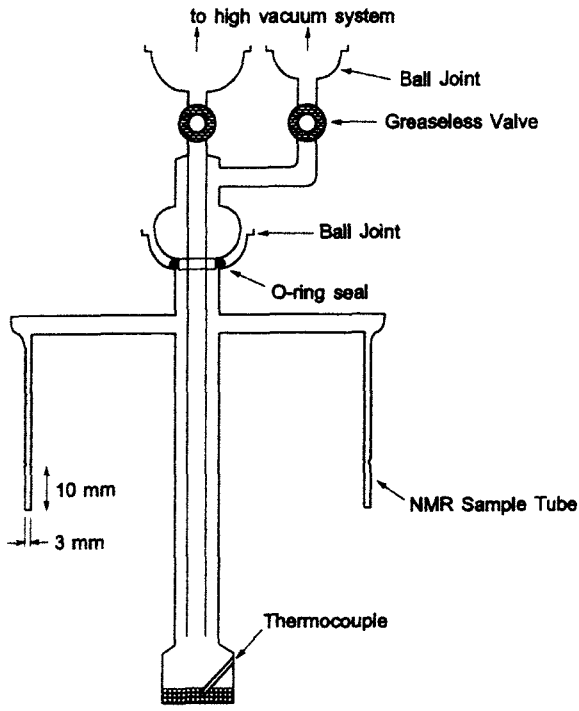

Fig. 1. NMR sample preparation cell.

can be transferred into the glass capsule from the glass tube, where the sample is pre-treated.

NH_4^+-exchanged zeolites such as NH_4-ZSM-5 were calcined to convert into H^+-exchanged type zeolites as shown by Eq. (1). The sample was then heated under vacuum at 673K for 3 h. After cooling the sample to room temperature, it was transferred into a glass capsule under vacuum to fill it completely and evenly. The neck of the capsule was then sealed, while the sample itself was maintained at 77K.

^1H MAS NMR spectra were recorded on a Chemagnetics CMX-Infinity spectrometer operating at 300 MHz equipped with a 5-mm CRAMPS probe. Sealed sample in a glass tube was inserted into zirconia rotor (5-mm diameter). In order to reduce ^1H background signal from probe material, the DEPTH2 pulse sequence was used.[77] The $\pi/2$ pulse width, the recycle delay were 2.0 μs, and 20 s, respectively. The rotation frequency of the glass capsule was 4.0 kHz as far as otherwise mentioned. The spectra were recorded upon raising the sample temperature stepwise from 298 to 473K. The chemical shift was expressed relative to tetramethylsilane (TMS) with the usual conventions.

6. DYNAMIC PROPERTIES OF ACIDIC PROTONS IN SOLID ACIDS

6.1. Temperature dependence of ^{1}H MAS NMR spectra of H-ZSM-5

Figure 2 shows the temperature dependence of ^{1}H MAS NMR spectra of H-ZSM-5 with SiO_2/Al_2O_3 ratio of 39.[4] The spectra were recorded upon raising the temperature of measurements stepwise from 298 to 473K. A peak was observed at (4.2 ± 0.1) ppm at 298K (Fig. 2a) while a very small and broad peak was observed around 1.8 ppm. The former is attributed to bridging OH groups (acidic protons) and the latter is attributed to silanol OH groups (Si-OH, nonacidic protons).[43]

The chemical shift values due to acidic protons did not change upon raising the temperature (Fig. 2a–i), while the change in the chemical shift value due to nonacidic protons is not clear because of its small intensity.

The lineshape due to acidic protons strongly depended on the temperature. Upon raising the temperature of measurements, the linewidth increased and through maximum around 390K, it decreased. The change of the lineshape with temperature was completely reversible. Upon lowering temperature from 473K to 298K, the original spectrum was restored (Fig. 2j).

The spinning sidebands due to acidic protons were clearly observed at 298K. Their intensities monotonously decreased and the linewidths were broadened upon raising the temperature. At temperature higher than 393K, the clear spinning sidebands were not observed.

The temperature dependence of ^{1}H MAS NMR spectra of H-ZSM-5 with SiO_2/Al_2O_3 ratio of 106, is shown in Fig. 3. Two signals were observed at (4.3 ± 0.1) and (2.0 ± 0.1) ppm, which are attributed to acidic and nonacidic protons, respectively.

The chemical shift values of both peaks did not change with temperature. On the other hand, the linewidth of the peak at 4.3 ppm increased and through a maximum around 353K, it decreased. The variation of the linewidth of the peak at 2.0 ppm was not observed upon raising temperature.

The peaks of 4.3 ppm and 2.0 ppm partially overlapped. To determine the linewidth of the peak precisely, the peaks were deconvoluted by using Lorentzian lines, as shown in Fig. 4.[4] ^{1}H MAS NMR spectra of other H-ZSM-5 zeolites were also deconvoluted similarly.

The variation of the line width of the peak due to acidic protons was also observed in H-ZSM-5 with the SiO_2/Al_2O_3 ratios of 39 and 72 (Fig. 5), while the chemical shift values due to acidic protons in these H-ZSM-5 were independent of SiO_2/Al_2O_3 ratios as well as the temperature of measurements.

Since the correlation time decreases with temperature, the spectroscopic features of acidic protons in H-ZSM-5 as shown in Figs 2, 3 and 5 are in conformity with those of the theoretical description. Thus, upon raising temperature, the linewidth increases and through a maximum it decreases.

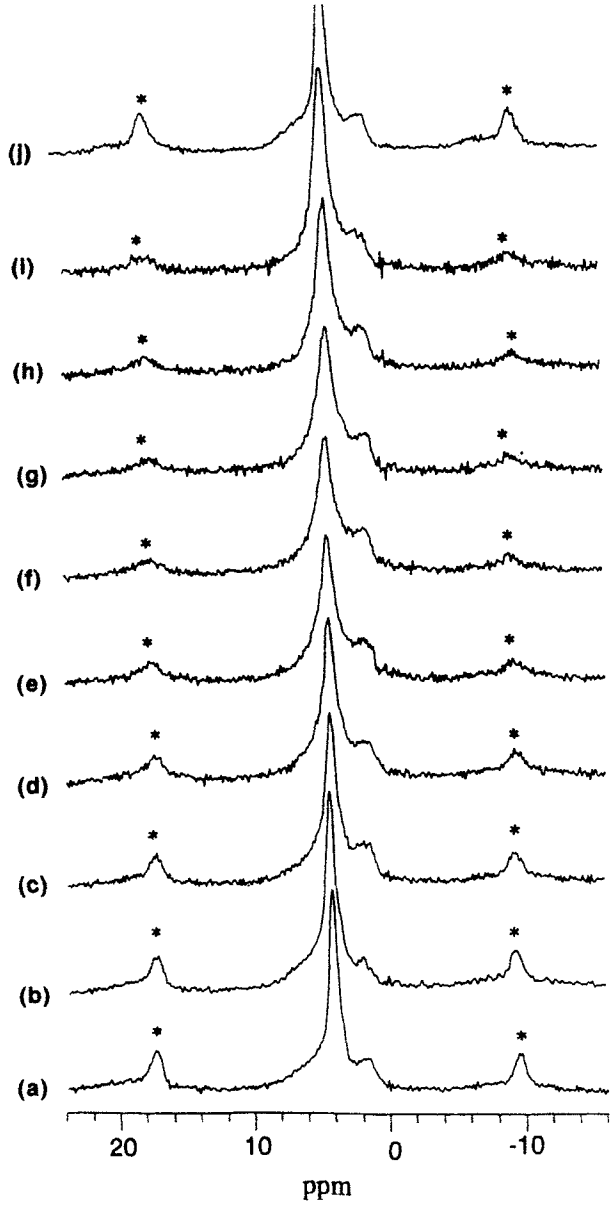

Fig. 2. ^{1}H MAS NMR spectra of H-ZSM-5 (SiO_2/Al_2O_3 = 39). (a) 298K, (b) 313K, (c) 333K, (d) 353K, (e) 373K, (f) 393K, (g) 423K, (h) 453K, (i) 473K, (j) the sample (i) cooled to 298K. The spinning frequency of the sample was 4 kHz. (*) denotes a spinning sideband.

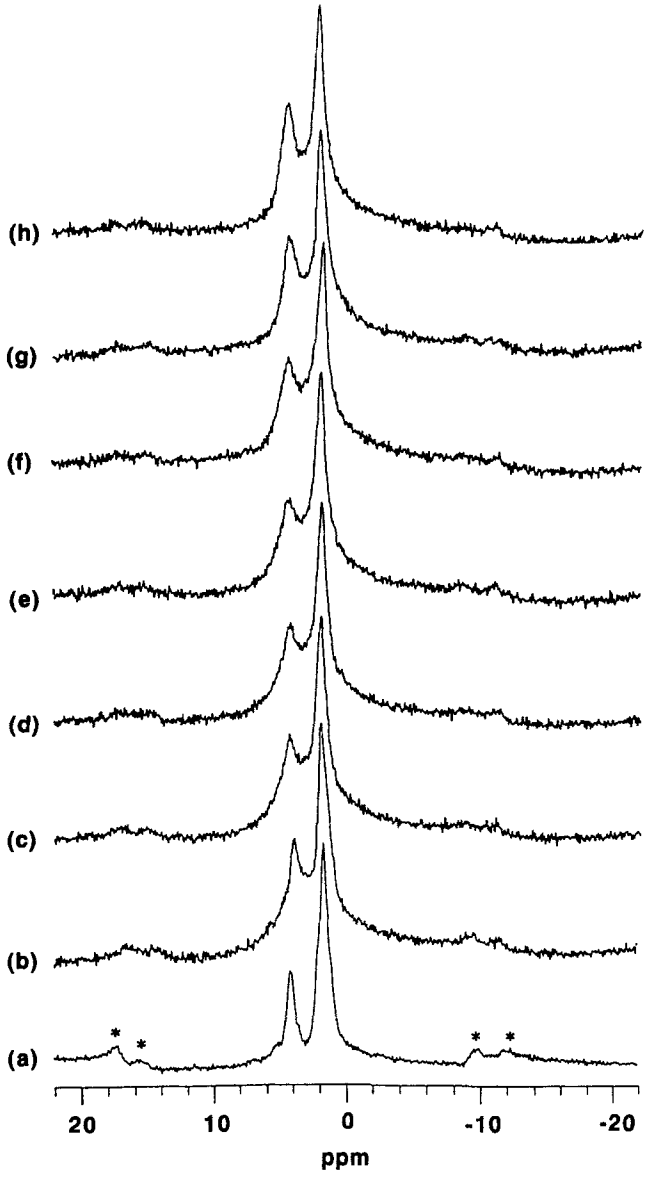

Fig. 3. ^{1}H MAS NMR spectra of H-ZSM-5 (SiO_2/Al_2O_3 = 106). (a) 298K, (b) 333K, (c) 353K, (d) 373K, (e) 393K, (f) 423K, (g) 453K, (h) 473K. (*) denotes a spinning sideband.

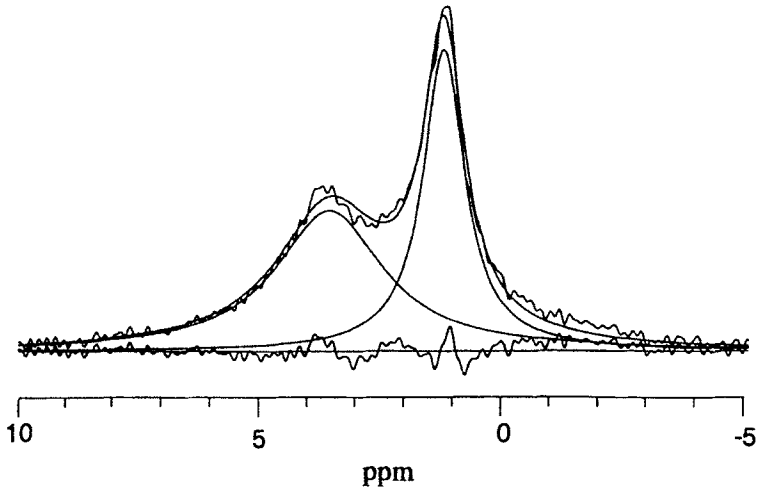

Fig. 4. The peak separation of ^{1}H MAS NMR spectrum. The spectrum of H-ZSM-5 (SiO_2/Al_2O_3 = 106) recorded at 393K.

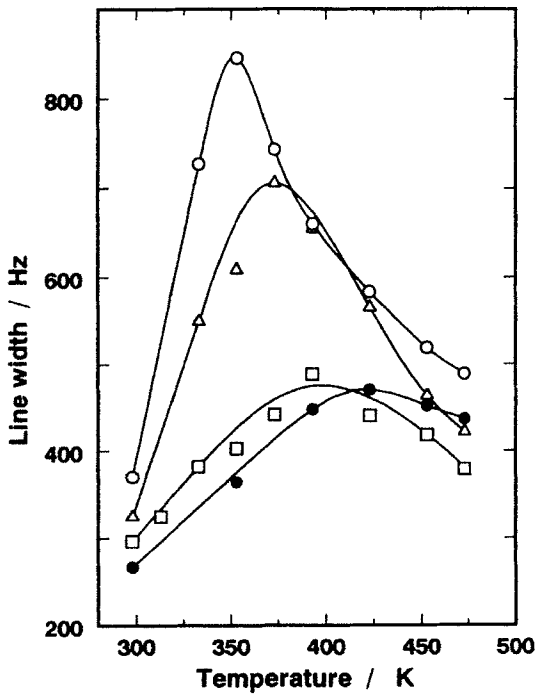

Fig. 5. Effect of temperature on the linewidth of the peak due to acidic protons in H-ZSM-5 zeolites. (●) SiO_2/Al_2O_3 = 24, (□) SiO_2/Al_2O_3 = 39, (△) SiO_2/Al_2O_3 = 72, (○) SiO_2/Al_2O_3 = 106.

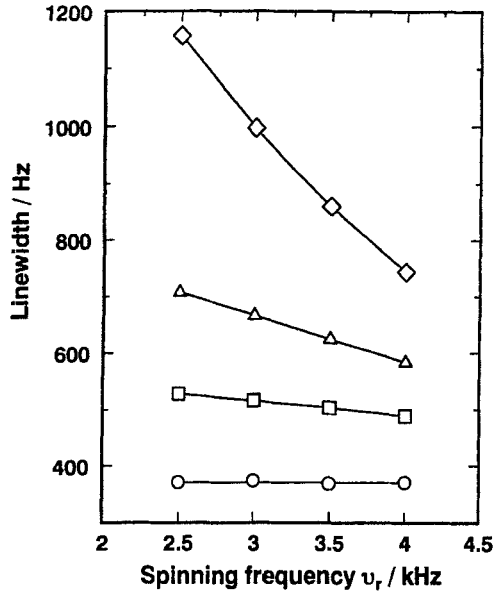

Fig. 6. Linewidth of the peak due to acidic protons in H-ZSM-5 (SiO_2/Al_2O_3 = 106) plotted against the spinning frequency of the sample. (○) 298K, (◇) 373K, (△) 423K, (□) 473K.

Equation (2) also shows that the linewidth depends on the spinning frequency by the isotropic thermal motion of protons. The ^{1}H MAS NMR spectra of H-ZSM-5 (SiO_2/Al_2O_3 = 106) were recorded at 298, 373, 423 and 473K by changing the spinning frequency of the sample from 2.5 to 4.0 kHz. As shown in Fig. 6, the linewidth of the peak due to acidic protons was sharply influenced by changing the spinning frequency from 2.5 to 4 kHz at 373–473K. This dependence of the lineshape is further evidence for the contribution of thermal motion to the lineshape. The protons may move from one bridging oxygen atom to another around Al^{3+} ion. From the dependence of the line-width on spinning frequency, the correlation time and the activation energy for hopping were estimated as listed in Table 1, where the values for H-ZSM-5 with SiO_2/Al_2O_3 ratio of 39 and 72.[4] The activation energy was 17–20 kJ mol^{-1}. Sarv *et al.* estimated the activation energy of proton mobility as 45 kJ mol^{-1} by the lineshape analysis of the spinning sidebands.[76] Sauer gave the activation energy for hopping of 53 kJ mol^{-1} from a theoretical calculation.[78]

At 298K, however, the linewidth did not change by changing the spinning frequency, being 3.6×10^2 Hz as shown in Fig. 6. This result indicates that the acidic protons are fixed on the bridging oxygen atoms in the zeolite lattice as shown in Eq. (1) and are not mobile at 298K. Brunner also reported that the

Table 1. ^{1}H MAS NMR parameters of H-ZSM-5 and H-mordenite.

Material	Temperature (K)	τ (μs)	M_2 (10^8 s^{-2})	E (kJ mol^{-1})
H-ZSM-5				
SiO_2/Al_2O_3 = 106				
	373	42		
	423	19		
	473	13		
			1.4	17
H-ZSM-5				
$SiO_2Al_2O_3$ = 72				
	393	39		
	423	22		
	473	14		
			1.2	19
H-ZSM-5				
SiO_2/Al_2O_3 = 39				
	393	41		
	423	21		
	473	14		
			1.1	20
H-mordenite				
SiO_2/Al_2O_3 = 106				
	373	64		
	423	26		
	453	14		
			1.1	28

linewidth was independent of the spinning rate for the bridging OH groups of H-ZSM-5 at room temperature.[70]

The linewidth of acidic protons in H-mordenite (SiO_2/Al_2O_3 = 106) depended also on temperature and spinning frequency. The activation energy for hopping of protons in H-mordenite is higher than those in H-ZSM-5 samples (Table 1). However, the linewidth of acidic protons in H-mordenite of SiO_2/Al_2O_3 = 19 and 40 only slightly depended on temperature and did not change with spinning frequency. This indicates that the mobility of protons in these zeolites is not a major factor for determining the residual linewidth. The protons in all three mordenite samples show the same chemical shift (4.2 ppm).

The acidic protons in H-MCM-22 (SiO_2/Al_2O_3 = 31) exhibits the chemical shift of 4.1 ppm. As in the case of mordenite samples of SiO_2/Al_2O_3 = 19, and 40 the linewidth of acidic protons in H-MCM-22 slightly depended on temperature but did not depend on the spinning frequency. Thus, the mobility of protons in H-MCM-22 is much lower than that in H-ZSM-5.

The linewidth of the peak due to silanol protons in every zeolite did not

change upon raising temperature. It was also independent of the spinning frequency even at higher temperature as expected. These results show that silanol protons are fixed and the thermal motion does not contribute to the linewidth.

6.2. Mobility of protons in metallosilicates

The metallosilicates molecular sieves, [Ga]-ZSM-5, [B]-ZSM-5, and [B,Al]-ZSM-5 are also used as solid-acid catalysts as well as zeolites. There is a possibility that the mobility of protons is influenced by incorporating Ga and B atoms into the ZSM-5 zeolite skeleton instead of Al atom, because the extent of incorporation of the isomorphous replacement affects the catalytic properties, e.g. the activities of the zeolites.[79] Quantification can be attained by appropriate test reactions.[80]

^{1}H MAS NMR spectra of [Ga]-ZSM-5, [B]-ZSM-5, and [B,Al]-ZSM-5 were measured by raising the temperature stepwise from 298 to 473K. In the case of [Ga]-ZSM-5, the chemical shift value of acidic protons is 4.2 ppm, which is the same as those in H-ZSM-5. As shown in Fig. 7, the sharp dependence of the linewidth on temperature was observed for [Ga]-ZSM-5, indicating that protons in [Ga]-ZSM-5 are mobile. On the other hand, the linewidth did not depend on temperature in the case of [B]-ZSM-5 below 473K, indicating that protons in [B]-ZSM-5 are not mobile in this temperature range.

Figure 8 shows the temperature dependence of the ^{1}H MAS NMR spectrum of [Al,B]-ZSM-5 (SiO_2/Al_2O_3 = 90, SiO_2/B_2O_3 = 288), where three types of protons are observed at 4.2 ppm, 2.2 ppm and 1.8 ppm. These are attributed to protons in ≡Al–OH–Si≡, in ≡B–OH–Si≡ and silanol groups. Upon raising the temperature of measurements, the chemical shifts of these three protons did not change. This indicates that three types of protons are apparently independent of each other. No chemical exchange occurs among different types of protons in [Al,B]-ZSM-5. As expected, no broadening of the signals due to ≡B–OH–Si≡ and silanols was observed even at 473K. Broadening was observed for protons ≡Al–OH–Si≡ upon raising temperature. However, the extent of broadening was small compared with protons in H-ZSM-5, indicating that the mobility of Al-originating protons is suppressed by incorporating boron atoms in the framework. The mobility of protons is affected by subtle difference in zeolite composition.

6.3. Effect of a small amount of Na^+ cations on properties of protons in H-ZSM-5

Influence of a small amount of Na^+ cations on catalytic activity of zeolites

Hall and co-workers have reported on the poisoning effect of ammonia on neopentane cracking over high-silica zeolites, i.e. H-ZSM-5,

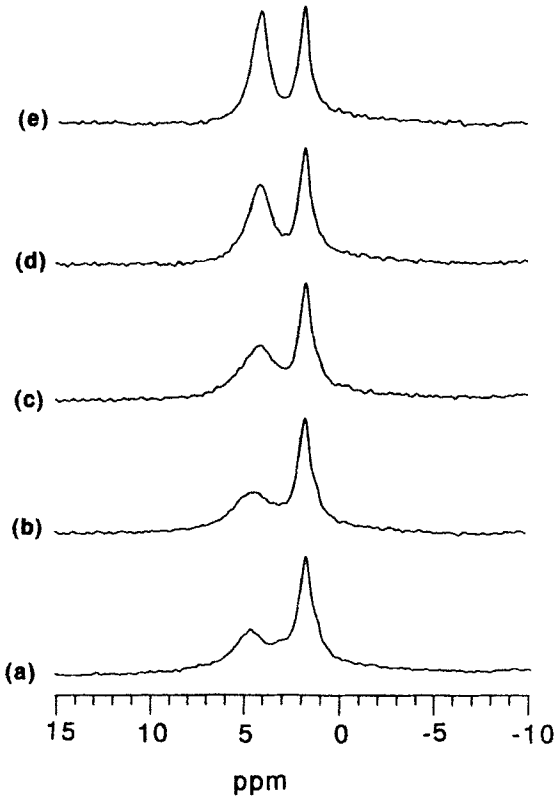

Fig. 7. Temperature dependence of the ^1H MAS NMR spectrum of H-Ga-ZSM-5. $SiO_2/Ga_2O_3 = 72$, (a) 298K, (b) 333K, (c) 373K, (d) 423K, (e) 473K. The spinning frequency of the sample was 4 kHz.

H-mordenite and H-Y at 673K.[81,82] They found that poisoning no more than 10% of the sites was sufficient to eliminate the catalytic activity. A similar salient feature of the poisoning has been observed also by introduction of a small amount of Na^+ by ion exchange. For example, Friz and Lunsford reported that the introduction of one Na^+ ion was equivalent to removal of the about five aluminium ions from the framework in hexane cracking over dealuminated Y-type zeolites at 623K.[83] A similar effect of Na^+ poisoning was reported also for heptane cracking over ZSM-20 at 623K.[84] These results suggest that the catalytic activities are not always proportional to the number of acid sites (or the amount of acidic protons). These poisoning phenomena have often been discussed in terms of heterogeneity of the acidic sites.

We have also studied the dependence of the catalytic activity of H-ZSM-5 on Na^+ content of H-ZSM-5.[6]

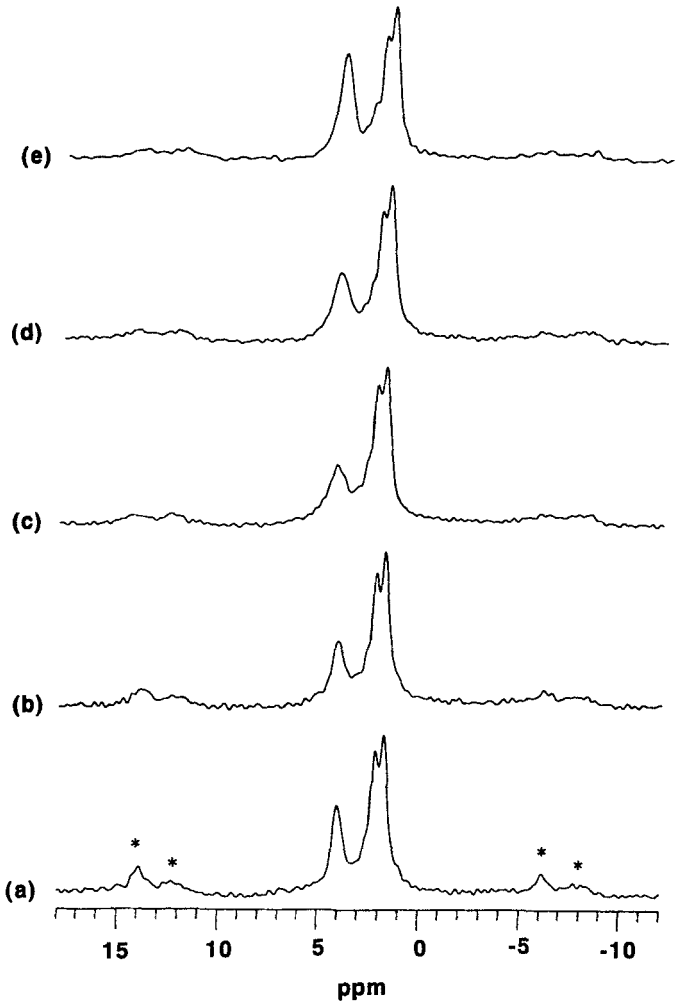

Fig. 8. Temperature dependence of the ^{1}H MAS NMR spectrum of H-[Al, B]-ZSM-5. SiO_2/Al_2O_3 = 158, SiO_2/B_2O_3 = 256. (a) 298K, (b) 353K, (c) 373K, (d) 423K, (e) 493K. The spinning frequency of the sample was 4 kHz.

Isomerization of cyclopropane over Na-H-ZSM-5

The isomerization of cyclopropane was carried out at 373K over H-ZSM-5, Na(1%)-H-ZSM-5 and Na(20%)-H-ZSM-5 under an initial cyclopropane pressure of 39 kPa in a conventional gas-circulation system.[6] In every case, the cyclopropane conversion linearly increased with reaction time in the low conversion range (Fig. 9). The initial rate was plotted against the degree of

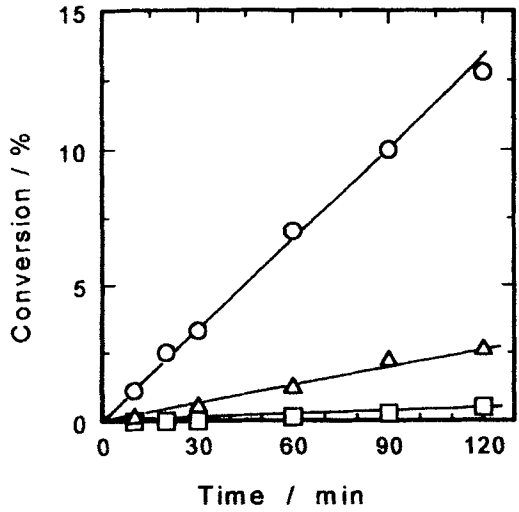

Fig. 9. The percentage conversion of cyclopropane isomerization into propene over H-ZSM-5 (○), Na(1%)-H-ZSM-5 (△) and Na(20%)-H-ZSM-5 (□). Reaction conditions: temperature 373K, cyclopropane pressure 40 kPa.

Na^+ exchange. Only 1% substitution of Na^+ for H^+ resulted in 80% loss of the catalytic activity of the original H-ZSM-5. By increasing the degree of Na^+ content to 20%, most of the activity was quenched. These results confirm that a minute amount of alkali cations in H-ZSM-5 is very effective in reducing the catalytic activity.

^1H MAS NMR spectra of Na-H-ZSM-5

^1H MAS NMR measurements of H-ZSM-5 partially exchanged with Na^+ ions were performed at different temperatures. Figure 10 shows the temperature dependence of the linewidth of the ^1H MAS NMR signal of H-ZSM-5 (SiO_2/Al_2O_3 = 106) and the same zeolite where 7% of protons are replaced by Na^+ ions. The variation of linewidth with temperature is very small as compared with that for original H-ZSM-5, as shown in Fig. 10. The suppression of the temperature dependence was also observed when only 1% of protons of H-ZSM-5 (SiO_2/Al_2O_3 = 42) was replaced by NH_4^+ ions.[6] These results indicate that a small amount of Na^+ or NH_4^+ ions effectively suppresses the thermal motion of the whole of the remaining protons. In other words, a long-range interaction exists between Na^+ ions and remaining protons.

The chemical shift of acidic protons was not affected by Na^+ introduction. The dynamic property of protons can be a more sensitive measure for the activity of protons than the static parameters such as NMR chemical shift and IR band position of OH bonds.

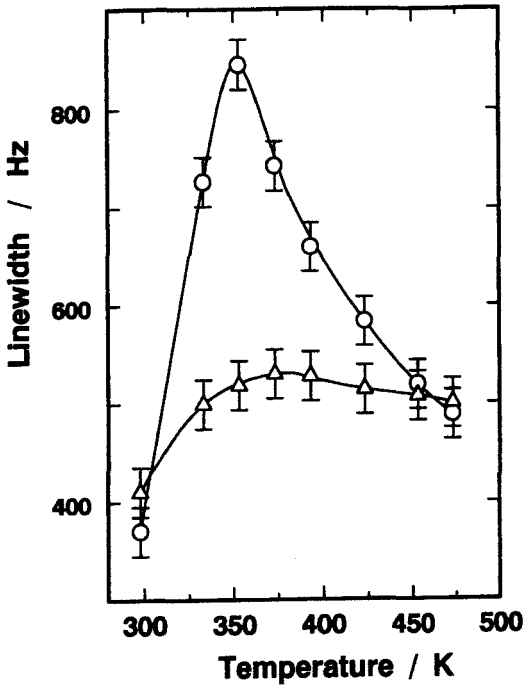

Fig. 10. Effect of Na^+ cations on the linewidth of the peak due to acidic protons in ZSM-5. SiO_2/Al_2O_3 = 106. (○) H-ZSM-5, (△) Na(7%)-H-ZSM-5.

The variable temperature measurements of ^{1}H MAS NMR offer very variable information on the dynamic character of the protons of zeolites as solid-acid catalysts. The temperature-dependent lineshape of ^{1}H MAS NMR spectra of acidic protons (acidic OH groups) in zeolites shows the first and unambiguous evidence for proton migration in zeolite structure. There is a possibility that the mobility of protons influences a catalytic activity of solid-acid catalysts.

7. HETEROPOLYACIDS AND RELATED COMPOUNDS AS SOLID ACIDS

Heteropolyacids such as dodecatungstophosphoric acid ($H_3PW_{12}O_{40}$, denoted as HTP hereafter) are strongly acidic solids and can be used as catalysts for a variety of organic reactions,[85–90] while their silver salts such as silver salt of dodecatungstophosphoric acid ($Ag_3PW_{12}O_{40}$, denoted as AgTP hereafter) themselves have no catalytic activity as a solid acid.[91] However, AgTP under hydrogen atmosphere is more active than the parent acid, HTP for several

acid-catalysed reactions.[91,92] Moreover, the catalytic activity of palladium metal (Pd^0) loaded on HTP (denoted as Pd^0/HTP) in the presence of hydrogen is also higher than that of HTP.[93] In this chapter, the properties of protons in HTP, AgTP and Pd^0/HTP in the presence of H_2 are examined by ^1H MAS NMR. There is a possibility that the dynamic property of protons influences their catalytic activities as well as zeolites.

7.1. Structure of heteropolyacids

Heteropolyacids are polyoxometalates incorporating anions (heteropolyanions) having metal-oxygen octahedra as the basic structural units.[94,95] Among a wide variety of heteropoly acids those belonging to the so-called Keggin series are the most important for catalysis. They include heteropolyanions $XM_{12}O_{40}^{y-8}$ where X is the central atoms (P^{5+}, Si^{4+}, etc.), y is its oxidation state and M is the metal ion (W^{6+}, Mo^{6+}, etc.). These heteropolyanions have a well-known Keggin structure which is composed of a central tetrahedron XO_4 surrounded by 12 edge-sharing metal-oxygen octahedra MO_6, as shown in Fig. 11. The MO_6 octahedra are grouped in four M_3O_{13} triads, which are connected by common vertices. The radius of the heteropoly anion is ~0.6 nm. The anion contains 12 quasilinear M–O–M linkages between the octahedra forming part of different M_3O_{13} triads, 12 angular M–O–M bonds between the octahedra within a single triad, four X–O–M bonds whereby the triads are joined to the central atoms, and 12 terminal M=O bonds. These bonds exhibit characteristic vibration frequency in the IR spectrum in the range 600–1100 cm^{-1}.[95]

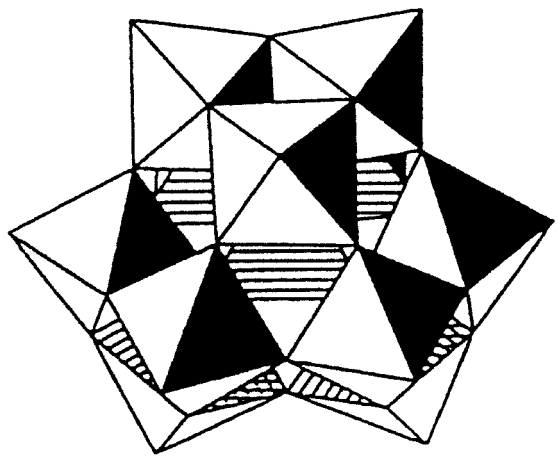

Fig. 11. The structure of heteropolyanion $XM_{12}O_{40}^{y-8}$.

The Keggin-type heteropoly acids such as $H_3PW_{12}O_{40}$ are stable. In addition to their well-defined structure, heteropoly acids have special properties which are of great value for catalysis, such as strong Brönsted acidity,[85–90] and high solubility in water and oxygenated organic solvents, fairly high stability in the solid state, a "pseudoliquid phase".[88–90] These properties render heteropoly acids potentially promising acid catalysts in heterogeneous system.

7.2. Proton sites and acid strength

Structural characterization of the proton sites in heteropolyacids is an important step towards understanding the catalytic activity. ^{17}O NMR date indicates that in the polyanion in solution, the bridging oxygen atoms have a higher electron density than the terminal oxygen atoms.[96,97] In the Keggin anion, edge-bridging M–O–M oxygens are assumed to be the predominant protonation sites. In solid heteropolyacids, the protons take part in the formation of the heteropolyacid crystal structure, linking the neighbouring heteropoly anions. In this case, the more accessible terminal oxygens can be protonated. Thus, from single-crystal X-ray and neutron diffraction date, the proton sites in the crystalline $H_3PW_{12}O_{40} \cdot 6H_2O$ are represented as diaquahydrogen ions, $H_5O_2^+$, each of which links four neighbouring $PW_{12}O_{40}^{3-}$ by forming hydrogen bonds with the terminal W=O oxygens.[98] In the dehydrated $H_3PW_{12}O_{40}$, according to ^{17}O NMR date, the protons are also predominantly localized on the terminal oxygens around room temperature.[96,97]

The acid strength of Keggin-type heteropolyacids is stronger than such conventional solid acids such as SiO_2–Al_2O_3 and H–Y zeolites.[99] The acid strength of crystalline heteropolyacids decreases in the series.[95]

$$H_3PW_{12}O_{40} > H_4SiW_{12}O_{40} > H_3PMo_{12}O_{40} > H_4SiMo_{12}O_{40}$$

8. CATALYTIC AND DYNAMIC PROPERTIES OF PROTONS IN HETEROPOLY COMPOUNDS

8.1. Catalytic properties of protons in $H_3PW_{12}O_{40}$

As mentioned above, $H_3PW_{12}O_{40}$ (HTP) is very active solid acid for various reactions. It is also known that polar molecules are absorbed in the solid bulk phase and the polar reactants undergo chemical transformations in the solid bulk as well as on the surface.[88–90] This behaviour of heteropoly compounds is called a "pseudo liquid phase" phenomenon.

In order to find the behaviour of protons in pseudoliquid phase, the effect

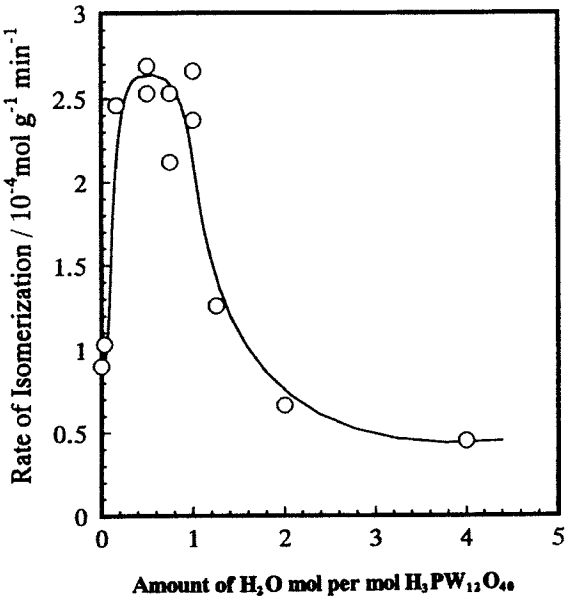

Fig. 12. Influence of the amount of water on the rate of isomerization of cyclopropane to propene over $H_3PW_{12}O_{40} \cdot nH_2O$. Reaction temperature: 354K, cyclopropane 40 kPa.

of absorbed water on the catalyst was examined. Figure 12 shows the change in the catalytic activity for cyclopropane isomerization to propene as a function of the amount of water absorbed in HTP. The catalytic activity reached its maximum when a small amount of water was absorbed (~0.5 mol mol^{-1} HTP). Enhancement of the activity by water is plausibly due to the increased mobility of protons in HTP. The decline of the activity at higher loading of water is ascribed to the decreased activity of protons by hydration.

8.2. Dynamic properties of protons in $H_3PW_{12}O_{40}$

Figure 13 shows ^1H MAS NMR of HTP in which water molecules are absorbed in a different degree. ^1H MAS NMR spectra were measured on samples sealed in a glass capsule as in the case of zeolites.

The spectra of HTP·nH_2O were recorded at 298K. The chemical shift of protons in HTP was observed at 9.0 ppm. Even when the values of n in HTP·nH_2O were 0.25, 0.50, 1.0 and 2.0, only a single peak was observed at 9.4, 9.2, 9.0 and 8.9 ppm, respectively, and the signal was sharpened. This indicates that rapid exchange of protons occurs between protons in absorbed water and those originated from the acid.

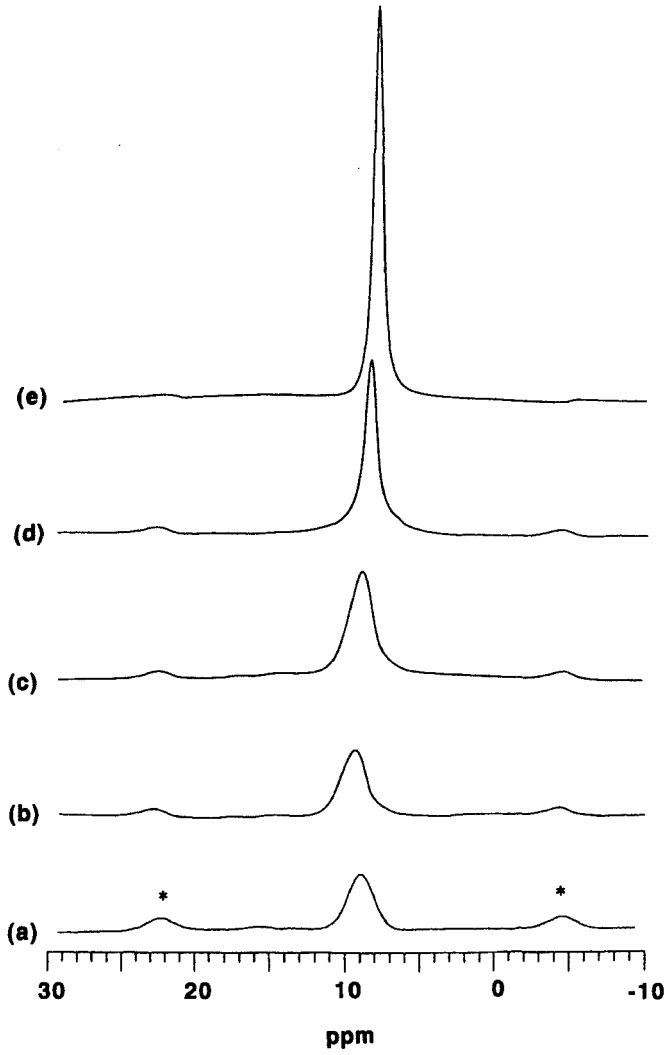

Fig. 13. ^{1}H MAS NMR spectra of $H_3PW_{12}O_{40}$ and $H_3PW_{12}O_{40} \cdot nH_2O$ at 298K. The spinning rate of the sample was 4 kHz. (a) $H_3PW_{12}O_{40}$, (b) $H_3PW_{12}O_{40} \cdot 0.25H_2O$, (c) $H_3PW_{12}O_{40} \cdot 0.5H_2O$, (d) $H_3PW_{12}O_{40} \cdot H_2O$, (e) $H_3PW_{12}O_{40} \cdot 2H_2O$. (*) denotes a spinning sideband.

9. PROPERTIES OF PROTONS IN $Ag_3PW_{12}O_{40}$

9.1. Generation of acidic protons in $Ag_3PW_{12}O_{40}$

$Ag_3PW_{12}O_{40}$ (AgTP) itself has no catalytic activity at all as solid acid catalysts. The acidic protons are generated in AgTP when Ag^+ ions are reduced with hydrogen.[100]

$$2Ag^+ + H_2 \rightarrow 2Ag^0 + 2H^+ \quad (3)$$

In this chapter, the interaction between H_2 molecules and Ag^+ cations is investigated by ^1H MAS NMR.

9.2. ^1H MAS NMR measurements of $Ag_3PW_{12}O_{40}$ under hydrogen atmosphere

^1H MAS NMR spectra were measured on samples sealed in a glass capsule as in the case of zeolites. After the reduction of AgTP, under hydrogen atmosphere, the sample was transferred to the glass capsule under hydrogen atmosphere, and sealed with a flame. AgTP reduced with hydrogen is denoted as R-AgTP. The degree of reduction of Ag^+ in R-AgTP is 33%, which is corresponded to reduction of one of the three Ag^+ ions in AgTP.

^1H MAS NMR spectra were recorded between 298K and 373K on a Bruker AM 400 or an MSL 270 spectrometer. The repetition time was 20 s and the rotation frequency of the glass capsule was 4.0 kHz.

9.3. ^1H MAS NMR spectra of $Ag_3PW_{12}O_{40}$ partially reduced with hydrogen

^1H MAS NMR spectrum of R-AgTP in the presence of hydrogen (40 kPa) was recorded at 298K. Two peaks were observed at (9.3 ± 0.1) ppm and (6.4 ± 0.1) ppm, as shown in Fig. 14(a). The peaks observed at 9.3 ppm and 6.4 ppm are hereinafter denoted as H (high frequency) peak and L (low frequency) peak, respectively. When hydrogen in the gas phase was evacuated at room temperature for 2 h, L-peak disappeared as shown in Fig. 14(b).

A unique feature of R-AgTP is the effect of hydrogen on the property of acidic protons and the catalytic activities. These findings are summarized as follows:[6,7]

1. The amount of the protons at 6.4 ppm reversibly changed with hydrogen pressure, while the amount of protons at 9.3 ppm was independent of the hydrogen pressure.
2. R-AgTP exhibits a catalytic activity for the isomerization of hexane only in the presence of hydrogen.

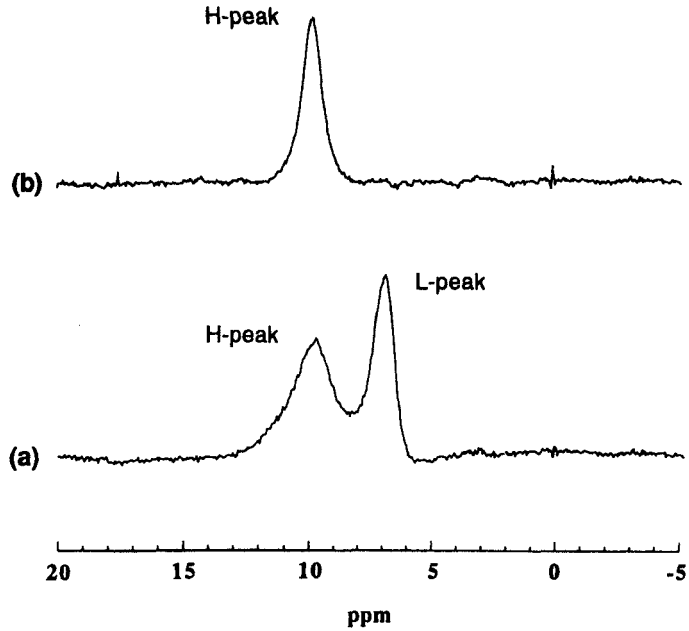

Fig. 14. ^{1}H MAS NMR spectra of R-AgTP at 298K. (a) R-AgTP recorded under 40 kPa of hydrogen. (b) Recorded after evacuating hydrogen at 298K for 2 h.

3. The activities of R-AgTP for the isomerization of hexane reversibly with hydrogen pressure. Thus, the catalytic activity disappears when hydrogen is eliminated from the gas phase and reappears upon reintroducing hydrogen.
4. The catalytic activity of R-AgTP in the presence of hydrogen for the isomerization of hexane is much higher than that of HTP, whose activity is independent of hydrogen pressure.

These findings indicate that the properties of the protons formed by the reduction of AgTP are quite different from those in HTP, and that hydrogen molecules are reversibly converted into acidic protons over AgTP. Moreover, the protons at 6.4 ppm are active for hexane isomerization, but the protons at 9.3 ppm are not active. In general, the protons with chemical shifts higher values are considered to be more electron deficient and are expected to be more active as solid acids. For example, the chemical shifts attributed to the protons in zeolites are correlated with the positions of the IR stretching bands of the acidic OH groups.[40,41] The findings in R-AgTP apparently contradict with this general rule. Therefore, there must be some other important factors which determine the activities of protons, other than the chemical shift or the electron density of the protons. A possible factor may be the dynamic

property of the protons as well as zeolites. The dynamic phenomenon between interconversion of hydrogen into protons might be observed by ^{1}H MAS NMR.

9.4. Spinning frequency dependence of ^{1}H MAS NMR of $Ag_3PW_{12}O_{40}$ at 298K

In order to know if the thermal motion of the protons contributes to the linewidth of ^{1}H MAS NMR spectrum of R-AgTP, the effect of the spinning frequency on the linewidths of the two signals was examined at 298K in the presence of hydrogen. As shown in Fig. 15, the linewidth of L-peak significantly changes with the spinning frequency, while H-peak does not.

The linewidth of the L-peak decreased from $(6.4 \pm 0.4) \times 10^2$ Hz to $(3.6 \pm 0.3) \times 10^2$ Hz by increasing the spinning frequency (ν_r) from 2.5 kHz to 4.0 kHz. Moreover, the linewidth was nearly proportional to $(\nu_r)^{-2}$, which relation is observed at $\omega \tau_c \gg 1$ in Eq. (2). This implies that the thermal motion of protons even at 298K determines the linewidth of L-peak. On the other

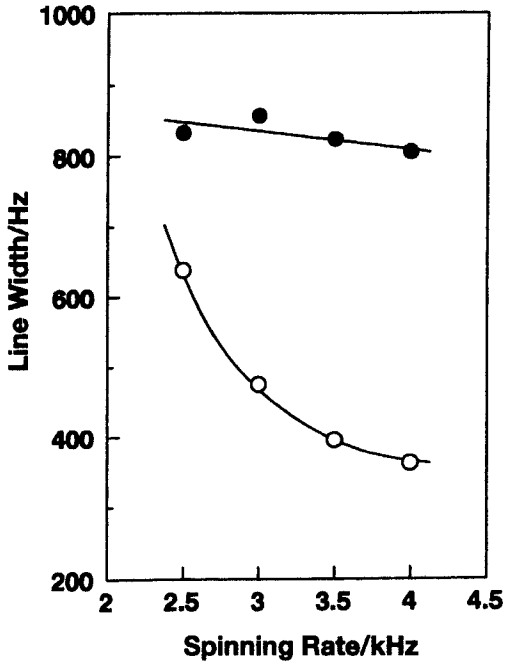

Fig. 15. Dependence of linewidth on the spinning rate for ^{1}H MAS NMR signal of the protons at 9.3 ppm (●) and 6.4 ppm (○) in R-AgTP in the presence of hydrogen (40 kPa). The spectra were recorded at 298K.

hand, the linewidth of H-peak in the absence of hydrogen was not influenced by the spinning frequency either and was smaller than that measured in the presence of hydrogen. Thus, the linewidths in the absence and presence of hydrogen were $(4.6 \pm 0.3) \times 10^2$ Hz and $(8.0 \pm 0.3) \times 10^2$ Hz, respectively.

The results described above indicate that the protons at 6.4 ppm are mobile in an NMR time scale even at room temperature, and that the protons at 9.3 ppm are fixed at $PW_{12}O_{40}^{3-}$ anions.

9.5. Temperature dependence of ^{1}H MAS NMR spectra of $Ag_3PW_{12}O_{40}$ in the presence of hydrogen

Further evidence for high mobility of 6.4 ppm protons was obtained from the temperature dependence of the spectra in the presence of hydrogen. Figure 16(a) shows the spectrum at 298K. As described above, two kinds of protons were observed at 6.4 ppm and 9.3 ppm. When temperature was raised, both peaks shifted, and at the same time, both peaks broadened significantly as shown in Fig. 16(b)–(d). The peak at 6.4 ppm shifted to the higher frequency field, while the peak at 9.3 ppm to the lower frequency field. At 373K, "6.4 ppm peak" was further broadened and merged into "9.3 ppm peak" as a shoulder. The original lineshape was completely reproduced by cooling the sample down to 298K again (Fig. 16(e)), indicating that the linebroadening phenomenon is reversible.

The temperature dependence of the spectrum clearly indicates that the exchange reaction proceeds between the two types of protons.

Moreover, the extent of broadening of 6.4 ppm peak was more pronounced than that of 9.3 ppm peak, indicating that the mobility of 6.4 ppm protons is higher than that of 9.3 ppm protons in accord with the conclusion from the effect of the spinning frequency at 298K. This suggests that the exchange reaction is caused by migration of the mobile protons (6.4 ppm) to the sites of nonmobile protons (9.3 ppm).

To examine further the nature of the protons due to the H-peak, the temperature dependence of the linewidth of H-peak was examined. Thus, the spectrum of R-AgTP was measured after the system was evacuated for 2 h at room temperature. By this treatment, L-peak was completely eliminated and thus H-peak could be observed without complication from the effect of the proton exchange.

As shown in Fig. 14(b), a signal of the protons of H-peak was observed at 9.3 ppm at 298K in the absence of hydrogen. The temperature dependence of the spectrum was examined by raising the sample temperature stepwise (Fig. 17(a)–(e)). The value of chemical shift shifted only slightly; it changed from 9.3 ppm to 9.1 ppm upon raising the temperature from 298K to 373K. The linewidth of the peak was increased only slightly from $(4.6 \pm 0.3) \times 10^2$ Hz to $(6.1 \pm 0.4) \times 10^2$ Hz. This indicates that the mobility of the protons responsible

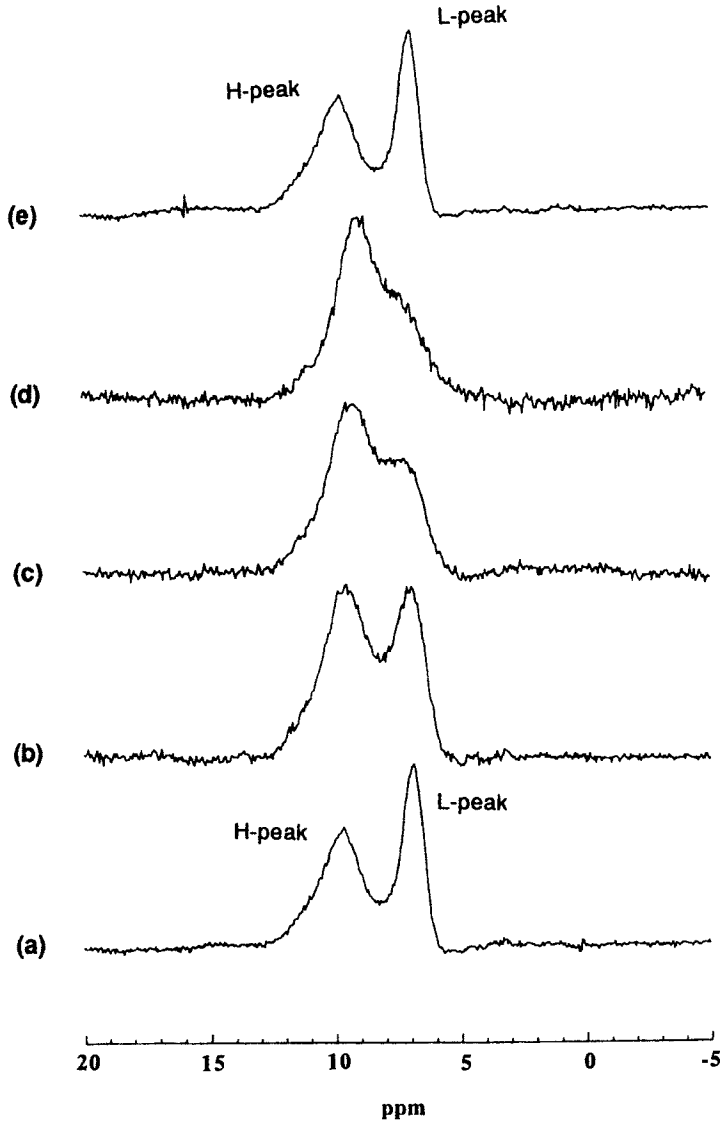

Fig. 16. Change in the ^1H MAS NMR spectrum of R-AgTP with temperature. Each spectrum was recorded by heating the sample stepwise from 298K to 373K under hydrogen (40 kPa). Temperature: (a) 298K, (b) 333K, (c) 353K and (d) 373K. The spectrum (e) recorded at 298K, after the spectrum was measured at 373K.
(*) denotes a spinning sidebond.

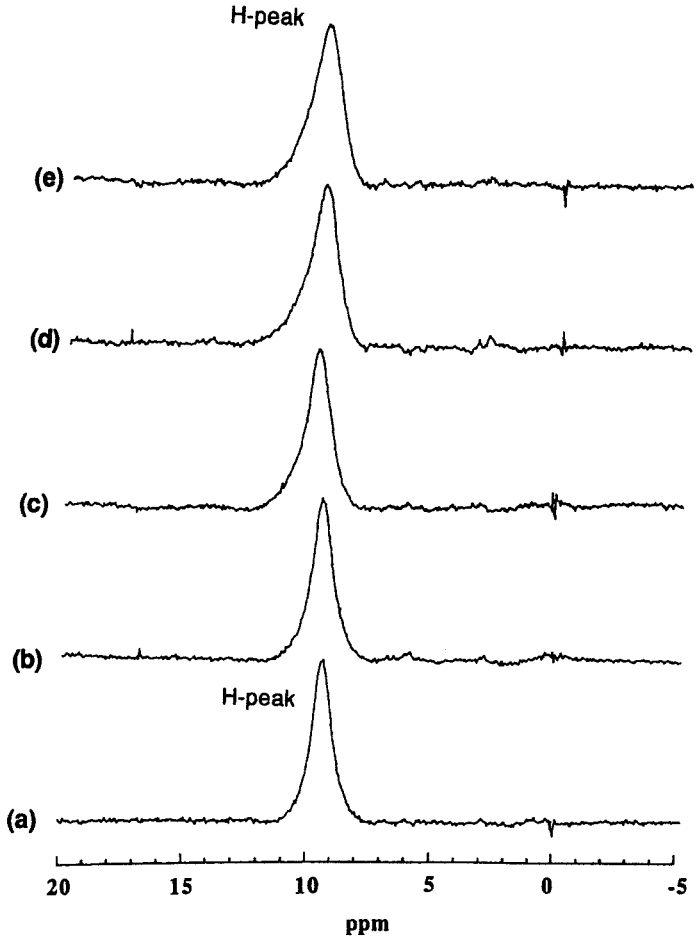

Fig. 17. Change in ^{1}H MAS NMR spectra of R-AgTP with temperature in the absence of hydrogen in the gas phase. R-AgTP was evacuated at 298K for 30 min. Temperature: (a) 298K, (b) 313K, (c) 333K, (d) 353K and (e) 373K.

for H-peak is low even at 373K, and that only protons responsible for L-peak have a high mobility. Therefore, it is concluded that the exchange occurs by migration of the mobile protons observed at 6.4 ppm to immobile protons observed at 9.3 ppm. Moreover, the linewidth of H-peak in the absence of L-peak (Fig. 17(a)) was smaller than that in the presence of L-peak (Fig. 16(a)). This is probably because the proton exchange contributes to the linewidth of H-peak even at room temperature. Only the variable temperature ^{1}H MAS NMR gives the information of the dynamic process between protons and hydrogen molecules.

10. COMPOSITE CATALYST CONSISTING OF Pd^0 AND $H_3PW_{12}O_{40}$

The catalytic activity of a composite catalyst consisting of palladium metal (Pd^0) and $H_3PW_{12}O_{40}$ (denoted as Pd^0/HTP) was higher than that of HTP.[93] The presence of H_2 is necessary to maintain the high activity as well as R-AgTP. H_2 molecules dissociate into hydrogen atoms over Pd^0, while they do not dissociate over Ag^+ cation and Ag^0 metal. This suggests that the mechanism of the generation of protons in Pd^0/HTP is different from that in AgTP and/or the dynamic property of protons in Pd^0/HTP might be different from that of R-AgTP and that of HTP. In the case of Pd^0/HTP, hydrogen atoms formed over Pd^0 spillover and might interact with surrounding heteropoly anions. In this chapter, the interaction of hydrogen atoms with $PW_{12}O_{40}^{3-}$ is examined by ^1H MAS NMR in the presence and absence of hydrogen.

10.1. Preparation of $Pd^0/H_3PW_{12}O_{40}$ and ^1H MAS NMR measurements

Pd^0/HTP was prepared as follows. $Pd(NO_3)_2$ was loaded on http by impregnation method from the solution of http and $Pd(NO_3)_2$. $Pd(NO_3)_2$ loaded on HTP is denoted as Pd(II)/HTP. Pd^0/HTP was prepared by the reduction of Pd(II)/HTP with hydrogen.

10.2. ^1H MAS NMR spectra of $Pd^0/H_3PW_{12}O_{40}$

The spectrum of Pd(II)/HTP is shown in Fig. 18(a). The peak at 9.1 ppm due to protons in HTP was observed. This means that Pd(II)/HTP is a mixture of $Pd(NO_3)_2$ and HTP.

When Pd(II)/HTP was reduced with hydrogen, a small peak was observed at 19.8 ppm beside the peaks at 9.1 ppm and 4.7 ppm. The peak at 19.8 ppm was assigned to be hydrogen atoms adsorbed on metallic palladium. The other two kinds of protons are attributed to acidic protons (9.1 ppm) and water molecules (4.7 ppm) (Fig. 18(b)).

The intensity of the peak at 9.1 ppm was increased by the reduction of Pd(II)/HTP with hydrogen (Fig. 18(b)). The acidic protons are generated by following mechanism.

$$H_2 \xrightarrow{Pd^0} 2H \tag{4}$$

$$H + PW_{12}O_{40}^{3-} \rightarrow H^+ + PW_{12}O_{40}^{4-} \tag{5}$$

Thus, H_2 molecules from the gas phase dissociate into hydrogen atoms over Pd^0 metal. The hydrogen atoms thus formed spillover and interact with surrounding heteropolyanions, $PW_{12}O_{40}^{3-}$ to be converted into protons.

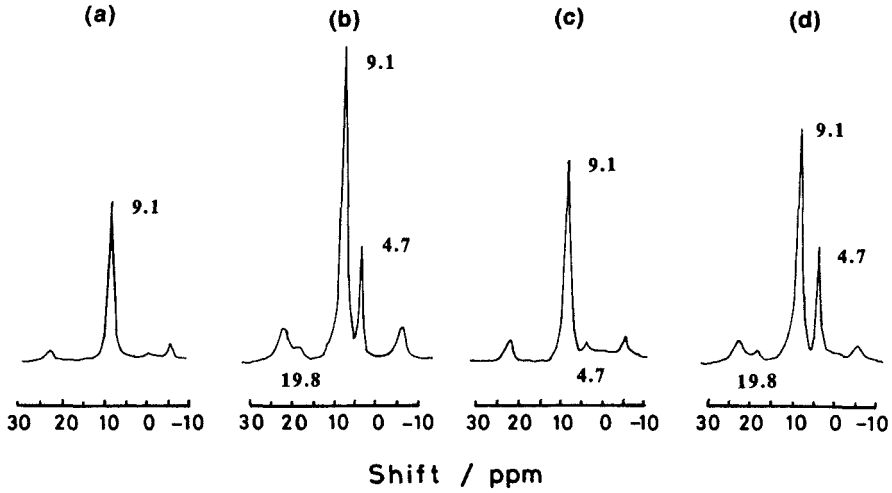

Fig. 18. The reversible generation of protons. (a) Pd(II)/HTP, (b) Pd^0/HTP in the presence of hydrogen (13.3 kPa), (c) Pd^0/HTP evacuated at 423K for 1 h. (d) The sample (c) re-exposed to hydrogen (13.3 kPa) at 423K for 30 min. The spectra measured at 298K. The resonance frequency was 300 MHz. (*) denotes a spinning sideband. The molar ratio of Pd/HTP was 1.5.

According to the above mechanism, metallic palladium serves as a catalyst for the interconversion between hydrogen atoms and acidic protons.

The protons due to water observed at 4.7 ppm were formed by the reduction of HTP with H atom or H_2.

$$H_3PW_{12}O_{40} + 2\ H\ (\text{or}\ H_2) \rightarrow H_2O + H_3PW_{12}O_{39} \qquad (6)$$

To know how the three types of protons behave with the adsorption–desorption cycle of hydrogen, ^{1}H MAS NMR spectra of Pd^0/HTP were recorded at 298K in the presence and absence of hydrogen. Upon evacuation of the sample (b) in Fig. 18 at 423K for 1 h, the peak due to hydrogen atoms on Pd^0 metal disappeared. The intensity of the peak due to water molecules decreased considerably, and the peak intensity of the acidic protons decreased to about two-thirds of that before evacuation (Fig. 18(c)).

The sample (c) in Fig. 18 was then re-exposed to hydrogen (13.3 kPa) at 423K. As shown in Fig. 18(d), the peak at 19.8 ppm due to hydrogen atoms dissociated over Pd^0 reappeared, and its intensity was recovered. This result indicates that the dissociation of H_2 into H atoms over Pd^0 is reversible. On the other hand, the intensity of the peak at 9.1 ppm was not completely recovered to the original intensity of Fig. 18(b), though it is about 1.3 times larger than that of the peak due to Pd(II)/HTP (Fig. 18(a)). The intensity did not completely recover to that before hydrogen evacuation. This shows that

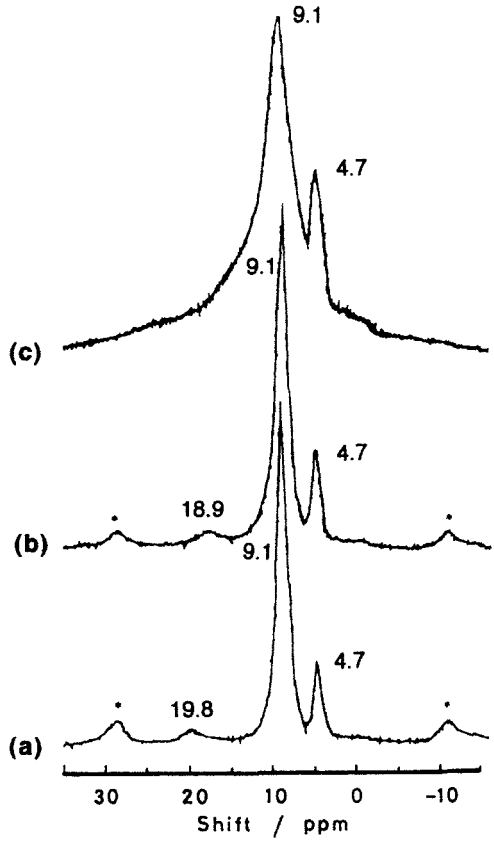

Fig. 19. The temperature dependence of ^1H MAS NMR spectrum of Pd^0/HTP in the presence of hydrogen. (a) 298K, (b) 333K and (c) 373K. The spinning frequency of the sample was 5.8 kHz. The resonance frequency was 300 MHz. (*) denotes a spinning sideband. The molar ratio of Pd/HTP was 1.5.

the protons which are reversibly formed, disappear by the desorption of hydrogen. Upon re-exposure to hydrogen, the intensity of the peak at 19.8 ppm was recovered. The reappeared peak at 4.7 ppm shows that the reduction of the heteropoly anion further proceeds by the second exposure to hydrogen.

10.3. Influence of temperature on the ^1H MAS NMR spectra of $Pd^0/H_3PW_{12}O_{40}$ in the presence of hydrogen

To examine further the conversion of H atoms into protons, the spectra of Pd^0/HTP under hydrogen atmosphere were recorded by raising the sample

temperature (Fig. 19). The peaks at 9.1 and 18.9 ppm were broadened by raising the temperature to 333K, and further broadened at 373K. The peak at 19.8 ppm shifted to lower frequency field by raising temperature, and merged into the peak at 9.1 ppm at 373K. These spectra changes suggest that the exchange of the two types of protons occurs at higher temperatures. The intensities of the spinning sidebands decreased at 333K and disappeared at 373K.

To know whether the thermal motion of the protons contributes to the linewidth of ^{1}H MAS NMR spectrum of Pd^0/HTP, the effect of the spinning frequency on the linewidth of the signal in the presence of hydrogen was examined at 298K and 373K. The molar ratio of Pd^0 to HTP was 0.1. The linewidth of the peak at 9.1 ppm in Pd^0/HTP significantly changed with the spinning frequency at 373K, decreasing from $(7.4 \pm 0.3) \times 10^2$ Hz to $(5.4 \pm 0.3) \times 10^2$ Hz by increasing the spinning rate from 2.0 kHz to 3.5 kHz. The dependence of linewidth on the spinning frequency implies that the thermal motion greatly contributes to the linewidth of the peak at 9.1 ppm. The values of τ_c and M_2^{IS} are obtained as (31 ± 3) μs and $(1.1 \pm 0.2) \times 10^8 s^{-2}$ at 373K, respectively.

On the other hand, the linewidth was not influenced by spinning frequency at 298K, indicating that the thermal motion is not responsible for the linewidth at this temperature.

The linewidth of HTP was independent of the spinning frequency at both 298K and 373K, being $(4.8 \pm 0.2) \times 10^2$ Hz and $(5.0 \pm 0.2) \times 10^2$ Hz, respectively.

The results described above indicate that the protons in Pd^0/HTP under hydrogen are more mobile than those in HTP. The difference of the mobility between the protons in Pd^0/HTP and those of HTP may explain the difference in the catalytic activities of the two catalysts for methanol conversion and hexane isomerization.[85]

11. SUMMARY

The various experimental facts described above show that the temperature variable ^{1}H MAS NMR could reveal the dynamics of protons in solid acids. Information obtained by this technique offers new insights, which could not be obtained by other means, on the acidic properties of solid acids and their catalysis. The significance of proton mobility in catalysts will be able to be discussed in the future.

REFERENCES

1. For example, A. T. Bell and A. Pines, *NMR Techniques in Catalysis*, Marcel Dekker, New York, Basel, Hong Kong, 1994.

2. E. Lippmaa, M. Magi, A. Samoson, A. R. Grimner and G. Engelhardt, *J. Am. Chem. Soc.*, 1980, **102**, 4889.
3. T. Baba, Y. Inoue, H. Shoji, T. Uematsu and Y. Ono, *Microporous Mater.*, 1995, **3**, 647.
4. T. Baba, N. Komatsu, H. Sugisawa and Y. Ono, *J. Phys. Chem.*, 1998, **102**, 804.
5. T. Baba, N. Komatsu, H. Sugisawa, T. Takahashi and Y. Ono, *Microporous and Mesoporous Mater.*, 1998, **22**, 203.
6. T. Baba, Y. Inoue and Y. Ono, *J. Catal.*, 1996, **159**, 230.
7. T. Baba, M. Nomura, Y. Kansaki and Y. Ono, *J. Chem. Soc., Faraday Trans.*, 1992, **88**, 71.
8. T. Baba, M. Nomura, Y. Oono and Y. Ono, *J. Phys. Chem.*, 1993, **97**, 12888.
9. T. Baba and Y. Ono, *J. Phys. Chem.*, 1996, **100**, 9064.
10. D. W. Breck, *Zeolites Molecular Sieves, Structure, Chemistry and Use*, Wiley, London, 1974.
11. W. M. Meier and D. H. Olson, *Atlas of Zeolite Structure Types*, 3rd edn, Butterworth, London, 1992.
12. W. Loewenstein, *Am. Mineral.*, 1954, **39**, 92.
13. M. Rubin, *U.S. Patent*, 1990, 4,954,325.
14. R. M. Barrer, *Hydrothermal Chemistry of Zeolites*, Academic Press, London, 1982.
15. G. Bellussi and M. S. Rigutto, *Stud. Surf. Sci. Catal.*, 1994, **84**, 177.
16. F. Hölderrich, M. Hesse and F. Naumann, *Angew. Chem. Int. Ed. Engl.*, 1988, **27**, 226.
17. W. F. Hölderrich and H. van Bekkum, *Stud. Surf. Sci. Catal.*, 1991, **58**, 631.
18. P. B. Venute, *Microporous Mater.*, 1994, **2**, 297.
19. P. B. Venuto, *Stud. Surf. Sci. Catal.*, 1997, **105 B**, 811.
20. W. O. Haag, *Stud. Surf. Sci. Catal.*, 1994, **84**, 1375.
21. W. O. Haag, R. M. Lago and P. B. Weise, *Nature*, 1984, **309**, 589.
22. H. G. Karge, J. Ladebeck and Z. Srbak, in *Proc. 7th International Congress on Catalysis* (eds T. Siyama and K. Tanabe), Tokyo, Japan, Kodansha Ltd, Tokyo, Elsevier, Amsterdam, 1981, p. 1408.
23. W. J. Mortier, *J. Catal.*, 1978, **55**, 138.
24. P. A. Jacobs, *Catal. Rev. Sci. Eng.*, 1982, **24**, 415.
25. D. Barthomeuf, *Mater. Chem. Phys.*, 1987, **17**, 49.
26. R. A. van Santen, *Catal. Today*, 1997, **38**, 377.
27. W. J. Moritier, J. Sauer, J. A. Lerchen and H. Noller, *J. Phys. Chem.*, 1984, **88**, 905.
28. J. Sauer, *J. Mol. Catal.*, 1989, **54**, 312.
29. J. Dwyer, *Stud. Surf. Sci. Catal.*, 1988, **37**, 333.
30. J. A. Rabo and G. J. Gajda, *NATO ASI Section B*, 1990, **221**, 273.
31. J. L. Flaconer and J. A. Schwarz, *Catal. Rev. Sci. Eng.*, 1983, **25**, 141.
32. H. G. Karge and V. Dondar, *J. Phys. Chem.*, 1990, **94**, 765.
33. K. Tsutsumi, H. Q. Koh, S. Hagiwara and H. Takahashi, *Bull. Chem. Soc. Jpn.*, 1975, **48**, 3576.
34. A. Auroux, P. Wierzchowski and D. C. Gravelle, *Thermochimica Acta*, 1979, **32**, 165.
35. A. Auroux, *Topics Catal.*, 1997, **4**, 71.
36. D. Bartheuf, *Stud. Surf. Sci. Catal.*, 1980, **5**, 55.
37. G. Boudillon, G. Gueguene and M. Gusinet, *Appl. Catal.*, 1990, **6**, 123.
38. D. Freude, M. Hunger and H. Pfeifer, *Z. Phys. Chem. (Neue Folge)*, 1987, **152**, 429.
39. H. Ernst, D. Freude, M. Hunger, H. Pfeifer and B. Seiffert, *Z. Phys. Chem. (Leipzig)*, 1987, **268**, 304.
40. H. Pfeifer, D. Freude and M. Hunger, *Zeolites*, 1985, **5**, 274.
41. H. Pfeifer, *J. Chem. Soc., Faraday Trans.*, 1, 1987, **84**, 3777.
42. H. Pfeifer, *Colloids Surf.*, 1989, **36**, 169.
43. D. Freude, M. Hunger and H. Pfeifer, *Chem. Phys. Lett.*, 1986, **128**, 62.
44. J. Klinowski, *Chem. Rev.*, 1991, **91**, 1459.
45. H. Pfeifer, *NATO AIS Series C* (ed. G. E. Maciel), 1994, **447**, 499.

46. E. Brunner, *J. Mol. Struct.*, 1995, **355**, 61.
47. M. Hunger, *Solid State Nucl. Magn. Reson.*, 1996, **6**, 1.
48. E. Brunner, H. G. Karge and H. Pfeifer, *Z. Phys. Chem.*, 1992, **76**, 173.
49. E. Brunner, *Catal. Today*, 1997, **38**, 361.
50. U. Fleischer, W. Kutzelnigg, A. Bleiber and J. Sauer, *J. Am. Chem. Soc.*, 1993, **115**, 7833.
51. D. Freude, M. Hunger and H. Pfeifer, *Z. Phys. Chem. (Neue Folge)*, 1987, **152**, 171.
52. H. Pfeifer, *NMR Basic Principles and Progress*, Vol. 31, Springer, Berlin, p. 31, 1994.
53. J. Klinowski, *Chem. Rev.*, 1991, **91**, 1459.
54. G. Engelhardt, *Stud. Surf. Sci. Catal.*, 1991, **58**, 285.
55. C. Tsiao, D. R. Corbin, V. Duraunte, D. Walker and C. D. Dybowski, *J. Phys. Chem.*, 1990, **94**, 4195.
56. C. Tsiao, D. R. Corbin, L. Hbrans, E. E. Carroell, V. Duraunte, D. Walker and C. D. Dybowski, *J. Phys. Chem.*, 1991, **95**, 5586.
57. R. Grosse, R. Brumeister, B. Bodenberg, A. Ctedeon and J. Fressard, *J. Phys. Chem.*, 1991, **95**, 2243.
58. J. H. Lunsford, W. P. Rothwell and W. Shen, *J. Am. Chem. Soc.*, 1985, **107**, 1540.
59. J. F. Haw, J. B. Nicholas, T. Xu, L. B. Beck and D. B. Ferguson, *Acc. Chem. Res.*, 1996, **29**, 259.
60. H. M. Kao and C. P. Grey, *J. Phys. Chem.*, 1996, **100**, 5105.
61. L. Heeribout, P. Batamack, C. D. Morin, R. Vincent and J. Fraissard, *Colloid Surf. A*, 1996, **115**, 229.
62. D. Freude, M. Hunger and H. Pfeifer, *J. Magn. Reson.*, 1991, **95**, 477.
63. M. Hunger, M. W. Anderson, A. Ojo and H. Pfeifer, *Microporous Mater.*, 1993, **1**, 17.
64. D. Barthomeuf, *Stud. Surf. Sci. Catal.*, 1985, **20**, 75.
65. J. W. Ward, *J. Catal.*, 1967, **9**, 396 and 1968, **64**, 1093.
66. N. W. Cant and W. K. Hall, *Trans. Faraday Soc.*, 1968, **64**, 1093.
67. R. A. Schoonheydt and J. B. Uytterhoeven, *J. Catal.*, 1970, **19**, 55.
68. B. Lee, J. K. Nomura, F. Wakabayashi and K. Domen., *Bull. Chem. Soc. Jpn.*, 1998, **71**, 2149.
69. D. Fenzke, B. C. Gerstein and H. Pfeifer, *J. Magn. Reson.*, 1992, **98**, 469.
70. E. Brunner, *J. Chem. Soc., Faraday Trans.*, 1990, **86**, 3957.
71. M. M. Mestdagh, W. E. E. Stone and J. J. Fripiat, *J. Phys. Chem.*, 1972, **76**, 1220.
72. M. M. Mestdagh, W. E. E. Stone and J. J. Fripiat, *J. Chem. Soc., Faraday Trans. 1*, 1976, **72**, 154.
73. D. Freude, W. Oehme, W. Schmiedel and B. Staudte, *J. Catal.*, 1974, **32**, 137.
74. H. J. Rauscher, D. Michel and H. Pfeifer, *J. Mol. Catal.*, 1981, **12**, 159.
75. D. Freude and H. Pfeifer, *Proc. 5th Intern. Conf. Zeolites* (ed. L. V. C. Rees), Heydon, London, p. 732, 1980.
76. P. Sarv, T. Tuhern, E. Lippmaa, K. Keskinen and A. Root, *J. Phys. Chem.*, 1995, **99**, 13763.
77. D. G. Cory and W. M. Ritchey, *J. Magn. Reson.*, 1998, **80**, 128.
78. J. Sauer, C. N. Kolmel, J. R. Hill and R. Ahlrichs, *Chem. Phys. Lett.*, 1989, **164**, 193.
79. T. W. Chu and C. D. Chang, *J. Phys. Chem.*, 1985, **89**, 1569.
80. J. A. Martens, M. Thienlen, P. A. Jacobs and J. Weitkamp, *Zeolites*, 1984, **4**, 98.
81. K. Hall, J. Engellhardt and G. A. Sill, *Stud. Surf. Sci. Catal.*, 1989, **49**, 1253.
82. E. A. Lombardo, G. A. Sill and W. K. Hall, *J. Catal.*, 1989, **119**, 420.
83. P. O. Friz and J. H. Lunsford, *J. Catal.*, 1989, **118**, 85.
84. F. R. Rebeiro, F. Alvarez, C. Henriques, F. Lemos, J. M. Lopes and M. F. Reberio, *J. Mol., Catal.*, 1995, **96**, 245.
85. I. V. Kozhevnikov, *Russ. Chem. Rev.*, 1987, **56**, 811.
86. I. V. Kozhevnikov, *Catal. Rev. Sci. Eng.*, 1995, **37**, 311.
87. Y. Ono, in *Prospective in Catalysis* (eds J. M. Thomas and K. I. Zamaraev), p. 431, Blackwey, London, 1992.
88. M. Misono, *Catal. Rev. Sci. Eng.*, 1987, **29**, 269.

89. M. Misono, *Catal. Rev. Sci. Eng.*, 1988, **30**, 339.
90. T. Okuhara, N. Mizuno and M. Misono, *Adv. Catal.*, 1996, **41**, 113.
91. T. Baba, M. Nomura, Y. Kansaki and Y. Ono, *J. Chem. Soc., Faraday Trans.*, 1992, **88**, 71.
92. T. Baba and Y. Ono, *Appl. Catal.*, 1989, **55**, 301.
93. T. Baba, S. Hasada, M. Nomura, Y. Ohno and Y. Ono, *J. Mol. Catal. A*, 1996, **114**, 247.
94. G. A. Tsigdnios, *Topics Current Chemistry*, vol. 76, p. 1., Springer, Berlin, 1978.
95. M. T. Pope, *Heteropoly and Isopoly Oxometalates*, Springer, Berlin, 1983.
96. I. V. Kozhevnikov, A. Sinnema, R. J. J. Jansen and H. van Bekkum, *Mendeleev Commun.*, 92, 1994.
97. I. V. Kozhevnikov, A. Sinnema, R. J. J. Jansen and H. van Bekkum, *Catal. Lett.*, 1994, **27**, 187.
98. G. M. Brown, M. R. Noe-Spirlet, W. R. Bushing and H. A. Levy, *Acta. Crystallogr., Sect. B*, 1977, **33**, 1038.
99. M. Misono, N. Mizuno, K. Katamura, A. Kasai, K. Konishi, K. Sakata, T. Okuhara and Y. Yoneda, *Bull. Chem. Soc. Jpn.*, 1982, **55**, 400.
100. T. Baba, H. Watanabe and Y. Ono, *J. Phys. Chem.*, 1983, **87**, 2406.